



Black-Hole Microstates in String Theory : Black is the Color but Smooth are the Geometries?

Pierre Heidmann

► To cite this version:

Pierre Heidmann. Black-Hole Microstates in String Theory : Black is the Color but Smooth are the Geometries?. High Energy Physics - Theory [hep-th]. Université Paris Saclay (COMUE), 2019. English. NNT : 2019SACLS109 . tel-02169793

HAL Id: tel-02169793

<https://theses.hal.science/tel-02169793>

Submitted on 1 Jul 2019

HAL is a multi-disciplinary open access archive for the deposit and dissemination of scientific research documents, whether they are published or not. The documents may come from teaching and research institutions in France or abroad, or from public or private research centers.

L'archive ouverte pluridisciplinaire **HAL**, est destinée au dépôt et à la diffusion de documents scientifiques de niveau recherche, publiés ou non, émanant des établissements d'enseignement et de recherche français ou étrangers, des laboratoires publics ou privés.

Black-Hole Microstates in String Theory: Black is the Color but Smooth are the Geometries?

Thèse de doctorat de l'Université Paris-Saclay
préparée à l'Université Paris-Sud

Ecole doctorale n°564 École Doctorale Physique en Île-de-France (PIF)
Spécialité de doctorat: Physique

Thèse présentée et soutenue à Gif-sur-Yvette, le 27 Juin 2019, par

Pierre Heidmann

Composition du Jury :

Boris Pioline

Directeur de Recherche, CNRS, Sorbonne Université,
Laboratoire de Physique Théorique

Président

Henning Samtleben

Professeur, CNRS, École Normale Supérieure de Lyon,
Laboratoire de Physique

Rapporteur

Bert Vercnocke

Assistant professeur, KU Leuven, Institut de Physique Théorique

Rapporteur

Stefano Giusto

Assistant professeur, Université de Padoue, Département de
Physique et d'Astronomie

Examineur

Andrea Puhm

Chargé de Recherche, CNRS, Ecole Polytechnique, CPHT

Examineur

Rodolfo Russo

Professeur, Queen's Mary, Ecole de Physique et d'Astronomie

Examineur

Iosif Bena

Chercheur CEA, CEA, Université Paris Saclay, IPhT

Directeur de thèse

There's only one direction in the faces that I see
Its upward to the ceiling, where the chamber's said to be.
Like the forest fight for sunlight, that takes root in every tree.
They are pulled up by the magnet, believing they are free.
The carpet crawlers heed their callers.
We've got to get in to get out,
We've got to get in to get out.

Genesis, *The Carpet Crawlers*

À Laurène,

Acknowledgments

A thesis may appear to be a long winding and lonely road from the outside, but it is far from true behind the scenes. This thesis could not have been realized without the many aids and supports I was fortunate to receive on a professional and personal level.

First and foremost, I would like to express my gratitude to my PhD supervisor, Iosif Bena. I have no idea if it is a classic phenomenon to admire the behavior of your supervisor. First, he has been an attentive teacher, always eager to dedicate times to making me understand, by his own inimitable way, the challenges of the field (and also a bit of Romanian History). His rhythm of explanations, propelled by a Formula-one engine, allowed me to quickly move from a master student to where I am today. He also taught me to be autonomous, to exploit the best of myself by ignoring my shortcomings, to propose and contribute to collaborations. I also thank him for his unfailing support in the search for postdocs, which allowed me to approach this stressful moment with confidence. These are the main points I will remember in the future.

I would like also to thank all the collaborators with whom I had the opportunity to work. Pedro Ramirez for being my first interlocutor. David Turton for the very rich project with Iosif and for the very long skype calls (endless?) that I essentially spent learning, learning and learning. Swapno Mondal for sharing a project that both of us do not totally understand what we were obtaining. Ruben Monten for his always optimistic approach for dealing with problems and for the time we spent trying to make this bloody WKB technique to work. And finally, I am pleased to have had the opportunity to work with Nick Warner. Even if it was only for a short period of my PhD, the clarity of his explanations and his constant good humour have made our scientific discussions the best I have ever had so far.

I am also grateful to Saclay's string group for the perfect working atmosphere, without too much pressure and always attentive: Alessandro Bombini, Johan Blaback, Adam Bzowski, Lilian Chabrol, Andrea Galliani, Monica Guica, Mariana Grana, Stefanos Katmadas, Eva Llabres Llambias, Severin Lüst, Daniel Mayerson, Ruben Minasian, Ander Retolaza, Chiara Toldo, Robert Walker.

I am thankful to the administration of IPhT and in particular to the IPhT secretaries, Anne Angles, Loic Bervas, Emmanuelle De Laborderie, François Gelis, Laure Sauboy, Sylvie Zaffanella. I have never experienced such an efficient administration before. Any french bureaucracy, famous throughout the world for its complexity, has never been a problem and has always been well managed.

For more personal thanks, it is more convenient for me to switch to french.

Je remercie mes parents, mon frère et ma soeur pour le cocon familial privilégié qui m'entoure, d'avoir respecter mon indépendance silencieuse mais en me soutenant sans faille au moindre besoin.

Je me sens également très chanceux d'avoir été accompagné d'un cercle fort d'amis qui m'ont permis de m'évader par tous les moyens, en vacances, en week-end ou lors de simples soirées et de m'avoir rendu certains matins compliqués. Premières pensées pour ma coloc de rêve avec Max, François et Laurène dont je garderai en mémoire simplement une image de rires, d'allégresse et de fléchettes. Pensée toute particulière pour Martin, ma muse accidentelle, mon partageur de tisane préféré, pour ses questions et incompréhensions permanentes du monde des sciences dans notre jeunesse qui m'ont certainement poussé à m'interroger à mon tour et d'en être arrivé là aujourd'hui. Pensée spéciale également à l'hebdomadaire, Rachel, Mathieu et Laurène, pour avoir fait de nos moments routiniers des moments mémorables. Je remercie mes amis, Anis, Aurelie, Alice, Caro, Cracra, Clem, Dada,

Delphine, Guigz, Guillaume, Lara, Pierre, Marie, Paulo, Erick, Sacha, Sophie, Vicouille pour tous les bons moments partagés. Vous allez me manquer par-delà l’atlantique.

Je remercie également mes camarades doctorants. De Saclay, Tavarish Kemal, Benoit pour les nombreuses pauses passées à déconner et Luca, Niall, Santiago, Severin et Christian, unis par les liens de la Chouffe et du frisbe. Et de Polytechnique, Charles, Luca et Quentin.

Pour finir, ma dernière pensée, et la plus importante, revient à Laurène pour avoir coloré mon quotidien. Qu’auraient-été ces dernières années sans toi ? Tout dans le moins très certainement. Tu m’as poussé quand je traînais des pieds, et ralenti quand j’étais trop pressé. Notre complicité me fut vitale. Tu es mon métronome, mon battement, ma raison.

Publications

Published papers

- **Four-center bubbled BPS solutions with a Gibbons-Hawking base,**
P. Heidmann
JHEP 10 (2017) 009 [1703.10095].
- **A systematic construction of microstate geometries with low angular momentum,**
I. Bena, P. Heidmann and P. F. Ramirez
JHEP 10 (2017) 217 [1709.02812]
- **AdS2 Holography: Mind the Cap,**
I. Bena, P. Heidmann and D. Turton
JHEP 12 (2018) 028 [1806.02834]
- **Bubbling the NHEK,**
P. Heidmann
JHEP 01 (2019) 108 [1811.08256]

Preprints

- **The full space of BPS multicenter states with pure D-brane charges,**
P. Heidmann and S. Mondal
Accepted by JHEP [1810.10019].
- **Superstratum Symbiosis,**
P. Heidmann and N.P. Warner
[1903.07631].
- **Thermal Decay without Information Loss in Horizonless Microstate Geometries,**
I. Bena, P. Heidmann, R. Monten and N. P. Warner
[1905.05194].

Contents

0	Introduction	1
1	Introduction en Français	9
Part I	Black holes and their microstates in Supergravity	18
2	Black holes in General Relativity and black-hole thermodynamics	19
2.1	Black holes in General Relativity	19
2.1.1	The Einstein-Hilbert action	20
2.1.2	The Schwarzschild black hole	20
2.1.3	The Kerr-Newman black hole	20
2.2	Black hole thermodynamics and Hawking radiation	21
2.2.1	The laws of black hole thermodynamics	22
2.2.2	Hawking radiation	23
3	Supergravity	24
3.1	Supergravity frameworks	24
3.1.1	Eleven-dimensional Supergravity	24
3.1.2	Type IIA and IIB Supergravity	29
3.2	Dualities and dimensional reduction	32
3.2.1	Kaluza-Klein reduction	32
3.2.2	T-duality	33
3.2.3	S-duality	33
3.2.4	Generalized spectral flows	34
3.3	Compactification to lower dimensions	34
3.3.1	Five-dimensional $\mathcal{N} = 2$ Supergravity	35
3.3.2	Six-dimensional $\mathcal{N} = (1, 0)$ Supergravity	36
4	Classical solutions in Supergravity	40
4.1	BPS solutions in five dimensions	40
4.1.1	Generic BPS solutions	40
4.1.2	Three-charge supersymmetric black hole	52
4.1.3	Smooth multicenter bubbling solutions	54

4.2	BPS solutions in six dimensions	59
4.2.1	Generic BPS solutions	60
4.2.2	Supersymmetric black string and the BTZ black hole	66
4.2.3	Two-charge Supertube	68
4.2.4	Momentum-generating technique	71
4.2.5	Superstrata	72
4.3	Three-charge non-BPS solutions	78
4.3.1	Extremal rotating black holes in type IIB	78
4.3.2	Almost-BPS solutions	80
4.4	Final comment	85
Part II Construction of microstate geometries		87
5	Systematic construction of scaling multicenter solutions	88
5.1	Walls of marginal stability of collinear centers in the scaling limit	89
5.1.1	A change of background preserving the $U(1) \times U(1)$ isometry	90
5.1.2	A change of background breaking a $U(1)$ isometry	95
5.2	Systematic construction of a large family of smooth four-center solutions	97
5.2.1	Three-supertube scaling BPS solutions in Taub-NUT	97
5.2.2	Microstate geometries from three-supertube configurations	99
5.3	Multicenter solutions with arbitrarily low angular momentum	102
5.3.1	Analysis with four GH centers	103
5.3.2	Analysis with three GH centers and one Supertube	103
5.4	Final comment	105
6	Counting Multicenter solutions at low charges	106
6.1	Setting the problem	106
6.2	Counting zero-momentum multicenter states with pure D2 and D6 charges	108
6.2.1	The family of three-center solutions	109
6.2.2	The family of four-center solutions	109
6.2.3	The family of five-center solutions	110
6.2.4	Summary	110
6.3	Discussion	110
6.3.1	Features of the twelve solutions	110
6.3.2	Quantum Effects	113
6.3.3	The solutions with $Q_{D6} = 2$	115
6.4	Final comment	115

7	The ultimate single-mode Superstratum	117
7.1	Supercharged Superstrata	118
7.1.1	The first layer	118
7.1.2	The second layer	119
7.1.3	Regularity and conserved charges	120
7.2	Hybrid Superstrata	120
7.2.1	The first layer	120
7.2.2	The second layer	121
7.2.3	Regularity and conserved charges	122
7.3	The $(2, 1, n)$ example	123
7.3.1	The metric	124
7.3.2	Limiting geometries	124
7.4	Generic multi-mode Superstrata	126
7.4.1	The multi-mode problem	126
7.4.2	The high-frequency sources in the second BPS layer	127
7.5	Final comment	129
8	Microstates of extremal Kerr black holes	130
8.1	Generating technique	130
8.1.1	From $\text{AdS}_3 \times \text{S}^3$ to $\text{WAdS}_3 \times \text{SqS}^3$	130
8.1.2	The recipe	131
8.1.3	The family of almost-BPS three-supertube solutions in \mathbb{R}^4	132
8.2	Asymptotically $\text{WAdS}_3 \times \text{SqS}^3$ bubbling geometries	135
8.2.1	The ultraviolet geometry	136
8.2.2	The infrared geometry	138
8.2.3	The construction procedure	140
8.2.4	An explicit example	140
8.3	Asymptotically NHEK bubbling geometries	141
8.3.1	Matching the WAdS_3 UV geometry to NHEK	142
8.3.2	The construction procedure	143
8.3.3	An explicit example	143
8.4	Final comment	144
Part III	Scattering from microstate geometries and application to AdS/CFT	145
9	AdS_2 Holography: Mind the Cap	146
9.1	State of the art and proposal	146
9.2	AdS_2 limit of capped solutions of five- and six-dimensional Supergravity	148

9.2.1	The AdS_2 limit	148
9.2.2	Asymptotically AdS_2 multicenter solutions	149
9.2.3	Asymptotically AdS_2 Superstrata	150
9.3	Excitations of asymptotically AdS_2 Superstrata	154
9.3.1	The minimally coupled massless scalar wave equation	154
9.3.2	Constructing finite-energy solutions	156
9.3.3	Analytic bound-state solutions for large n	157
9.3.4	Numerical bound-state solutions for arbitrary n	159
9.3.5	An AdS_3 perspective	161
9.4	Discussion	164
9.4.1	Backreaction	164
9.4.2	Holographic description of the solutions and excitations	165
10	Scattering from microstate geometries in the black-hole regime	167
10.1	Holographic response functions	168
10.1.1	Brief review of holographic correlators	168
10.1.2	Brief review of WKB	168
10.1.3	The WKB hybrid technique	170
10.2	Details of the WKB analysis	173
10.2.1	Derivation of the response function using hybrid WKB	173
10.2.2	Response function in asymptotically extremal BTZ geometries	177
10.2.3	Model response function in the interior: global AdS_3	180
10.3	The $(1,0,n)$ Superstrata	184
10.3.1	The metric	184
10.3.2	The massless scalar wave perturbation	185
10.3.3	WKB analysis	186
10.4	Response function for $(1,0,n)$ Superstrata	188
10.4.1	Summary of results	188
10.4.2	The cap regime	190
10.4.3	The extremal-BTZ regime	191
10.4.4	The intermediate extremal-BTZ regime	192
10.4.5	The centrifugal-barrier regime	193
10.5	Position-space Green functions	195
10.5.1	Position space Green function in $(1,0,n)$ Superstrata	195
10.6	Final comment	197
A	Appendix	1
A.1	Integration in \mathbb{R}^3	1

A Appendix of Chapter 5	3
A.2 Numerical analysis of the entropy parameter of four-GH-center solutions	3
A.3 Numerical analysis of the entropy parameter of solutions with one Supertube and three Gibbons-Hawking centers	7
A Appendix of Chapter 6	10
A.4 Analysis of three-center solutions	10
A.4.1 Analytic investigation of solutions with two Supertubes and one GH center . .	10
A.4.2 Numerical analysis of solutions with one Supertube and two GH centers and solutions with three GH centers	12
A.5 Analysis of four-center and five-center solutions	12
A.5.1 Analysis of four-center solutions	12
A.5.2 Analysis of five-center solutions	13
A.6 Configurations with $Q_{D6} = 2$	13
A.7 Three-node abelian quiver with general (a,b,c)	15
A Appendix of Chapter 8	17
A.8 The example of asymptotically $WAdS_3 \times SqS^3$ bubbling solution	17
A.9 The example of asymptotically NHEK bubbling solution	19
A Appendix of Chapter 9	22
A.10 Analytic solution of the wave equation for large n	22
A Appendix of Chapter 10	27
A.11 Potentials with arbitrarily many turning points	27
A.12 Comparison of the exact and approximate response functions	28
A.12.1 The exact and approximate BTZ response functions	28
A.12.2 The exact and approximate AdS_3 response functions	28
A.13 Position-space Green functions	29
A.13.1 Position space Green's functions in extremal BTZ	29
A.13.2 Position space Green's functions in AdS_3	32
Bibliography	35

Introduction

Foreword

In science, the Universe defines what can be governed univocally through fundamental laws. In that sense, our notion of Universe has never stopped growing through the centuries. In ancient times, it was very limited in space and time by the theory of the five classical elements, earth, water, air, fire and aether, and by geocentrism. Thanks to countless breakthroughs, such as the Newton's laws, Kepler's laws, Maxwell theory, Mendeleïev's classification, etc., our Universe has evolved to describe the atom scale to the solar-system scale. Each step forward has always been made possible by exploiting singular behaviours lying at the edge of our prevailing conception of the Universe. Those singular behaviours have been either observed through experiments or have emerged from theoretical divergences from previous prevailing theories. In physics, new theories always arise by including the essential degrees of freedom needed to resolve singularities.

In the 20th century, the list of fundamental elements and the four fundamental interactions composing the Universe were well-established. On one side, the *Standard model* unified the electromagnetic, weak and strong interactions at high energy within a quantum-field-theory framework. It described with great success the dynamics of the elements under those interactions at any scale where gravity is negligible. On the other side, the gravitational interaction was captured as a spacetime deformation in *General Relativity* from the scale of the atom to the size of the observable universe. Inspired by the Standard model, the notion of a theory of everything unifying all interactions at high energy emerged. This requires to quantize gravity into a theory of *Quantum Gravity*. However, due to the geometric nature of gravity, direct quantization has faced major issues. String Theory is a quantum theory of gravity based on the classification of the fundamental elements as extended objects in higher dimensions such as strings.

Unifying General Relativity and Quantum mechanics is not a theorist's fantasy. Even if both frameworks have been experimentally tested with great precision in their domains of validity, the picture of the Universe remains scattered and their incompatibility gives rise to unsolved paradoxes. First, from observation, the matter well-described by those theories accounts only for 15% of the overall density and 68% of the energy allowing the expansion of the Universe to accelerate is unknown. Their names, dark matter and dark energy, are the only characteristics widely shared by the scientific community. Second, the understanding of our world is limited by the scales where the theoretical description breaks down. If the Standard model is naturally protected from divergences, General Relativity is not. General Relativity has two inherent singular behaviours delimiting the edge of the Universe as we know it today. First, the initial singularity, or big bang, corresponds to the furthest spacetime slice when the Universe was Planck size. Second, the theory contains also "black-hole-type" singularities where the curvature of spacetime diverges under strong deformations of compact masses. Those two singularities lie at the common theoretical border between General Relativity and Quantum Mechanics and must be resolved by a quantum theory of gravity. Because time travel back to the first nanoseconds of our Universe is not yet planned, black holes are the main theoretical and experimental laboratory for testing quantum theories of gravity such as String Theory.

Black-hole mystery

Black holes were first predicted theoretically before being recently observed via gravitational-wave detection [1] or via direct observation [2]. They are supposed to be produced by the gravitational collapse of supermassive stars. In General Relativity, stationary black holes are described as a compact mass and charge inducing a spacetime singularity and an angular momentum rotating the spacetime. The singularity is dressed by a null hypersurface, called the *event horizon* delimiting two regions: the interior of the black hole and the exterior. In the interior, nothing, not even light, can escape and the black hole is purely absorbing. Therefore, for a distant observer, a black hole is completely characterized by its three macroscopic quantities. However, black holes behave as black bodies. Their entropy, or *Bekenstein-Hawking entropy* is proportional to the area of the horizon and they have a temperature. A semiclassical computation by Hawking suggests that this temperature is accompanied by a thermal radiation until complete evaporation.

We did not go into details for the first description, but let us now develop the three main puzzles of black-hole physics:

- The black-hole entropy:

The entropy of a black hole is enormous, of the order of its mass squared in Planck-length unit. As for any entropic object, a microscopic description in terms of large degeneracy of states should exist. The “ e^S ” microstates should be related via statistical ensemble to the macroscopic description of black holes in General Relativity. It is naively questionable whether General Relativity can also provide a description of those microstates. The no-hair theorem stipulates that a black hole is uniquely defined by the external quantities and all other information thrown inside is lost. This forms a no-go theorem for constructing non-trivial horizon-scale structures within General Relativity.

Therefore, a quantum theory of gravity must provide the degrees of freedom that are necessary to describe the microstate nature of black holes.

- The information loss:

Black-hole evaporation gives rise to a conceptual conflict between Quantum Mechanics and General Relativity. A black hole can be produced by the gravitational collapse of a pure state whereas it radiates only thermal mixed states. Thus, the unitarity principle of Quantum Mechanics is apparently undermined by gravity. Two choices are at hand: either one can construct quantum gravity without the unitarity cornerstone of Quantum Mechanics as Hawking suggested, or one can construct a unitary quantum gravity theory and find a process by which information can escape from a black hole. The latter is usually the preferred scenario for most quantum theories of gravity and addressing the *information loss puzzle* is a major challenge for their consistency.

- The central singularity:

The sun does not collapse under its own weight thanks to nuclear reactions in its nucleus. The stability of the sun can be modelled by activating the right degrees of freedom within General Relativity. The black-hole singularity results from the lack of quantum degrees of freedom and should be replaced by considering quantum corrections. The main question is to determine at which scale from the singularity the classical picture starts to break down. This issue is also closely related to the question of the microstate structure. Indeed, if this structure can have a geometrical meaning, it is supposed to naturally solve the singularity.

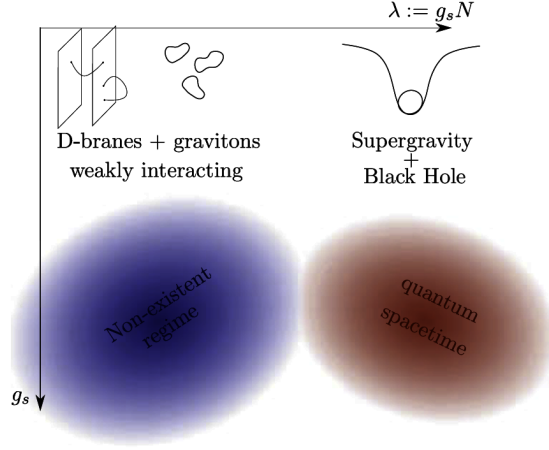


Figure 1: The regimes of parameters in String Theory (the graph is taken from [5]).

The approach of String Theory

Since the 60s, String Theory has been a very promising candidate for a theory of Quantum Gravity. Its progressive development over the years has provided a powerful framework for understanding the nature of black holes. String Theory is based on the existence of Supersymmetries relating fermions and bosons. This allows for the non-trivial connection between the spacetime symmetry of the Poincaré group and the internal gauge symmetries of the other interactions. The consistency of the theory fixes the total number of spacetime dimensions at 10 or possibly 11. Let us stick to the ten-dimensional String theories for the sake of clarity. The six extra-dimensions must form a relatively small compact manifold in order to match our four-dimensional everyday world. Moreover, a point particle in four dimensions can now have a non-trivial geometry along the extra dimensions. The fundamental string is the most primitive one but higher-dimensional objects such as *branes* also exist. A string is described by its *string length*, l_s , and its *string coupling*, g_s . Interactions between strings defines two-dimensional surfaces, called world-sheets, which obviate the usual local singularities of particle scattering in quantum field theories. Thus, String Theory is UV complete. Moreover, String Theory requires the presence of a spin-2 field, the graviton, and thus incorporates General Relativity at low energy. On the other side, the Standard-model gauge groups and their associated matter contents can also be encompassed within String Theory even if there is no special requirement to have the specific $SU(3) \times SU(2) \times U(1)$.

In String Theory, fundamental objects are represented as branes interacting with open or closed strings. Supersymmetric configurations of N branes have the great advantage of having moduli-free quantities such as their entropy for instance. Thus, those quantities can be obtained for any values of g_s that are suitable for the computation. Two regimes are particularly interesting (see Fig.1.1). Both are at $g_s \ll 1$ where stringy corrections are negligible and where the Newton constant, G , is negligible. The Supergravity regime is at large $g_s N$. This corresponds to have fixed “ $G.M$ ”, the branes backreact and deform the spacetime (see Fig.1.1). At low $g_s N$, the branes do not backreact and are heavy static objects with weakly-coupled open strings stretched between them. The physics of the branes is given by a free field theory. Thus, a supersymmetric brane bound state has two equivalent descriptions in two apparently different frameworks. This is what guided the discovery of the AdS/CFT correspondence. The correspondence had initially established a link between weakly-coupled Super Yang-Mills at $g_s N \ll 1$ to AdS₅ gravity at $g_s N \gg 1$ [3] before being considerably enriched (see [4] for a review).

Thus, String Theory offers a consistent framework of Quantum Gravity for answering the black-hole mystery. We briefly review the state-of-the-art and the remaining open questions in the following:

- The black-hole entropy:

One of the most important achievements of String Theory is the construction of the microscopic degrees of freedom of supersymmetric black holes as bound states of strings and branes at very low string coupling.

This was first achieved for the supersymmetric two-charge system. It was initially derived in the F1-P frame where the system corresponds to a large number N of fundamental strings F1 with momentum P on them. At low $g_s N$, the entropy results from the different ways in which the momentum can be distributed among the harmonics of the strings. Each microstate has a well-defined and unique representation. The entropy can be calculated exactly via the Cardy's formula within the underlying CFT. At large $g_s N$, the configurations collapse to a point and their microscopic structures disappear by forming a two-charge black hole. The black hole does not have enough types of charges to support a macroscopically non-vanishing horizon area. However, it has been argued by Sen [6] and confirmed by Dabholkar [7] that stringy corrections to the horizon area give a Bekenstein-Hawking entropy exactly equal to the entropy obtained at low $g_s N$.

Strominger and Vafa extended Sen's conclusions to the supersymmetric three-charge system [8]. They worked in the D1-D5-P frame where the system corresponds to one-dimensional branes D1 with five-dimensional branes D5 sharing a common compact direction and momentum charges P¹. Similarly, at low $g_s N$, each brane bound state is identifiable and the entropy is obtained via Cardy's formula. By increasing $g_s N$, the branes backreact and deform their six-dimensional transverse space. At large $g_s N$, the supergravity framework contains the six-dimensional supersymmetric black-string solutions. The black string can be dimensionally reduced to the five-dimensional supersymmetric black hole or D1-D5-P black hole. The derivation of its horizon area exactly matches the microscopic result.

Those outstanding results showed that black holes are formed by brane bound states. At the “no-gravity” point of the moduli space, their microscopic degrees of freedom are manifest. They correspond to configurations of branes with weakly-coupled open strings stretched between them. However, their fate once gravity is turned on is still subject to debate. Do the microstate structures fall behind the horizon and essentially disappear from the view of distant observers? Or are they still manifest through non-trivial horizon-scale physics? Let us admit that the latter scenario could give us more confidence in resolving the two next black-hole puzzles.

The second scenario has been proposed by Mathur and is known as the *Fuzzball proposal* [9]. The proposal stipulates that, in the classical regime, there exist “ e^S ” horizonless non-singular solutions that resemble a black hole from afar but differ in the vicinity of the horizon. Based on this statement, the classical black-hole solution corresponds to the average description of a system of solutions which match the black-hole geometry outside the horizon but cap off as “fuzzy” smooth geometries in the infrared (see Fig.1.2). Such solutions obviously cannot exist in classical General Relativity; one needs objects which grow and do not collapse as gravity increases and such objects are provided within String Theory [10].

Starting once again with the two-charge system, the “ e^S ” F1-P singular solutions can be dualized into “ e^S ” D1-D5 solutions, called *wiggly Supertubes* [11–14]. In this frame, the singularity is resolved by being mapped to a Kaluza-Klein monopole. Each solution is horizon-free and develops a specific smooth geometry close to the would-be horizon. Thus, the microstate structure of the two-charge black hole is still visible in the supergravity regime and the microstates are all represented as non-singular smooth geometries.

To be validated, the proposal must successfully address the three-charge system. The *microstate geometry program* was developed to accomplish this vast task. Since then, many supersymmetric

¹The F1-P system considered by Sen can be dualized to the D1-D5 system. In that sense, the Strominger-Vafa black hole is adding another type of charge to the Sen black hole.

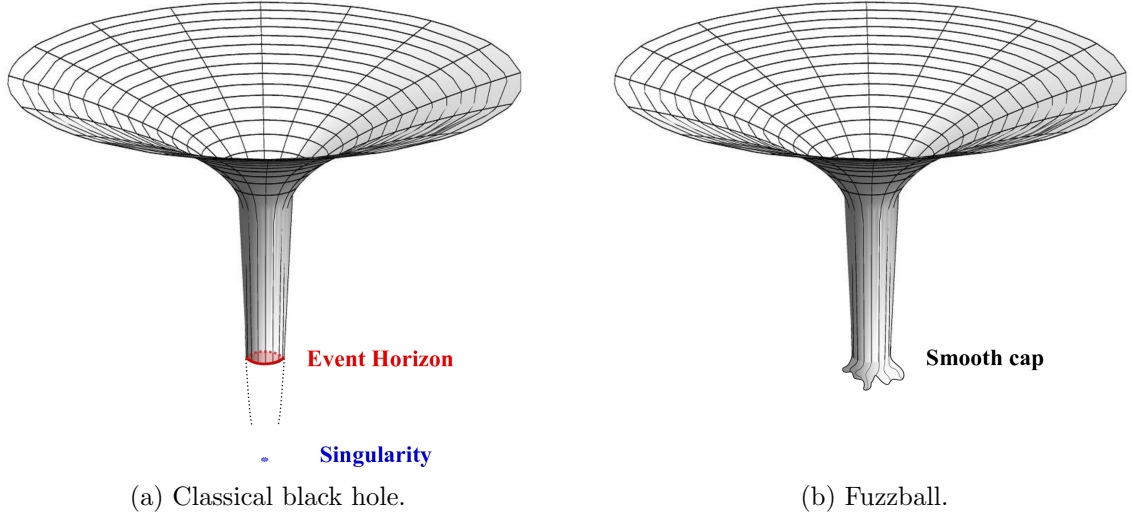


Figure 2: The Fuzzball proposal and the schematic description of the two-dimensional embedding of the classical black hole as an average description of “ e^S ” smooth fuzzballs.

smooth horizonless three-charge solutions have been constructed as we will see in detail in the main parts of the thesis (see [15, 16] for reviews).

- The central singularity:

The discovery of the microscopic degrees of freedom of black holes is an important achievement, but it does not provide any insight regarding the information loss paradox or the resolving of the singularity. Those questions can only be addressed in the classical regime.

A preliminary step is to elucidate at which scale the classical picture of black hole breaks down. For most quantum systems, the classical description is reliable up to Planck scale, $l_P \sim 10^{-35}\text{m}$. One can naturally think that the description of black holes in General Relativity is valid until a Planck distance from the singularity [17]. In that regard, the microstate structure should be confined below this scale. Another approach, related to the Fuzzball proposal, is to conjecture that a highly-entropic quantum system has a reliable classical description up to a scale of $N^\alpha l_P$. For instance, the scale of reliability of the two-charge F1-P system is $N^{1/3}l_P$ [9]. Moreover, all the three-charge smooth horizonless solutions differ from the black-hole geometry at Planck’s length from the horizon. Although their description as black-hole microstates is still subject to discussions, they show at least that the singularity can be resolved much further than the Planck’s length. Moreover, String Theory is dotted with many well-known examples where singularities are resolved at large scales such as Polchinski Strassler [10], Klebanov-Strassler [18] or the LLM geometries [19]. Therefore, it can be confidently stated that the effects of quantum gravity can occur at macroscopic distance from the classical singularity and possibly at the horizon scale.

- The information loss:

The last statement helps considerably to resolve the paradox of the information loss. In the original Hawking calculation, the radiation is emitted in the vicinity of the horizon, in the vacuum, away from the location of the black-hole singularity. The Hawking quanta can not easily carry information from the interior. However, if the near-horizon geometry should be replaced by some fuzzy structures, the radiation can carry information about the microstates and can be unitary [20].

Once again, this is still at the level of a postulate and explicit computations and evidence are needed. Moreover, other scenarios have developed unitary mechanisms allowing information to escape

or partially escape without the need for fuzzballs. One can refer non-exhaustively to the soft hair on black holes [21] or to the information recovery from double-trace deformations [22].

However, the most naive scenario, that consists in quantum corrections to the semiclassical Hawking’s computation, has been excluded. Indeed, Hawking’s computation is based on quantum field theories on a classical curved background. In [20], it has been shown that quantum corrections on the near-horizon region of black holes cannot completely restore unitarity.

A curious reader may also wonder why the failure of unitarity is not considered a plausible scenario. String Theory is a quantum theory of gravity that naturally preserves unitarity. In addition, the AdS/CFT correspondence provides a direct counterexample. Indeed, asymptotically AdS black hole must have a dual description within a unitary conformal field theory. In that sense, any physical process must be unitary.

All those arguments and new open questions represent a major step further in our understanding of black holes. However, they were conducted in the context of supersymmetric and extremal solutions. They must be considered as guidelines for addressing similar issues to non-supersymmetric and non-extremal solutions, which are much less understood.

Contributions and Organization of the Manuscript

This thesis addresses black-hole physics through the lens of the fuzzball proposal and the microstate geometry program. The major part of the discussion will be conducted in the low-energy limit of String Theory, that is in Supergravity. We will self-consistently introduce and review the works [23–29] that we hope have given more weight to the proposal.

The thesis is made up of three main parts. Part I introduces the basic materials and gives a review of the microstate geometry program. Part II gathers the works [23, 24, 26–28] which aimed at constructing new classes of smooth horizonless geometries, supersymmetric or non-supersymmetric ones. Finally, Part III tackles deeper questions related to the black-hole puzzles discussed above [25, 29].

In the first chapter, we introduce basic notions of General relativity leading to the construction of black holes. We also discuss the laws of black-hole thermodynamics. We describe their properties and their paradoxes in slightly more details than in the present introduction.

In Chapter 3, we review the supergravity frameworks used in this thesis. We self-consistently start with the “mother” theory in eleven dimensions and the ten-dimensional type IIA and type IIB Supergravities. We review the different dualities that relate them. We aim to construct three-charge solutions valid in the same regime as the five-dimensional black hole or six-dimensional black string. We construct five- and six-dimensional ungauged Supergravities by dimensional reduction of type IIB and eleven-dimensional Supergravities.

In Chapter 4, we derive the equations of motion for supersymmetric solutions in five and six dimensions. We give the brane-bound-state pictures of those solutions from an eleven- and ten-dimensional perspective. We show that the three-charge supersymmetric black-hole solutions coexist with smooth horizonless solutions that resemble the black holes up to the horizon scale. In particular, we review the construction of smooth *bubbling solutions* in five dimensions and *Superstrata* in six dimensions and describe them as brane bound states in eleven and ten dimensions. In the last section of this chapter, we briefly discuss the non-supersymmetric solutions. We first detail the properties of the Cvetič-Youm black hole and its *near-horizon extremal Kerr geometry*. Then, we construct the family of *almost-BPS bubbling solutions*.

According to the fuzzball proposal, those smooth solutions must be viewed as black-hole microstates. The “Holy Grail” of the microstate geometry program is to construct “ e^S ” such solutions or, in the first instance, to construct very large classes of them.

Chapter 5 is devoted to the smooth bubbling solutions in five dimensions at $g_s N \gg 1$. First of all, we show that a class of such solutions has peculiar properties that have not been noticed so far. It is well-known that brane bound states can decay at *walls of marginal stability* by changing the background at large distance. For instance, a brane configuration can perfectly live in an asymptotically flat background but a change to asymptotically AdS_3 can make the configuration disappear. Obviously, a black hole is independent on the asymptotics in which it is embedded. Typical black-hole microstates must then share this characteristic. We show that some bubbling solutions are still highly dependent on the asymptotic background, even when the solutions develop a very long throat. In a second section, we construct the largest known family of smooth bubbling solutions [23]. Such a construction is complicated to achieve due to the hardly-manageable regularity constraints governing bubbling solutions. Then, by analyzing the properties of this family, we show that bubbling solutions can have an arbitrarily low angular momentum [24]. Before this work, it was commonly thought that such solutions were almost-maximally spinning and that Superstrata were the only known microstate geometries with low angular momentum.

In Chapter 6 we construct the “ e^S ” brane bound states of a specific brane system at $g_s N \ll 1$ [26]. We consider the system with pure D6-D2-D2-D2 charges. At large charges, this system corresponds to a black hole dual to the D1-D5-P black hole. With pure charges, that is charges equal one, the number of states is microscopically 12. We construct the 12 brane bound states in the Coulomb branch as bubbling solutions. For large charges, they might describe “near-horizon limit” of fuzzballs. Thus, for this specific low-charge example, we show that the “ e^S ” states of a “primitive” three-charge black hole are recovered as fuzzball-like states.

In Chapter 7, we review a crucial step forward in the construction of “the most general” single-mode Superstratum [28]. We use a hybrid of the original superstratum mode [30] and the supercharged mode [31] to construct single-mode Superstrata that still have free classical moduli after fixing the asymptotic charges of the system. We show that those hybrid modes are the elementary building blocks of generic multi-mode Superstrata parametrized by arbitrary functions of three independent variables. These multi-mode Superstrata form the largest family of solutions to the Einstein’s equation ever constructed.

In Chapter 8, we build the first family of smooth bubbling microstate geometries that are asymptotic to the near-horizon region of extremal five-dimensional Kerr black holes [27]. Nearly extremal Kerr black holes were observed in the sky. This work represents an important advance towards describing the microstate structure of observable black holes.

The strategy of the microstate geometry program is not only about recovering the phase space with smooth horizonless solutions in the black-hole regime. First, it is crucial to examine how it clarifies the information loss paradox. Second, microstate geometries are also very useful tools for testing and learning about AdS/CFT correspondences in various dimensions.

Chapter 9 investigates the implication of microstate geometries in the context of the $\text{AdS}_2/\text{CFT}_1$ correspondence [25]. The extremal supersymmetric three-charge black holes develop an AdS_2 near-horizon limit. However, any finite-energy perturbations in global AdS_2 destroy either the ultraviolet (UV) or the infrared (IR). This unusual feature led the community to think that holography in AdS_2 is subtle and very different from other $\text{AdS}_{D+1}/\text{CFT}_D$ correspondences. That is, understanding quantum gravity in asymptotically AdS_2 spacetimes is crucial. We show that the microstate geometries have a “near-horizon” limit similar to that of the black hole. This leads to asymptotically AdS_2 geometries which cap off smoothly in the IR. These geometries satisfy the zero-angular momentum conjecture

according to which any typical black-hole microstates in five dimensions must have one zero angular momentum out of two. Moreover, we argue that all the ground states of a non-trivial CFT_1 must have dual geometries which break conformal invariance in the IR. In other words, the geometries must cap off like fuzzballs. A corollary is that uncapped Poincaré AdS_2 is not dual to any ground state of a non-trivial CFT_1 . From this statement, we argue that the $\text{AdS}_2/\text{CFT}_1$ correspondence follows the usual holographic philosophy. We show that the geometries dual to the CFT_1 ground states support an infinite tower of non-supersymmetric excitations thanks to the presence of an IR cap. Thus, the work of [25] gives the beginning of a proof for the fuzzball proposal. It does not show that all “ e^S ” black-hole microstates are fuzzballs. It shows that, if the CFT_1 that gives rise to the black-hole entropy is not trivial, the “ e^S ” ground states are dual to geometries that end with a cap in the IR.

In Chapter 10, we study the scattering process in microstate geometries by computing boundary-to-boundary scalar Green functions [29]. This helps to elucidate how unitarity is restored and how information escapes from black-hole backgrounds. It is commonly accepted that black holes are very chaotic objects due to a large number of microstates. For the D1-D5-P black hole, when a scalar wave is emitted from the boundary, the Green function decays exponentially over time as the wave is absorbed by the hole. Then, after a long period of time, it is expected that the microstate structure will begin to influence the physics: the Green function increases again and reaches a plateau with large random fluctuations. This long period is of the order of $N_1 N_5$ for a D1-D5-P black hole where N_1 and N_5 corresponds to the number of D1 and D5 branes respectively. In this chapter, we develop a brand-new technique that allows to compute Green functions in arbitrarily-complicated asymptotically-AdS backgrounds. We apply this technique to a specific family of Superstrata. We show that the response function of a probe scalar, in momentum space, is essentially given by the pole structure of the cap modulated by the black-hole response function. In position space, this translates into a sharp exponential black-hole-like decay at short time followed by evenly spaced “echoes from the cap,” with period $\sim N_1 N_5$. Those echoes differ from the sporadic expectations. This is mainly due to the fact that we are probing only one highly-coherent microstate geometry with a specific highly-redshifted AdS_3 cap. Thus, considering an ensemble of microstates should average slightly-different echoes and gives the expected random fluctuations. Nevertheless, this is the first computation in the black-hole regime showing how non-trivial structure at the horizon-scale allows the information to escape in a unitary process.

We join in the Appendix all the additional materials of the different chapters. The appendixes are classified according to the chapters they correspond to.

In the last chapter, we briefly take stock of what has been done in this thesis. We also sketch few open questions that we would like to explore in the near future.

Introduction en Français

En science, l'Univers définit ce qui peut être gouverné de façon univoque par des lois fondamentales. En ce sens, notre notion d'Univers n'a jamais cessé de croître au cours des siècles. Dans l'Antiquité, elle était très limitée dans l'espace et dans le temps par la théorie des cinq éléments classiques, la terre, l'eau, l'air, le feu et l'éther, et par le géocentrisme. Grâce à d'innombrables percées, telles que les lois de Newton, les lois de Kepler, la théorie de Maxwell, la classification de Mendeleïev, etc., notre Univers a évolué de l'échelle atomique à celle du système solaire. Chaque pas en avant a toujours été rendu possible par l'exploitation de comportements singuliers à la limite de notre conception dominante de l'Univers. Ces comportements singuliers ont été observés à travers des expériences ou ont émergé de divergences théoriques par rapport aux théories existantes. En physique, de nouvelles théories surgissent toujours en incluant les degrés de liberté essentiels et nécessaires pour résoudre les singularités.

Dans le 20^{ème} siècle, la liste des éléments fondamentaux et les quatre interactions fondamentales composant l'Univers étaient bien établies. D'un côté, le modèle standard a unifié à haute énergie les interactions électromagnétiques, faibles et fortes dans un cadre de théorie des champs quantiques. Elle a décrit avec grand succès la dynamique des éléments sous ces interactions à n'importe quelle échelle où la gravité est négligeable. D'un autre côté, l'interaction gravitationnelle a été capturée comme une déformation spatio-temporelle de l'échelle de l'atome à la taille de l'univers observable. Inspirée par le modèle Standard, la notion d'une théorie du tout unifiant toutes les interactions à haute énergie a émergé. Il faut pour cela quantifier la gravité dans une théorie de la gravité. Cependant, en raison de la nature géométrique de la gravité, la quantification directe a été confrontée à des problèmes majeurs. La théorie des cordes est une théorie quantique de la gravité basée sur la classification des éléments fondamentaux en objets étendus dans des dimensions supérieures comme les cordes.

L'unification de la Relativité Générale et de la Mécanique Quantique n'est pas le fantasme de théoriciens. Même si les deux cadres ont été testés expérimentalement avec une grande précision dans leurs domaines de validité, l'image de l'Univers reste limitée et leur incompatibilité donne lieu à des paradoxes non résolus. Tout d'abord, d'après les observations, la matière bien décrite par ces théories ne représente que 15% de la densité globale et 68% de l'énergie permettant à l'expansion de l'Univers d'accélérer est inconnue. Leurs noms, matière noire et énergie noire, sont les seules caractéristiques largement partagées par la communauté scientifique. Deuxièmement, la compréhension de notre monde est limitée par les échelles où la description théorique cesse d'être valide. Si le modèle Standard est naturellement protégé des divergences, la Relativité Générale ne l'est pas. La Relativité Générale a deux comportements singuliers inhérents qui délimitent le bord de l'Univers tel que nous le connaissons aujourd'hui. Premièrement, la singularité initiale, ou big bang, correspond au moment la plus éloignée lorsque la taille de l'Univers était de l'ordre de l'échelle de Planck. Deuxièmement, la théorie contient aussi des singularités de type "trou noir" où la courbure de l'espace-temps diverge sous de fortes déformations de masses compactes. Ces deux singularités se situent à la frontière théorique commune entre la relativité générale et la mécanique quantique et doivent être résolues par une théorie quantique de la gravité. Parce que le voyage dans le temps jusqu'aux premières nanosecondes de notre Univers n'est pas encore planifié, les trous noirs sont le principal laboratoire théorique et expérimental pour

tester les théories quantiques de la gravité comme la théorie des cordes.

Le mystère des trous noirs

Les trous noirs ont d'abord été prédits théoriquement avant d'être observés récemment par détection des ondes gravitationnelles [1] ou par observation directe [2]. Ils sont censés être produits par l'effondrement gravitationnel d'étoiles supermassives. Dans la Relativité Générale, les trous noirs stationnaires sont décrits comme une masse et une charge compactes induisant une singularité spatio-temporelle et un moment angulaire induisant une rotation de l'espace-temps. La singularité est habillée d'une hypersurface nulle, appelée *horizon des événements*, délimitant deux régions : l'intérieur du trou noir et l'extérieur. A l'intérieur, rien, pas même la lumière, ne peut s'échapper et le trou noir est purement absorbant. Par conséquent, pour un observateur éloigné, un trou noir est complètement caractérisé par ses trois grandeurs macroscopiques. Cependant, les trous noirs se comportent comme des corps noirs. Leur entropie, ou entropie de Beckestein-Hawking, est proportionnelle à la surface de l'horizon et ils ont une température. Un calcul semi-classique mené par Hawking suggère que cette température est accompagnée d'un rayonnement thermique jusqu'à évaporation complète.

Nous avons été vague dans la description, nous allons maintenant développer les trois principales énigmes de la physique des trous noirs :

- Le paradoxe de l'entropie:

L'entropie d'un trou noir est énorme, de l'ordre de sa masse au carré. Comme pour tout objet entropique, une description microscopique en termes de grande dégénérescence d'états devraient exister. Les micro-états " e^S " doivent être reliés via un ensemble statistique à la description macroscopique des trous noirs dans la Relativité Générale. On peut naïvement se demander si la Relativité Générale peut aussi fournir une description de ces micro-états. Le "no-hair theorem" stipule qu'un trou noir est défini de façon unique par les quantités externes et que toutes les autres informations qui y sont jetées sont perdues. Ceci forme un "no-go theorem" pour construire des structures non triviales à l'échelle de l'horizon à l'intérieur de la relativité générale.

Par conséquent, une théorie quantique de la gravité doit fournir les degrés de liberté nécessaires pour décrire la nature microéstatique des trous noirs.

- Le paradoxe de l'information:

L'évaporation des trous noirs donne lieu à un conflit conceptuel entre la Mécanique quantique et la Relativité générale. Un trou noir peut être produit par l'effondrement gravitationnel d'un état pur alors qu'il ne rayonne que des états mixtes thermiques. Ainsi, le principe d'unitarité de la Mécanique Quantique est apparemment miné par la gravité. Deux choix s'offrent à nous : soit on peut construire la gravité quantique sans la pierre angulaire de l'unitarité de la Mécanique quantique comme l'a suggéré Hawking, soit on peut construire une théorie de la gravité quantique unitaire et trouver un processus par lequel l'information peut sortir d'un trou noir. Ce dernier scénario est généralement le scénario préféré pour la plupart des théories quantiques de la gravité et le fait de s'attaquer au paradoxe de l'information est un défi majeur pour leur consistance.

- La singularité centrale:

Le soleil ne s'effondre pas sous son propre poids grâce à des réactions nucléaires dans son noyau. La stabilité du soleil peut être modélisée en activant les bons degrés de liberté en relativité générale. La singularité du trou noir résulte de l'absence de degrés quantiques de liberté et devrait être remplacée par la prise en compte des corrections quantiques. La question principale est de déterminer à quelle

échelle de la singularité l'image classique commence à ne plus être valide. Cette question est également étroitement liée à celle de la structure des micro-états. En effet, si cette structure peut avoir un sens géométrique, elle est censée résoudre naturellement la singularité.

L'approche de la Théorie des Cordes

Depuis les années 60, la théorie des cordes est un candidat très prometteur pour la gravité quantique. Son développement progressif au fil des ans a fourni un cadre puissant pour comprendre la nature des trous noirs. La théorie des cordes est basée sur l'existence de supersymétries entre les fermions et les bosons. Cela permet la connexion non triviale entre la symétrie spatio-temporelle du groupe de Poincaré et les symétries internes de jauge des autres interactions. La cohérence de la théorie fixe le nombre total de dimensions spatio-temporelles à 10 ou peut-être 11. Tenons-nous en aux théories des cordes à dix dimensions pour plus de clarté. Les six dimensions supplémentaires doivent former une variété compacte relativement petite afin de ne pas être en contradiction avec notre monde quotidien en quatre dimensions. De plus, une particule ponctuelle en quatre dimensions peut maintenant avoir une géométrie non triviale le long des dimensions supplémentaires. La corde fondamentale est la plus primitive mais il existe aussi des objets de plus grande dimension tels que *membranes*. Une corde est décrite par sa *string length*, l_s , et son *string coupling*, g_s . Les interactions entre les cordes définissent des surfaces bidimensionnelles, appelées “world-sheets”, qui évitent la présence de singularités locales, singularités coutumières dans les théories quantiques des champs habituelles. Ainsi, la Théorie des Cordes est naturellement “UV complete”. De plus, la Théorie des cordes requiert la présence d'un champ de spin 2, le graviton, et incorpore ainsi la Relativité Générale à basse énergie. De l'autre côté, les groupes de jauge du modèle standard et leur contenu de matières peuvent également être inclus dans la théorie des cordes même s'il n'y a pas d'exigence spéciale pour avoir le groupe $SU(3) \times SU(2) \times U(1)$.

Dans la Théorie des cordes, les objets fondamentaux sont représentés par des membranes interagissant avec des cordes ouvertes ou fermées. Les configurations supersymétriques de N membranes ont le grand avantage d'avoir des quantités invariantes selon leurs modules comme l'entropie par exemple. Ainsi, ces quantités peuvent être obtenues pour toute valeur de g_s qui convient le mieux au calcul. Deux régimes sont particulièrement intéressants (voir Fig. 1.1). Les deux sont à $g_s \ll 1$ où les “stringy” corrections sont négligeables et où la constante de Newton, G , est négligeable comme dans la limite classique de la Relativité Générale. Le régime de supergravité est de $g_s N$. Cela correspond à avoir fixé “ $G.M$ ”, les membranes réagissent en retour et déforment l'espace-temps (voir Fig.1.1). À $g_s N$ faible, les membranes n'influencent pas leur environnement et sont des objets statiques lourds dont des cordes ouvertes faiblement couplées sont tendues entre elles. La physique des membranes est donnée par une théorie de champ libre. Ainsi, les micro-états de systèmes supersymétriques de membranes ont deux descriptions équivalentes dans deux cadres apparemment différents. C'est ce qui a guidé la découverte de la correspondance AdS/CFT. La correspondance avait initialement établi un lien entre des théories de Super Yang-Mills faiblement couplés à $g_s N \ll 1$ à des théories de gravité AdS₅ à $g_s N \gg 1$ [3] avant de s'enrichir considérablement (voir [4] pour un aperçu).

Ainsi, la théorie des cordes offre un cadre cohérent de gravité quantique pour répondre au mystère du trou noir. Nous passons brièvement en revue l'état de l'art et les questions en suspens dans ce qui suit :

- Le paradoxe de l'entropie:

L'une des réussites les plus importantes de la Théorie des cordes est la construction des degrés microscopiques de liberté des trous noirs supersymétriques en tant qu'états liés de cordes et de membranes à très faible couplage.

Tout d'abord, cela a été fait pour le système supersymétrique à deux charges. Il a été initialement

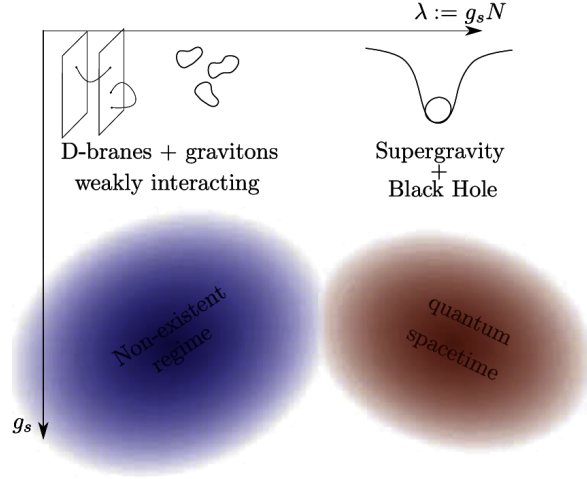


Figure 1.1: Les régimes de paramètres en théorie des cordes (le graphique est tiré de [5]).

dérivé dans le cadre F1-P où le système correspond à un grand nombre N de cordes fondamentales F1 avec des momentum modes P sur elles. À $g_s N$ faibles, l'entropie résulte des différentes manières dont les modes P peuvent être répartis entre les différentes harmoniques des cordes. Chaque micro-état a une représentation bien définie et unique. L'entropie peut être calculée exactement à l'aide de la formule de Cardy dans la CFT sous-jacente. À $g_s N$ large, les configurations s'effondrent en un point et leurs structures microscopiques disparaissent en formant un trou noir à deux charges. Le trou noir n'a pas assez de types de charges pour soutenir un horizon d'air non-nul. Cependant, Sen [6] et Dabholkar [7] ont montré que les “stringy” corrections à l'horizon donnent une entropie de Bekenstein-Hawking exactement égale à celle obtenue à $g_s N$ faible.

Quelques années plus tard, Strominger et Vafa ont étendu les conclusions de Sen au système supersymétrique à trois charges [8]. Ils ont travaillé dans le cadre D1-D5-P où le système correspond à des membranes unidimensionnelles D1 avec des membranes à cinq dimensions D5 partageant une direction compacte commune et des charges de momentum P¹. De même, à $g_s N$ faible, chaque état lié au membrane est identifiable et l'entropie est obtenue par la formule de Cardy. En augmentant $g_s N$, les membranes déforment leur espace transversal de six dimensions. À $g_s N$ large, la théorie de supergravité contient les solutions de “cordes noires” supersymétriques à six dimensions. La corde noire peut être réduite dimensionnellement à un trou noir supersymétrique à cinq dimensions autrement appelé trou noir D1-D5-P. L'air de son horizon des événements correspond exactement au résultat microscopique.

Ces résultats remarquables ont montré que les trous noirs sont formés par des états liés de membranes. À l’“orbifold point”, leurs degrés de liberté microscopiques sont manifestes. Ils correspondent à des configurations de membranes avec des cordes ouvertes faiblement couplées. Cependant, leur sort une fois que la gravité est activée fait toujours l'objet de débats. Les structures des micro-états disparaissent-elles derrière l'horizon et d'effacent-elles radicalement de la vue des observateurs éloignés ? Ou se manifestent-elles encore à travers une physique non-triviale à l'échelle de l'horizon ? Admettons que ce dernier scénario pourrait nous donner plus de confiance pour résoudre les deux prochaines énigmes des trous noirs.

Le second scénario a été soutenu par Mathur et la formulation de la “proposition de Fuzzball”. [9]. La proposition stipule que, dans le régime classique, il existe “ e^S ” solutions non singulières sans horizon qui ressemblent à un trou noir de loin mais qui diffèrent à proximité de l'horizon. Sur la base de cette

¹Le système F1-P considéré par Sen peut être dualisé au système D1-D5. En ce sens, le trou noir Strominger-Vafa ajoute un autre type de charge au trou noir Sen.

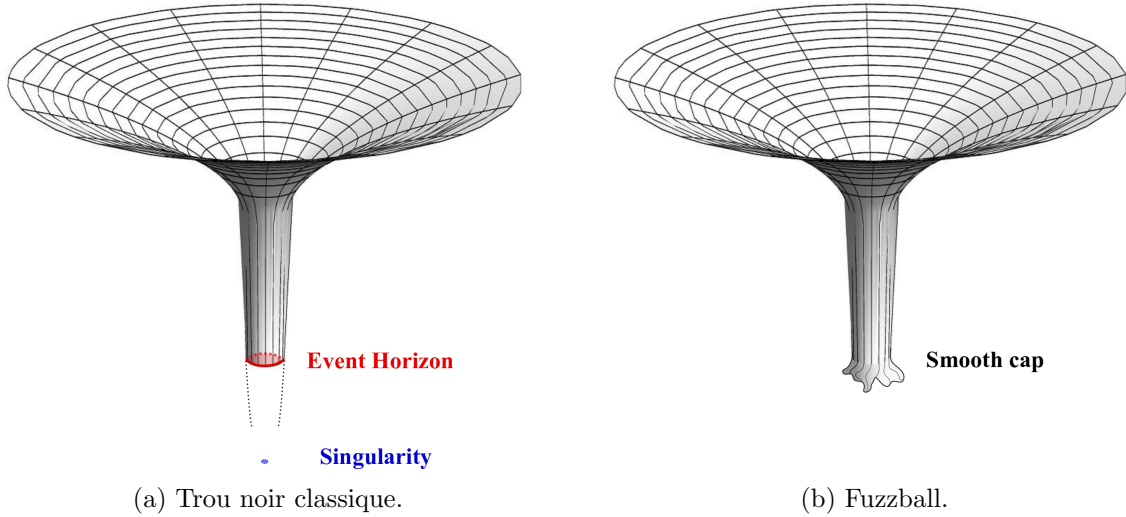


Figure 1.2: La proposition Fuzzball et la description schématique de l’intégration bidimensionnelle du trou noir classique en tant que description moyenne des fuzzballs lisses “ e^S ”.

affirmation, la solution de trou noir classique correspond à la description moyenne d’un système de solutions qui correspondent à la géométrie du trou noir à l’extérieur de l’horizon, mais qui se terminent par des géométries lisses dans l’infrarouge (voir Fig.1.2). De telles solutions ne peuvent évidemment pas exister dans le contexte de la Relativité Générale classique; car cela demande des objets qui grandissent et ne s’effondrent pas à mesure que la gravité augmente et de tels objets sont fournis par la Théorie des cordes [10].

De nouveau, en commençant par le système à deux charges, les “ e^S ” solutions singulières F1-P peuvent être dualisées en “ e^S ” solutions D1-D5, appelées Supertubes. [11–14]. Dans ce cadre, la singularité est résolue en étant mappée en un monopôle Kaluza-Klein. Chaque solution est sans horizon et développe une géométrie lisse spécifique proche de l’éventuel horizon. Ainsi, la structure de micro-états du trou noir à deux charges est encore visible dans le régime de supergravité et les micro-états sont tous représentés comme des géométries lisses non singulières.

Pour être validée, la proposition doit aborder avec succès le système à trois charges. Le programme de recherche, “programme de géométrie des micro-état”, a été développé pour accomplir cette vaste tâche. Depuis lors, de nombreuses solutions à trois charges sans horizon régulières et supersymétriques ont été construites, comme nous le verrons en détail dans les parties principales de la thèse (voir [15,16] pour des revues).

- La singularité centrale:

La découverte des degrés microscopiques de liberté des trous noirs est une étape importante, mais elle ne donne aucune idée à propos du paradoxe de la perte d’information ou de la résolution de la singularité. Ces questions ne peuvent être traitées que dans le régime classique.

Une étape préliminaire consiste à élucider à quelle échelle l’image classique du trou noir n’est plus valide. Pour la plupart des systèmes quantiques, la description classique est fiable jusqu’à l’échelle de Planck, $l_P \sim 10^{-35}\text{m}$. On peut naturellement penser que la description des trous noirs dans la Relativité Générale est valable jusqu’à une distance de Planck de la singularité [17]. À cet égard, la structure du micro-état devrait être limitée en dessous de cette échelle. Une autre approche, liée à la proposition de Fuzzball, consiste à supposer qu’un système quantique hautement entropique a une description classique fiable jusqu’à une échelle de $N^\alpha l_P$. Par exemple, l’échelle de fiabilité du système

F1-P à deux charges est de $N^{1/3}l_P$ [9]. De plus, toutes les solutions sans horizon lisse à trois charges diffèrent de la géométrie du trou noir à la longueur de Planck de l'horizon. Bien que leur description en tant que micro-états à trous noirs fasse encore l'objet de discussions, ils montrent au moins que la singularité peut être résolue beaucoup plus loin qu'à une distance de Planck de l'horizon. De plus, la Théorie des cordes est parsemée de nombreux exemples bien connus où les singularités sont résolues à grande échelle comme Polchinski Strassler [10], Klebanov-Strassler [18] ou LLM géométries [19]. Par conséquent, on peut affirmer en toute confiance que les effets de la gravité quantique peuvent se produire à une distance macroscopique de la singularité classique et éventuellement à l'échelle de l'horizon.

- Le paradoxe de la perte d'information:

Le dernier énoncé aide considérablement à résoudre le paradoxe de la perte d'information. Dans le calcul original de Hawking, le rayonnement est émis à proximité de l'horizon, dans le vide, loin de l'emplacement du trou noir. Un quanta d'Hawking ne peut pas facilement transporter l'information de l'intérieur. Cependant, si la géométrie proche de l'horizon doit être remplacée par des structures de type fuzzball, le rayonnement peut transporter des informations sur les micro-états et peut être unitaire [20].

Encore une fois, ceci est encore au niveau d'un postulat et des calculs et des preuves explicites sont nécessaires. De plus, d'autres scénarios ont développé des mécanismes unitaires permettant à l'information de s'échapper ou de s'échapper partiellement sans avoir besoin de fuzzballs. On peut se référer de manière non exhaustive aux "soft hair" des trous noirs [21] ou à la récupération d'information par des déformations de type double-trace [22].

Cependant, le scénario le plus naïf, qui consiste en des corrections quantiques au calcul de Hawking semi classique, a été exclu. En effet, le calcul de Hawking est basé sur des théories de champs quantiques dans une géométrie courbe. Dans [20], il a été démontré que les corrections quantiques dans la région de l'horizon des trous noirs ne peuvent pas restaurer complètement l'unitarité.

Un lecteur curieux peut aussi se demander pourquoi des défauts de l'unitarité ne sont pas considérés comme un scénario plausible. La théorie des cordes est une théorie quantique de la gravité qui préserve naturellement l'unitarité. En outre, la correspondance AdS/CFT fournit un contre-exemple direct. En effet, asymptotiquement, le trou noir AdS doit avoir une double description dans le cadre d'une théorie de champ conforme unitaire. En ce sens, tout processus physique doit être unitaire.

Tous ces arguments et toutes ces nouvelles questions ouvertes représentent un grand pas en avant dans notre compréhension des trous noirs. Cependant, elles ont été menées dans le contexte de solutions supersymétriques et extrêmes. Elles doivent être considérées comme des lignes directrices pour aborder des questions similaires à celles des solutions non supersymétriques et non extrêmes, qui sont beaucoup moins bien comprises.

Contributions et Organisation de la Thèse

Cette thèse porte sur la physique des trous noirs à travers la proposition de fuzzball et du programme de géométrie des micro-états. La majeure partie de la discussion se déroulera dans la limite de basse énergie de la théorie des cordes, c'est-à-dire en supergravité. Nous présenterons et examinerons de manière consistantes les travaux [23–29] que nous espérons avoir donné plus de poids à cette proposition.

La thèse se compose en trois parties principales. La partie I présente les matériaux de base et donne un aperçu du programme de géométrie des micro-états. La partie II rassemble les travaux [23, 24, 26–28] qui visaient à construire de nouvelles classes de géométries sans horizon lisse, supersymétrique ou non

supersymétrique. Enfin, la partie III aborde des questions plus profondes liées aux énigmes des trous noirs discutées ci-dessus [25, 29].

Dans le premier chapitre, nous introduisons les notions de base de la relativité générale menant à la construction de trous noirs. Nous discutons également des lois de la thermodynamique du trou noir. Nous décrivons leurs propriétés et leurs paradoxes un peu plus en détail que dans la présente introduction.

Dans le chapitre 2, nous passons en revue les théories de supergravité utilisés dans cette thèse. Nous commençons par la théorie de la "mère" en onze dimensions et les supergravités de type IIA et IIB en dix dimensions. Nous passons en revue les différentes dualités qui les relient. Notre objectif est de construire des solutions à trois charges dans le même régime que le trou noir à cinq dimensions ou l'anneau noir à six dimensions. Nous construisons des supergravités non jaugées à cinq et six dimensions par réduction dimensionnelle du type IIB et des supergravités à onze dimensions.

Dans le chapitre 3, nous dérivons les équations du mouvement pour les solutions supersymétriques en cinq et six dimensions. Nous donnons les représentations de ses solutions à onze et dix dimensions. Nous montrons que les solutions de trous noirs supersymétriques à trois charges coexistent avec des solutions régulières sans horizon qui ressemblent aux trous noirs jusqu'à l'échelle de l'horizon. En particulier, nous passons en revue la construction de solutions régulières en cinq dimensions et en six dimensions et les décrivons en onze et dix dimensions comme des états liés de membranes. Dans la dernière section de ce chapitre, nous abordons brièvement les solutions non supersymétriques. Nous détaillons d'abord les propriétés du trou noir Cvetič-Youm et sa géométrie proche de l'horizon de type extrême Kerr. Ensuite, nous construisons la famille des solutions "almost-BPS".

Selon la proposition de fuzzball, ces solutions régulières doivent être considérées comme des micro-états de trous noirs. Le "Saint-Graal" du programme de géométrie des micro-états est de construire " e^S " solutions de ce type ou, dans un premier temps, d'en construire de très grandes classes.

Le chapitre 4 est consacré aux solutions "bubbling" régulières en cinq dimensions à $g_s N \gg 1$. Tout d'abord, nous montrons qu'une classe de telles solutions a des propriétés particulières qui n'ont pas été remarquées jusqu'à présent. Il est bien connu que les états liés de membranes peuvent se désintégrer à des *murs de stabilité marginale* en changeant la géométrie à large distance. Par exemple, une configuration de membranes peut parfaitement vivre dans une géométrie asymptotiquement plat mais un changement vers asymptotiquement AdS_3 peut faire disparaître la configuration. Évidemment, un trou noir est indépendant de l'asymptotique dans laquelle il est incrusté. Les micro-états typiques de trous noirs doivent alors partager cette caractéristique. Nous montrons que certaines solutions "bubbling" sont encore très dépendantes du fond asymptotique, même lorsque les solutions développent une très longue gorge. Dans une deuxième section, nous construisons la plus grande famille de solutions de "bubbling" régulières [23]. Une telle construction est compliquée à réaliser en raison des contraintes de régularité difficilement gérables des solutions de "bubbling". Ensuite, en analysant les propriétés de cette famille, nous montrons que les solutions "bubbling" peuvent avoir un moment angulaire arbitrairement faible [24]. Avant ces travaux, on pensait généralement que ces solutions tournaient presque de façon maximale et que les Superstrata étaient les seules géométries de micro-états connues à faible moment angulaire.

Dans le chapitre 5 nous construisons les " e^S " états liés de membranes d'un système de membrane spécifique à $g_s N \ll 1$ [26]. Nous considérons le système avec des charges pures D6-D2-D2-D2-D2. Pour des valeurs de charges plus élevées, ce système correspond à un trou noir dual au trou noir D1-D5-P. Avec des charges pures, le nombre d'états est microscopiquement de 12. Nous construisons les 12 états liés de membranes dans le régime de Coulomb en tant que solutions "bubbling". Dans le cas de larges charges, ils pourraient décrire la "limite proche de l'horizon" des fuzzball. Ainsi, pour cet

exemple spécifique de faible charges, nous montrons que les “ e^S ” états d’un trou noir “primitif” à trois charges sont récupérés.

Dans le chapitre 6, nous passons en revue une étape cruciale dans la construction du Superstratum monomode ” le plus général ”, cité dans [28]. Nous utilisons un hybride du mode superstratum original [30] et du mode “supercharged” [31] pour construire des Superstrata à un mode qui ont encore des modules libres après fixation des charges asymptotiques du système. Nous montrons que ces modes hybrides possèdent toutes les caractéristiques nécessaires pour être les éléments constitutifs élémentaires des superstructures à plusieurs modes génériques fluctuant en fonction de trois variables indépendantes.

Dans le chapitre 7, nous construisons la première famille de géométries de micro-états “bubbling” régulières qui sont asymptotiques à la région proche de l’horizon des trous noirs extrêmes de Kerr à cinq dimensions [27]. Des trous noirs Kerr presque extrêmes ont été observés dans le ciel. Ce travail représente un progrès important dans la description de la structure des micro-états de trous noirs observables.

La stratégie du programme de géométrie des micro-états ne consiste pas seulement à construire l’espace des états avec des solutions sans horizon régulières dans le régime du trou noir. Premièrement, il est crucial d’examiner comment il clarifie le paradoxe de la perte d’information. Deuxièmement, les géométries de micro-états sont également des outils très utiles pour tester et apprendre les correspondances AdS/CFT dans différentes dimensions.

Le chapitre 8 examine l’implication des géométries des micro-états dans le contexte de la correspondance AdS₂/CFT₁ [25]. Les trous noirs supersymétriques à trois charges développent une limite AdS₂ dans la région de l’horizon. Cependant, toute perturbation d’énergie finie dans AdS₂ détruit soit l’ultraviolet (UV), soit l’infrarouge (IR). Cette caractéristique inhabituelle amène la communauté à penser que l’holographie dans AdS₂ est subtile et très différente des autres correspondances AdS_{D+1}/CFT_D. Autrement dit, il est crucial de comprendre la gravité quantique dans des espaces-temps asymptotiques AdS₂. Nous montrons que les géométries des micro-états suivent une limite ”proche de l’horizon” semblable à celle du trou noir. Ceci conduit à des géométries asymptotiquement AdS₂ qui se terminent de manière régulière dans l’IR. Ces géométries satisfont à la conjecture du moment angulaire zéro selon laquelle tout microétat typique de trou noir en cinq dimensions doit avoir un de ses deux moments angulaires nul. De plus, nous soutenons que tous les états de base d’une CFT₁ non triviale doivent avoir des géométries duales qui cassent l’invariance conforme dans l’IR. En d’autres termes, les géométries doivent être de type fuzzball. Un corollaire est que AdS₂ n’est dual à aucun état de base d’une CFT₁ non-triviale. De cette déclaration, nous soutenons que la correspondance AdS₂/CFT₁ suit la philosophie holographique habituelle. Nous montrons que les géométries duales aux états de CFT₁ soutiennent une tour infinie d’excitations non supersymétriques grâce à la présence d’un cap dans l’IR. Ainsi, le travail de [25] donne le début d’une preuve pour la proposition fuzzball. Il ne montre pas que tous les “ e^S ” micro-états de trous noirs sont des fuzzballs. Il montre que, si la CFT₁ qui donne lieu à l’entropie du trou noir n’est pas triviale, les “ e^S ” états de base sont duals aux géométries qui se terminent par un cap dans l’IR.

Dans le chapitre 9, nous étudions le processus de diffusion des ondes dans les géométries de micro-états en calculant les Green functions scalaires [29]. Cela permet d’élucider comment l’unitarité est rétablie et comment l’information s’échappe des micro-états de trous noirs dans le régime des trous noirs. Il est communément admis que les trous noirs sont des objets très chaotiques en raison du grand nombre de micro-états. Pour le trou noir D1-D5-P, lorsqu’une onde scalaire est émise à partir des bords de la géométrie, la Green function décroît exponentiellement au fil du temps à mesure que l’onde est absorbée par le trou. Puis, après une longue période, on s’attend à ce que la structure des micro-états commence à influencer : la Green function augmente à nouveau et atteint un plateau avec de larges fluctuations sporadiques. Cette longue période est de l’ordre de $N_1 N_5$ pour un trou noir D1-D5-P

où N_1 et N_5 correspondent respectivement au nombre de membranes D1 et D5. Dans ce chapitre, nous développons une toute nouvelle technique qui permet de calculer les Green functions dans des géométries arbitrairement compliqués asymptotiquement AdS. Nous appliquons cette technique à une famille spécifique de Superstrata. Nous montrons que la “fonction de réponse” d’une onde scalaire est essentiellement donnée par la structure de pôles du cap par la fonction de réponse du trou noir. En coordonnées spatiales, cela se traduit par une forte décroissance exponentielle à court terme suivie d’échos uniformément espacés venant du cap, toutes les périodes $\sim N_1 N_5$. Ces échos diffèrent des attentes sporadiques. Ceci est principalement dû au fait que nous ne sondons qu’une seule géométrie de micro-état hautement cohérente avec un cap AdS_3 spécifique. Ainsi, si l’on considère un ensemble de micro-états, on obtient une moyenne d’échos légèrement différents et on obtient les fluctuations sporadiques attendues. Néanmoins, il s’agit du premier calcul dans le régime du trou noir montrant comment une structure non triviale à l’échelle de l’horizon permet à l’information de s’échapper dans un processus unitaire.

Dans le dernier chapitre, nous faisons brièvement le point sur ce qui a été fait dans cette thèse. Nous esquissons également quelques questions ouvertes que nous aimerions explorer dans un proche avenir.

Part I

Black holes and their microstates in Supergravity

Black holes in General Relativity and black-hole thermodynamics

Formulated by Einstein in 1915 [32], General Relativity (GR) is the theory of space, time and gravitation based on differential geometry. Its eminent breakthrough is to describe spacetime as a four-dimensional manifold which can be deformed by whatever fields in the background. The dynamics of the deformation is captured by the Einstein-Hilbert action relating the Riemann curvature tensor to the energy-momentum tensors of the fields. GR has been an incredibly efficient framework to describe the structure of spacetime from the scale of an atom-length ($\sim 10^{-10}$ m) to the scale of the universe ($\sim 10^{25}$ m). The first developments of GR have been lead with great success, even with too great success, to the description of highly-energetic astrophysical objects and phenomena as Quasars, X-ray sources, gravitational lensing, gravitational waves and many others. However, the most remarkable GR outcome is in the prediction of two different singular behaviours inherent of spacetime which must be resolved by theories beyond GR:

- First, the prediction of the initial singularity or Big Bang. The expanding nature or the de Sitter nature of our universe leads to a point in the far past at the edge of the validity of GR where the size of universe matches the size of an atom.
- Second, the prediction of the black-hole singularity from the tragic fate of gravitational collapse of massive stars.

This thesis principally aims to detail some progresses in the understanding of the second type of singularity within the framework of String Theory. In this chapter, we introduce the reader to some basic notions of black-hole physics in General Relativity (GR) in four-dimensions. This is essential to have them in mind for the overall discussion. Interested readers are greatly advised to browse through the high-quality books [33, 34].

2.1 Black holes in General Relativity

In GR, a black hole is produced by gravitational collapse of matter characterized by a spacetime singularity separated from the rest of the universe by an *event horizon* from which no information can escape. The presence of a horizon makes a stationary solution to be uniquely defined by its macroscopical quantities which are the mass, charge and angular momentum. This uniqueness theorem is a corollary of the “no-hair theorem”. This reduces the number of GR black holes to four categories:

- The Schwarzschild black hole ($M, Q = 0, J = 0$).
- The Kerr black hole ($M, Q = 0, J$).
- The Reissner-Nordström black hole ($M, Q, J = 0$).
- The Kerr-Newman black hole (M, Q, J).

We first review the Einstein-Hilbert action and how it leads to the Schwarzschild and the more-general Kerr-Newman solutions. Second, we discuss the thermodynamical description of black holes.

2.1.1 The Einstein-Hilbert action

The key element of GR is to describe gravity as a geometric property of spacetime. The spacetime is a four-dimensional Riemannian manifold defined by its metric tensor $g_{\mu\nu}$, $\mu, \nu = 1, 2, 3, 4$. It can be deformed in presence of matter fields characterized by their energy-momentum tensors, $T_{\mu\nu}$, following the principle of least action of the Einstein-Hilbert action¹

$$S_{EH} = \int d^4x \sqrt{-\det g} \left[\frac{1}{16\pi G_4} R - \mathcal{L}_M \right], \quad (2.1.1)$$

where G_4 is the four-dimensional Newton constant, R is the Ricci scalar, and \mathcal{L}_M is a Lagrangian depending on the nature of the matter fields. The principle of least action leads to the Einstein equation

$$R_{\mu\nu} - \frac{1}{2} g_{\mu\nu} R = 8\pi G_4 T_{\mu\nu}, \quad (2.1.2)$$

where $T_{\mu\nu}$ is the energy-momentum tensor of the matter fields defined by

$$T_{\mu\nu} \equiv -\frac{2}{\sqrt{-\det g}} \frac{\delta(\sqrt{-\det g} \mathcal{L}_M)}{\delta g_{\mu\nu}}. \quad (2.1.3)$$

In what will follow, we will be interested in GR with vacuum $T_{\mu\nu} = 0$ or in GR coupled to an electromagnetic gauge field A_μ , $T_{\mu\nu} = F_{\mu\rho} F_\nu^\rho - \frac{1}{4} g_{\mu\nu} F_{\rho\sigma} F^{\rho\sigma}$.

2.1.2 The Schwarzschild black hole

The first black hole solution was found by Schwarzschild in 1916. It is a stationary vacuum solution to Einstein equation with a spherically symmetric mass distribution of mass M . The four-dimensional metric is

$$ds^2 = -\left(1 - \frac{2G_4 M}{r}\right) dt^2 + \left(1 - \frac{2G_4 M}{r}\right)^{-1} dr^2 + r^2 d\Omega_2^2, \quad (2.1.4)$$

where $d\Omega_2^2$ is the metric of the round two-sphere. The origin, $r = 0$, is the singularity of the black hole where the curvature becomes infinite. The Schwarzschild radius $r_H = 2G_4 M$ corresponds to a coordinate singularity and the curvature is finite at this location (see Fig. 2.1a for the two-dimensional picture of the geometry). The surface $r = r_H$ is the event horizon where t goes from a time-like coordinate for $r > r_H$ to a space-like coordinate $r < r_H$ and reversely for r . Moreover, a straightforward computation of radial null geodesics shows that the light-cones close up when approaching the horizon. A black hole is made of a singularity and a horizon, the horizon delimits two distinct regions: the interior and the exterior of the black hole. By studying geodesic motion in the background one can show that the black hole is purely absorbing and nothing can escape from the interior to the exterior.

2.1.3 The Kerr-Newman black hole

The most general stationary axially symmetric black hole solution in GR with a non-vanishing mass M , angular momentum J and charge Q is the Kerr-Newman black hole. The spacetime metric is

$$ds^2 = -\frac{\Delta - a^2 \sin^2 \theta}{\Sigma} dt^2 - 2a \frac{r^2 + a^2 - \Delta}{\Sigma} \sin^2 \theta dt d\phi + \frac{\Sigma}{\Delta} dr^2 + \Sigma d\theta^2 + \frac{(r^2 + a^2)^2 - a^2 \Delta \sin^2 \theta}{\Sigma} \sin^2 \theta d\phi^2, \quad (2.1.5)$$

¹We have chosen the cosmological constant to be zero.

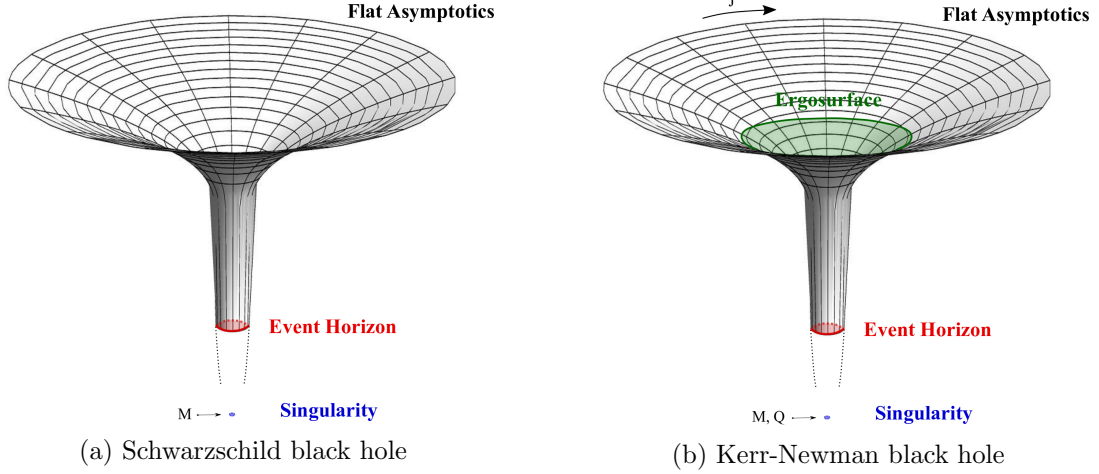


Figure 2.1: Schematic description of the two-dimensional embedding of black holes in GR.

where we have defined

$$\begin{aligned}\Sigma &\equiv r^2 + a^2 \cos^2 \theta, \\ \Delta &\equiv r^2 - 2MG_4 r + Q^2 G_4 + a^2, \\ a &\equiv JM^{-1}.\end{aligned}\tag{2.1.6}$$

The electromagnetic gauge field is

$$A_\mu = \left(Q\sqrt{G_4} \frac{r}{\Sigma}, 0, 0, -aQ\sqrt{G_4} \frac{r \sin^2 \theta}{\Sigma} \right).\tag{2.1.7}$$

Like the Schwarzschild solution, $\Sigma = 0$ corresponds to a ring-like curvature singularity. Moreover, there are two coordinate singularities corresponding to the locations where g_{rr} diverges. This determines two three-surfaces of constant r delimited by an outer horizon, r_+ , and an inner horizon r_-

$$r_\pm \equiv G_4 M \pm \sqrt{G_4^2 M^2 - G_4 Q^2 - a^2}.\tag{2.1.8}$$

The Kerr-Newman solution is *extremal* if those two radii coincide $G_4^2 M^2 - G_4 Q^2 - a^2 = 0$. If $G_4^2 M^2 - G_4 Q^2 - a^2 < 0$, there is no horizon and the singularity is naked which is in violation of the *cosmic censorship conjecture* [35]. Another point of interest is where g_{tt} vanishes. This corresponds to the radius²

$$r_+^E(\theta) \equiv G_4 M + \sqrt{G_4^2 M^2 - G_4 Q^2 - a^2 \cos^2 \theta}.\tag{2.1.9}$$

This defines a stationary limit surface usually called ergosurface and the region $r_+ < r < r_+^E$ is usually referred as the ergosphere. The ergosurface delimits the radius where the time Killing vector, ∂_t , goes from time-like for $r > r_+^E$ to space-like for $r < r_+^E$ (see Fig. 2.1b). Hence, no physical trajectory can remain stationary within the ergosphere in any time-independent coordinate system.

2.2 Black hole thermodynamics and Hawking radiation

General Relativity conveys the idea that black holes are purely absorbing objects and any inherent structure inside the event horizon cannot be accessed from a distant observer. There exists only one

²We take only the largest root of g_{tt} since the other one lies inside the horizon.

state for a given mass, angular momentum and charge. However, in the early 70s, Bekenstein and Hawking showed that black holes behave as thermodynamical objects. The word “behave” is carefully chosen in a sense that a black hole is not described as a gas in a room but a strong analogy and a one-to-one map between the classical thermodynamics and the black-hole thermodynamics can be made.

2.2.1 The laws of black hole thermodynamics

Classically, a black hole cannot emit anything and the mass only increases. This led Bekenstein to give a thermodynamic interpretation by suggesting that [36]

$$dM = TdS, \quad (2.2.1)$$

where T is the black hole temperature and S its entropy. The temperature can be classically computed by requiring that the “Euclideanized” metric is regular at the horizon. Concretely, it requires to take the near-horizon limit of the Euclidean metric and read the periodicity of the Euclidean time required by the absence of conical defect

$$ds^2|_{\theta=\phi=0} \propto dr^2 + r^2 \left(\frac{2\pi}{\beta} d\tau \right)^2,$$

where $\beta \equiv T^{-1}$. For a Schwarzschild and a Kerr-Newman black hole, we have

$$T_{\text{Sch}} = \frac{1}{8\pi M G_4}, \quad T_{\text{KN}} = \frac{r_+ - r_-}{4\pi (r_+^2 + a^2)},$$

where r_{\pm} are the inner and outer horizons of the Kerr-Newman black hole (2.1.8). By integrating (2.2.1), we obtain

$$S_{\text{Sch}} = 4\pi M^2 G_4, \quad S_{\text{KN}} = \pi (r_+^2 + a^2).$$

For both solutions, the entropy can be written as a function of the horizon area, A ,

$$S = \frac{A}{4 G_4}. \quad (2.2.2)$$

This relation is the *Bekenstein-Hawking entropy formula*. It is universally valid for an arbitrary black hole with a large area in D dimensions by replacing the four-dimensional Newton constant, G_4 , by the D -dimensional equivalent, G_D . This leads also to associate to the temperature a universal geometric property at the horizon called *surface gravity*, κ_s :

$$T = \frac{\kappa_s}{2\pi}. \quad (2.2.3)$$

Moreover, Penrose suggested a classical process which allows to extract rotational energy of a black hole [37]. This modifies the expression (2.2.1) to the *first law* of black hole thermodynamics

$$dM = \frac{\kappa_s}{8\pi G_4} dA + \Omega dJ + \Phi dQ, \quad (2.2.4)$$

where Ω is the angular velocity and Φ is the electrostatic potential. The *second law* states that the horizon area can never decrease

$$dA \geq 0,$$

in analogy with the positive variation of entropy for thermodynamical objects. Finally, the *third law* stipulates that it is impossible to reduce κ_s to zero by physical process in finite time.

2.2.2 Hawking radiation

From a thermodynamical point of view, an object at finite temperature emits thermal radiation until it evaporates. For a black hole, a radiation will necessarily imply a loss of mass and so a decrease of its horizon area which is in violation of the second law. Thus, the classical description should break down. This led Hawking to consider quantum corrections at the vicinity of the horizon. The Hawking's semi-classical computation consists in computing quantum-pair creation in classical curved background [38]. Broadly speaking, one part of the pair can be absorbed by the black hole whereas the other part will escape as a physical on-shell particle. From an outside observer, the black hole behaves as a black body emitting thermal radiation at the temperature computed earlier.

To reconcile Hawking radiation and the second law of black hole thermodynamics, the *generalized second law* states that

$$dS_{\text{tot}} = dS_{\text{emit}} + dS_{\text{BH}} \geq 0.$$

The GR picture which claims that nothing can escape from an event horizon is undermined by quantum effects. Moreover, as a finite black body, black hole should evaporate in finite time. Because black hole can be produced by a gravitational collapse of a pure state whereas it only radiates thermal mixed states, Hawking argued that pure states can evolve into mixed states in a quantum gravity theory. This would imply that the unitary property of quantum mechanics should break down when gravity is considered. This is referred as the *information loss* and depicts one of the great conflict between General Relativity and quantum mechanics.

This chapter should be considered as a technical complement to the Introduction. We have detailed the prevailing pictures of black holes and we refer the reader to the Introduction for the enunciation of the three main black-hole mysteries that result from these descriptions.

Supergravity

In 1967, the Coleman-Mandula theorem [39] gave hard time to the unification of quantum mechanics and gravity by proving the impossibility of connecting in a non-trivial way the Poincaré group (space-time symmetries) with internal symmetries (gauge symmetries) into a Lie algebra. A loophole was given by considering Lie superalgebra by adding generators of a symmetry, called supersymmetry, relating the bosons and fermions of the theory. Since then, supersymmetry is considered a key ingredient for a quantum theory of gravity.

Supergravity is based on the gauge principle of local supersymmetry and gives a supersymmetric theory of gravity. It arises as the low-energy limit of Superstring Theory and is then a UV complete theory. There exist different types of String Theory in ten dimensions: the type I, type IIA, the type IIB, and the heterotic string theories. The second superstring revolution has unified those theories in a mother theory in eleven dimensions, the M-theory. The low-energy limit of M-theory is the eleven-dimensional Supergravity. All other supergravity theories can be obtained by dimensional reduction and dualities. In this chapter, we review the supergravity frameworks necessary for this thesis. We self-consistently start with the eleven-dimensional, type IIA and type IIB theories and discuss the methodology to construct simple classical solutions in Section 3.1. We then review the duality and dimensional-reduction rules which relate them in Section 3.2. In Section 3.3, we review the $\mathcal{N} = (1, 0)$ six-dimensional ungauged Supergravity and $\mathcal{N} = 2$ five-dimensional ungauged Supergravity.

3.1 Supergravity frameworks

3.1.1 Eleven-dimensional Supergravity

Eleven-dimensional Supergravity has the largest number of spacetime dimension for a supergravity theory and was initially constructed by Cremmer, Julia and Scherk [40]. This theory has one supersymmetry ($\mathcal{N} = 1$) and 32 supercharges carrying an index in the 32-dimensional spinor representation of $SO(1, 10)$ [41] (see [42] for more details). The theory contains the following massless fields, all in the supermultiplet of the graviton:

- A spin-2 gravitational field g with 44 degrees of freedom in the traceless symmetric tensor representation of $SO(9)$.
- A Majorana spinor gravitino Ψ with 128 degrees of freedom in a vector-spinor representation of $SO(9)$.
- A three-form gauge field A_3 and its field strength $F_4 = d_{11}A_3$ with 84 degrees of freedom in the rank-three antisymmetric tensor representation of $SO(9)$.

One can now wonder what types of objects can source the fields. The gravitational field captures the dynamics of the spacetime. The off-diagonal terms with a leg along time are scalar fields sourced by *momentum charges* P whereas the spatial cross-terms are vector fields sourced by *Kaluza-Klein*

monopoles (KKm).

By analogy with electromagnetism, The field F_4 can be sourced by magnetic charges. The electric field is conveniently studied by dualizing into a seven-form:

$$F_7 = \star_{11} F_4 - \frac{1}{2} A_3 \wedge F_4.$$

In this context, the field F_7 can be sourced by electric charges. The magnetic and electric charges are obtained from the flux-integral of F_4 and F_7 over the boundary of a five-dimensional and eight-dimensional volume. Each volume defines a transverse worldvolume of a two-dimensional brane configuration (M2) or a five-dimensional brane configuration (M5). In other word, the gauge field A_3 couples electrically to *M2-branes* and magnetically to *M5-branes*.

The dynamics of the background in the bosonic sector is given by the following action

$$(16\pi G_{11}) S_{11} = \int d^{11}x \sqrt{-g} R - \frac{1}{2} \int F_4 \wedge \star_{11} F_4 + \frac{1}{6} \int A_3 \wedge F_4 \wedge F_4, \quad (3.1.1)$$

where \star_{11} is the Hodge dual with respect to the eleven-dimensional space and the eleven-dimensional Newton constant is given according to the eleven-dimensional Planck length as

$$16\pi G_{11} = (2\pi)^{-1} (2\pi l_P^{(11)})^9. \quad (3.1.2)$$

In comparison with the Einstein-Hilbert action (2.1.1), the first integral is the purely gravitational term and the second corresponds to the Lagrangian of the matter fields. In eleven-dimensional Supergravity, supersymmetry requires that the only bosonic field is a three-dimensional gauge field. This field is the analogue of the electromagnetic gauge field in four dimensions. The third integral does not contain the metric and is topological. It is the *Chern-Simons* term required by supersymmetry. In the next chapter, we will see how crucial this term will be to construct smooth black-hole-like geometries, obviating the GR no-go theorem to construct non-singular structure at the horizon scale.

3.1.1.1 Solutions of the equations of motion

In this thesis, we are interested in constructing supergravity solutions which have the same charges, mass and angular momenta as a black hole. This obviously requires to solve the equations of motion. The Einstein-Maxwell equations of the eleven-dimensional supergravity action are given by

$$\begin{aligned} R_{\mu\nu} - \frac{1}{12} \left(F_{4\mu\rho\sigma\tau} F_{4\nu}{}^{\rho\sigma\tau} - \frac{1}{12} g_{\mu\nu} F_4^2 \right) &= 0, \\ d_{11} \star_{11} F_4 + \frac{1}{2} F_4 \wedge F_4 &= 0. \end{aligned} \quad (3.1.3)$$

Their compact forms hide a very complex structure since the Einstein equations are second-order coupled non-linear differential equations. Finding solutions directly is a lost cause. An easier way is to look for solutions which preserve some of the supersymmetries. Such solutions will saturate the Bogomol'nyi-Prasad-Sommerfield bound (BPS) [43, 44] and have then a mass equal to the sum of its charges. The number of unbroken supersymmetries is encoded in a set of 32-component Killing spinors ϵ^i which obey the supersymmetric transformation rules

$$\begin{aligned} \delta e_\mu^A &= \bar{\epsilon}_i \Gamma^A \Psi_\mu, \\ \delta A_{3\mu\nu\rho} &= -3 \bar{\epsilon}_i \Gamma_{[\mu\nu} \Psi_{\rho]}, \\ \delta \Psi_\mu &= \nabla_\mu \epsilon^i + \frac{1}{288} \left(\Gamma_\mu{}^{\nu\rho\sigma\tau} F_{4\nu\rho\sigma\tau} - 8 \Gamma^{\rho\sigma\tau} F_{4\mu\rho\sigma\tau} \right) \epsilon^i, \end{aligned} \quad (3.1.4)$$

where we have defined the eleven-dimensional vielbeins e^A according to the gravitational field and the $SO(1, 10)$ Minkowski metric as

$$g_{\mu\nu} dx^\mu dx^\nu = \eta_{AB} e^A e^B,$$

the 32×32 gamma matrices Γ^μ and their antisymmetric products

$$\Gamma^{\mu_1 \mu_2 \dots \mu_n} = \Gamma^{[\mu_1} \Gamma^{\mu_2} \dots \Gamma^{\mu_n]},$$

and ∇_μ is the covariant derivative. We look for classical configurations. This means that the expectation value of the fermionic fields should be zero (otherwise, a Lorentz symmetry would not conserve the vacuum). Thus we assume that the gravitini is frozen, the supersymmetric variations (3.1.4) reduce to $\delta\Psi_\mu = 0$. This led to a simpler first order equation. The second step consists in working with bosonic quantities quadratic in ϵ^i called bilinears: $\bar{\epsilon}_i \Gamma_{\mu_1 \dots \mu_n} \epsilon^j$. The simplest non-zero bilinear is

$$\mathcal{K}_\mu = \bar{\epsilon}_i \Gamma_\mu \epsilon^i, \quad (3.1.5)$$

where the indices i are contracted. A rather technical algebraic computation, using Fierz identity and $\delta\Psi_\mu = 0$, shows that \mathcal{K} is either a time-like or a null Killing vector. If it is time-like and the equation $\delta\Psi_\mu = 0$ is satisfied, all the components of the Einstein equations of motion are satisfied. If it null, all the components except the 00 component are satisfied [45]. Consequently, solutions of eleven-dimensional Supergravity which preserve Killing spinors ϵ^i , where \mathcal{K} is time-like, are obtained by solving the following first order equations

$$\begin{aligned} d_{11} \star_{11} F_4 + \frac{1}{2} F_4 \wedge F_4 &= 0, \\ \nabla_\mu \epsilon^i + \frac{1}{288} (\Gamma_\mu^{\nu\rho\sigma\tau} F_{4\nu\rho\sigma\tau} - 8 \Gamma^{\rho\sigma\tau} F_{4\mu\rho\sigma\tau}) \epsilon^i &= 0. \end{aligned} \quad (3.1.6)$$

In order to get familiar with the construction of supersymmetric solutions, we discuss the solutions of coincident M2-branes, solutions of coincident M5-branes and the extension to an intersection of three orthogonal stacks of M2-branes. They are the basic ingredients of the three-charge black hole solutions and three-charge bubbled solutions. We parametrize the eleven-dimensional space with the Cartesian coordinates $(t, x_1, x_2, \dots, x_{10})$.

- A basic example: a configuration of M2-branes.

We consider a stack of M2-branes at the same locus along the directions (t, x_1, x_2) . The $SO(1, 10)$ symmetry group is broken into $SO(1, 2) \times SO(8)$. As explained in the previous section, the three-form gauge field is electrically sourced along $dt \wedge dx_1 \wedge dx_2$. The Ansatz which is consistent with the symmetry is

$$\begin{aligned} ds_{11}^2 &= Z_{M2}^\parallel(r) (-dt^2 + dx_1^2 + dx_2^2) + Z_{M2}^\perp(r) (dx_3^2 + \dots + dx_{10}^2), \\ F_4 &= d \left(Z_{M2}^{(e)}(r) \right) dt \wedge dx_1 \wedge dx_2, \end{aligned} \quad (3.1.7)$$

where r is the radial coordinate of the eight-dimensional transverse space and $Z_{M2}^{\parallel/\perp/(e)}(r)$ are scalar *warp factors*. The stack of branes is at $r = 0$. The supersymmetric equation of motion in (3.1.6) implies, when $\mu = M = 0, 1, 2$,¹

$$\partial_M \epsilon = 0, \quad Z_{M2}^{(e)}(r) = Z_{M2}^\parallel(r)^{\frac{3}{2}}, \quad (\mathbb{1} + \Gamma^{012}) \epsilon = 0, \quad (3.1.8)$$

and when $\mu = 3, 4, \dots, 10$

$$Z_{M2}^\parallel(r)^{-1} = Z_{M2}^\perp(r)^2, \quad \epsilon = Z_{M2}^{(e)}(r)^{\frac{1}{6}} \epsilon_0, \quad (3.1.9)$$

¹We drop the index “ i ” of the Killing spinors for readability.

where ϵ_0 are constant spinors. Then, the Maxwell equation in (3.1.6) implies

$$\star_8 d_8 \star_8 d_8 \left(Z_{M2}^{(e)}(r)^{-1} \right) = 0,$$

where d_8 and \star_8 are the exterior derivative and the Hodge dual with respect to the eighth-dimensional transverse flat space. Thus, we define the scalar warp factor $Z_{M2}(r)$ as

$$Z_{M2}(r) \equiv Z_{M2}^{(e)}(r)^{-1} = Z_{M2}^{\parallel}(r)^{-\frac{3}{2}} = Z_{M2}^{\perp}(r)^3.$$

The metric and the field strength give

$$\begin{aligned} ds_{11}^2 &= Z_{M2}(r)^{-\frac{2}{3}} (-dt^2 + dx_1^2 + dx_2^2) + Z_{M2}(r)^{\frac{1}{3}} (dx_3^2 + \dots + dx_{10}^2), \\ F_4 &= d(Z_{M2}(r)^{-1}) dt \wedge dx_1 \wedge dx_2. \end{aligned} \quad (3.1.10)$$

The solution is associated to a constant Killing spinor and to a warp factor which satisfy

$$\begin{aligned} (\mathbb{1} + \Gamma^{012}) \epsilon_0 &= 0, \\ \star_8 d_8 \star_8 d_8 Z_{M2}(r) &= 0, \end{aligned} \quad (3.1.11)$$

The first equation is just a projection equation: half of the components of ϵ_0 must be set to zero whereas the other half remain free. Thus, the solution preserves 16 supersymmetries of the 32 initial ones. They are denoted as 1/2-BPS solutions. The second equation is simply a harmonic equation over an eight-dimensional base space which is sourced at the brane locus. Generic solutions are

$$Z_{M2}(r) = 1 + \frac{\alpha_{M2}}{r^6}.$$

The coefficient α_{M2} can be related to the electric M2-charge, Q_{M2} from the flux-integral of the magnetic field strength over the boundary of an eight-dimensional volume transverse to the branes

$$Q_{M2} = \int_{S_\infty^7} F_7 = 6 \text{Area}(S^7) \alpha_{M2}. \quad (3.1.12)$$

Moreover, α_{M2} can be related to the number of M2-branes, N_{M2} , through the generic asymptotic expansion of the tt metric component for N_p p -branes of tension T_p in D dimensions [46]

$$g_{tt} = -1 + \frac{16\pi G_D N_p T_p}{(D-2)\text{Area}(S^{D-p-2})} \frac{1}{r^{D-p-3}}. \quad (3.1.13)$$

The tension of a M2-brane is $T_{M2} = 2\pi \left(2\pi l_P^{(11)} \right)^{-3}$. From the large-distance behavior of the metric (3.1.10), this gives

$$\alpha_{M2} = 32\pi^2 l_P^{(11)6} N_{M2}. \quad (3.1.14)$$

As advertised in the preamble of the chapter and in the Introduction, Supergravity is the low-energy limit of String Theory. One can illustrate this fact and the validity of the supergravity description using our simple example. The Ricci scalar of the metric (3.1.10) gives

$$R = -\frac{6\alpha_{M2}^2}{(r^6 + \alpha_{M2})^{\frac{7}{3}}} \underset{r \rightarrow 0}{\sim} -6(\alpha_{M2})^{-\frac{1}{3}} \propto \left(l_P^{(11)6} N_{M2} \right)^{-\frac{1}{3}}. \quad (3.1.15)$$

Consequently, the curvature becomes very large at the origin for small $l_P^{(11)6} N_{M2}$ and stringy excitation starts to be non-negligible. The validity of the classical description requires to have a large number of branes $N_{M2} \gg 1$.

- A basic example: a configuration of M5-branes

We consider now a stack of M5-branes at the same locus along the direction (t, x_1, \dots, x_5) . We then assume a symmetry $SO(1, 5) \times SO(5)$. The M5-branes magnetically source the gauge field, this is better suited to a dual perspective. The Ansatz is then

$$\begin{aligned} ds_{11}^2 &= Z_{M5}^{\parallel}(r) (-dt^2 + dx_1^2 + \dots + dx_5^2) + Z_{M5}^{\perp}(r) (dx_6^2 + \dots + dx_{10}^2), \\ F_7 &= d\left(Z_{M5}^{(m)}(r)\right) dt \wedge dx_1 \wedge \dots \wedge dx_5, \end{aligned} \quad (3.1.16)$$

where r is now the radial coordinate of the five-dimensional transverse space. The equations of motion (3.1.6) are solved following the same arguments as before. The solution is determined by an unique warp factor, $Z_{M5}(r)$ and constant Killing spinors ϵ_0

$$\begin{aligned} ds_{11}^2 &= Z_{M5}(r)^{-\frac{1}{3}} (-dt^2 + dx_1^2 + \dots + dx_5^2) + Z_{M5}(r)^{\frac{2}{3}} (dx_6^2 + \dots + dx_{10}^2), \\ F_7 &= d\left(Z_{M5}(r)^{-1}\right) dt \wedge dx_1 \wedge \dots \wedge dx_5, \end{aligned} \quad (3.1.17)$$

which satisfy the following equations

$$\begin{aligned} (\mathbb{1} + \Gamma^{012345}) \epsilon_0 &= 0, \\ \star_5 d_5 \star_5 d_5 Z_{M5}(r) &= 0, \end{aligned} \quad (3.1.18)$$

The solution is also 1/2-BPS and $Z_{M5}(r)$ is a harmonic function of the five-dimensional base space

$$Z_{M5} = 1 + \frac{\alpha_{M5}}{r^3}.$$

The coefficient α_{M5} is related to the magnetic M5-brane charge, Q_{M5} from the flux-integral of the electric field strength over the boundary of a five-dimensional volume

$$Q_{M5} = \int_{S_{\infty}^4} F_4 = 3 \text{Area}(S^4) \alpha_{M5}. \quad (3.1.19)$$

The tension of a M5-brane is $T_{M5} = 2\pi \left(2\pi l_P^{(11)}\right)^{-6}$. We apply (3.1.13) with the large-distance behavior of the metric (3.1.17),

$$\alpha_{M5} = \pi l_P^{(11)3} N_{M5}.$$

- A basic example: M-brane intersection

An interesting extension of the previous solutions is to consider different stacks of M-branes at the same location. This is a foretaste of generic 1/8-BPS three-charge solutions and of the construction of the STU model. Let us consider three orthogonal stacks of M2 branes, along (x_1, x_2) , (x_3, x_4) and (x_5, x_6) . The spacetime symmetry is broken into $SO(2)_{1,2} \times SO(2)_{3,4} \times SO(2)_{5,6} \times SO(2)_{7,\dots,10}$ which leads to the Ansatz

$$\begin{aligned} ds_{11}^2 &= -Z^{\parallel}(\hat{r}) dt^2 + Z_1^{\parallel}(\hat{r}) (dx_1^2 + dx_2^2) + Z_2^{\parallel}(\hat{r}) (dx_3^2 + dx_4^2) + Z_3^{\parallel}(\hat{r}) (dx_5^2 + dx_6^2) \\ &\quad + Z^{\perp}(\hat{r}) (dx_7^2 + dx_8^2 + dx_9^2 + dx_{10}^2), \\ F_4 &= d\left(Z_1(\hat{r})^{-1}\right) dt \wedge dx_1 \wedge dx_2 + d\left(Z_2(\hat{r})^{-1}\right) dt \wedge dx_3 \wedge dx_4 + d\left(Z_3(\hat{r})^{-1}\right) dt \wedge dx_5 \wedge dx_6, \end{aligned} \quad (3.1.20)$$

where \hat{r} is the radial coordinate of the four-dimensional transverse space to the branes. As before, we decompose the supersymetric equation (3.1.6) along the time coordinate, the two-cycles wrapped by

the branes and the transverse space. This leads to express the metric deformations according to the electric sources, Z_I , $I = 1, 2, 3$, and to identify constant Killing spinors ϵ_0 :

$$\begin{aligned} Z^\parallel(\hat{r}) &= (Z_1(\hat{r}) Z_2(\hat{r}) Z_3(\hat{r}))^{-\frac{2}{3}}, & Z^\perp(\hat{r}) &= (Z_1(\hat{r}) Z_2(\hat{r}) Z_3(\hat{r}))^{\frac{1}{3}}, \\ Z_I^\parallel(\hat{r}) &= \frac{|\epsilon_{IJK}|}{2} \left(\frac{Z_J(\hat{r}) Z_K(\hat{r})}{Z_I(\hat{r})^2} \right)^{\frac{1}{3}}, & \star_4 d_4 \star_4 d_4 Z_I(\hat{r}) &= 0, \quad I = 1, 2, 3, \\ (\mathbb{1} + \Gamma^{012}) \epsilon_0 &= (\mathbb{1} + \Gamma^{034}) \epsilon_0 = (\mathbb{1} + \Gamma^{056}) \epsilon_0 = 0, \end{aligned} \quad (3.1.21)$$

where ϵ_{IJK} is three-dimensional Levi-Civita symbol. The projection relations imply that there are only four Killing spinors and that the solution is indeed 1/8-BPS. The metric and the field strength is then given by²

$$\begin{aligned} ds_{11}^2 &= -(Z_1 Z_2 Z_3)^{-\frac{2}{3}} dt^2 + (Z_1 Z_2 Z_3)^{\frac{1}{3}} (dx_7^2 + dx_8^2 + dx_9^2 + dx_{10}^2) \\ &\quad + \left(\frac{Z_2 Z_3}{Z_1^2} \right)^{\frac{1}{3}} (dx_1^2 + dx_2^2) + \left(\frac{Z_1 Z_3}{Z_2^2} \right)^{\frac{1}{3}} (dx_3^2 + dx_4^2) + \left(\frac{Z_1 Z_2}{Z_3^2} \right)^{\frac{1}{3}} (dx_5^2 + dx_6^2) \\ F_4 &= d(Z_1^{-1}) dt \wedge dx_1 \wedge dx_2 + d(Z_2^{-1}) dt \wedge dx_3 \wedge dx_4 + d(Z_3^{-1}) dt \wedge dx_5 \wedge dx_6. \end{aligned} \quad (3.1.22)$$

Each warp factor is determined by a harmonic equation on the four-dimensional transverse space which can be sourced only at the brane locus $\hat{r} = 0$. Thus,

$$Z_I(\hat{r}) = 1 + \frac{\alpha_I}{\hat{r}^2}, \quad I = 1, 2, 3.$$

The coefficient α_I is related to the electric charge of the corresponding stack of M2-branes, Q_I , from the flux-integral of the magnetic field strength over the boundary of the eight-dimensional volume transverse to the branes. This leads to the same computation as for a single stack of M2-branes:

$$\alpha_I = 32\pi^2 l_P^{(11)^6} N_I, \quad I = 1, 2, 3, \quad (3.1.23)$$

where N_I is the number of M2-branes in the I^{th} stack.

There are other possible BPS solutions that belong to the class of intersecting branes, which can be derived by suitably composing with the solutions above. In Section 3.3.1, we will discuss the general solutions of an arbitrary number of stacks of M2-branes and M5-branes with additional KKm and P charges within the dimensional reduction to $\mathcal{N} = 2$ five-dimensional Supergravity. The stacks of M2-branes and M5-branes will be wrapping appropriate two-cycles and five-cycles in order to preserve 4 supercharges. Before going into that discussion, let us review the two other supergravity frames used in this thesis and their duality relations.

3.1.2 Type IIA and IIB Supergravity

The ten-dimensional type IIA and type IIB supergravity theories were discovered in the eighties by Schwarz and West for IIB [47–49] and Romans for IIA [50]. Type IIA (resp. type IIB) has $\mathcal{N} = (1, 1)$ (resp. $\mathcal{N} = (2, 0)$) supersymmetries with opposite chirality (resp. same chirality). Both theories have 16 real supercharges corresponding to two Majorana-Weyl spinors. The bosonic degrees of freedom can be decomposed in a Neveu-Schwarz Neveu-Schwarz sector (NS-NS) and a Ramond-Ramond (R-R) sector. Their field content in the NS-NS sector is identical:

- A spin-2 gravitational field g .

²We omit the “ (\hat{r}) ” for readability.

Theory	M	IIA					IIB			
Fields	A_3	B_2	$C^{(1)}$	$C^{(3)}$	$C^{(5)}$	$C^{(7)}$	B_2	$C^{(2)}$	$C^{(4)}$	$C^{(6)}$
Electric	M2	F1	D0	D2	D4	D6	F1	D1	D3	D5
Magnetic	M5	NS5	D6	D4	D2	D0	NS5	D5	D3	D1

Table 3.1: Branes and gauge fields in eleven-dimensional and ten-dimensional supergravity theories. We have omitted the field $C^{(0)}$ (resp. $C^{(8)}$) which couples electrically (resp. magnetically) to D(-1)-branes and magnetically (resp. electrically) to D7-branes. They are special and required a particular treatment.

- An antisymmetric two-form gauge field B_2 and its three-form field strength $H_3 = d_{10}B_2$.
- A scalar field Φ called dilaton.

The R-R sector contains antisymmetric p -form gauge fields, $C^{(p)}$, and their field strengths $F^{(p+1)}$, $p \leq 8$. Type IIA contains the forms with p odd whereas type IIB contains the p even.

As the eleven-dimensional Supergravity, the gravitational field gives rise to the spacetime metric. The off-diagonal terms with a leg along time are sourced by P waves whereas the spatial off-diagonal vector fields corresponds to KKm charges. The value of the dilaton at the boundary encodes the string coupling through the relation $e^{\Phi} = g_s$. Furthermore, type IIA and IIB supergravity theories have a larger number of type of gauge fields compared to eleven-dimensional Supergravity. This also enlarges the number of classical objects which couple to them. The NS-NS gauge fields will couple with objects related to strings with NS boundary conditions whereas the R-R gauge fields will couple with objects related to Dirichlet boundary condition. Following the same arguments as in Section 3.1.1, the NS-NS gauge field, B_2 , couples electrically to a *fundamental strings* (F1) and magnetically to a five-dimensional branes called *NS5-branes*. The R-R gauge field, $C^{(p)}$, couples electrically to D($p-1$)-branes and magnetically to D($7-p$)-branes. A D p -brane traces out a $p+1$ dimensional worldvolume in space-time. By simple inversion, a D($3+q$)-brane, $-4 \leq q \leq 4$, induces an electric charge in $C^{(4+|q|)}$ and a magnetic charge in $C^{(4-|q|)}$. This leads to the duality rules

$$\bar{F}^{(5+|q|)} = \star_{10} \bar{F}^{(5-|q|)}, \quad -4 \leq q \leq 4, \quad (3.1.24)$$

where we have defined

$$\bar{F}^{(p)} = \begin{cases} F^{(p)} + H_3 \wedge C^{(p-3)} & \text{if } p \geq 3 \\ F^{(p)} & \text{if } p < 3 \end{cases}. \quad (3.1.25)$$

The duality relation fixes entirely the $C^{(4+|q|)}$ gauge fields. In the Table 3.1, we have summarized the fundamental electric-magnetic elements in the ten-dimensional and eleven-dimensional Supergravities and their couplings with the gauge fields.

The bosonic sector of the ten-dimensional action can be decomposed naturally as follows

$$S_{10} = S_{\text{NS}} + S_{\text{R}} + S_{\text{CS}}. \quad (3.1.26)$$

The NS-NS part is common to type IIA and type IIB

$$(16\pi G_{10}) S_{\text{NS}} = \int d^{10}x \sqrt{-g} e^{-2\Phi} (R + 4 d_{10}\Phi \wedge \star_{10} d_{10}\Phi) - \int e^{-2\Phi} H_3 \wedge \star_{10} H_3, \quad (3.1.27)$$

where the ten-dimensional Newton constant is given according to the string length l_s and the string coupling as

$$16\pi G_{10} = (2\pi)^{-1} g_s^2 (2\pi l_s)^8.$$

The contributions differ for the R-R and for the Chern-Simons terms

$$\begin{aligned}
(16\pi G_{10}) S_{\text{R}}^{\text{IIA}} &= - \int F^{(2)} \wedge \star_{10} F^{(2)} + \bar{F}^{(4)} \wedge \star_{10} \bar{F}^{(4)}, & (16\pi G_{10}) S_{\text{CS}}^{\text{IIA}} &= - \int B_2 \wedge F^{(4)} \wedge F^{(4)}, \\
(16\pi G_{10}) S_{\text{R}}^{\text{IIB}} &= - \int F^{(1)} \wedge \star_{10} F^{(1)} + \bar{F}^{(3)} \wedge \star_{10} \bar{F}^{(3)} + \frac{1}{2} \bar{F}^{(5)} \wedge \star_{10} \bar{F}^{(5)}, \\
(16\pi G_{10}) S_{\text{CS}}^{\text{IIB}} &= - \int C^{(4)} \wedge H_3 \wedge F^{(3)}.
\end{aligned} \tag{3.1.28}$$

The NS-NS and R-R parts of the action are the extension of the Einstein Hilbert action (2.1.1). The NS-NS action, (3.1.27), contains the purely gravitational term $\sqrt{-g}R$, the Lagrangian of a massless scalar field Φ and the Lagrangian of a two-form gauge fields whereas the R-R actions, (3.1.28), contain several Lagrangian of interacting p -form gauge fields. One notices a slight difference in the purely gravitational term which is a consequence of the choice of metric frame. The actions are written in the *string frame*. The *Einstein frame*, characterized by a term $\sqrt{-g_E} R$, is obtained by rescaling

$$g_{E\mu\nu} = e^{\frac{\Phi}{2}} g_{\mu\nu}.$$

In type IIB Supergravity, the self-duality of the five-form field strength $\bar{F}^{(5)}$ which couples electrically and magnetically to D3-branes is required in addition to the equations of motion.

- Supersymmetric solution example: a stack of Dp-branes

In a similar fashion to M-brane solutions, one can derive the background and the fields sourced by a stack of coincident Dp-branes in type II Supergravity. We consider the Cartesian coordinates (t, x_1, \dots, x_{10}) . The $SO(1, 9)$ symmetry is broken into $SO(1, p) \times SO(9 - p)$. The solutions can be obtained from the type IIA or type IIB action assuming that the solution preserves Killing spinors and working with the bilinears. They can be also derived by performing a sequence of duality transformations from the M-brane solutions that we will review in the next section. The Ansatz for the gauge fields and the metric in the string frame is

$$\begin{aligned}
ds_{10}^2 &= Z_{Dp}^{-\frac{1}{2}} (-dt^2 + dx_1^2 + \dots + dx_p^2) + Z_{Dp}^{\frac{1}{2}} (dx_{p+1}^2 + \dots + dx_{10}^2), \\
e^{2\Phi} &= Z_{Dp}^{\frac{3-p}{2}}, \quad B_2 = 0, \\
C^{(p+1)} &= - (Z_{Dp}^{-1} - 1) dt \wedge dx_1 \wedge \dots \wedge dx_p, \quad C^{(p')} = 0, \quad p' \neq p+1, 7-p,
\end{aligned} \tag{3.1.29}$$

The solution is a 1/2-BPS solution of the Einstein equation if it satisfies the Maxwell equation which reduces to a Laplace equation in the $9 - p$ transverse space

$$\star_{9-p} d_{9-p} \star_{9-p} d_{9-p} Z_{Dp} = 0, \quad \implies \quad Z_{Dp} = 1 + \frac{\alpha_{Dp}}{r^{7-p}},$$

where r is the radial coordinate of the transverse space. The supergravity charge α_{Dp} can be related to the number of Dp branes by integrating the flux on a boundary of the transverse space as for M-branes. The end result gives

$$\alpha_{Dp} = (4\pi)^{\frac{5-p}{2}} \Gamma\left(\frac{7-p}{2}\right) l_s^{7-p} g_s N_{Dp}.$$

Once again, one can evaluate the regime of validity of the supergravity description. The geometry is singular at $r \rightarrow 0$ and then the geometry cannot be reliable everywhere. By computing the Ricci scalar, one can check that if one wants the geometry to be trustable for $r \gtrsim l_s$, we need $\alpha_{Dp} r^{p-7} \sim 1$. This requires $g_s N_{Dp} \gg 1$ as advertised in the Introduction of the thesis.

In the next section, we review the dualities existing between supergravity theories and the Kaluza-Klein dimensional reduction. This will allow to connect type IIA and type IIB to the mother eleven-dimensional Supergravity and to have a precise one-to-one map connecting the different ingredients of Table 3.1.

3.2 Dualities and dimensional reduction

During the “second superstring revolution” [51], the various string-theory frames were unified by new equivalences, called dualities. Nowadays, those dualities are very useful to relate theories and spectra of very different appearance at various limits (as strong-weak dualities). In this section we review the Kaluza-Klein reduction, the T-duality and the S-duality. We also review the generalized spectral flows, which are not dualities but transformations built on dualities and which allow to relate very different spectra of solutions.

3.2.1 Kaluza-Klein reduction

A one-dimensional Kaluza-Klein compactification is the compactification of a $(D + 1)$ -dimensional theory on a product spacetime $\mathcal{M}_{D+1} = \mathcal{M}_D \times S^1$, where S^1 is a compact circle along a coordinate y with the periodicity $y \sim y + 2\pi R_o$. Fields of the lower dimensional theory arise from harmonic expansion on S^1 of the various higher-dimensional fields. In a Kaluza-Klein compactification, one keeps the entire infinite set of harmonic modes, which describe both massless and massive fields in D dimensions. For the purpose of this thesis, we consider that the fields at higher dimensions are independent of y and then that the harmonic expansion reduces to the massless modes. Moreover, for readability, we focus on the eleven-dimensional Supergravity. Generalization to arbitrary dimensions with arbitrary y -independent gauge fields can be found in [52].

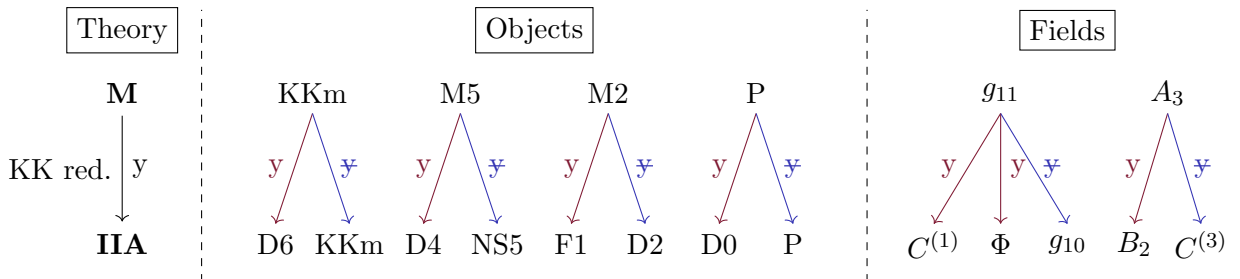
We consider eleven-dimensional Supergravity with a compact 11th dimension, y , with a radius $R_o = g_s l_s$ where g_s and l_s are the string coupling and the string length respectively³. The choice of radius is motivated to make a concrete relation between type IIA and eleven-dimensional Supergravity, especially by relating the Newton constants

$$G_{11} = 2\pi R_o G_{10}.$$

We decompose the bosonic fields along y as

$$\begin{aligned} ds_{11}^2 &= e^{-\frac{2\Phi}{3}} ds_{10}^2 + e^{\frac{4\Phi}{3}} \left(dy + C^{(1)}\right)^2, \\ A_3 &= C^{(3)} + B_2 \wedge dy, \end{aligned} \tag{3.2.1}$$

where the decomposition has been arranged to have a lower-dimensional theory with the field content of type IIA Supergravity. Remind that $C^{(5)}$ and $C^{(7)}$ are obtained from the duality relation (3.1.24). One can draw the map from the objects in eleven-dimensional supergravity to type IIA objects depending if they have a leg along y or not. We outline the KK reduction on the gauge fields and on the objects in the following:



where the blue arrows with “ \overline{y} ” correspond to the reduction of objects or fields with no legs along y whereas the red arrows with “ y ” correspond to objects or fields with a leg along y . The remaining R-R gauge fields are obtained from the duality relations (3.1.24).

³The size of the circle gives rise to only one degree of freedom since $l_s = g_s^3 l_P^{(11)}$.

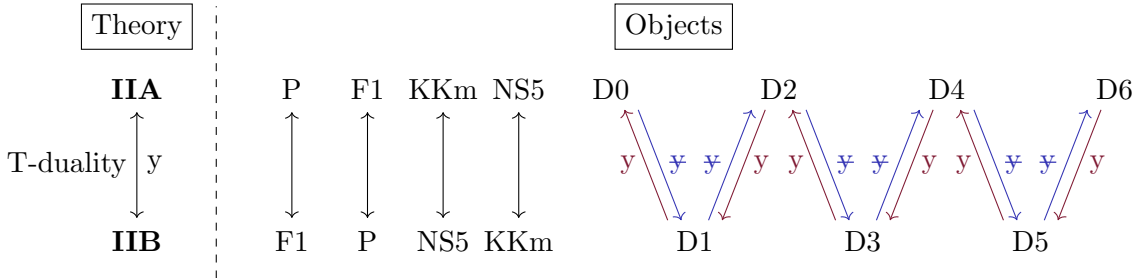
3.2.2 T-duality

T-duality is a symmetry which maps the string spectra of different string theories into each other, in particular the string spectrum of type IIA String Theory to the string spectrum of type IIB String Theory. If we consider type IIA and type IIB with a compact circle of radius R_A and R_B respectively. The fundamental strings F1 wrapping the circle are quantized in unit of $R_{A/B} l_s^{-2}$ whereas the momentum waves P are quantized in $(R_{A/B})^{-1}$. Thus, by mapping

$$\frac{R_A}{l_s} = \frac{l_s}{R_B},$$

the quanta of fundamental string of type IIA gets map into the quanta of momentum wave of type IIB and inversely. T-duality is then a strong coupling - weak coupling duality: it maps a stringy regime when $R_{A/B} \ll l_s$ to low-energy regime $R_{B/A} \gg l_s$.

A similar reasoning applies to D-branes. If a Dp -brane is wrapped along the circle, it T-dualizes into a $D(p-1)$ -brane whereas if it is not, it T-dualizes into a $D(p+1)$ -brane. We then have the following mapping:



where we have used the same convention for the arrows. To compute the effect of a T-duality along y on the fields, it is convenient to decompose them in the following forms

$$\begin{aligned} ds_{10}^2 &= \hat{g}_{\mu\nu} dx^\mu dx^\nu + g_{yy} (dy + A_\mu dx^\mu)^2, \\ B_2 &= \hat{B}_2 + B_{\mu y} dx^\mu \wedge (dy + A_\mu dx^\mu), \\ C^{(p)} &= \hat{C}^{(p)} + C_y^{(p-1)} \wedge (dy + A_\mu dx^\mu). \end{aligned} \quad (3.2.2)$$

The T-dualized fields that we note with “ \sim ” are given by the Buscher’s rules [53]

$$\begin{aligned} d\tilde{s}_{10}^2 &= \hat{g}_{\mu\nu} dx^\mu dx^\nu + g_{yy}^{-1} (dy + B_{\mu y} dx^\mu)^2, \\ e^{2\tilde{\Phi}} &= g_{yy}^{-1} e^{2\Phi}, \\ \tilde{B}_2 &= \hat{B}_2 + A_\mu dx^\mu \wedge dy, \\ \tilde{C}^{(p)} &= C_y^{(p)} + \hat{C}^{(p-1)} \wedge (dy + B_{\mu y} dx^\mu). \end{aligned} \quad (3.2.3)$$

3.2.3 S-duality

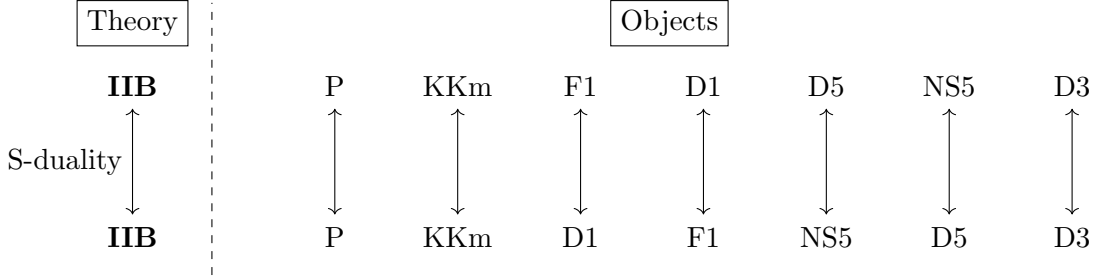
The S-duality is constructed in type IIB String Theory as a \mathbb{Z}_2 symmetry of the fields. It flips the dilaton and interchanges R-R and NS-NS fields as follows

$$\Phi \rightarrow -\Phi, \quad g_{\mu\nu} \rightarrow e^{-\Phi} g_{\mu\nu}, \quad B_2 \rightarrow C^{(2)}, \quad C^{(2)} \rightarrow -B_2, \quad (3.2.4)$$

with all the other $\bar{F}^{(p)}$ unchanged. The transformation of the dilaton actually shows, when evaluated at the boundary, the nature of the S-duality: it is actually a weak coupling - strong coupling which maps

$$g_s \rightarrow \frac{1}{g_s}.$$

Moreover, S-duality relates type-IIB objects as:



3.2.4 Generalized spectral flows

Generalized spectral flows are not duality transformations. Even if they allow to move from a spectrum of solutions to another, the map can lead to very different types of solutions. Generalized spectral flows can be constructed in various formulations whom several will be discussed in this thesis. One of their primary construction uses sequences of T-dualities, S-dualities and shifts of coordinates. The S-dualities make the construction naturally defined in type IIB. However, according to the duality rules detailed above, it can be translated into any frame by adding an initial T-duality or KK-reduction. Let us consider type IIB Supergravity with 6 compact directions and let us denote two of them as y and φ .

- The first type of generalized spectral flow is a simple shift of coordinates which we denote “s”, $\varphi \rightarrow \varphi + \gamma y$, where γ is a constant.
- The second type of generalized spectral flow consists in a S-duality, a T-duality along y followed by a shift of $\varphi \rightarrow \varphi + \gamma y$, a T-duality back along y and finally a S-duality. We usually denote such a transformation as “STsTS”.
- Using the previous notation, the third generalized spectral flow can be denoted as a $T^4\text{STsTST}^4$ transformation where the “ T^4 ” refers to four T-dualities on the four other compact directions.

In the main parts of the thesis, we will have direct illustrations of possible effects of spectral flows on supergravity solutions.

3.3 Compactification to lower dimensions

In this thesis, we will construct and study classical solutions in five or six dimensions. Even if our attempts will concentrate on solutions with four unbroken supersymmetries as the three-charge 1/8-BPS black hole, we will also construct eight-supercharge solutions and non-BPS solutions. Five-dimensional Supergravities arise as dimensional reduction of eleven-dimensional Supergravity on a Calabi-Yau three-fold whereas six-dimensional Supergravities are obtained from ten-dimensional Supergravities, as type IIB, on a Calabi-Yau two-fold. The truncated fields from ten or eleven dimensions give rise to a large variety of field contents in six or five dimensions (for a very general discussion see [54]). For the purpose of the thesis, we consider only consistent truncations which lead to specific contents that we are interested in. In particular, we are interested in $\mathcal{N} = 2$ five-dimensional Supergravity coupled to n_V vector multiplets with $n_V \geq 2$ and in $\mathcal{N} = (1, 0)$ six-dimensional Supergravity coupled to n_T tensor multiplets with $n_T \geq 1$. Both frameworks have 8 supercharges in total. In this section, we briefly review their field contents and how they arise from dimensional reduction of type IIB Supergravity or eleven-dimensional Supergravity.

3.3.1 Five-dimensional $\mathcal{N} = 2$ Supergravity

Five-dimensional $\mathcal{N} = 2$ Supergravity coupled to n_V vector multiplets with $n_V \geq 2$ has the following bosonic-field content:

- A gravitational field g .
- $n_V + 1$ U(1) vector gauge fields A_μ^I and their field strengths $F^I = d_5 A^I$. One is coming from the graviton multiplet and is usually referred as the “graviphoton” and the others come from the extra vector multiplets.
- $n_V + 1$ scalars X^I in the symmetric space $SO(1, 1) \times (SO(1, n_V)/SO(n_V))$.

It results from compactification of eleven dimensional Supergravity on a Calabi-Yau three-fold \mathcal{C}_6 [55]. The bosonic fields in eleven dimensions are the gravitational field and the three-form gauge potential $\{g_{MN}, A_{3MNR}\}$ as detailed in Section 3.1.1. We assume that the fields are independent on the coordinates of \mathcal{C}_6 and then only the zero modes will contribute to the KK reduction. Those zero modes correspond to the harmonic forms on \mathcal{C}_6 . Let us recall that a Calabi-Yau three-fold is uniquely defined by the non-zero Hodge numbers ($h^{(1,1)} = h^{(2,2)}$, $h^{(2,1)} = h^{(0,0)} = h^{(3,0)} = h^{(3,3)} = 1$) and the intersection numbers C_{IJK} , with $I, J, K = 1, \dots, h^{(1,1)}$ (see table below). The number of independent harmonic n -forms on a Calabi-Yau m -fold is given by the Betti numbers,

$$b_n = \sum_{p+q=n} h^{(p,q)} = b_{m-n}. \quad (3.3.1)$$

Therefore, \mathcal{C}_6 contains $h^{(1,1)}$ independent two-forms and four-forms. The number of independent harmonic three-forms is $2(h^{(2,1)} + 1)$, the number of zero-forms and six-forms is one and there is no one-forms and five-forms. We only consider vector descendants and then freeze all degrees of freedom coming from $h^{(2,1)}$. If we call D_I the $h^{(1,1)}$ independent two-forms, the *structure constants* is the volume of the product of three:

$$C_{IJK} \equiv \int_{\mathcal{C}_6} D_I \wedge D_J \wedge D_K. \quad (3.3.2)$$

We denote the compact coordinates with Latin letters ($a, \bar{a} = 1, 2, 3$) and the five-dimensional coordinates with Greek letters ($\mu = 1, \dots, 5$). According to the number of independent forms on \mathcal{C}_6 , three scalars correspond to the volume of \mathcal{C}_6 , \mathcal{V}_6 , and to the two gauge field components, A_{3abc} and $A_{3\mu\nu\rho}$. They belong to the universal hypermultiplet. Each of the $n_V + 1 = h_{(1,1)}$ independent two-forms gives a vector, $A_\mu^I \sim A_{3\mu a\bar{b}}$. They are associated to the scalars arising from the gravitational field, $X^I \sim g_{a\bar{b}}$. Those scalars determine the size of the two-form inside \mathcal{C}_6 . Because we have turned off all hypermultiplet degrees of freedom, the Calabi-Yau volume deformation is set to zero and \mathcal{V}_6 is constant. The volume cannot be zero, this implies that one of the vector multiplet belongs to the gravity multiplet of five-dimensional $\mathcal{N} = 2$ Supergravity and the n_V others are additional vector multiplets. Moreover, the fixed volume constrains the metric on \mathcal{C}_6 and the $n_V + 1$ scalars must satisfy⁴

$$\frac{1}{6} C_{IJK} X^I X^J X^K = 1 \quad \implies \quad X_I = \frac{1}{6} C_{IJK} X^J X^K. \quad (3.3.3)$$

The intersection constants induce non-trivial gauge coupling from the Chern-Simons term in the eleven-dimensional action

$$\int A_3 \wedge F_4 \wedge F_4 \sim C_{IJK} \int A^I \wedge F^J \wedge F^K.$$

We summarize the compactification descendants in the following table:

⁴We have consider everything in unit of \mathcal{V}_6 which is equivalent to take $\mathcal{V}_6 = 1$.

<u>Hodge diamonds of \mathcal{C}_6:</u>				<u>Harmonic forms:</u>	<u>Fields $\{g_{MN}, A_{3MNP}\}$:</u>
	1	—————→		six-forms	\mathcal{V}_6 , 1 scalar
	0		0 —————→	five-forms	\emptyset
0	$h^{(1,1)}$		0 —————→	four-forms	\emptyset
1	$h^{(2,1)}$	$h^{(1,2)}$	1 —→	three-forms	$(A_{3abc}, A_{3ab\bar{c}}, g_{ab})$, $(2, h^{(2,1)}, h^{(2,1)})$ scalars
	0	$h^{(1,1)}$	0 —————→	two-forms	$(A_{3\mu a\bar{b}}, g_{a\bar{b}})$, $(h^{(1,1)}, h^{(1,1)})$ vectors, scalars
	0		0 —————→	one-forms	\emptyset
	1	—————→		zero-forms	$A_{3\mu\nu\rho}$, 1 scalar

The compactification can be also described from a brane point of view by translating the “form language” to a “cycle language”. We decompose \mathcal{C}_6 in $h_{(1,1)} = n_V + 1$ two-cycles wrapped by M2-branes and their transverse four-cycles wrapped by M5 branes. The M5-branes are five-dimensional extended objects and have one remaining leg in the five-dimensional space inducing fluxes. The stacks of branes are smeared in their transverse directions inside \mathcal{C}_6 . They source specifically the three-form gauge field A_3 which the KK reduction leads to the $n_V + 1$ U(1) gauge fields A^I . The sizes of the cycles are the free moduli giving rise to the scalars X^I .

Finally, one can write down the five-dimensional action for the bosonic fields [56, 57]

$$(16\pi G_5) S_5 = \int d^5x \sqrt{-g} R - Q_{IJ} \int (F^I \wedge \star_5 F^J - d_5 X^I \wedge \star_5 d_5 X^J) + \frac{C_{IJK}}{6} \int A^I \wedge F^J \wedge F^K, \quad (3.3.4)$$

where the coupling Q_{IJ} depends on the scalars via [56, 57]

$$Q_{IJ} = \frac{9}{2} X_I X_J - \frac{1}{2} C_{IJK} X^K, \quad (3.3.5)$$

the structure constants are required to satisfy the constraint

$$C_{IJK} C_{J'(LM} C_{PQ)K'} \delta^{JJ'} \delta^{KK'} = \frac{4}{3} \delta_{I(L} C_{MPQ)}, \quad (3.3.6)$$

and the five-dimensional Newton constant is given according to the eleven-dimensional one as

$$G_5 = \mathcal{V}_6^{-1} G_{11}. \quad (3.3.7)$$

The two first integrals in (3.3.4) correspond to the five-dimensional Einstein-Hilbert action coupled to $n_V + 1$ scalar fields and $n_V + 1$ U(1) gauge fields with a non-trivial coupling constant. The third integral is the purely topological Chern-Simons integral. This term makes the difference from a purely GR description and gives hope for constructing solutions with non-trivial structure at the horizon scale.

As we will derive in detail in the next chapter, this action contains 1/8-BPS three-charge five-dimensional solutions. Constructing supersymmetric solutions in this framework is similar to the eleven-dimensional framework discussed in Section 3.1.1.1. If one assumes that some of the supersymmetries are preserved and that the bilinear, \mathcal{K}_μ (3.1.5), is a time-like Killing vector, a first order differential equation guarantees that the Einstein equations are satisfied. The remaining equation is the Maxwell equation for the gauge fields. This issue will be addressed in the next chapter.

3.3.2 Six-dimensional $\mathcal{N} = (1, 0)$ Supergravity

Six-dimensional $\mathcal{N} = (1, 0)$ Supergravity coupled to n_T tensor multiplets has the following bosonic fields coming from the graviton multiplet and the n_T extra tensor multiplets [58–61]:

- A gravitational field g .
- $n_T + 1$ two-form gauge fields $B_{\mu\nu}^I$ and their field strengths $G^I = d_6 B^I$.
- $n_T + 1$ scalars v^I in the coset space $SO(1, n_T)/SO(n_T)$. It is convenient to associate them into a $SO(1, n_T)$ matrix with constraints:

$$\mathcal{S} = \begin{pmatrix} v_I \\ x_I^M \end{pmatrix}, \quad I = 0, \dots, n_T, \quad M = 1, \dots, n_T, \quad (3.3.8)$$

$$v_I v^I = 1, \quad v_I v_J - x_I^M x_J^M = \eta_{IJ}, \quad v^I x_I^M = 0,$$

where the scalar indices, I or J , are raised by the $SO(1, n_T)$ Minkowski metric in light-cone coordinates with the mostly-minus signature,

$$\eta = \begin{pmatrix} 0 & 1 & 0 & \dots & 0 \\ 1 & 0 & 0 & \dots & 0 \\ 0 & 0 & -1 & \dots & 0 \\ \vdots & \vdots & \vdots & \ddots & \vdots \\ 0 & 0 & 0 & \dots & -1 \end{pmatrix}. \quad (3.3.9)$$

This choice of scalar basis may seem awkward from what can be found in the literature where the usual Minkowski metric $\text{diag}(1, -1, \dots, -1)$ is used. However, it will be motivated later as the right choice to relate spectra of BPS solutions in $\mathcal{N} = (1, 0)$ six-dimensional Supergravity to BPS solutions in $\mathcal{N} = 2$ five-dimensional Supergravity. The scalars are involved in the tensor dynamics through the metric

$$\mathcal{M}_{IJ} = (\eta \mathcal{S}^T \mathcal{S} \eta)_{IJ} = v_I v_J + x_I^M x_J^M = 2 v_I v_J - \eta_{IJ},$$

which dictates the twisted self-duality conditions of the tensors

$$\mathcal{M}_{IJ} G^J = \eta_{IJ} \star_6 G^J. \quad (3.3.10)$$

This implies that the tensor $v_I G^I$ is self-dual and then belongs to the gravity multiplet whereas the n_T tensors $x_I^M G^I$ are anti self-dual and then belong to the n_T tensor multiplets. The different number of self-dual and anti self-dual tensors (except for $n_T = 1$) implies that there is no Lorentz-invariant lagrangian formulation. However, one can write down a “pseudo-action” [59, 61]

$$(16\pi G_6) S_6 = \int d^6 x \sqrt{-g} \left(R - \eta_{IJ} \partial_\mu v^I \partial_\mu v^J - \frac{1}{3} \mathcal{M}_{IJ} G_{\mu\nu\rho}^I G^{J\mu\nu\rho} \right), \quad (3.3.11)$$

As it has been discussed for five-dimensional Supergravity, one may wonder how six-dimensional $\mathcal{N} = (1, 0)$ Supergravity results from compactification of ten-dimensional Supergravity on a Calabi-Yau two-fold. By contrast with the family of Calabi-Yau three-folds, $K3$, \mathbb{T}^4 and their orbifold limits are the only examples of compact Calabi-Yau two-folds. Different six-dimensional Supergravities can be obtained from compactification of type IIA, type IIB or even type I or heterotic Supergravities [62–66] (for a review see [67]). Moreover, for the six-dimensional Lagrangian to be anomaly-free, hypermultiplets and vector multiplets need to be turned on and their numbers must satisfy an algebraic condition. We will not go into such details and consider only consistent truncations that contain only tensor multiplets in addition to the gravity multiplet.

Let us consider type IIB Supergravity on \mathbb{T}^4 or $K3$. The bosonic fields are the gravity field g_{MN} , the R-R zero-form and the dilaton $(\Phi, C^{(0)})$, the NS-NS and R-R two-forms $(B_2, C^{(2)})$ and the R-R four-forms $C^{(4)}$ ⁵. We assume that they are independent on the transverse space. Only the zero modes which correspond to harmonic forms on \mathbb{T}^4 or $K3$ are involved in the KK reduction. Their numbers are fixed by the Hodge numbers.

⁵One does not need to consider $C^{(6)}$ and $C^{(8)}$. They are fixed by the duality rules (3.1.24).

- On \mathbb{T}^4 : A four-torus has $h^{(0,0)} = h^{(2,2)} = h^{(2,0)} = 1$, $h^{(1,0)} = h^{(2,1)} = 2$ and $h^{(1,1)} = 4$ (see the table below). The numbers of independent harmonic n -forms are given by the Betti numbers (3.3.1). Thus, \mathbb{T}^4 contains one zero-form and one four-form. The number of one-forms and three-forms is four each while the number of two-forms is six. We focus on the fields corresponding to two-forms and to scalars from the six-dimensional perspective. In six dimensions, two-forms must have a (anti) self-dual field strengths. Therefore, one must count the self-dual and anti self-dual components of the two-form descendants. The components of B_2 and $C^{(2)}$ with legs on the six-dimensional space can be decomposed in one self-dual two-form and one anti self-dual two-form each. Their components on \mathbb{T}^4 induce 2×6 scalars. The number of scalar descendants and two-form descendants of $C^{(4)}$ follows the number of harmonic zero-forms and two-forms of \mathbb{T}^4 respectively. They give rise to one scalar, three self-dual two-forms and three anti self-dual two-forms. The remaining scalars come from $(\Phi, C^{(0)})$ and the ten scalars of the metric on \mathbb{T}^4 . The total count gives then 5 anti self-dual two-forms, 5 self-dual two-forms and 25 scalars. The gravity multiplet contains the 5 self-dual two-forms while the tensor multiplets contain one anti self-dual two-form each. This corresponds to $\mathcal{N} = (2, 2)$ six-dimensional Supergravity with $SO(5, 5)$ global symmetry. Moreover, if one considers the \mathbb{T}^4 to be “rigid” in a sense that we consider only the harmonic four-form and the harmonic zero-form of \mathbb{T}^4 . Then, $C^{(4)}$ induces only scalars and the compactification leads to $\mathcal{N} = (2, 2)$ six-dimensional Supergravity with $SO(2, 2)$ global symmetry. The compactification on a rigid \mathbb{T}^4 is sufficient to study six-dimensional solutions with not more than two extra tensor multiplets.

We summarize the tensor and scalar descendants from the compactification in the following table:

Hodge diamonds \mathbb{T}^4 :		Harmonic forms:	Fields $\{g_{MN}, \Phi, B_2, C^{(0)}, C^{(2)}, C^{(4)}\}$:
1	————→	four-forms	$(\mathcal{V}_4, C_{abcd}^{(4)})$ 2 scalars
2	2 ———→	three-forms	g_{ab} 4 scalars
1	4 1 —→	two-forms	$(C_{\mu\nu a\bar{b}/b}^{(4)}, (C_{a\bar{b}/b}^{(2)}, B_{2a\bar{b}/b}, g_{a\bar{b}})$ $(3^+, 3^-)$ tens., 16 sca.
2	2 ———→	one-forms	...
1	————→	zero-forms	$(C_{\mu\nu}^{(2)}, B_{2\mu\nu}), (\Phi, C^{(0)}, C_{\mu\nu\rho\sigma}^{(4)})$ $(2^+, 2^-)$ tens., 3 sca.

where n^\pm gives the number of self-dual (resp. anti self-dual) corresponding tensors.

One way to have less than $\mathcal{N} = (2, 2)$ supersymmetries is to consider orbifold limits of \mathbb{T}^4 , as $\mathbb{T}^4/\mathbb{Z}_2 \simeq \mathbb{T}^2 \times \mathbb{T}^2$. Only one combination of the left-moving and the right-moving supercharges is preserved by the choice of orientation [64–66]. We can also consider consistent truncation of the field contents. Roughly speaking, this consists in freezing all but one self-dual two-forms by carefully fixing their associated scalars in the scalar moduli space (see for instance Appendix B of [68] for an example of truncation to $SO(1, 2)$). Thus, six-dimensional $\mathcal{N} = (1, 0)$ Supergravity with $n_T \leq 5$ extra tensor multiplets can be obtained from consistent truncation of type IIB Supergravity on \mathbb{T}^4 .

Moreover, the BPS solutions can be interpreted as brane bound states of type IIB. For instance, the BPS solutions with $n_T = 2$ correspond to D1 branes wrapping a one-curve in the six-dimensional space with momentum charge P along this curve and to D5 branes wrapping the same curve and \mathbb{T}^4 .

- On $K3$: The compactification on $K3$ is similar and only the numbers of descendants differ. The Hodge numbers of $K3$ are $h^{(0,0)} = h^{(2,2)} = h^{(2,0)} = 1$, $h^{(1,0)} = h^{(2,1)} = 0$ and $h^{(1,1)} = 20$. Thus, the KK reduction of $C^{(4)}$ induces 22 two-forms of which 3 are self-dual and 19 are anti self-dual. The gravity multiplet contains 5 self-dual two-forms, while we have 21 tensor multiplets with one anti self-dual two-form each. This corresponds to $\mathcal{N} = (2, 0)$ six-dimensional Supergravity with $SO(5, 21)$ global symmetry.

Once again, one can reduce supersymmetry to $\mathcal{N} = (1, 0)$ Supergravity coupled to $n_T \leq 21$ tensor multiplets by considering orientifold $K3$ or by consistent truncation of the field content.

The relation between type IIB and six-dimensional Supergravity allows to derive the six-dimensional Newton constant from the ten-dimensional one:

$$G_6 = (\mathcal{V}_4)^{-1} G_{10} . \tag{3.3.12}$$

We now have settled all the frameworks needed to construct classical solutions. This is the subject of the next chapter.

Classical solutions in Supergravity

We work in the context of the supergravity theories reviewed in the previous chapter to construct classical solutions describing black holes, black strings and smooth geometries.

In Section 4.1, we will work in the context of $\mathcal{N} = 2$ five-dimensional Supergravity equivalently seen as eleven-dimensional Supergravity on a Calabi-Yau three-fold. We show that the equations of motion of BPS solutions have a linear structure that allows to construct large classes of BPS supergravity solutions. We exploit the symplectic structure of the solutions to derive symplectic transformations corresponding to generalized spectral flows and gauge transformations. They allow a wide spectrum of solutions to be explored. We construct the well-known 1/8-BPS three-charge black hole in five dimensions, or BMPV black hole, and show that the spectrum contains also multicenter solutions which look like the BMPV black hole but caps off smoothly in the IR. The main features of the geometries that replace the singularity are topologically non-trivial cycles called *bubbles* maintained by fluxes. We will also discuss the two-charge 1/4-BPS round Supertubes which are singular from the five-dimensional perspective but smooth in six dimensions.

In Section 4.2, we work in the context of $\mathcal{N} = (1, 0)$ six-dimensional supergravity equivalently seen as a consistent truncation of type IIB Supergravity on a Calabi-Yau two-fold. We first derive the equations of motion of BPS solutions which are slightly more complex in that it can depend non-trivially upon the extra direction. They can be decomposed in a first layer of equations with a linear structure and a second layer with quadratic source terms. We review the basic construction of the D1-D5-P 1/8-BPS black string dual to the BMPV black hole and the two-charge Supertubes with arbitrary shapes. Finally, we discuss the construction of supergravity Superstrata. Superstrata are smooth solutions of the equations of motions that can have same mass, charges and angular momenta as the D1-D5-P 1/8-BPS black hole. They are obtained by generating momentum charge P on specific two-charge Supertubes.

In Section 4.3, we discuss an extension to non-supersymmetric solutions in five or six dimensions. First we review the construction of the non-BPS three-charge over-rotating Cvetič-Youm black string in six dimensions. Then, we review a class of non-BPS smooth solutions called almost-BPS solutions. Supersymmetry is broken in a subtle way and the almost-BPS equations of motion are “similar” to the BPS equations in five dimensions.

4.1 BPS solutions in five dimensions

4.1.1 Generic BPS solutions

We consider $\mathcal{N} = 2$ five-dimensional Supergravity coupled to n_V extra vector multiplets. We use the conventions detailed in Section 3.3.1. The dynamics of solutions of the action given in (3.3.4) is

governed by the following Einstein-Maxwell-scalar equations [69]

$$\begin{aligned} R_{\mu\nu} + Q_{IJ} \left(\partial_\mu X^I \partial_\nu X^J + F_{\mu\rho}^I F_\nu^{J\rho} - \frac{1}{6} g_{\mu\nu} F_{\rho\sigma}^I F^{J\rho\sigma} \right) &= 0, \\ d_5 (Q_{IJ} \star_5 F^J) + \frac{1}{4} C_{IJK} F^J \wedge F^K &= 0, \\ -d_5 \star_5 d_5 X_I + \left(C_{IJK} X_L X^K - \frac{1}{6} C_{ILJ} \right) (F^L \wedge \star_5 F^J - dX^L \wedge \star_5 dX^J) &= 0. \end{aligned} \quad (4.1.1)$$

4.1.1.1 BPS equations of motion

As with supersymmetric solutions in eleven-dimensional Supergravity, we solve the Einstein equation by turning off the gravitini Ψ_μ and by assuming that the BPS solutions preserve Killing spinors with a time-like bilinear $\mathcal{K}_\mu = \bar{\epsilon} \Gamma^\mu \epsilon$. The supersymmetry transformation leads to a first order differential equation [70, 71]

$$\delta \Psi_\mu = \nabla_\mu \epsilon + \frac{1}{8} X_I (\Gamma_\mu^{\nu\rho} - 4 \delta_\mu^\nu \Gamma^\rho) F^I_{\nu\rho} \epsilon = 0, \quad (4.1.2)$$

where Γ^μ are the 8×8 Gamma matrices and ∇_μ is the covariant derivative in five dimensions. The time-like Killing vector \mathcal{K} gives the time direction and one can build all the vielbeins from the other non-zero bilinears. The Ansatz that is consistent with the structure of the equations of motion consist in decomposing the metric and the U(1) vector gauge fields as follows

$$\begin{aligned} ds_5^2 &= -H^{-2} (dt + \omega)^2 + H ds(\mathcal{B})^2, \\ F^I &= d_5 A^I = d_4 (X^I H^{-1} (dt + \omega)) + \Theta^I, \end{aligned} \quad (4.1.3)$$

where Θ^I , ω and H are two-forms, a one-form and a scalar on \mathcal{B} respectively. We use the notation d_4 and \star_4 for the exterior derivative and the Hodge dual on \mathcal{B} and we conveniently define the $n_V + 1$ warp factors

$$Z_I = H X_I \quad \implies \quad H = \left(\frac{1}{6} C_{IJK} Z_I Z_J Z_K \right)^{\frac{1}{3}}. \quad (4.1.4)$$

The gravitino variation and algebraic conditions obtained from Fierz identities imply that \mathcal{B} is a Ricci-flat and Kähler manifold (hyper-Kähler), Θ^I is self dual and that [69]

$$d_4 \omega + \star_4 d_4 \omega = Z_I \Theta^I.$$

This condition corresponds to the geometric requirement that the two angular momenta in the four-dimensional base space must be equal to preserve supersymmetry (when $Z_I \Theta^I = 0$). The left-hand side corresponds to the rotation of the spacetime whereas the right-hand side is, by analogy with electromagnetism, the ‘‘Poynting vector’’ of the charges.

These conditions are sufficient to ensure that the solutions preserve at least 4 of the 8 supersymmetries of $\mathcal{N} = 2$ five-dimensional Supergravity which corresponds to 1/8-BPS solutions in eleven dimensions. Moreover, the Bianchi identities for the gauge fields require

$$d_4 F^I = 0 \quad \implies \quad d_4 \Theta^I = 0.$$

The remaining equation is the Maxwell equation for the $n_V + 1$ gauge fields in (4.1.1).

To summarize, supersymmetric solutions in $\mathcal{N} = 2$ five dimensional supergravity coupled to n_V extra gauge fields with structure constant C_{IJK} are determined by $n_V + 1$ couples of electric warp

factors and magnetic self-dual two-forms (Z_I, Θ^I) , an angular-momentum one-form ω , and a hyper-Kähler manifold \mathcal{B} as follows

$$\begin{aligned} ds_5^2 &= - \left(\frac{1}{6} C_{IJK} Z_I Z_J Z_K \right)^{-\frac{2}{3}} (dt + \omega)^2 + \left(\frac{1}{6} C_{IJK} Z_I Z_J Z_K \right)^{\frac{1}{3}} ds(\mathcal{B})^2, \\ F^I &= d_4 A^I = d_4 (Z_I^{-1} (dt + \omega)) + \Theta^I. \end{aligned} \quad (4.1.5)$$

The dynamics of the fields is captured by the *first layer of BPS equations*

$$\star_4 d_4 \star_4 d_4 Z_I = \frac{1}{2} C_{IJK} \star_4 (\Theta^J \wedge \Theta^K), \quad d_4 \Theta^I = 0, \quad \star_4 \Theta^I = \Theta^I, \quad I = 1, \dots, n_V + 1, \quad (4.1.6)$$

and the *second layer of BPS equations* determining the angular-momentum one-form

$$d_4 \omega + \star_4 d_4 \omega = Z_I \Theta^I. \quad (4.1.7)$$

The term $\star_4 (\Theta^J \wedge \Theta^K)$ in the first layer comes directly from the Chern-Simons term in the action (3.3.4). This allows the fields to be electrically sourced by magnetic fluxes without adding singular charges. As announced in the previous chapter, the presence of Chern-Simons terms and non-trivial spacetime topology will avoid the ‘no-go’ theorem that excludes non-singular soliton solutions in four dimensions.

4.1.1.2 Four-dimensional Gibbons-Hawking space

As already said, supersymmetry imposes \mathcal{B} to be hyper-Kähler. In this thesis, we will consider only three types of base manifold: flat space, Taub-NUT space, and the more general Gibbons-Hawking space. Those four-dimensional hyper-Kähler manifolds are the unique manifolds with a triholomorphic Killing vector ∂_ψ , i.e. a Killing vector that preserves the hyper-Kähler structure. The metric is a S^1 fibration along ψ over a flat \mathbb{R}^3 and is determined by a harmonic function V and a one-form A as follows [72, 73]

$$\begin{aligned} ds(\mathcal{B})^2 &= V^{-1} (d\psi + A)^2 + V [d\rho^2 + \rho^2 (d\vartheta^2 + \sin^2 \vartheta d\phi^2)], \\ \star_3 d_3 A &= d_3 V \quad \Rightarrow \quad \star_3 d_3 \star_3 d_3 V = 0, \end{aligned} \quad (4.1.8)$$

where d_3 and \star_3 denotes the exterior derivative and the Hodge dual on the three-dimensional base space. We have introduced the spherical system of coordinates (ρ, ϑ, ϕ) of \mathbb{R}^3 . The harmonic function V can be sourced at different centers on the base space. We use the notation

$$\star_3 d_3 \star_3 d_3 V = \sum_{j=1}^n q_j \delta^{(3)}(\vec{\rho}_j),$$

where $\vec{\rho}_j$ is the vector distance from the j^{th} center on \mathbb{R}^3 and q_j its charge. The generic solutions are

$$V(\vec{\rho}) = h_\infty + \sum_{j=1}^n \frac{q_j}{\rho_j}, \quad A = \sum_{j=1}^n q_j \cos \vartheta_j d\phi, \quad (4.1.9)$$

where $(\rho_j, \vartheta_j, \phi)$ is the shifted spherical coordinates around the j^{th} center. The choice of $V(\vec{\rho})$ gives different possible geometries:

- Flat \mathbb{R}^4 :

If we consider

$$V(\vec{\rho}) = \frac{1}{\rho}, \quad A = \cos \vartheta d\phi, \quad (4.1.10)$$

the four-dimensional base space is trivially flat (see Fig.4.1)

$$ds(\mathcal{B})^2 = ds(\mathbb{R}^4)^2 = d\hat{r}^2 + \hat{r}^2 \left(d\hat{\theta}^2 + \sin^2 \hat{\theta} d\varphi_1^2 + \cos^2 \hat{\theta} d\varphi_2^2 \right), \quad (4.1.11)$$

where $(\hat{r}, \hat{\theta}, \varphi_1, \varphi_2)$ are the usual spherical coordinates of \mathbb{R}^4 . They are related to $(\rho, \vartheta, \phi, \psi)$ by

$$\rho = \frac{\hat{r}^2}{4}, \quad \vartheta = 2\hat{\theta}, \quad \psi = \varphi_2 + \varphi_1, \quad \phi = \varphi_2 - \varphi_1. \quad (4.1.12)$$

- Taub-NUT space:

If we consider

$$V(\vec{\rho}) = 1 + \frac{1}{\rho}, \quad A = \cos \vartheta d\phi, \quad (4.1.13)$$

the four-dimensional base space is Taub-NUT. It is a special type of U(1) fibration over \mathbb{R}^3 [74, 75]. At large distance, the S^1 radius stabilizes and the space is asymptotically $S^1 \times \mathbb{R}^3$. At the origin, the singularity of $V(\vec{\rho})$ is not a spacetime singularity: the S^1 pinches off smoothly and gives a flat \mathbb{R}^4 . For arbitrary ρ , we usually say that the geometry takes a “cigar” form which grows with ρ (see Fig.4.1).

- Generic Gibbons-Hawking space:

The general form of Gibbons-Hawking metric given by (4.1.9) is a generalization of a Taub-NUT space (see Fig.4.1). At large distance, the S^1 radius either stabilizes if $h_\infty \neq 0$ and gives $S^1 \times \mathbb{R}^3$ or grows with ρ if $h_\infty = 0$ and is asymptotically a discrete $\mathbb{Z}_{|\sum q_j|}$ quotient of \mathbb{R}^4 . For the latter case, we usually impose the full \mathbb{R}^4 which requires

$$\sum_{j=1}^n q_j = 1. \quad (4.1.14)$$

At the center loci, the S^1 fiber pinches off as in Taub-NUT. There is no spacetime singularity but conical defect can occur. If we define the local spherical coordinates, $(\hat{r}^{(j)}, \hat{\theta}^{(j)}, \varphi_1^{(j)}, \varphi_2^{(j)})$, according to ψ and to the local \mathbb{R}^3 coordinates as

$$\rho_j = \frac{(\hat{r}^{(j)})^2}{4}, \quad \vartheta_j = 2\hat{\theta}^{(j)}, \quad \psi = q_j \left(\varphi_2^{(j)} + \varphi_1^{(j)} \right), \quad \phi = \varphi_2^{(j)} - \varphi_1^{(j)},$$

we recover locally the flat \mathbb{R}^4 metric

$$ds(\mathcal{B})^2 \sim q_j \left(d\hat{r}^{(j)2} + \hat{r}^{(j)2} \left(d\hat{\theta}^{(j)2} + \sin^2 \hat{\theta}^{(j)} d\varphi_1^{(j)2} + \cos^2 \hat{\theta}^{(j)} d\varphi_2^{(j)2} \right) \right).$$

The angles are identified as $\varphi_{1/2}^{(j)} = \frac{1}{2} \left(\frac{\psi}{q_j} \mp \phi \right)$, so their periodicities are not 2π : we have a discrete $\mathbb{Z}_{|q_j|}$ quotient of \mathbb{R}^4 . This quotient is smooth if and only if

$$q_j \in \mathbb{Z}, \quad j = 1, \dots, n. \quad (4.1.15)$$

The repetitively-shrinking S^1 forms topologically non-trivial two-cycles called *bubbles*. Those bubbles will allow fluxes wrapping them which will induce charges from the three-dimensional point of view as we will see when constructing smooth solutions.

However, the sign of q_j can be either positive or negative which drastically changes the sign of the signature of the metric. This is a feature of an ambipolar metric. We will see in concrete examples

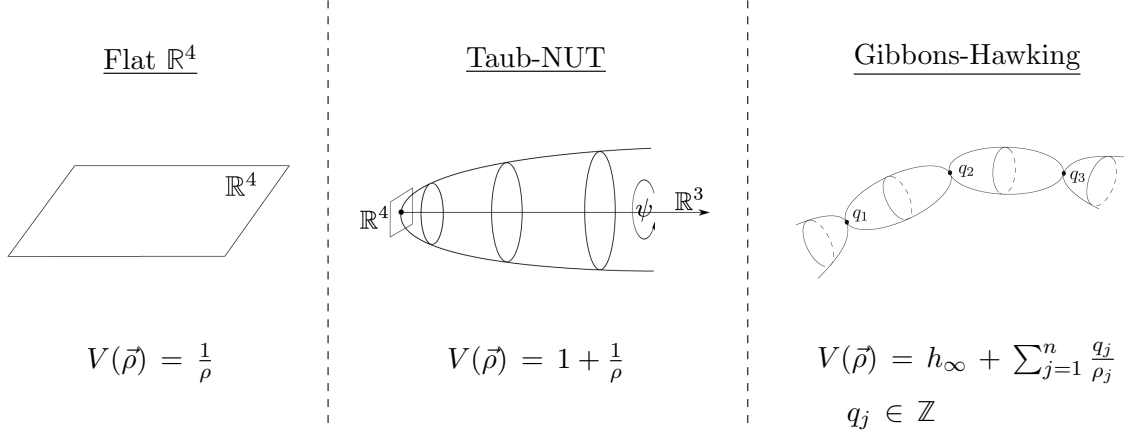


Figure 4.1: The three four-dimensional hyper-Kähler manifold considered and their topology.

how the full five-dimensional metric keeps a constant signature.

As a remark, unlike the three-dimensional base space of GR, a four-dimensional space induces two rotations, one for each \mathbb{R}^2 factor. The motion of stationary classical solutions will then be determined by two “left” and “right” conserved angular momenta associated with the angles ψ and ϕ and noted J_L and J_R in the thesis.

4.1.1.3 ψ -independent solutions

Now, we have all the ingredients to solve the BPS equations. We assume that the vector fields and the angular-momentum one-form preserve the ∂_ψ Killing vector of the four-dimensional base space. This extra assumption restricts the spectrum of BPS solutions studied. However, this has the benefit to have relatively user-friendly BPS equations while maintaining a very large space of solutions. We proceed step by step to find generic solutions to (4.1.6) and (4.1.7).

- The self-dual magnetic two-forms Θ^I :

First, we define the vielbeins of the Gibbons-Hawking space

$$e^0 = V^{-\frac{1}{2}} (d\psi + A), \quad e^a = V^{\frac{1}{2}} dx_a, \quad a = 1, 2, 3, \quad (4.1.16)$$

where x_a , $a = 1, 2, 3$, are the cartesian coordinates of the flat \mathbb{R}^3 base space. A basis of self-dual two-forms is

$$\Omega^a = e^0 \wedge e^a + \epsilon_{abc} e^b \wedge e^c, \quad a = 1, 2, 3. \quad (4.1.17)$$

With the Ansatz

$$\Theta^I = \partial_a (V^{-1} K^I) \Omega^a, \quad (4.1.18)$$

the Bianchi identities (4.1.6) transform into harmonic equations on \mathbb{R}^3 :

$$d_4 \Theta^I = 0 \quad \implies \quad \star_3 d_3 \star_3 d_3 K^I = 0 \quad \implies \quad K^I = k_\infty^I + \sum_{j=1}^n \frac{k_j^I}{\rho_j}. \quad (4.1.19)$$

Thus, the self-dual two-forms, Θ^I , are obtained from $n_V + 1$ magnetic harmonic functions, K^I , which are sourced by magnetic dipole charges k_j^I at the centers. When embedded in eleven dimensions, those

charges have a good understanding as M5-brane charges. As it has been argued in Section 3.3.2, the magnetic contribution of the gauge fields results from M5-branes wrapping n_V five-cycles described as four-cycles inside \mathbb{T}^6 and one non-trivial closed curve in the five-dimensional space. Thus, the computation of the flux integral of the eleven-dimensional field strength, F_4 , around each center and over the five-dimensional boundary transverse to the M5-branes relates the magnetic dipole charges k_j^J to the number of M5-branes at the j^{th} center. This implies that the k_j^J are quantized. Moreover, the magnetic sources are singular from the three-dimensional base-space perspective but they actually correspond to charges dissolved in fluxes along the non-trivial closed curve of the Gibbons-Hawking space.

- The warp factors Z_I :

The magnetic dipole charges source quadratically the electric warp factors (4.1.6). More concretely, the electric charges are induced by the magnetic fluxes. It is then possible to have asymptotically charged solutions without explicit sources, i.e. singularities. This is the key point for the construction of smooth geometries in five-dimension Supergravity. The equations for the warp factors are solved with the Ansatz

$$Z_I = L_I + \frac{C_{IJK}}{2} \frac{K^J K^K}{V} \xRightarrow{(4.1.6)} \star_3 d_3 \star_3 d_3 L_I = 0 \implies L_I = l_\infty^I + \sum_{j=1}^n \frac{l_j^I}{\rho_j}. \quad (4.1.20)$$

The warp factors have a magnetic and an electric contribution. The electric part is given by the harmonic function, L_I , sourced by the electric charges l_j^I at the centers. Those charges are described as M2-brane charges when embedded in eleven dimensions. Each charge l_j^I is related to the number of M2-branes at the j^{th} center and is consequently quantized.

- The angular-momentum one-form ω :

We decompose the one-form ω along the $U(1)$ ψ -fiber as follows

$$\omega \equiv \mu (d\psi + A) + \varpi \quad (4.1.21)$$

where ϖ is a one-form on \mathbb{R}^3 . The second layer of BPS equations (4.1.7) splits in two pieces. The first piece is solved by considering

$$\mu = \frac{M}{2} + \frac{K^I L_I}{2V} + \frac{C_{IJK}}{6} \frac{K^I K^J K^K}{V^2} \xRightarrow{(4.1.7)} \star_3 d_3 \star_3 d_3 M = 0 \implies M = m_\infty + \sum_{j=1}^n \frac{m_j}{\rho_j}. \quad (4.1.22)$$

Once again, the angular-momentum charges in M can be described in eleven-dimensional Supergravity. From the dictionary drawn in Section 3.1.1, this momentum charges are KKM charges and are then quantized. The second piece is determined by the following equation

$$\star_3 d_3 \varpi = \frac{1}{2} (V d_3 M - M d_3 V + K^I d_3 L_I - L_I d_3 K^I). \quad (4.1.23)$$

This equation defines a symplectic structure for the BPS equations. It can be made explicit by defining a $2n_V + 4$ -dimensional vector of harmonic functions, Γ , and a symplectic product

$$\Gamma \equiv (V, K^1, \dots, K^{n_V+1}; L_1, \dots, L_{n_V+1}, M) \equiv \Gamma_\infty + \sum_{j=1}^n \frac{\Gamma_j}{\rho_j}, \quad (4.1.24)$$

$$\langle A, B \rangle \equiv A^0 B_0 - A_0 B^0 + A^I B_I - A_I B^I, \quad A, B \in \mathbb{R}^{2n_V+4},$$

where Γ_∞ defines the *background moduli* of the solution and the Γ_j define the *charge vectors* at the j^{th} center. The equation for ϖ is then

$$\star_3 d_3 \varpi = \frac{1}{2} \langle \Gamma, d_3 \Gamma \rangle \quad (4.1.25)$$

This equation is left unsolved for the moment since it strongly depends on the center configuration.

- Regularity:

The solutions derived above do not necessarily correspond to physical solutions. The equation (4.1.25) induces an integrability condition imposed by requiring that $d_3^2 \varpi = 0$ which implies $\langle \Gamma, d_3^2 \Gamma \rangle = 0$. This leads to n equations referred as the *Denef equations* or *bubble equations* [76, 77]

$$\sum_{j=1}^n \frac{\langle \Gamma_i, \Gamma_j \rangle}{\rho_{ij}} = \langle \Gamma_\infty, \Gamma_i \rangle, \quad i = 1, \dots, n, \quad (4.1.26)$$

where ρ_{ij} are the distance between the i^{th} center and the j^{th} center in the three-dimensional base space $\rho_{ij} = |\vec{\rho}_i - \vec{\rho}_j|$. The last physical condition to satisfy is the *absence of closed time-like curves* (CTC's) by requiring that there is a well-defined global time function [78, 79]

$$\mathcal{I}_4 \equiv \frac{C_{IJK}}{6} Z_I Z_J Z_K V - \mu^2 V^2 \geq |\varpi|^2, \quad (4.1.27)$$

where \mathcal{I}_4 is referred as the *quartic invariant*. A necessary condition is to have $\mathcal{I}_4 \geq 0$. This can be subsumed into

$$Z_I V \geq 0, \quad I = 1, 2, 3, \quad (4.1.28)$$

which only guarantees that $\frac{C_{IJK}}{6} Z_I Z_J Z_K V \geq 0$. This usually seems sufficient. Indeed, one wants to construct classical solutions in the black hole regime where the cosmic censorship bound is satisfied. In addition to Denef equations, this generally implies that μ and ϖ decay faster than the warp factors as large distance and have smaller poles at the centers.

The regularity conditions drastically constrain the geometry of the center configuration and the phase space of the charges. The positivity of the quartic invariant has been the main obstacle to the construction of a phase space of parameters defining regular multicenter solutions. Without parameter space, it is very complicated to study their overall properties as the behavior of their conserved charges. In Chapter 5, we review the work done in [23, 24] where a well-defined procedure was used to construct large families of regular four-center solutions and to study their properties.

To summarize, BPS solutions in five dimensions with ∂_t and ∂_ψ as Killing vectors have a metric and U(1) gauge fields of the form of (4.1.5). They are uniquely defined by a set of $2n_V + 4$ harmonic functions $\Gamma = (V, L_I; K^I, M)$. The vector Γ is sourced by integer charges at given centers in the three-dimensional base space. From an eleven-dimensional perspective, the charges at the center arise from from KKm and P charges in the five-dimensional space, M2-branes wrapping two-cycles in \mathbb{T}^6 , and from M5-branes wrapping five-cycles with four components in \mathbb{T}^6 and one in the base space:

$$\Gamma_j = \left(q_j, k_j^1, \dots, k_j^{n_v+1}; l_j^1, \dots, l_j^{n_v+1}, m_j \right) \leftarrow \left(\text{KKm}, \text{M5}^1, \dots, \text{M5}^{n_v+1}; \text{M2}^1, \dots, \text{M2}^{n_v+1}, \text{P} \right) \quad (4.1.29)$$

As we will see, those solutions can describe five-dimensional three-charge black holes, circular black rings and round Supertubes as well as smooth bubbling solutions and arbitrary superposition of these objects. Before deriving explicit solutions, we first exploit the symplectic structure to construct symplectic transformations which allows to go from one spectrum of BPS solutions to another by simple linear transformations. Then, we will apply the construction above for specific values of n_V . We first discuss the *STU model* corresponding to $n_V = 2$ before considering an extra species, $n_V = 3$.

4.1.1.4 Symplectic transformations

Any vector of harmonic functions defines a solution, and any linear transformation, $\Gamma' = G\Gamma$ with $G \in GL(2n_V + 4, \mathbb{R})$ ¹, maps a solution of the BPS equations to another solution. A special subgroup of these transformations is $Sp(2n_V + 4, \mathbb{R})$, corresponding to linear transformations that preserve the symplectic product and, therefore, leave the Denef equations invariant. Among all possible $Sp(2n_V + 4, \mathbb{R})$ transformations, the most attractive are those that also leave the function \mathcal{I}_4 invariant. We are interested in two subgroups with these characteristics [80]:

- Generalized spectral flows:

In Section 3.2.4, we have broadly described three types of sequences of S-dualities, T-dualities and coordinate transformations, referred as generalized spectral flows, in ten-dimensional Supergravity. One can dualize the five-dimensional solutions above into ten-dimensional Supergravity by simply considering their embeddings in eleven dimensions on \mathcal{C}_6 and by compactifying along one closed curve of the \mathcal{C}_6 . The dual solutions will be embedded in type IIA on $S^1 \times \mathcal{C}_4$ where generalized spectral flows can be applied. The coordinate transformation will then consist in a shift $\psi \rightarrow \psi + \gamma y$ where ψ is the Gibbons-Hawking fiber coordinate and y is the coordinate along S^1 . From the different choices of closed curves and from the three types of generalized spectral flows available, the generalized spectral flows induce $n_V + 1$ independent transformations from the perspective of the five-dimensional solutions [81]. Those transformations are linear transformations of $Sp(2n_V + 4, \mathbb{R})$ defined by $n_V + 1$ constant shifts γ^I as [82]

$$\begin{aligned} V &\longrightarrow V + \gamma^I K^I - \frac{1}{2} C_{IJK} \gamma^I \gamma^J L_K + \frac{1}{6} C_{IJK} \gamma^I \gamma^J \gamma^K M, \\ L_I &\longrightarrow L_I - \gamma^I M, \\ M &\longrightarrow M, \\ K^I &\longrightarrow K^I - C_{IJK} \gamma^J L_K + \frac{1}{2} C_{IJK} \gamma^J \gamma^K M. \end{aligned} \tag{4.1.30}$$

One can straightforwardly check that those transformations belong to $Sp(2n_V + 4, \mathbb{R})$. Moreover, even though they act non-trivially on Z_I and μ , one can check that \mathcal{I}_4 remains invariant under the action of (4.1.30).

- Gauge transformations:

Gauge transformations leave the physical properties of the solution unchanged and their sole effect is a gauge transformation of the vector fields. They are a reflection of the fact that the construction of solutions in terms of $2n_V + 4$ harmonic functions contains redundancies. There are $n_V + 1$ independent gauge transformations (one for each vector) parametrized by g^I , acting as

$$\begin{aligned} V &\longrightarrow V, \\ L_I &\longrightarrow L_I - C_{IJK} g^J K^K - \frac{1}{2} C_{IJK} g^J g^K V, \\ K^I &\longrightarrow K^I + g^I V, \\ M &\longrightarrow M - g^I L_I + \frac{1}{2} C_{IJK} g^I g^J K^K + \frac{1}{6} C_{IJK} g^I g^J g^K V. \end{aligned} \tag{4.1.31}$$

One can straightforwardly check that Z_I , Θ^I , ϖ and μ are invariant and therefore the quartic invariant as well. There is one additional subgroup of $Sp(2n_V + 4, \mathbb{R})$ that leaves \mathcal{I}_4 invariant that

¹To preserve the quantization of the charges, one should reduce to $GL(2n_V + 4, \mathbb{Q})$ or even $GL(2n_V + 4, \mathbb{Z})$.

involves rescalings of the harmonic functions, but since we are not going to make use of this type of transformations we refer the interested reader to [80].

4.1.1.5 $n_V = 2$, the STU model

The $\mathcal{N} = 2$ five-dimensional Supergravity coupled to two extra gauge fields, referred as the STU model, corresponds to the minimum gauge fields in order to construct three-charge solutions. The model can be embedded in eleven-dimensional Supergravity on $\mathbb{T}^6 = \mathbb{T}^2 \times \mathbb{T}^2 \times \mathbb{T}^2$ where the \mathbb{T}^2 are orthogonal between each other. Each \mathbb{T}^2 and its transverse $\mathbb{T}^4 = \mathbb{T}^2 \times \mathbb{T}^2$ can be wrapped by M2-branes and M5-branes respectively. The resulting five-dimensional theory contains three vector gauge fields with the structure constant

$$C_{IJK} = \int_{\mathbb{T}^6} \text{Vol}(\mathbb{T}_I^2) \wedge \text{Vol}(\mathbb{T}_J^2) \wedge \text{Vol}(\mathbb{T}_K^2) = |\epsilon_{IJK}| ,$$

where ϵ_{IJK} is the three-dimensional Levi-Civita symbol. One can trivially check that this satisfies the constraint (3.3.6).

We consider that the four-dimensional space is a generic Gibbons-Hawking space. There exist n centers on the three-dimensional base space carrying Gibbons-Hawking charges. The five-dimensional metric and the U(1) gauge fields (4.1.5) give

$$\begin{aligned} ds_5^2 &= -(Z_1 Z_2 Z_3)^{-\frac{2}{3}} (dt + \mu(d\psi + A) + \varpi)^2 + V^{-1} (Z_1 Z_2 Z_3)^{\frac{1}{3}} (d\psi + A)^2 \\ &\quad + V (Z_1 Z_2 Z_3)^{\frac{1}{3}} \left[d\rho^2 + \rho^2 (d\vartheta^2 + \sin^2 \vartheta d\phi^2) \right], \\ F^I &= d_3 (Z_I^{-1} (dt + \mu(d\psi + A) + \varpi)) + \Theta^I, \end{aligned} \quad (4.1.32)$$

The BPS solutions are uniquely determined by an eight-dimensional vector of harmonic functions $\Gamma = (V, K^1, K^2, K^3; L_1, L_2, L_3, M)$. The harmonic functions source (Z_I, Θ^I) (4.1.20), μ (4.1.22) and ϖ (4.1.25).

In Section 3.3.1, we have detailed how $\mathcal{N} = 2$ five-dimensional Supergravity arises from eleven dimensions. Let us now go backwards and give the description of the STU solutions as brane bound states in type IIA, IIB and eleven-dimensional Supergravities. This requires the use of the dualities detailed in Section 3.2. These descriptions provide a complete understanding of the nature of the eight harmonic functions. In the following paragraphs, we give a non-exhaustive list of brane bound states corresponding to BPS solutions of the STU model. All solutions derived until now have been assumed to have ψ -independent gauge fields. With the exception of the D0-D2-D4-D6 frame, the metric and the fields in the various duality frames are still valid for ψ -dependent fields.

- The STU model in eleven-dimensional Supergravity.

As explained in Section 3.3.1 and in (4.1.29), the warp factors are sourced electrically by M2-branes and magnetically by M5 branes. The five-dimensional transverse space carries KKm charges corresponding to the Gibbons-Hawking charges and P charges giving rise to the angular momenta. The eleven-dimensional metric and the four-form field strength F_4 are similar to the intersecting-brane example in Section 3.1.1.1:

$$\begin{aligned} ds_{11}^2 &= -(Z_1 Z_2 Z_3)^{-\frac{2}{3}} (dt + \mu(d\psi + A) + \varpi)^2 + (Z_1 Z_2 Z_3)^{\frac{1}{3}} \left[V^{-1} (d\psi + A)^2 + V ds(\mathbb{R}^3)^2 \right] \\ &\quad + \left(\frac{Z_2 Z_3}{Z_1^2} \right)^{\frac{1}{3}} (dx_1^2 + dx_2^2) + \left(\frac{Z_1 Z_3}{Z_2^2} \right)^{\frac{1}{3}} (dx_3^2 + dx_4^2) + \left(\frac{Z_1 Z_2}{Z_3^2} \right)^{\frac{1}{3}} (dx_5^2 + dx_6^2) \\ F_4 &= F^1 \wedge dx_1 \wedge dx_2 + F^2 \wedge dx_3 \wedge dx_4 + F^3 \wedge dx_5 \wedge dx_6. \end{aligned} \quad (4.1.33)$$

The charge vectors Γ_j , that give the supergravity charges at the centers of the three-dimensional base space (4.1.24), can be related to M-brane, KKm or P charges in eleven dimensions by integrating appropriately the fluxes in the vicinity of the centers. This gives

$$\Gamma_j = (q_j, k_j^1, k_j^2, k_j^3; l_j^1, l_j^2, l_j^3, m_j) \leftarrow (\text{KKm}, M5^1, M5^2, M5^3; M2^1, M2^2, M2^3, P) \quad (4.1.34)$$

The STU solutions describe bound states of M2-branes, M5-branes, P and KKm charges in eleven dimensions. Each center on the three-dimensional base space can carry a KKm charge, three magnetic M5-brane charges, three electric M2-brane charges and one momentum P charge (see Table 4.1).

- The STU model in type IIA and type IIB Supergravity.

One can perform a KK reduction to type IIA Supergravity. The reductions along one of the six-torus directions will produce identical solutions by permutation of the vector fields. However, the solutions also have a U(1) isometry along ψ . The KK reduction along ψ is then also feasible. Thus, one can obtain two different descriptions depending on whether we reduce along ψ or x_6 . The former gives type IIA on \mathbb{T}^6 while the latter gives type IIA on $S^1 \times \mathbb{T}^4$. Furthermore, one can apply a bunch of T-dualities to go to different frames. In the thesis, we are interested in two frames: the D1-D5-P frame in type IIB and the D0-D4-F1 frame in type IIA.

- Type IIA on \mathbb{T}^6 from M/ S_ψ :

We consider a Kaluza-Klein reduction along ψ . Following the reduction rules in Section 3.2.1, the metric and fields (4.1.33) leads to the following system of relations for the ten-dimensional metric (in the string frame), dilaton, the R-R and NS-NS gauge fields [83]:

$$\begin{aligned} ds_{10}^2 &= - (Z_1 Z_2 Z_3 V - \mu^2 V^2)^{-\frac{1}{2}} (dt + \varpi)^2 + (Z_1 Z_2 Z_3 V - \mu^2 V^2)^{\frac{1}{2}} ds(\mathbb{R}^3)^2 \\ &\quad + (Z_1 Z_2 Z_3 V^{-1} - \mu^2)^{\frac{1}{2}} \left[Z_1^{-1} (dx_1^2 + dx_2^2) + Z_2^{-1} (dx_3^2 + dx_4^2) + Z_3^{-1} (dx_5^2 + dx_6^2) \right], \\ e^{-2\Phi} &= \frac{Z_1 Z_2 Z_3}{(Z_1 Z_2 Z_3 V^{-1} - \mu^2)^{\frac{3}{2}}}, \end{aligned} \quad (4.1.35)$$

$$\begin{aligned} B_2 &= \left(\frac{K^1}{V} - \frac{\mu}{Z_1} \right) dx_1 \wedge dx_2 + \left(\frac{K^2}{V} - \frac{\mu}{Z_2} \right) dx_3 \wedge dx_4 + \left(\frac{K^3}{V} - \frac{\mu}{Z_3} \right) dx_5 \wedge dx_6, \\ C^{(1)} &= A - \mu (Z_1 Z_2 Z_3 V^{-1} - \mu^2) (dt + \varpi), \\ C^{(3)} &= C_1^{(3)} \wedge dx_1 \wedge dx_2 + C_2^{(3)} \wedge dx_3 \wedge dx_4 + C_3^{(3)} \wedge dx_5 \wedge dx_6, \end{aligned} \quad (4.1.36)$$

where we have defined

$$C_I^{(3)} \equiv -\frac{dt + \varpi}{Z_I} + \left(\frac{K^I}{V} - \frac{\mu}{Z_I} \right) A + w^I,$$

and w^I are one-forms on the three-dimensional base space

$$\Theta^I = d_3 \left(\frac{K^I}{V} (d\psi + A) + w^I \right).$$

The two other R-R gauge fields, $C^{(5)}$ and $C^{(7)}$, are obtained using the electric-magnetic duality (3.1.24). Moreover, according to KK-reduction rules, the brane bound states (4.1.34) reduce to

$$(\text{KKm}, M5^1, M5^2, M5^3; M2^1, M2^2, M2^3, P) \xleftrightarrow{\text{KK } S_\psi} (D6, D4^1, D4^2, D4^3; D2^1, D2^2, D2^3, D0) \quad (4.1.37)$$

The STU solutions describe bound states of D0-D2-D4-D6 branes in type IIA on \mathbb{T}^6 . Each center on the three-dimensional base space can carry a D6 charge, three magnetic D4-brane charges, three electric D2-brane charges and one momentum D0 charge.

Notice that now the base space is three-dimensional. The angular momentum associated to ψ has been dualized into a D0 charge (J_L) and the four-dimensional solutions have only one angular momentum, J_R .

- Type IIA on $S^1 \times \mathbb{T}^4$ from M/S_{x_6} :

The KK reduction along x_6 transforms the eleven-dimensional bound states (4.1.34) into

$$(\text{KKm}, M5^1, M5^2, M5^3; M2^1, M2^2, M2^3, P) \xleftrightarrow{\text{KK } S_{x_6}} (\text{KKm}, D4^1, D4^2, NS5^3; D2^1, D2^2, F1^3, P) \quad (4.1.38)$$

The metric, the NS-NS and R-R fields are [83]

$$\begin{aligned} ds_{10}^2 &= -\frac{1}{Z_3\sqrt{Z_1Z_2}}(dt + \mu(d\psi + A) + \varpi)^2 + \sqrt{Z_1Z_2} \left[V^{-1}(d\psi + A)^2 + V ds(\mathbb{R}^3)^2 \right] \\ &\quad + \frac{\sqrt{Z_1Z_2}}{Z_3} dy^2 + \sqrt{\frac{Z_2}{Z_1}}(dx_1^2 + dx_2^2) + \sqrt{\frac{Z_1}{Z_2}}(dx_3^2 + dx_4^2), \\ e^{-2\Phi} &= \frac{Z_3}{\sqrt{Z_1Z_2}}, \quad B_2 = -A^3 \wedge dy, \quad C^{(1)} = 0, \\ C^{(3)} &= A^1 \wedge dx_1 \wedge dx_2 + A^2 \wedge dx_3 \wedge dx_4. \end{aligned} \quad (4.1.39)$$

We have noted y instead of x_5 to make the S^1 fiber manifest and we remind that the A^I are the vector fields associated to the field strength F^I in five dimensions

$$A^I = -\frac{dt + \omega}{Z_I} + \frac{K^I}{V}(d\psi + A) + w^I, \quad F^I = d_5 A^I.$$

Thus, the STU solutions correspond to bound states of electric D2-D2-F1 branes and magnetic D4-D4-NS5 branes in type IIA on $S^1 \times \mathbb{T}^4$.

- Type IIA on $S^1 \times \mathbb{T}^4$ from $M/S_{x_6} + T_{x_1}T_{x_2}$:

In addition, we apply two T-dualities along x_1 and x_2 . According to KK-reduction rules, the bound states of branes are transformed into

$$(\text{KKm}, M5^1, M5^2, M5^3; M2^1, M2^2, M2^3, P) \xleftrightarrow[T_{x_1}T_{x_2}]{\text{KK } S_{x_6}} (\text{KKm}, D6^1, D2^2, NS5^3; D0^1, D4^2, F1^3, P) \quad (4.1.40)$$

The metric and NS-NS and R-R fields are²

$$\begin{aligned} ds_{10}^2 &= -\frac{1}{Z_3\sqrt{Z_1Z_2}}(dt + \mu(d\psi + A) + \varpi)^2 + \sqrt{Z_1Z_2} \left[V^{-1}(d\psi + A)^2 + V ds(\mathbb{R}^3)^2 \right] \\ &\quad + \frac{\sqrt{Z_1Z_2}}{Z_3} dy^2 + \sqrt{\frac{Z_1}{Z_2}}(dx_1^2 + dx_2^2 + dx_3^2 + dx_4^2), \\ e^{-2\Phi} &= \frac{Z_2^{\frac{1}{2}} Z_3}{Z_1^{\frac{3}{2}}}, \quad B_2 = -A^3 \wedge dy, \quad F^{(2)} = -F^1, \\ F^{(4)} &= -\left(\frac{Z_2^5}{Z_1^3 Z_3^2} \right)^{\frac{1}{4}} \star_5 (F^2) \wedge dy, \end{aligned} \quad (4.1.41)$$

Thus, the STU solutions describe bound states of electric D0-D4-F1 and dipole moments corresponding to D6-D2-NS5 branes in type IIA on $S^1 \times \mathbb{T}^4$.

²We decide to write the R-R fields using their field strengths since the computation of the gauge fields require more work. We refer the interested reader to the Appendix A of [83] for more details.

- Type IIB on $S^1 \times \mathbb{T}^4$ from $M/S_{x_6} + T_{x_1}T_{x_2}T_{x_5}$:

We perform one last T-duality along $y = x_5$. This dualizes the solutions to a bound states of branes in the D1-D5-P frame:

$$(\text{KKm}, M5^1, M5^2, M5^3; M2^1, M2^2, M2^3, P) \xleftrightarrow[T_{x_1}T_{x_2}T_{x_5}]{\text{KK } S_{x_6}} (\text{NS5}, D5^1, D1^2, \text{KKm}^3; D1^1, D5^2, P^3, F1) \quad (4.1.42)$$

In string frame, the metric, the NS-NS and R-R fields are [83]

$$\begin{aligned} ds_{10}^2 &= -\frac{1}{Z_3\sqrt{Z_1Z_2}}(dt + \mu(d\psi + A) + \varpi)^2 + \sqrt{Z_1Z_2} \left[V^{-1}(d\psi + A)^2 + V ds(\mathbb{R}^3)^2 \right] \\ &\quad + \frac{Z_3}{\sqrt{Z_1Z_2}}(dy + A^3)^2 + \sqrt{\frac{Z_1}{Z_2}}(dx_1^2 + dx_2^2 + dx_3^2 + dx_4^2), \\ e^{-2\Phi} &= \frac{Z_2}{Z_1}, \quad B_2 = 0, \quad F^{(1)} = 0, \quad F^{(5)} = 0, \\ F^{(3)} &= -\left(\frac{Z_2^5}{Z_1^3Z_3^2}\right)^{\frac{1}{4}} \star_5 F^2 - F^1 \wedge (dz - A^3), \end{aligned} \quad (4.1.43)$$

Thus, the STU solutions describe bound states with D1, D5 and P charges and dipole moments corresponding to D5, D1 and KKm charges in type IIB on $S^1 \times \mathbb{T}^4$.

We have summarized the dual bound states of branes which are related to the STU model in Table 4.1. Even if the model is constructed from the minimum number of vector fields, the spectrum of STU

Charges \ Frame	M on \mathbb{T}^6	IIA on \mathbb{T}^6 : M/S_ψ	IIA on $\mathbb{T}^4 \times S^1$: M/S_{x_6}
Electric: $l^1 - l^2 - l^3$	M2 - M2 - M2	D2 - D2 - D2	D2 - D2 - F1
Magnetic: $k^1 - k^2 - k^3$	M5 - M5 - M5	D4 - D4 - D4	D4 - D4 - NS5
Momentum: m	P	D0	P
GH: q	KKm	D6	KKm

Charges \ Frame	IIA on $\mathbb{T}^4 \times S^1$: $M/S_{x_6} + T_{x_1}T_{x_2}$	IIB on $\mathbb{T}^4 \times S^1$: $M/S_{x_6} + T_{x_1}T_{x_2}T_{x_5}$
Electric: $l^1 - l^2 - l^3$	D0 - D4 - F1	D1 - D5 - P
Magnetic: $k^1 - k^2 - k^3$	D6 - D2 - NS5	D5 - D1 - KKm
Momentum: m	P	F1
GH: q	KKm	NS5

Table 4.1: Brane interpretation of a charge vector in the STU model in different duality frames. The coordinate of the eleven-dimensional space on \mathbb{T}^6 is $(t, \rho, \vartheta, \phi, \psi, x_1, x_2, x_3, x_4, x_5, x_6)$. We have used the notations T_{x_i} for a T-duality along x_i whereas M/S_{x_i} corresponds the KK reduction along the x_i direction.

solutions remains rich. We review the BMPV black hole [84] and the family of bubbling multicenter geometries [79, 78, 85, 15] in Section 4.1.2 and 4.1.3 respectively.

4.1.1.6 $n_V = 3$, an extra species

In this section, we consider three extra vector fields. The third extra species will have a crucial role in building superstratum solutions in $\mathcal{N} = (1, 0)$ six-dimensional Supergravity. As the previous section, we start with eleven-dimensional Supergravity on \mathbb{T}^6 . We define the coordinates of \mathbb{T}^6 as (x_1, x_2, \dots, x_6) . We start first with three transverse \mathbb{T}^2 , and the fourth two-cycle has legs inside one of the \mathbb{T}^4 appropriately chosen to satisfy (3.3.6). We define the following volume two-forms

$$D_1 = x_1 \wedge x_2, \quad D_2 = x_3 \wedge x_4, \quad D_3 = x_5 \wedge x_6, \quad D_4 = x_1 \wedge x_3 + x_2 \wedge x_4. \quad (4.1.44)$$

This implies that the only non-zero components of the structure constants are

$$C_{3JK} = \begin{pmatrix} 0 & 1 & 0 \\ 1 & 0 & 0 \\ 0 & 0 & -2 \end{pmatrix} \implies \frac{C_{IJK}}{6} Z_I Z_J Z_K = Z_3 (Z_1 Z_2 - Z_4^2). \quad (4.1.45)$$

Assuming that the four-dimensional space is Gibbons-Hawking and that the solutions preserve the ∂_ψ Killing vector of the base, BPS solutions of $\mathcal{N} = 2$ five-dimensional Supergravity coupled to three vector fields are uniquely determined by ten-dimensional vectors of harmonic functions in \mathbb{R}^3 , $\Gamma = (V, K^1, K^2, K^3, K^4; L_1, L_2, L_3, L_4, M)$. Such solutions can be also described as brane bound states in type IIA, type IIB and eleven-dimensional Supergravities by performing a sequence of duality transformations as it has been done for the STU model.

4.1.2 Three-charge supersymmetric black hole

The 1/8-BPS five-dimensional rotating black hole with a macroscopic horizon or BMPV black hole [84] has three types of electric charges Q_I , a non-vanishing $SU(2)_L$ angular momentum J_L , no $SU(2)_R$ angular momentum and no magnetic charges. The solution can be embedded in eleven-dimension Supergravity on $\mathbb{T}^6 = \mathbb{T}^2 \times \mathbb{T}^2 \times \mathbb{T}^2$ with three types of M2-branes wrapping the 2-tori and gravitational wave charges P inducing the rotation. This solution is most simply described within the STU model with a flat \mathbb{R}^4 base space. The single-center solutions are determined by the following harmonic functions³

$$V = \frac{1}{\rho}, \quad L_I = 1 + \frac{Q_I}{4\rho}, \quad K^I = 0, \quad M = \frac{J_L}{4\rho}. \quad (4.1.46)$$

In the \mathbb{R}^4 spherical coordinates (4.1.12), the warp factors, the angular momentum one-form and the magnetic two-forms are

$$Z_I = 1 + \frac{Q_I}{\hat{r}^2}, \quad \omega = \frac{J_L}{\hat{r}^2} \left(\sin^2 \hat{\theta} d\varphi_1 + \cos^2 \hat{\theta} d\varphi_2 \right), \quad \Theta^I = 0. \quad (4.1.47)$$

This solution trivially satisfies the Denef equations (4.1.26) and the absence of CTC's (4.1.27) is guaranteed if

$$J_L^2 < Q_1 Q_2 Q_3. \quad (4.1.48)$$

This corresponds to the cosmic censorship bound for three-charge supersymmetric solutions. The five-dimensional metric and the field strengths are

$$\begin{aligned} ds_{BMPV}^2 &= -(Z_1 Z_2 Z_3)^{-\frac{2}{3}} \left(dt + \frac{J_L}{\hat{r}^2} \left(\sin^2 \hat{\theta} d\varphi_1 + \cos^2 \hat{\theta} d\varphi_2 \right) \right)^2 \\ &\quad + (Z_1 Z_2 Z_3)^{\frac{1}{3}} \left[d\hat{r}^2 + \hat{r}^2 \left(d\hat{\theta}^2 + \sin^2 \hat{\theta} d\varphi_1^2 + \cos^2 \hat{\theta} d\varphi_2^2 \right) \right], \\ F^I &= d_3 (Z_I^{-1} (dt + \omega)), \end{aligned} \quad (4.1.49)$$

³The non-zero constant terms in the harmonic functions have been set to one since they can be absorbed by a coordinate transformation.

The metric is asymptotic to five-dimensional flat Minkowski for $\hat{r} \gg \{Q_1, Q_2, Q_3\}$. The *near-horizon geometry* is obtained by taking the limit $\hat{r} \ll \{Q_1, Q_2, Q_3\}$. The geometry is $\text{AdS}_2 \times S^3$ and the event horizon is at $\hat{r} = 0$. The ADM mass of the solution, given by the asymptotic expansion $-g_{tt} = 1 - \frac{2}{3} \frac{M}{\hat{r}^2} + \mathcal{O}(\hat{r}^{-4})$, is

$$M = Q_1 + Q_2 + Q_3,$$

which saturates the BPS bound as expected. The solutions are extremal and have zero temperature. However this does not mean that it is not entropic. The entropy can be derived from the Bekenstein-Hawking formula

$$S = \frac{A_H}{4G_5}.$$

The area of the event horizon is given by the area of the three-sphere $S^{\hat{\theta}\varphi_1\varphi_2}$ at $\hat{r} = 0$. We get

$$A_H = \int_{S^3|_{\hat{r}=0}} \text{Vol}(S^3) = 2\pi^2 \sqrt{Q_1 Q_2 Q_3 - J_L^2} \quad \Rightarrow \quad S = \frac{\pi^2}{2G_5} \sqrt{Q_1 Q_2 Q_3 - J_L^2}.$$

Let us consider the non-rotating solutions, $J_L = 0$, for simplicity. From an eleven-dimensional perspective, the supergravity charges can be related to the M2-brane charges and to the number of M2-branes wrapping the transverse 2-tori as it has been done in Section 3.1.1.1 for M-brane examples. We remind that the five-dimensional Supergravity has been obtained by requiring that the volume of the transverse \mathbb{T}^6 is constant (3.3.3). Its area is not necessary one and adds a contribution to the area of the horizon computed in five dimensions. Thus, we consider the metric of the solutions when embedded in eleven dimensions (4.1.33). We define the length of the closed one-curve along x_i as L_i . Thus, the eleven-dimensional area of the horizon, $A_H^{(11)}$ is given by

$$A_H^{(11)} = A_H \int_{\mathbb{T}^6} \text{Vol}(\mathbb{T}^6) = A_H \prod_{i=1}^6 (2\pi L_i)$$

The number of M2-branes can be read off by integrating the magnetic gauge field strength over a surface that surrounds the M2-branes as in Section 3.1.1.1. We obtain

$$Q_1 = \frac{l_P^{(11)6}}{L_3 L_4 L_5 L_6} N_1, \quad Q_2 = \frac{l_P^{(11)6}}{L_1 L_2 L_5 L_6} N_2, \quad Q_3 = \frac{l_P^{(11)6}}{L_1 L_2 L_3 L_4} N_3,$$

where N_I is the number of M2 branes wrapping the I^{th} 2-torus. From the expression of the Newton constant (3.1.2), the entropy in eleven dimensions is

$$S = \frac{A_H^{(11)}}{4G_{11}} = 2\pi \sqrt{N_1 N_2 N_3}. \quad (4.1.50)$$

The entropy neither depends on the transverse space nor on the Planck length and is then moduli-free. The first property implies that the entropy is invariant under compactification and T-dualities on the \mathbb{T}^6 . For instance, we perform the duality chain detailed in Section 4.1.1.5: a KK reduction along x_6 and three T-dualities along x_1, x_2 and x_5 . The dual solution of the BMPV black hole is a *D1-D5-P black hole* in type IIB on $S^1 \times \mathbb{T}^4$. The metric, the NS-NS and R-R fields are given in (4.1.43). The entropy is identical with now $N_1 \rightarrow N_1, N_2 \rightarrow N_5$ and $N_3 \rightarrow N_P$. In the supergravity regime, the microstate structure encoding the entropy is not manifest. However, as advertised in the Introduction, one can use the invariance under the string coupling to “turn off” gravity and describe the physics of the brane bound states at weak coupling where the microstate structure is explicit, $g_s N \ll 1$. This is the open string - closed string duality. The open-string description corresponds to the $\text{AdS}_3 \times S^3$ near-horizon

⁴Section 4.2.2 will be devoted to the description of the 1/8-BPS three-charge black hole in the D1-D5-P frame.

limit of the D1-D5-P supergravity solutions. The closed-string description is a two-dimensional CFT given by the shared circle of the D1 branes and the D5 branes and the time direction valid at weak coupling (zero gravity). At this regime, the microstates are well-known and are simply given by the different ways the momentum charge P can be partitioned on the D1-D5 strings. The entropy is given by the Cardy's formula [8] and exactly matches the supergravity result. The match of the entropy is a consequence of the non-renormalization of protected quantities by supersymmetry.

4.1.3 Smooth multicenter bubbling solutions

All BPS solutions in five dimensions with no magnetic charges lead to singular solutions of the type studied above. One can add centers and species of vector fields, one can change the base space to a Gibbons-Hawking space, this will not resolve the singular electric sources. Another way to think about this is that, in black-hole physics and in holographic renormalization group flows, singularities arise when one does not include the essential degrees of freedom needed to resolve singularities. The microstate geometry programme *exists* because String Theory and Supergravity have enough degrees of freedom to resolve black-hole singularities. In the present discussion, these degrees of freedom are exactly allowing magnetic fluxes on the non-trivial two-cycles induced by the Gibbons-Hawking topology (see Fig.4.1). Let us consider the most general asymptotically flat 1/8-BPS solution in the STU model. We consider n centers in the three-dimensional base space sourcing the Gibbons-Hawking function V , the electric and magnetic harmonic functions, L_I and K^I , and the momentum harmonic function M as follows

$$V = \sum_{j=1}^n \frac{q_j}{\rho_j}, \quad L_I = 1 + \sum_{j=1}^n \frac{l_j^I}{\rho_j}, \quad K^I = \sum_{j=1}^n \frac{k_j^I}{\rho_j}, \quad M = m_\infty + \sum_{j=1}^n \frac{m_j}{\rho_j}, \quad (4.1.51)$$

The constant terms, i.e. the background vector $\Gamma_\infty = (0, 0, 0, 0; 1, 1, 1, m_\infty)$, have been chosen to have an asymptotically flat geometry. One could have started with a generic point in the background moduli space. However, this specific choice is more convenient to read off the conserved charges and to match the asymptotics to the BMPV solution.

We assume that the charge vectors Γ_j and the center configuration satisfy the Denef equations (4.1.26) and the no-CTC condition (4.1.27). A straightforward consequence of the Denef equations is that

$$m_\infty = - \sum_{j=1}^n (k_j^1 + k_j^2 + k_j^3). \quad (4.1.52)$$

The five-dimensional metric and the field strengths are given by

$$\begin{aligned} ds_5^2 = & - (Z_1 Z_2 Z_3)^{-\frac{2}{3}} (dt + \mu (d\psi + A) + \varpi)^2 + V^{-1} (Z_1 Z_2 Z_3)^{\frac{1}{3}} (d\psi + A)^2 \\ & + V (Z_1 Z_2 Z_3)^{\frac{1}{3}} \left[d\rho^2 + \rho^2 (d\vartheta^2 + \sin^2 \vartheta d\phi^2) \right], \\ F^I = & d_3 (Z_I^{-1} (dt + \omega)) + \Theta^I, \end{aligned} \quad (4.1.53)$$

where the quantities above have been derived from the harmonic functions in Section 4.1.1.2. We now consider the interesting regime of parameters in which the inter-center distance is much smaller than the underlying charges:

$$\rho_{ij} \ll \mathcal{O}(q_j, l_j^I, k_j^I).$$

This assumption has implications in the Denef equations. We define the *aspect ratios* between the centers, $d_{ij} = \mathcal{O}(1)$, and the overall scale of the center configuration, $\lambda \ll 1$, as $\rho_{ij} = \lambda d_{ij}$. The Denef equations require at leading order in λ that

$$\sum_{j=1}^n \frac{\langle \Gamma_i, \Gamma_j \rangle}{d_{ij}} = \mathcal{O}(\lambda), \quad i = 1, \dots, n, \quad (4.1.54)$$

The family of solutions which satisfies the limit $\lambda \rightarrow 0$ are called *scaling solutions* [85–87]. Those solutions have the particularity that their cluster of centers shrinks to zero size from a three-dimensional perspective. However, as the points get closer and closer the throat becomes longer and longer, and the proper size in five dimensions of the various cycles supported by flux at the bottom of the throat stays finite in physical units [85, 86]. For those solutions, the relevant quantities have three behaviors. In the UV region, they converge to constant values and the five-dimensional spacetime is asymptotically flat Minkowski. In the intermediate region where they behave as “ ρ^{-1} ”, the solution will be a S^3 fibration over an AdS_2 throat. More specifically, the UV region and the intermediate region together approximates the geometry of a BMPV black hole whose the mass, the charges and angular momenta are functions of the charges at the centers. In the IR region, the bubble structure shows a resolution of the black-hole-type singularity via the blow up of topologically non-trivial two-cycles that are supported against collapse by fluxes (see Fig. 4.2b).

4.1.3.1 The asymptotic geometry

We start with the simplest limit: $\rho \gtrsim \mathcal{O}(q_j, l_j^I, k_j^I) \gg \rho_{ij}$. In this regime of parameter, we have⁵

$$Z_I \sim 1 + \frac{Q_I}{\rho}, \quad \omega \sim \frac{J_L + J_R \cos \vartheta}{\rho} d\psi + \frac{J_R + J_L \cos \vartheta}{\rho} d\phi, \quad \Theta^I = \mathcal{O}(\rho^{-2}), \quad V \sim \frac{1}{\rho}, \quad (4.1.55)$$

where

$$\begin{aligned} Q_I &= \sum_{j=1}^n l_j^I + C_{IJK} \sum_{(i,j)=1}^n k_i^J k_j^K, \\ J_L &= \frac{1}{2} \sum_{j=1}^n m_j + \frac{1}{2} \sum_{(i,j)=1}^n l_i^I k_j^I + \frac{C_{IJK}}{6} \sum_{(i,j,k)=1}^n k_i^I k_j^J k_k^K, \\ J_R &= \frac{1}{2} \left| \sum_{i < j} \langle \Gamma_i, \Gamma_j \rangle \hat{\rho}_{ij} \right| = \frac{1}{2} \left| \sum_i \langle \Gamma_\infty, \Gamma_i \rangle \vec{\rho}_i \right| = \mathcal{O}(\lambda), \quad \hat{\rho}_{ij} \equiv \frac{\vec{\rho}_i - \vec{\rho}_j}{|\vec{\rho}_i - \vec{\rho}_j|} \end{aligned} \quad (4.1.56)$$

Thus, the scaling solutions approach the BMPV solution (4.1.47) at large distance taking into account the change of coordinates from the Gibbons-Hawking coordinates $(\rho, \vartheta, \phi, \psi)$ to the spherical coordinates $(\hat{r}, \hat{\theta}, \varphi_1, \varphi_2)$ of \mathbb{R}^4 (4.1.12). We use carefully the word “approach” because the angular momentum J_R is not exactly zero but negligible.

Note that the asymptotic geometry depends on the background moduli Γ_∞ (4.1.24) or in other words to the choice of constant terms in the harmonic functions (4.1.51). If one adds a “1” in V for instance, the five-dimensional metric will be asymptotically $\mathbb{R}^{1,3} \times S^1$. If one removes all the constant terms in the harmonic function, that is $\Gamma_\infty = 0$, a quick analysis of the metric shows that the solutions are asymptotic to $\text{AdS}_2 \times S^3$, that is to the near-horizon geometry of a BMPV black hole. In this latter limit, $J_R = 0$, which matches the black hole result. Other kinds of asymptotics can be built up that way. However, this is not a free change. Indeed, the Denef equations relate the configuration of centers and their charges to the background moduli. Transforming the background changes the center configuration while the charge must remain fix. The section 5.1 will be dedicated to this issue.

4.1.3.2 The smooth cap and the Gibbons-Hawking centers

In the IR region $\rho = \mathcal{O}(\rho_{ij})$, the harmonic functions have order-one poles. To have a smooth geometry, the warp factors and μ must be regular everywhere. Around the j^{th} center, the regularity of Z_I fixes

⁵We remind that the Gibbons-Hawking space requires that $\sum_{j=1}^n q_j = 1$.

the electric charges l_j^I and the regularity of μ fixes the momentum charges m_j as follows⁶

$$l_j^I = -\frac{1}{2}C_{IJK}\frac{k_j^J k_j^K}{q_j}, \quad m_j = \frac{1}{12}C_{IJK}\frac{k_j^I k_j^J k_j^K}{q_j^2}. \quad (4.1.57)$$

This implies also that ϖ is regular. This type of center is called a *three-charge Gibbons-Hawking center*. They are locally 1/2-BPS⁷ and source the charge vector Γ_j as follows

$$\Gamma_j = \left(q_j, k_j^1, k_j^2, k_j^3; -\frac{k_j^2 k_j^3}{q_j}, -\frac{k_j^1 k_j^3}{q_j}, -\frac{k_j^1 k_j^2}{q_j}, \frac{k_j^1 k_j^2 k_j^3}{q_j^2} \right). \quad (4.1.58)$$

Thus, unlike the BMPV solution, the product $Z_1 Z_2 Z_3$ and the angular momentum one-form is “harmless” where the harmonic functions diverge and the topology is given by the Gibbons-Hawking base space that we have studied in Section 4.1.1.1. The five-dimensional spacetime is locally a smooth discrete $\mathbb{Z}_{|q_j|}$ quotient of $\mathbb{R}^{1,4}$ at each center.

As a remark, the regularity (4.1.57) can only be achieved by turning on dipole charges in K^I as expected. By focusing on the constraint on the electric charges l_j^I and comparing to the structure of the Maxwell equation (4.1.6)

$$\star_4 d_4 \star_4 d_4 Z_I = \frac{1}{2}C_{IJK} \star_4 (\Theta^J \wedge \Theta^K),$$

we notice that $\star_4 (\Theta^J \wedge \Theta^K)$ has been fixed to cancel the electric singularity. This term comes directly from the Chern-Simons term of the five-dimensional action (3.3.4). As advertised, the Chern-Simons term is the key ingredient that obviates the GR ‘no-go’ theorem and that allows non-trivial structure at the scale of the horizon. If one does not impose the regularity condition (4.1.57), the solution is multi-centered singular black holes.

As detailed in Section 4.1.1.1, the Gibbons-Hawking base space is ambipolar and one can wonder how the five-dimensional space keeps its $(-, +, +, +, +)$ signature all over the space. This is a consequence of the no-CTC’s inequalities (4.1.28). Thus, the absence of closed time-like curves requires that the warp factors flip sign when the Gibbons-Hawking metric changes signature. According to (4.1.53), the signature of the five-dimensional solutions remains constant.

Let us make a step back and determine what has been achieved so far. In General Relativity, all classical solutions which look like a black hole from the horizon scale to infinity are necessary black holes themselves or multi-centered black holes as a consequence of the no-hair theorem. In the framework of five-dimensional Supergravity and its dual frames, we have shown that supersymmetric black-hole solutions with a macroscopic horizon area and smooth horizonless solutions coexist in the same regime of parameters (see Fig.4.2). The latter look like a black hole from above the horizon scale. However, they cap off smoothly at the horizon scale thanks to magnetic charges that prevent the structure to collapse (see Fig.4.2b). The main question is if they do account significantly in the entropy computed in the closed-string description $S \sim \sqrt{N_1 N_2 N_3 - J_L^2}$. Unfortunately, no direct computation has been performed so far in that direction but general arguments tend to the negative answer as a consequence of the highly-isometric nature of the solutions. Nevertheless, smoothness should be only imposed in the D1-D5-P frame where the microscopic brane-bound-state counting is performed. One can expect that our requirement of smoothness in five dimensions is too rigid and that six-dimensional Supergravity contains less isometric smooth solutions that account more in the entropy.

⁶These regularity conditions are actually valid for smooth BPS multicenter solutions with an arbitrary number of vector fields.

⁷They preserve 16 supercharges.

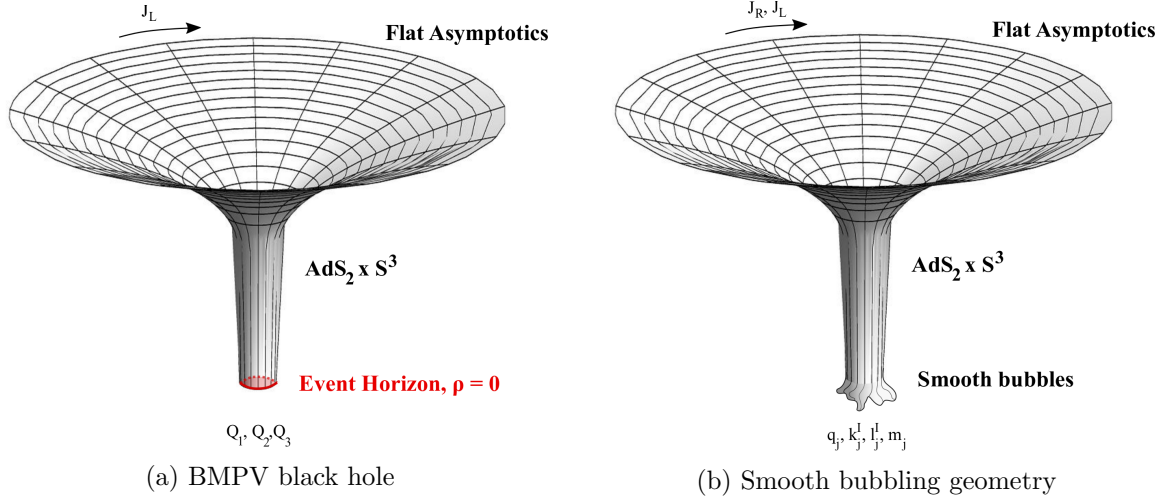


Figure 4.2: Schematic description of the two-dimensional embedding of a BMPV black hole and a smooth bubbling geometry.

The Gibbons-Hawking centers are the only centers that are regular from a five-dimensional perspective. In Section 4.1.1.5, we have discussed several dual frames containing the STU model. When the solutions are uplifted to ten dimensions, other types of regular centers exist. The *two-charge Supertubes* are brane bound states carrying two electric charges, a magnetic charge and one angular momentum [88–90]. They are 1/4-BPS objects⁸, and their angular momentum is fixed by regularity. In the next subsection, we will describe the two-charge supertube solutions in the context of the STU model. The isometric nature of the model restricts the solutions to the “round” supertubes whereas it has been shown that supersymmetry is preserved for arbitrary shapes [91, 89]. Moreover, the counting of “wiggly” supertubes reproduces exactly the entropy of the two-charge system as already said in the Introduction [92, 11–14]. Furthermore we will see that the “wiggly” supertubes are the foundation stones of Superstrata.

4.1.3.3 Two-charge round Supertube

Round supertubes were initially introduced in the context of type IIA Supergravity as D2-branes with a compact direction, carrying F1 and D0 charges (4.1.41). Translated into the STU language, the F1 and D0 induce two electric charges l^1 and l^2 and the D2 induces a dipole magnetic charge k^3 . The regularity of the ten-dimensional geometry imposes a non-zero angular momentum m sourced by a P charge:

$$m = \frac{l^1 l^2}{k^3}. \quad (4.1.59)$$

As it has been explained in Section 4.1.1.5, those 1/4-BPS brane bound states in type IIA on $S^1 \times \mathbb{T}^4$ are well-described as supergravity solutions within the STU model (4.1.41). However, for a reason that will become evident when we construct Superstrata, we will review the construction of two-charge round supertubes in the D1-D5-P frame (4.1.43).

- The two-charge round-supertube center:

In the D1-D5-P frame, a two-charge round Supertube is sourced electrically by D1-branes wrapping the transverse S^1 and D5 branes wrapping $S^1 \times \mathbb{T}^4$. The magnetic charge is induced by a KKm charge

⁸The Supertube preserves 16 supercharges and is locally 1/2-BPS but the \mathbb{R}^4 base space breaks half of the supersymmetries.

while the angular momentum is induced by a F1 charge. We recall the six-dimensional part of the metric (4.1.43)

$$\begin{aligned} ds_6^2 &= -\frac{1}{Z_3\sqrt{Z_1Z_2}}(dt + \omega)^2 + \sqrt{Z_1Z_2} \left[V^{-1} (d\psi + A)^2 + V ds(\mathbb{R}^3)^2 \right] + \frac{Z_3}{\sqrt{Z_1Z_2}} (dy + A^3)^2, \\ A^3 &= -\frac{dt + \omega}{Z_3} + \frac{K^3}{V} (d\psi + A) + w^3, \end{aligned} \quad (4.1.60)$$

According to the preamble, a supertube center is given by the following charge vector in the STU model

$$\Gamma_S^{(3)} = (0, 0, 0, k^3; l^1, l^2, 0, m). \quad (4.1.61)$$

The linearity of the BPS equations allows us to consider the supertube center in flat \mathbb{R}^4 with no other centers. Considering more centers will just add linear contributions to the harmonic function and will not affect the regularity of the solution around the supertube locus⁹. Thus, the single supertube center is determined by the following eight harmonic functions¹⁰

$$V = \frac{1}{\rho}, \quad L_1 = 1 + \frac{l^1}{\rho_S}, \quad L_2 = 1 + \frac{l^2}{\rho_S}, \quad L_3 = 1, \quad K^1 = K^2 = 0, \quad K^3 = \frac{k^3}{\rho_S}, \quad M = -k^3 + \frac{m}{\rho_S}, \quad (4.1.62)$$

where ρ_S is the distance from the supertube center in the three-dimensional base space. The Denef equations (4.1.26) fixes the supertube radius which we call a

$$a = \frac{\sqrt{l^1 l^2}}{k^3}. \quad (4.1.63)$$

To check regularity along the Supertube one must inspect potential singularities along the $(d\psi + A)^2$ fiber. This leads to the condition

$$\lim_{\rho_S \rightarrow 0} \rho_S^2 \left[Z_3 K^{3^2} - 2\mu V K^3 + Z_1 Z_2 V \right] = 0 \quad \implies \quad m = \frac{l^1 l^2}{k^3}. \quad (4.1.64)$$

This condition makes the six-dimensional metric regular. In the vicinity of the supertube center the geometry is a S^3 fibration along (ϑ, ϕ, ψ) over AdS_3 given by (ρ, t, y) . Notice that, unlike Gibbons-Hawking center, the ψ -circle does not pinch off at the round-supertube locus and has a fixed radius. If we add an arbitrary number of Gibbons-Hawking centers, the round Supertube represents a round circle wrapping the ψ -fiber as depicted in Fig.4.3. A similar picture can be drawn in flat \mathbb{R}^4 : instead of bubbles the ψ -fiber does not stop growing and the round Supertube stands at a distance a from the origin of \mathbb{R}^4 .

Moreover, one may consider two other centers which are identical to (4.1.61) by permutation of the vector fields:

$$\Gamma_S^{(1)} = \left(0, k^1, 0, 0; 0, l^2, l^3, \frac{l^2 l^3}{k^1} \right), \quad \Gamma_S^{(2)} = \left(0, 0, k^2, 0; l^1, 0, l^3, \frac{l^1 l^3}{k^2} \right). \quad (4.1.65)$$

The centers are singular in the D1-D5-P metric above. However, permuting similarly the vector fields in the metric (4.1.60) leads to regular frames. For instance, permuting the label $1 \leftrightarrow 3$ in (4.1.60), gives a D1-D5-P frame in which the supertube center $\Gamma_S^{(1)}$ is regular. Concretely, when we dualized the eleven-dimensional frame on $\mathbb{T}^6 = \mathbb{T}^2 \times \mathbb{T}^2 \times \mathbb{T}^2$ to the type IIB D1-D5-P frame, we discriminated

⁹This will also divide by two the number of unbroken supersymmetries.

¹⁰We have chosen the constant terms in order to obtain an asymptotically flat solution. A different choice will not affect the supertube regularity.

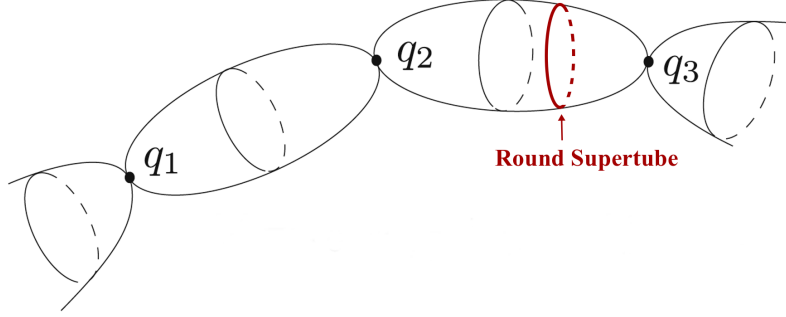


Figure 4.3: The round Supertube from the perspective of a four-dimensional base space with arbitrary many Gibbons-Hawking centers.

between the undistinguishable two-tori¹¹. Indeed, the KK reduction along a one-curve of one two-torus makes the corresponding vector field be “magnetically” sourced by a KKm charge. There are three possible choices of torus, therefore there exist three different D1-D5-P frames. Each frame has their own regular round Supertube. Thus, in the STU model, there are three *species of two-charge Supertubes* given by (4.1.61) and (4.1.65). Each one is regular in the specific D1-D5-P frame where their magnetic charge corresponds to a KKm charge of the base.

- Spectrally-flowed Supertube:

An interesting property of round Supertubes is that they can be mapped to Gibbons-Hawking centers by generalized spectral flows (4.1.30) and reciprocally. In the STU model, there are three generalized spectral flow transformations given by three constants γ^I . We perform the following transformation

$$\left(0, 0, 0, k^3; l^1, l^2, 0, \frac{l^1 l^2}{k^3}\right) \xrightarrow{(\gamma^1, \gamma^2, \gamma^3) = \left(0, 0, \frac{q}{k^3}\right)} \left(q, -\frac{q l^2}{k^3}, -\frac{q l^1}{k^3}, k^3; l^1, l^2, -\frac{q l^1 l^2}{k^3}, \frac{l^1 l^2}{k^3}\right) \quad (4.1.66)$$

One can check that the resulting charge vector satisfies the smoothness conditions of a Gibbons-Hawking center (4.1.57). One also find a sequence of generalized spectral flows transforming a generic Gibbons-Hawking center (4.1.58) to a round Supertube. Therefore, the equations that determine the smoothness of a Supertube in six dimensions are related by spectral flow to the smoothness conditions of a usual bubbling solution in five dimensions. This is trivial for the Denef equations and the CTC condition (4.1.26) and (4.1.27) as they are invariant under spectral flows but this is less trivial for the supertube regularity (4.1.64).

4.2 BPS solutions in six dimensions

The five-dimensional smooth solutions described in the previous section have a tri-holomorphic U(1) isometry. This isometry has the advantage to make simpler equations of motion, but in return, they are too rigid to account significantly for the entropy of the three-charge black hole. It should only be in six dimensions that the solutions would be complex enough to describe a significant phase space of black hole microstates due to the dependence along the extra dimension. However, the price to pay is to have more complicated equations. In this section, we derive the equations of motion of

¹¹The two-tori in the eleven-dimensional frame are undistinguishable in a sense that they map to each other under permutation of the vector fields.

solutions with unbroken supersymmetries in six-dimensional $\mathcal{N} = (1, 0)$ Supergravity coupled to tensor multiplets [59–61, 93, 94] and detail a linear procedure to solve them [95–97]. We review the D1-D5-P black-hole in this framework and we finally construct the superstratum solutions [30, 98–101, 31, 28]. They are obtained by generating momentum charges on two-charge wiggly Supertubes.

4.2.1 Generic BPS solutions

We start by considering $\mathcal{N} = (1, 0)$ six-dimensional Supergravity coupled to n_T extra tensor multiplets. We use the conventions detailed in Section 3.3.2. The dynamics of the solutions of the action given in 3.3.11 is governed by the following Einstein-Maxwell-scalar equations [59, 61]¹²

$$\begin{aligned} R_{\mu\nu} + \partial_\mu v^I \partial_\nu v_I - \mathcal{M}_{IJ} G_{\mu\alpha\beta}^I G_\nu^{J\alpha\beta} &= 0, \\ x_I^M d_6 \star_6 d_6 v^I + 4 x_I^M v_J G^I \wedge \star_6 G^J &= 0, \\ d_6 G^I &= 0. \end{aligned} \quad (4.2.1)$$

One also needs to add the self-duality condition and the $SO(1, n_T)/SO(n_T)$ constraint on the scalar:

$$\mathcal{M}_{IJ} G^J = \eta_{IJ} \star_6 G^J, \quad v_I v^I = 1. \quad (4.2.2)$$

4.2.1.1 BPS equations of motion

We derive the BPS equations. This essentially works in two steps as we have done before. We first derive all the conditions from the conservation of supersymmetries. This allows to simplify the form of the fields and to satisfy automatically all, or all but one, Einstein equations¹³. And second, we derive the BPS equations from the remaining equations.

- Supersymmetry and self-duality:

We assume that the solutions preserve Killing spinors. In six dimensions, spinors are Majorana-Weyl and then are in pairs. The gravitini and tensorini variations lead to first-order differential equations [60]:

$$\nabla_\mu \epsilon^i + \frac{1}{4} v_I G_{\mu\nu\rho}^I \Gamma^{\nu\rho} \epsilon^i = 0, \quad (4.2.3)$$

$$x_I^M \partial_\mu v^I \Gamma^\mu \epsilon^i + \frac{1}{6} x_I^M G_{\mu\nu\rho}^I \Gamma^{\mu\nu\rho} \epsilon^i = 0, \quad (4.2.4)$$

where Γ^μ are the 8×8 Gamma matrices. We construct the bilinear one-form

$$\mathcal{K}_\mu = \bar{\epsilon}_i \Gamma_\mu \epsilon^i. \quad (4.2.5)$$

The indices are contracted as symplectic Majorana spinors $\chi^i = \epsilon^{ij} \chi_j$, where ϵ^{ij} is the rank-two Levi-Civita tensor. A rather technical algebraic computation, using the Fierz identity and (4.2.3), shows that \mathcal{K} is a null Killing vector [60]. This defines a null coordinate u and its associated vielbein e^+ , $\mathcal{K} = \partial_u$. All the fields are independent of u . We also define the hypersurface nowhere tangent to \mathcal{K} by its normal vector e^- : $\mathcal{K} \cdot e^- = 1$. The metric decomposes as a two-dimensional space over a four-dimensional base space defined by the vielbein e^m , $m = 1, 2, 3, 4$ as

$$ds_6^2 = 2 e^- e^+ - \delta_{mn} e^m e^n.$$

¹²We used the self-duality condition to simplify the equations. This also reduces the usual Maxwell equations for the tensor fields to the Bianchi identity.

¹³As we have discussed in the context of eleven-dimensional Supergravity, one component of the Einstein equation might remain unsolved.

The most general Ansatz leads to [60]

$$ds_6^2 = \frac{2}{H} (dv + \beta) \left(du + \omega + \frac{1}{2} \mathcal{F} (dv + \beta) \right) - H ds(\mathcal{B})^2, \quad (4.2.6)$$

where $ds(\mathcal{B})^2$ is the metric of the base space \mathcal{B} , \mathcal{F} and \mathcal{P} are scalars on \mathcal{B} , ω and β are one-forms on \mathcal{B} . This corresponds to

$$e^+ = H^{-1} (dv + \beta), \quad e^- = du + \omega + \frac{1}{2} \mathcal{F} H e^+.$$

We use the Cartesian coordinates, x_m , on \mathcal{B} . If we work now with the other non-zero three-form bilinears $\tilde{\epsilon}^i \Gamma_{\mu\nu\rho} \epsilon^j$, one can show that the base space \mathcal{B} must be almost hyper-Kähler, that is the three anti self-dual two-forms,

$$J^A \equiv \frac{1}{2} J_{mn}^A dx^m \wedge dx^n, \quad (4.2.7)$$

satisfy the algebraic condition and the differential equation

$$J_p^{Am} J_n^{Bp} = \epsilon^{ABC} J_n^{Cm} - \delta_n^m \delta_n^A, \quad d_4 J^A = \partial_v (\beta \wedge J^A). \quad (4.2.8)$$

We have defined d_4 as the exterior derivative on \mathcal{B} . It is convenient to introduce the KK covariant differential operator \mathcal{D} as

$$\mathcal{D}\Phi \equiv d_4\Phi - \beta \wedge \dot{\Phi} \quad \Rightarrow \quad d_6\Phi = \mathcal{D}\Phi + H e^+ \wedge \dot{\Phi}, \quad (4.2.9)$$

where the dot “ $\dot{}$ ” means ∂_v . Finally, one can manipulate the tensorini equation using the self-duality relations and the supersymmetry condition on \mathcal{B} to rewrite the tensor fields [60, 61, 95, 93, 94]

$$\begin{aligned} G^I = \frac{1}{2} \left[\star_4 \left[\mathcal{D} (v^I H) + v^I H \dot{\beta} \right] + e^+ \wedge \left[v^I H^2 \Psi - \frac{1}{2} v^I (\mathcal{D}\omega - \star_4 \mathcal{D}\omega) + \hat{G}^I \right] \right. \\ \left. + v^I H^{-1} e^- \wedge \mathcal{D}\beta - e^+ \wedge e^- \wedge \left[v^I (H^{-1} \mathcal{D}H + \dot{\beta}) - \mathcal{D}v^I \right] \right], \end{aligned} \quad (4.2.10)$$

where we have introduced

$$\Psi \equiv \frac{1}{8} \epsilon^{ABC} J^{Amn} j_{mn}^B J^C, \quad \hat{G}^I \equiv (G_{+mn}^I - v^I v_J G_{+mn}^J) e^m \wedge e^n. \quad (4.2.11)$$

The self-duality conditions on the tensors and on J^A imply

$$\star_4 \mathcal{D}\beta = \mathcal{D}\beta, \quad \star_4 \mathcal{D}\hat{G}^I = \mathcal{D}\hat{G}^I, \quad \star_4 \hat{G}^I = \hat{G}^I, \quad v_I \hat{G}^I = 0, \quad \star_4 \Psi = -\Psi. \quad (4.2.12)$$

One can show, using the integrability conditions, that the scalar equation (4.2.1) is satisfied if the supersymmetric equations, (4.2.3) and (4.2.4), and the Bianchi identities are satisfied [60, 93, 94]. Moreover, all but the “++” components of the Einstein equation (4.2.1) are satisfied because the bilinear \mathcal{K} is null. The equations of motion for BPS solutions reduce to

$$\begin{aligned} R_{++} &= -\partial_+ v^I \partial_+ v_I + \mathcal{M}_{IJ} G_{+ab}^I G_+^{Jab}, \\ d_6 G^I &= 0, \\ \mathcal{M}_{IJ} G^J &= \eta_{IJ} \star_6 G^J, \\ v_I v^I &= 1. \end{aligned} \quad (4.2.13)$$

- Bianchi identity:

We substitute the expression for G^I (4.2.10) in the Bianchi identities. This leads to two sets of equations:

$$\begin{aligned} d_4(v^I H \Psi + \mathcal{G}^{+I}) &= \partial_v \left[\beta \wedge (v^I H \Psi + \mathcal{G}^{+I}) + \star_4 (\mathcal{D}(v^I H) + v^I H \dot{\beta}) \right], \\ \mathcal{D} \star_4 [\mathcal{D}(v^I H) + v^I H \dot{\beta}] &= -\mathcal{G}^{+I} \wedge \mathcal{D}\beta, \end{aligned} \quad (4.2.14)$$

where we have defined the $n_T + 1$ self-dual two-forms

$$\mathcal{G}^{+I} \equiv \frac{1}{2} H^{-1} \left[v^I (\mathcal{D}\omega + \star_4 \mathcal{D}\omega + \mathcal{F} \mathcal{D}\beta) + 2\hat{G}^I \right]. \quad (4.2.15)$$

• Einstein equation:

The Einstein equation requires some work. After simplification, we obtain [60, 61, 93, 94]

$$\begin{aligned} \star_4 \mathcal{D} \star_4 \left(\dot{\omega} + \frac{1}{2} \mathcal{F} \dot{\beta} - \frac{1}{2} \mathcal{D} \mathcal{F} \right) &= -2 \left(\dot{\omega} + \frac{1}{2} \mathcal{F} \dot{\beta} - \frac{1}{2} \mathcal{D} \mathcal{F} \right)^m \partial_v (\beta_m) + \frac{1}{2} H h^{mn} \partial_v^2 (H h_{mn}) \\ &\quad + \frac{1}{4} \partial_v (H h^{mn}) \partial_v (H h_{mn}) - \frac{1}{8} H^{-2} (2\mathcal{D}\omega + \mathcal{F} \mathcal{D}\beta)^2 \\ &\quad + \frac{1}{8} (2H\Psi - H^{-1} (\mathcal{D}\omega - \star_4 \mathcal{D}\omega))^2 \\ &\quad - \frac{1}{2} H^{-2} \eta_{IJ} \hat{G}_{mn}^I \hat{G}^{Jmn} - \eta_{IJ} H^2 \partial_v v^I \partial_v v^J, \end{aligned} \quad (4.2.16)$$

where h_{mn} is the metric on \mathcal{B} in Cartesian coordinates,

$$ds(\mathcal{B})^2 = h_{mn} dx^m dx^n.$$

The natural way to solve the equations (4.2.14), (4.2.15) and (4.2.16) is first to choose an almost hyper-Kähler four-dimensional base and its fibration vector β , giving h_{mn} and the two-form Ψ , then to solve the equations for $v^I H$, \mathcal{G}^{+I} , \mathcal{F} and ω and. As it has been shown in [95, 96], the complicated form of the equations can be simplified to equations where a linear structure is manifest. For that purpose, we define

$$Z_I \equiv \sqrt{2} \eta_{IJ} v^J H, \quad \Theta^I \equiv \sqrt{2} (v^I H \Psi + \mathcal{G}^{+I}), \quad G^{(I)} \equiv \sqrt{2} G^I. \quad (4.2.17)$$

We choose the same notations as the electric gauge fields and the magnetic two-forms in five dimensions on purpose. We will see later that they have the same properties and under certain assumptions, the six-dimensional BPS solutions can be compactified into a five-dimensional BPS solutions. We also assume that the labelling given by “ I ” goes like $I = 1, 2, 4, 5, \dots, n_T + 2$ for the same reason. With these definitions, the scalar constraint, $v_I v^I = 1$, and the tensor fields translate into¹⁴

$$\begin{aligned} \mathcal{P} \equiv H^2 &= \frac{1}{2} \eta^{IJ} Z_I Z_J = Z_1 Z_2 - \frac{1}{2} Z_4^2 - \frac{1}{2} Z_5^2 - \dots - \frac{1}{2} Z_{n_T+2}^2, \\ G^{(I)} &= \frac{1}{2} \left[\eta^{IJ} \star_4 [\mathcal{D} Z_J + Z_J \dot{\beta}] - d_6 \left(\frac{\eta^{IJ} Z_J}{\mathcal{P}} (du + \omega) \wedge (dv + \beta) \right) + (dv + \beta) \wedge \Theta^I \right]. \end{aligned} \quad (4.2.18)$$

In order to have the usual $(-, +, +, \dots, +)$ signature for the six-dimensional metric (4.2.6), we set

$$H = -\sqrt{\mathcal{P}}.$$

The equations that determine the four-dimensional base geometry are called the *zeroth layer of BPS equations*. They involve the metric on \mathcal{B} , and the one-form β as follows

$$J_p^{Am} J_n^{Bp} = \epsilon^{ABC} J_n^{Cm} - \delta^{AB} \delta_n^m, \quad \mathcal{D} J^A = \dot{\beta} \wedge J^A, \quad \star_4 \mathcal{D}\beta = \mathcal{D}\beta. \quad (4.2.19)$$

¹⁴We recall that we have chosen a basis of scalar v^I of $SO(1, n_T)$ with the light-cone metric η (3.3.9).

The equations (4.2.14) and the self-duality of the two-forms give the *first layer of BPS equations*¹⁵

$$\begin{aligned}\eta^{IJ} \mathcal{D} \star_4 \left[\mathcal{D} Z_J + Z_J \dot{\beta} \right] &= -\Theta^I \wedge \mathcal{D} \beta, \\ \eta^{IJ} \star_4 \partial_v \left[\mathcal{D} Z_J + Z_J \dot{\beta} \right] &= \mathcal{D} \Theta^I - \dot{\beta} \wedge \Theta^I, \\ \star_4 \left[\Theta^I - \eta^{IJ} Z_J \Psi \right] &= \Theta^I - \eta^{IJ} Z_J \Psi.\end{aligned}\tag{4.2.20}$$

The last two equations result from inverting (4.2.15) and from introducing (Z_I, Θ^I) in the Einstein equation (4.2.16) [95]. They are called *second layer of BPS equations*:

$$\begin{aligned}\mathcal{D} \omega + \star_4 \mathcal{D} \omega + \mathcal{F} \mathcal{D} \beta &= \eta_I^J Z_J \Theta^I - 2H^2 \Psi, \\ \star_4 \mathcal{D} \star_4 \left(\dot{\omega} + \frac{1}{2} \mathcal{F} \dot{\beta} - \frac{1}{2} \mathcal{D} \mathcal{F} \right) &= -2 \left(\dot{\omega} + \frac{1}{2} \mathcal{F} \dot{\beta} - \frac{1}{2} \mathcal{D} \mathcal{F} \right)^m \partial_v (\beta_m) + \frac{1}{2} H h^{mn} \partial_v^2 (H h_{mn}) \\ &\quad + \frac{1}{4} \partial_v (H h^{mn}) \partial_v (H h_{mn}) - \eta^{IJ} \frac{H^2}{2} \partial_v \left(\frac{Z_I}{H} \right) \partial_v \left(\frac{Z_J}{H} \right) \\ &\quad - \frac{1}{2} \star_4 \left[\eta_{IJ} (\Theta^I - \eta^{IK} Z_K \Psi) \wedge (\Theta^J - \eta^{JL} Z_L \Psi) \right. \\ &\quad \left. + H^2 \Psi \wedge \Psi - 2\Psi \wedge \mathcal{D} \omega \right].\end{aligned}\tag{4.2.21}$$

Note that the first layer is linear in Z_I and Θ^I and that the second layer is linear in \mathcal{F} and ω with quadratic sources. Thus, once the base geometry and its fibration vector β are fixed, the first layer fixes the $n_T + 1$ scalars and two-forms (Z_I, Θ^I) and then the second layer fixes the six-dimensional background geometry (\mathcal{F}, ω) .

- The BPS equations with a base space independent on v :

All the six-dimensional BPS solutions we study in this thesis have a v -independent base geometry. Thus, the four-dimensional base space is hyper-Kähler. This drastically simplifies the layers of equations. The zeroth layer becomes

$$J_p^{Am} J_n^{Bp} = \epsilon^{ABC} J_n^{Cm} - \delta^{AB} \delta_n^m, \quad d_4 J^A = 0, \quad \star_4 d_4 \beta = d_4 \beta.\tag{4.2.22}$$

The first layer is

$$\eta^{IJ} \mathcal{D} \star_4 \mathcal{D} Z_J = -\Theta^I \wedge d_4 \beta, \quad \eta^{IJ} \star_4 \mathcal{D} \dot{Z}_J = \mathcal{D} \Theta^I, \quad \star_4 \Theta^I = \Theta^I.\tag{4.2.23}$$

As for the second layer, by noticing that $h^{mn} h_{mn} = 4$, we have

$$\begin{aligned}\mathcal{D} \omega + \star_4 \mathcal{D} \omega + \mathcal{F} d_4 \beta &= \eta_I^J Z_J \Theta^I, \\ \star_4 \mathcal{D} \star_4 \left(\dot{\omega} - \frac{1}{2} \mathcal{D} \mathcal{F} \right) &= \frac{\eta^{IJ}}{2} \left[\partial_v^2 (Z_I Z_J) - \dot{Z}_I \dot{Z}_J \right] - \frac{\eta_{IJ}}{2} \star_4 (\Theta^I \wedge \Theta^J).\end{aligned}\tag{4.2.24}$$

As a remark, if we assume that the full solution is independent of v . The first and second layers correspond to the BPS equations of solutions in five-dimensional Supergravity coupled to $n_T + 1$ extra vector multiplets, (4.1.6) and (4.1.7). This requires identifying (Z_3, Θ^3) as $(-\mathcal{F}/2, d_4 \beta)$, rescaling all $(Z_I, \Theta^I) \rightarrow (Z_I, \Theta^I)/\sqrt{2}$ for $I \geq 4$ and the non-zero five-dimensional structure constants C_{IJK} is determined according to η_{IJ} as follows

$$C_{3JK} = \eta_{JK} \quad \text{and cyclic permutations with } J, K = 1, 2, 4, \dots, n_T + 1.\tag{4.2.25}$$

¹⁵To obtain those equations, we recall that the contraction of a self-dual and an anti self-dual two-forms vanishes.

Thus, the spectrum of v -independent BPS solutions of six-dimensional Supergravity with n_T extra tensor multiplets maps to the spectrum of BPS solutions of five dimensional Supergravity with $n_T + 1$ extra vector multiplets. The map can be achieved by KK reduction along v . However, it is not a one-to-one map due to the strong constraint on the structure constants. Generic five-dimensional BPS solutions cannot be mapped to v -independent six-dimensional solutions with only tensor multiplets. This constraint has a clear picture from the eleven-dimensional perspective. We have shown that five-dimensional Supergravity arises from eleven-dimensional Supergravity on a Calabi-Yau three-fold \mathcal{C}_6 . The choice of structure constants (4.2.25) translates into that \mathcal{C}_6 has a \mathbb{T}^2 factor, $\mathcal{C}_6 = \mathbb{T}^2 \times \mathcal{C}_4$ where \mathcal{C}_4 is a Calabi-Yau two-fold. Under this assumption, one can perform a KK reduction on a one-curve of \mathbb{T}^2 and a sequence of T/S-dualities to type IIB on $S^1 \times \mathcal{C}_4$. The dualized solutions will be embedded in six-dimensional Supergravity with only tensor multiplets. An example of sequence has been detailed in the context of the STU model in Section 4.1.1.5. An extension to solutions with four vector multiplets ($n_T = 2$) can be found in [102]. On the contrary, a generic \mathcal{C}_6 can induce non-trivial vector multiplets and hypermultiplets from the six-dimensional perspective.

To conclude, we derived the equations of motion of BPS solutions of $\mathcal{N} = (1, 0)$ six-dimensional Supergravity coupled to n_T extra tensor multiplets. We also considered the BPS solution with a v -independent hyper-Kähler base. In the next subsection, we investigate the solutions with $n_T = 2$ and we detail their description in type IIB Supergravity.

4.2.1.2 Solutions with two extra tensor multiplets

The BPS solutions that we will consider in this thesis have a v -independent four-dimensional hyper Kähler base space and are embedded in $\mathcal{N} = (1, 0)$ Supergravity coupled to two extra tensor multiplets. In this section, we just specify the results obtained for generic number of extra tensor multiplets and consider $n_T = 2$. We also discuss the description of the solutions as ten-dimensional solutions in the D1-D5-P frame. To have a consistent notation with the BPS solutions in five dimensions discussed in Section 4.1, we rescale the scalar metric η as follows

$$\eta \rightarrow \eta = \begin{pmatrix} 0 & 1 & 0 \\ 1 & 0 & 0 \\ 0 & 0 & -2 \end{pmatrix}. \quad \xRightarrow{(4.2.18)} \quad \mathcal{P} = Z_1 Z_2 - Z_4^2 \quad (4.2.26)$$

We recall the expressions for the six-dimensional metric and the three extra tensor fields

$$\begin{aligned} ds_6^2 &= -\frac{2}{\sqrt{\mathcal{P}}} (dv + \beta) \left(du + \omega + \frac{1}{2} \mathcal{F} (dv + \beta) \right) + \sqrt{\mathcal{P}} ds(\mathcal{B})^2, \\ G^{(I)} &= \frac{1}{2} \left[\eta^{IJ} \star_4 \mathcal{D} Z_J - d_6 \left(\frac{\eta^{IJ} Z_J}{\mathcal{P}} (du + \omega) \wedge (dv + \beta) \right) + (dv + \beta) \wedge \Theta^I \right]. \end{aligned} \quad (4.2.27)$$

As already said, the BPS equations split into three layers. The zeroth layer requires that \mathcal{B} is hyper-Kähler and $d_4 \beta$ is self-dual. The first layer gives the dynamics of the electric-magnetic pairs (Z_I, Θ^I) , $I = 1, 2, 4$,

$$\begin{aligned} \star_4 \mathcal{D} \dot{Z}_1 &= \mathcal{D} \Theta^2, & \mathcal{D} \star_4 \mathcal{D} Z_1 &= -\Theta^2 \wedge d_4 \beta, & \Theta^2 &= \star_4 \Theta^2, \\ \star_4 \mathcal{D} \dot{Z}_2 &= \mathcal{D} \Theta^1, & \mathcal{D} \star_4 \mathcal{D} Z_2 &= -\Theta^1 \wedge d_4 \beta, & \Theta^1 &= \star_4 \Theta^1, \\ \star_4 \mathcal{D} \dot{Z}_4 &= \mathcal{D} \Theta^4, & \mathcal{D} \star_4 \mathcal{D} Z_4 &= -\Theta^4 \wedge d_4 \beta, & \Theta^4 &= \star_4 \Theta^4, \end{aligned} \quad (4.2.28a)$$

while the second layer determines the angular-momentum one-form ω and the warp factor \mathcal{F} as follows

$$\begin{aligned} \mathcal{D} \omega + \star_4 \mathcal{D} \omega + \mathcal{F} d\beta &= Z_1 \Theta^1 + Z_2 \Theta^2 - 2Z_4 \Theta^4, \\ \star_4 \mathcal{D} \star_4 \left(\dot{\omega} - \frac{1}{2} \mathcal{D} \mathcal{F} \right) &= \partial_v^2 (Z_1 Z_2 - Z_4^2) - (\dot{Z}_1 \dot{Z}_2 - \dot{Z}_4^2) - \frac{1}{2} \star_4 (\Theta^1 \wedge \Theta^2 - \Theta^4 \wedge \Theta^4). \end{aligned} \quad (4.2.29)$$

The equations are non-linear first or second order differential equations. However, they can be tackled through a linear process by fixing the pairs (Z_I, Θ^I) with the first layer and consider them as quadratic sources for (ω, \mathcal{F}) in the second layer.

In Section 3.3.2, we have discussed how BPS solutions of $\mathcal{N} = (1, 0)$ six-dimensional Supergravity with 2 extra tensor multiplets are obtained by dimensional reduction and consistent truncation of type IIB Supergravity on a Calabi-Yau two-fold, particularly on a rigid \mathbb{T}^4 . Such solutions in type IIB Supergravity are described by the following Ansatz [96, 97]¹⁶

$$\begin{aligned}
ds_{10}^2 &= \frac{\sqrt{Z_1}}{\mathcal{P}^{1/4}} \left[\frac{\sqrt{Z_2}}{\mathcal{P}^{1/4}} ds_6^2 + \frac{\mathcal{P}^{1/4}}{\sqrt{Z_2}} ds(\mathbb{T}^4)^2 \right], \\
e^{2\Phi} &= \frac{Z_1^2}{\mathcal{P}}, \\
B_2 &= -\frac{Z_4}{\mathcal{P}} (du + \omega) \wedge (dv + \beta) + a_4 \wedge (dv + \beta) + \delta_4, \\
C^{(0)} &= \frac{Z_4}{Z_1}, \\
C^{(2)} &= -\frac{Z_2}{\mathcal{P}} (du + \omega) \wedge (dv + \beta) + a_1 \wedge (dv + \beta) + \delta_1, \\
C^{(4)} &= \frac{Z_4}{Z_2} \text{Vol}(\mathbb{T}^4) - \frac{Z_4}{\mathcal{P}} \delta_1 \wedge (du + \omega) \wedge (dv + \beta) + x_3 \wedge (dv + \beta), \\
C^{(6)} &= \text{Vol}(\mathbb{T}^4) \wedge \left[-\frac{Z_1}{\mathcal{P}} (du + \omega) \wedge (dv + \beta) + a_2 \wedge (dv + \beta) + \delta_2 \right].
\end{aligned} \tag{4.2.30}$$

The Ansatz introduces one-forms, a_1, a_2, a_4 , two-forms, $\delta_1, \delta_2, \delta_4$, and a three-form, x_3 , all on \mathcal{B} . These quantities may depend on the coordinates of \mathcal{B} and on v . The truncation is hidden in the Ansatz by fixing some coefficients according to Z_I and \mathcal{P} . The six-dimensional tensor fields (4.2.27) descend from the NS-NS and R-R gauge fields, they can be easily read by identifying

$$G^{(2)} = d_6 C^{(2)}, \quad G^{(4)} = d_6 B_2, \quad \text{Vol}(\mathbb{T}^4) \wedge G^{(1)} = d_6 C^{(6)}.$$

This also allows to relate $a_1, a_2, a_4, \delta_1, \delta_2$ and δ_4 to β and Θ^I ,

$$\Theta^I = \mathcal{D}a_I + \dot{\delta}_I.$$

The three-form x_3 is fixed by requiring $C^{(4)}$ to have a self-dual field strength.

The solutions correspond to D1-branes wrapping the S^1 inside the (u, v) surface sourcing electrically Z_1 and magnetically Θ^2 ($G^{(2)}$), to D5-branes wrapping $S^1 \times \mathbb{T}^4$ and sourcing similarly Z_2 and Θ^1 ($G^{(1)}$) and to P momentum charge along S^1 sourcing \mathcal{F} and β . The warp factor Z_4 is an “auxillary” field which will play a crucial role in the smoothness of the solutions. The solutions can also have KKm charges corresponding to the two left and right five-dimensional angular momenta. As matter of notations, we introduce the coordinate y along the S^1 and R_y its radius. We fix the time direction as follows¹⁷

$$u \equiv \frac{t - y}{\sqrt{2}}, \quad v \equiv \frac{t + y}{\sqrt{2}}. \tag{4.2.31}$$

¹⁶The uplift to type IIB can be done exactly the same way for v -dependent basis.

¹⁷The metric on the (u, v) surface is invariant under coordinate redefinition

$$u = u' + U(x, v'), \quad v = v' + V(x),$$

if one rescales \mathcal{F} and ω appropriately. One can then choose many different forms of u and v as functions of t and y .

The D1, D5 and P charges are denoted by Q_1 , Q_5 and Q_P respectively. They are derived from the asymptotic behaviors of the fields¹⁸

$$Z_1 \sim (\text{cst}) + \frac{Q_1}{\hat{r}^2}, \quad Z_2 \sim (\text{cst}) + \frac{Q_5}{\hat{r}^2}, \quad \mathcal{F} \sim (\text{cst}) - \frac{2Q_P}{\hat{r}^2}. \quad (4.2.32)$$

The left and right angular momenta are denoted by J_L and J_R . They are obtained from the asymptotic behavior of ω and β but they are obtained differently depending on the coordinate system. As usual, the macroscopic conserved charges are related to the integer multiples of the elementary D1, D5 and P charges, N_1 , N_5 and N_P , and to the quantized angular momenta j_L and j_R by flux integrations

$$\begin{aligned} Q_1 &= \frac{(2\pi)^4 g_s (\alpha')^3}{V_4} N_1, \quad Q_5 = g_s \alpha' N_5, \quad Q_P = \frac{(2\pi)^4 g_s^2 (\alpha')^4}{V_4 R_y^2} N_P, \\ J_{L/R} &= \frac{(2\pi)^4 g_s^2 \alpha'^4}{V_4 R_y} j_{L/R} = \frac{Q_1 Q_5}{R_y N_1 N_5} j_{L,R}, \end{aligned} \quad (4.2.33)$$

where V_4 is the volume of \mathbb{T}^4 .

The equations of motion of these BPS solutions in type IIB on rigid \mathbb{T}^4 have been computed in [96]. They lead to the three layers of BPS equations we derived in the context of $\mathcal{N} = (1, 0)$ six-dimensional Supergravity (4.2.28) and (4.2.29).

Now that everything is settled, one can think about finding solutions to the layers of BPS equations. Despite the linear structure and the assumption of a v -independent base space, the solutions have not yet been solved in a general form as it has been done for 1/8- or 1/4-BPS solutions in five dimensions. Before 2015 [30], the known solutions were the most trivial, such as the solutions uplifted from five dimensions or the two-charge solutions. In this category, we have already studied the BMPV black hole in Section 4.1.2, the smooth multicenter solution in Section 4.1.3 and the round two-charge Supertube solution in 4.1.3.3. As a warm-up, in the next section, we study the supersymmetric six-dimensional black string solutions dual to the BMPV black hole and equivalently seen as the 1/8-BPS D1-D5-P black hole of type IIB on $S^1 \times \mathbb{T}^4$. In Section 4.2.3, we study the 1/4-BPS Supertubes in six dimensions and in type IIB. Based on the pioneer works [103, 96, 97, 30], a generating-technique has been developed to build large families of three-charge 1/8-BPS solutions depending on v and the four coordinates of \mathcal{B} . We detail their construction in Sections 4.2.3 and 4.2.4.

4.2.2 Supersymmetric black string and the BTZ black hole

The BPS equations of six-dimensional $\mathcal{N} = (1, 0)$ Supergravity contain the supersymmetric black-string solution that is dual to the BMPV black hole. Even if the BMPV black hole is already discussed in Section 4.1.2, the six-dimensional uplift has an important role in this thesis, and therefore it is worth writing the solution here and its picture in type IIB on $S^1 \times \mathbb{T}^4$ where the torus is much smaller than the one-sphere. The solution needs only one extra tensor multiplet but we will work in the context of two extra tensor multiplets to be consistent with the overall discussion. The four-dimensional base space is flat \mathbb{R}^4 (4.1.12),

$$ds(\mathcal{B})^2 = ds(\mathbb{R}^4)^2 = d\hat{r}^2 + \hat{r}^2 \left(d\hat{\theta}^2 + \sin^2 \hat{\theta} d\varphi_1^2 + \cos^2 \hat{\theta} d\varphi_2^2 \right).$$

We consider that the black string is located at the origin of the spherical coordinate system of \mathbb{R}^4 . The black string has three electric charges Q_I , no magnetic dipole charges and one non-zero angular

¹⁸We remind that \hat{r} is the radial coordinate of \mathbb{R}^4 (4.1.12). The fields behave as \hat{r}^{-2} compared to ρ^{-1} in the STU model because ρ corresponds to the radial distance of the \mathbb{R}^3 part of the base space.

momentum only, J_L . The six-dimensional metric and the tensor gauge fields (4.2.27) are determined by the following fields

$$\begin{aligned} Z_1 &= 1 + \frac{Q_1}{\hat{r}^2}, & Z_2 &= 1 + \frac{Q_5}{\hat{r}^2}, & Z_4 &= 0, & \mathcal{F} &= -\frac{2Q_P}{\hat{r}^2} \\ \omega &= \frac{\sqrt{2} J_L}{\hat{r}^2} (\sin^2 \hat{\theta} d\varphi_1 + \cos^2 \hat{\theta} d\varphi_2), & \beta &= 0, & \Theta^1 &= \Theta^2 = \Theta^4 = 0. \end{aligned} \quad (4.2.34)$$

The horizon is at $\hat{r} = 0$ and has a S^1 topology. As with the BMPV black hole, the solution has no CTC if the cosmic censorship bound is satisfied

$$Q_1 Q_5 Q_P - J_L^2 = \left(\frac{(2\pi)^4 g_s^2 \alpha'^4}{V_4 R_y} \right)^2 (N_1 N_5 N_P - j_L^2) \geq 0.$$

From the type IIB Ansatz (4.2.30), the singularity is all along the transverse S^1 and the solution corresponds to the D1-D5-P rotating black hole on $S^1 \times \mathbb{T}^4$. The Bekenstein-Hawking entropy is computed via the area of the transverse space at $\hat{r} = 0$ and this gives the same moduli-free entropy as the BMPV solution

$$S = 2\pi \sqrt{N_1 N_5 N_P - j_L^2}.$$

The six-dimensional solution is asymptotically $\mathbb{R}^{1,4} \times S^1$,

$$ds_6^2 \sim -2 du dv + ds(\mathcal{B})^2.$$

In the IR, $\hat{r} \lesssim \sqrt{Q_1 Q_5}$, the metric tends to

$$\begin{aligned} ds_6^2 \sim \sqrt{Q_1 Q_5} \left[\left(\frac{d\hat{r}_{BTZ}}{\hat{r}_{BTZ}} \right)^2 - \hat{r}_{BTZ}^2 dt^2 + \hat{r}_{BTZ}^2 dy^2 + \frac{Q_1 Q_5 Q_P - J_L^2}{Q_1 Q_5} (dt + dy)^2 \right. \\ \left. + d\hat{\theta}^2 + \sin^2 \hat{\theta} \left(d\varphi_1 - \frac{J_L}{Q_1 Q_5} (dt + dy) \right)^2 + \cos^2 \hat{\theta} \left(d\varphi_2 - \frac{J_L}{Q_1 Q_5} (dt + dy) \right)^2 \right], \end{aligned} \quad (4.2.35)$$

where we have introduced $\hat{r}_{BTZ} \equiv \frac{\hat{r}}{\sqrt{Q_1 Q_5}}$. We recognize a S^3 fibration over an *extremal Banados-Teitelboim-Zanelli (BTZ) black hole* [104]. The three-dimensional black hole is characterized by its AdS radius, ℓ_{AdS} , and the left and right temperatures

$$\ell_{AdS} = (Q_1 Q_5)^{\frac{1}{4}}, \quad T_L = \frac{R_y}{2\pi} \frac{\sqrt{Q_1 Q_5 Q_P - J_L^2}}{(Q_1 Q_5)^{3/4}} = \ell_{AdS} \frac{\sqrt{N_1 N_5 N_P - j_L^2}}{2\pi N_1 N_5}, \quad T_R = 0. \quad (4.2.36)$$

A BTZ geometry has an AdS_3 region at $\hat{r}_{BTZ} \gtrsim T_L^2$ where the y -circle grows as a function of \hat{r}_{BTZ} . Then, for $\hat{r}_{BTZ} \lesssim T_L^2$, the y -circle stabilises to a radius $(2\pi T_L)^2$ and the geometry is $AdS_2 \times S^1$ until $\hat{r}_{BTZ} = 0$ where the horizon stands.

For asymptotically-flat D1-D5-P black hole, if $Q_P \sim \{Q_1, Q_5\}$, the $AdS_3 \times S^3$ region has zero size and the overall solution goes directly from the flat asymptotics to the $AdS_2 \times S^1 \times S^3$. The interesting regime of parameters is when $Q_P \ll \{Q_1, Q_5\}$ where the geometry contains all the characteristic of a $BTZ \times S^3$ throat.

One could have also restricted the D1-D5-P black hole to its decoupling limit by removing the “1” in the definition of the fields (4.2.34) which would have transformed (4.2.35) into a strong equality. The six-dimensional part of the asymptotically- AdS_3 D1-D5-P rotating black hole is a S^3 fibration over a BTZ black hole.

4.2.3 Two-charge Supertube

In Section 4.1.3.3, we reviewed the construction of the 1/4-BPS two-charge Supertubes in the context of the STU model. The angle independence restricted the solutions to the round ones. Supertubes can have arbitrary shape and they reproduce exactly the entropy of the D1-D5 system [92, 11–14]. More intriguingly, all solutions are smooth in this D1-D5 frame with an $\text{AdS}_3 \times S^3 \times \mathbb{T}^4$ geometry at the supertube locus.

The two-charge solutions have been initially constructed in the F1-P frame (4.1.41) [105, 90]. The entropy results from the different ways the momentum can be distributed among the various harmonics of the string. A specific supergravity geometry is parametrized by a curve $g_A(v')$ describing its profile in the eight-dimensional transverse space to the string. In this frame, the solutions have no macroscopic horizons and have a singularity corresponding to the string source, which is understood to be a physical source in the theory.

A sequence of S/T-dualities map the solutions to D1-D5 bound states [106, 107]. The string source is mapped to a KKm source, which is a smooth gravitational solution with a topological twist as illustrated in Section 4.1.3.3 for round Supertubes. In this frame, the “auxiliary” profiles $g_A(v')$ do not have any direct geometric meaning but the solutions can be derived with the same intuition. In this thesis, we focus on the subclass of D1-D5 solutions with rigid \mathbb{T}^4 , and then are invariant under the rotations of \mathbb{T}^4 . Moreover, we also construct the solution from a flat base, $\mathcal{B} = \mathbb{R}^4$. Under this assumption, the most general two-charge configuration is given in terms of five functions: four $g_m(v)$ corresponding to the F1 profile in \mathbb{R}^4 and one extra function, denoted $g_5(v)$, describing the F1 profile in a particular direction of \mathbb{T}^4 that plays a special role in the sequence of dualities relating the F1-P and D1-D5 frames. The parameter along the curve is v' and has a periodicity $L = 2\pi \frac{Q_5}{R_y}$. This class of two-charge solutions is written in terms of the Ansatz (4.2.30) and (4.2.27), taking

$$\begin{aligned}
Z_2 &= 1 + \frac{Q_5}{L} \int_0^L \frac{1}{|x_m - g_m(v')|^2} dv', & Z_4 &= -\frac{Q_5}{L} \int_0^L \frac{\dot{g}_5(v')}{|x_m - g_m(v')|^2} dv', \\
Z_1 &= 1 + \frac{Q_5}{L} \int_0^L \frac{|\dot{g}_m(v')|^2 + |\dot{g}_5(v')|^2}{|x_m - g_m(v')|^2} dv', & d_4\gamma_2 &= \star_4 d_4 Z_2, & d_4\delta_2 &= \star_4 d_4 Z_4, \\
A &= -\frac{Q_5}{L} \int_0^L \frac{\dot{g}_n(v') dx^n}{|x_m - g_m(v')|^2} dv', & d_4 B &= -\star_4 d_4 A, \\
\beta &= \frac{-A + B}{\sqrt{2}}, & \omega &= \frac{-A - B}{\sqrt{2}}, & \mathcal{F} &= 0, & \Theta^1 &= \Theta^2 = \Theta^4 = 0,
\end{aligned} \tag{4.2.37}$$

4.2.3.1 Retrieving the round-supertube solution

The round Supertube, derived within the STU model in Section 4.1.3.3, is obtained by taking a circular string profile in the plane (x_1, x_2) and the other components of the profile are set to zero:

$$g_1(v') = a \cos\left(\frac{2\pi v'}{L}\right), \quad g_2(v') = a \sin\left(\frac{2\pi v'}{L}\right), \tag{4.2.38}$$

where a is a free real parameter that gives the radius of the Supertube from a four-dimensional perspective. It is more convenient to work with the spheroidal coordinates that split the two plans (x_1, x_2) and (x_3, x_4) of the base as follows

$$x_1 + ix_2 = \sqrt{r^2 + a^2} \sin \theta e^{i\varphi_1}, \quad x_3 + ix_4 = r \cos \theta e^{i\varphi_2}. \tag{4.2.39}$$

They are related to the spherical \mathbb{R}^4 coordinates $(\hat{r}, \hat{\theta}, \varphi_1, \varphi_2)$ that we have already introduced by

$$\hat{r}^2 = r^2 + a^2 \sin^2 \theta, \quad \hat{r} \cos \hat{\theta} = r \cos \theta.$$

The locus $r = 0$ describes a disk of radius a parameterized by θ and φ_1 with the origin of \mathbb{R}^4 at $(r = 0, \theta = 0)$ while the tube lies at the perimeter of this disk ($r = 0, \theta = \pi/2$). With these coordinates, the flat \mathbb{R}^4 metric is

$$ds(\mathcal{B})^2 = (r^2 + a^2 \cos^2 \theta) \left(\frac{dr^2}{r^2 + a^2} + d\theta^2 \right) + (r^2 + a^2) \sin^2 \theta d\varphi_1^2 + r^2 \cos^2 \theta d\varphi_2^2, \quad (4.2.40)$$

We also introduce the distance to the origin of \mathbb{R}^4

$$\Sigma \equiv r^2 + a^2 \cos^2 \theta. \quad (4.2.41)$$

The fields (4.2.37) give

$$\begin{aligned} Z_1 &= 1 + \frac{Q_1}{\Sigma}, & Z_2 &= 1 + \frac{Q_5}{\Sigma}, & Z_4 &= 0, \\ \omega &= \frac{R_y a^2}{\sqrt{2} \Sigma} (\sin^2 \theta d\varphi_1 + \cos^2 \theta d\varphi_2), & \beta &= \frac{R_y a^2}{\sqrt{2} \Sigma} (\sin^2 \theta d\varphi_1 - \cos^2 \theta d\varphi_2), \\ \mathcal{F} &= 0, & \Theta^1 &= \Theta^2 = \Theta^4 = 0. \end{aligned} \quad (4.2.42)$$

The relation between the radius R_y , the two charges Q_I and the parameter a is

$$R_y = \frac{\sqrt{Q_1 Q_5}}{a}. \quad (4.2.43)$$

This relation is equivalent to the regularity condition imposed by the Denef equation in the STU model (4.1.63). One can push the parallel a little further by changing to the Gibbons-Hawking system of coordinates. We find that the electric charges, l^1 and l^2 , and the magnetic dipole charge k^3 introduced in (4.1.61) are related to the two charges Q_I and R_y as

$$l^1 = \frac{Q_1}{4}, \quad l^2 = \frac{Q_5}{4}, \quad k^3 = \frac{R_y}{2}.$$

The magnetic dipole charge is only given by the radius R_y since it corresponds to a KKm charge in this frame.

4.2.3.2 An example of wiggly Supertube

There is a large diversity of supertube string profiles. In this thesis, we focus on the two-charge configurations that have a circular profile in \mathbb{R}^4 , but can have a non-trivial $g_5(v')$ component on \mathbb{T}^4 :

$$g_1(v') = a \cos\left(\frac{2\pi v'}{L}\right), \quad g_2(v') = a \sin\left(\frac{2\pi v'}{L}\right), \quad g_5(v') = -\frac{b}{k} \sin\left(\frac{2\pi k v'}{L}\right), \quad (4.2.44)$$

where b is an extra real coefficient and k is a positive integer. The profile induces the following fields

$$\begin{aligned} Z_1 &= \frac{R_y^2}{Q_5 \Sigma} \left[a^2 + \frac{b^2}{2} + \frac{b^2}{2} \left(\frac{a^2 \sin^2 \theta}{r^2 + a^2} \right)^k \cos(2k\varphi_1) \right], & Z_4 &= \frac{R_y b}{\Sigma} \left(\frac{a^2 \sin^2 \theta}{r^2 + a^2} \right)^{\frac{k}{2}} \cos(k\varphi_1), \\ Z_2 &= \frac{Q_5}{\Sigma}, & \beta &= \frac{R_y a^2}{\sqrt{2} \Sigma} (\sin^2 \theta d\varphi_1 - \cos^2 \theta d\varphi_2), & \omega &= \frac{R_y a^2}{\sqrt{2} \Sigma} (\sin^2 \theta d\varphi_1 + \cos^2 \theta d\varphi_2), \\ \mathcal{F} &= 0, & \Theta^1 &= \Theta^2 = \Theta^4 = 0, \end{aligned} \quad (4.2.45)$$

where we are restricting to the decoupling region and hence have dropped the “1” in Z_1 and Z_2 . It is fairly straightforward to check that the ten-dimensional geometry is asymptotically $\text{AdS}_3 \times S^3 \times \mathbb{T}^4$ under the change of coordinates

$$\widetilde{\varphi}_1 = \varphi_1 - \frac{t}{R_y}, \quad \widetilde{\varphi}_2 = \varphi_2 - \frac{y}{R_y}, \quad (4.2.46)$$

where t and y are related to u and v in (4.2.31). This corresponds to a boost along φ_1 and a spectral flow transformation on φ_2 . The relation between the parameters a , b , the charges Q_I , and the S^1 radius R_y is now

$$R_y = \sqrt{\frac{Q_1 Q_5}{a^2 + \frac{b^2}{2}}}. \quad (4.2.47)$$

We note the appearance of a non-trivial, φ_1 -dependent Z_4 , in addition to a φ_1 -dependent deformation in Z_1 at second order in b . The function Z_2 remains unchanged. It is also very interesting to note that the combination $Z_1 Z_2 - Z_4^2$ is deformed at order b^2 , but the form of the φ_1 -dependent terms in Z_4 and Z_1 is such that $Z_1 Z_2 - Z_4^2$ is φ_1 -independent. This cancelation is called *coiffuring*. As a result, the six-dimensional metric does not depend on φ_1 . This is very similar to the mechanism that plays a central role in obtaining neutral black hole microstate geometries [108] and smooth “coiffured” black rings [109].

4.2.3.3 The CFT description

For the moment, we have restrained the discussion of brane bound states to a supergravity description. The geometries we have constructed have an $\text{AdS}_3 \times S^3 \times \mathbb{T}^4$ decoupling limit. According to the AdS/CFT duality, they admit a dual description in terms of a two-dimensional superconformal field theory (SCFT), commonly called the D1-D5 CFT, with a large central charge [110, 111]

$$c = 6N \equiv 6N_1 N_5.$$

We will be very brief in the description of the D1-D5 CFT since we only want to sketch the overall picture and understand how the CFT description can help us generate three-charge solutions from two-charge seeds with known CFT duals. We refer the interested reader to the exhaustive discussion in [30] that we summarize here.

The D1-D5 CFT has $\mathcal{N} = (4, 4)$ supersymmetries, a $SL(2, \mathbb{R})_L \times SL(2, \mathbb{R})_R$ symmetry and a \mathcal{R} -symmetry $SO(4)_{\mathcal{R}} \simeq SU(2)_L \times SU(2)_R$. The anomaly-free part of the small superconformal algebra contains a finite number of generators. The $SU(2)$ factors give algebra with bosonic generators $\{J_0^i, \tilde{J}_0^i\}$, $i = \{\pm, 3\}$, and correspond to rotations of S^3 in the gravity side. The $SL(2, \mathbb{R})$ algebra are generated by the bosonic operators $\{L_0, L_{\pm 1}, \tilde{L}_0, \tilde{L}_{\pm 1}\}$, and correspond to conformal transformations in AdS_3 . One can extend these transformations to the full chiral algebra with $\{J_{-n}^i, \tilde{J}_{-n}^i, L_{-n}, \tilde{L}_{-n}\}$, $n \in \mathbb{Z}$ as discussed, from the gravity point of view, in [112].

At the point of the moduli space where $g_s N \rightarrow 0$, the D1-D5 CFT is described by a non-linear sigma model with target space the orbifold $(\mathbb{T}^4)^N / S_N$. This theory splits into two sectors for each chirality: a Neveu-Schwarz and a Ramond sector, connected by a spectral flow transformation. The R-R supersymmetric sector of the theory contains the states that are relevant for the statistical ensemble of states describing the D1-D5-P black hole [113, 97].

It is convenient to think of the CFT orbifold point as N distinct *strings* of length one, on each of which live four bosons and four fermions. The R-R ground states are formed by joining strings into *strands* of arbitrary length by twist operators. Moreover, they can be charged under the \mathcal{R} -symmetry and are eigenstates of (J_0^3, \tilde{J}_0^3) with half-integer eigenvalues. Each strand of the R-R ground states then has eigenvalues (j_ℓ, \tilde{j}_ℓ) under the reduction of (J_0^3, \tilde{J}_0^3) on that strand. To form a ground state, the only possible quantum numbers are $j_\ell, \tilde{j}_\ell = -\frac{1}{2}, 0, \frac{1}{2}$. We then introduce the ket notation for a strand

$$|j_\ell \tilde{j}_\ell\rangle_k, \quad j_\ell, \tilde{j}_\ell = -, 0, +,$$

where k is the length of the single strand.

We are interested in the CFT duals of 1/4-BPS geometries determined by a periodic profile $g_i(v')$ in \mathbb{R}^5 which are invariant under \mathbb{T}^4 rotations. They are R-R ground states and are constructed according to the following dictionary [114, 107, 30]:

- The mode numbers of the Fourier expansion of $g_i(v')$ correspond to the lengths of the strands.
- The different non-zero components, $i = 1, \dots, 5$, correspond to different quantum numbers j_ℓ, \tilde{j}_ℓ .
- The amplitudes of the Fourier modes are related to the numbers of the corresponding strands.

This can be summarized in the following duality table

$$\begin{aligned}
 g_1 + i g_2 &= \frac{a}{k} e^{\pm i \frac{2\pi k v'}{L}} & \longleftrightarrow & \prod_{N_{\pm\pm}} |\pm \pm\rangle_k, \\
 g_3 + i g_4 &= \frac{a}{k} e^{\pm i \frac{2\pi k v'}{L}} & \longleftrightarrow & \prod_{N_{\pm\mp}} |\pm \mp\rangle_k, \\
 g_5 &= -\frac{b}{k} \sin\left(\frac{2\pi k v'}{L}\right) & \longleftrightarrow & \prod_{N_k} |00\rangle_k,
 \end{aligned} \tag{4.2.48}$$

where $N_{\pm\pm}, N_{\pm\mp} \sim a^2$ and $N_k \sim b^2$ are the numbers of $|\pm \pm\rangle_k, |\pm \mp\rangle_k$ and $|00\rangle_k$ in the configuration taking into account that the total “strand budget” is limited to N . The CFT duals of the round Supertube and the round Supertube with a non-trivial profile on \mathbb{T}^4 studied above are

$$|\text{round}\rangle = \prod_N |++\rangle_1, \quad |\text{round} + g_5\rangle = \prod_{N_{++}} |++\rangle_1 \cdot \prod_{N_k} |00\rangle_k, \tag{4.2.49}$$

For the latter, the “strand budget” constrains N_{++} and N_k to satisfy

$$N_{++} + k N_k = N_1 N_5 \equiv N, \tag{4.2.50}$$

This expression is the CFT dual of the supergravity regularity condition (4.2.47).

Although the regime of validity of the CFT orbifold point, $g_s N \ll 1$, is far outside the regime where Supergravity is a reliable approximation, $g_s N \gg 1$, it remains a very valuable framework for describing states. In particular, unbroken supersymmetries make certain useful quantities invariant under change of moduli: the conformal dimensions of states preserving more than four supercharges, their three-point correlators [115] and four-point correlators with states preserving more than eight supercharges are protected. The matching of those quantities in the two descriptions gives a non-trivial test for the AdS/CFT correspondence. Moreover, adding momentum-carrying perturbations to some two-charge R-R ground states using appropriate generators of the superconformal algebra is well-controlled in the CFT side. On the gravity side, each CFT transformation is realized by a diffeomorphism that is non-trivial at the AdS boundary. This program has been initiated in [103] and had brought many successes in the construction of large families of three-charge smooth six-dimensional solutions since then [30, 98–101, 31, 28].

4.2.4 Momentum-generating technique

Three-charge solutions can be obtained by adding momentum-carrying perturbations to some two-charge Supertubes. The Supertube will be called the *seed solution*. This has the benefit to keep track of their CFT dual states and also to give important clues for the construction of the geometries in Supergravity. By acting with chiral algebra generators of the left-moving sector $SU(2)_L \times SL(2, \mathbb{R})_L$, the R-R ground states will be excited with P charge and will still preserve four of the eight supersymmetries.

In this thesis, the seed solutions are the two-charge Supertubes that are invariant under \mathbb{T}^4 rotations. However, they are allowed to have a generic Fourier expansion in $g_5(v')$

$$g_1(v') + i g_2(v') = a e^{i \frac{2\pi v'}{L}}, \quad g_5(v') = - \sum_i \frac{b_i}{k_i} \sin\left(\frac{2\pi k_i v'}{L}\right). \quad (4.2.51)$$

According to (4.2.48), their CFT duals at the orbifold point are

$$\prod_{N_{++}} |++\rangle_1 \cdot \prod_i \prod_{N_{k_i}} |00\rangle_{k_i}. \quad (4.2.52)$$

The momentum perturbations are obtained by applying m_i times with J_{-1}^+ and n_i times $L_{-1} - J_{-1}^3$ on each $|00\rangle_{k_i}$. In the CFT side, their strand configurations are easy to derive:

$$\prod_{N_{++}} |++\rangle_1 \cdot \prod_i \prod_{N_{k_i}, m_i, n_i} \frac{(J_{-1}^+)^{m_i}}{m_i!} \frac{(L_{-1} - J_{-1}^3)^{n_i}}{n_i!} |00\rangle_{k_i}. \quad (4.2.53)$$

The product is well-defined because $L_{-1} - J_{-1}^3$ and J_{-1}^+ commute. The main goal is to dualize those perturbations in the gravity side. The cheapest procedure is to translate everything in the NS-NS sector. The NS-NS generators belong to the anomaly-free part of the small superconformal algebra and have a simple picture as transformations in $\text{AdS}_3 \times S^3$. In the gravity side, the map from R-R to NS-NS is done by a coordinate change (4.2.46), while it corresponds to spectral flow using J^3 and \tilde{J}^3 in the CFT:

$$\begin{aligned} J_{-1}^+ &\xrightarrow{R \rightarrow NS} J_0^+, \\ L_{-1} - J_{-1}^3 &\xrightarrow{R \rightarrow NS} L_{-1}. \end{aligned} \quad (4.2.54)$$

The generators of the small algebra correspond to the following transformations in $\text{AdS}_3 \times S^3$

$$\begin{aligned} L_0 &= \frac{i R_y}{2} (\partial_t + \partial_y), \\ L_{\pm 1} &= i e^{\pm \frac{i}{R_y} (t+y)} \left[-\frac{R_y}{2} \left(\frac{r}{\sqrt{r^2 + a^2}} \partial_t + \frac{\sqrt{r^2 + a^2}}{r} \partial_y \right) \pm \frac{i}{2} \sqrt{r^2 + a^2} \partial_r \right], \\ J_0^3 &= -\frac{i}{2} (\partial_{\tilde{\varphi}_1} + \partial_{\tilde{\varphi}_2}), \quad J_0^\pm = \frac{i}{2} e^{\pm i(\tilde{\varphi}_1 + \tilde{\varphi}_2)} (\mp i \partial_\theta + \cot \theta \partial_{\tilde{\varphi}_1} - \tan \theta \partial_{\tilde{\varphi}_2}). \end{aligned} \quad (4.2.55)$$

where t and y are related to u and v in (4.2.31). Thus, the solution-generating technique proceeds as follows in the gravity side:

- Start with a six-dimensional and ten-dimensional specific supertube seed.
- Change coordinates to the NS-NS sector (4.2.46).
- Act on the fields with the NS-NS generators (4.2.55) at linear order.
- Change back the coordinates to the R-R sector.
- Recast the fields into a new Ansatz.

In the next section, we review one of the greatest success of this construction technique, which is the construction of Superstrata.

4.2.5 Superstrata

Superstrata are 1/8-BPS solutions of six-dimensional Supergravity with 2 extra tensor multiplets or ten-dimensional type IIB Supergravity with D5-branes wrapping a S^1 and an internal rigid \mathbb{T}^4 , D1-branes wrapping the S^1 and left-moving momentum P charges along the common S^1 . They are constructed by performing the momentum-generating technique above on asymptotically- AdS_3 Supertubes corresponding to the string profiles (4.2.51). Their CFT duals at the orbifold point are (4.2.53).

4.2.5.1 Zeroth-layer and first-layer fields

At linear order in b_i , only (Z_4, Θ^4) is perturbed by the momentum-generating technique. However, thanks to the linearity of the first layer of BPS equations (4.2.28), one can reproduce the perturbation of (Z_4, Θ^4) in the pairs (Z_1, Θ^2) and (Z_2, Θ^1) and keep the zeroth-layer fields β and $ds(\mathcal{B})^2$ unchanged. Therefore, a very general set of zeroth-layer and first-layer fields is given by the four-dimensional metric (4.2.40) and [30, 98–101]

$$\begin{aligned} Z_1 &= \frac{Q_1}{\Sigma} + \sum_i b_1^{k_i, m_i, n_i} \tilde{z}_{k_i, m_i, n_i}, & Z_2 &= \frac{Q_5}{\Sigma} + \sum_i b_2^{k_i, m_i, n_i} \tilde{z}_{k_i, m_i, n_i}, & Z_4 &= \sum_i b_4^{k_i, m_i, n_i} \tilde{z}_{k_i, m_i, n_i}, \\ \Theta^1 &= \sum_i b_2^{k_i, m_i, n_i} \tilde{\vartheta}_{k_i, m_i, n_i}, & \Theta^2 &= \sum_i b_1^{k_i, m_i, n_i} \tilde{\vartheta}_{k_i, m_i, n_i}, & \Theta^4 &= \sum_i b_4^{k_i, m_i, n_i} \tilde{\vartheta}_{k_i, m_i, n_i}, \\ \beta &= \frac{R_y a^2}{\sqrt{2} \Sigma} (\sin^2 \theta d\varphi_1 - \cos^2 \theta d\varphi_2), \end{aligned} \quad (4.2.56)$$

where the $b_I^{k, m, n}$'s define a set of Fourier coefficients, while $\tilde{z}_{k, m, n}$ and $\tilde{\vartheta}_{k, m, n}$ are respectively scalars and two-forms with quantum numbers (k, m, n) depending on v and the coordinates of the four-dimensional flat base space as follows

$$\begin{aligned} \tilde{z}_{k, m, n} &= R_y \frac{\Delta_{k, m, n}}{\Sigma} \cos v_{k, m, n}, \\ \tilde{\vartheta}_{k, m, n} &= -\sqrt{2} \Delta_{k, m, n} \left[\left((m+n) r \sin \theta + n \left(\frac{m}{k} - 1 \right) \frac{\Sigma}{r \sin \theta} \right) \Omega^{(1)} \sin v_{k, m, n} \right. \\ &\quad \left. + \left(m \left(\frac{n}{k} + 1 \right) \Omega^{(2)} + \left(\frac{m}{k} - 1 \right) n \Omega^{(3)} \right) \cos v_{k, m, n} \right], \end{aligned}$$

with

$$\begin{aligned} \Delta_{k, m, n} &\equiv \left(\frac{a}{\sqrt{r^2 + a^2}} \right)^k \left(\frac{r}{\sqrt{r^2 + a^2}} \right)^n \cos^m \theta \sin^{k-m} \theta, \\ v_{k, m, n} &\equiv (m+n) \frac{\sqrt{2} v}{R_y} + (k-m) \varphi_1 - m \varphi_2. \end{aligned} \quad (4.2.57)$$

The Ω 's are the basis of self-dual 2-forms on the base space. They have been early introduced in the context of five-dimensional BPS solutions (4.1.17) for generic Gibbons-Hawking base space. In the spheroidal coordinate system of \mathbb{R}^4 , they give

$$\begin{aligned} \Omega^{(1)} &\equiv \frac{dr \wedge d\theta}{(r^2 + a^2) \cos \theta} + \frac{r \sin \theta}{\Sigma} d\varphi_1 \wedge d\varphi_2, \\ \Omega^{(2)} &\equiv \frac{r}{r^2 + a^2} dr \wedge d\varphi_2 + \tan \theta d\theta \wedge d\varphi_1, \\ \Omega^{(3)} &\equiv \frac{dr \wedge d\varphi_1}{r} - \cot \theta d\theta \wedge d\varphi_2. \end{aligned} \quad (4.2.58)$$

The complicated dependence on the six-dimensional coordinates shows how non-trivial it would have been to solve the first layer of BPS equations directly. However, now, it is fairly straightforward to check that the fields (4.2.57) satisfy the equations (4.2.28)

$$*_4 \mathcal{D} \tilde{z}_{k, m, n} = \mathcal{D} \tilde{\vartheta}_{k, m, n}, \quad \mathcal{D} *_4 \mathcal{D} \tilde{z}_{k, m, n} = -\tilde{\vartheta}_{k, m, n} \wedge d_4 \beta, \quad \tilde{\vartheta}_{k, m, n} = *_4 \tilde{\vartheta}_{k, m, n}. \quad (4.2.59)$$

For the moment, the $b_I^{k, m, n}$ are arbitrary. They will be related to each other by coiffuring constraints. The solutions with several triplets of quantum numbers as in (4.2.56) are called *multi-mode Superstrata*.

A very interesting subclass is the solutions with only one triplet of mode numbers (k, m, n) called *single-mode Superstrata*. Their first-layer fields are

$$\begin{aligned} Z_1 &= \frac{Q_1}{\Sigma} + b_1 \frac{R_y}{2Q_5} \tilde{z}_{2k,2m,2n}, & Z_2 &= \frac{Q_5}{\Sigma}, & Z_4 &= b_4 \tilde{z}_{k,m,n}, \\ \Theta^1 &= 0, & \Theta^2 &= b_1 \frac{R_y}{2Q_5} \tilde{\vartheta}_{2k,2m,2n}, & \Theta^4 &= b_4 \tilde{\vartheta}_{k,m,n}, \end{aligned} \quad (4.2.60)$$

Note that we have only excited the pairs (Z_1, Θ^2) and (Z_4, Θ^4) , and that the former has twice the mode numbers of the latter. As we will see, this choice simplifies the second layer and makes the coiffuring relatively easy. The modes in (Z_1, Θ^2) represent a secondary modes will be fixed by the smoothness of the supergravity solution.

4.2.5.2 Second-layer fields

The second layer of BPS equations (4.2.29) is sourced quadratically by the first-layer fields. Even if the homogeneous equations are fairly easy to solve, the source terms that may depend on v and the four coordinates of \mathbb{R}^4 make the task of finding generic solutions for the second layer very complex. The second layer has been generically solved for single-mode Superstrata [30, 98]. However, finding generic solutions for two-mode or multi-mode Superstrata is still work in progress. We will detail a significant breakthrough in that direction in Chapter 7 [28].

From now on, we restrict the discussion to single-mode Superstrata (4.2.60). The second-layer sources have both a non-oscillating “RMS” component and an oscillating part that depends only upon $v_{2k,2m,2n}$. Experience shows that such oscillating sources generically lead to singular angular momentum vectors and so we remove these terms by “coiffuring.” That is, the Fourier coefficient of the oscillating source is proportional to $b_1 - b_4^2$ and so we take:

$$b_1 = b_4^2. \quad (4.2.61)$$

The solution for ω and \mathcal{F} is now given by the sum of the seed supertube solution (4.2.45) and the solution for the new pieces¹⁹:

$$\omega = \omega_0 + \tilde{\omega}_{k,m,n}, \quad \mathcal{F} = 0 + \tilde{\mathcal{F}}_{k,m,n}. \quad (4.2.62)$$

The equations (4.2.29) for $\tilde{\omega}_{k,m,n}$ and $\tilde{\mathcal{F}}_{k,m,n}$ reduce to

$$\begin{aligned} d_4 \tilde{\omega}_{k,m,n} + *_4 d_4 \tilde{\omega}_{k,m,n} + \tilde{\mathcal{F}}_{k,m,n} d_4 \beta &= \sqrt{2} b_4^2 R_y \frac{\Delta_{2k,2m,2n}}{\Sigma} \left(\frac{m(k+n)}{k} \Omega^{(2)} - \frac{n(k-m)}{k} \Omega^{(3)} \right), \\ \mathcal{L} \tilde{\mathcal{F}}_{k,m,n} &= \frac{4 b_4^2}{(r^2 + a^2) \cos^2 \theta \Sigma} \left[\left(\frac{m(k+n)}{k} \right)^2 \Delta_{2k,2m,2n} + \left(\frac{n(k-m)}{k} \right)^2 \Delta_{2k,2m+2,2n-2} \right], \end{aligned} \quad (4.2.63)$$

where \mathcal{L} is the scalar Laplacian on the base space \mathcal{B} , $\mathcal{L} = - *_4 d_4 *_4 d_4$:

$$\mathcal{L} F \equiv \frac{1}{r \Sigma} \partial_r (r(r^2 + a^2) \partial_r F) + \frac{1}{\Sigma \sin \theta \cos \theta} \partial_\theta (\sin \theta \cos \theta \partial_\theta F). \quad (4.2.64)$$

Note that these $\tilde{\mathcal{F}}_{k,m,n}$ and $\tilde{\omega}_{k,m,n}$ depend on the mode numbers but do not fluctuate themselves: coiffuring means that the metric only responds to the RMS values of the fluctuating modes.

Since the right-hand side of the first line in (4.2.63) has no component in the $\Omega^{(1)}$ direction, we can set the legs of $\tilde{\omega}_{k,m,n}$ along dr and $d\theta$ to be zero and take:

$$\tilde{\omega}_{k,m,n} \equiv \tilde{\mu}_{k,m,n} (d\varphi_2 + d\varphi_1) + \tilde{\zeta}_{k,m,n} (d\varphi_2 - d\varphi_1), \quad (4.2.65)$$

¹⁹We renamed the seed-solution one-form ω by ω_0 for obvious reason of notation.

for some functions $\tilde{\mu}_{k,m,n}$ and $\tilde{\zeta}_{k,m,n}$. The scalars, $\tilde{\mu}_{k,m,n}$ and $\tilde{\zeta}_{k,m,n}$, can be solved separately by defining

$$\tilde{\mu}_{k,m,n}^S \equiv \tilde{\mu}_{k,m,n} + \frac{R_y}{4\sqrt{2}} \frac{r^2 + a^2 \sin^2 \theta}{\Sigma} \tilde{\mathcal{F}}_{k,m,n} + \frac{R_y b_4^2}{4\sqrt{2}} \frac{\Delta_{2k,2m,2n}}{\Sigma}, \quad (4.2.66)$$

Then $\tilde{\mu}_{k,m,n}^S$ satisfies

$$\mathcal{L} \tilde{\mu}_{k,m,n}^S = \frac{R_y b_4^2}{\sqrt{2}} \frac{1}{(r^2 + a^2) \cos^2 \theta \Sigma} \left(\frac{(k-m)^2 (k+n)^2}{k^2} \Delta_{2k,2m+2,2n} + \frac{(nm)^2}{k^2} \Delta_{2k,2m,2n-2} \right), \quad (4.2.67)$$

and $\tilde{\zeta}_{k,m,n}$ is determined by ($s_\theta = \sin \theta$, $c_\theta = \cos \theta$)

$$\begin{aligned} \partial_r \tilde{\zeta}_{k,m,n} &= \frac{r^2 \cos 2\theta - a^2 s_\theta^2}{r^2 + a^2 s_\theta^2} \partial_r \tilde{\mu}_{k,m,n} - \frac{r \sin 2\theta}{r^2 + a^2 s_\theta^2} \partial_\theta \tilde{\mu}_{k,m,n} \\ &\quad + \frac{\sqrt{2} R_y r}{\Sigma (r^2 + a^2 s_\theta^2)} \left[b_4^2 \left(m s_\theta^2 + n c_\theta^2 - \frac{mn}{k} \cos 2\theta \right) \Delta_{2k,2m,2n} - \frac{a^2 (2r^2 + a^2) s_\theta^2 c_\theta^2}{\Sigma} \tilde{\mathcal{F}}_{k,m,n} \right], \\ \partial_\theta \tilde{\zeta}_{k,m,n} &= \frac{r(r^2 + a^2) \sin 2\theta}{r^2 + a^2 s_\theta^2} \partial_r \tilde{\mu}_{k,m,n} + \frac{r^2 \cos 2\theta - a^2 s_\theta^2}{r^2 + a^2 s_\theta^2} \partial_\theta \tilde{\mu}_{k,m,n} \\ &\quad + \frac{R_y \sin 2\theta}{\sqrt{2} \Sigma (r^2 + a^2 s_\theta^2)} \left[b_4^2 \left(-mr^2 + n(r^2 + a^2) - \frac{mn}{k} (2r^2 + a^2) \right) \Delta_{2k,2m,2n} \right. \\ &\quad \left. + \frac{a^2 r^2 (r^2 + a^2) \cos 2\theta}{\Sigma} \tilde{\mathcal{F}}_{k,m,n} \right]. \end{aligned} \quad (4.2.68)$$

To solve the equations for $\tilde{\mathcal{F}}_{k,m,n}$ and $\tilde{\mu}_{k,m,n}^S$, we find the generating function $F_{2k,2m,2n}$ that solves the equation

$$\mathcal{L} F_{2k,2m,2n} = \frac{\Delta_{2k,2m,2n}}{(r^2 + a^2) \cos^2 \theta \Sigma}. \quad (4.2.69)$$

The solution to this problem is given by

$$F_{2k,2m,2n} = - \sum_{j_1, j_2, j_3=0}^{j_1+j_2+j_3 \leq k+n-1} \binom{j_1+j_2+j_3}{j_1, j_2, j_3} \frac{\binom{k+n-j_1-j_2-j_3-1}{k-m-j_1, m-j_2-1, n-j_3}^2}{\binom{k+n-1}{k-m, m-1, n}^2} \frac{\Delta_{2(k-j_1-j_2-1), 2(m-j_2-1), 2(n-j_3)}}{4(k+n)^2 (r^2 + a^2)}, \quad (4.2.70)$$

where

$$\binom{j_1+j_2+j_3}{j_1, j_2, j_3} \equiv \frac{(j_1+j_2+j_3)!}{j_1! j_2! j_3!}. \quad (4.2.71)$$

In terms of $F_{2k,2m,2n}$, the form of $\tilde{\mathcal{F}}_{k,m,n}$ and $\tilde{\mu}_{k,m,n}$ for general k, m, n is

$$\begin{aligned} \tilde{\mathcal{F}}_{k,m,n} &= 4 b_4^2 \left[\frac{m^2 (k+n)^2}{k^2} F_{2k,2m,2n} + \frac{n^2 (k-m)^2}{k^2} F_{2k,2m+2,2n-2} \right], \\ \tilde{\mu}_{k,m,n} &= \frac{R_y b_4^2}{\sqrt{2}} \left[\frac{(k-m)^2 (k+n)^2}{k^2} F_{2k,2m+2,2n} + \frac{m^2 n^2}{k^2} F_{2k,2m,2n-2} - \frac{\Delta_{2k,2m,2n}}{4 \Sigma} \right] \\ &\quad - R_y \frac{r^2 + a^2 \sin^2 \theta}{4\sqrt{2} \Sigma} \tilde{\mathcal{F}}_{k,m,n} + \frac{R_y b^2}{4\sqrt{2} \Sigma}. \end{aligned} \quad (4.2.72)$$

In this expression for $\tilde{\mathcal{F}}_{k,m,n}$ and $\tilde{\mu}_{k,m,n}$ it should be understood that, when the coefficient of one of the F functions is zero, the term is zero. The term proportional to b in the last line of (4.2.72) is a harmonic piece that we can freely add to the solution of the Poisson equation for $\tilde{\mu}_{k,m,n}^S$. Once $\tilde{\mathcal{F}}_{k,m,n}$ and $\tilde{\mu}_{k,m,n}$ are determined, $\tilde{\zeta}_{k,m,n}$ can be found by integrating (4.2.68) on a case-by-case basis. The coefficient b will be fixed by regularity in the next subsection.

4.2.5.3 Regularity

Generic solutions to the BPS equations are not necessarily regular. Much of the singular behavior is already removed by coiffuring the modes in the sources for the second layer. However, there is still a final step in which harmonic solutions (zero-modes) are chosen so as to cancel any remaining singular behaviour. Singularities typically occur at the Supertube and where coordinates degenerate. This means one should start by examining $r = 0$, $\theta = 0$ where the whole angular S^3 shrinks and $r = 0$, $\theta = \pi/2$ at the supertube locus.

Since one does not have the generic form of multi-mode Superstrata, we discuss the regularity of the single-mode solutions derived above. According to [30, 101], to remove the singularities one should require $\tilde{\mu}_{k,m,n}$ and $\tilde{\zeta}_{k,m,n}$ to vanish at $r = 0$, $\theta = 0$. This fixes the constant, b , in $\tilde{\mu}_{k,m,n}$ to be

$$b = b_4 \left[\binom{k}{m} \binom{k+n-1}{n} \right]^{-\frac{1}{2}}, \quad (4.2.73)$$

and the same condition for $\tilde{\zeta}_{k,m,n}$ fixes the integration constant of (4.2.68). By examining the metric near the supertube locus one finds that the regularity condition is identical to the one obtained for the seed supertube solution (4.2.47):

$$\frac{Q_1 Q_5}{R_y^2} = a^2 + \frac{b^2}{2}. \quad (4.2.74)$$

4.2.5.4 Conserved charges

The superstratum solutions described above are asymptotic to $\text{AdS}_3 \times S^3$ from a six-dimensional perspective. The conserved charges can be extracted from the large-distance behavior of the scalars Z_1 , Z_2 and Z_4 and the one-forms β and ω (4.2.32). The fluctuating modes fall off much faster than the charge monopoles and so the D-brane charges Q_1 and Q_5 , given by the asymptotic behavior of Z_1 and Z_2 do not change compared to the seed Supertube.

The momentum charge is derived from the large-distance behavior of \mathcal{F} (4.2.32). The left and right five-dimensional angular momenta of the solutions are computed from the $d\varphi_1 d\varphi_2$ component of the metric which can be obtained by looking at the $d\varphi_1 + d\varphi_2$ legs of the one-form $\beta + \omega$. We have the generic expressions

$$\beta_{\varphi_1} + \beta_{\varphi_2} + \omega_{\varphi_1} + \omega_{\varphi_2} \sim \sqrt{2} \frac{J_L - J_R \cos 2\theta}{r^2}, \quad (4.2.75)$$

which gives

$$J_L = \frac{R_y}{2} \left(a^2 + \frac{m}{k} b^2 \right), \quad J_R = \frac{R_y}{2} a^2, \quad Q_P = \frac{m+n}{2k} b^2. \quad (4.2.76)$$

Finally, one can use (4.2.33) to derive their quantized values. This gives

$$j_L = \frac{\mathcal{N}}{2} \left(a^2 + \frac{m}{k} b^2 \right), \quad j_R = \frac{\mathcal{N}}{2} a^2, \quad N_P = \frac{\mathcal{N}}{2} \frac{m+n}{k} b^2, \quad (4.2.77)$$

where \mathcal{N} is defined by

$$\mathcal{N} \equiv \frac{R_y^2 N_1 N_5}{Q_1 Q_5}. \quad (4.2.78)$$

These solutions are in the black-hole regime if the cosmic censorship bound is satisfied $N_1 N_5 N_P - j_L^2 > 0$, which happens if

$$\frac{b^2}{a^2} > \frac{k}{n + \sqrt{(k-m+n)(m+n)}}. \quad (4.2.79)$$

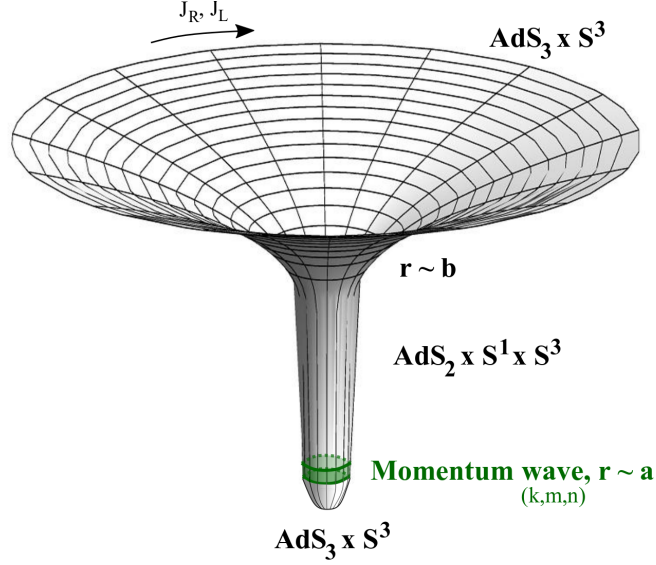


Figure 4.4: The six-dimensional geometry of Superstrata

4.2.5.5 The three regions

As already said, the fluctuations modes in the first-layer fields decay much faster than the charge monopoles. However, they are summed in the second-layer fields, therefore they induce a leading behavior that results in a left-moving momentum charge and an increase of the left angular momentum. Moreover, one can show that the subleading contributions are localized at $r \sim a$. Thus at $r \gg a$ the geometry is determined by the leading behaviors dictated by the conserved charges.

In the regime of parameter where $\frac{b}{a} \gg 1$ and $a \ll 1$, J_R is negligible and the superstratum geometries approximate the D1-D5-P black-hole geometry (4.2.35) at $r \gg a$. In this region, the single-mode Superstrata are asymptotically $BTZ \times S^3$. At $r \sim a$, the geometries are deformed by a momentum wave which depends on v and the four coordinates of the base space. For $r \ll a$, the fluctuating modes are once again subleading and we retrieve the IR geometry of the smooth supertube seed. Thus, in the IR, the geometry caps off smoothly as $AdS_3 \times S^3$. We have depicted those three regions in Fig.4.4.

Although it becomes more complicated for multi-mode Superstrata, those features are also present and the three-dimensional geometry can be decomposed in three pieces: a BTZ region, an intermediate momentum-wave region and a smooth AdS_3 cap.

Superstrata form a large family of solutions which look like the D1-D5-P black hole and which cap off smoothly in the IR. They determine a large phase space of microstate geometries of the D1-D5-P black hole.

There are seven free parameters for the single-mode Superstratum: Q_1, Q_5, k, m, n, a and b and there are five bulk charges: Q_1, Q_5, Q_P, j_L and j_R as well as the regularity condition (4.2.74), and so there can be, at most, one free “rational” parameter. Indeed, suppose Q_1 and Q_5 are fixed, and note that j_R fixes a . The regularity condition (4.2.74) then fixes b , which means that j_L fixes $\frac{m}{k}$ and so Q_P fixes $\frac{n}{k}$. Ignoring the issues of rational arithmetic, one can take k to be the remaining free parameter. Thus, for a given D1-D5-P black hole, single-mode Superstrata describe a one-parameter family of black hole microstates.

The simplest classes of single-mode solutions that have been studied to date are the $(1, 0, n)$ [99, 116, 117, 25, 29], $(2, 1, n)$ [100, 116, 28] and $(k, 0, 1)$ [118] families. They have brought several breakthrough in our understanding of microstate geometries with the same mass, charges and angular momenta of

the three-charge supersymmetric black hole.

4.3 Three-charge non-BPS solutions

In the two previous sections, unbroken supersymmetries were used to considerably simplify the search for classical solutions to Einstein equations. This has led to many breakthroughs in the understanding of supersymmetric black holes and their microstates in String Theory as brane bound states. However, to describe realistic solutions, one needs to get away from supersymmetry and extremality. Most of the solution-generating technique consists of starting with a class of well-known solutions, generally supersymmetric and extremal, and deforming the geometries with boosts and non-extremal well-controlled transformations [119–122, 113].

In this section, we focus only on some non-BPS solutions and their properties rather than the techniques used to generate them. In Section 4.3.1, we review the extremal Kerr-Newman black hole in five dimensions as a six-dimensional non-BPS over-rotating black string in type IIB on $S^1 \times \mathbb{T}^4$. In Section 4.3.1, we review the class of smooth almost-BPS solutions. This class of solutions is the key ingredient of the work [27], that we will discuss in Chapter 6, in which the first family of smooth bubbling microstate geometries that are asymptotic to the near-horizon region of extremal five-dimensional Kerr black holes (NHEK) is constructed.

4.3.1 Extremal rotating black holes in type IIB

In this section we briefly review the description of non-supersymmetric three-charge over-rotating Cvetič-Youm black holes that appear within the low-energy limit of type IIB String Theory compactified on $\mathbb{T}^4 \times S^1$ [120–122]. We describe their near-horizon or NHEK limit and the more general family of warped-AdS₃ geometries (WAdS₃) to which those NHEK solutions belong to [123–127].

4.3.1.1 Non-supersymmetric extremal D1-D5-P black holes

We work in the context of type IIB String Theory on a $\mathbb{T}^4 \times S^1$. We assume that the torus is much smaller than the one-sphere. As a consequence, the five-dimensional black-hole solutions can be viewed as six-dimensional black string solutions. We consider a four-parameter family of non-supersymmetric extremal spinning black holes characterized by a mass M , two $SU(2)_L$ and $SU(2)_R$ angular momenta J_L and J_R and three charges Q_I , with $I = 1, 5, P$, as follows

$$\begin{aligned} M &= 2 r_H^2 (c_1^2 + s_1^2 + c_5^2 + s_5^2 + c_P^2 + s_P^2), \\ J_R &= 0, \\ J_L &= 4 r_H^3 (c_1 c_5 c_P + s_1 s_5 s_P), \\ Q_I &= 4 r_H^2 s_I c_I, \quad I = 1, 5, P, \end{aligned} \tag{4.3.1}$$

where $s_I = \sinh \delta_I$ and $c_I = \cosh \delta_i$. The Bekenstein-Hawking entropy and the left and right temperatures are

$$\begin{aligned} S_{BH} &= 2\pi \sqrt{J_L^2 - Q_1 Q_5 Q_P} = 8\pi r_H^3 (c_1 c_5 c_P - s_1 s_5 s_P), \\ T_R &= 0, \\ T_L &= \frac{1}{\pi} \sqrt{1 - \frac{Q_1 Q_5 Q_P}{J_L^2}}. \end{aligned} \tag{4.3.2}$$

The metric of the six-dimensional black string is [122, 123]

$$\begin{aligned}
ds_6^2 = & - \left(1 - \frac{4a^2 c_P^2}{\hat{r}^2 + r_H^2}\right) \frac{d\hat{t}^2}{\sqrt{Z_1 Z_5}} + \left(1 + \frac{4a^2 s_P^2}{\hat{r}^2 + r_H^2}\right) \frac{d\hat{y}^2}{\sqrt{Z_1 Z_5}} \\
& + \frac{8r_H^2 s_{PCP}}{(\hat{r}^2 + r_H^2)\sqrt{Z_1 Z_5}} d\hat{t} d\hat{y} + (\hat{r}^2 + r_H^2)\sqrt{Z_1 Z_5} \left(\frac{\hat{r}^2}{(\hat{r}^2 - r_H^2)^2} d\hat{r}^2 + d\hat{\theta}^2 \right. \\
& \left. + \cos^2 \hat{\theta} d\hat{\varphi}_2^2 + \sin^2 \hat{\theta} d\hat{\varphi}_1^2 \right) + \frac{4r_H^4}{(\hat{r}^2 + r_H^2)\sqrt{Z_1 Z_5}} \left(\cos^2 \hat{\theta} d\hat{\varphi}_2 + \sin^2 \hat{\theta} d\hat{\varphi}_1 \right)^2 \\
& - \frac{8r_H^3}{(\hat{r}^2 + r_H^2)\sqrt{Z_1 Z_5}} ((c_1 c_5 c_P + s_1 s_5 s_P) d\hat{t} + (s_1 s_5 c_P + c_1 c_5 s_P) d\hat{y}) \left(\cos^2 \hat{\theta} d\hat{\varphi}_2 + \sin^2 \hat{\theta} d\hat{\varphi}_1 \right)
\end{aligned} \tag{4.3.3}$$

where

$$Z_I = 1 + \frac{4a^2 s_I^2}{\hat{r}^2 + r_H^2}, \quad I = 1, 5. \tag{4.3.4}$$

The coordinates $(\hat{r}, \hat{\theta}, \hat{\varphi}_1, \hat{\varphi}_2)$ are the spherical coordinates of the four-dimensional base space and \hat{y} is the KK direction. The periodicities of the angles \hat{y} , $\hat{\varphi}_2$ and $\hat{\varphi}_1$ are²⁰

$$(\hat{y}, \hat{\varphi}_2, \hat{\varphi}_1) = \begin{cases} (\hat{y}, \hat{\varphi}_2, \hat{\varphi}_1) + 2\pi (1, 0, 0) \\ (\hat{y}, \hat{\varphi}_2, \hat{\varphi}_1) + 2\pi (0, 1, 0) , \\ (\hat{y}, \hat{\varphi}_2, \hat{\varphi}_1) + 2\pi (0, 0, 1) \end{cases} \tag{4.3.5}$$

The geometry is asymptotically $\mathbb{R}^{1,4} \times S^1$ and has an event horizon at $\hat{r} = r_H$.

4.3.1.2 Near-horizon extremal Kerr geometry

The near-horizon geometry of the six-dimensional uplift of the five-dimensional black hole solutions given in (4.3.3) has been shown to be a *near-horizon extremal Kerr* geometry (NHEK) [123, 128, 124, 126, 127]. It is a squashed S^3 fibered over warped AdS_3 with specific angle periodicities.

The near-horizon limit is obtained by changing the coordinates as follows

$$\begin{aligned}
t &= \frac{4\pi \epsilon}{S} \hat{t}, & \rho &= \frac{\hat{r}^2 - r_H^2}{\epsilon}, & y &= \frac{S}{\pi Q_1 Q_5} (\hat{y} - V_H \hat{t}), \\
\psi &= \hat{\varphi}_2 + \hat{\varphi}_1 - \frac{8\pi r_H^2}{S} \hat{t} - \frac{4J_L}{Q_1 Q_5} (\hat{y} - V_H \hat{t}), & \phi &= \hat{\varphi}_2 - \hat{\varphi}_1, & \vartheta &= 2\hat{\theta},
\end{aligned} \tag{4.3.6}$$

where V_H is the linear velocity $V_H = -\frac{8\pi r_H^3 (c_1 c_5 s_P - s_1 s_5 c_P)}{S}$. Thus, the periodicities of y , ψ and ϕ are given by the following identifications

$$(y, \psi, \phi) = \begin{cases} (y, \psi, \phi) + 2\pi (T_y, -T_\psi, 0) \\ (y, \psi, \phi) + 2\pi (0, 2, 0) \\ (y, \psi, \phi) + 2\pi (0, 1, 1) \end{cases}, \tag{4.3.7}$$

with

$$T_y \equiv \frac{S}{\pi Q_1 Q_5}, \quad T_\psi \equiv \frac{4J_L}{Q_1 Q_5}. \tag{4.3.8}$$

²⁰We have chosen the unit $R_{\hat{y}} = 1$.

By taking the limit $\epsilon \rightarrow 0$, the near-horizon metric in terms of the above coordinates leads to a \mathbb{T}^2 fibration over $\text{AdS}_2 \times \text{S}^2$

$$ds_{\text{NHEK}}^2 = \frac{\kappa^2}{4} \left[-\rho^2 dt^2 + \frac{d\rho^2}{\rho^2} + \gamma (dy + \rho dt)^2 + \gamma (d\psi + \cos \theta d\phi)^2 + 2\alpha (dy + \rho dt)(d\psi + \cos \theta d\phi) + d\vartheta^2 + \sin^2 \vartheta d\phi^2 \right]. \quad (4.3.9)$$

where the warp constant factors γ and α and the length κ are given by

$$\gamma = 1 + \frac{1}{(c_1^2 + s_1^2)(c_5^2 + s_5^2)}, \quad \alpha = \frac{1}{c_1^2 + s_1^2} + \frac{1}{c_5^2 + s_5^2}, \quad (4.3.10)$$

$$\kappa^2 = 2r_H^2 \sqrt{(c_1^2 + s_1^2)(c_5^2 + s_5^2)}.$$

This background belongs to the family of deformations of $\text{AdS}_3 \times \text{S}^3$ into squashed S^3 (SqS^3) over warped AdS_3 (WAdS_3) [129–131]. However, for generic $\text{WAdS}_3 \times \text{SqS}^3$ backgrounds, the periods T_y and T_ψ (4.3.7) are arbitrary.

One can rewrite the solutions in terms of the $\text{SU}(2)_L$ -invariant one-forms on S^3

$$\begin{aligned} \sigma_1 &= \cos \psi d\vartheta + \sin \vartheta \sin \psi d\phi, & \sigma_2 &= -\sin \psi d\vartheta + \sin \vartheta \cos \psi d\phi, \\ \sigma_3 &= d\psi + \cos \vartheta d\phi, \end{aligned} \quad (4.3.11)$$

and the $\text{SL}(2, \mathbb{R})_L$ -invariant one-forms on AdS_3

$$w_+ = -e^{-y} \left(\frac{d\rho}{\rho} + \rho dt \right), \quad w_- = e^y \left(\frac{d\rho}{\rho} - \rho dt \right), \quad w_3 = dy + \rho dt, \quad (4.3.12)$$

to make the $\text{WAdS}_3 \times \text{SqS}^3$ geometry manifests

$$ds_{\text{NHEK}}^2 = \frac{\kappa^2}{4} (-w_+ w_- + \gamma w_3^2 + \sigma_1^2 + \sigma_2^2 + \gamma \sigma_3^2 + 2\alpha w_3 \sigma_3). \quad (4.3.13)$$

4.3.2 Almost-BPS solutions

We work in the context of $\mathcal{N} = 2$ five-dimensional Supergravity coupled to two extra vector fields but the generalization to an arbitrary number of vector fields is fairly straightforward. One can also consider the uplift to six dimensions as discussed for BPS solutions of the STU model in Section 4.1.1.5. We start with the same Ansatz for the five-dimensional metric and the field strengths:

$$\begin{aligned} ds_5^2 &= -(Z_1 Z_2 Z_3)^{-\frac{2}{3}} (dt + \mu (d\psi + A) + \varpi)^2 + V^{-1} (Z_1 Z_2 Z_3)^{\frac{1}{3}} (d\psi + A)^2 \\ &\quad + V (Z_1 Z_2 Z_3)^{\frac{1}{3}} \left[d\rho^2 + \rho^2 (d\vartheta^2 + \sin^2 \vartheta d\phi^2) \right], \\ F^I &= d_5 A^I = d_3 (Z_I^{-1} (dt + \omega)) + \Theta^I, \end{aligned} \quad (4.3.14)$$

4.3.2.1 Almost-BPS equations of motion

It was observed in [132] and extended in [133, 134, 82, 135], that a class of non-supersymmetric solutions of the equations of motion is obtained from the BPS equations by reversing the duality of the Θ^I and of ω relative to the duality of the curvature of the four-dimensional base. That is, one preserves the

hyper-Kähler metric, $ds(\mathcal{B})$, and the duality of its Riemann tensor but flips $\star_4 \rightarrow -\star_4$ in (4.1.6) and (4.1.7). Therefore, the almost-BPS equations are given by

$$\begin{aligned} \star_4 d_4 \star_4 d_4 Z_I &= -\frac{1}{2} C_{IJK} \star_4 (\Theta^J \wedge \Theta^K), & d_4 \Theta^I &= 0, & \star_4 \Theta^I &= -\Theta^I, \\ d_4 \omega - \star_4 d_4 \omega &= Z_I \Theta^I. \end{aligned} \quad (4.3.15)$$

From an eleven-dimensional perspective, the supersymmetry is broken by making incompatible the supersymmetry preserved by the M-branes with the supersymmetry preserved by the base space (the KKm charges). Consequently, if the base space is only flat \mathbb{R}^4 and does not carry KKm charges, the almost-BPS equations and the BPS equations are actually equivalent.

Even if the structure of the almost-BPS equations seems similar to the BPS equations, the change of orientation has annihilated the symplectic structure of the equations and generic solutions cannot be derived. We consider that the base space is Gibbons-Hawking with n centers as described in Section 4.1.1.2. Moreover, we assume that the vector fields preserve the ∂_ψ Killing vector of the base. We define the basis of anti-self dual two-forms as functions of the Gibbons-Hawking vielbeins (4.1.16)

$$\Omega_-^a = e^0 \wedge e^a - \epsilon_{abc} e^b \wedge e^c, \quad a = 1, 2, 3. \quad (4.3.16)$$

With the Ansatz

$$\Theta^I = \partial_a (K^I) \Omega_-^a \equiv d_3 (K^I (d\psi + A) + w^I), \quad (4.3.17)$$

then Θ^I is anti-self dual and

$$d_4 \Theta^I = 0 \quad \implies \quad \star_3 d_3 \star_3 d_3 K^I = 0 \quad \implies \quad K^I = k_\infty + \sum_{j=1}^n \frac{k_j^I}{\rho_j}. \quad (4.3.18)$$

Unfortunately, one cannot go much further. By introducing the functions K^I in the almost-BPS equations and with the decomposition $\omega = \mu (d\psi + A) + \varpi$, where μ and the one-form ϖ are functions on \mathbb{R}^3 , we have

$$\begin{aligned} d_3 \star_3 d_3 Z_I &= \frac{C_{IJK}}{2} V d \star_3 d (K^J K^K), \\ \star_3 d_3 w^I &= V d_3 K^I - K^I d_3 V, \\ d_3 \star_3 d_3 (\mu V) &= -d_3 (V Z_I) \star_3 d_3 K^I, \\ d_3 (\mu V) + \star_3 d_3 \varpi &= V Z_I d_3 K^I. \end{aligned} \quad (4.3.19)$$

Those equations do not admit closed-form solutions and they strongly depend on the center configuration. However, in practice, it is still relatively easy to obtain exact solutions for Z_I in a case-by-case manner. We will solve the equations in Taub-NUT for center configurations with an axial symmetry.

4.3.2.2 Axially symmetric multicenter solutions in Taub-NUT

In this section, we review the solutions derived in [133] for axially symmetric configurations in Taub-NUT where the centers are denoted by a coordinate a_j on the z axis of \mathbb{R}^3 , $j = 1 \dots n$. We consider the Taub-NUT at the center of the \mathbb{R}^3 base space and we use the spherical coordinates (ρ, ϑ, ϕ) :

$$V = h_\infty + \frac{q}{\rho}, \quad A = q \cos \vartheta d\phi.$$

We assume that the centers that source the vector fields are all distinct from the Taub-NUT center, $a_j \neq 0$. The shifted spherical coordinates around the j^{th} center, $(\rho_j, \vartheta_j, \phi)$, are given by

$$\rho_j = \sqrt{\rho^2 + a_j^2 - 2\rho a_j \cos \vartheta} \quad \vartheta_j = \arccos \left(\frac{\rho \cos \vartheta - a_j}{\rho_j} \right). \quad (4.3.20)$$

We proceed step by step by resolving first the magnetic field strengths before the warp factors and the angular momentum one-form. We end the discussion by deriving the regularity constraints.

- The anti-self dual magnetic two-forms Θ^I :

The two-form field strengths, Θ^I , are closed and anti-self dual in the Taub-NUT space and have the generic form given by (4.3.17). For axially symmetric centers, we have

$$*_3 dw^I = V dK^I - K^I dV \quad \Rightarrow \quad w^I = \sum_{j=1}^n k_j^I \left(h_\infty \cos \vartheta_j + q \frac{\rho - a_j \cos \vartheta}{\rho_j a_j} \right) d\phi. \quad (4.3.21)$$

- The warp factors Z^I :

The warp factors, Z_I , are determined by the harmonic equations with quadratic sources (4.3.19). For axially symmetric centers in Taub-NUT, the generic solutions are

$$Z_I = L_I + \frac{C_{IJK}}{2} \sum_{j,k=1}^n \left(h_\infty + \frac{q \rho}{a_j a_k} \right) \frac{k_j^J k_k^K}{\rho_j \rho_k}. \quad (4.3.22)$$

The functions L_I are the electric harmonic functions one can freely add to the equations. We use the same convention as in (4.1.20):

$$L_I = l_\infty^I + \frac{l_0^I}{\rho} + \sum_{j=1}^n \frac{l_j^I}{\rho_j}.$$

- The angular momentum one-form ω :

The last equations in (4.3.19) determine the two components, μ and ϖ , of the angular momentum one-form, ω . We will use the library of generating functions in Appendix A.1. The source terms are

$$\begin{aligned} V Z_I d_3 K^I &= \sum_j l_\infty^I k_j^I \left(h_\infty s_j^{(1)} + q s_j^{(2)} \right) + \sum_j l_j^I k_j^I \left(h_\infty s_j^{(3)} + q s_j^{(5)} \right) \\ &\quad + \sum_{i \neq j} l_i^I k_j^I \left(h_\infty s_{ij}^{(4)} + q s_{ij}^{(6)} \right) + \frac{C_{IJK}}{2} \sum_{i,j,k} k_i^I k_j^J k_k^K \left(h_\infty^2 s_{ijk}^{(7)} + q^2 s_{ijk}^{(8)} + h_\infty q s_{ijk}^{(9)} \right). \end{aligned} \quad (4.3.23)$$

According to the Appendix A.1, we have

$$\begin{aligned} \mu V &= \sum_j l_\infty^I k_j^I \left(h_\infty f_j^{(1)} + q f_j^{(2)} \right) + \sum_j l_j^I k_j^I \left(h_\infty f_j^{(3)} + q f_j^{(5)} \right) \\ &\quad + \sum_{i \neq j} l_i^I k_j^I \left(h_\infty f_{ij}^{(4)} + q f_{ij}^{(6)} \right) + \frac{C_{IJK}}{2} \sum_{i,j,k} k_i^I k_j^J k_k^K \left(h_\infty^2 f_{ijk}^{(7)} + q^2 f_{ijk}^{(8)} + h_\infty q f_{ijk}^{(9)} \right) + M, \\ \varpi &= \sum_j l_\infty^I k_j^I \left(h_\infty t_j^{(1)} + q t_j^{(2)} \right) + \sum_j l_j^I k_j^I \left(h_\infty t_j^{(3)} + q t_j^{(5)} \right) \\ &\quad + \sum_{i \neq j} l_i^I k_j^I \left(h_\infty t_{ij}^{(4)} + q t_{ij}^{(6)} \right) + \frac{C_{IJK}}{2} \sum_{i,j,k} k_i^I k_j^J k_k^K \left(h_\infty^2 t_{ijk}^{(7)} + q^2 t_{ijk}^{(8)} + h_\infty q t_{ijk}^{(9)} \right) + t^{(10)}, \end{aligned} \quad (4.3.24)$$

where M is the angular-momentum harmonic function one can freely add to the equation. We use the same convention as in (4.1.22):

$$M = m_\infty + \frac{m_0}{\rho} + \sum_{j=1}^n \frac{m_j}{\rho_j}.$$

The complete expression for μ and ϖ is then²¹

$$\begin{aligned} \mu = & \sum_j \frac{l_\infty^I k_j^I}{2\rho_j} + \sum_j \frac{l_j^I k_j^I}{2V\rho_j^2} \left(h_\infty + \frac{q \cos \vartheta}{a_j} \right) + \sum_{i \neq j} \frac{l_i^I k_j^I}{2V\rho_i \rho_j} \left(h_\infty + q \frac{\rho^2 + a_i a_j - 2a_j \rho \cos \vartheta}{a_j(a_i - a_j)} \right) \\ & + \sum_{i,j,k} \frac{k_i^1 k_j^2 k_k^3}{V\rho_i \rho_j \rho_k} \left(h_\infty^2 + q^2 \frac{\rho \cos \vartheta}{a_i a_j a_k} + h_\infty q \frac{\rho^2(a_i + a_j + a_k) + a_i a_j a_k}{2a_i a_j a_k \rho} \right) + \frac{M}{V}, \end{aligned} \quad (4.3.25)$$

$$\begin{aligned} \varpi = & \sum_j \frac{l_\infty^I k_j^I}{2\rho_j} \left(h_\infty(\rho \cos \vartheta - a_j) + q \frac{\rho - a_j \cos \vartheta}{a_j} \right) d\phi + \sum_j l_j^I k_j^I \frac{q\rho \sin^2 \vartheta}{2a_j \rho_j^2} d\phi \\ & + \sum_{i \neq j} \frac{l_i^I k_j^I}{2(a_j - a_i)\rho_i \rho_j} \left(h_\infty(\rho^2 + a_i a_j - (a_i + a_j)\rho \cos \vartheta) \right. \\ & \quad \left. - q \frac{\rho(a_i + a_j \cos 2\vartheta) - (\rho^2 + a_i a_j) \cos \vartheta}{a_j} \right) d\phi \\ & + \sum_{i,j,k} \frac{k_i^1 k_j^2 k_k^3}{a_i a_j a_k \rho_i \rho_j \rho_k} \left(q^2 \rho^2 \sin^2 \vartheta \right. \\ & \quad \left. + h_\infty q \frac{\rho^3 + \rho(a_i a_j + a_i a_k + a_j a_k) - (\rho^2(a_i + a_j + a_k) + a_i a_j a_k) \cos \vartheta}{2} \right) d\phi \\ & + \varpi_0 d\phi - m_0 \cos \vartheta d\phi - \sum_j m_j \cos \vartheta_j d\phi. \end{aligned} \quad (4.3.26)$$

- The regularity constraints:

The solutions constructed above are regular if:

- The one-form ϖ does not have Dirac-Misner string and must vanish on the z -axis.
- The metric is regular everywhere.
- The quartic invariant, \mathcal{I}_4 (4.1.27), must be positive everywhere.

The first condition implies $n + 1$ algebraic equations. One can make these constraints explicit, for example, by solving them with respect to the $n + 1$ variables ϖ_0 , m_0 and m_i for $i = 1, \dots, n$. If one considers, for definiteness, a configuration in which all the poles a_i lie on one side of the Taub-NUT center ($0 < a_1 < \dots < a_n$), then the regularity constraints are:

$$\begin{aligned} \varpi_0 &= -q \sum_j \frac{l_\infty^I k_j^I}{2a_j} - h_\infty \sum_{i \neq j} \frac{l_i^I k_j^I}{2(a_j - a_i)} - h_\infty q \sum_{i,j,k} \frac{k_i^1 k_j^2 k_k^3}{2a_i a_j a_k}, \\ m_0 &= -q \sum_i \frac{l_\infty^I k_i^I}{2a_i} - h_\infty \sum_i \frac{l_0^I k_i^I}{2a_i} + q \sum_{i \neq i', i \neq 0} \frac{l_i^I k_{i'}^I}{2a_{i'}(a_{i'} - a_i)} - h_\infty q \sum_{i,j,k} \frac{k_i^1 k_j^2 k_k^3}{2a_i a_j a_k}, \\ m_i &= \frac{l_\infty^I k_i^I}{2} \left(h_\infty + \frac{q}{a_i} \right) + \sum_j \frac{1}{2|a_i - a_j|} \left[l_j^I k_i^I \left(h_\infty + \frac{q}{a_i} \right) - l_i^I k_j^I \left(h_\infty + \frac{q}{a_j} \right) \right] \\ &\quad + \frac{h_\infty q}{2} \left[\frac{k_i^1 k_i^2 k_i^3}{a_i^3} + \frac{|\epsilon_{IJK}|}{2} \frac{k_i^I}{a_i} \sum_{j,k} \text{sign}(a_j - a_i) \text{sign}(a_k - a_i) \frac{d_j^{(J)} d_k^{(K)}}{a_j a_k} \right] \quad (i \geq 1), \end{aligned} \quad (4.3.27)$$

Those equations are equivalent to the Denef equations, (4.1.26), for almost-BPS solutions. The requirement that the quartic invariant is everywhere positive does not translate in a set of algebraic conditions

²¹Note that we are using a different convention for the angular-momentum harmonic function compared to the BPS multicenter solutions (4.1.22). We have removed the factor 2 in the definition of M in μ .

and must be checked at any point on three-dimensional part of Taub-NUT base space. As their BPS cousins, this condition makes the task of finding a phase space of regular almost-BPS solutions very complicated.

Finally, the harmonic functions have order-one poles. The regularity of the five-dimensional metric and the field strengths (4.3.14) requires that the warp factors Z_I and μ are regular. However, we have restricted the almost-BPS solutions to have a Taub-NUT base. Thus, all the n additional centers do not have any charge in V . The Gibbons-Hawking charges were crucial to ensure that the BPS solutions are regular in five dimensions. For a similar reason, our almost-BPS solutions are necessarily singular at the n centers in five-dimensions. However, the embedding in six dimensions through the sequence of duality transformations into the D1-D5-P frame (4.1.43) allows the existence of smooth centers. They are the almost-BPS equivalents of the 1/2-BPS round-supertube centers. The discussion in Section 4.1.3.3 can be identically reproduced in the context of almost-BPS solutions. The smooth almost-BPS centers in six dimensions carry two electric charges l^I, l^J and one magnetic dipole charge k^K with I, J and K all different. Regularity required a non-zero angular momentum m given by the relation

$$m = \frac{l^I l^J}{2 k^K}. \quad (4.3.28)$$

The difference of factor 2 compared to the regularity condition of BPS round Supertubes (4.1.59) is due to the difference of definition of the harmonic part, M , in μ .

4.3.2.3 Generalized spectral flows and gauge transformations

The three generalized spectral flows detailed in 3.2.4 can be translated in the formalism of multicenter almost-BPS solutions. We consider the embedding of the solutions in the D1-D5-P frame where the sequence of dualities corresponding to spectral flows can be performed. The metric, the NS-NS fields and the R-R fields are given in (4.1.43). Let us define the three constant shifts γ_1, γ_2 and γ_3 of the three types of spectral flows and the following new functions [82, 127]

$$T_I \equiv 1 + \gamma_I K^I, \quad N_I = \frac{C_{IJK}}{2} \gamma_I^2 Z_J Z_K + V T_I^2 Z_I - 2\gamma_I V T_I \mu, \quad I = 1, 2, 3. \quad (4.3.29)$$

We also introduce the short-hand notations $T^3 = T_1 T_2 T_3$, $N^3 = N_1 N_2 N_3$, $\gamma^3 = \gamma_1 \gamma_2 \gamma_3$ and $Z^3 = Z_1 Z_2 Z_3$. The spectrally flowed six-dimensional metric and the U(1) vector gauge fields are given by [82]

$$\begin{aligned} d\tilde{s}_6^2 &= - \frac{1}{\tilde{Z}_3 \sqrt{\tilde{Z}_1 \tilde{Z}_2}} \left(dt + \tilde{\mu}(d\psi + \tilde{A}) + \varpi \right)^2 + \frac{\tilde{Z}_3}{\sqrt{\tilde{Z}_1 \tilde{Z}_2}} (\tilde{A}^3 + dy)^2 \\ &\quad + \sqrt{\tilde{Z}_1 \tilde{Z}_2} \left(\tilde{V}^{-1} (d\psi + \tilde{A})^2 + \tilde{V} ds(\mathbb{R}^3)^2 \right), \\ \tilde{A}^I &= - \frac{dt + \varpi}{\tilde{W}_I} + \tilde{P}^I (d\psi + \tilde{A}) + \tilde{w}^I, \end{aligned} \quad (4.3.30)$$

where

$$\begin{aligned}
\tilde{V} &= \left[T^6 V^2 + 8\gamma^3 T^3 V \mu - T^3 V (C_{IJK} \gamma_J \gamma_K T_I Z_I) \right. \\
&\quad \left. + \frac{C_{IJK}}{2} \gamma_J^2 \gamma_K^2 T_I^2 Z_I^2 - C_{IJK} \gamma_I^2 \gamma_J \gamma_K T_J Z_J T_K Z_K \right]^{1/2}, \\
\tilde{A} &= A - \gamma_I w^I - \frac{C_{IJK}}{2} \gamma_J \gamma_K v_I + \gamma^3 v_0, \\
\tilde{Z}_I &= \frac{N_I}{\tilde{V}}, \\
\tilde{\mu} &= \tilde{V}^{-2} \left(T^3 V^2 \mu - \gamma^3 Z^3 + \frac{C_{IJK}}{2} \gamma_J \gamma_K Z_I T_I V \mu - \frac{C_{IJK}}{2} \gamma_I V T_J Z_J T_K Z_K \right), \\
\tilde{W}_I &= \frac{N_I}{T^3 V + \frac{C_{IJK}}{2} \gamma_J \gamma_K T_I Z_I - C_{IJK} \gamma_I \gamma_J T_K Z_K}, \\
\tilde{P}^I &= \frac{V Z_I T_I K^I + \frac{C_{IJK}}{2} \gamma_I Z_J Z_K - (2T_I - 1) V \mu}{N_I}, \\
\tilde{w}^I &= w^I + C_{IJK} \gamma_J v_K - \frac{C_{IJK}}{2} \gamma_J \gamma_K v_0.
\end{aligned} \tag{4.3.31}$$

We have defined four magnetic and electric one-forms, v_I and v_0 , determined by the following equations

$$\begin{aligned}
\star_3 dv_I &\equiv -dZ_I + \frac{C_{IJK}}{2} (V d(K^J K^K) - K^J K^K dV), \\
\star_3 dv_0 &\equiv K^I dZ_I - Z_I dK^I + \frac{C_{IJK}}{6} (K^I K^J K^K dV - V d(K^I K^J K^K)).
\end{aligned} \tag{4.3.32}$$

Generalized spectral flows produce a non-trivial modification of the functions. However, the spectrally-flowed solutions still satisfy the regularity conditions. Indeed, the one-form ϖ is unchanged that guarantees the absence of Dirac-Misner string at $\vartheta = 0, \pi$. Moreover, the quartic invariant is preserved under spectral flows $\tilde{\mathcal{I}}_4 = \mathcal{I}_4$. Hence, a regular almost-BPS multicenter solution is transformed by a generic spectral flows into a regular extremal non-supersymmetric solution.

Furthermore, if the initial almost-BPS solution has a supertube curvature singularity the corresponding generalized spectral flow transforms the singular local geometries to quotients of $\mathbb{R}^4 \times S^1$ [81] as in the BPS case.

In the context of BPS solutions, the generalized spectral flows were just linear transformations between solutions of the same class. In the context of almost-BPS, we see that the spectrally-flowed solution no longer belongs to the same class and has a very different structure. Generalized spectral flows allow to move to very different spectra of non-BPS solutions. Some of these spectra were studied in [82]. In this thesis, we will see to what extent they can be used to construct non-BPS solutions asymptotically NHEK or WAdS₃ [27].

4.4 Final comment

In this chapter, we have detailed one of the most important aspect of the microstate geometry program: exploiting degrees of freedom in Supergravity to build large number of smooth solutions that differ from the black-hole at the horizon scale.

Over the years, larger and larger families of such solutions have been found for supersymmetric and extremal black holes, for non-supersymmetric and extremal black holes, as we have reviewed here, but also non-supersymmetric and non-extremal black holes [136–138].

There is no guarantee that these solutions are indeed black-hole microstates. Another aspect of the microstate geometry program is also to address the black-hole paradoxes by considering ensemble of such solutions, and to see how they fit into various AdS/CFT correspondences.

Part II

Construction of microstate geometries

Systematic construction of scaling multicenter solutions

In the previous chapter, we have detailed the construction of smooth horizonless multicenter 1/8-BPS geometries in five dimensions that have the same charges and angular momenta as a BMPV black hole with a macroscopically-large horizon. They were obtained by resolving the black hole singularity via the blow-up of topologically-nontrivial bubbles that are supported against collapse by fluxes.

Finding a closed form for generic solutions was surprisingly simple thanks to the linearity of the BPS equations. However, no explicit family of regular solutions have been constructed and only a few explicit examples are known [85, 139, 99, 23]. This is due to the hardly-manageable regularity constraints that can be decomposed into four categories:

- The Denef equations (4.1.26).
- The absence of closed timelike curves (CTC) (4.1.27).
- The regularity of the metric at each center in five dimensions (Gibbons-Hawking center) or six dimensions (Gibbons-Hawking or round-supertube center).
- The scaling condition (4.1.54).

Most solutions one can construct by putting fluxes on a multi-center Gibbons-Hawking (GH) base have an angular momentum larger than the black hole cosmic censorship bound, $J_L^2 \gtrsim Q_1 Q_2 Q_3$. This does not mean that they are irregular but only that they do not a priori correspond to black-hole microstates. This was first discovered in [77], where it was pointed out that BPS solutions with a large number of GH centers have angular momenta at and slightly above the cosmic censorship bound. So far the only solutions corresponding to microstate geometries for black holes with arbitrary-low angular momentum have been obtained via Superstrata. Since all bubbling solutions have charges dissolved in fluxes, and since these fluxes have different signs, the most likely outcome of trying to obtain a solution by putting random values of fluxes on various cycles is a solution with regions of positive and negative charge densities. Such solutions are not supersymmetric, and imposing a supersymmetric Ansatz on them gives in general a solution with CTC's. Furthermore, since the flux on every cycle interacts with the flux on every other cycle, making sure there are no regions of negative charge density is a very complicated problem, that has not been solved yet¹.

In this chapter, we present two published results [23, 24] and an unpublished result that allowed a better understanding of the properties of multicenter smooth solutions. The first two belong to the same project and will be reviewed in Sections 5.2 and 5.3. In [23], a generic recipe was given to construct the largest known family of scaling regular multicenter solutions with four GH centers. By studying the large parameter space, it has been shown that generic solutions with four GH centers correspond to microstate of a black hole with an angular momentum around 99% of its maximal value confirming [77]. The notion of *hierarchy of scale* between the centers has been introduced: the angular momentum can be lowered for center configurations divided in several clusters of close centers. Moreover, in [24], a

¹In [140] a strategy to solve this problem is proposed.

similar method applied to smooth solutions with three GH centers and one Supertube showed that those solutions can have arbitrarily low angular momentum. As explained in the previous chapter, those solutions are smooth in six dimensions, in the D1-D5-P frame.

These constructions required a good understanding of the structure of the regularity constraints listed above. The unpublished result is a consequence of this study and is discussed in Section 5.1. Denef equations give a strong relation between the center configuration, their charges and the background moduli determining the asymptotics of the solution (4.1.3.1). Depending on the background moduli, a generic solution may be forced to decay at *walls of marginal stability* [141] and some D-brane bound states cease to exist when the asymptotics are changed. A black hole does not have this feature and the solution is independent of the background. A typical microstate should then share this characteristic. The standard lore is that families of scaling solutions represent the good candidates to be typical microstates are also background-independent. We will discuss the limit of this assessment by showing that configuration with collinear centers might have walls of marginal stability even in the scaling limit.

5.1 Walls of marginal stability of collinear centers in the scaling limit

In this section, we discuss the mathematical structure of Denef equations for BPS solutions with collinear centers. Collinearity has advantages in many aspects. First, it preserves the $U(1) \times U(1)$ isometry of the GH base space in a sense that the configuration does not break the ϑ/ϕ -independence². This assumption considerably simplifies the resolution of Denef equations since the degrees of freedom of the configuration (the relative distance on the line between the centers) matches the number of equations. Second, they do not belong to a strange corner of the phase space of multicenter solutions. It has been even proven that the index of multicenter solutions is reproduced by counting only collinear solutions [142].

BPS solutions which do not satisfy scaling conditions have a moduli space divided by walls of marginal stability that delimit zones where the moduli is incompatible with the set of charges $\{\Gamma_i\}$ [76, 141]. When crossing a wall, the centers are forced to pair up or to split and the solution changes drastically. For instance, if one takes the simplest example of a two-center solution where the Denef equations reduce to one equation $\langle \Gamma_1, \Gamma_2 \rangle = -\langle \Gamma_1, \Gamma_\infty \rangle \times \rho_{12}$, the inter-center distance is diverging when the background moduli is approaching the wall defined by $\langle \Gamma_1, \Gamma_\infty \rangle = 0$. Beyond the wall the two centers merge to a single-center solution $\Gamma_1 + \Gamma_2 \rightarrow \Gamma = \Gamma_1 + \Gamma_2$ [141]. However, it has been argued that solutions with a scaling limit do not have walls of marginal stability because they are indistinguishable from a single-center solution and therefore all possible values of moduli at infinity are available.

We consider a multicenter solution with n centers uniquely defined by $n + 1$ symplectic vectors Γ_i and Γ_∞ (4.1.24). The centers are on the z -axis of \mathbb{R}^3 and are given by their distance to the origin ordered as follows

$$a_1 > \dots > a_{n-2} > a_{n-1} > a_0 = 0. \quad (5.1.1)$$

We assume that the solution belongs to a family of scaling solutions. Then, we introduce a scale $\lambda \ll 1$ such that

$$a_j = \lambda d_j, \quad d_j = \mathcal{O}(1), \quad d_1 > \dots > d_{n-1} > d_0 = 0, \quad (5.1.2)$$

We rewrite the Denef equations by replacing $\rho_{ij} = |a_i - a_j|$

$$\sum_{j=0}^{n-1} \frac{\langle \Gamma_i, \Gamma_j \rangle}{|a_i - a_j|} = \langle \Gamma_\infty, \Gamma_i \rangle \quad \implies \quad \sum_{j=0}^{n-1} \frac{\langle \Gamma_i, \Gamma_j \rangle}{|d_i - d_j|} = \mathcal{O}(\lambda) \quad i = 1, \dots, n, \quad (5.1.3)$$

²We remind that these are the two spherical angles of \mathbb{R}^3 .

A direct consequence of the equations is that the background moduli satisfies

$$\sum_{j=0}^{n-1} \langle \Gamma_\infty, \Gamma_j \rangle = 0. \quad (5.1.4)$$

The question we address in this section is: is the solution insensitive to a change of asymptotics Γ_∞ like any expected black hole microstates? The standard lore answers yes. It comes from the simple observation that if $a_i \ll 1$, an infinitesimal transformation of center positions induces a change of order one in $\frac{\langle \Gamma_i, \Gamma_j \rangle}{|a_i - a_j|}$ which might annihilate a change of order one in Γ_∞ . We will rigorously show to what extent this naive idea is false and to what extent such a solution can be sensitive to the asymptotic.

5.1.1 A change of background preserving the $U(1) \times U(1)$ isometry

We want to compute the deformation of the center configuration under a change of background moduli by keeping the charge vectors fixed. For that purpose, we consider another symplectic vector \hat{l} of the same order of magnitude as Γ_∞ that defines the direction of the change of background in the eight-dimensional moduli space. We perform the transformation $\Gamma_\infty \rightarrow \Gamma_\infty + x \hat{l}$ where x is a real variable. The only constraint on \hat{l} is the same as the constraint on Γ_∞ :

$$\sum_{j=0}^{n-1} \langle \hat{l}, \Gamma_j \rangle = 0. \quad (5.1.5)$$

5.1.1.1 Disproof of the standard lore

In this subsection, we investigate the standard lore stating that any background change can be solved by infinitely small changes of center positions into the Denef equations. We show that this reasoning is (unfortunately) wrong. For that purpose, let us assume it is true and consider the following family of transformations:

$$\begin{aligned} \Gamma_\infty &\rightarrow \Gamma_\infty + x \hat{l} \\ a_i &\rightarrow a_i (1 + \delta_i(x)), \quad \delta_i(x) \ll 1 \\ \Gamma_i &\rightarrow \Gamma_i. \end{aligned} \quad (5.1.6)$$

To solve Denef equations, we have $n - 1$ variables δ_i for $n - 1$ independent equations. Therefore, the system of equations is solvable. We linearize the equations (5.1.3) in terms of the δ_i , by noticing that

$$\frac{1}{\rho_{ij}} \rightarrow \frac{1}{|a_i - a_j|} \left(1 + \frac{a_j \delta_j - a_i \delta_i}{|a_i - a_j|} \right), \quad i \neq j.$$

At leading-order, in a matrix form we have

$$M \cdot \begin{bmatrix} \delta_1 \\ \delta_2 \\ \delta_3 \\ \vdots \\ \delta_{n-1} \end{bmatrix} = x \begin{bmatrix} \langle \Gamma_0, \hat{l} \rangle \\ \langle \Gamma_1, \hat{l} \rangle \\ \langle \Gamma_2, \hat{l} \rangle \\ \vdots \\ \langle \Gamma_{n-2}, \hat{l} \rangle \end{bmatrix}, \quad (5.1.7)$$

with

$$\begin{aligned}
 M &\equiv \begin{bmatrix} \frac{\Gamma_{01}}{a_1} & \frac{\Gamma_{02}}{a_2} & \frac{\Gamma_{03}}{a_3} & \cdots & \frac{\Gamma_{0\,n-1}}{a_{n-1}} \\ \sum_{j=0}^{n-1} \frac{\Gamma_{1j}}{\rho_{1j}} \frac{a_1}{a_1-a_j} & -\frac{\Gamma_{12}}{\rho_{12}} \frac{a_2}{a_1-a_2} & -\frac{\Gamma_{13}}{\rho_{13}} \frac{a_3}{a_1-a_3} & \cdots & -\frac{\Gamma_{1\,n-1}}{\rho_{1\,n-1}} \frac{a_{n-1}}{a_1-a_{n-1}} \\ -\frac{\Gamma_{21}}{\rho_{21}} \frac{a_1}{a_2-a_1} & \sum_{j=0}^{n-1} \frac{\Gamma_{2j}}{\rho_{2j}} \frac{a_2}{a_2-a_j} & -\frac{\Gamma_{23}}{\rho_{23}} \frac{a_3}{a_2-a_3} & \cdots & -\frac{\Gamma_{2\,n-1}}{\rho_{2\,n-1}} \frac{a_{n-1}}{a_2-a_{n-1}} \\ \vdots & \ddots & \ddots & \ddots & \vdots \\ -\frac{\Gamma_{n-2\,1}}{\rho_{n-2\,1}} \frac{a_1}{a_{n-2}-a_1} & -\frac{\Gamma_{n-2\,2}}{\rho_{n-2\,2}} \frac{a_2}{a_{n-2}-a_2} & -\frac{\Gamma_{n-2\,3}}{\rho_{n-2\,3}} \frac{a_3}{a_{n-2}-a_3} & \cdots & -\frac{\Gamma_{n-2\,n-1}}{\rho_{n-2\,n-1}} \frac{a_{n-1}}{a_{n-2}-a_{n-1}} \end{bmatrix} \\
 &\equiv \begin{bmatrix} C_1 & C_2 & C_3 & \cdots & C_{n-1} \end{bmatrix}, \quad (5.1.8)
 \end{aligned}$$

where C_i is the i^{th} column of M . We apply the Cramer formula to solve the system of equations (5.1.7). We only express δ_1 for readability:

$$\delta_1 = x \frac{\det[M_l]}{\det[M]}. \quad (5.1.9)$$

We obtain M_l from M by replacing C_1 by the vector on the right hand side of the equation (5.1.7) that we denote $\langle \hat{\Gamma}, \hat{l} \rangle$:

$$\begin{aligned}
 M_l &\equiv \begin{bmatrix} \langle \hat{\Gamma}, \hat{l} \rangle & C_2 & C_3 & \cdots & C_{n-1} \end{bmatrix} \\
 &= \begin{bmatrix} \langle \Gamma_0, \hat{l} \rangle & \frac{\Gamma_{02}}{a_2} & \frac{\Gamma_{03}}{a_3} & \cdots & \frac{\Gamma_{0\,n-1}}{a_{n-1}} \\ \langle \Gamma_1, \hat{l} \rangle & -\frac{\Gamma_{12}}{\rho_{12}} \frac{a_2}{a_1-a_2} & -\frac{\Gamma_{13}}{\rho_{13}} \frac{a_3}{a_1-a_3} & \cdots & -\frac{\Gamma_{1\,n-1}}{\rho_{1\,n-1}} \frac{a_{n-1}}{a_1-a_{n-1}} \\ \langle \Gamma_2, \hat{l} \rangle & \sum_{j=0}^{n-1} \frac{\Gamma_{2j}}{\rho_{2j}} \frac{a_2}{a_2-a_j} & -\frac{\Gamma_{23}}{\rho_{23}} \frac{a_3}{a_2-a_3} & \cdots & -\frac{\Gamma_{2\,n-1}}{\rho_{2\,n-1}} \frac{a_{n-1}}{a_2-a_{n-1}} \\ \vdots & \vdots & \ddots & \ddots & \vdots \\ \langle \Gamma_{n-2}, \hat{l} \rangle & -\frac{\Gamma_{n-2\,2}}{\rho_{n-2\,2}} \frac{a_2}{a_{n-2}-a_2} & -\frac{\Gamma_{n-2\,3}}{\rho_{n-2\,3}} \frac{a_3}{a_{n-2}-a_3} & \cdots & -\frac{\Gamma_{n-2\,n-1}}{\rho_{n-2\,n-1}} \frac{a_{n-1}}{a_{n-2}-a_{n-1}} \end{bmatrix}. \quad (5.1.10)
 \end{aligned}$$

Furthermore, by performing the column operation $C_1 \rightarrow C_1 + C_2 + \cdots + C_{n-1}$ on the first column of M , the components of the first column become the $n-1$ left-hand side of the Denef equations (5.1.3). So the determinant of M is equal to the determinant of $-M_\infty$ where M_∞ is given by

$$M_\infty \equiv \begin{bmatrix} \langle \Gamma_0, \Gamma_\infty \rangle \\ \langle \Gamma_1, \Gamma_\infty \rangle \\ \langle \Gamma_2, \Gamma_\infty \rangle & C_2 & C_3 \cdots C_{n-1} \\ \vdots \\ \langle \Gamma_{n-2}, \Gamma_\infty \rangle \end{bmatrix} = [\langle \hat{\Gamma}, \Gamma_\infty \rangle \ C_2 \ C_3 \cdots C_{n-1}]. \quad (5.1.11)$$

Since $a_i = \mathcal{O}(\lambda)$ with $\lambda \ll 1$, all the coefficients of C_i are of order λ^{-1} while the coefficients of $\langle \hat{\Gamma}, \Gamma_\infty \rangle$ or $\langle \hat{\Gamma}, \hat{l} \rangle$ are of order one. Thus, according to (5.1.10) and (5.1.11), the determinant of M_l and the determinant of M_∞ are of the same order of magnitude. Therefore,

$$\delta_1 = -x \frac{\det[\langle \hat{\Gamma}, \hat{l} \rangle \ C_2 \ C_3 \cdots C_{n-1}]}{\det[\langle \hat{\Gamma}, \Gamma_\infty \rangle \ C_2 \ C_3 \cdots C_{n-1}]} = -x \frac{\det[M_l]}{\det[M_\infty]} = \mathcal{O}(1). \quad (5.1.12)$$

We repeat the same arguments for each δ_i and we get with the same conventions:

$$\delta_i = -x \frac{\det[C_1 \cdots C_{i-1} \ \langle \hat{\Gamma}, \hat{l} \rangle \ C_{i+1} \cdots C_{n-1}]}{\det[C_1 \cdots C_{i-1} \ \langle \hat{\Gamma}, \Gamma_\infty \rangle \ C_{i+1} \cdots C_{n-1}]} = \mathcal{O}(1). \quad (5.1.13)$$

This is in contradiction with the assumption $\delta_i \ll 1$. Thus, the transformation (5.1.6) is not valid: changing the background moduli changes significantly the positions of the centers even in the scaling regime.

5.1.1.2 The right transformation

In this section, we describe rigorously how the center positions vary $a_i \rightarrow a_i(x)$ under a change of background $\Gamma_\infty \rightarrow \Gamma_\infty + x \hat{l}$ that preserves the axisymmetry of the centers. We only assume that the positions $a_i(x)$ are analytic functions of x and we proceed step by step to obtain differential equations:

$$\begin{aligned} \Gamma_\infty + x \hat{l} &\rightarrow \Gamma_\infty + (x + dx) \hat{l}, & dx &\ll 1 \\ a_i(x) &\rightarrow a_i(x + dx) = a_i(x) \left(1 + \frac{1}{a_i(x)} \frac{da_i}{dx} dx \right) \\ \Gamma_i &\rightarrow \Gamma_i. \end{aligned} \quad (5.1.14)$$

Now we have an infinitesimally small parameter dx , we can rigorously reproduce the previous arguments by replacing in all formulas the initial configuration $\{\Gamma_\infty, a_i, \Gamma_i\}$ by $\{\Gamma_\infty + x \hat{l}, a_i(x), \Gamma_i\}$ and the final background $\Gamma_\infty + x \hat{l}$ by $\Gamma_\infty + (x + dx) \hat{l}$. We obtain according to (5.1.13):

$$\frac{1}{a_i(x)} \frac{da_i}{dx} dx = - \frac{\det \left[C_1(x) \dots C_{i-1}(x) \langle \Gamma, \hat{l} \rangle C_{i+1}(x) \dots C_{n-1}(x) \right]}{\det \left[C_1(x) \dots C_{i-1}(x) \langle \Gamma, \Gamma_\infty \rangle + x \langle \Gamma, \hat{l} \rangle C_{i+1}(x) \dots C_{n-1}(x) \right]} dx, \quad (5.1.15)$$

where $C_i(x)$ is obtained from C_i (5.1.8) by replacing ρ_{ij} and a_i by $\rho_{ij}(x)$ and $a_i(x)$. Finally, this leads to the following $n - 1$ differential non-linear equations:

$$\frac{d \ln a_i}{dx} = - \frac{A_i(x)}{B_i(x) + x A_i(x)}, \quad (5.1.16)$$

where

$$\begin{aligned} A_i(x) &\equiv \det \left[C_1(x) \dots C_{i-1}(x) \langle \Gamma, \hat{l} \rangle C_{i+1}(x) \dots C_{n-1}(x) \right] \\ B_i(x) &\equiv \det \left[C_1(x) \dots C_{i-1}(x) \langle \Gamma, \Gamma_\infty \rangle C_{i+1}(x) \dots C_{n-1}(x) \right]. \end{aligned} \quad (5.1.17)$$

Those equations are hard to solve directly. Nonetheless, the scaling-limit assumption $a_i(x) = \mathcal{O}(\lambda(x))$ with $\lambda(x) \ll 1$ greatly simplifies the equations. All the coefficients of $C_i(x)$ are of order $\lambda(x)^{-1}$ whereas the coefficients of $\langle \Gamma, \Gamma_\infty \rangle$ or $\langle \Gamma, \hat{l} \rangle$ are of order one. We first remark by performing an operation on the columns in (5.1.17), that

$$\begin{aligned} A_i(x) &= \underbrace{A_1(x)}_{\mathcal{O}(\lambda^{2-n})} + (-1)^i \underbrace{\det \left[\langle \Gamma, \hat{l} \rangle \quad \langle \Gamma, \Gamma_\infty \rangle \quad C_2(x) \dots C_{i-1}(x) \quad C_{i+1}(x) \dots C_{n-1}(x) \right]}_{\mathcal{O}(\lambda^{3-n})} \\ B_i(x) &= \underbrace{B_1(x)}_{\mathcal{O}(\lambda^{2-n})} - (-1)^i x \underbrace{\det \left[\langle \Gamma, \hat{l} \rangle \quad \langle \Gamma, \Gamma_\infty \rangle \quad C_2(x) \dots C_{i-1}(x) \quad C_{i+1}(x) \dots C_{n-1}(x) \right]}_{\mathcal{O}(\lambda^{3-n})}. \end{aligned} \quad (5.1.18)$$

Thus, in the scaling regime:

$$A_i(x) = A_1(x), \quad B_i(x) = B_1(x). \quad (5.1.19)$$

By replacing everything in (5.1.16) we obtain:

$$\frac{d \ln a_i}{dx} = \frac{d \ln a_1}{dx}, \quad (5.1.20)$$

and by integrating:

$$\frac{a_i(x)}{a_i(0)} = \frac{a_1(x)}{a_1(0)} \equiv f(x). \quad (5.1.21)$$

We call $f(x)$ the *distance factor*. This means that the centers change as a compact block and the aspect ratios do not change at leading order. Furthermore, one can now find $f(x)$ in terms of the initial center positions, $a_i = a_i(0)$, the initial background vector, Γ_∞ , and the charge vectors, Γ_i . Indeed, thanks to (5.1.21), we have $C_i(x) = f(x)^{-1} C_i$ where C_i is given in (5.1.8), so $A_i(x) = f(x)^{2-n} A_1$ and $B_i(x) = f(x)^{2-n} B_1$. Thus, (5.1.16) becomes

$$\frac{d \ln f}{dx} = -\frac{A_1}{B_1 + x A_1}, \quad (5.1.22)$$

which can be easily integrated:

$$f(x) = \frac{B_1}{B_1 + x A_1}. \quad (5.1.23)$$

To conclude, when a background transformation is performed along the direction \hat{l} on an initial solution defined by $\{a_i, \Gamma_\infty, \Gamma_i\}$ in the scaling regime,

$$\begin{aligned} \Gamma_\infty &\rightarrow \Gamma_\infty + x \hat{l} \\ a_i &\rightarrow a_i(x) \\ \Gamma_i &\rightarrow \Gamma_i, \end{aligned} \quad (5.1.24)$$

a distance factor, $a_i \rightarrow a_i(x) \approx f(x) a_i$, appears given by

$$f(x) = -\frac{x_c}{x - x_c}, \quad (5.1.25)$$

with

$$x_c \equiv -\frac{\det [\langle \Gamma, \Gamma_\infty \rangle C_2 \dots C_{n-1}]}{\det [\langle \Gamma, \hat{l} \rangle C_2 \dots C_{n-1}]} = -\frac{\det [M_\infty]}{\det [M_l]}. \quad (5.1.26)$$

The vectors C_i , $\langle \Gamma, \hat{l} \rangle$ and $\langle \Gamma, \Gamma_\infty \rangle$ and the matrices M_l and M_∞ are expressed in terms of the initial $\{a_i, \Gamma_\infty, \Gamma_i\}$ in (5.1.8), (5.1.10) and (5.1.11).

Surprising as it may seem, the expression (5.1.25) is the equation of a hyperbola. So the positions of the centers in the three-dimensional base space of the solution are deeply sensitive to modifications of background. We can distinguish between three different transformations according to the value of x . We suppose $x_c > 0$ but the statement is identical with $x_c < 0$.

- $x < 0$:

The distance factor $f(x)$ is below one (yellow part in the illustration Fig.5.1). This is a *scaling-like* situation: the transformation $\Gamma_\infty \rightarrow \Gamma_\infty + x \hat{l}$ makes the inter-center distances decrease by a factor of $f(x)$. The geometry of the bubbles is compatible with the asymptotics given by $\Gamma_\infty + x \hat{l}$.

- $0 < x < x_c$:

The distance factor $f(x)$ is finite but greater than one (blue part in Fig.5.1). This corresponds to a *semi-critical* situation. Performing the transformation $\Gamma_\infty \rightarrow \Gamma_\infty + x \hat{l}$ increases the inter-center distances. So the geometry of the bubbles is compatible with the behavior of the solution from far away given by $\Gamma_\infty + x \hat{l}$. However, moving further the background towards the direction of \hat{l} makes the distances blow up.

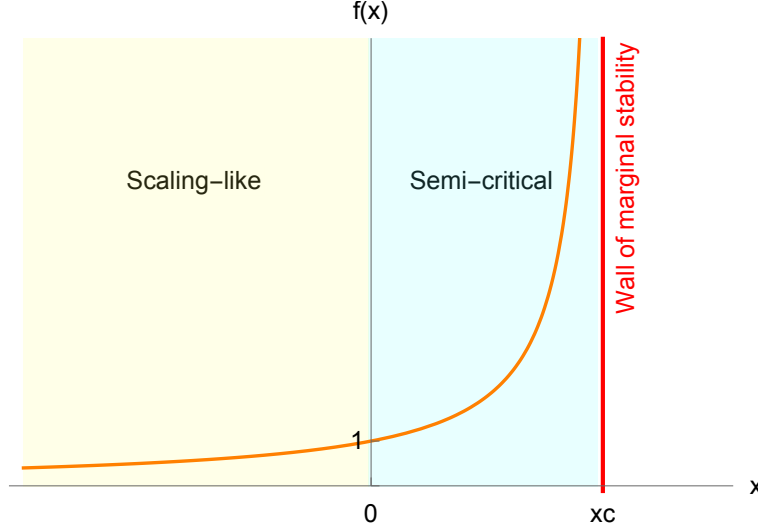


Figure 5.1: The three different phases of the impact of a background change $\Gamma_\infty \rightarrow \Gamma_\infty + x\hat{l}$ on the geometry of the axisymmetric configuration as a function of x with $x_c > 0$.

- $x = x_c$ and $x > x_c$:

At $x = x_c$, there is a *wall of marginal stability* (red line in Fig.5.1). At that point, the distance factor diverges and so the cluster of the centers blows up. Above x_c , analytic center positions $\{a_i(x)\}$ no longer exist.

Thus, along each direction \hat{l} starting from Γ_∞ , a wall of marginal stability exists at the location $\Gamma_\infty + x_c\hat{l}$. We illustrate this result in Fig.5.2 by projecting the eight-dimensional moduli space into a two-dimensional space. We choose three directions \hat{l} where $\det[M_l] = 0$ which implies $x_c \rightarrow \infty$ (5.1.26). Thus, the wall of marginal stability goes to infinity along those directions (see Fig.5.2). We have three zones that are incompatible with the center configuration of the solution (in red).

It is very hard to predict the behaviors of the walls of marginal stability because they are highly dependent on the initial center configuration, initial charge vectors and the initial background vector. The only thing we know is about the origin of the background moduli. First, if we assume $\Gamma_\infty = 0$, the equality (5.1.22) gives $\partial_x \ln f(x) = -x^{-1}$ which is not integrable. So, no other backgrounds can be accessed by transformation preserving the $U(1) \times U(1)$ isometry. Second, if $\Gamma_\infty \neq 0$, we straightforwardly have $x_c = -1$ along the direction $\hat{l} = \Gamma_\infty$. Thus, $\Gamma_\infty + x_c\hat{l} = 0$ belongs to a wall of marginal stability. From a supergravity point of view, this point of the moduli space corresponds to harmonic functions with no constant terms. According to the discussion in Section 4.1.3.1, the D-brane bound state is asymptotically $\text{AdS}_2 \times S^3$ in five dimensions. Thus a corollary of our result is that any solutions with collinear centers cannot go to their AdS_2 limit or move away from their AdS_2 limit at least by preserving their $U(1) \times U(1)$ isometry.

One may wonder if the walls of marginal stability can be bypassed by performing a change of background that breaks one of the $U(1)$ isometry.

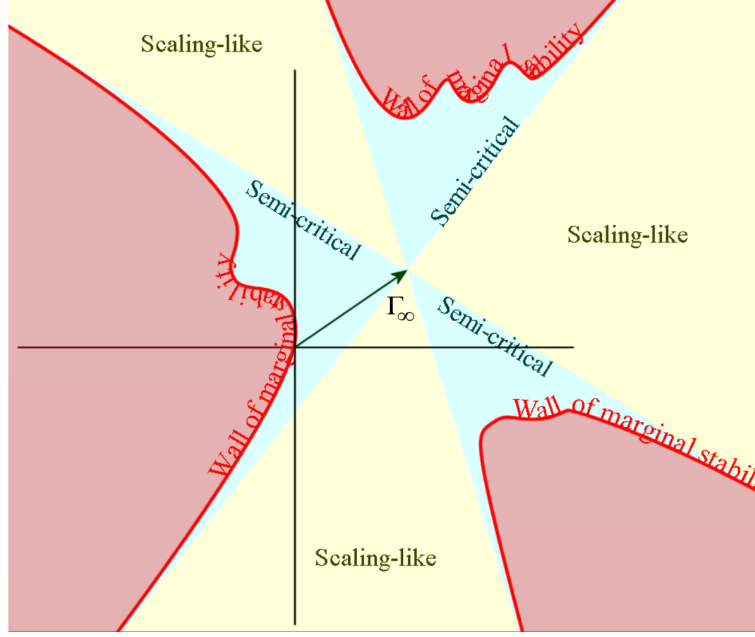


Figure 5.2: A two-dimensional schematic description of the background moduli space of an initial solution with a background vector Γ_∞ . The three different possible zones of background changes are depicted. The red zones correspond to the backgrounds which are incompatible with the initial charge vectors and center configuration.

5.1.2 A change of background breaking a $U(1)$ isometry

In this Section, we perform a change of background $\Gamma_\infty \rightarrow \Gamma_\infty + \hat{l}$ allowing the transformation to break the axisymmetry. So, the centers can move away from the z -axis and have a non-zero angle ϑ_j . We consider the transformations whose only $\{\vartheta_1, a_2, \dots, a_{n-1}\}$ can vary but any other transformation with one angle and $n - 2$ distances can be treated in the same way. We do not discuss the transformation involving more than one angle, because non-diagonal terms $\delta\vartheta_i\delta\vartheta_j$ appear in the linearization of the Denef equations which makes the problem more difficult without affecting the main result. We consider the following transformation

$$\begin{aligned}
 \Gamma_\infty &\rightarrow \Gamma_\infty + \hat{l} \\
 \vartheta_1 &\rightarrow \delta\vartheta_1, & \delta\vartheta_1 &\ll 1 \\
 i \neq 1, & \quad a_i \rightarrow a_i (1 + \delta_i), & \delta_i &\ll 1 \\
 \Gamma_i &\rightarrow \Gamma_i.
 \end{aligned} \tag{5.1.27}$$

The inverse inter-center distances transforms as

$$\begin{aligned}
 \frac{1}{\rho_{ij}} &\rightarrow \frac{1}{|a_i - a_j|} \left(1 + \frac{a_j \delta_j - a_i \delta_i}{|a_i - a_j|} \right), & i &\neq j, \\
 \frac{1}{\rho_{i1}} &\rightarrow \frac{1}{|a_i - a_1|} \left(1 - \frac{a_i}{|a_i - a_j|} \delta_i - \frac{a_i a_1}{2|a_i - a_1|^2} (\delta\vartheta_1)^2 \right), & i &\neq 1,
 \end{aligned} \tag{5.1.28}$$

The linearization of Denef equations is slightly different from the previous section since we need to go to second order in $\delta\vartheta_1$:

$$M_{\vartheta} \cdot \begin{bmatrix} \delta\vartheta_1^2 \\ \delta_2 \\ \delta_3 \\ \vdots \\ \delta_{n-1} \end{bmatrix} = \begin{bmatrix} \langle \Gamma_0, \hat{l} \rangle \\ \langle \Gamma_1, \hat{l} \rangle \\ \langle \Gamma_2, \hat{l} \rangle \\ \vdots \\ \langle \Gamma_{n-2}, \hat{l} \rangle \end{bmatrix}, \quad (5.1.29)$$

with

$$M_{\vartheta} \equiv \begin{bmatrix} 0 & \frac{\Gamma_{02}}{a_2} & \frac{\Gamma_{03}}{a_3} & \dots & \frac{\Gamma_{0\,n-1}}{a_{n-1}} \\ \sum_{j \neq 1} \frac{\Gamma_{1j}}{\rho_{1j}^3} \frac{a_1 a_j}{2} & -\frac{\Gamma_{12}}{\rho_{12}} \frac{a_2}{a_1 - a_2} & -\frac{\Gamma_{13}}{\rho_{13}} \frac{a_3}{a_1 - a_3} & \dots & -\frac{\Gamma_{1\,n-1}}{\rho_{1\,n-1}} \frac{a_{n-1}}{a_1 - a_{n-1}} \\ \frac{\Gamma_{21}}{\rho_{21}^3} \frac{a_1 a_2}{2} & \sum_{j=0}^{n-1} \frac{\Gamma_{2j}}{\rho_{2j}} \frac{a_2}{a_2 - a_j} & -\frac{\Gamma_{23}}{\rho_{23}} \frac{a_3}{a_2 - a_3} & \dots & -\frac{\Gamma_{2\,n-1}}{\rho_{2\,n-1}} \frac{a_{n-1}}{a_2 - a_{n-1}} \\ \vdots & \vdots & \ddots & \ddots & \vdots \\ \frac{\Gamma_{n-2\,1}}{\rho_{n-2\,1}^3} \frac{a_1 a_{n-2}}{2} & -\frac{\Gamma_{n-2\,2}}{\rho_{n-2\,2}} \frac{a_2}{a_{n-2} - a_2} & -\frac{\Gamma_{n-2\,3}}{\rho_{n-2\,3}} \frac{a_3}{a_{n-2} - a_3} & \dots & -\frac{\Gamma_{n-2\,n-1}}{\rho_{n-2\,n-1}} \frac{a_{n-1}}{a_{n-2} - a_{n-1}} \end{bmatrix}. \quad (5.1.30)$$

We apply the Cramer formula and solve the system of equations (5.1.29):

$$\begin{aligned} \delta_k &= \frac{\det[M_{\vartheta k}]}{\det[M_{\vartheta}]} \\ \delta\vartheta_1^2 &= \frac{\det[M_{\vartheta 1}]}{\det[M_{\vartheta}]}, \end{aligned} \quad (5.1.31)$$

where $M_{\vartheta k}$ is obtained from M_{ϑ} by replacing its k^{th} column by the vector on the right hand side of the equation (5.1.29). The operation $C_1 \rightarrow C_1 + C_2 + \dots + C_{n-1}$ on the first column of M_{ϑ} no longer makes Denef equations appear. In addition, a straightforward computation leads to

$$\begin{aligned} \det[M_{\vartheta k}] &= \mathcal{O}(\lambda^{2-n}) \\ \det[M_{\vartheta}] &= \mathcal{O}(\lambda^{1-n}). \end{aligned} \quad (5.1.32)$$

So,

$$\begin{aligned} \delta_k &= \mathcal{O}(\lambda) \\ \delta\vartheta_1^2 &= \mathcal{O}(\lambda). \end{aligned} \quad (5.1.33)$$

The infinitesimal expansion (5.1.27) is well defined. Nevertheless, notice that if the right hand side of the second line in (5.1.31) is negative, no real solutions exist for $\delta\vartheta_1$ and the transformation (5.1.27) is not valid. It is hard to predict the sign of this quantity due to the complexity of the matrices $M_{\vartheta 1}$ and M_{ϑ} . However, if one sends $\hat{l} \rightarrow -\hat{l}$, then $\det[M_{\vartheta 1}] \rightarrow -\det[M_{\vartheta 1}]$ whereas $\det[M_{\vartheta}]$ remains fixed. Thus, in one or the other direction along \hat{l} , $\delta\vartheta_1^2$ is negative and the transformation is not valid.

Even if the transformation (5.1.27) is not valid, it is complicated to conclude something about possible walls of marginal stability. Indeed, one can choose a slightly different transformation by letting another angle to vary and this will give another positivity condition. By allowing the transformation to break the collinearity, we have many more degrees of freedom than equations and we did not find an overall criterion to evaluate whether or not the background transformation can be performed. However, numerical test or concrete examples in Chapter 6 show that it is likely that some changes of background moduli are subject to walls of marginal stability even if the collinearity of the centers is broken.

Moreover, these features are really specific to the axisymmetric solutions and this does not apply to center configurations that do not initially preserve the $U(1) \times U(1)$ isometry. For instance, one can reproduce the computation of this section by assuming that the center configuration is planar. A transformation of the type (5.1.27) will lead to a result similar to (5.1.33) but with $\delta\vartheta_1$ instead of $\delta\vartheta_1^2$. Any change of background can be then compensated by an infinitesimal change of the bubble geometry in the Denef equations.

Thus, we have shown that BPS solutions with centers on a line are peculiar solutions. Even if they belong to a family of scaling solutions, they are non-trivially sensitive to the background moduli. Typical black hole microstates should not be. If one requires that the solutions remain axisymmetric, there are walls of marginal stability where the D-brane bound states are forced to decay. One of the $U(1)$ isometry must be broken to bypass those walls but this does not guarantee the existence of the bound states at any point of the moduli space.

5.2 Systematic construction of a large family of smooth four-center solutions

In this section, we present a systematic construction of the largest known family of scaling four-center smooth horizonless solutions that have the same charges as large black holes. Our construction allows us to easily build scaling four-center BPS solutions with any aspect ratios between the centers. Moreover, we focus on solutions which are asymptotically $\mathbb{R}^{1,4}$ but the method can be adapted to any asymptotics. The main idea is to start with BPS solutions with three collinear supertube centers in Taub-NUT. As we will see, defining a parameter space where those solutions satisfy the Denef equations, the no-CTC condition and the scaling condition is rather easy. Then, the next step is to regularize the solutions at the supertube centers. As detailed in Section 4.1.3.3, this can be done by performing two or three generalized spectral flows (4.1.30). Each generalized spectral flow transforms a singular magnetic charge of its corresponding species of Supertube to a smooth KKM charge and then transforms a species of Supertube to a smooth GH center. Thus, with two spectral flows we obtain a solution with three GH centers and a Supertube. This solution is smooth in the D1-D5-P frame as explained in Section 4.1.3.3. With three spectral flows, we have a solution of four smooth GH centers in five-dimensions. Because generalized spectral flows also change the asymptotics, the last step consists in applying gauge transformations and change of background moduli to have asymptotically flat solutions.

5.2.1 Three-supertube scaling BPS solutions in Taub-NUT

Let us apply the generic discussion of Section 4.1 to the specific family of three Supertubes in Taub-NUT. Each Supertube carries a dipole charge k_I and two electric charges $Q_j^{(I)}$ at the centers $j \neq I$. Consequently, the eight harmonic functions that characterize such a field configuration are given by

$$V = h_\infty + \frac{q_0}{\rho_0}, \quad K^I = \alpha^I + \sum_{j=1}^3 \frac{k_j}{\rho_j} \delta_j^I, \quad L_I = 1 + \sum_{j=1}^3 \frac{Q_j^{(I)}}{4\rho_j} (1 - \delta_j^I), \quad M = m_\infty + \sum_{j=1}^3 \frac{m_j}{\rho_j}. \quad (5.2.1)$$

We consider axisymmetric supertube configurations. The positions of the supertube centers and the Taub-NUT center are given by the distances a_1, a_2, a_3 and a_0 on the z-axis of the three-dimensional base space with the same convention as in (5.1.1). The Denef equations can be conveniently written

as

$$\begin{aligned}
\frac{\Gamma_{12}}{a_1 - a_2} + \frac{\Gamma_{13}}{a_1 - a_3} - 4q_0 \frac{m_1}{a_1} &= 4h_\infty m_1 - 4k_1 + Q_1^{(2)} \alpha_2 + Q_1^{(3)} \alpha_3, \\
\frac{\Gamma_{21}}{a_1 - a_2} + \frac{\Gamma_{23}}{a_2 - a_3} - 4q_0 \frac{m_2}{a_2} &= 4h_\infty m_2 - 4k_2 + Q_2^{(1)} \alpha_1 + Q_2^{(3)} \alpha_3, \\
\frac{\Gamma_{32}}{a_2 - a_3} + \frac{\Gamma_{31}}{a_1 - a_3} - 4q_0 \frac{m_3}{a_4} &= 4h_\infty m_3 - 4k_3 + Q_3^{(1)} \alpha_1 + Q_3^{(2)} \alpha_2, \\
\sum_{j=1}^3 \frac{m_j}{a_j} &= -m_\infty,
\end{aligned} \tag{5.2.2}$$

where we have introduced the short-hand notation $\Gamma_{ij} = \langle \Gamma_i, \Gamma_j \rangle$. Moreover, we want the solutions to belong to a family of scaling solutions. The aspect ratios, defined in 5.1.2, must satisfy the following scaling condition

$$\begin{aligned}
\frac{\Gamma_{12}}{d_1 - d_2} + \frac{\Gamma_{13}}{d_1 - d_3} - 8q_0 \frac{m_1}{d_1} &\sim 0, \\
\frac{\Gamma_{21}}{d_1 - d_2} + \frac{\Gamma_{23}}{d_2 - d_3} - 8q_0 \frac{m_2}{d_2} &\sim 0, \\
\frac{\Gamma_{32}}{d_2 - d_3} + \frac{\Gamma_{31}}{d_1 - d_3} - 8q_0 \frac{m_3}{d_4} &\sim 0, \\
\sum_{j=1}^3 \frac{m_j}{d_j} &\sim 0,
\end{aligned} \tag{5.2.3}$$

The regularity of the Supertubes (4.1.59) fixes the angular-momentum charges as follows

$$m_1 = \frac{Q_1^{(2)} Q_1^{(3)}}{16k_1^{(1)}}, \quad m_2 = \frac{Q_2^{(1)} Q_2^{(3)}}{16k_2^{(2)}}, \quad m_3 = \frac{Q_3^{(2)} Q_3^{(1)}}{16k_3^{(3)}}, \tag{5.2.4}$$

Moreover, the constant terms α_I are constrained by summing the four Denef equations. We want the minimum number of non-zero constant terms in the K 's³. So we choose

$$\alpha^1 = -2h_\infty m_\infty, \quad \alpha^2 = \alpha^3 = 0. \tag{5.2.5}$$

Denef equations can be easily solved by considering the electric charges $Q_j^{(I)}$ as variables instead of the inter-center distances. This drastically simplifies the structure of the equations. The last regularity condition is the absence of CTC (4.1.27). As already said, this can be reduced to $Z_I V \geq 0$, $I = 1, 2, 3$, for generic solutions in the black-hole regime. By expanding the conditions around each pole and at the boundary, one can transform those inequalities on a set of algebraic inequalities on the charges and dipole charges:

$$q_0 \frac{Q_J^{(I)}}{a_J} + \frac{k_I k_J}{|a_I - a_J|} \geq 0 \quad \text{and} \quad q_0 \left(\frac{Q_J^{(I)}}{a_J} + \frac{Q_K^{(I)}}{a_K} \right) \geq 0, \quad I \neq J \neq K. \tag{5.2.6}$$

At infinity, this implies that $h_\infty \geq 0$.

Finally, the last line in (5.2.3) requires that at least one m_j is negative and then that a dipole charge k_j is negative. To conclude, we ensure the quartic invariant to be positive everywhere by restricting q_0 to be positive, $Q_j^{(I)}$ to satisfy the above inequalities and one of the dipole charges, say k_2 , to be negative.

³Constant terms in the K 's can induce CTC.

We delimited a large parameter space of regular three-supertube solutions in Taub-NUT. The parameter space is specified by seven charge parameters $k_1, k_2, k_3, q_0, \frac{Q_2^{(1)}}{Q_1^{(3)}}, \frac{Q_3^{(2)}}{Q_1^{(2)}}, \frac{Q_2^{(3)}}{Q_3^{(1)}}$ and the relative distance ratios $\frac{a_1}{a_2}$ and $\frac{a_2}{a_3}$. The missing point is that they are not smooth neither in five dimensions nor in six dimensions. This will be fixed using generalized spectral flows in the next subsection.

5.2.2 Microstate geometries from three-supertube configurations

We use generalized spectral flows (4.1.30), gauge transformations (4.1.31), and change of background moduli to transform the solutions into configurations of three GH centers and one Supertube or into configurations of four GH centers. The techniques to generate these configurations only differ in the number of generalized spectral flows. We require the transformed solutions to satisfy the following conditions:

- The constant terms in V and K^I are zero to have asymptotically flat solutions.
- The sum of all charges in V is one.
- The values of the charges and dipole charges are integer.

Our recipe is the following:

1. We choose a value for the seven degrees of freedom of the three-supertube solutions, $k_1, k_2, k_3, q_0, \frac{Q_2^{(1)}}{Q_1^{(3)}}, \frac{Q_3^{(2)}}{Q_1^{(2)}}, \frac{Q_2^{(3)}}{Q_3^{(1)}}$. We give also a starting value for the aspect ratios between the centers. They will be modified slightly in the next steps. Remind that we can only obtain scaling solutions if one of the k 's has a sign different from the other two. We also give a non-vanishing value to h_∞ , which is necessary in order to cancel the constant terms of all K^I in a later step. Therefore, the base space is Taub-NUT.
2. We impose the scaling condition (5.2.3) as three exact equations from which we obtain the precise value of all the $Q_j^{(I)}$ parameters. Afterwards, we round these values to some close rational numbers and solve the Denef equations (5.2.2) to determine the positions of the centers a_1, a_2 and a_3 . Thus, (5.2.3) cease to be equalities and become approximations, as intended. The aspect ratios are also slightly changed compared to their initial values. This step ensures that we construct a scaling three-supertube solution free of CTC's.
3. We perform three generalized spectral flows and three gauge transformations (or two generalized spectral flows and two gauge transformations). We fix the values of the spectral flow parameters γ^I by imposing specific integer values of the Gibbons-Hawking charges q_1, q_2 and q_3 (or q_1 and q_2) such that $\sum q_j = 1$. The values of the gauge parameters g_I are fixed requiring that the constant terms in all the functions K^I are zero.

At this stage, we have a BPS scaling solution with four Gibbons-Hawking centers (or three Gibbons-Hawking centers and one Supertube). However, there are still two issues that need to be fixed. First, the harmonic function V still has a constant term. This means that the four-dimensional base space is asymptotically $\mathbb{R}^3 \times S^1$ instead of flat \mathbb{R}^4 . Second, all the parameters of the transformations γ_I and g_I are fixed by polynomial equations, so the resulting charges and dipole charges of the solution are real numbers. Since they are expected to be quantized when interpreted in the full context of String Theory, it is crucial that they take integer values.

4. It is not possible to remove the constant in V using transformations that preserve the Denef equations. We therefore remove it by performing a background-moduli transformation as discussed in the previous section. The centers are on a line, so they belong to the category where the transformation can cross a wall of marginal stability. In our construction we will carefully select the solutions for which it is possible to perform this truncation preserving the axisymmetry of the center configuration.

5. We want the monopole and dipole charges to be integer numbers. The first step consists in obtaining solutions whose harmonic functions have rational poles. For that purpose, we round the values of the parameters k_j^I to be rational and obtain all the other charges l_j^I and m_j using the Gibbons-Hawking condition (4.1.57). Since one can find rational numbers arbitrarily close to any irrational number, this procedure is guaranteed not to change significantly the properties of the solution. Hence, we have a fair bit of freedom in rounding the irrational numbers to rational ones, and we can use it to obtain k_j^I that have the same denominator. This rounding does not leave the Denef equations invariant, and we need to solve them again and check the absence of CTC's. The second step is to obtain solutions whose harmonic functions have integer poles. We use the following transformations parametrized by any real numbers $\{s_1, s_2, s_3\}$,

$$\begin{aligned} M &\rightarrow \frac{1}{6} C_{IJK} s_I s_J s_K M, & L_I &\rightarrow \frac{1}{2} C_{IJK} s_J s_K L_I, \\ V &\rightarrow V, & K^I &\rightarrow s_I K^I, & \{s_1, s_2, s_3\} &\in \mathbb{R}^3. \end{aligned} \quad (5.2.7)$$

They preserve the regularity of the solution. Indeed, the regularity of Gibbons-Hawking centers (4.1.57) or the regularity of the round Supertube (4.1.59) are still satisfied and the Denef equations and the quartic invariant are multiplied by an overall factor $s_1 s_2 s_3$ and $(s_1 s_2 s_3)^2$ respectively. Thus, one chooses the three s_I to be the smallest integers needed to obtain integer charges from the rational charges.

6. The factors s_I are usually large numbers, so multiplying the harmonic functions L^I and M makes their constant terms very large. Asymptotic flatness of the five-dimensional metric (4.1.32) demands having the constant terms of all L^I equal to one⁴. To obtain such solutions one again has to perform a background-moduli transformation on the constant terms of all the L^I . We are in a situation where the background vector shift \hat{l} is almost collinear to the background vector Γ_∞ in the eight-dimensional moduli space. According to our discussion in Section 5.1.2, such a change is not critical, and results in a global dilatation of the multicenter configuration. To make the inter-center distances small again, we simply fine-tune the value of some of the dipole charges (keeping them integer) to make the solution scale [85].

This method produces asymptotically-flat solutions with four Gibbons-Hawking centers that have integer charges in the scaling regime (or asymptotically flat solutions with one round Supertube and three GH centers). Using this systematic procedure we have an “almost” complete map from three-supertube solutions in Taub-NUT to smooth solutions. By “almost” we consider that some of the solutions can decay at walls of marginal stability when performing the background transformations. Moreover, the parameter space is well defined by the set of parameters of the initial solutions $k_1, k_2, k_3, \frac{Q_2^{(1)}}{Q_1^{(3)}}, \frac{Q_3^{(2)}}{Q_1^{(2)}}, \frac{Q_2^{(3)}}{Q_3^{(1)}}, q_0$, by the aspect ratios between the centers, and by the spectral flow parameters giving the GH charges q_1 and q_2 . We remind that the parameters of the initial solutions are constrained to be CTC-free.

5.2.2.1 Explicit examples

Here we give the explicit form of the harmonic functions characterizing two BPS scaling microstate geometries: one with four Gibbons-Hawking centers and one with three Gibbons-Hawking center and a Supertube center. The solutions have been found following the recipe detailed above.

- An example with four Gibbons-Hawking centers:

⁴Actually only their product has to be equal to one, but this subtlety is not particularly relevant.

We have chosen the initial parameters to have a particularly low angular momentum for a configuration of four GH centers. As we will see in a moment, this requires a large hierarchy of scales in the inter-center distances and small charges in V .

The solution is determined by the following harmonic functions,

$$\begin{aligned}
V &= \frac{1}{\rho_0} + \frac{1}{\rho_1} - \frac{2}{\rho_2} + \frac{1}{\rho_3} \\
K^1 &= -\frac{36}{\rho_0} + \frac{100}{\rho_1} + \frac{18}{\rho_2} - \frac{1}{\rho_3} \\
K^2 &= \frac{278}{\rho_0} - \frac{4997}{\rho_1} - \frac{1702}{\rho_2} + \frac{220}{\rho_3} \\
K^3 &= \frac{344}{\rho_0} + \frac{342}{\rho_1} - \frac{2154}{\rho_2} + \frac{1644}{\rho_3} \\
L_1 &= 1 - \frac{95632}{\rho_0} + \frac{1708974}{\rho_1} + \frac{1833054}{\rho_2} - \frac{361680}{\rho_3} \\
L_2 &= 1 + \frac{12384}{\rho_0} - \frac{34200}{\rho_1} - \frac{19386}{\rho_2} + \frac{62472}{\rho_3} \\
L_3 &= 1 + \frac{10008}{\rho_0} + \frac{499700}{\rho_1} - \frac{15318}{\rho_2} + \frac{8360}{\rho_3} \\
M &= 5981 - \frac{3442752}{\rho_0} - \frac{170897400}{\rho_1} + \frac{16497486}{\rho_2} - \frac{13743840}{\rho_3}.
\end{aligned} \tag{5.2.8}$$

The bubble equations can be solved numerically for the location of the centers,

$$a_1 = 5.9600 \dots \times 10^{-1}, \quad a_2 = 1.1367 \dots \times 10^{-3}, \quad a_3 = 7.5586 \dots \times 10^{-6}. \tag{5.2.9}$$

Performing an asymptotic expansion of Z_I and μ we obtain the three electric charges and the angular momentum of the solution, which can be read from the $\mathcal{O}(\rho^{-1})$ coefficients (4.1.55)⁵.

$$\begin{aligned}
Q_1 &= 1993340 \\
Q_2 &= 29014 \\
Q_3 &= 229906 \\
J_L &= -87655680.
\end{aligned} \tag{5.2.10}$$

The angular momentum is 58% of its maximal value. While this value is not close to 0%, we can definitely affirm that it is far from 100%. Thus, this microstate geometry corresponds to a rotating black hole whose angular momentum is significantly below the cosmic censorship bound (4.1.48). The solution has been constructed thanks to a fine-tuning of the initial parameters following the numerical analysis that we will review in the next section.

- An example with three Gibbons-Hawking centers and a Supertube:

We build here a solution with one Supertube and three Gibbons-Hawking centers with a very low angular momentum. The solution has been also found from the coming numerical analysis. As an illustration, our procedure allows us to fine-tune appropriately the scale difference between the inter-center distances and the values of the initial charges and dipole charges of the three initial Supertubes.

⁵We do not write down J_R since it is almost vanishing of the order of the inter-center distance.

We take

$$\begin{aligned}
V &= \frac{1}{\rho_0} + \frac{1}{\rho_2} - \frac{1}{\rho_3} \\
K^1 &= -\frac{114}{\rho_0} - \frac{5}{\rho_1} - \frac{110}{\rho_2} + \frac{115}{\rho_3} \\
K^2 &= -\frac{111}{\rho_0} + \frac{4698}{\rho_2} + \frac{642}{\rho_3} \\
K^3 &= \frac{3}{\rho_0} - \frac{87}{\rho_2} + \frac{84}{\rho_3} \\
L_1 &= 1 + \frac{333}{\rho_0} + \frac{408726}{\rho_2} + \frac{53928}{\rho_3} \\
L_2 &= 1 + \frac{342}{\rho_0} + \frac{10}{\rho_1} - \frac{9570}{\rho_2} + \frac{9660}{\rho_3} \\
L_3 &= 1 - \frac{12654}{\rho_0} + \frac{381142}{\rho_1} + \frac{516780}{\rho_2} + \frac{73830}{\rho_3} \\
M &= -5115 + \frac{37981}{\rho_0} - \frac{762284}{\rho_1} + \frac{44959860}{\rho_2} + \frac{6201720}{\rho_3}.
\end{aligned} \tag{5.2.11}$$

The bubble equations give the positions of the centers:

$$a_1 = 7.3189 \dots \times 10^{-2}, \quad a_2 = 3.6046 \dots \times 10^{-3}, \quad a_3 = 9.7241 \dots \times 10^{-5}. \tag{5.2.12}$$

The three charges and the angular momentum are:

$$\begin{aligned}
Q_1 &= 462987 \\
Q_2 &= 442 \\
Q_3 &= 362992 \\
J_L &= -16021,
\end{aligned} \tag{5.2.13}$$

giving, as advertised, an angular momentum at 0.17% of the cosmic censorship bound.

5.3 Multicenter solutions with arbitrarily low angular momentum

The method reveals itself as a very powerful tool to study the spectrum of four-center microstate geometries. This has never been done before for any multicenter solutions with more than two centers because of the lack of a well-defined parameter space of regular solutions. In this section we are interested in the angular momentum of the solutions. For that purpose, we define the *entropy parameter*,

$$\mathcal{H} \equiv \frac{Q_1 Q_2 Q_3 - J_L^2}{Q_1 Q_2 Q_3}, \tag{5.3.1}$$

which measures how far the microstate angular momentum is below the cosmic censorship bound of the black hole with the same charges⁶. We perform a scan of the parameter spaces and try to elucidate some general properties for multicenter solutions.

We have generated automatically a huge number of regular solutions following the recipe until the step 3. All the steps coming after do not affect significantly the solutions and are unnecessary for a numerical analysis.

⁶Of course, microstate geometries have no horizons and their angular momentum can easily be above the cosmic censorship bound [77], so the name “entropy parameter” is a bit of a misnomer. We use it nonetheless because it facilitates the comparison between the microstate geometry and the corresponding black hole.

5.3.1 Analysis with four GH centers

We first focus on solutions without scale differences between the inter-center distances:

$$\begin{aligned}\frac{a_1 - a_2}{a_3} &\approx 1 \\ \frac{a_2 - a_3}{a_3} &\approx 1.\end{aligned}\tag{5.3.2}$$

We divided our analysis in three parts, considering the effect of modifying three sets of parameters: the Gibbons-Hawking charges (q_0, q_1, q_2) , the initial supertube dipole charges (k_1, k_2, k_3) and the supertube charge ratios $(\frac{Q_2^{(1)}}{Q_1^{(3)}}, \frac{Q_3^{(2)}}{Q_1^{(2)}}, \frac{Q_2^{(3)}}{Q_3^{(1)}})$. All the details of the numerical analysis can be found in Appendix A.2. We reach the following conclusions:

- The entropy parameter approaches zero drastically when the absolute value of the Gibbons-Hawking charges is large. The optimal value we observed for the Gibbons-Hawking charges is 1,1,1 and -2.
- For the initial supertube dipole charges, we observed that configurations with k_2 negative and k_1 and k_3 positive are the optimal ones. With the two other sign configurations, we did not find domains of charge ratios with an entropy parameter bigger than 0.1. We also noticed that the entropy parameter does not depend significantly on k_2 and it depends essentially on $\frac{k_1}{k_3}$. Furthermore, we observed that for any charge ratios one can find a particular dipole ratio $\frac{k_1}{k_3}$ where the entropy parameter is maximal and the upper bound seems to be $\mathcal{H} \sim 0.3$.
- With the optimal configuration of dipole charge signs and Gibbons-Hawking charges, we have found several domains of charge ratios where the entropy parameter is above 0.2.

Moreover, we performed an analysis to study the impact of the hierarchy of scales. In Figure 5.3, we show one of the main results of the analysis. It illustrates how the entropy parameter can significantly increase with the aspect ratios. The entropy parameter is represented with respect to two variables, one is a charge ratio and the other is the hierarchy parameter m :

$$\frac{a_1}{a_2} \approx 10^m, \quad \frac{a_2}{a_3} \approx 10^m.\tag{5.3.3}$$

The rest of parameters are chosen to optimize the entropy parameter, according to the numerical results just presented (see Appendix A.2 for more details). The graph shows that when m is around 0 the solutions are near-maximally spinning, with \mathcal{H} very close to 0. Furthermore, in all the solutions we examined the entropy parameter increases as the hierarchy between the distances gets more pronounced, converging toward a value below one. We have confirmed this behavior for several other domains of the parameter space.

The analysis supports the conclusion that microstate geometries with an angular momentum that is at a finite fraction of the cosmic censorship bound must have a difference in scale between their inter-center distances and the lowest possible charges in V .

5.3.2 Analysis with three GH centers and one Supertube

The details of the numerical analysis are in Appendix A.3. We first focus on solutions without scale differences between the inter-center distances (5.3.2). After scanning relevant domains of the space of parameters, we have reached the following conclusions when looking for the best value of \mathcal{H} :

- The optimal location of the Supertube is the outermost one: $(0, 0, a_1)$.

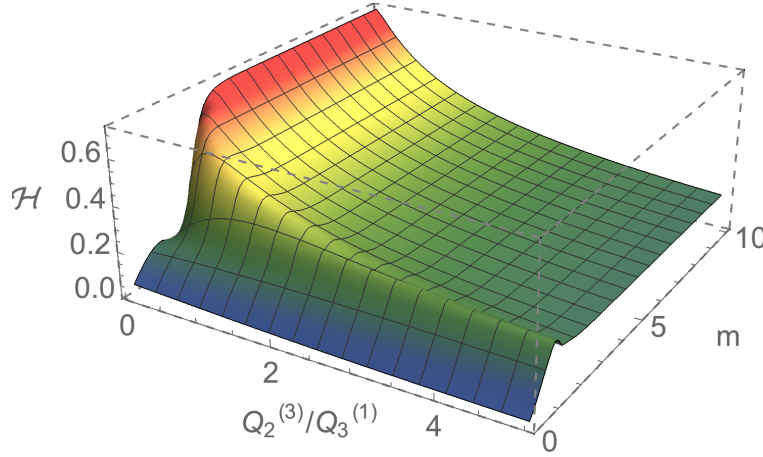


Figure 5.3: The entropy parameter \mathcal{H} as a function of $\frac{Q_2^{(3)}}{Q_3^{(1)}}$ and the initial hierarchy parameter $m = \log_{10} \left[\frac{a_1}{a_2} \right] = \log_{10} \left[\frac{a_2}{a_3} \right]$. The other parameters are fixed to the following values $q_0 = q_1 = q_2 = 1$, $k_1 = -k_2 = k_3 = 1$, $\frac{Q_2^{(1)}}{Q_1^{(3)}} = 0.9$ and $\frac{Q_3^{(2)}}{Q_1^{(2)}} = 2$.

- The Gibbons-Hawking charges q_a should have the smallest possible absolute value, $|q_2| = |q_3| = |q_0| = 1$, in agreement with what we found for four GH centers.
- All sign configurations for the initial dipole charges k_a appear to be equally favored. We find that, when k_2 is taken negative, the entropy parameter reaches a maximum for a particular value of $\frac{k_1}{k_3}$, regardless of the values of the other parameters.
- For aspect ratios satisfying (5.3.2), the maximal value of \mathcal{H} is around 0.25.

The analysis confirms what we anticipated: When only two generalized spectral flows are performed, the resulting solutions have lower angular momentum. Thus, one can reach a finite value of \mathcal{H} even without a hierarchy of scales.

We just found in the previous section that hierarchic configurations can improve the value of the entropy parameter, at least for four GH centers. So we would like to investigate how adding a hierarchy of scales affects the angular momentum. For that purpose, let us consider the scale m as in (5.3.3). We can then evaluate the value of the entropy parameter for a large set of solutions with different values of m and the charge ratio $\frac{Q_3^{(2)}}{Q_1^{(2)}}$. The other parameters are fixed to optimal values according to the analysis performed for $m \approx 0$. The result is very surprising. As the value of m increases the value of the entropy parameter improves significantly and can stay arbitrarily close to $\mathcal{H} = 1$ in a large region of the moduli space. This maximal value is obtained for $m \sim 1.5$, so the hierarchy of scales is not too pronounced. Unexpectedly, the value of the entropy parameter decreases if we go beyond that optimal hierarchy, see Fig.5.4.

Solutions with $m \sim 1.5$ are non-spinning. Indeed, one can find CTC-free scaling solutions with one supertube and three Gibbons-Hawking centers for which the spectral flow transformations completely annihilate the original angular momentum. However, those solutions typically have irrational charges.

To obtain solutions with integer charges and fluxes, one has to round these charges to nearby rational ones, and this typically brings back some angular momentum. However, the value of this angular momentum is proportional to the rounding, and hence can be made arbitrarily small by tightening the rounding. Hence, one can find regular scaling solutions with an entropy parameter infinitesimally close to one.

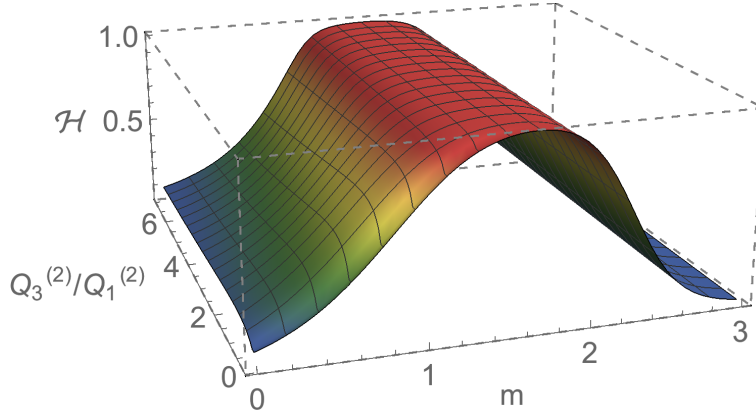


Figure 5.4: Representation of the entropy parameter \mathcal{H} as a function of the charge ratio $\frac{Q_3^{(2)}}{Q_1^{(2)}}$ and the order of magnitude of the inter-center distance ratio. The other parameters are $q_0 = q_2 = 1$, $k_1 = -k_2 = k_3 = 1$, $\frac{Q_2^{(1)}}{Q_1^{(3)}} = 0.85$ and $\frac{Q_2^{(3)}}{Q_3^{(1)}} = 0.009$.

5.4 Final comment

In this chapter, we have reviewed works about smooth 1/8-BPS multicenter solutions in the black-hole regime. First, we have highlighted a strong dependence between the bubbling geometry of scaling solutions with collinear centers and their background moduli. We have shown that walls of marginal stability might exist, which is contrary to the properties expected for typical microstates. Second, we have constructed the largest known family of multicenter smooth microstate geometries from three Supertubes in Taub-NUT. Thanks to a well-defined parameter space, we have shown that multicenter smooth solutions in six dimensions can have arbitrarily low angular momentum, which was thought to be only possible using Superstrata. We have stressed the need for a hierarchy of scales in the center configuration.

Counting Multicenter solutions at low charges

The “Holy Grail” of the microstate-geometry program and the fuzzball proposal is to build “ e^S ”, or even a significant fraction, of smooth horizonless supersymmetric geometries in the black-hole regime. In the previous sections, we have constructed many of such solutions. Counting them is an other issue out of reach.

In this chapter, we review the work of [26] which addresses a less ambitious problem but with meaningful conclusions. We study the space of BPS states in type IIA String Theory on a $\mathbb{T}^6 = \mathbb{T}^2 \times \mathbb{T}^2 \times \mathbb{T}^2$ wrapped by one D6 brane and three D2 branes wrapping the a two-torus each. The configuration is the low-charge equivalent of the non-rotating BMPV¹. A microscopic counting showed that, for this low-charge configuration, the number of ground states is 12 [143–145]. We show that these 12 states are all recovered as Coulomb branch BPS multicenter bound states, in which each center preserves 16 supercharges. They are the low-charge equivalent of what might describe “near-horizon limit” of fuzzballs.

We will describe those 12 multicenter bound states using the STU language of charge vectors, centers and background vector reviewed in Section 4.1 and the picture in the D0-D2-D4-D6 frame is given in (4.1.37). In Section 6.1 we will define the problem in detail. In Section 6.2 we give our methodology for building all multicenter bound states corresponding to the asymptotic pure D6-D2-D2-D2 charges. Finally, in Section 6.3, we discuss the main features of the 12 solutions, their description within the quiver-quantum-mechanics framework and the extension of our construction to D-brane bound states with $Q_{D6} = 2$.

6.1 Setting the problem

Type II String Theory on a Calabi-Yau three-fold with D-branes wrapped on various cycles has been an extensively studied for state counting [146, 147, 145, 148]. There are essentially three regimes in which one can work, depending on the value of g_s and the number of D-branes N (see Fig.6.1).

Thus far, we have essentially focused the discussion on the regime of validity of Supergravity, $g_s N \gg 1$. The Higgs branch is the one supporting the microscopic single D-brane picture of bound states and leads to exact results at infinitesimally small g_s . By increasing g_s , two scenarios are possible. The first one is that the Higgs-branch states are recovered as single center black hole solutions. The second possible scenario is that the D-brane charges gather in several centers forming a molecule-like BPS bound states described by quiver quantum mechanics. We denote this branch as the multicenter

¹One can dualize the BMPV solution of the STU model reviewed in Section 4.1.2 in type IIA on \mathbb{T}^6 (4.1.35). In this frame the D0-charge corresponds to the five-dimensional left-moving angular momentum J_L .

“Coulomb” branch². One can still define two regimes inside this branch: the supergravity regime, valid as long as $g_s N \gg 1$ which is now familiar to us, and the quiver regime, in which the system is described by a quiver quantum mechanics³.

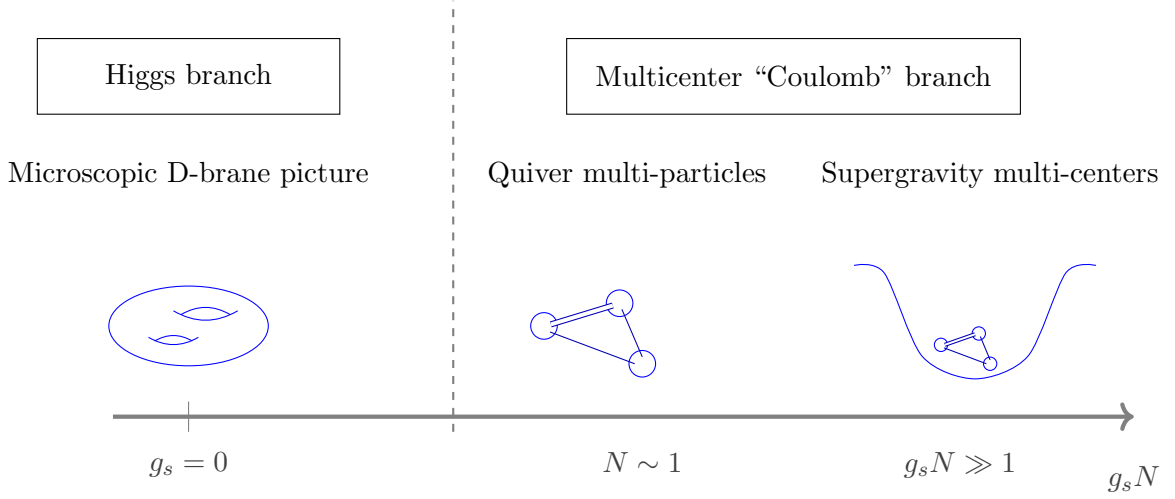


Figure 6.1: The description of a D-brane system in different regimes of parameters where g_s is the string coupling and N is the total number of branes.

The D6-D2-D2-D2 1/8-BPS bound states one wants to describe are determined, in the charge-vector notation, by the following global charges:

$$(Q_{D6}, Q_{D4}^1, Q_{D4}^2, Q_{D4}^3; Q_{D2}^1, Q_{D2}^2, Q_{D2}^3, Q_{D0}) = (Q_{D6}, 0, 0, 0; 1, 1, 1, 0), \quad Q_{D6} = 1 \text{ or } 2. \quad (6.1.1)$$

In the Higgs branch, the number of states is 12 and 56 for $Q_{D6} = 1$ and $Q_{D6} = 2$ respectively [143–145]. At a generic point of moduli space, the angular momentum of the microscopic D-brane states was found to be strictly zero⁴. Motivated by this result at $g_s N \ll 1$, it was conjectured that typical microstates of supersymmetric black holes continue to carry zero angular momentum at a generic point of the moduli space⁵. The conjecture seems to relegate all smooth horizonless solutions found so far to the rank of atypicality. We will see in Chapter 9, in full generality, that this is actually not true.

We test the conjecture in the multicenter Coulomb branch by building all the BPS multicenter bound states with global charges (6.1.1) and by investigating their possible moduli at infinity⁶. Strictly speaking, we are in a multicenter Coulomb branch, far from the supergravity regime ($g_s N \ll 1$) and one should construct these configurations as solutions of quiver quantum mechanics. However, thanks to the work done in [76, 149, 150, 87, 151, 141], one knows that the conditions of existence for quiver BPS multi-particle solutions are exactly the same as the ones for BPS multicenter solutions in the supergravity picture even if the supergravity solution is not reliable. As long as the geometry is not considered, the picture of charge vectors located at some centers still holds true for $g_s N \ll 1$. Thus, for a counting problem, one can use the STU framework reviewed in Section 4.1.1.5 to build the BPS solutions and study their general properties.

²The Coulomb branch is not the same as the Coulomb branch obtained by moving the D2 and D6 branes away from each other. We are referring to the multicenter Coulomb branch where the separations between the centers cannot be modified freely.

³See [87] for an exhaustive description of the different regimes.

⁴Remind that in the D0-D2-D4-D6 frame, there is only one angular momentum. Compared to our notation in the STU model, J_R is this angular momentum and J_L is now a D0-charge.

⁵Which includes g_s .

⁶Remind that the background moduli given by Γ_∞ determines the angular momentum J_R (4.1.56).

In this chapter we will then consider generic 1/8-BPS multicenter solutions with an arbitrary center configuration. As already said, a state in the STU model is uniquely defined by a set of eight-dimensional charge vectors Γ_j and inter-center distances ρ_{ij} . We first write down all the physical constraints to construct bound states with the global charges (6.1.1):

- The regularity conditions.

First and foremost, the solutions have to be regular. They must satisfy the Denef equations (4.1.26) and the absence of CTC (4.1.27).

- The global charges.

Being interested in specific D-brane charge configurations we express the quantized asymptotic D-brane charges according to the charges at each center [152]. They are derived from flux-integrals of the R-R gauge field forms $C^{(1)}$ and $C^{(3)}$ and their dual gauge fields $C^{(5)}$ and $C^{(7)}$ (4.1.35):

$$\begin{aligned} Q_{D6} &= \int_{S_\infty^2} dC^{(1)} = \sum_j q_j, & Q_{D4}^I &= \int_{S_\infty^2 \times \mathbb{T}_I^2} dC^{(3)} = \sum_j k_j^I, \\ Q_{D0} &= \int_{S_\infty^2 \times \mathbb{T}^6} dC^{(7)} = \sum_j m_j, & Q_{D2}^I &= C_{IJK} \int_{S_\infty^2 \times \mathbb{T}_J^2 \times \mathbb{T}_K^2} dC^{(5)} = \sum_j l_j^I. \end{aligned} \quad (6.1.2)$$

The condition on the charge vectors is then

$$\sum_j \Gamma_j = (Q_{D6}, 0, 0, 0; 1, 1, 1, 0), \quad Q_{D6} = 1 \text{ or } 2. \quad (6.1.3)$$

- Physical center configurations.

The inter-center distances that are solutions of Denef equations must correspond to physical sets of centers. With three centers for instance, the distances must satisfy the triangle inequality. With more centers, the condition gets more complicated and consists in several triangle and angle inequalities.

- The types of centers.

We are looking for BPS multicenter solutions with four supercharges, the choice of charge vectors is restricted to the one that preserves supersymmetry. Following the Bena-Warner ansatz [153], it is more likely that a system of low or pure D-brane charges (6.1.2) is fully or largely composed of maximally-supersymmetric BPS objects. The maximally-supersymmetric centers are the two-charge round Supertubes (4.1.61), the GH centers (4.1.58) and the simple D-brane centers. Since simple D-brane centers can be obtained from Supertubes by taking some of the charges to be zero, we will misuse the generic term supertube center, even for these objects.

- The background moduli.

We will construct our solutions at a point of the background moduli space where $\Gamma_\infty = 0$. From a supergravity point of view, this corresponds to impose AdS_2 asymptotics. This choice is motivated by the fact that the angular momentum J_R is vanishing in this situation (4.1.56) while other background moduli generally gives in a non-zero value. However, once the solutions are constructed, we plan to move away from this point by performing background transformations that we have studied in Section 5.1 and to test the zero-angular-momentum conjecture.

In the next section, we give our methodology to construct the BPS multicenter solutions satisfying all those constraints.

6.2 Counting zero-momentum multicenter states with pure D2 and D6 charges

Our approach consists in scanning analytically or numerically all the valid multicenter solutions starting with the family of three-center solutions then the family of four-center solutions and finally the five-

center solutions⁷. The growing complexity of the analysis does not allow to scan solutions with more than five centers but we have a strong intuition that adding centers increases necessarily the global D-brane charges of the solution. Thus, if solutions exist, they should consist in few centers. We have found exactly 12 distinct three-center solutions satisfying all those constraints. This matches exactly the microscopic counting. Readers interested only in the main ideas of our analysis can skip the next subsections until Section 6.2.4.

6.2.1 The family of three-center solutions

One needs at least one GH center in the configuration to have a non-zero D6 charge. We divide our analysis in three subfamilies:

- Solutions with one GH center and two supertube centers.
- Solutions with two GH centers and a Supertube.
- Solutions with three GH centers.

For the first subfamily, an analytic approach is possible. All the details of this analysis are given in Appendix A.4.1. The main result is that there exist 12 inequivalent solutions in this subfamily. As for the second and the third families, the number of parameters makes the analytic approach impossible. However, we have performed an efficient numerical analysis, fully detailed in Appendix A.4.2. We have scanned a significant part of the parameter space of the solutions by varying each GH charge q_j , k_j^1 , k_j^2 , k_j^3 and supertube charges k_j , $Q_j^{(I)}$ from -500 to 500. We didn't find any solution satisfying all the constraints in this domain of values.

In [154], the authors have tackled a similar issue by analyzing the parameter space of three-GH center solutions whose the total D6 charge is three and the three D2 charges are one. Interestingly, they have found that the total number of such multicenter solutions is also 12. This is half a coincidence with our computation. Even if the three-center solutions they study have a larger Q_{D6} ⁸, the form of their specific solutions are governed by the same type of permutations that gives to the 12 states we found here.

6.2.2 The family of four-center solutions

A four-center solution has more degrees of freedom than the previous solutions and the constraints are more complicated to deal with. This makes any analytic investigation very hard to perform. However, we have done a numerical analysis of the following subfamilies:

- Solutions with one GH center and three supertube centers.
- Solutions with two GH centers and two Supertubes.
- Solutions with three GH centers and a Supertube.
- Solutions with four GH centers.

For each subfamily, we have analyzed a significant part of the parameter space by varying all the parameters from -10 to 10. The details are given in the Appendix A.5.1. Our final result is that there are no valid solutions with four centers.

⁷Two-center solutions with GH centers or supertube centers have 8 remaining supercharges. Hence they do not correspond to the system we study.

⁸Total number of microscopic states with $Q_{D6} = 3$, $Q_{D4}^I = 0$, $Q_{D2}^I = 1$, $Q_{D0} = 0$ is actually 208 [145].

6.2.3 The family of five-center solutions

For five-center solutions, even a scan of the parameter space is complicated. This is principally due to the number of parameters available and the complexity of the constraints. However, we have been able to pick randomly a huge number of solutions with the right global D-brane charges and check if they can satisfy the bubble equations and the absence of closed timelike curves at the same time. We did not find any. This gives good intuition that no solutions with five centers exist as well.

6.2.4 Summary

We have analyzed analytically and numerically a huge number of BPS multicenter solutions to find only 12 solutions satisfying all the constraints. This exactly matches the exact counting of the 12 Higgs-branch states [143]. They are all recovered as Coulomb branch multicenter bound states. They belong to the family of three-center solutions with one GH center and two Supertubes of different species. The 12 solutions are given in full detail in Table 6.1. Moreover, as explained in Section 6.1, for most of the solutions found, the two-charge-supertube centers are actually simple fluxed D-brane centers⁹. For instance, the six first solutions in Table 6.1 have a GH center and two D4-brane centers with an induced D2 charge. The six other solutions have one GH center, one two-charge-supertube center and one simple D2-brane center with an induced D0 charge.

We do not have indisputable arguments that having more centers will not give rise to other valid solutions but only good intuition. Usually, adding centers increases the global D-brane charges. Another difficulty in adding centers follows from the fact that these centers must carry negative D-brane charges, in order to keep the total D-brane charges intact. However usually centers with negative D-brane charges are tricky, when it comes to the $Z_I V \geq 0$, i.e. absence of closed timelike curves. For these reasons, we can consider our analysis exhaustive even if we have analyzed configuration with few centers.

6.3 Discussion

6.3.1 Features of the twelve solutions

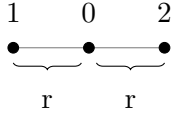
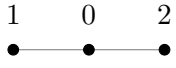
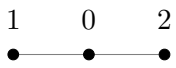
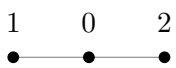
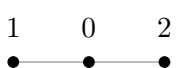

The 12 solutions found are all BPS three-center solutions formed by one GH center and two other 16-supercharge centers. Although we looked for all possible center configurations, it happens that the regular solutions we found have their centers lying on a line and hence are all axisymmetric. The fact that the index is reproduced by counting configurations with collinear centers was also observed in [142] and, given the very complicated algebra that required our physical solutions to be collinear, we do not believe this is a coincidence.

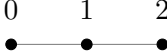
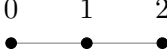
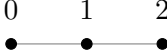
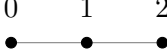
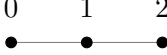
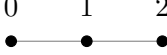
We can now investigate what kind of moduli at infinity determined by Γ_∞ are compatible with our multicenter solutions. The fact that microstates of black holes have necessarily zero angular momentum at any point of the moduli space has been conjectured in [155, 156, 144]. Nevertheless, we will argue that a single-center black hole does not correspond to any pure state of the CFT_1 dual to AdS_2 in the Chapter 9 [25], and the zero-angular momentum asymptotically AdS_2 solutions dual to pure states of the CFT_1 will have a non-trivial angular momentum when embedded in asymptotically AdS_3 geometries.

We would like to understand whether our 12 multicenter solutions can also develop a non trivial angular

⁹This means that some of D-brane charges of the two-charge Supertube are zero.

Table 6.1: The 12 multicenter solutions with global D-brane charges $(Q_{D6}, Q_{D4}^1, Q_{D4}^2, Q_{D4}^3; Q_{D2}^1, Q_{D2}^2, Q_{D2}^3, Q_{D0}) = (1, 0, 0, 0; 1, 1, 1, 0)$.

N	Charge vectors at each center $\Gamma_j = (Q_{D6}, Q_{D4}^1, Q_{D4}^2, Q_{D4}^3; Q_{D2}^1, Q_{D2}^2, Q_{D2}^3, Q_{D0})_j$	Center configuration
1	$\Gamma_0 = (1, 1, -1, 0; 0, 0, 1, 0)$ $\Gamma_1 = (0, -1, 0, 0; 0, 1, 0, 0)$ $\Gamma_2 = (0, 0, 1, 0; 1, 0, 0, 0)$	
2	$\Gamma_0 = (1, -1, 1, 0; 0, 0, 1, 0)$ $\Gamma_1 = (0, 1, 0, 0; 0, 1, 0, 0)$ $\Gamma_2 = (0, 0, -1, 0; 1, 0, 0, 0)$	
3	$\Gamma_0 = (1, 0, 1, -1; 1, 0, 0, 0)$ $\Gamma_1 = (0, 0, -1, 0; 0, 0, 1, 0)$ $\Gamma_2 = (0, 0, 0, 1; 0, 1, 0, 0)$	
4	$\Gamma_0 = (1, 0, -1, 1; 1, 0, 0, 0)$ $\Gamma_1 = (0, 0, 1, 0; 0, 0, 1, 0)$ $\Gamma_2 = (0, 0, 0, -1; 0, 1, 0, 0)$	
5	$\Gamma_0 = (1, 1, 0, -1; 0, 1, 0, 0)$ $\Gamma_1 = (0, -1, 0, 0; 0, 0, 1, 0)$ $\Gamma_2 = (0, 0, 0, 1; 1, 0, 0, 0)$	
6	$\Gamma_0 = (1, -1, 0, 1; 0, 1, 0, 0)$ $\Gamma_1 = (0, 1, 0, 0; 0, 0, 1, 0)$ $\Gamma_2 = (0, 0, 0, -1; 1, 0, 0, 0)$	

7	$\Gamma_0 = (1, -1, 0, 0; 0, 0, 0, 0)$ $\Gamma_1 = (0, 1, 0, 0; 0, 1, 1, 1)$ $\Gamma_2 = (0, 0, 0, 0; 1, 0, 0, -1)$	
8	$\Gamma_0 = (1, 1, 0, 0; 0, 0, 0, 0)$ $\Gamma_1 = (0, -1, 0, 0; 0, 1, 1, -1)$ $\Gamma_2 = (0, 0, 0, 0; 1, 0, 0, 1)$	
9	$\Gamma_0 = (1, 0, -1, 0; 0, 0, 0, 0)$ $\Gamma_1 = (0, 0, 1, 0; 1, 0, 1, 1)$ $\Gamma_2 = (0, 0, 0, 0; 0, 1, 0, -1)$	
10	$\Gamma_0 = (1, 0, 1, 0; 0, 0, 0, 0)$ $\Gamma_1 = (0, 0, -1, 0; 1, 0, 1, -1)$ $\Gamma_2 = (0, 0, 0, 0; 0, 1, 0, 1)$	
11	$\Gamma_0 = (1, 0, 0, -1; 0, 0, 0, 0)$ $\Gamma_1 = (0, 0, 0, 1; 1, 1, 0, 1)$ $\Gamma_2 = (0, 0, 0, 0; 0, 0, 1, -1)$	
12	$\Gamma_0 = (1, 0, 0, 1; 0, 0, 0, 0)$ $\Gamma_1 = (0, 0, 0, -1; 1, 1, 0, -1)$ $\Gamma_2 = (0, 0, 0, 0; 0, 0, 1, 1)$	

momentum when embedded in an asymptotically AdS_3 space, or whether they are incompatible with $J_R \neq 0$. We have discussed in great detail the effect of background transformations on collinear configurations in Section 5.1. We illustrate the result with our specific examples here.

- Due to the numerous zeroes in the charge vectors, there are many possible Γ_∞ that preserve $J_R = 0$. However, one needs to carefully check that these Γ_∞ 's do not induce closed timelike curves. We give the list of possible moduli at infinity compatible with our solutions and preserving the vanishing-angular momentum. Because all the 12 solutions have similar properties, it suffices to list the possibilities corresponding to the first solution in the Table 6.1. We list only the interesting moduli at infinity and their holographic meaning:
 - $\Gamma_\infty = 0$. The 12 bound states are thus holographically dual to the 12 ground states of a CFT_1 . In anticipation of Chapter 9, Our results corroborate the conjecture that the “ e^S ” ground states of a non-topological CFT_1 must break conformal invariance [25]. So, all their bulk duals must have a scale, as it is actually the case for multicenter or superstratum solutions¹⁰.
 - $\Gamma_\infty = (0, 0, 0, 0; 0, 0, 1, 0)$. The meaning of this choice can be seen only from a six-dimensional point of view in the dual D1-D5-P frame. In this frame, the solution turns out to be an asymptotically AdS_3 state.

Both kinds of moduli at infinity impose $J_R = 0$ and do not have any impact on the center configuration.

- There are also moduli at infinity which do not preserve the symplectic products $\langle \Gamma_\infty, \Gamma_j \rangle$ and therefore give rise to a finite angular momentum, J_R , without affecting the D-brane charges. According to the methodology developed in Section 5.1, this type of background transformation necessarily breaks the $U(1)$ isometry of the centers. A configuration with 3 centers has two angles to vary. One can prove that any moduli at infinity which has $\langle \Gamma_\infty, \Gamma_j \rangle \neq 0$ and which does not induce closed timelike curves is incompatible with our solutions. Our multicenter solutions illustrate perfectly the background sensitivity of collinear configuration. Therefore, all solutions are incompatible with having a non-zero angular momentum.

This corroborates in a different regime of g_s the zero-angular-momentum conjecture [155, 156, 144]. However, from an holographic point of view, the solutions can be either asymptotically AdS_3 ¹¹ or asymptotically AdS_2 solutions.

6.3.2 Quantum Effects

Thus far, our analysis has been classical. However the charges considered being small, one might expect quantum effects to significantly modify our analysis. Of particular interest is the fate of angular momentum when quantum mechanical effects are taken into account. A classical configuration with angular momentum J_3 is known to furnish a spin $J_3 - 1/2$ representation of $SO(3)$, when quantum effects are taken into account [87]. This makes the present case, which corresponds to $J_3 = 0$, particularly puzzling. Since there is nothing called a spin $-1/2$ representation, either the angular momentum does not receive quantum correction in this particular case, or there are no supersymmetric ground states corresponding to the multicenter configurations carrying classically zero angular momentum.

To settle this question, one must analyse these multicenter configurations quantum mechanically. The framework for this has been laid down in [87], where it has been shown that such multicenter configurations (equivalently intersecting D-branes wrapping various cycles of a Calabi-Yau threefold) are described by $\mathcal{N} = 4$ quiver quantum mechanics. For an exhaustive discussion, we refer the interested reader to [157, 87, 141, 158, 159].

¹⁰For multicenter solutions, the scale is determined by the inter-center distances.

¹¹When dualized to the D1-D5-P duality frame in type IIB.

Briefly, field content of a quiver quantum mechanics is encoded in a quiver diagram, which has as many nodes as centers and as arrows between nodes. The j^{th} node corresponds to a vector multiplet with $U(N_j)$ gauge symmetry, with N_j being determined by the charge vector Γ_j . For primitive Γ_j , which is the case at hand, one has $N_j = 1$. Thus we shall restrict to Abelian quivers. For $\langle \Gamma_j, \Gamma_i \rangle > 0$, there are $\langle \Gamma_j, \Gamma_i \rangle$ arrows stretching from j^{th} node to i^{th} node, each corresponding to a hypermultiplets in the $U(1) \times \overline{U(1)}$ bifundamental. The dynamics of the fields is captured by a quiver Lagrangian fully determined by the charge vectors, their intersection products, Fayet-Iliopoulos parameters (henceforth referred to as FI parameters) and superpotential (when the quiver has loops).

Each of the 12 solutions corresponds to a three node Abelian quiver. For each quiver, we define the unique triplet of integer intersection product $(a, b, c) \equiv (\langle \Gamma_i, \Gamma_j \rangle, \langle \Gamma_j, \Gamma_k \rangle, \langle \Gamma_k, \Gamma_i \rangle)$ where i, j, k are three different integers between 0 and 2 in order to satisfy $a \geq b > 0$ and $c > 0$. Each quiver has a closed loop and (a, b, c) satisfies the three triangle inequalities, $a + b \geq c$ and permutations. Three-nodes quivers have been extensively studied in the literature, particularly the ones with a closed loop [87, 141, 158, 159], for non-zero FI parameters. However we have vanishing FI parameters, which makes a lot of difference. In the following we analyze the relevant quiver.

All 12 solutions correspond to $(a, b, c) = (2, 1, 1)$ or some permutations thereof. Thus, the quiver under discussion is the following

$$\begin{array}{ccc}
 & \textcircled{1} & \\
 X \nearrow & & \searrow Y \\
 \textcircled{1} & \xleftarrow{C_1, C_2} & \textcircled{1}
 \end{array} . \tag{6.3.1}$$

The D-term equations read as follows

$$\begin{aligned}
 |X|^2 - |C_1|^2 - |C_2|^2 &= 0 \\
 |Y|^2 - |X|^2 &= 0 \\
 -|Y|^2 + |C_1|^2 + |C_2|^2 &= 0.
 \end{aligned} \tag{6.3.2}$$

Following [158], we assume a generic cubic superpotential

$$W = w_i X Y C_i, \tag{6.3.3}$$

which gives the following F-term equations

$$w_i Y C_i = 0, \quad w_i X C_i = 0, \quad X Y = 0.$$

The last equation requires either X or Y to vanish. But the second D-term equation implies that both X and Y vanishes. The remaining D-term equations imply $C_i = 0$. Thus, the moduli space is a single point and hence furnishes a spin 0 representation of Lefschetz $SU(2)$. Thus we indeed have one quantum ground state with vanishing angular momentum. It is interesting to note that the vacuum preserves $U(1) \times U(1)$.

In order to decide whether this should be counted as pure-Higgs state or not, it is instructive to briefly describe the similar computation carried out in [158], but with non-zero FI parameters. After one of the three variables has been set to zero, in order to satisfy F-term equations, the D-term equations define a product of two projective spaces and the remaining F-term equation define a complete intersection manifold in this product of projective spaces. The Betti numbers of the complete intersection manifold, can be read out from those of the ambient space, except middle cohomology, where there can be extra states called “pure-Higgs states”.

In the present case, the FI parameters are zero and then the projective space collapses to a point. Consequently, the cohomology of the ambient space consists of a single state, which lies in the middle cohomology. So it is not very clear whether to count this state as pure-Higgs or not. We have however showed that each of the 12 quivers has only one ground state which hopefully leave the total of 12 states as expected from [143, 144].

The argument for general (a, b, c) is not very different as discussed in Appendix A.7.

6.3.3 The solutions with $Q_{D6} = 2$

As it has been done in [144], one can extend our construction to compute the number of BPS states in supergravity framework with global D-brane charges:

$$Q_{D6} = 2, \quad Q_{D4}^I = 0, \quad Q_{D2}^I = 1, \quad Q_{D0} = 0 \quad (6.3.4)$$

The index is known to be 56 for these charges [145, 144]. We have been able to find only 18 BPS bound states formed by three centers similar to the ones described in Section 6.2 and 12 BPS unbound states formed by four axisymmetric centers. The special aspect of those 12 unbound states is that one of the centers does not interact with the other centers and can be placed anywhere on the axis of the center configuration. We did not consider these solutions because they are similar to the “real Coulomb” branch where the centers can move freely. Since we did not count the unbound Coulomb-branch configuration with non-interacting D6 center and three D2 centers, we are not counting these unbound states either. The charge vectors of the 18 three-center bound states are given in Table A.1 in the Appendix A.6.

One can also describe the 18 states as three-node quivers with a closed loop and vanishing FI parameters. The only difference is that for $Q_{D6} = 2$, 9 solutions are given by the triplet $(a, b, c) = (3, 2, 1)$ and the 9 others give $(a, b, c) = (3, 1, 2)$ (see Table A.1). This does not affect our general argument discussed in Appendix A.7. Each quiver has only one ground state which keeps the total of 18 states.

Our present construction technique does not allow easily to go beyond the multicenter solutions with GH centers or supertube centers and to find the 38 missing states. This will require more work in future projects. However, one can already have an idea of where these states may come from:

- Adding extra gauge fields and preserving the $U(1) \times U(1)$ isometry of the base space. Following [160, 161], one can add for example a fourth massless abelian gauge field to the configuration, which corresponds to changing the fluxes on the T^6 . The solutions will be slightly more complex but they will remain $U(1) \times U(1)$ invariant and one may hope, along the line of [142], that these will contribute to the index.
- Constructing configurations which break the $U(1) \times U(1)$ isometry. Such objects may include wiggly Supertubes [139] or superstratum configurations [30, 99]. In four dimensions, these solutions give rise to KK modes along the two $U(1)$ fibers of the base space and do not correspond to supergravity solutions.

6.4 Final comment

In this chapter, we have investigated the space of states of one or two D6 branes with pure D2-D2-D2 branes (6.1.1).

For $Q_{D6} = 1$, we have found exactly 12 BPS multicenter bound states. We have confirmed the counting from a quiver description by showing that the corresponding 12 quivers have only one supersymmetric ground state each. In this instance, all the microscopic D-brane states are recovered as BPS multicenter bound states and no single-center state should exist. This conveys the idea that BPS multicenter

microstates which are types of fuzzballs in the macroscopic regime do not correspond to a peculiar part of the overall space of states of a certain D-brane system. Furthermore, we have shown that the 12 multicenter solutions carry necessarily zero angular momentum at this point of the moduli space giving greater weight to the zero angular momentum conjecture. From a supergravity point of view, this means that they are incompatible with having flat asymptotics.

For $Q_{D6} = 2$, only 18 BPS multicenter bound states have been found. We expect more multicenter solutions to exist. Indeed, our construction essentially focuses on $U(1) \times U(1)$ invariant centers carrying 16-supercharges. One can expect, for configurations with more than pure D-brane charges, that less-isometric solutions exist. Such centers may be more exotic and less supersymmetric, such as wiggly Supertubes. Nevertheless, the 18 solutions found also confirm the zero angular momentum conjecture.

The ultimate single-mode Superstratum

The construction of superstratum states in the CFT requires the generators of the “small,” anomaly-free $\mathcal{N}=4$ superconformal algebra act on a particular “length- k ” strand in the NS-NS ground state of the D1-D5 CFT. This technique generates a non-vanishing momentum P charge. In Section 4.2.4, we restricted the generators to the left-moving sector of the SCFT and to the bosonic generators as it has been done in the pioneer works [30, 98–101]. However, the left-moving sector of the small SCFT contains also fermionic generators that can be used as bosonic operators by acting twice [31]. The fermionic operators of interest in the NS-NS sector are $G_{-1/2}^{+A}$ where $A = 1, 2$ is the index for an $SU(2)_B$ group related to the internal manifold. By acting with $G_{-1/2}^{+1}G_{-1/2}^{+2}$ on the two-charge seed solutions, the states are “supercharged” and momentum charge is generated [31]. We introduce then a fourth quantum number q of excitation modes associated to these generators. This quantum number is limited to 0 or 1 due to the fermionic nature of the generators. In the NS-NS sector, the single-mode superstratum states are then given by

$$|k, m, n, q\rangle^{\text{NS}} = \begin{cases} (J_0^+)^m (L_{-1})^n |O^{--}\rangle_k, & q = 0 \\ (J_0^+)^{m-1} (L_{-1})^{n-1} \left(G_{-1/2}^{+1} G_{-1/2}^{+2} + \frac{1}{k} J_0^+ L_{-1} \right) |O^{--}\rangle_k, & q = 1, \end{cases} \quad (7.0.1)$$

where $n \geq 1$ and $k > 0, k - q \geq m \geq 1$. The generators $\frac{1}{k} J_0^+ L_{-1}$ were introduced to make the operators commute. The first line in (7.0.1) corresponds to the original superstratum modes constructed in Section 4.2.5 while the second line is the supercharged modes constructed in [31]. In the gravity side, the duals of the pair of fermionic generators are slightly more complicated than diffeomorphisms on $\text{AdS}_3 \times S^3$ and correspond to modifications of the Killing spinors on $\text{AdS}_3 \times S^3 \times \mathbb{T}^4$. We will not review the fermionically generating technique here and refer the interested reader to [31] for an exhaustive discussion. In Section 7.1, we simply review the essential elements of the single-mode supercharged Superstrata in six-dimensions Supergravity.

For the rest of the chapter, we will review the work [28] and the construction of the *most general “single-mode” superstratum* using supercharged excitation modes. That is, we will make a “hybrid” of the original single-mode superstratum, dual to $|k, m, n, q = 0\rangle^{\text{NS}}$, and the supercharged superstratum state, dual to $|k, m, n, q = 1\rangle^{\text{NS}}$:

$$|k, m, n, q = 0\rangle^{\text{NS}} \otimes |k, m, n, q = 1\rangle^{\text{NS}}.$$

This will still be a “single-mode” superstratum as it depends only on one Fourier mode. However the two distinct states enter the supergravity through different tensor structures in Θ^4 and thus are represented by two distinct Fourier coefficients. As we will see, these two tensor structures are extraordinarily miscible and their combined back-reaction remains relatively simple.

We denote those modes as the “most general” single-modes since they appear to have the right form to be the essential building blocks for the construction of multi-mode Superstrata, unlike the

original single-mode Superstrata. More specifically, we will show that including the supercharged ($q = 1$) superstratum modes leads us to introduce new “leading” and “secondary” Fourier modes into the supergravity solution. In particular, the additional secondary Fourier coefficients allow us to solve the essential coiffuring constraints and leave us with precisely the correct set of free leading Fourier coefficients, b_{k_i, m_i, n_i, q_i} , that are the duals of the freely choosable N_{k_i, m_i, n_i, q_i} in the CFT (4.2.53). We thus have exactly the right number of free parameters to describe a generic multi-moded superstratum that is a function of three independent variables and is dual to a generic state of the form (4.2.53). This echoes the fact that the original single-mode Superstrata have no free moduli once smoothness is imposed, the remaining parameters are completely determined by the bulk thermodynamic variables: the charges and the angular momenta of the system. Our new “hybrid” single-mode superstrata have a modulus that varies the amount of each species of states.

7.1 Supercharged Superstrata

We now review the supergravity solutions for supercharged Superstrata recently obtained in [31]. Our discussion will closely parallel that of Section 4.2.5, but all the “supercharged” quantities will be denoted with a “ $\hat{}$ ” as opposed to a “ \sim ”.

7.1.1 The first layer

The non-trivial excitations in the first layer of the BPS system now have the form:

$$\hat{z}_{k,m,n} = 0, \quad \hat{\vartheta}_{k,m,n} = \sqrt{2} \Delta_{k,m,n} \left[\frac{\Sigma}{r \sin \theta} \Omega^{(1)} \sin v_{k,m,n} + \left(\Omega^{(2)} + \Omega^{(3)} \right) \cos v_{k,m,n} \right], \quad (7.1.1)$$

where $\Delta_{k,m,n}$ and $v_{k,m,n}$ are defined in (4.2.57) and the self-dual basis, $\Omega^{(i)}$, $i = 1, 2, 3$, is defined in (4.2.58). It is elementary to check that these modes satisfy the first layer of BPS equations (4.2.28):

$$\mathcal{D} \hat{\vartheta}_{k,m,n} = 0, \quad \hat{\vartheta}_{k,m,n} \wedge d_4 \beta = 0, \quad \hat{\vartheta}_{k,m,n} = *_4 \hat{\vartheta}_{k,m,n}. \quad (7.1.2)$$

This new fluctuating structure is remarkably simple. Indeed, one should note the orthogonality in the middle equation of (7.1.2) allows one to take $\hat{z}_{k,m,n} = 0$ in solving the first layer of the BPS equations. Moreover, the exterior products $\hat{\vartheta}_{k,m,n} \wedge \hat{\vartheta}_{k,m,n}$ and $\hat{\vartheta}_{k,m,n} \wedge \hat{\vartheta}_{k,m,n}$ are “self-coiffuring” in that the oscillations cancel and the only residual part are the RMS values of the excitations. This will be important in the “hybrid superstrata,” discussed in Section 7.2. We also note that the expression for $\hat{\vartheta}_{k,m,n}$ is precisely the coefficient of $\frac{mn}{k}$ in $\hat{\vartheta}_{k,m,n}$ (see (4.2.57)). This was important for orthogonalizing and mixing the original and supercharged superstrata states in the dual CFT. For rather similar reasons, this observation will play an essential role in Section 7.4, where we show how to coiffure generic, multi-mode superstrata.

The field content of the first layer of the supercharged superstratum is¹:

$$\begin{aligned} \hat{Z}_1 &= \frac{Q_1}{\Sigma}, & \hat{\Theta}_2 &= c_2 \frac{R_y}{2 Q_5} \hat{\vartheta}_{2k, 2m, 2n}, & \hat{Z}_2 &= \frac{Q_5}{\Sigma}, & \hat{\Theta}_1 &= 0, \\ \hat{Z}_4 &= 0, & \hat{\Theta}_4 &= c_4 \hat{\vartheta}_{k,m,n}. \end{aligned} \quad (7.1.3)$$

In analogy with the original superstrata, we have introduced a secondary mode in $\hat{\Theta}_2$. However, as we described above, the supercharged modes are “self-coiffuring” and so we will ultimately set $c_2 = 0$. On the other hand, such a term will be essential once in the hybrid superstratum solutions.

¹Compared to [31], we have replaced $\{m+1, n+1\} \rightarrow \{m, n\}$ and we have added a $\sqrt{2}$ factor to make the comparison with the original superstratum solution on an equal footing.

7.1.2 The second layer

As with the original superstrata, one expects the sources of the second layer of BPS equations to have an RMS part and an oscillating part that depends upon $v_{2k,2m,2n}$. However, because $\hat{Z}_4 = 0$ and $\hat{\Theta}_4$ is “self-coiffuring,” there are no terms that depend on $v_{2k,2m,2n}$ generated by \hat{Z}_4 and $\hat{\Theta}_4$. Thus the only oscillating source is proportional to c_2 and so we take:

$$c_2 = 0. \quad (7.1.4)$$

The solution for ω and \mathcal{F} is given by the sums of the seed supertube solutions and the solution for the new pieces:

$$\omega = \omega_0 + \hat{\omega}_{k,m,n}, \quad \mathcal{F} = 0 + \hat{\mathcal{F}}_{k,m,n}. \quad (7.1.5)$$

The equations (4.2.29) for $\hat{\omega}_{k,m,n}$ and $\hat{\mathcal{F}}_{k,m,n}$ reduce to:

$$\begin{aligned} d_4 \hat{\omega}_{k,m,n} + *_4 d_4 \hat{\omega}_{k,m,n} + \hat{\mathcal{F}}_{k,m,n} d_4 \beta &= 0, \\ \mathcal{L} \hat{\mathcal{F}}_{k,m,n} &= \frac{4c_4^2}{(r^2 + a^2) \cos^2 \theta \Sigma} [\Delta_{2k,2m,2n} + \Delta_{2k,2m+2,2n-2}], \end{aligned} \quad (7.1.6)$$

As in Section 4.2.5.2, one can solve directly the equation for $\hat{\mathcal{F}}_{k,m,n}$ using the generating function $F_{k,m,n}$, (4.2.70). As for $\hat{\omega}_{k,m,n}$, we define

$$\hat{\omega}_{k,m,n} \equiv \hat{\mu}_{k,m,n} (d\varphi_2 + d\varphi_1) + \hat{\zeta}_{k,m,n} (d\varphi_2 - d\varphi_1). \quad (7.1.7)$$

By shifting $\hat{\mu}_{k,m,n}$

$$\hat{\mu}_{k,m,n}^S \equiv \hat{\mu}_{k,m,n} + \frac{R_y}{4\sqrt{2}} \frac{r^2 + a^2 \sin^2 \theta}{\Sigma} \hat{\mathcal{F}}_{k,m,n}, \quad (7.1.8)$$

we have

$$\mathcal{L} \tilde{\mu}_{k,m,n}^S = \frac{R_y c_4^2}{\sqrt{2}} \frac{\Delta_{2k,2m+2,2n} + \Delta_{2k,2m,2n-2}}{(r^2 + a^2) \cos^2 \theta \Sigma}. \quad (7.1.9)$$

In terms of $F_{2k,2m,2n}$, (4.2.70), the form of $\hat{\mathcal{F}}_{k,m,n}$ and $\hat{\mu}_{k,m,n}$ is

$$\begin{aligned} \hat{\mathcal{F}}_{k,m,n} &= 4c_4^2 \left[F_{2k,2m,2n} + F_{2k,2m+2,2n-2} \right], \\ \hat{\mu}_{k,m,n} &= \frac{R_y c_4^2}{\sqrt{2}} \left[F_{2k,2m+2,2n} + F_{2k,2m,2n-2} \right] - R_y \frac{r^2 + a^2 \sin^2 \theta}{4\sqrt{2} \Sigma} \hat{\mathcal{F}}_{k,m,n} + \frac{R_y c^2}{4\sqrt{2} \Sigma}, \end{aligned} \quad (7.1.10)$$

where the term proportional to c is a harmonic piece that we can add to the solution of the Poisson equation for $\hat{\mu}_{k,m,n}^S$ and will be fixed by regularity in the next sub-section. Then, $\hat{\zeta}_{k,m,n}$ is determined by integrating ($s_\theta = \sin \theta$, $c_\theta = \cos \theta$)

$$\begin{aligned} \partial_r \hat{\zeta}_{k,m,n} &= \frac{r^2 \cos 2\theta - a^2 s_\theta^2}{r^2 + a^2 s_\theta^2} \partial_r \hat{\mu}_{k,m,n} - \frac{r \sin 2\theta}{r^2 + a^2 s_\theta^2} \partial_\theta \hat{\mu}_{k,m,n} - \frac{\sqrt{2} a^2 R_y r (2r^2 + a^2) s_\theta^2 c_\theta^2}{\Sigma^2 (r^2 + a^2 s_\theta^2)} \hat{\mathcal{F}}_{k,m,n}, \\ \partial_\theta \hat{\zeta}_{k,m,n} &= \frac{r(r^2 + a^2) \sin 2\theta}{r^2 + a^2 s_\theta^2} \partial_r \hat{\mu}_{k,m,n} + \frac{r^2 \cos 2\theta - a^2 s_\theta^2}{r^2 + a^2 s_\theta^2} \partial_\theta \hat{\mu}_{k,m,n} \\ &\quad + \frac{R_y a^2 r^2 (r^2 + a^2) \sin 2\theta \cos 2\theta}{\sqrt{2} \Sigma^2 (r^2 + a^2 s_\theta^2)} \hat{\mathcal{F}}_{k,m,n}. \end{aligned} \quad (7.1.11)$$

7.1.3 Regularity and conserved charges

The smoothness of supercharged solutions closely follows that of the original superstrata and are detailed in Section 4.2.5.3. The scalar $\hat{\mu}_{k,m,n}$ must vanish at $(r = 0, \theta = 0)$ which requires that

$$c = c_4 \frac{k}{\sqrt{mn(k-m)(k+n)}} \left[\binom{k}{m} \binom{k+n-1}{n} \right]^{-\frac{1}{2}}. \quad (7.1.12)$$

Moreover, the absence of singularity at $(r = 0, \theta = \pi/2)$ relates the charges of the solution to the Fourier coefficients

$$\frac{Q_1 Q_5}{R_y^2} = a^2 + \frac{c^2}{2}. \quad (7.1.13)$$

As before, the conserved charges can be extracted from the large-distance behavior of the scalars Z_1 , Z_2 and \mathcal{F} (4.2.32) and the one-forms β and ω (4.2.75). Indeed, from the supercharged analogue of (4.2.75) we can read off

$$J_L = \frac{R_y}{2} \left(a^2 + \frac{m}{k} c^2 \right), \quad J_R = \frac{R_y}{2} a^2, \quad Q_P = \frac{m+n}{2k} c^2. \quad (7.1.14)$$

The relations between the conserved charges and the Fourier coefficients of the supercharged superstrata, a and c , are exactly the same as the ones for the original superstrata (4.2.76) but with b replaced by c .

7.2 Hybrid Superstrata

As we described in the preamble, constructing multi-mode superstrata affords the possibility of making microstate geometries with additional moduli that represent the numbers, $N_{k,m,n,q}$, of excited strands with each kind of excitation. In supergravity, these numbers are related, via $N_{k_i,m_i,n_i,q_i} \sim (b_{k_i,m_i,n_i,q_i})^2$, to the “leading” Fourier coefficients that appear in Θ^4 . We will investigate generic multi-mode superstrata in Section 7.4. Here our goal is more modest, but more completely executed: we will combine the original single-mode superstratum solution, detailed in Section 4.2.5, with the single-mode supercharged superstratum solution, detailed in the previous section to obtain a hybrid superstratum with an extra modulus obtained through the independent Fourier coefficients. In Section 7.4, those hybrid superstrata will prove to be the crucial elementary components to construct multi-mode superstrata.

Combining two single-mode superstrata is straightforward for the first layer of BPS equations (4.2.28) thanks to linearity but it usually requires a great deal of effort to obtain the explicit solution to the second layer (4.2.29) because of the quadratic terms that non-trivially mix the modes. However, as we noted before, the supercharged modes and their original partners are “self-coiffuring” in that $\hat{\vartheta}_{k,m,n} \wedge \hat{\vartheta}_{k,m,n}$, is actually independent of v , φ_1 and φ_2 . This makes the computation, and the resulting solution, much simpler. In this section, we will obtain explicit solutions for new hybrid single-mode superstrata with *eight* parameters: Q_1, Q_5, k, m, n, a and the Fourier coefficients b_4 and c_4 of the superstratum modes. The only constraint on smoothness will be a single equation generalizing (4.2.74) and (7.1.13). Thus there will be one constraint and five bulk state functions: Q_1, Q_5, Q_P, J_L and J_R this leaved two variables, which may be thought of as k and the relative magnitude of b_4 and c_4 .

7.2.1 The first layer

The first layer of BPS equations, (4.2.28), is made of linear equations. At this level, pairing two BPS solutions simply consists in adding both solutions. Thus, our initial Ansatz for the field content is

simply the sum of (4.2.60) and (7.1.3)

$$\begin{aligned} Z_1 &= \frac{Q_1}{\Sigma} + b_1 \frac{R_y}{2Q_5} \tilde{z}_{2k,2m,2n}, & \Theta^2 &= b_1 \frac{R_y}{2Q_5} \tilde{\vartheta}_{2k,2m,2n} + c_2 \frac{R_y}{2Q_5} \hat{\vartheta}_{2k,2m,2n}, \\ Z_2 &= \frac{Q_5}{\Sigma}, & \Theta^1 &= 0, & Z_4 &= b_4 \tilde{z}_{k,m,n}, & \Theta^4 &= b_4 \tilde{\vartheta}_{k,m,n} + c_4 \hat{\vartheta}_{k,m,n}, \end{aligned} \quad (7.2.1)$$

where the original-superstratum contribution, $\tilde{z}_{k,m,n}$ and $\tilde{\vartheta}_{k,m,n}$, is given in (4.2.57) and the supercharged-superstratum contribution, $\hat{\vartheta}_{k,m,n}$, is given in (7.1.1).

7.2.2 The second layer

The quadratic terms in the second layer of BPS equations can induce oscillating parts that depend only upon $v_{2k,2m,2n}$, which one wants to cancel to ensure regularity. They come from the original superstratum, via $\tilde{\vartheta}_{k,m,n} \wedge \tilde{\vartheta}_{k,m,n}$, $\tilde{\vartheta}_{2k,2m,2n}$, $\tilde{z}_{k,m,n} \tilde{\vartheta}_{k,m,n}$ and $\tilde{z}_{2k,2m,2n}$, from the supercharged superstratum, via $\hat{\vartheta}_{k,m,n} \wedge \hat{\vartheta}_{k,m,n}$ and $\hat{\vartheta}_{2k,2m,2n}$ and also from mixed terms, $\tilde{\vartheta}_{k,m,n} \wedge \hat{\vartheta}_{k,m,n}$ and $\tilde{z}_{k,m,n} \hat{\vartheta}_{k,m,n}$. As advertised in the preamble, the mixed term $\tilde{\vartheta}_{k,m,n} \wedge \hat{\vartheta}_{k,m,n}$ is intriguingly self-coiffuring. However, $\tilde{z}_{k,m,n} \hat{\vartheta}_{k,m,n}$ is not. This is why we have reinstated the secondary excitation mode with the Fourier coefficient c_2 . Indeed, one can show that the Fourier coefficient of the oscillating sources vanish if

$$b_1 = b_4^2, \quad c_2 = 2b_4 c_4. \quad (7.2.2)$$

One can now solve the second layer in a similar fashion as in Section 4.2.5.2 and 7.1.2. The solution for ω and \mathcal{F} is given by the sums of the supertube solutions and the solution for the new pieces:

$$\omega = \omega_0 + \omega_{k,m,n}, \quad \mathcal{F} = 0 + \mathcal{F}_{k,m,n}. \quad (7.2.3)$$

The equations (4.2.29) for $\omega_{k,m,n}$ and $\mathcal{F}_{k,m,n}$ reduce to:

$$\begin{aligned} d_4 \omega_{k,m,n} + *_4 d_4 \omega_{k,m,n} + \mathcal{F}_{k,m,n} d_4 \beta &= \sqrt{2} b_4 R_y \frac{\Delta_{2k,2m,2n}}{\Sigma} \left[\left(\frac{m(k+n)}{k} b_4 - c_4 \right) \Omega^{(2)} \right. \\ &\quad \left. - \left(\frac{n(k-m)}{k} b_4 + c_4 \right) \Omega^{(3)} \right], \\ \mathcal{L} \mathcal{F}_{k,m,n} &= \frac{4}{(r^2 + a^2) \cos^2 \theta \Sigma} \left[\left(\frac{m(k+n)}{k} b_4 - c_4 \right)^2 \Delta_{2k,2m,2n} \right. \\ &\quad \left. + \left(\frac{n(k-m)}{k} b_4 + c_4 \right)^2 \Delta_{2k,2m+2,2n-2} \right], \end{aligned} \quad (7.2.4)$$

We can straightforwardly check that taking $c_4 = 0$ or $b_4 = 0$ in the foregoing equations reduces to the original-superstratum equations, (4.2.63), or the supercharged-superstratum equations, (7.1.6), respectively. Moreover, one can also note how non-trivial the pairing of the two solutions and its coiffuring (7.2.2) are. For instance, if one looks to the coefficients in front of the functions Δ in the second equation in (7.2.4), one can see that the pairing does not simply consist in adding the contribution from the supercharged superstratum, which is c_4^2 , with the contribution from the original superstratum, which is of the form $\gamma_{k,n,m}^2 b_4^2$ for some coefficient $\gamma_{k,n,m}$. The source terms, rather remarkably, conspire to complete the squares and lead to coefficients of the form $(\gamma_{k,n,m} b_4 \pm c_4)^2$.

To solve the equations, we define, as before:

$$\omega_{k,m,n} \equiv \mu_{k,m,n} (d\varphi_2 + d\varphi_1) + \zeta_{k,m,n} (d\varphi_2 - d\varphi_1). \quad (7.2.5)$$

Then, by shifting $\mu_{k,m,n}$

$$\mu_{k,m,n}^S \equiv \mu_{k,m,n} + \frac{R_y}{4\sqrt{2}} \frac{r^2 + a^2 \sin^2 \theta}{\Sigma} \mathcal{F}_{k,m,n} + \frac{R_y b_4^2}{4\sqrt{2}} \frac{\Delta_{2k,2m,2n}}{\Sigma}, \quad (7.2.6)$$

we have

$$\begin{aligned} \mathcal{L} \mu_{k,m,n}^S = \frac{R_y b_4^2}{\sqrt{2}} \frac{1}{(r^2 + a^2) \cos^2 \theta \Sigma} & \left[\left(\frac{(k-m)(k+n)}{k} b_4 + c_4 \right)^2 \Delta_{2k,2m+2,2n} \right. \\ & \left. + \left(\frac{mn}{k} b_4 - c_4 \right)^2 \Delta_{2k,2m,2n-2} \right]. \end{aligned} \quad (7.2.7)$$

Then, $\zeta_{k,m,n}$ is determined by ($s_\theta = \sin \theta$, $c_\theta = \cos \theta$)

$$\begin{aligned} \partial_r \zeta_{k,m,n} &= \frac{r^2 \cos 2\theta - a^2 s_\theta^2}{r^2 + a^2 s_\theta^2} \partial_r \mu_{k,m,n} - \frac{r \sin 2\theta}{r^2 + a^2 s_\theta^2} \partial_\theta \mu_{k,m,n} \\ &+ \frac{\sqrt{2} R_y r}{\Sigma (r^2 + a^2 s_\theta^2)} \left[b_4 \left((m s_\theta^2 + n c_\theta^2) b_4 + \left(c_4 - \frac{mn}{k} b_4 \right) \cos 2\theta \right) \Delta_{2k,2m,2n} \right. \\ &\quad \left. - \frac{a^2 (2r^2 + a^2) s_\theta^2 c_\theta^2}{\Sigma} \mathcal{F}_{k,m,n} \right], \\ \partial_\theta \zeta_{k,m,n} &= \frac{r(r^2 + a^2) \sin 2\theta}{r^2 + a^2 s_\theta^2} \partial_r \mu_{k,m,n} + \frac{r^2 \cos 2\theta - a^2 s_\theta^2}{r^2 + a^2 s_\theta^2} \partial_\theta \mu_{k,m,n} \\ &+ \frac{R_y \sin 2\theta}{\sqrt{2} \Sigma (r^2 + a^2 s_\theta^2)} \left[b_4 \left((-mr^2 + n(r^2 + a^2)) b_4 + (2r^2 + a^2) \left(c_4 - \frac{mn}{k} b_4 \right) \right) \Delta_{2k,2m,2n} \right. \\ &\quad \left. + \frac{a^2 r^2 (r^2 + a^2) \cos 2\theta}{\Sigma} \mathcal{F}_{k,m,n} \right]. \end{aligned} \quad (7.2.8)$$

In terms of $F_{2k,2m,2n}$, (4.2.70), the form of $\mathcal{F}_{k,m,n}$ and $\mu_{k,m,n}$ for general k, m, n is

$$\begin{aligned} \mathcal{F}_{k,m,n} &= 4 \left[\left(\frac{m(k+n)}{k} b_4 - c_4 \right)^2 F_{2k,2m,2n} + \left(\frac{n(k-m)}{k} b_4 + c_4 \right)^2 F_{2k,2m+2,2n-2} \right], \\ \mu_{k,m,n} &= \frac{R_y}{\sqrt{2}} \left[\left(\frac{(k-m)(k+n)}{k} b_4 + c_4 \right)^2 F_{2k,2m+2,2n} + \left(\frac{mn}{k} b_4 - c_4 \right)^2 F_{2k,2m,2n-2} - \frac{b_4^2 \Delta_{2k,2m,2n}}{4 \Sigma} \right] \\ &- R_y \frac{r^2 + a^2 \sin^2 \theta}{4\sqrt{2} \Sigma} \mathcal{F}_{k,m,n} + \frac{R_y B^2}{4\sqrt{2} \Sigma}. \end{aligned} \quad (7.2.9)$$

Then, $\zeta_{k,m,n}$ can be found by integrating (4.2.68). The coefficient B will be fixed by regularity in the next subsection.

7.2.3 Regularity and conserved charges

As with the original superstratum solutions, the hybrid solutions must be smooth at the center of space and at the supertube locus. The conditions are essentially the same as the ones detailed in Section 4.2.5.3. The scalar $\hat{\mu}_{k,m,n}$ must vanish at ($r = 0$, $\theta = 0$) which requires that

$$B = \left(b_4^2 + \frac{k^2}{mn(k-m)(k+n)} c_4^2 \right)^{\frac{1}{2}} \left[\binom{k}{m} \binom{k+n-1}{n} \right]^{-\frac{1}{2}} = \sqrt{b^2 + c^2} \quad (7.2.10)$$

where b is the individual contribution from the original superstratum part (4.2.73) and c is the individual contribution from the supercharged superstratum part (7.1.12). Moreover, the absence of

singularity at $(r = 0, \theta = \pi/2)$ relates the charges of the solution to the Fourier coefficients

$$\frac{Q_1 Q_5}{R_y^2} = a^2 + \frac{b^2 + c^2}{2}. \quad (7.2.11)$$

From this expression one can easily see what the pairing of the two single-mode superstrata has produced. The resulting single-mode superstratum has the same integers number k , m and n and has combined the Fourier coefficients of the two initial solutions, b and c , into one regularity constraint. Moreover, as we will now describe, the values of the conserved charges are given by the addition of the two individual contributions of the superstratum modes.

As before, the conserved charges can be extracted from the metric from the large-distance behavior of the scalars Z_1 , Z_2 and \mathcal{F} and the one-forms β and ω . We find

$$J_L = \frac{R_y}{2} \left(a^2 + \frac{m}{k} (b^2 + c^2) \right), \quad J_R = \frac{R_y}{2} a^2, \quad Q_P = \frac{m+n}{2k} (b^2 + c^2). \quad (7.2.12)$$

As in Section 4.2.5.4, the quantized charges are given by:

$$j_L = \frac{\mathcal{N}}{2} \left(a^2 + \frac{m}{k} (b^2 + c^2) \right), \quad j_R = \frac{\mathcal{N}}{2} a^2, \quad N_P = \frac{\mathcal{N}}{2} \frac{m+n}{k} (b^2 + c^2), \quad (7.2.13)$$

where \mathcal{N} is defined in (4.2.78). All the conserved quantities depend on $b^2 + c^2$ only. We define

$$b \equiv B \cos \alpha, \quad c \equiv B \sin \alpha \quad (7.2.14)$$

where $\alpha \in [0, 2\pi]$ and $B \in \mathbb{R}_+$. All the asymptotic charges are independent of α which corresponds to an internal degree of freedom. However, α has a great impact on the IR geometry since it is the “interpolation” parameter between the single-mode original superstratum state at $\alpha = 0$ to a single-mode supercharged superstratum state at $\alpha = \frac{\pi}{2}$ with non-trivial pairing terms when α is in between. Thus, this new family of solutions allows one to study a phase space of superposition of two superstratum states by varying the phase α which have the same macroscopic mass, charges and angular momenta.

7.3 The $(2, 1, n)$ example

In this section, we illustrate the new type of superstratum solutions with a detailed example: the $(2, 1, n)$ hybrid. This is, in fact, the first non-trivial family since one must have $k \geq m + 1 \geq 2$ and $n \geq 1$. From here on, we will reparametrize the Fourier coefficients, b and c , with α and B (7.2.14) so as to make the internal degree of freedom manifest.

The modes and the functions in (4.2.57) are now simply

$$v_{2,1,n} = (n+1) \frac{\sqrt{2}v}{R_y} + \varphi_1 - \varphi_2, \quad \Delta_{2,1,n} = (1 - \Gamma) \Gamma^{\frac{n}{2}} \cos \theta \sin \theta, \quad (7.3.1)$$

where we have defined

$$\Gamma \equiv \frac{r^2}{a^2 + r^2}. \quad (7.3.2)$$

7.3.1 The metric

The scalar functions $\mathcal{P}_{2,1,n}$, $\mathcal{F}_{2,1,n}$ are given by:

$$\begin{aligned}\mathcal{P}_{2,1,n} &= \frac{R_y^2}{\Sigma^2} \left(a^2 + \frac{B^2}{2} - (n+1) B^2 \cos^2 \alpha (1-\Gamma)^2 \Gamma^n \cos^2 \theta \sin^2 \theta \right), \\ \mathcal{F}_{2,1,n} &= \frac{n(n+1) B^2}{2a^2(1-\Gamma)} \left[n \left(\cos \alpha + \sqrt{\frac{n+2}{n}} \sin \alpha \right)^2 \left(G_n^{(1)}(\Gamma) + G_n^{(2)}(\Gamma) \cos^2 \theta \right) \right. \\ &\quad \left. + (n+2) \left(\sin \alpha - \sqrt{\frac{n+2}{n}} \cos \alpha \right)^2 \left(G_{n+1}^{(1)}(\Gamma) + G_{n+1}^{(2)}(\Gamma) \sin^2 \theta \right) \right],\end{aligned}\tag{7.3.3}$$

where

$$\begin{aligned}G_n^{(1)}(\Gamma) &\equiv \frac{\Gamma(1-\Gamma^n) - n(1-\Gamma)}{n^2(1+n)^2}, \\ G_n^{(2)}(\Gamma) &\equiv \frac{-1-\Gamma + (1+n)^2 \Gamma^n + (1-2n(n+1)) \Gamma^{n+1} + n^2 \Gamma^{n+2}}{n^2(1+n)^2},\end{aligned}\tag{7.3.4}$$

The angular momentum one-form, $\omega_{2,1,n}$, is given by:

$$\omega_{2,1,n} = \omega_0 + B^2 \left[\cos^2 \alpha \tilde{\omega}_{2,1,n} + \frac{\sin^2 \alpha}{n(n+2)} \hat{\omega}_{2,1,n} + \frac{\sin \alpha \cos \alpha}{\sqrt{n(n+2)}} \omega_{2,1,n}^{\text{mix}} \right],\tag{7.3.5}$$

where ω_0 is the supertube contribution, (4.2.45), while $\tilde{\omega}_{2,1,n}$ and $\hat{\omega}_{2,1,n}$ are, respectively, the individual contributions from the original superstratum and the supercharged superstratum. There is also a mixing, $\omega_{2,1,n}^{\text{mix}}$, coming from the interactions between the original and supercharged modes. These are given by:

$$\begin{aligned}\tilde{\omega}_{2,1,n} &= \frac{R_y}{2\sqrt{2}\Sigma} \left[\Gamma^{n+1} (n+2 - (n+1)\Gamma - (n+1)(1-\Gamma) \cos 2\theta) \cos^2 \theta d\varphi_2 \right. \\ &\quad \left. + (2 - (n(1-\Gamma) + 1)\Gamma^n - (n+1)(1-\Gamma)\Gamma^n \cos 2\theta) \sin^2 \theta d\varphi_1 \right], \\ \hat{\omega}_{2,1,n} &= \frac{R_y}{2\sqrt{2}(1-\Gamma)^2\Sigma} \left[\Gamma(4 - (2+n(1-\Gamma))^2\Gamma^n) (\cos^2 \theta d\varphi_2 - \sin^2 \theta d\varphi_1) \right. \\ &\quad \left. + 2n(n+2)(\Gamma-1)^2 \sin^2 \theta d\varphi_1 \right], \\ \omega_{2,1,n}^{\text{mix}} &= \frac{R_y}{4\sqrt{2}(1-\Gamma)\Sigma} (2 - (n+1)(n+2)\Gamma^n + 2n(2+n)\Gamma^{1+n} - n(1+n)\Gamma^{2+n}) \\ &\quad \times \sin^2 2\theta (\Gamma d\varphi_2 + d\varphi_1).\end{aligned}\tag{7.3.6}$$

One can easily check that if one takes $\alpha = \frac{\pi}{2}$, then one recovers the fields of the $(2, 1, n, q = 1)$ supercharged superstratum [31]² whereas $\alpha = 0$ gives the fields of the $(2, 1, n, q = 0)$ original superstratum first constructed in [116]. Taking any value in between gives a non-trivial hybrid of those two solutions.

7.3.2 Limiting geometries

We now consider the interesting regime of parameters in which a^2 is much smaller than the underlying charges:

$$a^2 \ll \{Q_1, Q_5, Q_P\} \implies a^2 \ll B^2.\tag{7.3.7}$$

²We remind that in our notation the $(2, 1, n, q = 1)$ supercharged superstratum corresponds to the $(2, 0, n-1, q = 1)$ solution in [31].

In this regime, one has an AdS_3 at large r ($r \gg \sqrt{Q_P}$), which then transitions to a long extremal BTZ throat (for $\sqrt{n}a \ll r \ll \sqrt{Q_P}$), which ultimately ends with a smooth cap ($r \ll \sqrt{n}a$). We will essentially focus in the IR and UV limit of the metric. In the previous section we gave all the pieces of the metric and if one combines them all into the six-dimensional metric (4.2.27), it produces a very complicated and rather unedifying mess that we will not write explicitly. However, we will look at some physically interesting regions of the geometry in which the metric simplifies significantly. In particular, as observed in [25, 29], an important part of the physics of the solutions is contained in the geometry of the cap.

7.3.2.1 The asymptotic geometry

We start with the simplest limit: $r \gg \sqrt{n}a$, in which the metric reduces to:

$$ds_{\text{asym}}^2 = \sqrt{Q_1 Q_5} \left[\frac{dr^2}{r^2} - \frac{4r^2}{(2a^2 + B^2) R_y^2} du dv + \frac{2n+1}{2 R_y^2} dv^2 + d\theta^2 + \sin^2 \theta \left(d\varphi_1 - \frac{dv}{\sqrt{2} R_y} \right)^2 + \cos^2 \theta \left(d\varphi_2 - \frac{dv}{\sqrt{2} R_y} \right)^2 \right]. \quad (7.3.8)$$

This is simply a trivial S^3 fibration over a red-shifted extremal BTZ geometry (4.2.35). The left and right temperatures are

$$T_L = \frac{\sqrt{n + \frac{1}{2}}}{2\pi R_y}, \quad T_R = 0. \quad (7.3.9)$$

in unit of the AdS length $\ell = (Q_1 Q_5)^{1/4}$. Note that the BTZ region is independent of the parameter α . This parameter represents an internal degree of freedom and does not change the macroscopic charges, mass and angular momenta of the solutions.

7.3.2.2 The cap geometry

The cap geometry is obtained by taking the limit $r \ll \sqrt{n}a$. We decompose the six-dimensional cap metric according to the free parameter α as follows

$$ds_{\text{cap}}^2 = \sqrt{Q_1 Q_5} \left[\frac{dr^2}{r^2 + a^2} - \frac{2a^2(r^2 + a^2)}{(2a^2 + B^2)^2 R_y^2} (du + dv)^2 + \frac{2a^2 r^2}{(2a^2 + B^2)^2 R_y^2} \left(du - \left(1 + \frac{B^2}{a^2} \right) dv \right)^2 + d\theta^2 + \cos^2 \alpha d\tilde{\Omega}_2^2 + \sin^2 \alpha d\hat{\Omega}_2^2 + \sin \alpha \cos \alpha d\Omega_2^{\text{mix}2} \right]. \quad (7.3.10)$$

where

$$\begin{aligned} d\tilde{\Omega}_2^2 &= \sin^2 \theta \left(d\varphi_1 - \frac{\sqrt{2}a^2}{(2a^2 + B^2) R_y} (du + dv) \right)^2 + \cos^2 \theta \left(d\varphi_2 + \frac{\sqrt{2}a^2 (du - dv) - \sqrt{2}B^2 dv}{(2a^2 + B^2) R_y} \right)^2, \\ d\hat{\Omega}_2^2 &= \sin^2 \theta \left(d\varphi_1 - \frac{\sqrt{2}a^2}{(2a^2 + B^2) R_y} (du + dv) + \frac{2\sqrt{2}B^2 r^4}{n(n+2)a^4(2a^2 + B^2)R_y} dv \right)^2 \\ &\quad + \cos^2 \theta \left(d\varphi_2 + \frac{\sqrt{2}a^2 (du - dv) - \sqrt{2}B^2 dv}{(2a^2 + B^2) R_y} - \frac{2\sqrt{2}B^2 r^4}{n(n+2)a^4(2a^2 + B^2)R_y} dv \right)^2, \\ d\Omega_2^{\text{mix}2} &= \frac{2B^2}{(2a^2 + B^2)\sqrt{n(n+2)}} \left[-\sin^4 \theta \left(d\varphi_1 + \frac{\sqrt{2}r^2}{a^2 R_y} dv \right)^2 + \cos^4 \theta \left(d\varphi_2 - \frac{\sqrt{2}(a^2 + r^2)}{a^2 R_y} dv \right)^2 \right]. \end{aligned} \quad (7.3.11)$$

The first line of (7.3.10) defines a (hugely red-shifted and boosted) global AdS_3 . Indeed, the red-shift in front of the time coordinate is given by:

$$\left(1 + \frac{B^2}{2a^2}\right)^{-1} = \frac{2j_R}{N_1 N_5}. \quad (7.3.12)$$

The various of $d\Omega_2$ terms in (7.3.10) give the metric on the $U(1) \times U(1)$ defined by (φ_1, φ_2) . The φ_1 -circles and φ_2 -circles universally pinch-off at $\theta = 0$ and $\theta = \frac{\pi}{2}$, respectively and so the $(d\theta, d\varphi_1, d\varphi_2)$ components describe a squashed S^3 .

It is remarkable to note that all the off-diagonal components of the metric that mix $(d\varphi_1, d\varphi_2)$ with (du, dv) are independent of θ , and are either constant or depend solely upon r . This means that they can be reduced to non-trivial Kaluza-Klein massless electromagnetic fields on the three-dimensional base defined by the AdS_3 . Thus, the dynamics of the six-dimensional cap metric excitations reduces to dynamics of the metric and massless vector fields on the three-dimensional base space described by (r, u, v) . For $\alpha = 0$, the metric of the 3-sphere is reduces to that of the $(2, 1, n, q = 0)$ original superstratum, $d\theta^2 + d\tilde{\Omega}_2$. The S^3 is round and the Kaluza-Klein vector fields on the S^3 are constant and so the fibration is trivial. At $\alpha = \frac{\pi}{2}$ the solution is purely the $(2, 1, n, q = 1)$ supercharged superstratum. The S^3 is also round but now the fibration is non-trivial in that the vector fields depend on r . When α takes any other value, the mixed term, $d\Omega_2^{\text{mix}^2}$, warps the 3-sphere with, once again, non-trivial r -dependent vector fields.

The fact that the fibration of the cap metric has the simple Kaluza-Klein structure suggests that there may be some interesting consistent truncation of the six-dimensional physics of the cap to a gauged supergravity in three-dimensions. The Kaluza-Klein fields are all of the correct form while the squashing may reflect the role of a Kaluza-Klein scalar in three dimensions. Similar observations were made for complete metric of some of the original superstrata constructed in [116].

7.4 Generic multi-mode Superstrata

Here we consider the broad class of multi-mode hybrid superstrata:

$$\bigotimes_i \left[|k_i, m_i, n_i, 0\rangle^{\text{NS}} \otimes |k_i, m_i, n_i, 1\rangle^{\text{NS}} \right]. \quad (7.4.1)$$

That is, we will consider the hybrid superstrata of Section 7.2, but now with a superposition of any set of mode excitations in the first layer. While we will not present the complete solution, we will examine a potentially dangerous obstruction to making smooth solutions in the second layer of BPS equations that arises when one restricts purely to the original superstrata. We will also show how the supercharged modes play a crucial role in getting around this obstruction.

7.4.1 The multi-mode problem

The second layer of BPS equations is:

$$\mathcal{D}\omega + *_4 \mathcal{D}\omega + \mathcal{F}d_4\beta = \mathcal{S}_1, \quad *_4 \mathcal{D} *_4 \left(\dot{\omega} - \frac{1}{2} \mathcal{D}\mathcal{F} \right) = \mathcal{S}_2, \quad (7.4.2)$$

where the sources are defined by:

$$\mathcal{S}_1 \equiv Z_1 \Theta^1 + Z_2 \Theta^2 - 2Z_4 \Theta^4, \quad (7.4.3)$$

$$\mathcal{S}_2 \equiv \partial_v^2 (Z_1 Z_2 - Z_4^2) - (\dot{Z}_1 \dot{Z}_2 - (\dot{Z}_4)^2) - \frac{1}{2} *_4 (\Theta^1 \wedge \Theta^2 - \Theta^4 \wedge \Theta^4). \quad (7.4.4)$$

Since these sources are quadratic in the fundamental fields of the first BPS layer, the sources will only involve the interactions between pairs of modes. It therefore suffices to solve this system for the most general *two-mode, hybrid superstratum* because one can construct the general mode solution through superpositions of all the two-mode source interactions.

Recall the definitions of the first-layer modes, (4.2.57) and (7.1.1), that underpin the original and supercharged superstrata:

$$\begin{aligned}\tilde{z}_{k,m,n} &= R_y \frac{\Delta_{k,m,n}}{\Sigma} \cos v_{k,m,n}, \\ \tilde{v}_{k,m,n} &\equiv -\sqrt{2} \Delta_{k,m,n} \left[\left((m+n) r \sin \theta + n \left(\frac{m}{k} - 1 \right) \frac{\Sigma}{r \sin \theta} \right) \Omega^{(1)} \sin v_{k,m,n} \right. \\ &\quad \left. + \left(m \left(\frac{n}{k} + 1 \right) \Omega^{(2)} + \left(\frac{m}{k} - 1 \right) n \Omega^{(3)} \right) \cos v_{k,m,n} \right],\end{aligned}\tag{7.4.5}$$

and

$$\hat{v}_{k,m,n} \equiv \sqrt{2} \Delta_{k,m,n} \left[\frac{\Sigma}{r \sin \theta} \Omega^{(1)} \sin v_{k,m,n} + \left(\Omega^{(2)} + \Omega^{(3)} \right) \cos v_{k,m,n} \right].\tag{7.4.6}$$

The general two-mode, hybrid superstratum has a first BPS layer of the form:

$$\begin{aligned}Z_1 &= \frac{Q_1}{\Sigma} + \frac{R_y}{2Q_5} \left[b_1 \tilde{z}_{2k_1,2m_1,2n_1} + b_2 \tilde{z}_{2k_2,2m_2,2n_2} + b_3 \tilde{z}_{k_1+k_2,m_1+m_2,n_1+n_2} \right], \\ Z_2 &= \frac{Q_5}{\Sigma}, \quad Z_4 = b_4 \tilde{z}_{k_1,m_1,n_1} + b_5 \tilde{z}_{k_2,m_2,n_2}, \\ \Theta^1 &= 0, \quad \Theta^4 = b_4 \tilde{v}_{k_1,m_1,n_1} + b_5 \tilde{v}_{k_2,m_2,n_2} + c_4 \hat{v}_{k_1,m_1,n_1} + c_5 \hat{v}_{k_2,m_2,n_2}, \\ \Theta^2 &= \frac{R_y}{2Q_5} \left[b_1 \tilde{v}_{2k_1,2m_1,2n_1} + b_2 \tilde{v}_{2k_2,2m_2,2n_2} + b_3 \tilde{v}_{k_1+k_2,m_1+m_2,n_1+n_2} \right. \\ &\quad \left. + c_1 \hat{v}_{2k_1,2m_1,2n_1} + c_2 \hat{v}_{2k_2,2m_2,2n_2} + c_3 \hat{v}_{k_1+k_2,m_1+m_2,n_1+n_2} \right],\end{aligned}\tag{7.4.7}$$

7.4.2 The high-frequency sources in the second BPS layer

The sources, (7.4.3) and (7.4.4), contain terms that are products of pairs of oscillating terms. Using elementary identities, one can rewrite these products in terms of circular functions that involve sums and differences of the mode numbers. We will define the “high-frequency” and “low-frequency” sources to be those that result from the addition or, respectively, subtraction of mode numbers. Since one has $k_1, k_2, m_1, m_2, n_1, n_2 \geq 0$, the “high-frequency” sources do indeed have larger mode numbers than their “low-frequency” counterparts. We will also define the “high-frequency” sources to include the terms that come from the product of a non-fluctuating term (zero mode-number) with a fluctuating mode.

From a great deal of experience [30, 98–100, 116, 101] we know that the BPS equations for the non-oscillating sources and the “low-frequency” sources have non-singular solutions that lead to smooth superstrata. On the other hand, the “high-frequency” sources generically lead to singular solutions of the BPS equations. We should stress that this statement is not a theorem but reflects the results of many computations in which homogeneous solutions have been found to cancel putative singularities in “low-frequency” solutions but no such homogeneous solutions have been found for “high-frequency” solutions.

In supergravity, the technique of “coiffuring” [161, 109, 30, 101] was introduced to address this issue. The idea is that “high-frequency” sources that lead to singularities can be combined in such a manner as to cancel any singularity. In simpler examples, like asymptotically-AdS superstrata, this means cancelling all of the “high-frequency” sources. In more complicated examples, like asymptotically-flat superstrata, the high-frequency sources are not completely cancelled but are combined so as to remove singularities in the solutions.

Since we are considering asymptotically-AdS superstrata, our goal here is to isolate the “high-frequency” sources, $\bar{\mathcal{S}}_j$, and cancel them completely. It is relatively easy to compute these sources from (7.4.3) and (7.4.4), and we find:

$$\begin{aligned} \bar{\mathcal{S}}_1 = \frac{R_y}{2\Sigma} & \left[(b_1 - b_4^2) \tilde{\vartheta}_{2k_1, 2m_1, 2n_1} + (b_2 - b_5^2) \tilde{\vartheta}_{2k_2, 2m_2, 2n_2} + (b_3 - 2b_4 b_5) \tilde{\vartheta}_{k_1+k_2, m_1+m_2, n_1+n_2} \right. \\ & + (c_1 - 2b_4 c_4) \hat{\vartheta}_{2k_1, 2m_1, 2n_1} + (c_2 - 2b_5 c_5) \hat{\vartheta}_{2k_2, 2m_2, 2n_2} \\ & + \left(c_3 - 2(b_4 c_5 + b_5 c_4) \right. \\ & \left. \left. + \frac{2b_4 b_5}{k_1 k_2 (k_1 + k_2)} (k_1 n_2 - k_2 n_1)(k_1 m_2 - k_2 m_1) \right) \hat{\vartheta}_{k_1+k_2, m_1+m_2, n_1+n_2} \right], \end{aligned} \quad (7.4.8)$$

and

$$\begin{aligned} \bar{\mathcal{S}}_2 = \frac{4}{R_y \Sigma} & \left[(m_1 + n_1)^2 (b_4^2 - b_1) \tilde{z}_{2k_1, 2m_1, 2n_1} + (m_2 + n_2)^2 (b_5^2 - b_2) \tilde{z}_{2k_2, 2m_2, 2n_2} \right. \\ & \left. + \frac{1}{4} (m_1 + m_2 + n_1 + n_2)^2 (2b_4 b_5 - b_3) \tilde{z}_{k_1+k_2, m_1+m_2, n_1+n_2} \right]. \end{aligned} \quad (7.4.9)$$

The obvious coiffuring identities are

$$\begin{aligned} b_1 &= b_4^2, & b_2 &= b_5^2, & b_3 &= 2b_4 b_5, & c_1 &= 2b_4 c_4, & c_2 &= 2b_5 c_5, \\ c_3 &= 2(b_4 c_5 + b_5 c_4) - \frac{2b_4 b_5}{k_1 k_2 (k_1 + k_2)} (k_1 n_2 - k_2 n_1)(k_1 m_2 - k_2 m_1), \end{aligned} \quad (7.4.10)$$

which means that all the “high-frequency” sources do indeed vanish.

There are several important things to note at this point. First and foremost, there are still four free parameters in these solutions: b_4, b_5, c_4 and c_5 , which correspond to the fundamental, or “leading,” modes in Θ^4 and thus, at linear order, to the four independent sets of CFT states. Next we note that the expression for c_3 , (7.4.10), has a term proportional to $b_4 b_5 \sim b_3$. There is therefore no solution with all of the $c_j = 0$: the supercharged modes are essential to a non-singular, coiffured solution.

Put differently, there is no way to coiffure a generic set of two-mode superstrata using the original superstratum modes *only*. The dangerous source term is the one proportional to $b_4 b_5 \hat{\vartheta}_{k_1+k_2, m_1+m_2, n_1+n_2}$ in the last line of (7.4.8). This term comes from the fact the b_3 term produces a contribution to $\bar{\mathcal{S}}_1$ that is proportional to $\frac{(m_1+m_2)(n_1+n_2)}{k_1+k_2} \hat{\vartheta}$ whereas the corresponding $b_4 b_5$ term is proportional to $(\frac{m_1 n_1}{k_1} + \frac{m_2 n_2}{k_2}) \hat{\vartheta}$. There is thus an imperfect cancellation from setting $b_3 = b_4 b_5$ and the residual part is proportional to $(k_1 n_2 - k_2 n_1)(k_1 m_2 - k_2 m_1) \hat{\vartheta}$. This term is only non-trivial if neither of (m_1, m_2) and (n_1, n_2) are parallel to (k_1, k_2) . Such generic two-mode solutions of the original superstratum have not been investigated because they are complicated and there was still this unresolved issue with coiffuring. As we have seen, the supercharged modes provide an elegant resolution of this issue with *no additional constraints on the fundamental, physical Fourier coefficients*.

More broadly, there is now no further obstruction, in principal, to the construction of superstrata with an arbitrary number of excited modes. As we noted above, the BPS equations have sources that are quadratic in the fundamental modes and so a generic multi-mode solution will simply result in a superposition of many two-mode interactions. Thus, in addressing the most general two-mode problem one has necessarily captured all the pieces of a generic multi-mode solution. The analysis above therefore shows that, once one includes the supercharged modes, there are no longer any singular “high frequency” interactions that cannot be coiffured away easily.

If one were to restrict to the original ($q = 0$) superstrata alone then the most obvious way to remove the dangerous high frequency sources is to require

$$(k_1 n_2 - k_2 n_1)(k_1 m_2 - k_2 m_1) = 0, \quad (7.4.11)$$

which restricts the modes to two-dimensional subspaces. Such superstrata are thus restricted to intrinsically two-dimensional fluctuations and are consequently restricted in their ability to cover the dual CFT states. In the hybrid superstrata, we now have unconstrained modes with two families of unconstrained Fourier coefficients (the b 's and the c 's) which means that the superstratum fluctuations are described by two generic functions of three variables and can faithfully describe all the coherent CFT states (7.4.1).

7.5 Final comment

In this chapter, we have reviewed a crucial step further in the construction of the large class of microstate geometries in six dimensions called Superstrata. We have shown how the supercharged modes represent an essential missing piece of the puzzle in the construction of supergravity duals of generic superstratum states. This was put in place by constructing a new version of single-mode Superstrata called hybrid which still have moduli after the bulk thermodynamic charges are fixed. We also gave the roadmap for generically solving the second layer of BPS equation for multi-mode Superstrata which do fluctuate as a function of three independent variables and which have the right number of degrees of freedom as compared to their CFT duals (4.2.53).

Microstates of extremal Kerr black holes

In this chapter, we review the work of [27] and the construction of smooth bubbling microstate geometries that are asymptotic to the near-horizon region of extremal five-dimensional Kerr black holes (NHEK). The embedding of these black holes in type IIB Supergravity on $S^1 \times \mathbb{T}^4$ has been discussed in Section 4.3.1. Their near-horizon geometry is $\text{WAdS}_3 \times \text{SqS}^3$ (4.3.9) with specific angle periodicities (4.3.8). Our strategy resembles the construction of the family of smooth BPS microstate geometries with four GH center in Section 5.2. We will start with a family of three almost-BPS Supertubes in \mathbb{R}^4 and we will perform a sequence of generalized spectral flows to transform the asymptotics to $\text{WAdS}_3 \times \text{SqS}^3$ in addition to regularizing the IR geometry.

The Kerr/CFT correspondence was first conjectured in [162] and relates the near-horizon geometry of extremal Kerr black hole (NHEK) to a chiral 2-dimensional conformal CFT whose central charges are given by the angular momenta of the black hole. This conjecture correctly reproduces via Cardy's formula the Bekenstein-Hawking entropy of the black hole. Nevertheless, even if there are several possible candidates of dual “CFT₂” as a dipole CFT [126] or as warped-CFT [163], the Kerr/CFT holographic dictionary is still poorly understood. Hence, it is very useful to have concrete examples, if not of the CFT, then of asymptotically NHEK geometries, which are bulk duals of pure CFT states.

8.1 Generating technique

8.1.1 From $\text{AdS}_3 \times \text{S}^3$ to $\text{WAdS}_3 \times \text{SqS}^3$

In [127], it has been shown that $\text{WAdS}_3 \times \text{SqS}^3$ solutions, of which the NHEK spacetime is a particular example, can be obtained from $\text{AdS}_3 \times \text{S}^3$ by a specific sequence of supergravity transformations. As we have seen it already, building asymptotically $\text{AdS}_3 \times \text{S}^3$ geometries is well-known and one can then use this result as a cornerstone of our construction.

The sequence of transformations has been exhaustively detailed in [127]. We just give a brief summary here. The transformations can be seen as a series of \mathcal{STU} transformations or equivalently as a sequence of three generalized spectral flows detailed in Section 3.2.4. Each spectral flow transformation is made of a shift $\varphi \rightarrow \varphi + \gamma y$ where y is the S^1 coordinate and φ is either the Gibbons-Hawking fiber, ψ , or the ϕ angle of the \mathbb{R}^3 base space.

The two possible choices of φ differ significantly. If the gravity multiplet of the $\text{AdS}_3 \times \text{S}^3$ background has a dual three-form field strength, the \mathcal{STU} transformations associated to this background ($\text{SL}(2, \mathbb{R})_L \times \text{SU}(2)_L$ invariant) or the generalized spectral flows along ψ will preserve supersymmetry and the transformed geometry will remain $\text{AdS}_3 \times \text{S}^3$. Reversely, if the three-form field strength is anti self-dual, the \mathcal{STU} transformations associated to this background ($\text{SL}(2, \mathbb{R})_L \times \text{SU}(2)_R$ invariant) or the generalized spectral flows along ϕ will break supersymmetry and will transform the geometry

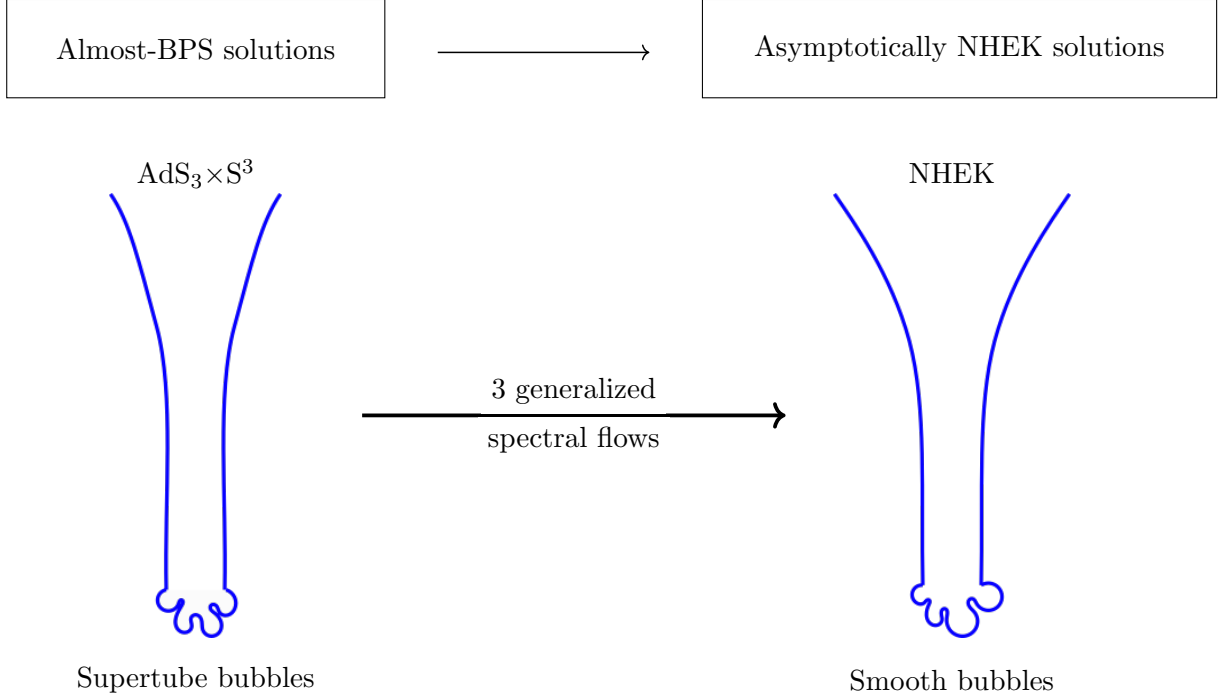


Figure 8.1: Schematic description of the construction of a family of smooth asymptotically NHEK solutions from the family of almost-BPS solutions.

to $\text{WAdS}_3 \times \text{SqS}^3$ (see Section 2.2 of [127] for more details).

Those two possibilities reflect the two types of generalized spectral flows in the context of the STU model. The BPS generalized spectral flows (4.1.1.4), are related to the angle ψ and are just linear transformations preserving supersymmetry whereas the almost-BPS generalized spectral flows (4.3.2.3) correspond to shifts along ϕ and break supersymmetry. This is the latter transformations which allow to map an asymptotically $\text{AdS}_3 \times \text{S}^3$ solutions to an asymptotically $\text{WAdS}_3 \times \text{SqS}^3$.

Having the same metric is not the only requirement. The periodicities of the angles of the squashed three-sphere and the angle of the warped AdS_3 must have a specific form (4.3.7). Imposing such periodicities to our solutions has a major impact on the smoothness of the geometry in the IR.

Furthermore, if the initial almost-BPS solution has supertube curvature singularities, the corresponding generalized spectral flows will transform the singular local geometries to quotients of $\mathbb{R}^4 \times \text{S}^1$ [81]. Nevertheless, the quotients are not necessarily smooth and conical singularities related to the angle periodicities can still occur at these locations. Indeed, the NHEK angle periodicities or the WAdS_3 angle periodicities (4.3.7) imposed in the UV can spoil the periodicities at the centers where the three-sphere shrinks and conical singularities can emerge.

8.1.2 The recipe

We sketch the overall idea about our construction of smooth bubbling asymptotically $\text{WAdS}_3 \times \text{SqS}^3$ or asymptotically NHEK geometries in Figure 8.1. The recipe has the following steps:

- We start with a specific family of almost-BPS solutions. They have four centers, one is the center of \mathbb{R}^4 and the three others are two-charge supertube centers of different species. This choice of solution is just a matter of simplicity since the systematic construction detailed for supersymmetric solutions in Section 5.2 can be easily extended to almost-BPS solutions. However,

nothing prevents from taking different almost-BPS configurations. We construct asymptotically $\text{AdS}_2 \times S^1 \times S^3$ solutions where the S^1 fibration over AdS_2 gives the full AdS_3 . Moreover, we require their left and right angular momenta to be zero.

- We perform three generalized spectral flows that transform the UV geometry into $\text{WAdS}_3 \times \text{SqS}^3$ and preserve the bubble feature in the IR.
- We identify the periodicities at infinity of $\text{WAdS}_3 \times \text{SqS}^3$ or NHEK and impose the absence of conical singularities at the centers.

Once all these steps are performed, we obtain a family of smooth bubbling geometries, asymptotically $\text{WAdS}_3 \times \text{SqS}^3$ or asymptotically NHEK in type IIB on T^4 .

We now have all the basic ingredients to construct extremal non-supersymmetric geometries which cap off smoothly in the IR and are asymptotically NHEK or WAdS_3 . Before going to the detail of each step, let us first review the extension of the systematic construction in Section 5.2 to the family of three two-charge Supertubes in \mathbb{R}^4 in the almost-BPS context.

8.1.3 The family of almost-BPS three-supertube solutions in \mathbb{R}^4

We consider the family of almost-BPS solutions with three two-charge Supertubes on a line of a \mathbb{R}^4 base space. Remember that almost-BPS solutions have been obtained by imposing an opposite self-duality between the background and the field strengths. Because the base space is \mathbb{R}^4 , the background is not oriented and its self-duality is just a matter of choice. Indeed, as it has been shown in [127, 132, 134], almost-BPS solutions in \mathbb{R}^4 can be mapped to a BPS solution by interchanging $\phi \leftrightarrow \psi$. Those solutions are supersymmetric, but can be constructed either as BPS or as almost-BPS solutions. Does it mean that our initial family of solutions is ill-chosen? It is not. The generalized spectral flows are the key element that will differentiate between both orientation. Because, we will need the spectral flows which break supersymmetry it is more convenient to write the solutions in the almost-BPS language where the transformations have been explicitly written as a transformation of the harmonic functions (4.3.31).

Thus, the construction of the initial solutions is just a matter of rewriting carefully the discussion of Section 5.2 in the context of almost-BPS solutions. We apply the general results obtained in Section 4.3.2 to our specific family of solutions. We first detail how the gauge fields are sourced by a configuration of three Supertubes of different species in \mathbb{R}^4 . We then derive the regularity conditions and show that they can be systematically satisfied.

8.1.3.1 The solution

A type “ I ” supertube, with $I = 1, 5, P$, has a singular magnetic source in K^I , two singular electric sources in Z_J and Z_K with $I \neq J \neq K$ and one angular-momentum charge in M (4.3.28)¹. The six-dimensional metric and the matter fields are given by (4.1.43). We assume that the \mathbb{R}^4 center is at the origin of the space and that a supertube of type 1 is at a second center with coordinate a_1 on the z -axis, a supertube of type 5 is at a third center with coordinate a_5 and a supertube of type P is at a fourth center with coordinate a_P . We consider that $a_I > 0$. We use the following notation for the

¹In the previous chapters, we have labelled the three vector fields of the STU model by $I = 1, 2, 3$. This was motivated by the absence of distinction between them. In this chapter, we work in the D1-D5-P frame from which the extremal Kerr black hole is constructed. In this frame, the vector fields have a different nature. In this chapter, we will label the vector fields by $I = 1, 5, P$ to make this distinction explicit. The map between the two labelling conventions is $(1, 2, 3) \leftrightarrow (1, 5, P)$

eight harmonic functions²

$$\begin{aligned}
V &= \frac{q}{\rho}, & M &= m_\infty + \frac{m_0}{\rho} + \sum_{I=1,5,P} \frac{|\epsilon_{IJK}|}{2} \frac{q Q_I^{(J)} Q_I^{(K)}}{2a_I \kappa_I} \frac{1}{\rho_I}, \\
K^1 &= k_\infty^1 + \frac{a_1 \kappa_1}{q \rho_1}, & L_1 &= l_\infty^1 + \frac{Q_5^{(1)}}{\rho_5} + \frac{Q_P^{(1)}}{\rho_P}, \\
K^5 &= k_\infty^5 + \frac{a_5 \kappa_5}{q \rho_5}, & L_5 &= l_\infty^5 + \frac{Q_1^{(5)}}{\rho_1} + \frac{Q_P^{(5)}}{\rho_P}, \\
K^P &= k_\infty^P + \frac{a_P \kappa_P}{q \rho_P}, & L_P &= l_\infty^P + \frac{Q_1^{(p)}}{\rho_1} + \frac{Q_5^{(p)}}{\rho_5},
\end{aligned} \tag{8.1.1}$$

We have defined on purpose the “effective” dipole charges κ_I as a function of the charges in K^I : $\kappa_I = \frac{q k_I}{a_I}$. Those effective dipole charges were argued to be the local magnetic charges obtained by integrating the fluxes of the gauge fields around the center [133, 135]. Using the expression of the warp factors (4.3.22), of μ (4.3.25) and ϖ (4.3.26), we obtain

$$\begin{aligned}
Z_1 &= \frac{Q_5^{(1)}}{\rho_5} + \frac{Q_P^{(1)}}{\rho_P} + \frac{\kappa_5 \kappa_P}{q} \frac{\rho}{\rho_5 \rho_P}, \\
Z_5 &= \frac{Q_1^{(5)}}{\rho_1} + \frac{Q_P^{(5)}}{\rho_P} + \frac{\kappa_1 \kappa_P}{q} \frac{\rho}{\rho_1 \rho_P}, \\
Z_P &= \frac{Q_1^{(p)}}{\rho_1} + \frac{Q_5^{(p)}}{\rho_5} + \frac{\kappa_1 \kappa_5}{q} \frac{\rho}{\rho_1 \rho_5}, \\
\mu &= \sum_I \sum_{J \neq I} \frac{Q_J^{(I)} \kappa_I}{2q} \frac{\rho^2 + a_I a_J - 2a_I \rho \cos \vartheta}{(a_J - a_I) \rho_I \rho_J} + \frac{\kappa_1 \kappa_5 \kappa_P}{q^2} \frac{\rho^2 \cos \vartheta}{\rho_1 \rho_5 \rho_P} + \frac{\rho M}{q}, \\
\varpi &= \left[\sum_I \sum_{J \neq I} \frac{Q_J^{(I)} \kappa_I}{2} \frac{\rho(a_J + a_I \cos 2\vartheta) - (\rho^2 + a_I a_J) \cos \vartheta}{(a_J - a_I) \rho_I \rho_J} + \frac{\kappa_1 \kappa_5 \kappa_P}{q} \frac{\rho^2 \sin^2 \vartheta}{\rho_1 \rho_5 \rho_P} \right. \\
&\quad \left. + \varpi_0 d\phi - \sum_I m_I \cos \vartheta_I - m_0 \cos \vartheta \right] d\phi,
\end{aligned} \tag{8.1.2}$$

In order to analyze the spectrally-flowed solutions (4.3.30), we must compute the U(1) vector gauge fields A^I for the initial solutions

$$\begin{aligned}
w^I &= \left(\kappa_I \frac{\rho - a_I \cos \vartheta}{\rho_I} - q k_\infty^I \cos \vartheta \right) d\phi, \\
A^I &= - \frac{dt + \mu(d\psi + q \cos \vartheta d\phi) + \varpi}{Z_I} + K^I(d\psi + q \cos \vartheta d\phi) + w^I.
\end{aligned} \tag{8.1.3}$$

For the same reason, the electromagnetic one-forms v_0 and v_I involved in the spectral flow transformations of the gauge fields must be derived. We solve their equations (4.3.32) in the context of our

²We remind that all the constant terms in V and L^I have been set to zero to have an asymptotically $\text{AdS}_2 \times \text{S}^1 \times \text{S}^3$ solution.

solutions using the library of generating functions in the Appendix A.1:

$$\begin{aligned} v_I &= \frac{|\epsilon_{IJK}|}{2} \left[-q k_\infty^J k_\infty^K T^{(0)} + 2 k_\infty^J \kappa^K T_J^{(1)} - 2 Q_J^{(I)} T_J^{(2)} - \frac{\kappa_J \kappa_K}{q} T_{JK}^{(3)} \right], \\ v_0 &= \frac{|\epsilon_{IJK}|}{6} \left[q k_\infty^I k_\infty^J k_\infty^K T^{(0)} + 6 k_\infty^I Q_J^{(I)} T_J^{(1)} - 3 k_\infty^I k_\infty^J \kappa_K T_K^{(2)} \right. \\ &\quad \left. + 6 \frac{\kappa_I Q_J^{(I)}}{q} T_{IJ}^{(3)} + 3 \frac{k_\infty^I \kappa_J \kappa_K}{q} T_{JK}^{(4)} + \frac{\kappa_I \kappa_J \kappa_K}{q^2} T_{IJK}^{(5)} \right]. \end{aligned} \quad (8.1.4)$$

At this point, we have the full description of the almost-BPS solutions we will use as input for our construction. In general, most of the solutions in this class are not regular. We investigate the regularity conditions in the next section after deriving the condition to have $\text{AdS}_3 \times \text{S}^3$ asymptotics.

8.1.3.2 The regularity conditions and conditions on the asymptotics

- Conditions on the asymptotics

We want to prepare our initial almost-BPS solutions to be asymptotically $\text{AdS}_3 \times \text{S}^3$. We derive the conditions to be asymptotic to the specific S^1 fibration over $\text{AdS}_2 \times \text{S}^3$ that gives the full $\text{AdS}_3 \times \text{S}^3$:

$$ds_{6\infty}^2 \propto -\rho^2 dt^2 + \frac{d\rho^2}{\rho^2} + (dy + \rho dt)^2 + d\Omega_3^2. \quad (8.1.5)$$

The series expansion of Z_I , V and ω involves the constant terms l_∞^I , the D1, D5 and P charges and the left and right angular momenta of the solution which we denote as q_1 , q_5 , q_P , j_L and j_R :

$$\begin{aligned} Z_1 &\underset{\rho \rightarrow \infty}{\sim} l_\infty^1 + \frac{q_1}{\rho}, & Z_5 &\underset{\rho \rightarrow \infty}{\sim} l_\infty^5 + \frac{q_5}{\rho}, & Z_P &\underset{\rho \rightarrow \infty}{\sim} l_\infty^P + \frac{q_P}{\rho}, \\ \omega &\underset{\rho \rightarrow \infty}{\sim} \frac{j_R + j_L \cos \vartheta}{\rho} d\psi + q \frac{j_L + j_R \cos \vartheta}{\rho} d\phi, & V &\underset{\rho \rightarrow \infty}{\sim} \frac{q}{\rho}. \end{aligned} \quad (8.1.6)$$

From the expression of the metric in the six-dimensional frame (4.1.43), we require the constant terms in the warp factors Z_I to be zero. Furthermore, to obtain the specific $\text{U}(1)$ -fiber, $(dy + \rho dt)$, the right and left angular momenta must be zero. The AdS_2 throat has an infinite length due to the vanishing constant terms. This means that $j_R = 0$ is straightforwardly satisfied. We obtain j_L from (8.1.2):

$$j_L = \frac{2}{q} \left(\frac{\kappa_1 \kappa_5 \kappa_P}{q} + \sum_{I \neq J \neq K} \frac{Q_I^{(J)} Q_I^{(K)}}{\kappa_I} + \frac{1}{2} \sum_{I \neq J} \kappa_I Q_J^{(I)} \right) = 0. \quad (8.1.7)$$

Our initial almost-BPS solutions must satisfy this equation and have no constant terms in L_I before applying the sequence of generalized spectral flows.

- Absence of Dirac-Misner strings at the centers:

The absence of Dirac-Misner string singularities in ϖ has been derived in (4.3.27). For our specific

solutions, this gives one condition on the constant term in ϖ and four Denef-like equations

$$\begin{aligned}
\varpi_0 &= 0 \\
2m_0 &= \frac{\Gamma_{15}}{a_1 - a_5} + \frac{\Gamma_{1P}}{a_1 - a_P} + \frac{\Gamma_{5P}}{a_5 - a_P}, \\
\frac{q Q_1^{(5)} Q_1^{(p)}}{a_1 \kappa_1} &= \frac{\Gamma_{15}}{|a_1 - a_5|} + \frac{\Gamma_{1P}}{|a_1 - a_P|}, \\
\frac{q Q_5^{(1)} Q_5^{(p)}}{a_5 \kappa_5} &= \frac{\Gamma_{51}}{|a_1 - a_5|} + \frac{\Gamma_{5P}}{|a_5 - a_P|}, \\
\frac{q Q_P^{(1)} Q_P^{(5)}}{a_P \kappa_P} &= \frac{\Gamma_{P1}}{|a_1 - a_P|} + \frac{\Gamma_{P5}}{|a_5 - a_P|},
\end{aligned} \tag{8.1.8}$$

where $\Gamma_{IJ} \equiv \kappa_I Q_J^{(I)} - \kappa_J Q_I^{(J)}$.

- Absence of closed timelike curves:

The absence of closed timelike curves in the rest of the space requires the positivity of the quartic invariant \mathcal{I}_4 (4.1.27). The condition is satisfied with the same arguments as for BPS three-supertube solutions in Taub-NUT (see Section 5.2.1). We use the condition (4.1.28):

$$Z_I V \geq 0, \quad I = 1, 5, p, \quad \mu \xrightarrow{\rho \rightarrow \infty} 0, \tag{8.1.9}$$

that requires straightforwardly that $m_\infty = 0$ and that the supertube monopole and dipole charges satisfy the inequalities (5.2.6) by replacing k_I by κ_I . Thus we take all the supertube electric charges and q to be positive. Moreover, if the sum of the three last equations (8.1.8) imposes at least one supertube dipole charge to be negative. Let us consider only one negative charge, say κ_5 . The conditions (5.2.6) will just define a significantly large domain of possible values.

In this section, we have described in full detail the family of almost-BPS three-supertube solutions with a flat \mathbb{R}^4 base space and with zero left and right angular momenta. We have shown a procedure to construct systematically bubbling solutions of this type. We expect from Section 8.1.1 that acting with three generalized spectral flows on those initial solutions will produce smooth bubbling asymptotically $\text{WAdS}_3 \times \text{SqS}^3$ or NHEK geometries. We will discuss this construction in the next section.

8.2 Asymptotically $\text{WAdS}_3 \times \text{SqS}^3$ bubbling geometries

We start with the solutions constructed in the previous section. We will perform three generalized spectral flows parametrized by the constant shifts γ_1 , γ_5 and γ_P . Even if the transition from an AdS_3 to a WAdS_3 with generalized spectral flows seems to be straightforward from the point of view of Section 8.1.1, things get more complicated for a bubbling geometry and we will need to massage the initial solutions and the spectral flows to satisfy different regularity conditions in the UV and IR geometries:

- The spectrally-flowed UV geometry differs from a $\text{WAdS}_3 \times \text{SqS}^3$ geometry by the angle periodicities (4.3.7). In Section 8.2.1, we will deal with the spectral flow parameters and the parameters of the initial solution to get a UV geometry exactly identified as a $\text{WAdS}_3 \times \text{SqS}^3$ geometry with the right angle periodicities (4.3.7).

- The spectrally flowed IR geometry is a smooth bubbling geometry. However, the modification of the angle periodicities in the UV region changes drastically the periods around the centers where the S^3 shrinks and conical singularities can occur. We will show in Section 8.2.2 that one can still systematically build geometries where the UV angle periods do not yield to conical singularities.

Several attempts on building bubbling geometries with a NHEK or $WAdS_3 \times SqS^3$ region have been performed in previous works [164, 127]. In [127], only very specific $WAdS_3$ geometries with limited field contents have been built. Furthermore, in both papers, the NHEK regions were built in the deep IR and the issue of conical singularities that can occur at the centers was not tackled. Here we give all the details of the construction of the largest known family of smooth general solutions with a $WAdS_3 \times SqS^3$ UV.

8.2.1 The ultraviolet geometry

We start with a solution of the family of almost-BPS solutions (detailed in 8.1.3) with all the constraints and regularity conditions satisfied. Thus, the asymptotic behavior of the initial solution is

$$Z_I \sim \frac{q_I}{\rho}, \quad K^I \sim k_\infty^I, \quad V \sim \frac{q}{\rho}, \quad \mu = \varpi = \mathcal{O}(\rho^{-2}), \quad \rho \gg 1, \quad (8.2.1)$$

By applying the spectral-flow rules (4.3.31), the spectrally-flowed solution has the following asymptotic expansion:

$$\begin{aligned} \tilde{Z}_I &\sim \frac{\tilde{q}_I}{\rho}, \quad \tilde{V} \sim \frac{\tilde{q}}{\rho}, \quad \tilde{\mu} \sim \frac{\tilde{J}}{\rho}, \quad \tilde{W}_I \sim \frac{\tilde{\chi}_I}{\rho}, \quad \tilde{P}^I \sim \tilde{k}_\infty^I \\ \tilde{A} &\sim \left(\tilde{A}_\infty^{(0)} + \tilde{A}_\infty \cos \vartheta \right) d\phi, \quad \tilde{w}^I \sim \left(\tilde{w}_{I\infty}^{(0)} + \tilde{w}_{I\infty} \cos \vartheta \right) d\phi, \quad \rho \rightarrow \infty, \end{aligned} \quad (8.2.2)$$

where each tilded quantity in the right-hand side is a constant that can be derived from (4.3.31) as a function of the conserved charges of the initial solution (8.2.1). Since these functions are rather complicated and of minor interest, we did not write them down in their general forms. However, it is noteworthy that \tilde{q} is generically a square root of a polynomial function. In anticipation of the constraints demanded by the regularity around the centers, one needs to impose all the quantities to be at least rational. For that purpose, we fix the polynomial to be a perfect square. Two simple choices are: $\gamma_P = 0$ and $\gamma_P = -\frac{1}{k_\infty^P}$. We have analyzed both possibilities and the second one leads to simpler solutions. From now on, we suppose that $\gamma_P = -\frac{1}{k_\infty^P}$. We define the constants

$$t_\infty^I \equiv 1 + k_\infty^I \gamma_I. \quad (8.2.3)$$

Then, we have³

$$\begin{aligned} \tilde{q} &= \left| \frac{q_1 \gamma_5 t_\infty^1 - q_5 \gamma_1 t_\infty^5}{k_\infty^P} \right|, & \tilde{q}_I &= \frac{q q_I (t_\infty^I)^2 + \frac{|\epsilon_{IJK}|}{2} \gamma_I^2 q_J q_K}{\tilde{q}}, \\ \tilde{J} &= \frac{q_1 q_5}{k_\infty^P \tilde{q}^2} (\gamma_1 \gamma_5 q_P + q t_\infty^1 t_\infty^5), & \tilde{\chi}_I &= |\epsilon_{IJK}| \frac{2 \tilde{q} \tilde{q}_I}{\gamma_J \gamma_K t_\infty^I q_I - 2 \gamma_I \gamma_J t_\infty^K q_K}, \\ \tilde{k}_\infty^I &= \frac{q q_I k_\infty^I t_\infty^I + \frac{|\epsilon_{IJK}|}{2} \gamma_I q_J q_K}{q q_I (t_\infty^I)^2 + \frac{|\epsilon_{IJK}|}{2} \gamma_I^2 q_J q_K} + \frac{\tilde{J}}{\tilde{\chi}_I}, & \tilde{A}_\infty &= -\frac{q_1 \gamma_5 t_\infty^1 + q_5 \gamma_1 t_\infty^5}{k_\infty^P}, \\ \tilde{w}_{I\infty} &= -\frac{|\epsilon_{IJK}|}{2} [q k_\infty^I t_\infty^J t_\infty^K + 2 q_J \gamma_K + \gamma_J \gamma_K \sum k_\infty^L q_L]. \end{aligned} \quad (8.2.4)$$

³We use $t_\infty^P = 1 + k_\infty^P \gamma_P = 0$.

The expressions of $\tilde{w}_{I\infty}^{(0)}$ and $\tilde{A}_{\infty}^{(0)}$ remain complicated functions of the charges of the initial solution and the interested reader can easily compute them from (8.1.3) and (8.1.4). One can check by curiosity that the asymptotic value of the quartic invariant $\mathcal{I}_{4\infty}$ (4.1.27) is indeed preserved

$$\mathcal{I}_{4\infty} = q q_1 q_5 q_P = \tilde{q} \tilde{q}_1 \tilde{q}_5 \tilde{q}_P - \tilde{q}^2 \tilde{J}^2 = \tilde{\mathcal{I}}_{4\infty}. \quad (8.2.5)$$

By inserting (8.2.2) in the spectrally-flowed six-dimensional metric (4.3.30), the WAdS₃×SqS³ asymptotic expansion of the metric is explicit

$$ds_{\infty}^2 = \frac{\kappa^2}{4} \left[-\rho^2 d\tau^2 + \frac{d\rho^2}{\rho^2} + \gamma (dy_{\infty} + \rho d\tau)^2 + \gamma (d\psi_{\infty} + \cos \vartheta d\phi)^2 \right. \\ \left. + 2\alpha (dy_{\infty} + \rho d\tau)(d\psi_{\infty} + \cos \vartheta d\phi) + d\vartheta^2 + \sin^2 \vartheta d\phi^2 \right] + \dots, \quad (8.2.6)$$

where we have defined the six-dimensional coordinates at infinity $(\tau, \rho, \vartheta, \phi, \psi_{\infty}, y_{\infty})$ using the initial coordinates $(t, \rho, \vartheta, \phi, \psi, y)$ as follows

$$y_{\infty} \equiv \sqrt{\mathcal{I}_{4\infty}} \tilde{\chi}_P \frac{\tilde{w}_{p\infty} (\psi + \tilde{A}_{\infty}^{(0)} \phi) - \tilde{A}_{\infty} (y + \tilde{w}_{p\infty}^{(0)} \phi)}{\tilde{A}_{\infty} (\mathcal{I}_{4\infty} - \tilde{q}^2 \tilde{\chi}_P \tilde{k}_{\infty}^P \tilde{J}) - \tilde{w}_{p\infty} \tilde{q}^2 \tilde{\chi}_P \tilde{J}}, \quad \tau \equiv \frac{t}{\sqrt{\mathcal{I}_{4\infty}}}, \quad (8.2.7)$$

$$\psi_{\infty} \equiv \frac{(\psi + \tilde{A}_{\infty}^{(0)} \phi) (\mathcal{I}_{4\infty} - \tilde{q}^2 \tilde{\chi}_P \tilde{k}_{\infty}^P \tilde{J}) - \tilde{q}^2 \tilde{\chi}_P \tilde{J} (y + \tilde{w}_{p\infty}^{(0)} \phi)}{\tilde{A}_{\infty} (\mathcal{I}_{4\infty} - \tilde{q}^2 \tilde{\chi}_P \tilde{k}_{\infty}^P \tilde{J}) - \tilde{w}_{p\infty} \tilde{q}^2 \tilde{\chi}_P \tilde{J}},$$

and where the warp constant factors, γ and α , and the length, κ , are given by

$$\gamma = \left(\frac{\tilde{q}_P}{\tilde{\chi}_P} \right)^2 \left[1 + \frac{\tilde{q} \tilde{J}^2}{\tilde{q}_1 \tilde{q}_5 \tilde{q}_P} \left(\left(\frac{\tilde{\chi}_P}{\tilde{q}_P} \right)^2 - 1 \right) \right], \quad (8.2.8)$$

$$\alpha = - \frac{\sqrt{\mathcal{I}_{4\infty}}}{\tilde{q}^3 \tilde{q}_1 \tilde{q}_5 \tilde{q}_P} \left(\tilde{A}_{\infty} (\tilde{k}_{\infty}^P \tilde{q}_P^2 + \tilde{\chi}_P \tilde{J}) + \tilde{q}_P^2 \tilde{w}_{p\infty} \right),$$

$$\kappa^2 = 4 \tilde{q} \sqrt{\tilde{q}_1 \tilde{q}_5}.$$

The last condition for having WAdS₃×SqS³ is on the periods for $(y_{\infty}, \psi_{\infty}, \phi)$

$$(y_{\infty}, \psi_{\infty}, \phi) = \begin{cases} (y_{\infty}, \psi_{\infty}, \phi) + 2\pi (T_y, -T_{\psi}, 0) \\ (y_{\infty}, \psi_{\infty}, \phi) + 2\pi (0, 2, 0) \\ (y_{\infty}, \psi_{\infty}, \phi) + 2\pi (0, 1, 1) \end{cases}. \quad (8.2.9)$$

It is rather complicated to have such periodicities while preserving the usual periods for (y, ψ, ϕ)

$$y = y + 2\pi, \quad \psi = \psi + 4\pi, \quad (\psi, \phi) = (\psi, \phi) + (2\pi, 2\pi). \quad (8.2.10)$$

However, one can just reverse the perspective by imposing directly the periods (8.2.9) for $(y_{\infty}, \psi_{\infty}, \phi)$ and express the corresponding periods of (y, ψ, ϕ) by inverting (8.2.7). This has the advantage of adding no new constraints on the parameters of the solution but the main drawback is that this drastic modification of periods for (y, ψ, ϕ) can induce conical singularities in the IR wherever the S³ shrinks.

8.2.2 The infrared geometry

Generalized spectral flows preserve the bubbling feature of the initial solution: the number of centers and their positions on the \mathbb{R}^3 base space are straightforwardly preserved. They also preserve all the conditions for the absence of closed timelike curves as detailed in Section 4.3.2.3. Moreover, they transform a singular supertube center to a smooth Gibbons-Hawking center. A series expansion of the spectrally-flowed solution around the center J (where $J = 0, 1, 5, P$) gives

$$\begin{aligned} \tilde{Z}_I &\sim \tilde{z}_{IJ}, & \tilde{V} &\sim \frac{\tilde{q}_J}{\rho_J}, & \tilde{\mu} &\sim \tilde{\mu}_J \rho_J, & \tilde{W}_I &\sim \tilde{\chi}_{IJ}, & \tilde{P}^I &\sim \tilde{k}_{IJ} \\ \tilde{A} &\sim \left(\tilde{A}_J^{(0)} + \tilde{A}_J \cos \vartheta_J \right) d\phi, & \tilde{w}^I &\sim \left(\tilde{w}_{IJ}^{(0)} + \tilde{w}_{IJ} \cos \vartheta_J \right) d\phi, & \rho_J &\rightarrow 0, \end{aligned} \quad (8.2.11)$$

where the tilded quantities in the right-hand sides are constant. It is not necessary for what will follow to write their complicated dependence on the parameters of the initial solution⁴. The three noteworthy points are

- The ratio $\frac{\tilde{A}_J}{\tilde{q}_J}$ is equal to 1. This is a key feature of an ambipolar Gibbons-Hawking metric. Indeed, in a generic Gibbons-Hawking metric (4.1.8), the term proportional to $\cos \vartheta d\phi$ in $\frac{A}{V}$ must be exactly $\cos \vartheta d\phi$.
- The quantity $\tilde{k}_{pJ} \tilde{A}_J + \tilde{w}_{pJ}$ is equal to zero. Thus, the U(1) fiber defined by $\tilde{A}^P + dy$ in (4.3.30) has no term proportional to $\cos \vartheta_J d\phi$ when we approach the center J . The local five-dimensional base space is then an exact direct product of a S^1 with a Gibbons-Hawking space.
- All the quantities in (8.2.11) except \tilde{z}_{IJ} are rational functions of the initial parameters. This will be an important ingredient for the local geometry to be a discrete quotient of $S^1 \times \mathbb{R}^4$.
- The warp factors \tilde{Z}_I do not blow at the centers preventing from spacetime singularities.

We can now use the expansions (8.2.11) and the three remarks above to compute the limit of the spectrally flowed six-dimensional metric around the center J :

$$\begin{aligned} ds_J^2 &= \tilde{q}_J \sqrt{\tilde{z}_{1J} \tilde{z}_{5J}} \left[-d\tau_J^2 + \frac{d\rho_J^2}{\rho_J} + \rho_J \left((d\psi_J + (1 + \cos \vartheta_J) d\phi)^2 + d\vartheta_J^2 + \sin^2 \vartheta_J d\phi^2 \right) \right. \\ &\quad \left. + \frac{\tilde{z}_{pJ}}{\tilde{q}_J \tilde{z}_{1J} \tilde{z}_{5J}} dy_J^2 \right], \end{aligned} \quad (8.2.12)$$

where we have defined the six-dimensional local coordinate system $(\tau_J, \rho_J, \vartheta_J, \psi_J, \phi, y_J)$ as a function of the initial coordinates $(t, \rho, \vartheta, \phi, \psi, y)$:

$$\begin{aligned} \tau_J &\equiv \frac{t}{\sqrt{\tilde{q}_J \tilde{z}_{1J} \tilde{z}_{5J} \tilde{z}_{pJ}}}, & \rho_J &\equiv \sqrt{\rho^2 + a_J^2 - 2a_J \rho \cos \vartheta}, & \cos \vartheta_J &\equiv \frac{\rho \cos \vartheta - a_J}{\rho_J}, \\ \psi_J &\equiv \frac{\psi + (\tilde{A}_J^{(0)} - 1) \phi}{\tilde{q}_J}, & y_J &\equiv y - \frac{t}{\tilde{\chi}_{pJ}} + \tilde{k}_{pJ} \psi + \left(\tilde{k}_{pJ} \tilde{A}_J^{(0)} + \tilde{w}_{pJ}^{(0)} \right) \phi. \end{aligned} \quad (8.2.13)$$

We recognize a U(1) fiber over a Gibbons-Hawking space. Thus, the local geometry has no curvature singularity. However, a conical singularity can occur depending on the periodicities of (y_J, ψ_J, ϕ) . If the periodicities were the usual Gibbons-Hawking periods (8.2.10), the base space would be a discrete $\mathbb{Z}_{|\tilde{q}_J|}$ quotient of $S^1 \times \mathbb{R}^4$. The absence of conical singularity at $\rho_J = 0$ would simply require that \tilde{q}_J is integer-valued and would impose some arithmetic constraints on the coefficients involved in

⁴For the interested reader, they can be easily derived with a calculation software using the transformation rules (4.3.31) on the initial almost-BPS supertube solution given in (8.1.2), (8.1.3) and (8.1.4) and then taking the limit $\rho_J \rightarrow 0$.

(8.2.13)⁵. However, the modification of the periodicities at infinity have drastically modified the periods of (y, ψ, ϕ) and the smoothness analysis will require the full mathematical machinery that we briefly detail following [165–167].

Let us first map the Gibbons-Hawking patch of angles $(\vartheta_J, \psi_J, \phi)$ to the S^3 patch $(\vartheta_J, \phi_{LJ}, \phi_{RJ})$ by taking

$$\phi_{RJ} = \frac{\psi_J}{2}, \quad \phi_{LJ} = \frac{\psi_J}{2} + \phi. \quad (8.2.14)$$

The spacelike components of the metric ($dt_J = 0$) gives the spherically symmetric metric on $S^1 \times \mathbb{R}^4$

$$\begin{aligned} \frac{1}{\tilde{q}_J \sqrt{\tilde{z}_{1J} \tilde{z}_{5J}}} ds_a^2 &= \frac{d\rho_J^2}{\rho_J} + \frac{\tilde{z}_{pJ}}{\tilde{q}_J \tilde{z}_{1J} \tilde{z}_{5J}} dy_J^2 \\ &+ \rho_J \left[d\vartheta_J^2 + 2(1 + \cos \vartheta_J) d\phi_{LJ}^2 + 2(1 - \cos \vartheta_J) d\phi_{RJ}^2 \right], \end{aligned} \quad (8.2.15)$$

The periodicities of $(y_J, \phi_{LJ}, \phi_{RJ})$ can be read off from the periodicities of $(y_\infty, \psi_\infty, \phi)$ (8.2.9) with the sequence of three linear changes of coordinates $(y_\infty, \psi_\infty, \phi) \rightarrow (y, \psi, \phi)$ in (8.2.7), $(y, \psi, \phi) \rightarrow (y_J, \psi_J, \phi)$ in (8.2.13) and $(y_J, \psi_J, \phi) \rightarrow (y_J, \phi_{LJ}, \phi_{RJ})$ in (8.2.14). After few lines of computation, the periodicities translate into the following identifications⁶

$$(y_J, \phi_{LJ}, \phi_{RJ}) = \begin{cases} (y_J, \phi_{LJ}, \phi_{RJ}) + 2\pi(\alpha_A, \beta_A, \beta_A) & (A) \\ (y_J, \phi_{LJ}, \phi_{RJ}) + 2\pi(\alpha_B, \beta_B, \beta_B) & (B) \\ (y_J, \phi_{LJ}, \phi_{RJ}) + 2\pi(\alpha_C, 1 + \beta_C, \beta_C) & (C) \end{cases}, \quad (8.2.16)$$

where the coefficients α_i and β_i are complicated but computable rational functions depending on:

- The parameters of the initial almost-BPS solution.
- The spectral flow parameters γ_I .
- The periods T_y and T_ψ of the angles of the UV WAdS₃ (4.3.7).
- The square root of the asymptotic value of the quartic invariant $\sqrt{\mathcal{I}_{4\infty}}$ (8.2.5).

The local geometry is a discrete quotient of $S^1 \times \mathbb{R}^4$ if α_J and β_J are rational numbers. Thus, all the initial parameters and $\sqrt{\mathcal{I}_{4\infty}}$ must be rational⁷. Choosing the other parameters to be rational is easy. However, imposing $\sqrt{\mathcal{I}_{4\infty}}$ to be rational requires a little bit of arithmetic.

Conical singularities only occur at points that are invariant under the operation

$$A^{n_A} B^{n_B} C^{n_C}, \quad (n_A, n_B, n_C) \in \mathbb{Z}. \quad (8.2.17)$$

Furthermore, they all arise at $\rho_J = 0$ where ϕ_{LJ} and ϕ_{RJ} are both degenerate, at $\vartheta_J = 0$ where ϕ_{RJ} is degenerate and at $\vartheta_J = \pi$ where ϕ_{LJ} is degenerate. The periods of ϕ_{RJ} and ϕ_{LJ} are almost identical with a difference of 2π for the periodicity C , so if the identifications (8.2.16) at $\rho_J = 0$ do not destroy smoothness, they will also ensure the absence of singularities at $\vartheta_J = 0$ or π .

At $\rho_J = 0$, in order for the shifts $\phi_{LJ} \rightarrow \phi_{LJ} + 2\pi$ and $\phi_{RJ} \rightarrow \phi_{RJ} + 2\pi$ at fixed y_J to be a closed orbit, any triplet of integers (n_A, n_B, n_C) where $y_J \rightarrow y_J$ under (8.2.17) must satisfy $n_A \beta_A + n_B \beta_B + n_C \beta_C \in \mathbb{Z}$. In more concrete terms, any operation (8.2.17) that leaves y_J invariant, that is to say where $n_A \alpha_A + n_B \alpha_B + n_C \alpha_C = 0$, must transform $\phi_{LJ} \rightarrow \phi_{LJ} + 2\pi N$ and $\phi_{RJ} \rightarrow \phi_{RJ} + 2\pi N'$ where N and N' are both integers. Using simple arithmetic arguments one can show that this is equivalent to prove

⁵See [137] for examples of this kind.

⁶For readability, we have dropped the index J referring to the center but the coefficient α_i and β_i are not identical for the four centers.

⁷This means that the entropy of the corresponding black hole given by $S = 2\pi\sqrt{\mathcal{I}_{4\infty}}$ belongs to $2\pi\mathbb{Q}$.

the condition for the three sets of integers $(0, n_B, n_C)$, $(n_A, 0, n_C)$ and $(n_A, n_B, 0)$. If the conditions are satisfied for each set, the action of the quotient is free and the local geometry around the center J is then a smooth discrete quotient of $S^1 \times \mathbb{R}^4$.

This analysis applies at every center. The total number of smoothness conditions is then 12 (3×4 centers). The number of parameters is still greater than the number of conditions, which gives good hope to draw a systematic construction procedure.

8.2.3 The construction procedure

We sketch briefly a technical summary of what we have done until now to build asymptotically $WAdS_3 \times SqS^3$ geometries:

- We start with the family of almost-BPS four-center solutions of three supertubes in \mathbb{R}^4 . Initially, it is a family of 15 rational parameters : q , $Q_I^{(J)}$, κ^I , a_I and k_∞^I . The regularity of the solution imposes three bubble equations (8.1.8), the condition on the asymptotics requires $j_L = 0$ (8.1.7) and the positivity of the quartic invariant \mathcal{I}_4 is satisfied by imposing all the initial charges and dipole charges to be positive except one. Furthermore, $\sqrt{\mathcal{I}_{4\infty}}$ needs to be a rational number which is not an equation but one can consider that this fixes a parameter. We have consequently a 10-parameter family of initial almost-BPS solutions.
- After three generalized spectral flows, we have three new parameters γ_I whose one is fixed to have rational spectrally flowed charges. Moreover, the periods T_y and T_ψ of the angles of the $WAdS_3 \times SqS^3$ region can also be considered as free parameters.
- We have in total a 14-parameter family of bubbling asymptotically $WAdS_3 \times SqS^3$ geometries. The smoothness of the geometry in the IR requires 12 arithmetic conditions as discussed in the previous section. These conditions do not exactly fix parameters so the parameter space of the resulting family of smooth solutions is complicated to define. However, many solutions can be easily generated by generating parameters and by checking for each set of parameters if the 12 arithmetic conditions can be satisfied. We give an example of such a solution in the next section.

8.2.4 An explicit example

We construct an explicit example of the procedure discussed above. We picked an almost-BPS three-supertube solution in \mathbb{R}^4 giving the solution that we use in the first step of the procedure:

$$\begin{aligned} q &= \Lambda, & \kappa_1 &= \frac{\Lambda}{2}, & \kappa_5 &= -\frac{2\Lambda}{3}, & \kappa_P &= \frac{\Lambda}{2}, & Q_5^{(1)} &= \Lambda, \\ Q_P^{(1)} &= \frac{2\Lambda}{3}, & Q_1^{(5)} &= \Lambda, & Q_P^{(5)} &= \Lambda, & Q_1^{(p)} &= \frac{\Lambda}{3}, & Q_5^{(p)} &= \frac{4\Lambda}{3}, \end{aligned} \quad (8.2.18)$$

where $\Lambda \in \mathbb{Q}^+$ is a degree of freedom of the charges that does not compromise the regularity of the solution and the condition on the asymptotics. We can consider Λ as a free parameter all along the construction. The coordinates of the three supertube centers on the z-axis are

$$a_1 = 1, \quad a_5 = \frac{36}{13}, \quad a_P = 24. \quad (8.2.19)$$

The solution is asymptotically $AdS_2 \times S^1 \times S^3$, which implies that the center positions are scaling invariant $a_I \rightarrow \lambda a_I$ [25]. Consequently, one can freely rescale (8.2.19) to make the inter-center distances as small as we want.

We did not fix yet the constant terms k_∞^I since they are not involved in the regularity of the solution. They are actually irrelevant from the point of view of the initial almost-BPS solution since they affect only the asymptotic values of the gauge, A^I , of the solution that can be gauge-fixed to zero. However, they affect greatly the solutions after spectral flows.

From (8.1.2), one can derive the asymptotic values of the D1, D5, P charges of the initial solution, the left and right angular momenta and the entropy of the corresponding three-charge black hole

$$\begin{aligned} q_1 &= \frac{4\Lambda}{3}, & q_5 &= \frac{9\Lambda}{4}, & q_P &= \frac{4\Lambda}{3}, \\ j_L &= j_R = 0, \\ S &= 2\pi\sqrt{\mathcal{I}_{4\infty}} = 4\pi\Lambda^2. \end{aligned} \tag{8.2.20}$$

One can now play with the spectral flow parameters γ_I and the constants k_∞^I to generate an extremal non-supersymmetric smooth asymptotically WAdS₃×SqS³ bubbling geometry. We found an infinite number of such solutions. To give an example, we pick one of these solutions:

$$\gamma_1 = \frac{1}{2}, \quad \gamma_5 = -1, \quad \gamma_P = -1, \quad k_\infty^1 = -\frac{3}{2}, \quad k_\infty^5 = 3, \quad k_\infty^P = 1. \tag{8.2.21}$$

We can derive the full geometry by computing the metric and the gauge fields (4.3.30) and (4.3.31). We will just focus on the WAdS₃×SqS³ asymptotic region that is given by

$$\begin{aligned} ds_{6\infty}^2 &= \frac{1}{3}\sqrt{\frac{485}{6}} \left[-\rho^2 d\tau^2 + \frac{d\rho^2}{\rho^2} + \frac{701}{485} (dy_\infty + \rho d\tau)^2 + \frac{701}{485} (d\psi_\infty + \cos\vartheta d\phi)^2 \right. \\ &\quad \left. + \frac{1302}{485} (dy_\infty + \rho d\tau)(d\psi_\infty + \cos\vartheta d\phi) + d\vartheta^2 + \sin^2\vartheta d\phi^2 \right]. \end{aligned} \tag{8.2.22}$$

We choose the periodicities of the angles to be⁸

$$(y_\infty, \psi_\infty, \phi) = \begin{cases} (y_\infty, \psi_\infty, \phi) + 2\pi \left(\frac{24}{43}T, -\frac{8}{11}T, 0 \right) \\ (y_\infty, \psi_\infty, \phi) + 2\pi (0, 2, 0) \\ (y_\infty, \psi_\infty, \phi) + 2\pi (0, 1, 1) \end{cases}, \tag{8.2.23}$$

where T is a free parameter. For the reader interested in the smoothness of the bubbling geometry in the IR, the metric and the periodicities of the angles around the centers are given in the Appendix A.8. We found that the IR bubbling geometry is smooth if and only if $T = \frac{a}{b} \in \mathbb{Q}$ and b is not divisible by 2 or 13.

8.3 Asymptotically NHEK bubbling geometries

In the previous section, we have constructed in detail a large family of extremal non-supersymmetric bubbling solutions that cap off smoothly in the IR and that are asymptotically WAdS₃×SqS³. In the present section, we push a bit further the construction to asymptotically NHEK bubbling solutions. The path from WAdS₃×SqS³ to NHEK requires to relate the WAdS₃ region to the near-horizon region of the over-rotating 5d D1-D5-P black hole detailed in Section 4.3.1. This essentially means that we have to express the charges, angular momentum and mass of the D1-D5-P black hole in terms of the parameters of our solutions. Once this is done, we have to impose the NHEK periodicities of the angles

⁸Many other possibilities were available.

at infinity (4.3.8) and check the smoothness of the IR geometry as it has been done for asymptotically WAdS₃ geometries in Section 8.2.2. At first sight, this might seem to be a mere formality. However, the fact that the periods of y_∞ and ψ_∞ were free parameters for asymptotically WAdS₃ solutions was practical to satisfy the twelve conditions of smoothness at the centers. Now that the periods are connected to the parameters defining the bubbling geometry, this requires more work.

In this section, we use all the results obtained in the previous section. We have started with the family of almost-BPS three-supertube solutions in \mathbb{R}^4 and performed the sequence of generalized spectral flows detailed in Section 8.2.1 to obtain an asymptotically WAdS₃×SqS³ bubbling geometry. In Section 8.3.1 we will match this asymptotic region to a near-horizon region of an extremal non-supersymmetric D1-D5-P black hole. We will identify the corresponding periodicities and see how such solutions can be systematically generated in Section 8.3.2. At the end of the section, we will give an explicit example of a solution.

8.3.1 Matching the WAdS₃ UV geometry to NHEK

After applying the sequence of generalized spectral flows to our family of almost-BPS solutions, the asymptotic metric is given by (8.2.6) where the constant warp factors γ and α and the length κ are defined in (8.2.8). We want to relate this geometry to the near-horizon geometry of an extremal non-supersymmetric D1-D5-P black hole determined by four parameters a , δ_1 , δ_5 and δ_P and given by the metric (4.3.9) where γ , α and κ are defined by (4.3.10). We use the three identities between γ , α and κ to relate a , δ_1 and δ_5 to the parameters of our solutions and we use the matching of the entropy to find δ_P . After few lines of computation, we obtain

$$\begin{aligned} a &= 2 (\mathcal{I}_{4\infty} \gamma_1 \gamma_5 t_\infty^1 t_\infty^5)^{1/4}, \\ s_1 &= \frac{1}{2} \left[\frac{q q_1 t_\infty^1{}^2 + \gamma_1 (\gamma_1 q_5 q_P - 2\sqrt{\mathcal{I}_{4\infty}} t_\infty^1)}{\gamma_1 t_\infty^1 \sqrt{\mathcal{I}_{4\infty}}} \right]^{1/2}, \\ s_5 &= \frac{1}{2} \left[\frac{q q_5 t_\infty^5{}^2 + \gamma_5 (\gamma_5 q_1 q_P - 2\sqrt{\mathcal{I}_{4\infty}} t_\infty^5)}{\gamma_5 t_\infty^5 \sqrt{\mathcal{I}_{4\infty}}} \right]^{1/2}, \\ s_P &= \frac{\mathcal{I}_{4\infty}}{4a^3} \frac{s_1 s_5 + c_1 c_5 \sqrt{\mathcal{H}}}{c_1^2 c_5^2 - s_1^2 s_5^2}, \end{aligned} \tag{8.3.1}$$

where $s_I = \sinh \delta_I$, $c_I = \cosh \delta_I$ and \mathcal{H} is defined as

$$\begin{aligned} \mathcal{H} &\equiv 1 - 16 \frac{a^6 (c_1^2 c_5^2 - s_1^2 s_5^2)}{\mathcal{I}_{4\infty}} \\ &= 1 - 256 \sqrt{\gamma_1 \gamma_5 t_\infty^1 t_\infty^5} (\gamma_1 q_5 t_\infty^5 + \gamma_5 q_1 t_\infty^1) (q t_\infty^1 t_\infty^5 + q_P \gamma_1 \gamma_5). \end{aligned} \tag{8.3.2}$$

The mass, the D1, D5 and P charges and the left angular momentum of the corresponding Cvetič-Youm black hole can be derived using (4.3.1). However, the most interesting quantities are the NHEK periods T_y and T_ψ (4.3.8). Using (8.3.1), we can show that they are rational numbers if:

- $\sqrt{\mathcal{I}_{4\infty}}$ is rational. This is the same condition as the one imposed for asymptotically WAdS₃ bubbling geometries.
- $\sqrt{\mathcal{H}}$ is rational. This is a more complicated condition to satisfy than the previous one. Tricky arithmetic is required.

Once the matching to NHEK is performed, one can look at the IR bubbling region of our solutions. The periodicities of the angles around each center depends on T_y and T_ψ . Thus the local geometries are quotients of $\mathbb{R}^4 \times S^1$ only if they are rational. Moreover, conical singularities might still occur as for asymptotically WAdS₃ bubbling geometries. We use the same smoothness analysis as in Section 8.2.1 to derive 12 conditions to have smooth discrete quotients on $\mathbb{R}^4 \times S^1$ around the centers.

8.3.2 The construction procedure

The procedure to build smooth asymptotically NHEK bubbling geometries is similar to the one depicted in Section 8.2.3:

- We start with the family of almost-BPS four-center solutions of three supertubes in \mathbb{R}^4 . Initially, it is a family parametrized by 15 rational parameters : $q, Q_I^{(J)}, \kappa^I, a_I$ and k_∞^I . We solve the three bubble equations (8.1.8), $j_L = 0$ (8.1.7) and we require the positivity of the quartic invariant \mathcal{I}_4 by imposing all the initial charges to be positive except one. Furthermore, $\sqrt{\mathcal{I}_{4\infty}}$ needs to be a rational number which fixes a parameter. We have consequently a 10-parameter family of initial almost-BPS solutions.
- After three generalized spectral flows, we have two more parameters γ_I (γ_P is fixed to have rational spectrally flowed charges). The condition on the periods T_y and T_ψ to be rational requires some arithmetic machinery which fixes 3 parameters (the two remaining spectral flow parameters and k_∞^5).
- We have in total an 8-parameter family of bubbling asymptotically NHEK₃ geometries. The smoothness of the geometry in the IR requires 12 arithmetic conditions. Even if the parameter space is not easy to determine, we can perform a loop generating technique to build a large number of such solutions. We give an example of such a solution in the next section.

8.3.3 An explicit example

We construct an explicit example of the procedure discussed above. We choose a smooth almost-BPS three-supertube solution in \mathbb{R}^4 satisfying the first point of the procedure:

$$\begin{aligned} q &= 1, & \kappa_1 &= \Lambda, & \kappa_5 &= -\frac{\Lambda}{2}, & \kappa_P &= \frac{\Lambda}{3}, & Q_5^{(1)} &= \Lambda^2, \\ Q_P^{(1)} &= \frac{\Lambda^2}{2}, & Q_1^{(5)} &= \frac{2\Lambda^2}{3}, & Q_P^{(5)} &= \frac{\Lambda^2}{3}, & Q_1^{(p)} &= \frac{\Lambda^2}{2}, & Q_5^{(p)} &= \Lambda^2, \end{aligned} \quad (8.3.3)$$

where $\Lambda \in \mathbb{Q}^+$ corresponds to the charge-scaling free parameter. We choose a slightly different charge-scaling Λ than in Section 8.2.4. They are actually equivalent. The present choice is just more adapted to the matching with NHEK. The coordinates of the three supertube centers on the z-axis are

$$a_1 = 1, \quad a_5 = \frac{3}{14} (17 + \sqrt{65}), \quad a_P = \frac{3}{4} (9 + \sqrt{65}). \quad (8.3.4)$$

Once again, the $\text{AdS}_2 \times \text{S}_1 \times \text{S}^3$ asymptotics of the solution allows us to rescale $a_I \rightarrow \lambda a_I$ as small as we want. The irrationality of the inter-center distances does not impact the smoothness of the solution around the centers.

From (8.1.2), one can derive the asymptotic values of the initial D1, D5, P charges of the solution, the left and right angular momenta and the entropy of the initial system

$$\begin{aligned} q_1 &= \frac{4\Lambda^2}{3}, & q_5 &= \frac{4\Lambda^2}{3}, & q_P &= \Lambda^2, \\ j_L &= j_R = 0, \\ S &= 2\pi\sqrt{\mathcal{I}_{4\infty}} = \frac{8\pi}{3}\Lambda^3. \end{aligned} \quad (8.3.5)$$

One can now play with the spectral flow parameters γ_I and the constants k_∞^I to generate an extremal non-supersymmetric smooth asymptotically NHEK₃ × SqS³ bubbling geometry. This requires $\sqrt{\mathcal{H}}$ in

(8.3.2) to be rational. After a rather technical arithmetic computation we found several values for γ_1 , γ_5 and k_∞^5 that lead to rational NHEK periods T_y and T_ψ without inducing any conical singularities at the centers:

$$\begin{aligned} \gamma_1 &= \frac{1}{3\Lambda - 2}, & \gamma_5 &= \frac{9\Lambda - 6}{40\Lambda^2}, & \gamma_P &= -1, \\ k_\infty^1 &= 2, & k_\infty^5 &= -\frac{\Lambda}{3} \frac{2 + 37\Lambda}{3\Lambda - 2}, & k_\infty^P &= 1. \end{aligned} \quad (8.3.6)$$

We can derive the full geometry by computing the metric and the gauge fields (4.3.30) and (4.3.31). We will just focus on the NHEK asymptotic region that is given by

$$\begin{aligned} ds_\infty^2 &= \frac{\Lambda^2}{3} \left[-\rho^2 d\tau^2 + \frac{d\rho^2}{\rho^2} + \frac{34}{25} (dy_\infty + \rho d\tau)^2 + \frac{34}{25} (d\psi_\infty + \cos\vartheta d\phi)^2 \right. \\ &\quad \left. + \frac{12}{5} (dy_\infty + \rho d\tau)(d\psi_\infty + \cos\vartheta d\phi) + d\vartheta^2 + \sin^2\vartheta d\phi^2 \right]. \end{aligned} \quad (8.3.7)$$

The NHEK angle periodicities are

$$(y_\infty, \psi_\infty, \phi) = \begin{cases} (y_\infty, \psi_\infty, \phi) + 2\pi \left(\frac{75}{32\Lambda}, -\frac{93}{32\Lambda}, 0 \right) \\ (y_\infty, \psi_\infty, \phi) + 2\pi (0, 2, 0) \\ (y_\infty, \psi_\infty, \phi) + 2\pi (0, 1, 1) \end{cases}. \quad (8.3.8)$$

The asymptotic NHEK region corresponds to the near-horizon region of an extremal Kerr black hole given by the following mass, angular momenta and charges:

$$\begin{aligned} M &= \frac{287\Lambda^2}{75}, \\ J_R &= 0, \quad J_L = \frac{124\Lambda^3}{75}, \\ Q_1 &= \frac{16\Lambda^2}{15}, \quad Q_5 = \frac{16\Lambda^2}{15}, \quad Q_P = \frac{21\Lambda^2}{25} \end{aligned} \quad (8.3.9)$$

For the reader interested in the feature of the bubbling geometry in the IR, we gave the local metrics and the periodicities of the angles around the centers in the Appendix A.9.

For any rational values of Λ , we found a smooth non-supersymmetric extremal geometry which is bubbling in the IR and NHEK in the UV.

8.4 Final comment

In this chapter, we have constructed a family of smooth bubbling solutions in six dimensions that are asymptotic to either generic $\text{WAdS}_3 \times \text{SqS}^3$ or NHEK spacetime. We gave explicit examples of the construction which can be used for different purposes:

- One can investigate their CFT dual states. They can give some hints on the nature of the CFT_2 dual to WAdS_3 or the CFT_2 dual to NHEK.
- Nearly extreme black hole have been seen in the sky [168]. From an astrophysical point of view, one can compute the Kerr multipole moments of our solutions to see if there exist deviations from the Kerr-Newman black hole solution. This could give interesting observable quantities in order to detect some imprints of the microstate structure of black holes in the gravitational wave emission after a collision of two black holes.

Part III

Scattering from microstate geometries and application to AdS/CFT

AdS₂ Holography: Mind the Cap

One of the most important statement that arised from modern theoretical physics is surely the AdS/CFT correspondence [3]. The correspondence relates String Theory on $D + 1$ AdS spacetime to D -dimensional CFT. It has led to the gravitational-holography field of research and its countless breakthroughs. If the $\text{AdS}_{D+1}/\text{CFT}_D$ is well-understood for $D \geq 2$, less is known for the $\text{AdS}_2/\text{CFT}_1$. In this chapter, we review the work in [25] that examined in what extend the microstate geometry program fits in a well-defined $\text{AdS}_2/\text{CFT}_1$ correspondence.

9.1 State of the art and proposal

First, String Theory has had great success in counting the microstates of extremal black holes whose near-horizon geometries contain a factor that is AdS_3 [8, 6, 169] or AdS_4 [170, 171], however many extremal black holes have an AdS_2 near-horizon limit that is not contained in a higher-dimensional AdS space, and the counting of the microstates of these black holes is poorly understood. Furthermore, many black holes have an AdS_3 near-horizon limit and a further AdS_2 very-near-horizon geometry deeper in the infrared. For these black holes, understanding the RG flow between AdS_3 and AdS_2 remains an important and challenging open problem [172–177].

Second, holography in AdS_2 is somewhat subtle: it is well known that the backreaction of finite-energy excitations in global AdS_2 necessarily diverges at one of the two asymptotic boundaries [178, 179]. Indeed, much of the recent interest in the Sachdev-Ye-Kitaev (SYK) model and its dual (see for example [180–184]) is driven by the desire to understand quantum gravity in AdS_2 . Since global AdS_2 has two disconnected boundaries, it appears that its holographic dual should be two copies of a CFT_1 .¹ By contrast, black hole entropy in String Theory is usually accounted for by enumerating bound states of a (single) system of branes, so one expects there to be an $\text{AdS}_2/\text{CFT}_1$ entropy calculation that involves counting ground states of a single CFT_1 (see for example [173, 187]). It does not appear to be understood in general whether the ground states of the CFT_1 preserve or break conformal invariance, whether the CFT_1 is topological, and whether or not one can construct a tower of non-supersymmetric states above a given ground state.

Third, as it has been already addressed in Chapter 4, five-dimensional supersymmetric black holes have an AdS_2 near-horizon region with $J_R = 0$. For such black holes, according to the zero-angular-momentum conjecture [156, 144], the only solutions that can be interpreted as pure black hole microstates (involving no additional degrees of freedom exterior to the black hole) are those that have zero angular momentum in four dimensions ($J_R = 0$ in five dimensions) and fit in an AdS_2 region.

The purpose of this chapter is to address all these three points at the same time. We will first

¹See [185, 186] for work on the construction of bubbling solutions that are asymptotic to global AdS_2 .

review what has been sparsely discussed in the thesis which is the construction of families of smooth solutions that have an $\text{AdS}_2 \times \mathcal{M}$ asymptotic region in the UV (allowing also for \mathcal{M} to be non-trivially fibered over AdS_2), that end in the IR with a smooth cap, and that have $J_R = 0$. It has been already discussed for smooth multicenter in five dimensions, one will extend the construction to six-dimensional smooth solutions as Superstrata. If one reduces these solutions to two-dimensional gravity coupled to matter, they appear to be geometrically singular. However, this singularity is resolved into smooth geometry supported by fluxes in five- or six-dimensional Supergravity as detailed in Chapter 4. The naive two-dimensional geometrical singularity of our solutions enables our solutions to have non-trivial features in their IR while preserving the AdS_2 UV, in contrast to the rigidity of global AdS_2 [178, 179]. According to the AdS-CFT correspondence, these supersymmetric solutions should be dual to pure states of (a single copy of) a CFT_1 .

By contrast, most of the recent attempts to understand quantum gravity in AdS_2 involve modifying the UV (by adding a running dilaton and working in a “Nearly- AdS_2 ” geometry) and preserving the IR [179, 181–184]. Indeed, if one works in two-dimensional theories with relatively simple field content, modifying the UV is the only option; our solutions require much richer field content from a two-dimensional perspective, as of course is natural in String Theory.

These two options: either keeping the UV fixed and resolving the IR singularity by brane polarization and bubbling (as in Polchinski-Strassler) or keeping the IR fixed and modifying the UV asymptotics (as in Almheiri-Polchinski), appear to be the only two possibilities to obtain non-trivial physics in AdS_2 . Our interest in the present work is in the CFT_1 description of asymptotically AdS_2 String Theory solutions, rather than irrelevant deformations of such a CFT_1 . We therefore choose the Polchinski-Strassler option over the Almheiri-Polchinski one.

Our map also clarifies the relation between deep scaling microstate geometries, the angular momentum J_R , and the discussions of [156, 144]. In particular, the key argument of [156, 144] was that all the information characterizing the microstates of supersymmetric black holes should fit inside an AdS_2 throat, and everything that does not do so represents degrees of freedom external to the black hole horizon. Our construction shows that all the information about the topology, fluxes and wiggles of the scaling black hole microstates constructed thus far passes this criteria. The only information that does not survive the AdS_2 limit is the non-zero J_R of the asymptotically AdS_3 solutions, which is proportional to the inverse of the length of the AdS_2 throat and thus vanishes in the AdS_2 scaling limit, consistent with the discussions in [156, 144]. The fact that these solutions fit inside an AdS_2 region, and that in this limit the angular momentum J_R vanishes, indicates that the non-zero J_R of the corresponding asymptotically AdS_3 solutions does not come from the structure that replaces the horizon, but rather from the gluing of the long AdS_2 throat to the ambient spacetime.

The presence of a smooth IR cap allows our supersymmetric solutions to support an infinite tower of non-supersymmetric linearized excitations. These excitations are localized very near the IR cap, and are normalizable. An important question that remains open is whether or not the backreaction of these excitations preserves the AdS_2 UV asymptotics. One possibility, consistent with the naive extrapolation of the results of [178, 179] to our capped solutions, is that the backreaction of these excitations necessarily modifies the AdS_2 UV asymptotics, meaning that these excitations are not dual to any states of the original CFT_1 . However, since there exist non-supersymmetric black hole solutions with a finite bulk stress-energy tensor that preserve the AdS_2 asymptotics [188], it is possible that the backreacted non-supersymmetric solutions will also preserve the AdS_2 asymptotics, and indeed this is our expectation. We rather expect that the data that determines whether the UV is modified is independent of the existence of our excitations, and will discuss this in more detail in Section 9.4.1.

If the backreaction of our time-dependent perturbations preserves the AdS_2 UV asymptotics, then these perturbations should be dual to time-dependent excitations of the CFT_1 . This in turn indicates

that this CFT₁ has nontrivial dynamics, and hence is not a topological theory. By contrast, if a given CFT₁ has a conformally invariant ground state (which would presumably be holographically dual to empty Poincaré AdS₂), it is necessarily topological. Hence, if the backreaction preserves the AdS₂ UV, this implies that the dual CFT₁ does not have a conformally invariant ground state. CFT₁ models that have no conformally invariant ground state have been discussed in [189].

The absence of a conformally invariant ground state would in turn indicate that empty Poincaré AdS₂ cannot be dual to any pure state of the microscopic CFT₁ under consideration. From this perspective Poincaré AdS₂ would have a similar status to Poincaré AdS₃, which is also not dual to any pure state of the D1-D5 CFT, but is a singular geometry that should be rather thought of as an approximation to a mixed state. The bulk duals of all the pure states of a single CFT₁ would therefore be asymptotically AdS₂ states of String Theory with nontrivial (and likely stringy and/or quantum) physics in the infrared that breaks conformal invariance. If one could prove that there is no conformally invariant CFT₁ ground state, this would establish beyond reasonable doubt that the fuzzball proposal is the correct description of extremal black holes.

The organization of the chapter is as follows. In Section 9.2.1 we formulate our general AdS₂ limit for smooth horizonless supergravity solutions in five or six dimensions. In Section 9.3 we solve the free massless scalar wave equation on a class of asymptotically AdS₂ Superstrata, finding an infinite tower of bound-state excitations. Finally, in Section 9.4 we discuss the backreaction of these excitations, their holographic description, and possible connections with other approaches to AdS₂ quantum gravity.

9.2 AdS₂ limit of capped solutions of five- and six-dimensional Supergravity

9.2.1 The AdS₂ limit

We describe a general limiting procedure to obtain asymptotically AdS₂ BPS solutions in five or six dimensions. Let us recall the metric and field Ansatz for the five-dimensional solutions (4.1.5)

$$ds_5^2 = - \left(\frac{1}{6} C_{IJK} Z_I Z_J Z_K \right)^{-\frac{2}{3}} (dt + \omega)^2 + \left(\frac{1}{6} C_{IJK} Z_I Z_J Z_K \right)^{\frac{1}{3}} ds(\mathcal{B})^2, \quad (9.2.1)$$

$$F^I = d_4 A^I = d_4 (Z_I^{-1} (dt + \omega)) + \Theta^I,$$

and the metric and field Ansatz for six-dimensional solutions (4.2.27)

$$ds_6^2 = - \frac{2}{\sqrt{\mathcal{P}}} (dv + \beta) \left(du + \omega + \frac{1}{2} \mathcal{F} (dv + \beta) \right) + \sqrt{\mathcal{P}} ds(\mathcal{B})^2, \quad (9.2.2)$$

$$G^{(I)} = \frac{1}{2} \left[\eta^{IJ} \star_4 \mathcal{D} Z_J - d_6 \left(\frac{\eta^{IJ} Z_J}{\mathcal{P}} (du + \omega) \wedge (dv + \beta) \right) + (dv + \beta) \wedge \Theta^I \right].$$

Both types of solutions are constructed on a four-dimensional base space \mathcal{B} which is asymptotic to flat \mathbb{R}^4 . We are interested in smooth horizonless solutions, which have non-trivial topological structure that is controlled by another length-scale, a , and where there is a large hierarchy between the scale a and the electric charges Q_I ,

$$a^2 \ll Q_I, \quad (9.2.3)$$

and where the J_L angular momentum is inside the regime of parameters where the black hole horizon is macroscopic,²

$$J_L^2 < Q_1 Q_2 Q_3. \quad (9.2.4)$$

²For the six-dimensional solutions, remind that we have used the D1-D5-P label for the charges: $(1, 2, 3) \rightarrow (1, 5, P)$.

We first extract the scale a^2 from the four-dimensional base metric,

$$ds(\mathcal{B})^2 = a^2 \bar{ds}(\mathcal{B})^2 \iff \hat{r} = a\bar{r}, \quad (9.2.5)$$

where \hat{r} is the four-dimensional radial coordinate defined in (4.1.11). We will be interested in taking a limit in which $a \rightarrow 0$ with $\bar{ds}(\mathcal{B})^2$ and Q_I fixed. The scaling limit we shall derive is closely related to the families of “scaling solutions” mentioned in previous chapters [85, 87], and is also closely related to other scaling limits considered previously in the literature for brane and black hole solutions (see for example [3, 172, 191–193]).

We require that the scaling limit results in a non-singular solution. Let us derive the implications of this requirement for the dependence of the ansatz quantities on the parameter a . First, given the scaling of the base metric with a , (9.2.5), in order to have a finite and non-trivial limit for the four-dimensional part, as $a \rightarrow 0$ we must have

$$Z_I \rightarrow \frac{\bar{Z}_I}{a^2}, \quad \mathcal{P} \rightarrow \frac{\bar{\mathcal{P}}}{a^4}, \quad (9.2.6)$$

In the (t) -part or (u, v) -part of the metrics, this implies that we must have

$$\omega \rightarrow \frac{\bar{\omega}}{a^2}, \quad \mathcal{F} \rightarrow \frac{\bar{\mathcal{F}}}{a^2}, \quad t = \frac{\tau}{a^2} \quad \text{or} \quad u = \frac{\bar{u}}{a^2}, \quad (9.2.7)$$

where $\bar{\omega}$, $\bar{\mathcal{F}}$ and β are finite and independent of a , and where τ , \bar{u} and v are held fixed as we take the limit.

We can thus define our AdS₂ limit on the five- or six- dimensional coordinates by:

$$\begin{aligned} r &= a\bar{r}, & t &= a^{-2}\tau; & a &\rightarrow 0 & \text{with } \bar{r}, \tau, \text{ angles fixed} & (5d), \\ r &= a\bar{r}, & u &= a^{-2}\bar{u}; & a &\rightarrow 0 & \text{with } \bar{r}, \bar{u}, v, \text{ angles fixed} & (6d). \end{aligned} \quad (9.2.8)$$

Examining the Ansatz for the vector and tensor fields (9.2.1) and (9.2.2), one requires in addition that the Θ^I are also finite and independent of a . The above behavior of the ansatz quantities then ensures the finite limit

$$ds_5^2 \rightarrow - \left(\frac{1}{6} C_{IJK} \bar{Z}_I \bar{Z}_J \bar{Z}_K \right)^{-\frac{2}{3}} (d\tau + \bar{\omega})^2 + \left(\frac{1}{6} C_{IJK} \bar{Z}_I \bar{Z}_J \bar{Z}_K \right)^{\frac{1}{3}} \bar{ds}(\mathcal{B})^2, \quad (9.2.9)$$

$$F^I \rightarrow d_4(\bar{Z}_I^{-1}(d\tau + \bar{\omega})) + \Theta^I, \quad (9.2.10)$$

for the five-dimensional solutions and

$$ds_6^2 \rightarrow - \frac{2}{\sqrt{\bar{\mathcal{P}}}} (dv + \beta) \left(d\bar{u} + \bar{\omega} + \frac{1}{2} \bar{\mathcal{F}} (dv + \beta) \right) + \sqrt{\bar{\mathcal{P}}} \bar{ds}(\mathcal{B})^2, \quad (9.2.11)$$

$$G^{(I)} \rightarrow \frac{1}{2} \left[\eta^{IJ} \bar{\star}_4 \mathcal{D} \bar{Z}_J - d_6 \left(\frac{\eta^{IJ} Z_J}{\mathcal{P}} (d\bar{u} + \bar{\omega}) \wedge (dv + \beta) \right) + (dv + \beta) \wedge \Theta^I \right]. \quad (9.2.12)$$

for the six-dimensional solutions where $\bar{\star}_4$ is the Hodge star with respect to $\bar{ds}(\mathcal{B})$. The limit $a \rightarrow 0$ has now been taken, and the solution is independent of a .

9.2.2 Asymptotically AdS₂ multicenter solutions

In Section 4.1.3.1, we have already observed that the asymptotics of a BPS multicenter solution is governed by their background vector Γ_∞ , that is, the constant terms in the harmonic functions. We have also noted that taking the limit for which all constant terms vanish corresponds to the limit where

the geometry is asymptotically $\text{AdS}_2 \times S^3$ and $J_R = 0$. Let us check that the AdS_2 limit above is equivalent.

The requirement on the warp factors (9.2.6) under the coordinate transformation (9.2.8), imposes the charge vectors and the background vector (4.1.24) to transform as

$$\bar{\Gamma} = a^2 \Gamma \quad \Longleftrightarrow \quad \bar{\Gamma}_\infty = a^2 \Gamma_\infty, \quad \bar{\Gamma}_j = \Gamma_j, \quad \bar{\rho}_j = a^{-2} \rho_j. \quad (9.2.13)$$

Thus, under the limit $a \rightarrow 0$, the constant terms are indeed sent to zero whereas the charges remain fixed. The right angular momentum of those solutions is given in (4.1.56) and is clearly zero when $\Gamma_\infty = 0$. Moreover, the requirement on the three-dimensional distance from the j^{th} center, ρ_j , implies that the inter-center distances must be rescaled similarly: $\rho_{ij} = a^2 d_{ij}$ where the aspect ratios d_{ij} are held fixed.

As for the regularity conditions, we can easily check that the quartic invariant \mathcal{I}_4 (4.1.27) is simply rescaled $\bar{\mathcal{I}}_4 = a^8 \mathcal{I}_4$ and the positivity is guaranteed along the transformation. However, in Section 5.1, we examined the impact of a change of background moduli on the center configuration. Even if one assumes that the initial solution satisfy the scaling condition (4.1.54), the solution can still decay at walls of marginal stability along the AdS_2 limit. However, we showed that this concerned only solutions with specific center configurations. We will then leave aside this subtlety from now on.

Therefore, microstate geometries at $J_R \neq 0$ are then constructed from an asymptotically AdS_2 solution with an identical charge content Γ_j and aspect ratios between the centers d_{ij} (see Fig.9.1). It is tempting to postulate that for every microstate of the CFT_1 there is a corresponding family of CFT_2 microstates, parameterized by the quantized value j_R^3 . It should be understood that this applies to states with relatively low values of J_R , that are dual to solutions with long throats.

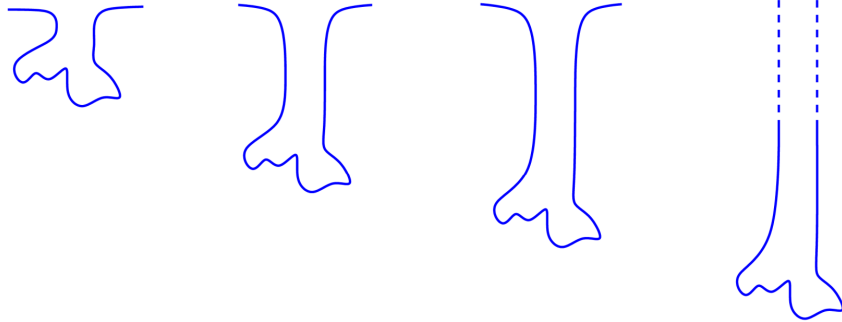


Figure 9.1: A schematic pictorial representation of a scaling geometry and the asymptotically AdS_2 limit. The proper size of the bubbles remains the same as the throat of the solutions becomes longer [85, 86]; the throat becomes infinite in the AdS_2 limit.

9.2.3 Asymptotically AdS_2 Superstrata

In this section we apply the six-dimensional AdS_2 limit defined in Section 9.2.1 to construct families of explicit supergravity solutions with near-horizon-BTZ $\times S^3$ asymptotics, which as described above can be written as S^1 fibered over the near-horizon D1-D5-P solution. We will exhibit an explicit family of examples that are asymptotically S^1 fibered over $\text{AdS}_2 \times S^3$.

³Even if one has taken continuous limit, J_R is determined by a quantized right angular momentum in half-integer unit, j_R .

9.2.3.1 Superstrata with a flat base metric

The procedure discussed in Section 9.2.1 is general, and can be applied to all solutions which have the hierarchy of charges (9.2.3). For concreteness, we will work with the family of superstratum solutions detailed in Section 4.2.5 for which the zeroth-layer fields, that is the four-dimensional \mathbb{R}^4 base and its fibration one-form β , are given in (4.2.40) and (4.2.56). Then, we see that in the limit (9.2.8),

$$\beta \rightarrow \bar{\beta} = \frac{R_y}{\sqrt{2}(\bar{r}^2 + \cos^2 \theta)} (\sin^2 \theta d\varphi_1 - \cos^2 \theta d\varphi_2), \quad (9.2.14)$$

which is of order a^0 , as required. For the four-dimensional flat metric, we obtain

$$\bar{ds}(\mathcal{B})^2 = (\bar{r}^2 + \cos^2 \theta) \left(\frac{d\bar{r}^2}{\bar{r}^2 + 1} + d\theta^2 \right) + (\bar{r}^2 + 1) \sin^2 \theta d\varphi_1^2 + \bar{r}^2 \cos^2 \theta d\varphi_2^2. \quad (9.2.15)$$

9.2.3.2 Single-mode Superstrata

We now focus attention further to the original single-mode Superstratum constructed in Section 4.2.5. We will soon focus for our explicit presentation on solutions that have $(k, m, n) = (1, 0, n)$, however for the moment, and where it is illuminating, we shall keep (k, m, n) general, to illustrate the generality of the procedure. Following the general discussion in Section 4.2.5.5, in the regime

$$a^2 \ll \{Q_1, Q_5, Q_P\}, \quad (9.2.16)$$

we have a BTZ-like near-horizon throat inside $\text{AdS}_3 \times S^3$. In order to more easily connect to the discussion of with the five-dimensional solution, we change the parametrization of (u, v) according to (t, y) where y is the coordinate of the common S^1 of the D1- and D5-branes:

$$u = t, \quad v = t + y. \quad (9.2.17)$$

As already said, this can be achieved from the initial coordinate definition $u/v = \frac{1}{\sqrt{2}}(t \mp y)$ by constant shift in \mathcal{F} and shift by β in ω [100]. The first- and second-layer fields of asymptotically AdS_3 solutions are given in (4.2.60) and (4.2.72) respectively.

We now take the AdS_2 limit of this family of solutions. We will continue to write the general (k, m, n) expressions for the first-layer data, specializing to $(1, 0, n)$ for the second layer. The phase $v_{k,m,n}$ is invariant (4.2.57); we define the quantities

$$\begin{aligned} \bar{\Sigma} &\equiv \bar{r}^2 + \cos^2 \theta, \\ \bar{\Delta}_{k,m,n} &\equiv \left(\frac{1}{\sqrt{\bar{r}^2 + 1}} \right)^k \left(\frac{\bar{r}}{\sqrt{\bar{r}^2 + 1}} \right)^n \cos^m \theta \sin^{k-m} \theta, \\ \bar{\vartheta}_{k,m,n} &\equiv -\bar{\Delta}_{k,m,n} \left[\left((m+n)\bar{r} \sin \theta + n \left(\frac{m}{k} - 1 \right) \frac{\bar{\Sigma}}{\bar{r} \sin \theta} \right) \bar{\Omega}^{(1)} \sin v_{k,m,n} \right. \\ &\quad \left. + \left(m \left(\frac{n}{k} + 1 \right) \bar{\Omega}^{(2)} + n \left(\frac{m}{k} - 1 \right) \bar{\Omega}^{(3)} \right) \cos v_{k,m,n} \right], \end{aligned} \quad (9.2.18)$$

where $\bar{\Omega}^{(i)}$ ($i = 1, 2, 3$) are given by:

$$\begin{aligned} \bar{\Omega}^{(1)} &\equiv \frac{d\bar{r} \wedge d\theta}{(\bar{r}^2 + 1) \cos \theta} + \frac{\bar{r} \sin \theta}{\bar{\Sigma}} d\varphi_1 \wedge d\varphi_2, \\ \bar{\Omega}^{(2)} &\equiv \frac{\bar{r}}{\bar{r}^2 + 1} d\bar{r} \wedge d\varphi_2 + \tan \theta d\theta \wedge d\varphi_1, \\ \bar{\Omega}^{(3)} &\equiv \frac{d\bar{r} \wedge d\varphi_1}{\bar{r}} - \cot \theta d\theta \wedge d\varphi_2. \end{aligned} \quad (9.2.19)$$

and we see that in the AdS₂ limit,

$$\Omega^{(1)} \rightarrow a\bar{\Omega}^{(1)}, \quad \Omega^{(2)} \rightarrow \bar{\Omega}^{(2)}, \quad \Omega^{(3)} \rightarrow \bar{\Omega}^{(3)}. \quad (9.2.20)$$

The “-” quantities defined in (9.2.6) for the first-layer data, become

$$\begin{aligned} \bar{Z}_1 &= \frac{Q_1}{\bar{\Sigma}} + \frac{b_1 R_y^2}{2Q_5} \frac{\bar{\Delta}_{2k,2m,2n}}{\bar{\Sigma}} \cos v_{2k,2m,2n}, & \bar{Z}_2 &= \frac{Q_5}{\bar{\Sigma}}, \\ \bar{Z}_4 &= R_y b_4^2 \frac{\bar{\Delta}_{k,m,n}}{\bar{\Sigma}} \cos v_{k,m,n}, \end{aligned} \quad (9.2.21)$$

and

$$\bar{\Theta}^1 = 0, \quad \bar{\Theta}^2 = \frac{b_4^2 R_y}{2Q_5} \bar{v}_{2k,2m,2n}, \quad \bar{\Theta}^4 = b_4 \bar{v}_{k,m,n}. \quad (9.2.22)$$

The solution to the second layer for general (k, m, n) can be similarly derived by replacing the usual quantities by their “barred” version (9.2.18). For ease of presentation, at this point we will specialize to the sub-family $(k, m, n) = (1, 0, n)$, as this will suffice for an explicit family of examples. It is straightforward to generalize the following discussion to the general (k, m, n) family. The solution to the second layer for the $(1, 0, n)$ family is [99]⁴:

$$\begin{aligned} \mathcal{F} &= 1 + \frac{b_4^2}{2a^2} \left(1 - \frac{r^{2n}}{(r^2 + a^2)^n} \right), \\ \omega &= \omega_0 + \frac{b_4^2 R_y}{2\Sigma} \left(1 - \frac{r^{2n}}{(r^2 + a^2)^n} \right) \sin^2 \theta d\varphi_1, \end{aligned} \quad (9.2.23)$$

where⁵

$$\omega_0 = \frac{a^2 R_y}{\Sigma} \sin^2 \theta d\varphi_1. \quad (9.2.24)$$

Applying the AdS₂ limit, we have

$$\begin{aligned} \bar{\mathcal{F}} &= \frac{b_4^2}{2} \left(1 - \frac{\bar{r}^{2n}}{(\bar{r}^2 + 1)^n} \right), \\ \bar{\omega} &= \frac{b_4^2 R_y}{2\bar{\Sigma}} \left(1 - \frac{\bar{r}^{2n}}{(\bar{r}^2 + 1)^n} \right) \sin^2 \theta d\varphi_1. \end{aligned} \quad (9.2.25)$$

Smoothness of the $(1, 0, n)$ solution (4.2.73) imposes the relation

$$b = b_4. \quad (9.2.26)$$

We observe that our AdS₂ limit can be described as “dropping the 1” in $Z_3 = \mathcal{F}$, and also dropping the associated supertube component of ω , namely ω_0 . It is not hard to see that the second layer of the BPS equations (4.2.29) are still satisfied, precisely because ω_0 balances the “1” in Z_3 . To write the full metric, we define the following shorthands:

$$\begin{aligned} \bar{F}_0(\bar{r}) &\equiv 1 - \frac{\bar{r}^{2n}}{(\bar{r}^2 + 1)^n}, & \bar{F}_1(\bar{r}) &\equiv 1 - \frac{\bar{r}^{2n}}{(\bar{r}^2 + 1)^{n+1}}, \\ \bar{\Lambda} &\equiv \frac{\bar{\Sigma}\sqrt{\bar{\mathcal{P}}}}{\sqrt{Q_1 Q_5}} = \sqrt{1 - \frac{\bar{r}^{2n}}{(\bar{r}^2 + 1)^{n+1}} \sin^2 \theta}. \end{aligned} \quad (9.2.27)$$

We will write the full metric in two ways. The first is more convenient for displaying the AdS₂ asymptotics, the second is more convenient to see the smoothness in the cap. In the first form of the

⁴We remind that the second-layer fields have been rescaled to redefine the u and v coordinates.

⁵Remind that ω has been rescaled to redefine (u, v) . That is why ω_0 does not correspond to the one computed from the seed Supertube in (4.2.45).

metric, the square is first completed on the dv terms, as appropriate for a reduction from six dimensions to five on the v fiber,

$$ds_6^2 = Q_1 Q_5 \frac{\bar{F}_0(\bar{r})}{\sqrt{\bar{\mathcal{P}}}} \left(\frac{dv}{R_y} - \frac{1}{\bar{F}_0(\bar{r})} \frac{2 d\tau}{b^2 R_y} - \frac{\cos^2 \theta}{\bar{\Sigma}} d\varphi_2 \right)^2 - \frac{2}{b^2 \sqrt{\bar{\mathcal{P}}}} \left(\frac{1}{\bar{F}_0(\bar{r})} + \frac{\sin^2 \theta}{\bar{\Sigma}} \right) d\tau^2 \\ + \sqrt{Q_1 Q_5} \bar{\Lambda} \left(\frac{d\bar{r}^2}{\bar{r}^2 + 1} + d\theta^2 + \frac{\bar{r}^2 \cos^2 \theta}{\bar{\Sigma}} d\varphi_2^2 \right) + \frac{\sqrt{Q_1 Q_5}}{\bar{\Lambda}} \sin^2 \theta \left(d\varphi_1 - \frac{2 d\tau}{b^2 R_y} \right)^2. \quad (9.2.28)$$

At large \bar{r} , this metric becomes that of the “very-near-horizon” limit of the six-dimensional non-rotating black string (4.2.35)⁶, in the form in which the v direction is fibered over the very-near-horizon limit of the five-dimensional non-rotating supersymmetric (Strominger-Vafa) black hole [172],

$$ds_6^2 = \frac{Q_P}{\sqrt{Q_1 Q_5}} \left(dv - \frac{\bar{r}^2}{Q_P} d\tau \right)^2 - \frac{\bar{r}^4 d\tau^2}{Q_P \sqrt{Q_1 Q_5}} + \sqrt{Q_1 Q_5} \left(\frac{d\bar{r}^2}{\bar{r}^2} + d\theta^2 + \sin^2 \theta d\varphi_1^2 + \cos^2 \theta d\varphi_2^2 \right) \\ = -2 \frac{\bar{r}^2 dv d\tau}{\sqrt{Q_1 Q_5}} + \frac{Q_P}{\sqrt{Q_1 Q_5}} dv^2 + \sqrt{Q_1 Q_5} \left(\frac{d\bar{r}^2}{\bar{r}^2} + d\theta^2 + \sin^2 \theta d\varphi_1^2 + \cos^2 \theta d\varphi_2^2 \right). \quad (9.2.29)$$

We next write the metric in a second form in the squares are completed first on the S^3 directions, demonstrating the smooth shrinking of the remaining directions in the cap. The metric in this form is given by

$$ds_6^2 = -\frac{2}{b^2} \frac{\bar{\Lambda}}{\sqrt{Q_1 Q_5}} \frac{\bar{r}^2 + 1}{\bar{F}_0(\bar{r})} d\tau^2 + \sqrt{Q_1 Q_5} \bar{\Lambda} \left(\frac{d\bar{r}^2}{\bar{r}^2 + 1} + d\theta^2 \right) + \frac{\sqrt{Q_1 Q_5}}{\bar{\Lambda}} \sin^2 \theta \left(d\varphi_1 - \frac{2 d\tau}{b^2 R_y} \right)^2 \\ + \frac{\sqrt{Q_1 Q_5}}{\bar{\Lambda}} \bar{F}_1(\bar{r}) \cos^2 \theta \left(d\varphi_2 - \frac{\bar{F}_0(\bar{r})}{\bar{F}_1(\bar{r})} \frac{dv}{R_y} + \frac{1}{\bar{F}_1(\bar{r})} \frac{2 d\tau}{b^2 R_y} \right)^2 \\ + \sqrt{Q_1 Q_5} \bar{\Lambda} \frac{\bar{F}_0(\bar{r})}{\bar{F}_1(\bar{r})} \bar{r}^2 \left(\frac{dv}{R_y} - \frac{1}{\bar{F}_0(\bar{r})} \frac{2 d\tau}{b^2 R_y} \right)^2. \quad (9.2.30)$$

At $\bar{r} \rightarrow 0$ we have $\bar{F}_0(\bar{r}) \rightarrow 1$, $\bar{F}_1(\bar{r}) \rightarrow 1$ and $\bar{\Lambda} \rightarrow 1$, the geometry is a red-shifted $\text{AdS}_3 \times S^3$ and the term on the final line combines with the $d\bar{r}^2$ term to describe the smooth shrinking of an S^1 at the center of a local \mathbb{R}^2 .

The AdS_2 limit of the matter fields can be similarly derived; since this is a straightforward implementation of the above procedure, we omit the details.

9.2.3.3 AdS_3 and AdS_2 perspectives

From the metric (9.2.28) one can read off that in the AdS_2 limit the J_R angular momentum has gone to zero, while the solution remains non-trivial. This indicates that the internal structure deep inside the core of the solutions indeed fits inside the AdS_2 throat, while the J_R angular momentum does not survive this limit. Thus for different values of a/b in the starting solution, we have the same representative in the AdS_2 limit.

Let us compare and contrast the above AdS_2 limit with a more naive $a \rightarrow 0$ limit. If one does not rescale coordinates as in (9.2.8), but rather holds r , t fixed and sends $a \rightarrow 0$, instead of the superstratum metric (9.2.28) one obtains the extremal black hole solution with a large horizon [99]. This can be interpreted as the solution effectively seen by an observer who remains at a fixed depth

⁶It corresponds to a non-rotating solutions since for asymptotically- AdS_3 (1,0,n) Superstrata, the left and right angular momenta are equal to $J_L = J_R = \frac{R_y}{2} a^2$ (4.2.76) and then both vanish in the AdS_2 limit. However, single-mode Superstrata with quantum number $m \neq 0$ will have a non-vanishing J_L after the limit.

of the extremal BTZ throat (measured from a fixed reference far from the black hole), while the total depth of the throat is taken longer and longer.

By contrast, the limit defined above can be interpreted as the solution effectively seen by an observer deep inside the throat, as the length of the throat is taken longer and longer. From such an observer's point of view, the original asymptotic AdS_3 region goes to infinity as the limit is taken, such that the asymptotics of the solution become those given in (9.2.29).

9.3 Excitations of asymptotically AdS_2 Superstrata

In this section we show that the asymptotically AdS_2 solutions constructed in the previous section admit an infinite tower of finite-energy non-BPS normalizable excitations. The results in this section are obtained for the family of $(1, 0, n)$ superstratum solutions, where the wave equation for minimally coupled massless scalar fields is separable [116]. However, we expect that the existence of towers of finite-energy excitations is a general feature of all asymptotically AdS_2 microstate geometries with a smooth IR cap. From the perspective of ten-dimensional Type IIB supergravity compactified on T^4 , the scalar fluctuations we consider come from traceless deformations of the internal manifold.

Our analysis involves an analytic solution for large n , presented in Section 9.3.3, and a numerical solution for general n , presented in Section 9.3.4. In Section 9.3.5 we discuss these results from the AdS_3 perspective. When glued back to AdS_3 , these excitations correspond to towers of CFT_2 excitations whose energies are evenly spaced. Interestingly, for the solutions with the longest throats, the gap between these energies is equal to the smallest possible gap of the dual CFT_2 .

9.3.1 The minimally coupled massless scalar wave equation

We start by considering the asymptotically $\text{AdS}_3 \times S^3$ $(1, 0, n)$ family of superstratum solutions constructed in [99] and reviewed in Section 9.2.3.2. In the D1-D5-P duality frame, the Type IIB string-frame metric is (4.2.30)

$$ds_{10}^2 = \sqrt{\frac{Z_1 Z_2}{\mathcal{P}}} ds_6^2 + \sqrt{\frac{Z_1}{Z_2}} \delta_{ij}^{(4)} dx^i dx^j, \quad i, j = 1, \dots, 4, \quad (9.3.1)$$

where the six-dimensional metric is given in (9.2.28) and (9.2.30). This choice of family is motivated by the fact that the wave equation of a massless minimally coupled scalar is separable and the null geodesic equations are integrable [116]. We consider a scalar deformation of the T^4 metric,

$$\delta_{ij}^{(4)} dx^i dx^j \rightarrow \left(\delta_{ij}^{(4)} + h_{ij} \right) dx^i dx^j. \quad (9.3.2)$$

The equations of motion at first order in h_{ij} require that h_{ij} is a minimally coupled scalar fluctuation in six dimensions (see for example Appendix B of [194]), obeying the six-dimensional Klein-Gordon equation:

$$\frac{1}{\sqrt{-\det g}} \partial_M \left(\sqrt{-\det g} g^{MN} \partial_N h_{ij} \right) = 0. \quad (9.3.3)$$

From a six-dimensional perspective the indices i, j label different scalar fields; we will take any one of these and denote it as Φ for the rest of the section. One can either directly compute the wave equation from the asymptotically AdS_2 superstratum metric (9.2.28) or use the wave equation for the $(1, 0, n)$ family of asymptotically AdS_3 Superstrata derived in [116], and take the AdS_2 limit of this wave equation. Both methods are equivalent. For later convenience we exhibit here the second method, recalling the main results of [116] in the process.

We separate variables as⁷

$$\Phi = K(r)S(\theta)e^{i\left(\frac{1}{R_y}\Omega t + \frac{1}{R_y}Pv + q_1\varphi_1 + q_2\varphi_2\right)}. \quad (9.3.4)$$

The frequency of the mode is given by Ω , P is the momentum and q_1 and q_2 are the quantum numbers along the S^2 . In the background of an asymptotically AdS₃ (1, 0, n) Superstratum, the wave equation separates [116] into:

$$\begin{aligned} \frac{1}{r}\partial_r(r(r^2 + a^2)\partial_r K(r)) + \left(\frac{a^2(\Omega + P + q_1)^2}{r^2 + a^2} - \frac{a^2(P + q_2)^2}{r^2}\right)K(r) \\ + \frac{b^2\Omega\left(a^2(\Omega + 2P) + F_0(r)(2a^2q_1 + (a^2 + \frac{b^2}{2})\Omega)\right)}{2a^2(r^2 + a^2)}K(r) = mK(r), \end{aligned} \quad (9.3.5)$$

$$\frac{1}{\sin\theta\cos\theta}\partial_\theta(\sin\theta\cos\theta\partial_\theta S(\theta)) - \left(\frac{q_1^2}{\sin^2\theta} + \frac{q_2^2}{\cos^2\theta}\right)S(\theta) = -mS(\theta), \quad (9.3.6)$$

where m corresponds to the constant eigenvalue of the Laplacian operator along the S^3 which results in an effective mass in the three dimensional space and where

$$F_0(r) \equiv 1 - \frac{r^{2n}}{(r^2 + a^2)^n}. \quad (9.3.7)$$

To describe fluctuations of the asymptotically AdS₂ Superstrata that we have constructed in Section 9.2.3 we take the same limit as (9.2.8), rescaling Ω appropriately:

$$r = a\bar{r}, \quad t = \frac{\tau}{a^2}, \quad \Omega = a^2\bar{\Omega}; \quad a \rightarrow 0 \quad \text{with } \bar{r}, \tau, v, P, b, q_1, q_2 \text{ fixed.} \quad (9.3.8)$$

The scalar wave equation for the mode

$$\Phi = K(\bar{r})S(\theta)e^{i\left(\frac{1}{R_y}\bar{\Omega}\tau + \frac{1}{R_y}Pv + q_1\varphi_1 + q_2\varphi_2\right)} \quad (9.3.9)$$

of course remains separable in our AdS₂ limit. The angular part of the wave equation (9.3.6) remains the same, and the radial wave equation becomes

$$\begin{aligned} \frac{1}{\bar{r}}\partial_{\bar{r}}(\bar{r}(\bar{r}^2 + 1)\partial_{\bar{r}} K(\bar{r})) + \left(\frac{(P + q_1)^2}{\bar{r}^2 + 1} - \frac{(P + q_2)^2}{\bar{r}^2}\right)K(\bar{r}) \\ + \frac{b^2\bar{\Omega}\left(P + \bar{F}_0(\bar{r})\left(q_1 + \frac{b^2}{4}\bar{\Omega}\right)\right)}{\bar{r}^2 + 1}K(\bar{r}) = mK(\bar{r}), \end{aligned} \quad (9.3.10)$$

where $\bar{F}_0(\bar{r})$ is defined in (9.2.27). The angular equation (9.3.6) is solvable and there is only one branch of well-defined solutions:

$$S(\theta) \propto (\sin\theta)^{|q_1|} (\cos\theta)^{|q_2|} {}_2F_1(-s, 1 + s + |q_1| + |q_2|; |q_2| + 1; \cos^2\theta), \quad (9.3.11)$$

where s is given by

$$m = \Delta(\Delta - 2), \quad s = \frac{1}{2}\left(|\Delta - 1| - 1 - |q_1| - |q_2|\right). \quad (9.3.12)$$

⁷Note that this separation ansatz appears slightly different to that of [116], because our six-dimensional coordinates ($\{t, v\} \equiv \{t, t + y\}$) are different from those of [116] ($\{u, v\} \equiv \frac{1}{\sqrt{2}}\{t - y, t + y\}$). For a discussion on these two choices of coordinates, see Appendix B of [98].

The solution is regular at $\cos^2 \theta = 1$ if and only if s is a non-negative integer. Consequently, the angular wave function is regular when

$$|\Delta - 1| \geq 1 + |q_1| + |q_2|, \quad q_1, q_2, \Delta, s \in \mathbb{Z}, \quad s \geq 0. \quad (9.3.13)$$

This significantly constrains the possible values of q_1 , q_2 and Δ . For instance the value $\Delta = 1$ which corresponds to tachyonic perturbations of AdS₂ ($m = -1$) is not allowed.

The radial wave equation (9.3.10) does not appear to be analytically solvable for general n . In what follows we shall therefore use a combination of numerical and analytical arguments to show that it has an infinite tower of finite-energy normalizable bound-state solutions.

9.3.2 Constructing finite-energy solutions

We perform a change of variables in order to map the infinite radial direction to a segment,

$$z \equiv \frac{\bar{r}^2}{1 + \bar{r}^2} \quad \Longleftrightarrow \quad \bar{r} \equiv \sqrt{\frac{z}{1 - z}}, \quad z \in [0, 1]. \quad (9.3.14)$$

The radial wave equation then becomes

$$\begin{aligned} \partial_z (z \partial_z K(z)) + \frac{1}{4(1 - z)} \left[(P + q_1)^2 - \frac{1}{z} (P + q_2)^2 \right. \\ \left. + b^2 \bar{\Omega} \left(P + (1 - z^n) \left(q_1 + \frac{b^2}{4} \bar{\Omega} \right) \right) - \frac{\Delta(\Delta - 2)}{1 - z} \right] K(z) = 0. \end{aligned} \quad (9.3.15)$$

We first investigate the behavior of the solutions to this equation around the ends of the segment ($z = 0$ and $z = 1$) to check whether there are any obvious restrictions to constructing bound states:

- The value $P + q_2$ gives the centrifugal barrier at the origin ($z = \bar{r} = 0$). When $P + q_2 \neq 0$, near $z = 0$ a solution of (9.3.15) must satisfy

$$z \partial_z (z \partial_z K(z)) - \left(\frac{P + q_2}{2} \right)^2 K(z) = 0. \quad (9.3.16)$$

The only branch of regular solutions is

$$K(z) \propto z^{\frac{|P + q_2|}{2}} \underset{\bar{r} \rightarrow 0}{\sim} \bar{r}^{|P + q_2|}. \quad (9.3.17)$$

Consequently, regular solutions necessarily go to 0 when $\bar{r} \rightarrow 0$ when the centrifugal barrier is vanishing. This is expected, since the spacetime caps off smoothly at this location.

- When $P + q_2 = 0$ one must consider the next-to-leading-order term in (9.3.15). The resulting equation also has a regular branch of solutions at $z = 0$. The main difference is that these regular solutions remain finite at $z = 0$.
- Near $z = 1$ (at the boundary $r \sim \infty$) and for $\Delta \neq \{0, 2\}$, Equation (9.3.15) becomes:

$$\partial_z (z \partial_z K(z)) - \frac{\Delta(\Delta - 2)}{4(1 - z)^2} K(z) = 0. \quad (9.3.18)$$

The branch of non-diverging solutions is

$$K(z) \propto (1 - z)^{\frac{1+\nu}{2}} {}_2F_1 \left(\frac{\nu}{2}, \frac{\nu}{2}; \nu; (1 - z) \right) \underset{z \rightarrow 1}{\sim} (1 - z)^{\frac{1+\nu}{2}} \underset{\bar{r} \rightarrow \infty}{\sim} \frac{1}{\bar{r}^{1+\nu}}, \quad (9.3.19)$$

with

$$\nu \equiv |\Delta - 1|. \quad (9.3.20)$$

These solutions decay at infinity for any value of Δ . In order to check whether they correspond to normalizable or non-normalizable modes one has to check whether the energy of this field is finite. The Hamiltonian density is composed of terms of the form $\sqrt{-g} g^{MN} \partial_M \Phi \partial_N \Phi$ (no sum over the indexes). The most important terms when $\bar{r} \rightarrow +\infty$ decay as

$$\sqrt{-g} g^{MN} \partial_M \Phi \partial_N \Phi = \mathcal{O}_{\bar{r} \rightarrow \infty} \left(\frac{1}{\bar{r}^{1+2\nu}} \right). \quad (9.3.21)$$

From Eq. (9.3.13) we have that $\Delta \neq 1$ and so $\nu \geq 1$. Consequently, the scalar field bound states have finite energy.

- When $\Delta = \{0, 2\}$, the behavior of K at $z = 1$ is dictated by the next-to-leading-order term in $\frac{1}{1-z}$ of equation (9.3.15). One can show that this equation admits square-integrable finite-energy solutions when $\bar{r} \rightarrow \infty$ that decay as $K(\bar{r}) \underset{\bar{r} \rightarrow \infty}{\sim} \bar{r}^{-2}$.

These two steps do not prove the existence of bound-state solutions. However, they are necessary conditions that ensure that there are no remaining obvious obstructions to building bound-state solutions. When $P + q_2 \neq 0$, if we find solutions of (9.3.15) that go to 0 at $z = 0$ and $z = 1$, then these solutions will behave as (9.3.17) and (9.3.19) at the boundaries and will be regular finite-energy excitations. When $P + q_2 = 0$, we have the same features but K can take a non-zero finite value at $z = 0$.

9.3.3 Analytic bound-state solutions for large n

We now analytically solve the wave equation (9.3.15) in a $(1, 0, n)$ -superstratum background with $n \gg 1$, in a $1/n$ expansion. For that purpose, we decompose the wave equation as

$$\mathcal{L}[\bar{\Omega}] K(z) - \frac{z^n}{1-z} \mathcal{E}[\bar{\Omega}] K(z) = 0, \quad (9.3.22)$$

where

$$\begin{aligned} \mathcal{L}[\bar{\Omega}] &\equiv \partial_z (z \partial_z) + \frac{1}{4(1-z)} \left[\left(P + q_1 + \frac{b^2 \bar{\Omega}}{2} \right)^2 - \frac{(P + q_2)^2}{z} - \frac{\Delta(\Delta - 2)}{1-z} \right], \\ \mathcal{E}[\bar{\Omega}] &\equiv \frac{b^2 \bar{\Omega} (4q_1 + b^2 \bar{\Omega})}{16}, \end{aligned} \quad (9.3.23)$$

and look for regular solutions with

$$K(0) = \text{const.}, \quad K(1) = 0. \quad (9.3.24)$$

Note that the wave equation given by $\mathcal{L}[\bar{\Omega}]$ corresponds to the wave equation in a global AdS₃ geometry. This AdS₃ wave equation is actually the equation we can derive by considering only the AdS₃ cap of the Superstrata. The other term proportional to $\mathcal{E}[\bar{\Omega}]$ corresponds to the momentum wave geometry and the junction to the AdS₂ region. However, we will postpone the questions related to the nature of the scattering in the next chapter and we concentrate here only on the existence of normalizable modes.

The details of the method and the mathematical proof of the $1/n$ expansion to solve this equation are given in Appendix A.10. We show there that the only condition for having bound-state solutions is to impose $\Delta \neq 1$ as required by (9.3.13). For any other value of Δ , we have found a tower of excitation modes $K_j(z)$ labeled by a mode number $j \in \mathbb{N}$. The large n expansion is valid as long as the mode

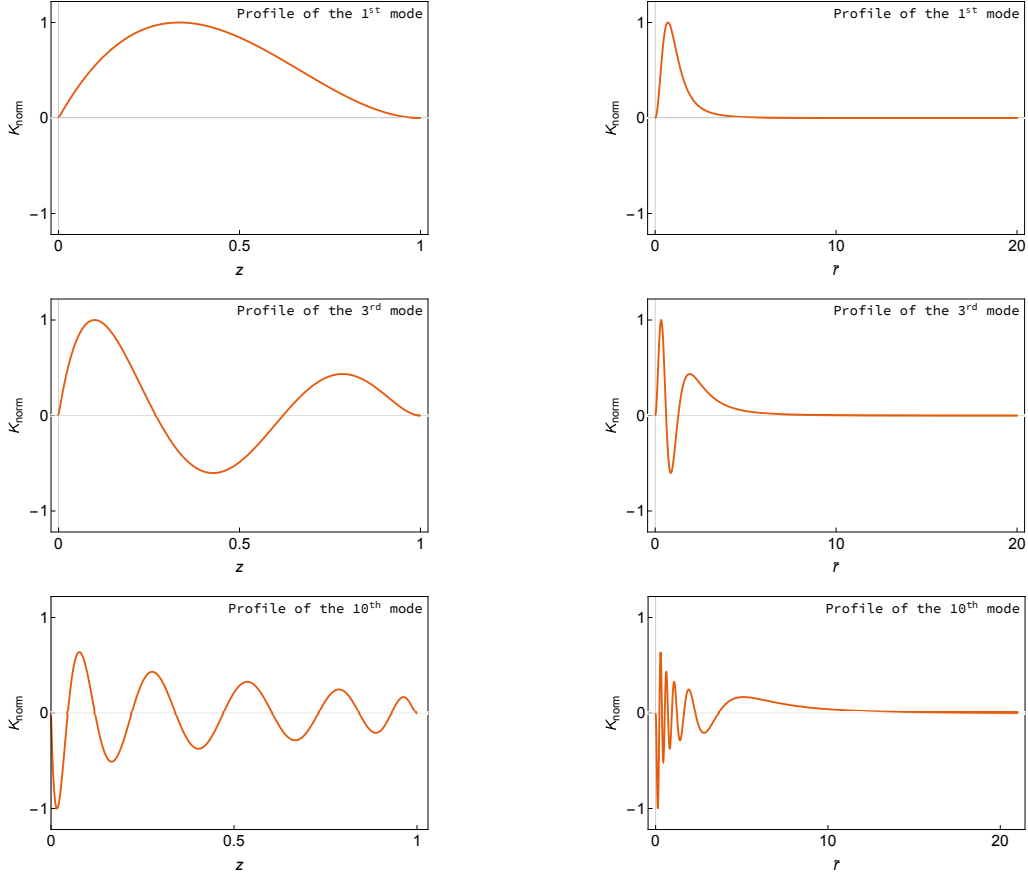


Figure 9.2: Analytic radial wavefunctions at large n for several scalar excitation modes of an asymptotically AdS₂ (1,0, n) Superstratum with $b = 1$, $n \gg 1$, $P = q_1 = q_2 = 1$ and $\Delta = 4$. The same wavefunctions are plotted as functions of z (left) and \bar{r} (right), where $z = \frac{\bar{r}^2}{\bar{r}^2 + 1}$.

number is smaller than $j \lesssim \sqrt{n}$. Thus the \sqrt{n} first normalizable modes are given by the AdS₃ cap geometry in the IR of our solutions. The regular solutions of (9.3.22) are

$$K_j(z) = \kappa_j (1-z)^{\frac{1+|\Delta-1|}{2}} z^{\frac{|P+q_2|}{2}} \left[\sum_{\ell=0}^j (-1)^\ell \binom{j}{\ell} \frac{(j+1+|\Delta-1|+|P+q_2|)_\ell}{(1+|P+q_2|)_\ell} z^\ell + \mathcal{O}\left(\frac{1}{n^\nu}\right) \right], \quad (9.3.25)$$

where $(k)_\ell \equiv \prod_{m=0}^{\ell-1} (k+m)$ and κ_j is a normalization constant. There are two possible values of $\bar{\Omega}$ for the function K_j to be a solution of (9.3.22). Both sets of frequencies describe the same wavefunctions, so as usual we restrict attention to the positive frequencies,

$$\bar{\Omega}_j = \frac{2}{b^2} \left[2j + 1 + |\Delta - 1| + |P + q_2| - (P + q_1) \right] + \mathcal{O}\left(\frac{1}{n^\nu}\right). \quad (9.3.26)$$

The leading-order term of the $\frac{1}{n}$ -expansion in (9.3.25) captures all the features of the wavefunction. It corresponds to the wave computed in the AdS₃ cap only. The behaviors at $z = 0$ and $z = 1$ depicted in (9.3.17) and (9.3.19) are explicit in (9.3.25). This proves the existence of solutions regular at both boundaries. One can re-express the modes K_j in the radial variable \bar{r} using $z = \frac{\bar{r}^2}{\bar{r}^2 + 1}$. The mode profiles are depicted in Fig. 9.2.

The polynomial of order j in (9.3.25) determines the number of oscillations of the wavefunction (one can explicitly show that the polynomial has exactly j roots in the range $0 < z < 1$). Much as for

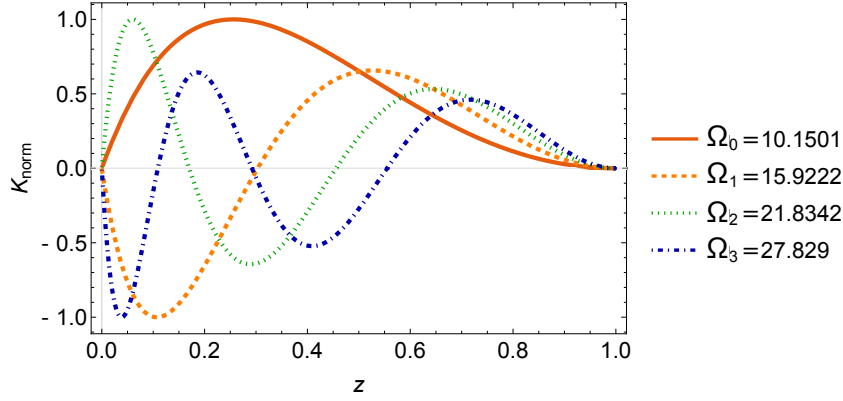


Figure 9.3: Numerically obtained radial wavefunctions of the first four excitation modes of an asymptotically AdS₂ (1,0,1) Superstratum with $b = 1$, $P = q_1 = q_2 = 1$ and $\Delta = 4$, plotted as functions of z .

solutions to the Schrödinger equation, the lowest mode of the radial wave function has no nodes, the next one has one node, etc. One can see both from Fig. 9.2 and from the form of the solution that the excitations are localized in the cap and decay rapidly as one goes up the throat.

Thus, we have shown that in the large n limit, the asymptotically AdS₂ (1,0, n)-superstratum solutions we have constructed support an infinite tower of finite-energy non-BPS excitations. We will now investigate the same issue for arbitrary n using numerical methods.

9.3.4 Numerical bound-state solutions for arbitrary n

We now describe the main steps of the procedure we use to solve Equation (9.3.15) numerically (using *Mathematica*), as follows:

- We fix particular values for $\{n, P, q_1, q_2, \Delta\}$. The remaining variable is the frequency $\bar{\Omega}$.
- When we imposed directly on $K(z)$ the Dirichlet boundary condition $K(0) = K(1) = 0$, this led the numerics to return the trivial solution $K(z) = 0$ everywhere. To evade this problem, we instead impose Dirichlet boundary conditions $K(0) = 0$ and $|K(\frac{1}{2})| = 1$. Since we do not expect the solution to have a node exactly at $z = \frac{1}{2}$, this boundary condition fixes the overall normalization.
- We then fine-tune the value of $\bar{\Omega}$ to find the values for which K goes to 0 when $z \rightarrow 1$.
- For each configuration $\{n, P, q_1, q_2, \Delta\}$ we have studied, we find a discrete set of positive $\bar{\Omega}$ for which K vanishes at $z = 1$. This set of positive frequencies $\bar{\Omega}_j$ characterizes the tower of non-supersymmetric excitations of our solutions.

We illustrate our procedure with a particular example:⁸

$$n = 1, \quad b = 1, \quad P = q_1 = q_2 = 1, \quad \Delta = 4. \quad (9.3.27)$$

The equations governing bound states for this choice of parameters are

$$\partial_z (z \partial_z K_j) - \left[\frac{1}{z} + \frac{2}{(1-z)^2} - \frac{\bar{\Omega}_j}{4(1-z)} - \frac{\bar{\Omega}_j}{4} \left(1 + \frac{\bar{\Omega}_j}{4} \right) \right] K_j = 0, \quad (9.3.28)$$

with $K_j(0) = K_j(1) = 0$.

⁸In principle, the value of b should be chosen to ensure that Q_P in (4.2.76) satisfies (9.2.16) (recall a has already taken to zero here), however we shall simply take $b = 1$ for the purpose of plotting the results. From (9.3.23) the physics of the modes depends only on the combination $b^2 \bar{\Omega}$, so one can easily rescale as desired.

We apply the procedure detailed above. We find a discrete set of values of $\bar{\Omega}$ for which $K(z)$ is regular at the boundaries. Figure 9.3 shows the radial wave functions for the first four modes of the tower in the z -coordinate system.

The plots in Fig. 9.4 show the radial component of the modes in the radial coordinate \bar{r} . Their features are very similar to the ones found analytically at large n , shown above in Fig. 9.2. In particular, the energy grows approximately linearly with the mode number and the excitations are localized near the IR cap and decay very quickly at large \bar{r} , even for high-energy excitations.

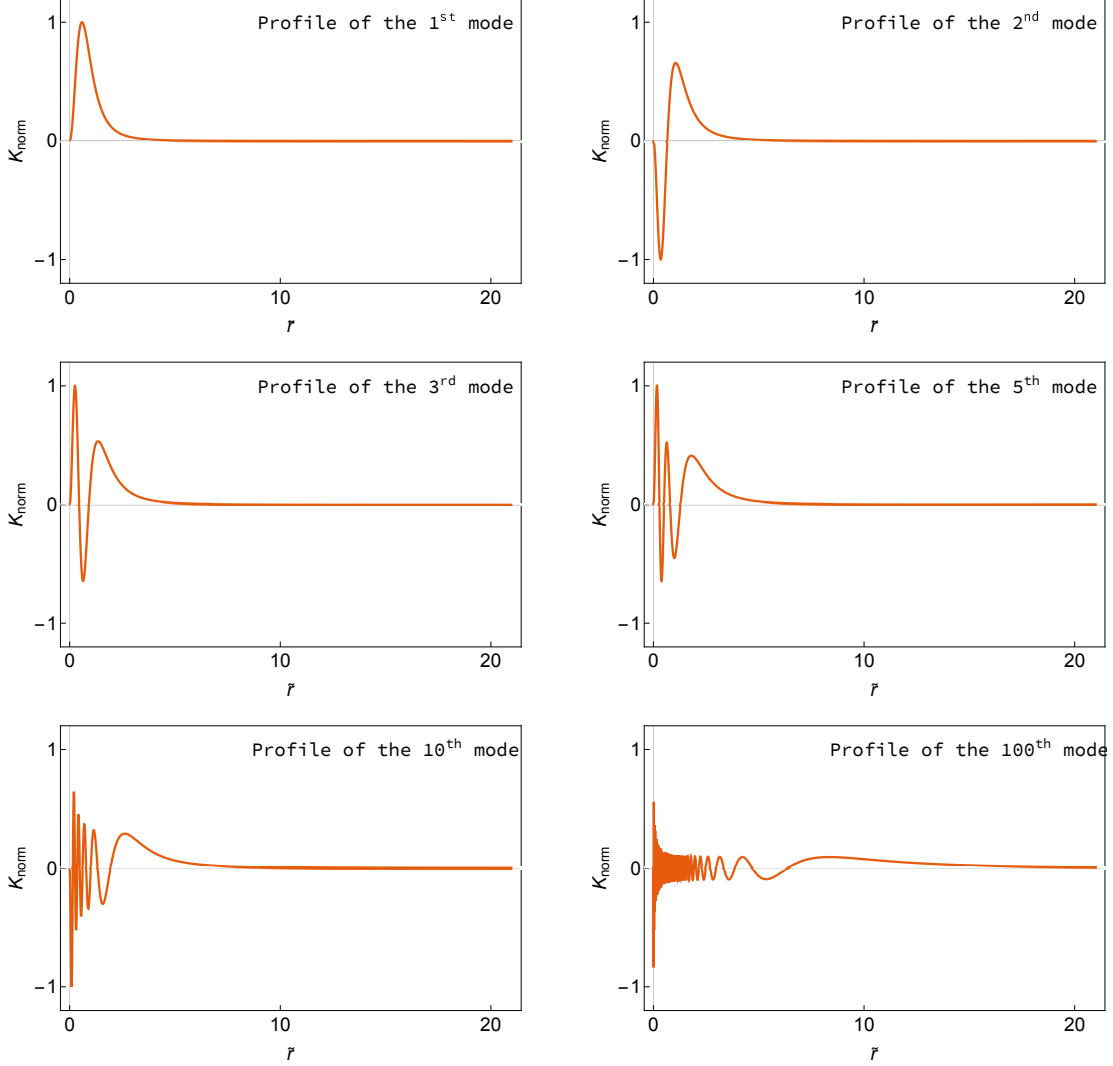


Figure 9.4: Numerically obtained radial wavefunctions of several different excitation modes of an asymptotically AdS₂ (1,0,1) superstratum solution with $b = 1$, $P = q_1 = q_2 = 1$ and $\Delta = 4$, plotted as functions of \bar{r} .

Interestingly, the frequencies have approximately the same linear dependence on the mode number, j , as that found at large n in Eq. (9.3.26) (see Fig. 9.5):

$$\bar{\Omega}_j \simeq 5.97(j + 1.67), \quad j \in \mathbb{N}. \quad (9.3.29)$$

We repeated the numerical procedure for different values of $\{n, P, q_1, q_2, \Delta\}$, and we obtained similar results to those shown here.

We thus see that the existence of an infinite tower of excitations can be established analytically at large n and numerically for finite n . It is remarkable how similar the mode profiles are for large n and

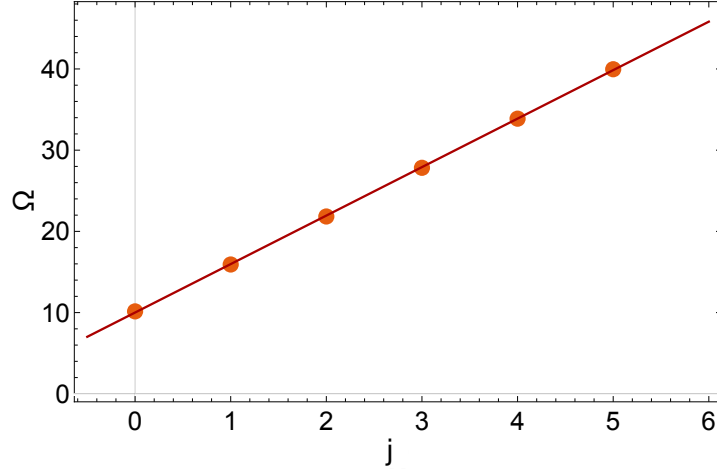


Figure 9.5: The frequencies of modes with number j , and the linear fitting function given in (9.3.29).

for $n = 1$ (compare Fig. 9.2 with Figs. 9.3 and 9.4). It is also interesting that the frequencies depend linearly on the mode number, both at large n (9.3.26) and at finite n (9.3.29). Despite the rather complicated form of the equations we are solving, the normalizable modes are essentially determined by the smooth AdS₃ IR cap.

9.3.5 An AdS₃ perspective

In previous subsections we studied scalar excitations of asymptotically AdS₂ Superstrata. It is also interesting to solve the wave equation of the corresponding asymptotically AdS₃ Superstrata and to examine the properties of the modes from the perspective of an AdS₃ observer. For that purpose, we consider the family of asymptotically AdS₃ (1, 0, n) Superstrata and the wave equation of a scalar field in this background (9.3.4)–(9.3.6).

9.3.5.1 Excitation modes of asymptotically AdS₃ solutions

We recall that the mode profile is

$$\Phi = K(r)S(\theta)e^{i\left(\frac{1}{R_y}\Omega t + \frac{1}{R_y}Pv + q_1\varphi_1 + q_2\varphi_2\right)}, \quad (9.3.30)$$

where $K(r)$ and $S(\theta)$ satisfy the radial and angular equations (9.3.5) and (9.3.6). The solutions of the angular equation are still given by (9.3.11) and (9.3.12). First, we perform a similar change of variables in order to map the infinite radial direction to a segment,

$$\hat{z} = \frac{r^2}{a^2 + r^2} \iff r = a\sqrt{\frac{\hat{z}}{1 - \hat{z}}}, \quad \hat{z} \in [0, 1]. \quad (9.3.31)$$

The radial wave equation (9.3.5) becomes

$$\hat{\mathcal{L}}[\Omega] K(\hat{z}) - \frac{\hat{z}^n}{1 - \hat{z}} \hat{\mathcal{E}}[\Omega] K(\hat{z}) = 0, \quad (9.3.32)$$

with the boundary condition $K(0) = K(1) = 0$, and where we have defined

$$\begin{aligned}\hat{\mathcal{L}}[\Omega] &\equiv \partial_{\hat{z}}(\hat{z}\partial_{\hat{z}}) + \frac{1}{4(1-\hat{z})} \left[(P+q_1 + (1+\hat{b}^2)\Omega)^2 - \frac{1}{\hat{z}}(P+q_2)^2 - \frac{\Delta(\Delta-2)}{1-\hat{z}} \right], \\ \hat{\mathcal{E}}[\Omega] &\equiv \frac{\hat{b}^2\Omega(2q_1 + (1+\hat{b}^2)\Omega)}{4}, \\ \hat{b} &\equiv \frac{b}{\sqrt{2}a}.\end{aligned}\tag{9.3.33}$$

This equation looks similar to the radial wave equation in the asymptotically AdS₂ background (9.3.22) and (9.3.23).

As in Section 9.3.3, we take n to be large and work to leading order in $1/n$. The only condition for having finite-energy excitations is to impose $\Delta \neq 1$. For any other value of Δ , we have found a tower of excitation modes $K_j(\hat{z})$ labeled by a mode number $j \in \mathbb{N}$:

$$K_j(\hat{z}) = \kappa_j (1-\hat{z})^{\frac{1+|\Delta-1|}{2}} \hat{z}^{\frac{|P+q_2|}{2}} \left[\sum_{\ell=0}^j (-1)^\ell \binom{j}{\ell} \frac{(j+1+|\Delta-1|+|P+q_2|)_\ell}{(1+|P+q_2|)_\ell} \hat{z}^\ell + \mathcal{O}\left(\frac{1}{n^\nu}\right) \right],\tag{9.3.34}$$

where $(k)_\ell \equiv \prod_{m=0}^{\ell-1} (k+m)$ and κ_j is a normalization constant. The wave function K_j is again a solution of (9.3.32) for two values of Ω . The tower of positive values of Ω is given by

$$\Omega_j = \frac{1}{1+\hat{b}^2} \left[2j+1+|\Delta-1|+|P+q_2|-(P+q_1) \right] + \mathcal{O}\left(\frac{1}{n^\nu}\right).\tag{9.3.35}$$

Furthermore, we have a relation between $1+\hat{b}^2$ and the quantized charges of the solution derived in Section 4.2.5.4

$$a^2 + \frac{b^2}{2} = \frac{Q_1 Q_5}{R_y^2} \quad \Rightarrow \quad \frac{1}{1+\hat{b}^2} = \frac{a^2 R_y^2}{Q_1 Q_5} = \frac{2j_R}{N_1 N_5},\tag{9.3.36}$$

where N_1, N_5 are the integer numbers of D1 and D5 branes, and where j_R is dimensionless and quantized in units of $1/2$ (so $j_R = 1/2$ corresponds to the solution with the longest throat from the AdS₃ perspective). One can now compute the mass gap, δ , of our perturbations, which is equal to the smallest excitation energy above the ground state:

$$\delta \equiv \min_{\Delta, P, q_2, q_1} \frac{\Omega_0}{R_y} = \frac{4j_R}{N_1 N_5 R_y}.\tag{9.3.37}$$

The mass gap was previously estimated by an order-of-magnitude calculation in [98] and by an infrared analysis of the wave equation in [117], where it was also pointed out this gap is of the same order of magnitude as the smallest mass gap in the D1-D5 CFT.

In fact, for non-BPS excitations of the D1-D5 CFT, the lowest gap in the theory is obtained by adding one unit of left-moving and one unit of right-moving energy to a ground state in the longest possible winding sector, of winding $N_1 N_5$, and is equal to $\frac{2}{N_1 N_5 R_y}$. Analytically solving the wave equation allows us to also pin down the exact coefficient of the bulk mass gap and to find that the solution with the longest throat has a gap exactly equal to the CFT₂ gap in this ‘long string’ sector: $\frac{2}{N_1 N_5 R_y}$.

By contrast, the dual CFT states at the orbifold point (4.2.53) have strands of length one, so the mass gap at the free orbifold point in the moduli space is $\frac{2}{R_y}$. Of course, the gap is not a protected quantity and so a mismatch is both expected and in line with previous findings [106, 98]. However, it is remarkable that in this example the gap appears to be renormalized by precisely the maximal amount $N_1 N_5$. We will examine this issue in more details in the next chapter.

9.3.5.2 Infinite-throat limit of the excitation modes

We next describe how the perturbations behave as $a \rightarrow 0$, when the length of the AdS₂ region increases indefinitely. First, we rewrite the mode profiles and their corresponding frequencies to make the a -dependence explicit,

$$\Phi_j = K_j(r) S(\theta) e^{i\left(\frac{1}{R_y} \Omega_j t + \frac{1}{R_y} P v + q_1 \varphi_1 + q_2 \varphi_2\right)}, \quad (9.3.38)$$

where

$$K_j(r) = \kappa_j \left(\frac{a^2}{r^2 + a^2} \right)^{\frac{1+|\Delta-1|}{2}} \left(\frac{r^2}{r^2 + a^2} \right)^{\frac{|P+q_2|}{2}} \times \left[\sum_{\ell=0}^j (-1)^\ell \binom{j}{\ell} \frac{(j+1+|\Delta-1|+|P+q_2|)_\ell}{(1+|P+q_2|)_\ell} \left(\frac{r^2}{r^2 + a^2} \right)^\ell + \mathcal{O}\left(\frac{1}{n^\nu}\right) \right], \quad (9.3.39)$$

$$\Omega_j = \frac{a^2 R_y^2}{Q_1 Q_5} [2j+1+|\Delta-1|+|P+q_2|-(P+q_1)] + \mathcal{O}\left(\frac{1}{n^\nu}\right), \quad (9.3.40)$$

and where $S(\theta)$ is given as before by (9.3.11) and (9.3.12).

- For an observer at the top of the AdS₂ throat, near the AdS₂–AdS₃ gluing region, the six-dimensional coordinate system is the original one $\{r, t, v, \theta, \phi_1, \phi_2\}$. The limit $a \rightarrow 0$ is trivial and gives $\Omega_j \rightarrow 0$. This means that the perturbations seen by such an observer are red-shifted to zero-energy perturbations. This confirms the point of view that the AdS₃ perspective is inappropriate to study asymptotically AdS₂ geometries.

- For an observer at the bottom of the throat, we use the rescaled coordinates (9.2.8): $\{\bar{r}, \tau, v, \theta, \phi_1, \phi_2\}$. In these coordinates, the leading terms in $1/n$ of the radial parts of the excitation modes are independent of a and the frequencies depend on a only through the combination $a^2 + b^2/2 = Q_1 Q_5 / R_y^2$,

$$\bar{\Phi}_j = \bar{K}_j(r) S(\theta) e^{i\left(\frac{1}{R_y} \bar{\Omega}_j \tau + \frac{1}{R_y} P v + q_1 \varphi_1 + q_2 \varphi_2\right)}, \quad (9.3.41)$$

where

$$\bar{K}_j(\bar{r}) = \kappa_j \left(\frac{1}{\bar{r}^2 + 1} \right)^{\frac{1+|\Delta-1|}{2}} \left(\frac{\bar{r}^2}{\bar{r}^2 + 1} \right)^{\frac{|P+q_2|}{2}} \times \left[\sum_{\ell=0}^j (-1)^\ell \binom{j}{\ell} \frac{(j+1+|\Delta-1|+|P+q_2|)_\ell}{(1+|P+q_2|)_\ell} \left(\frac{\bar{r}^2}{\bar{r}^2 + 1} \right)^\ell + \mathcal{O}\left(\frac{1}{n^\nu}\right) \right], \quad (9.3.42)$$

$$\bar{\Omega}_j = \frac{1}{a^2 + \frac{b^2}{2}} [2j+1+|\Delta-1|+|P+q_2|-(P+q_1)] + \mathcal{O}\left(\frac{1}{n^\nu}\right). \quad (9.3.43)$$

In the limit $a \rightarrow 0$, these expressions correspond precisely to the modes on top of the asymptotically AdS₂ (1,0, n) Superstrata (9.3.25), (9.3.26). In other words, the perturbations of the asymptotically AdS₃ solutions live in the cap at the bottom of the intermediate AdS₂ throat, and when the throat gets longer and longer they become the perturbations of an asymptotically AdS₂ solution as seen by an observer at the bottom of the infinite throat.

To conclude this section, the solution of the wave equation on the asymptotically AdS₃ solutions raises three interesting points. First, the mass gap of scalar excitations in the bulk is $\frac{4j_R}{N_1 N_5 R_y}$. For the solution with the longest throat, this matches exactly the lowest mass gap of non-BPS excitations of D1-D5 CFT₂, and is $N_1 N_5$ times larger than the value computed at the free orbifold point of the moduli space. Second, from the perspective of an observer at the bottom of the AdS₂ throat, the tower of excitations is the same as the tower of excitations on top of a asymptotically AdS₂ solution plus

small corrections. Thus, there is a one-to-one mapping between the excitation modes of asymptotically AdS₃ and the excitation modes of asymptotically AdS₂ microstate geometries.

Third, the frequencies of the modes and hence the spacing between different energy levels constructed on top of these solutions depend linearly on the mode number, which is quite remarkable given the intricate form of the equations we solved to obtain these energies. A linear spectrum agrees with what expects from a CFT₂ on a cylinder, and it would be interesting to understand whether this is a feature of more general superstratum solutions.

We note in passing that it has recently been argued that there is a tension between the fact that the spacing of excitations above the BPS D1-D5-P asymptotically AdS₃ Superstrata with the longest throats is of order $\frac{1}{N_1 N_5}$, and the fact that energy differences of non-BPS states away from the BPS bound are generically of order e^{-S} , where S is the entropy⁹ of the black hole [195]. However, these two facts are not in any sharp tension: above the many BPS states, different towers of excitations with spacings of order $\frac{1}{N_1 N_5}$ that are not exactly the same will generically give rise to differences in energies of non-BPS states of order e^{-S} because of the large degeneracy of states. Note that any given pair of non-BPS states with an energy difference of order e^{-S} could easily lie in different topological sectors and/or different regions of parameter space, so one should not expect such an energy difference to be visible in the perturbations of a single microstate geometry.

9.4 Discussion

In this chapter we have constructed two large classes of asymptotically AdS₂ supergravity solutions, and formulated a general procedure to construct even larger classes of such solutions. We have also solved for a tower of non-supersymmetric excitations above a family of capped asymptotically AdS₂ solutions. Returning to AdS₂ holography, we now discuss in detail the implications of our results, especially the non-supersymmetric bound state excitations we have found, focusing on the key question: *What is their backreaction of these modes, and what does this imply for the dual CFT₁?*

9.4.1 Backreaction

One possibility is that the backreaction of our modes necessarily modifies the AdS₂ UV asymptotics, and gives rise to “running dilation” or Nearly-AdS₂ solutions where the volume of the compact directions grows in the UV and the AdS₂ throat is glued to an AdS₃, AdS₄, or flat spacetime. In global AdS₂ and in simple theories (such as Jackiw-Teitelboim gravity) it has been argued that all finite-energy perturbations induce a running dilaton that modifies the AdS₂ UV asymptotics [178, 179]. However, our solutions cap off smoothly in the IR, so these arguments do not directly apply.

One might nevertheless imagine that the finite energy of any backreacted solution might mean that the UV is necessarily modified. However, it is known that there exist time-dependent non-extremal black hole solutions that have non-degenerate horizons in the IR and remain asymptotically AdS₂ in the UV [188]¹⁰. Thus the mere presence of a non-trivial energy-momentum tensor in the bulk is not enough to destroy the AdS₂ UV asymptotics. Indeed, if the backreacted solutions preserve the AdS₂ UV, they would be natural candidate microstates of these non-extremal black holes.¹¹

⁹The entropy of non-BPS D1-D5-P black holes is given by $S = 2\pi\sqrt{N_1 N_5 N_P - j_L^2} + 2\pi\sqrt{N_1 N_5 N_{\bar{P}} - j_R^2}$, where $N_P = L_0 - c/24$ and $N_{\bar{P}} = \bar{L}_0 - c/24$ are the left- and right-moving excitation numbers.

¹⁰The arguments of [178, 179] do not apply to these solutions either, because of the presence of a horizon.

¹¹These black holes can also be obtained from non-extremal asymptotically flat black holes by a similar limit to that defined in Section 9.2.1.

Furthermore, if the backreaction of the finite energy bound-state modes necessarily modifies the AdS₂ UV asymptotics, it gives rise to a puzzle: In such a scenario, the resulting finite length of the AdS₂ throat would depend on the energy above extremality, and the natural expectation is that this dependence should be inverse-linear. That is, from an AdS₃ perspective, the lowest state would still have energy $\frac{2}{N_1 N_5}$, coming from the lowest-energy mode in the longest throat. The next state would have twice more energy from the perspective of an observer at the bottom of the throat, but the throat itself would be shorter by a factor of two because of the inverse-linear dependence on the energy added. Hence, from the AdS₃ perspective the energy of the second mode would be $4 \times \frac{2}{N_1 N_5}$, and so on, leading to a quadratic spectrum of excitations that does not resemble the spectrum of any CFT₂ known to us. This conclusion could perhaps be avoided if the dependence of the throat length on the added energy is sufficiently weak, although we have not managed to construct a credible model for this possibility.

This puzzle, together with the existence of non-extremal black holes with AdS₂ UV asymptotics, is in our opinion a strong indication that the backreaction does not necessarily modify the AdS₂ UV. We now scrutinize this alternative possibility and show that it passes some basic tests.

First, one should identify the physics that controls whether or not the UV is modified into a throat of finite length. We propose that generically the throat length should be controlled by a combination of the overall angular momentum j_R and the contributions to j_R from the topological bubbles of the solution. The throat lengths of the asymptotically AdS₃ Superstrata studied in the previous section are indeed controlled by j_R , and we have seen that their energy gaps, as well as the difference between higher energy levels are $\frac{4j_R}{N_1 N_5}$. As described in the previous section, this is consistent with D1-D5 CFT physics.

Before taking the strict AdS₂ limit of the deep-scaling solutions studied in this chapter, the long AdS₂ throats and their gluing regions correspond, from an AdS₂ perspective, to running-dilaton solutions (where the dilaton encodes the size of a compact space transverse to AdS₂). Our method to construct asymptotically AdS₂ solutions has been to scale into a region of parameter space where the dilaton starts running further and further out in the AdS₂ UV, and to take the AdS₂ limit which restricts to a locus in parameter space where the dilaton becomes asymptotically constant.

In this language, one might imagine that introducing a non-supersymmetric perturbation and keeping all the parameters fixed on this locus in parameter space, may also induce a running dilaton. However it appears by parameter counting that there should be enough freedom to re-adjust parameters to compensate the non-supersymmetric contribution to the dilaton equation of motion and re-set the dilaton to asymptote to a constant value. Hence, both in the black-hole solutions of [188] and in our solutions, we expect that the parameters that control the running of the dilation in the UV are independent of the presence of a finite-energy configuration in the IR, and that finite-energy perturbations are compatible with AdS₂ UV asymptotics.

For the above reasons, the working hypothesis we consider for the remainder of our AdS₂-CFT₁ discussion is that our finite-energy excitations backreact into solutions that preserve the (constant dilaton) AdS₂ asymptotics, and that are dual to time-dependent configurations of the CFT₁.

9.4.2 Holographic description of the solutions and excitations

A fascinating question is to investigate whether or not the finite-energy bound state excitations correspond to finite-energy excitations in the dual CFT₁. In [177] it was argued that for certain simple two-dimensional Maxwell-dilaton theories, the holographic stress tensor is identically zero whenever the UV asymptotics is AdS₂, and hence all the constant-dilaton asymptotically AdS₂ solutions, including the time-dependent black holes of [188], have zero energy in the CFT₁. Since the CFT₁ configurations corresponding to these black holes have time-dependent VEVs, and since one usually associates time

dependence with finite energy, this would appear to be a distinctly unconventional property of the CFT_1 . However, a priori it does not appear to be ruled out.

Having said this, the asymptotically AdS_2 Superstrata descend from string-theory solutions with nontrivial harmonics along the compact directions and both R-R and NS-NS potentials turned on. Thus their field content from an AdS_2 perspective consists of a large (and possibly infinite) number of Kaluza-Klein modes, as well as several scalars and vectors, and hence is much more general than the field content of the solutions considered in [177]. Furthermore, our supersymmetric solutions do not have an everywhere-constant dilaton as in [177], but a dilaton that asymptotes to a constant. Thus, computing the holographic stress tensor for our theories may give a different result. A priori it seems more likely that the finite-energy bound state excitations we construct are dual to finite-energy time-dependent states of the CFT_1 . This would fit much better with the expectation that time dependence corresponds to finite energy, and would indicate that the CFT_1 is a more conventional theory.

Another reason to expect that our finite-bulk-energy bound states should be dual to finite-energy CFT_1 states is that we have an infinite tower of finite-energy perturbations on top of a family of bulk solutions, and we expect to have such a tower of perturbations on top of every such supersymmetric solution. Hence, if the CFT_1 energy of all these modes were zero, there would be a dramatic overcounting problem of the CFT ground states. Of course one could argue that only e^S of these states are supersymmetric and contribute to the index, while the other states do not, but this would again be a distinctly unusual situation.

Furthermore, the bulk theory also has an infinite number of black hole solutions, parameterized by an arbitrary function of one variable [188] and, if these black holes correspond to ensembles of CFT_1 zero-energy states, then again there would appear to be a serious overcounting problem of the CFT ground states.

If the finite-energy bulk perturbations had finite CFT_1 energies, this would solve all these problems: the CFT_1 would not have an infinite entropy at zero energy and no states at finite energy, but rather a finite entropy at each energy level. Furthermore, the entropy at each energy level might be captured by the non-extremal black holes of [188].

When the holographic CFT_1 has a parent holographic CFT_2 dual to AdS_3 , our construction can be used to better understand the relation between the CFT_1 and the parent CFT_2 . The asymptotically AdS_2 solutions constructed in Section 9.2.3 are obtained as a limit of families of asymptotically AdS_3 solutions with increasingly longer throats and progressively decreasing J_R . The asymptotically AdS_2 solutions are formally the $J_R = 0$ members of these families. It is tempting to postulate that for every microstate of the CFT_1 there is a corresponding family of CFT_2 microstates, parameterized by the value of J_R . It should be understood that this applies to states with relatively low values of j_R , that are dual to solutions with long throats.

From the perspective of the explicit families of D1-D5 orbifold CFT_2 states dual to asymptotically AdS_3 Superstrata (see [99, 101]), the expectation value of J_R is given by half the average number of $|+, +\rangle$ Ramond-Ramond ground state strands, so decreasing or increasing J_R corresponds to changing this average. Provided that the number of $|+, +\rangle$ strands remains small, this produces a small relative change in the physics of the other strands of the CFT_2 . Furthermore, it is tempting to imagine that, away from the orbifold point, the remaining strands form some kind of effective ‘long string’ that explains the small gap in the bulk.

One could then think of this one-to-many correspondence between AdS_2 and AdS_3 microstates, and our AdS_2 limit, as zooming on the information carried by the long string, which is the information encoding the bulk of the black hole entropy, and ignoring the information from the very small number of $|+, +\rangle$ strands. These strands could then be thought of as principally encoding the information pertaining to how the AdS_2 throat geometry is embedded inside AdS_3 .

Scattering from microstate geometries in the black-hole regime

In the previous chapter, the derivation of normalizable modes in superstratum background within the black-hole regime opened up several other interesting directions. One of them is the derivation of the *boundary-to-boundary four-point functions*, or response functions, in the bulk corresponding to *Heavy-Heavy-Light-Light correlators* in the dual D1-D5 CFT.

In the present chapter, we review the work of [29] in which a brand new technique was developed to compute boundary-to-boundary scalar Green function in a very large class of asymptotically AdS_D background. We apply this technique to $(1, 0, n)$ superstratum solutions. We show that the response function of a probe scalar, in momentum space, is essentially given by the pole structure of the highly-redshifted AdS_3 cap modulated by the BTZ black-hole response function. In position space, this translates into a sharp exponential decay at short time followed by evenly spaced “echoes from the cap,” with period $\sim N_1 N_5$.

This work bridges the gap between calculations of CFT HHLL four-point functions and information-theory-based arguments that the quantum unitarity requires the horizon of black holes to be replaced by a structure that allows information to escape.

In Section 10.1, we will review the class of boundary-to-boundary Green functions, or response functions, that are of interest and how they related to two-point functions of the holographic theory. We reduce the problem to the usual simple recipe that involves solving the scalar wave equation in the background geometry. We then briefly review the elements of the WKB method and introduce our hybrid WKB strategy.

In Section 10.2, we implement the hybrid WKB strategy in detail for a range of possible problems and we then focus on asymptotically-BTZ geometries for which we write the momentum-space Green function in terms of the corresponding BTZ Green function and the WKB integral that is associated with the bound-state structure of the background geometry.

In Section 10.3 we quickly review the geometry of $(1, 0, n)$ Superstrata and set up the application of our hybrid WKB method.

In Section 10.4 we compute the momentum-space Green function for the $(1, 0, n)$ Superstrata and examine the diverse limits and features of the geometry and how they emerge from the Green function.

In Section 10.5 we examine the position-space Green functions for the $(1, 0, n)$ Superstrata. The basic goal is to show how to adapt the Fourier transforms that relate position-space and momentum-space Green functions for AdS_3 and extremal BTZ to the corresponding Green functions for Superstrata.

10.1 Holographic response functions

10.1.1 Brief review of holographic correlators

A standard way to compute two-point correlation functions of an operator \mathcal{O} in QFT is to couple the QFT to an external source $\int J\mathcal{O}$ and compute the response function

$$\langle \mathcal{O} \mathcal{O} \rangle = \left. \frac{\delta}{\delta J} \langle \mathcal{O} \rangle_J \right|_{J=0}, \quad (10.1.1)$$

where $\langle \mathcal{O} \rangle_J$ is the one-point function of the operator \mathcal{O} , in the state of interest, in presence of the source J .

The holographic calculation of the two-point function of an operator \mathcal{O} can be performed in an identical manner, where one uses the holographic dictionary to read off the expectation value of the operator in presence of the source. Concretely, if one considers the bulk solution for a (free) scalar field with mass m dual to the boundary operator \mathcal{O} , near the AdS boundary ($r \rightarrow \infty$) this solution takes the form

$$\Phi(\vec{x}, t; r) = \beta(\vec{x}, t) r^{\Delta-d} (1 + \mathcal{O}(r^{-2})) + \alpha(\vec{x}, t) r^{-\Delta} (1 + \mathcal{O}(r^{-2})), \quad (10.1.2)$$

where $\Delta(\Delta - 2) = m^2 l^2$. The coefficient α is identified with the expectation value of \mathcal{O} , while β corresponds to the source. While α, β are independent as far as the asymptotic equations of motion are concerned, they become related through a boundary condition in the interior of the spacetime (e.g. smoothness), which encodes information about the state of the CFT. The holographic two-point function, (10.1.1), is then $\frac{\delta \alpha}{\delta \beta}$. Note that in order to compute two-point functions in the given state, a linearized analysis of the bulk scalar will suffice. The above discussion applies to $2\Delta \notin \mathbb{Z}$; the integer case is more subtle but is also well understood [196].

The above calculation can be performed in either Euclidean or Lorentzian signature. In Euclidean signature, operators commute, and there is a single two-point function one can define. The dual boundary condition in the bulk usually corresponds to smoothness in the interior of the geometry. In Lorentzian signature, several prescriptions are possible, corresponding to the different time orderings of the operators: retarded, advanced, Feynman, Wightman. In order to compute these various correlators one can work in a doubled formalism, both in the field theory and on the gravity side. If the supergravity background is a black hole, one uses the Schwinger-Keldysh formalism on the CFT side and on the gravity side one uses either the eternal black hole [197] or a doubled time contour [198, 199]. In this doubled formalism, it has been shown that the choice of sources on both contours precisely selects infalling boundary conditions at the black hole horizon [200]. The resulting correlator is the retarded propagator.

When there is no black hole in the bulk, bound states exist and it has been emphasized that the choice of initial and final conditions of the early and late time slices are important. One may nevertheless wonder about the result of a non-doubled formalism for the response function, ignoring said initial and final boundary conditions. In the case of geometries with a smooth interior, the response function we will obtain is the Feynman propagator, which is just the Wick rotation of the Euclidean correlator.

10.1.2 Brief review of WKB

For sufficiently complicated geometries, like the Superstratum, one cannot solve the scalar wave equation exactly and must resort to an approximate technique to obtain the boundary-to-boundary Green functions or response functions. Here we will describe our broader strategy in adapting WKB methods

to this purpose. As we will discuss, the naive application of WKB methods is, in fact, poorly suited to the computation of response functions using (10.1.2)¹. However, in this section, we will describe a hybrid strategy in which we match WKB approximations onto exact treatments of asymptotic structure. The result is a far more reliable, controlled and accurate technique for computing good approximations to response functions. We will apply these ideas to several examples in Sections 10.2 and 10.3. Here we simply wish to describe the technique and explain how suitably adapted WKB methods can actually be used to give detailed information about correlation functions.

10.1.2.1 The basics of the WKB method

We are interested in computing the response function in backgrounds which have a separable scalar wave equation

$$\square\Phi = m^2\Phi, \quad (10.1.3)$$

so that the non-trivial part of the wave equation is a second order differential equation for the “radial function,” $K(r)$, of the wave

$$\Phi(t, r, y_1, y_2, \dots) \equiv Y(y_1, y_2, \dots) K(r) e^{-i\omega t}.$$

Note that we are using ω for the frequency of the mode and not Ω like in Section 9.3. We are using capital letters Ω and P for the momentum conjugates when dealing with superstratum background only. For generic background we will use small letters. This will facilitate the discussion.

The function $K(r)$ contains all the details of the geometry from interior structure, $r \sim 0$, to the asymptotic region, $r \rightarrow \infty$. The next step is to rewrite this as a Schrödinger problem. We rescale $K(r)$ to a new wave function $\Psi(r) \equiv f(r)K(r)$, for some carefully chosen function $f(r)$. We will furthermore allow for a change of variables $r \rightarrow x = x(r)$ (for which we will specify requirements below) so that the radial equation is reduced to the standard Schrödinger problem:

$$\frac{d^2\Psi}{dx^2}(x) - V(x)\Psi(x) = 0, \quad (10.1.4)$$

for some potential, $V(x)$. This potential encodes all the details of the wave, including its energy, mass, charge and angular momenta. In practice, there can be many ways to reduce a given radial equation to Schrödinger form, but these choices do not affect the essential physics of the WKB approximation².

First, for the WKB wave functions, $\Psi_{WKB}(x)$, to be good approximations to the exact solutions one must require that the potential itself does not fluctuate wildly. That is, it should obey the following condition:

$$\left| V(x)^{-3/2} \frac{dV}{dx} \right| \ll 1, \quad \text{when } V(x) \neq 0. \quad (10.1.5)$$

The “boundaries” of the Schrödinger problem depend upon the choice of $x(r)$, but here we assume that the coordinate x has been chosen so that $x \rightarrow +\infty$ corresponds to the asymptotic region, $r \rightarrow \infty$ and that the other boundary is at $x \rightarrow -\infty$. In all of the problems we study, the potential, $V(x)$, will go to a constant, positive value as $x \rightarrow +\infty$:

$$\lim_{x \rightarrow +\infty} V(x) \equiv \mu^2, \quad \mu > 0. \quad (10.1.6)$$

This limit defines the parameter μ . For an asymptotically AdS background, we can choose f so that this parameter is related to the mass of the particle and the dual conformal dimension is $\mu = \sqrt{1 + m^2\ell^2} =$

¹Note that WKB methods have been used before to compute correlation functions using normalizable modes.

²However, choosing the reduction to Schrödinger form carefully can make WKB approximation algebraically simpler and, in some circumstances, more accurate.

$\Delta - 1$. The shift by 1 is due to the rescaling of the wave function. As mentioned before, we will treat the case $2\mu \notin \mathbb{Z}$.

We have now reduced the computation of the response function to the well-understood Schrödinger problem for which WKB was originally developed. In particular, the solution will break into oscillatory parts in the classically allowed region where $V(x) < 0$, and exponentially growing or decaying parts in the classically forbidden region $V(x) > 0$. The junctions between these regions, where $V(x) = 0$, are referred to as “(classical) turning points” because classical particles do not “penetrate barriers” but simply reverse course at these turning points. The requirement, (10.1.6), means that classical particles cannot escape to infinity, which is in accord with the behaviour of massive particles in asymptotically AdS spaces.

Significantly far from the classical turning points, when (10.1.5) is valid, the solutions, to first order in WKB, are of the form

$$\Psi(x) = |V(x)|^{-\frac{1}{4}} \exp\left(\pm i \int |V(x)|^{\frac{1}{2}} dx\right), \quad \text{or} \quad \Psi(x) = |V(x)|^{-\frac{1}{4}} \exp\left(\pm \int |V(x)|^{\frac{1}{2}} dx\right), \quad (10.1.7)$$

respectively. The solutions on the left are oscillating in two possible directions given by the $\pm i$. They are solutions in regions where $V(x) < 0$. The solutions on the right are decaying or growing depending on the \pm . They are solutions in regions where $V(x) > 0$. Since the potential converges asymptotically to a positive value, the solutions can be decomposed in a basis of growing or decaying solutions. We will denote them in what will follow as $\Psi_{WKB}^{\text{grow/dec}}$.

The non-trivial aspect of the WKB approximation is how to connect the classical, oscillatory solutions to the decaying and growing solutions at each turning point. This is done by expanding the potential at those points, x_* :

$$V(x) = V(x_*) + V'(x_*)(x - x_*) = V'(x_*)(x - x_*). \quad (10.1.8)$$

One then uses the fact that the Schrödinger problem, with a linear potential, has an exactly-known solution in terms of Airy functions. The oscillatory and decaying properties of Airy functions are then matched to the behavior of the corresponding WKB functions in (10.1.7).

This is extremely effective at computing bound-state and other “interior” structure but is typically quite problematic when it comes to asymptotic structure that is essential to the computation of a response function. Indeed, for large x where $V(x) > 0$, the physical WKB solution will have the form

$$\Psi_{WKB}^{\text{phys}}(x) = \Psi_{WKB}^{\text{grow}} + \mathcal{A} \Psi_{WKB}^{\text{dec}} = e^{\mu x}(1 + \dots + e^{-2\mu x} + \dots) + \mathcal{A} e^{-\mu x}(1 + \dots), \quad (10.1.9)$$

where \mathcal{A} is a constant determined by the physical boundary condition at $x \sim -\infty$. By comparison with (10.1.2), One can unambiguously identify the coefficient of the growing modes at infinity, $\beta = 1$, however, the identification of the full coefficient of the decaying mode may be hard in practice, since Ψ_{WKB}^{grow} may contain a piece. Thus α is very difficult, if not impossible, to extract purely from the WKB wave-function.

10.1.3 The WKB hybrid technique

There is a very effective way to adapt WKB techniques to the computation of response functions, and this approach works extremely well for much of the spectrum on Superstrata. For simplicity, we assume that there is at least one classical turning point where the potential vanishes and that (10.1.6) is satisfied. Let x_+ be the outermost classical turning point, that is, one has $V(x_+) = 0$ and $V(x) > 0$ for $x > x_+$. The position of x_+ depends on the background and on the energy and momenta of the wave, and, in particular, changes with the energy of the wave³.

³In many applications of the WKB method the energy is included explicitly and the integrals involve $|E - V(x)|$. In our formalism, E is absorbed into $V(x)$.

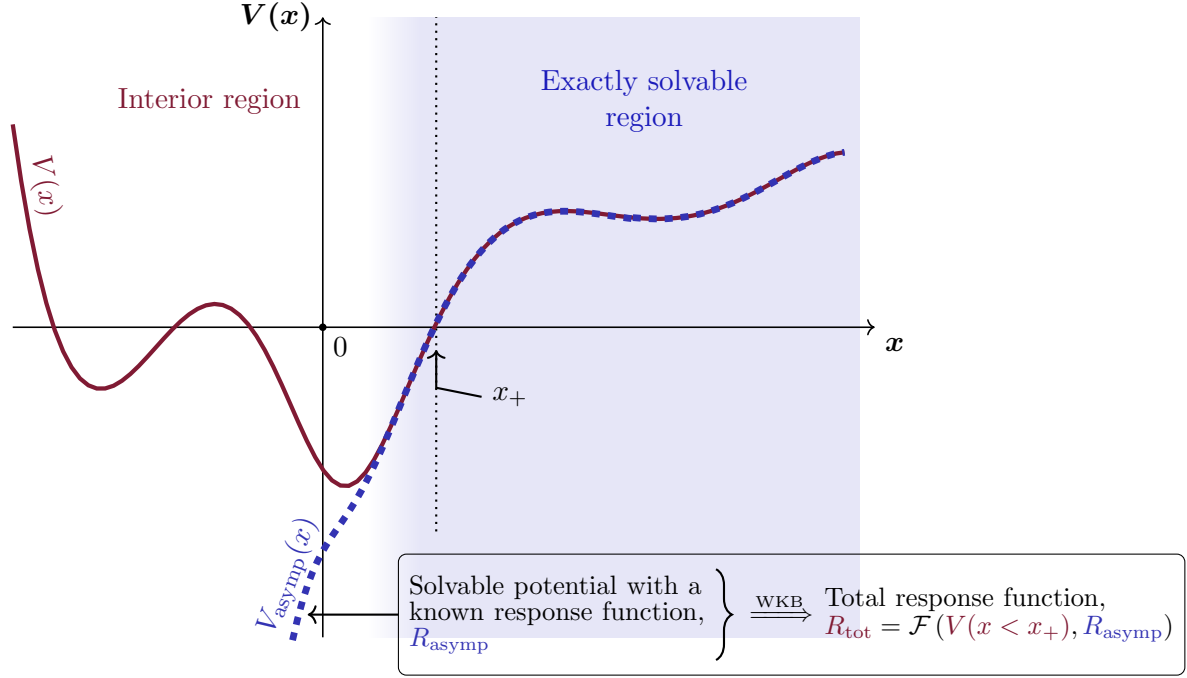


Figure 10.1: Schematic description of the WKB hybrid technique to derive the response function of a Schrödinger problem given by a potential $V(x)$ in red. The response function will be a deformation of the “asymptotic” response function given by the solvable asymptotic potential $V_{\text{asypm}}(x)$ with a term which only depends on the potential in the interior.

The WKB hybrid technique supposes that there is an asymptotic potential, $V_{\text{asypm}}(x)$, that very closely approximates $V(x)$ in the region $x > x_+$ and that the Schrödinger problem for $V_{\text{asypm}}(x)$ is *exactly* and analytically solvable (see Fig.10.1).

$$\Psi_E''(x) - V_{\text{asypm}}(x)\Psi_E(x) = 0. \quad (10.1.10)$$

These solutions closely approximate those of the original Schrödinger problem and they can be separated into distinct and *non-overlapping* growing and decaying modes, Ψ_E^{grow} and Ψ_E^{dec} , normalized according to

$$\Psi_E^{\text{grow}} = e^{+\mu x} (1 + \dots), \quad \Psi_E^{\text{dec}} = e^{-\mu x} (1 + \dots), \quad x \rightarrow \infty. \quad (10.1.11)$$

Importantly, Ψ_E^{grow} contains only the “purely growing” mode and has no sub-leading term involving Ψ_E^{dec} since $2\mu \notin \mathbb{Z}$. In the region $x > x_+$, an approximate solution to the original Schrödinger problem can now be written as in (10.1.2):

$$\Psi(x) \approx \beta \Psi_E^{\text{grow}} + \alpha \Psi_E^{\text{dec}} \sim [\beta e^{\mu x} + \alpha e^{-\mu x}]. \quad (10.1.12)$$

and, by construction and to the level of approximation of $V(x)$ by $V_{\text{asypm}}(x)$, the response function is indeed given by α/β . On the other hand, in the WKB formalism, the physical solution at any x takes the form (10.1.9). The main goal is now to determine α and β in terms of \mathcal{A} . This can be easily done by matching (10.1.9) which captures the inner structure of the wave to (10.1.12) where the response function can be read, continuously around x_+

$$\begin{aligned} \Psi_{\text{WKB}}^{\text{dec}}(x) &\approx a_1 \Psi_E^{\text{dec}}(x), \\ \Psi_{\text{WKB}}^{\text{grow}}(x) &\approx b_1 \Psi_E^{\text{grow}}(x) + b_2 \Psi_E^{\text{dec}}(x), \quad x \geq x_+, \end{aligned} \quad (10.1.13)$$

for some coefficients a_1, b_1 and b_2 which will be determined below. Obviously $\Psi_{WKB}^{\text{dec}}(x)$ cannot have term proportional to $\Psi_E^{\text{grow}}(x)$. The response function is then given by

$$R_{WKB} = \frac{\alpha}{\beta} = \frac{a_1}{b_1} \mathcal{A} + \frac{b_2}{b_1}. \quad (10.1.14)$$

The ratio a_1/b_1 only involves the relative normalizations of Ψ_{WKB} and Ψ_E in the asymptotic region, so it only depends on the asymptotic potential. The quantity \mathcal{A} is determined by the boundary condition in the deep interior, and will be calculated by WKB approximation. Finally, as we will see below, the ratio b_2/b_1 only cares about the matching condition between the exact and WKB wavefunctions in the region around x_+ .

In other words, one can use WKB methods to determine the solution in the region $x \leq x_+$ and then use the Airy function procedure around $x = x_+$ to match this WKB solution to the exactly solvable solution (10.1.12) in the region $x > x_+$. This will enable us to use the WKB method to capture all the interesting interior structure in the region $x < x_+$ and accurately extract the Green function by coupling this “interior data” to the exactly-solvable asymptotic problem.

In the next section, we will show that the WKB response function, R_{WKB} in (10.1.14), is given by

$$R_{WKB} = \left(\mathcal{A} + \frac{\sqrt{3}}{2} \right) e^{-2I_+} - \frac{\Psi_E^{\text{grow}}(x_+)}{\Psi_E^{\text{dec}}(x_+)}, \quad (10.1.15)$$

where I_+ is defined by:

$$I_+ \equiv -\mu x_+ + \int_{x_+}^{\infty} \left(|V(z)|^{\frac{1}{2}} - \mu \right) dz, \quad (10.1.16)$$

where we have “added and subtracted” μ to the integrand so as to handle the leading divergence in the integral, since we want to calculate α/β which remains finite. The quantity \mathcal{A} encodes the information about the potential $V(x)$ for $x < x_+$ as well as the physical boundary condition imposed as $x \rightarrow -\infty$:

- If $V(x)$ has only one turning point, x_+ , then one necessarily has $V(x) < 0$ for $x < x_+$. The interesting physical boundary conditions are those of a black hole in which the modes are required to be purely infalling as $x \rightarrow -\infty$. We will show that⁴

$$\mathcal{A} = \text{sign}(\omega) \frac{i}{2}. \quad (10.1.17)$$

- If $V(x)$ has only two turning points, x_- and x_+ , then one necessarily has $V(x) \geq 0$ in the “interior region,” $x < x_-$. The physical boundary condition as $x \rightarrow -\infty$ is that Ψ is smooth in this limit. These are the conditions relevant to global AdS_3 and the (1,0,n)-superstratum background. We will show that \mathcal{A} can be expressed in terms of the standard WKB “bound-state” integral:

$$\mathcal{A} = \frac{1}{2} \tan \Theta, \quad \Theta \equiv \int_{x_-}^{x_+} |V(z)|^{\frac{1}{2}} dz \quad (10.1.18)$$

If the potential has more than two turning points in the inner region, \mathcal{A} gets more complicated but can still be computed as a function of the integrals between successive turning points of the square root of the potential. The general expression of \mathcal{A} for a potential with arbitrarily many turning points is given in Appendix A.11.

The great strength of the WKB formula (10.1.15) is that it decouples the contribution of the geometry before the turning point (given by \mathcal{A}) from the contribution of the geometry outside the outermost turning point (given by I_+ , Ψ_E^{grow} and Ψ_E^{dec}). Since, the wave equation in the geometry

⁴Remind that ω is the momentum conjugate to time, $\Psi(x, t) = \Psi(x)e^{-i\omega t}$.

beyond the last turning point has been assumed to be solvable, the exact response function in this background, R_E , is known. One can then relate I_+ , Ψ_E^{grow} and Ψ_E^{dec} to this exact response function. Specifically, the response function in the full background, R_{WKB} , can be considered to be a function of the coefficient \mathcal{A} and the response function of the exactly solvable problem determined by $V_{\text{asympt}}(x)$, R_E ,

$$R_{\text{WKB}} = \mathcal{F}(R_E, \mathcal{A}) . \quad (10.1.19)$$

In this way we will show that for any asymptotically BTZ metric, like the Superstratum, the response function is well approximated, when x_+ lies in the BTZ region, by an expression of the form:

$$R_{\text{WKB}} \approx \text{Re} [R_E^{\text{BTZ}}] + 2 \text{sign}(\omega) \mathcal{A} \text{Im} [R_E^{\text{BTZ}}] , \quad (10.1.20)$$

where R_E^{BTZ} is the exactly-known BTZ response function and \mathcal{A} is determined by the WKB calculation in the “inner region,” $x < x_+$. There are some important subtleties in applying this expression, especially relating to the frequency ranges, pole structure and the validity of the WKB approximation. We will return to these later. For the moment we simply observe that this formula makes good intuitive sense: the structure of the interior, represented by \mathcal{A} , is carried up the BTZ throat by the BTZ response function.

We will now give the full derivation of the expressions for R_{WKB} , (10.1.15), for potentials with one turning point and for the potentials with two turning points. We will then discuss asymptotically BTZ problems and how the result (10.1.15) can be re-written as (10.1.20). The application of this technique to the superstratum background is detailed in Section 10.3.

10.2 Details of the WKB analysis

In this section, we explicitly compute the formula of the response function from our hybrid WKB method, (10.1.15), for potentials with one or two turning points. Then, we focus on backgrounds which have an extremal-BTZ or a global-AdS₃ regions as the superstratum geometries. We will show the adaptability of our method to compute the response function accurately. This will require to briefly review the exact computation of the response functions in those two well-known backgrounds [198, 199].

10.2.1 Derivation of the response function using hybrid WKB

10.2.1.1 Potentials with one turning point

We consider a Schrödinger equation of the type (10.1.4) satisfying the assumptions detailed in the previous section with one turning point, x_+ (see Fig.10.2). At first order of the WKB approximation, the generic solution is

$$\Psi(x) = \begin{cases} \frac{1}{|V(x)|^{\frac{1}{4}}} \left[D_+^{\text{I}} \exp \left(+i \int_x^{x_+} |V(z)|^{\frac{1}{2}} dz \right) + D_-^{\text{I}} \exp \left(-i \int_x^{x_+} |V(z)|^{\frac{1}{2}} dz \right) \right] , & x < x_+ , \\ d_+^{\text{I}} \text{Bi} \left(V'(x_+)^{\frac{1}{3}} (x - x_+) \right) + d_-^{\text{I}} \text{Ai} \left(V'(x_+)^{\frac{1}{3}} (x - x_+) \right) , & x \sim x_+ , \\ \frac{1}{|V(x)|^{\frac{1}{4}}} \left[D_+^{\text{II}} \exp \left(+ \int_{x_+}^x |V(z)|^{\frac{1}{2}} dz \right) + D_-^{\text{II}} \exp \left(- \int_{x_+}^x |V(z)|^{\frac{1}{2}} dz \right) \right] , & x > x_+ , \end{cases} \quad (10.2.1)$$

where $D_{\pm}^{\text{I/II}}$ and d_{\pm}^{I} are constants and Bi and Ai are the usual Airy functions. The usual WKB connection with Airy functions relates the constants $D_{\pm}^{\text{I/II}}$ and d_{\pm}^{I} in (10.2.1) via

$$\begin{pmatrix} d_+^{\text{I}} \\ d_-^{\text{I}} \end{pmatrix} \equiv e^{-i\frac{\pi}{4}} \sqrt{\pi} V'(x_+)^{-\frac{1}{6}} \begin{pmatrix} 1 & i \\ i & 1 \end{pmatrix} \begin{pmatrix} D_+^{\text{I}} \\ D_-^{\text{I}} \end{pmatrix} , \quad \begin{pmatrix} d_+^{\text{I}} \\ d_-^{\text{I}} \end{pmatrix} \equiv \sqrt{\pi} V'(x_+)^{-\frac{1}{6}} \begin{pmatrix} 1 & 0 \\ 0 & 2 \end{pmatrix} \begin{pmatrix} D_+^{\text{II}} \\ D_-^{\text{II}} \end{pmatrix} , \quad (10.2.2)$$

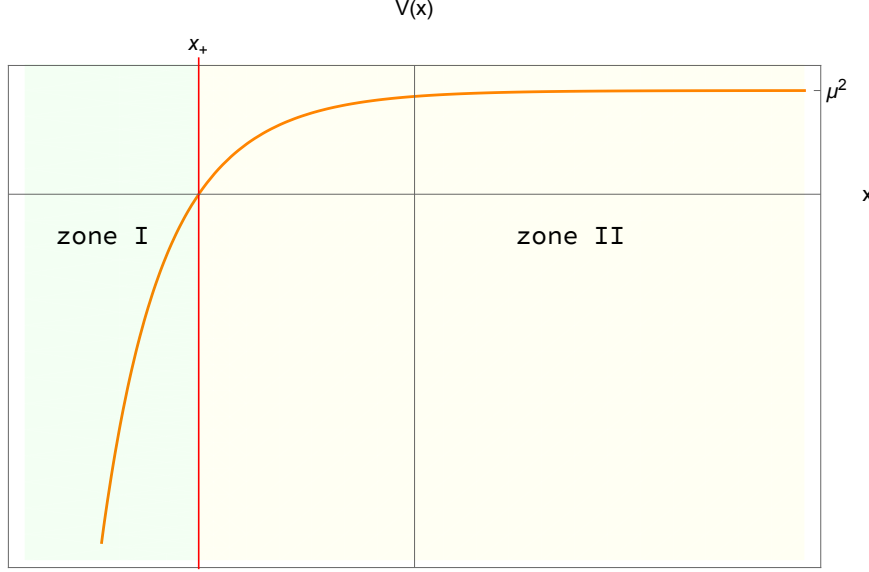


Figure 10.2: Schematic description of a potential $V(x)$ with one turning point, x_+ and the two zones depending on the sign of $V(x)$. For the illustration, we have considered that $V(x)$ tends to $-\infty$ at $-\infty$ but it is not necessary for the discussion. Any kind of behavior is possible as long as $V(-\infty) < 0$.

and hence one obtains

$$\begin{pmatrix} D_+^I \\ D_-^I \end{pmatrix} \equiv \begin{pmatrix} \frac{1}{2} e^{i\frac{\pi}{4}} & e^{-i\frac{\pi}{4}} \\ \frac{1}{2} e^{-i\frac{\pi}{4}} & e^{i\frac{\pi}{4}} \end{pmatrix} \begin{pmatrix} D_+^{\text{II}} \\ D_-^{\text{II}} \end{pmatrix} \quad (10.2.3)$$

We define $\Psi_{WKB}^{\text{grow}}(x)$ and $\Psi_{WKB}^{\text{dec}}(x)$ to be the WKB solutions that involve $\exp\left(\int_{x_+}^x |V|^{\frac{1}{2}}\right)$ and $\exp\left(-\int_{x_+}^x |V|^{\frac{1}{2}}\right)$ at large x . These are obtained by setting, respectively, $D_-^{\text{II}} = 0$ and $D_+^{\text{II}} = 1$ or $D_-^{\text{II}} = 1$ and $D_+^{\text{II}} = 0$, in (10.2.1) and, using (10.2.2), we obtain:

$$\Psi_{WKB}^{\text{grow}}(x) = \begin{cases} \frac{1}{|V(x)|^{\frac{1}{4}}} \cos\left(\int_x^{x_+} |V(z)|^{\frac{1}{2}} dz + \frac{\pi}{4}\right), & x < x_+, \\ \sqrt{\pi} V'(x_+)^{\frac{1}{6}} \text{Bi}\left(V'(x_+)^{\frac{1}{3}}(x - x_+)\right), & x \sim x_+, \\ \frac{1}{V(x)^{\frac{1}{4}}} \exp\left(+\int_{x_+}^x |V(z)|^{\frac{1}{2}} dz\right), & x > x_+, \end{cases} \quad (10.2.4)$$

and

$$\Psi_{WKB}^{\text{dec}}(x) = \begin{cases} \frac{2}{|V(x)|^{\frac{1}{4}}} \cos\left(\int_x^{x_+} |V(z)|^{\frac{1}{2}} dz - \frac{\pi}{4}\right), & x < x_+, \\ 2\sqrt{\pi} V'(x_+)^{\frac{1}{6}} \text{Ai}\left(V'(x_+)^{\frac{1}{3}}(x - x_+)\right), & x \sim x_+, \\ \frac{1}{V(x)^{\frac{1}{4}}} \exp\left(-\int_{x_+}^x |V(z)|^{\frac{1}{2}} dz\right), & x > x_+, \end{cases} \quad (10.2.5)$$

The response function is given by (10.1.14), where the coefficients a_1 and b_1 , defined in (10.1.13), are determined using the leading terms in (10.2.4) and (10.2.5) and the normalizations in (10.1.11). Indeed, one finds:

$$a_1 = \mu^{-1/2} e^{-I_+}, \quad b_1 = \mu^{-1/2} e^{I_+}, \quad (10.2.6)$$

where I_+ is given in (10.1.16). The coefficient b_2 can be obtained by evaluating both sides of (10.1.13) at any finite value of $x \geq x_+$. It is convenient to evaluate b_2 at $x = x_+$. One then obtains:

$$b_2 = a_1 \frac{\Psi_{WKB}^{\text{grow}}(x_+)}{\Psi_{WKB}^{\text{dec}}(x_+)} - b_1 \frac{\Psi_E^{\text{grow}}(x_+)}{\Psi_E^{\text{dec}}(x_+)}. \quad (10.2.7)$$

From (10.2.4) and (10.2.5) one finds

$$\frac{\Psi_{WKB}^{\text{grow}}(x_+)}{\Psi_{WKB}^{\text{dec}}(x_+)} = \frac{\text{Bi}(0)}{2 \text{Ai}(0)} = \frac{\sqrt{3}}{2}. \quad (10.2.8)$$

The constant \mathcal{A} is determined by the physical boundary condition that the wave must satisfy at $x \rightarrow -\infty$. For one turning point, we can ensure ingoing boundary conditions by choosing the physical WKB solution to be

$$\Psi_{WKB}^{\text{phys}}(x) \equiv \Psi_{WKB}^{\text{grow}}(x) + \text{sign}(\omega) \frac{i}{2} \Psi_{WKB}^{\text{dec}}(x), \quad (10.2.9)$$

where ω is the momentum conjugate to time at the horizon. This result corresponds to $\mathcal{A} = \text{sign}(\omega) \frac{i}{2}$ and observe that, by construction, one has, for $x < x_+$,

$$\Psi_{WKB}^{\text{phys}}(x) = |V(x)|^{-\frac{1}{4}} \exp \left[\text{sign}(\omega) i \left(\int_x^{x_+} |V(z)|^{\frac{1}{2}} dz + \frac{\pi}{4} \right) \right], \quad (10.2.10)$$

The important point is that because $V(x) < 0$ for $x < x_+$, the integral in (10.2.10) is monotonically decreasing as x increases. Therefore, when this wave-function is multiplied by time-dependent phase, $e^{-i\omega t}$, Ψ_{WKB}^{phys} is a purely “infalling” wave function at $x \rightarrow -\infty$. The resulting response function can be read off from (10.1.14)

$$R_{\text{WKB}} = \frac{1}{2} \left(\sqrt{3} + \text{sign}(\omega) i \right) e^{-2I_+} - \frac{\Psi_E^{\text{grow}}(x_+)}{\Psi_E^{\text{dec}}(x_+)}. \quad (10.2.11)$$

To illustrate this result, we will consider asymptotically extremal BTZ backgrounds as well as the exactly extremal BTZ background in Section 10.2.2.

10.2.1.2 Potentials with two turning points

We perform a similar computation by deriving the response function of a Schrödinger equation, (10.1.4), with now two classical turning points, x_- and x_+ (see Fig.10.3). In the WKB approximation, the generic solution consists of the usual growing or decaying exponentials in the regions where $V(x) > 0$, oscillatory solutions where $V(x) < 0$ which are then connected by Airy functions:

$$\Psi(x) = \begin{cases} \frac{1}{|V(x)|^{\frac{1}{4}}} \left[D_+^{\text{I}} \exp \left(\int_x^{x_-} |V(z)|^{\frac{1}{2}} dz \right) + D_-^{\text{I}} \exp \left(- \int_x^{x_-} |V(z)|^{\frac{1}{2}} dz \right) \right], & x < x_-, \\ d_+^{\text{I}} \text{Bi} \left(-|V'(x_-)|^{1/3} (x - x_-) \right) + d_-^{\text{I}} \text{Ai} \left(-|V'(x_-)|^{1/3} (x - x_-) \right), & x \sim x_-, \\ \frac{1}{|V(x)|^{\frac{1}{4}}} \left[D_+^{\text{II}} \exp \left(i \int_{x_-}^x |V(z)|^{\frac{1}{2}} dz \right) + D_-^{\text{II}} \exp \left(-i \int_{x_-}^x |V(z)|^{\frac{1}{2}} dz \right) \right], & x_- < x < x_+, \\ d_+^{\text{II}} \text{Bi} \left(|V'(x_-)|^{1/3} (x - x_-) \right) + d_-^{\text{II}} \text{Ai} \left(|V'(x_-)|^{1/3} (x - x_-) \right), & x \sim x_+, \\ \frac{1}{|V(x)|^{\frac{1}{4}}} \left[D_+^{\text{III}} \exp \left(\int_{x_+}^x |V(z)|^{\frac{1}{2}} dz \right) + D_-^{\text{III}} \exp \left(- \int_{x_+}^x |V(z)|^{\frac{1}{2}} dz \right) \right], & x > x_+, \end{cases} \quad (10.2.12)$$

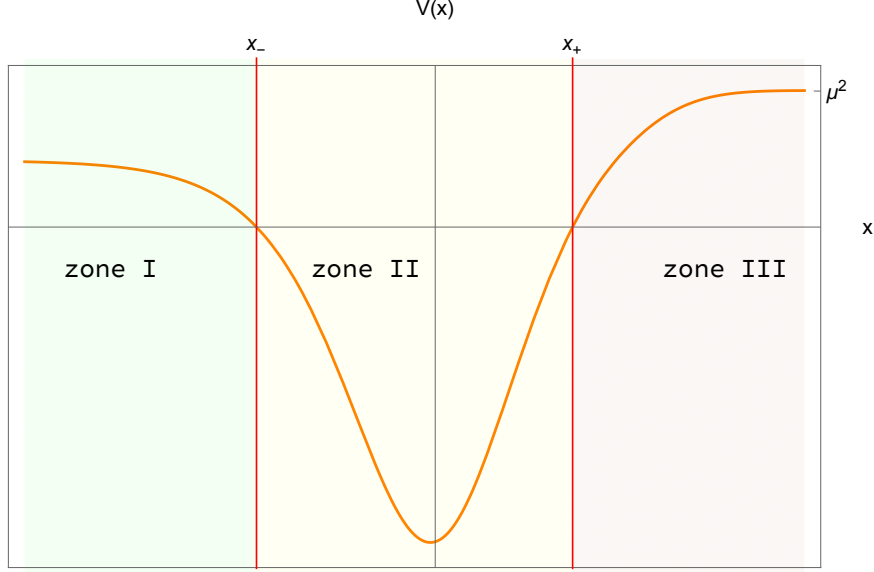


Figure 10.3: Schematic description of a potential $V(x)$ with the two turning points, x_- and x_+ and the three zones depending on the sign of $V(x)$. For the illustration, we have considered that $V(x)$ tends to a constant at $-\infty$ but it is not necessary for the discussion. Any kind of behavior is possible as long as $V(-\infty) \geq 0$.

The connection formulae at each junction determines all the unknown coefficients in terms of D_+^I and D_-^I :

$$\begin{aligned} \begin{pmatrix} d_+^I \\ d_-^I \end{pmatrix} &\equiv \frac{\sqrt{\pi}}{V'(x_-)^{\frac{1}{6}}} \begin{pmatrix} 1 & 0 \\ 0 & 2 \end{pmatrix} \begin{pmatrix} D_+^I \\ D_-^I \end{pmatrix}, & \begin{pmatrix} d_+^{II} \\ d_-^{II} \end{pmatrix} &\equiv \frac{\sqrt{\pi}}{V'(x_-)^{\frac{1}{6}}} \begin{pmatrix} -\sin \Theta & 2 \cos \Theta \\ \cos \Theta & 2 \sin \Theta \end{pmatrix} \begin{pmatrix} D_+^I \\ D_-^I \end{pmatrix}, \\ \begin{pmatrix} D_+^{II} \\ D_-^{II} \end{pmatrix} &\equiv \begin{pmatrix} \frac{1}{2} e^{i\frac{\pi}{4}} & e^{-i\frac{\pi}{4}} \\ \frac{1}{2} e^{-i\frac{\pi}{4}} & e^{i\frac{\pi}{4}} \end{pmatrix} \begin{pmatrix} D_+^I \\ D_-^I \end{pmatrix}, & \begin{pmatrix} D_+^{III} \\ D_-^{III} \end{pmatrix} &\equiv \begin{pmatrix} -\sin \Theta & 2 \cos \Theta \\ \frac{1}{2} \cos \Theta & \sin \Theta \end{pmatrix} \begin{pmatrix} D_+^I \\ D_-^I \end{pmatrix}, \end{aligned} \quad (10.2.13)$$

where

$$\Theta \equiv \int_{x_-}^{x_+} |V(z)|^{\frac{1}{2}} dz. \quad (10.2.14)$$

There are obvious parallels between these connection formula and those in (10.2.2). The only new element is Θ , whose origin is the trivial identity:

$$\exp\left(\pm i \int_{x_-}^x |V(z)|^{\frac{1}{2}} dz\right) = \exp(\pm i\Theta) \exp\left(\mp i \int_x^{x_+} |V(z)|^{\frac{1}{2}} dz\right). \quad (10.2.15)$$

The connection formulae at $x = x_+$ are simple expressions akin to those in (10.2.2) when the WKB wave-functions are written in terms of $\int_x^{x_+} |V(z)|^{\frac{1}{2}} dz$, however the expressions in (10.2.13) for Region II are written in terms of $\int_{x_-}^x |V(z)|^{\frac{1}{2}} dz$ and so (10.2.15) is needed to convert these expressions before using the simple connection formulae at x_+ .

The decaying and “growing” WKB modes can now be isolated by setting $D_+^{III} = 0$ or $D_-^{III} = 0$, respectively. Following our hybrid WKB strategy, we again assume that, for $x > x_+$ there is an exactly-known pair of wave-functions Ψ_E^{grow} and Ψ_E^{dec} . As in Section 10.2.1.1, one can match these to the decaying and growing WKB modes at x_+ , to arrive at essentially the same results as in (10.2.6) and (10.2.7).

The physical wave function should be regular in the interior of the geometry and so the physical wave function should not blow up as $x \rightarrow -\infty$. This means that Ψ_{WKB}^{phys} is given by (10.2.12) with

$D_+^I = 0$ and hence

$$\Psi_{WKB}^{\text{phys}}(x) = \cos \Theta \Psi_{WKB}^{\text{grow}}(x) + \frac{1}{2} \sin \Theta \Psi_{WKB}^{\text{dec}}(x), \quad (10.2.16)$$

This gives the response function in (10.1.15) with $\mathcal{A} = \frac{1}{2} \tan \Theta$.

To illustrate this result, we return to the global-AdS₃ geometry and compute the response function via the WKB approximation in Section 10.2.3. We examine the accuracy of the approximation in Appendix A.12, where we compare it to the exact result.

10.2.2 Response function in asymptotically extremal BTZ geometries

Our main goal is to apply our WKB hybrid technique on asymptotically extremal BTZ geometries, such as Superstrata. We will be able to relate their response functions to the response function of an extremal BTZ black hole. This naturally requires a good understanding of the later which we will quickly review here.

The standard form of the metric outside an extremal BTZ black hole in “Schwarzschild” coordinates is given by:

$$ds^2 = -\ell^2 f(\rho) dt^2 + \frac{d\rho^2}{f(\rho)} + \rho^2 \left(dy - \frac{r_H^2}{\rho^2} dt \right)^2, \quad f(\rho) = \frac{(\rho^2 - r_H^2)^2}{\ell^2 \rho^2}, \quad (10.2.17)$$

where the coordinate y is identified as $y \sim y + 2\pi R_y$ and the AdS length is given by ℓ . This solution has mass and angular momentum $J = M\ell = \frac{r_H^2}{4G\ell}$. It is more convenient to work in terms of a new radial coordinate $r^2 = (\rho^2 - r_H^2)$, so that $r = 0$ corresponds to the horizon, and $r \rightarrow \infty$ is the conformal boundary and with the null coordinates $u = y + t$ and $v = y - t$. The metric in this coordinate system is given by:

$$ds^2 = r^2 du dv + r_H^2 dv^2 + \ell^2 \frac{dr^2}{r^2}. \quad (10.2.18)$$

The wave equation for a scalar field Φ of mass $m^2 \ell^2 = \Delta(\Delta - 2)$, with $\Delta > 2$ can be solved with the Ansatz

$$\Phi = e^{-i(\omega u + p v)} K(r) \quad (10.2.19)$$

and is given by the Klein–Gordon equation:

$$\frac{1}{\ell^2 r} \partial_r (r^3 \partial_r K) - \left(\frac{\Delta(\Delta - 2)}{\ell^2} + \frac{4\omega p}{r^2} - \frac{4\omega^2 r_H^2}{r^4} \right) K = 0. \quad (10.2.20)$$

For convenience, we set the radius ℓ to 1 which can be also reabsorbed by scaling $(\ell\omega, \ell p) \rightarrow (\omega, p)$.

10.2.2.1 Exact treatment for extremal BTZ black holes

It is easy to see that in terms of a new variable $\tilde{r} = 1/r^2$, this is a confluent hypergeometric equation whose solutions are Whittaker functions⁵:

$$K(r) = c_1 M\left(\frac{ip}{2r_H}, \frac{1}{2}(\Delta - 1), \frac{2i\omega r_H}{r^2}\right) + c_2 M\left(\frac{ip}{2r_H}, \frac{1}{2}(1 - \Delta), \frac{2i\omega r_H}{r^2}\right). \quad (10.2.21)$$

⁵For $2\Delta \in \mathbb{Z}$, these two solutions are linearly dependent and it is necessary to use the Whittaker- W function instead.

The Whittaker M functions have the virtue of having a simple expansion around the conformal boundary ($r \rightarrow \infty$):

$$K = c_1 \left(\frac{2i\omega r_H}{r^2} \right)^{\Delta/2} [1 + \mathcal{O}(r^{-2})] + c_2 \left(\frac{2i\omega r_H}{r^2} \right)^{1-\Delta/2} [1 + \mathcal{O}(r^{-2})],$$

The response function is given by:

$$R^{\text{BTZ}} = \frac{c_1}{c_2} (2i\omega r_H)^{\Delta-1}. \quad (10.2.22)$$

The ratio c_1/c_2 is determined by the boundary conditions in the interior. For the BTZ black hole, the solution must be purely ingoing at the horizon ($r = 0$).

The expansion of the solution (10.2.21) at $r = 0$ is more complicated:

$$c_1 \Gamma(\Delta) \left[\frac{\left(\frac{2i\omega r_H}{r^2} \right)^{-\frac{ip}{2r_H}} e^{\frac{ir_H\omega}{r^2}}}{\Gamma(\frac{1}{2}(\Delta - \frac{ip}{r_H}))} + e^{i\frac{\pi}{2}\Delta \text{sign}(\omega)} \frac{\left(\frac{-2i\omega r_H}{r^2} \right)^{\frac{ip}{2r_H}} e^{-\frac{ir_H\omega}{r^2}}}{\Gamma(\frac{1}{2}(\Delta + \frac{ip}{r_H}))} \right] + c_2 (\Delta \leftrightarrow (2 - \Delta)). \quad (10.2.23)$$

To ensure ingoing boundary conditions at the horizon, the coefficient of $e^{-\frac{ir_H\omega}{r^2}}$ must vanish⁶ (remember that the horizon is at $r = 0$). This leads to the condition

$$c_1 \frac{\Gamma(\Delta) e^{i\frac{\pi}{2}\Delta \text{sign}(\omega)}}{\Gamma(\frac{1}{2}(\Delta + \frac{ip}{r_H}))} + c_2 \frac{\Gamma(2 - \Delta) e^{i\frac{\pi}{2}(2-\Delta) \text{sign}(\omega)}}{\Gamma(1 - \frac{1}{2}(\Delta - \frac{ip}{r_H}))} = 0. \quad (10.2.24)$$

Combining this with (10.2.22), we find the holographic “response” in momentum space:

$$R^{\text{BTZ}}(\omega, p) = -(-2i\omega r_H)^{\Delta-1} \frac{\Gamma(2 - \Delta) \Gamma(\frac{1}{2}(\Delta + \frac{ip}{r_H}))}{\Gamma(\Delta) \Gamma(1 - \frac{1}{2}(\Delta - \frac{ip}{r_H}))}. \quad (10.2.25)$$

This result can be compared to the thermal CFT two-point function (in the appropriate extremal limit). Ignoring an Δ -dependent factor, which can be absorbed in the normalization of the CFT operator \mathcal{O} , we recognize the retarded propagator with inverse left-moving temperature $\beta_L = R_y \pi / r_H$.

The Fourier transformation towards the Green function in position space is sensitive to the pole structure of (10.2.25). We have given all the details in Appendix A.13.1. Because of the ingoing boundary conditions, these poles correspond to the quasi-normal mode frequencies of the BTZ black hole (as opposed to normal modes in horizonless geometries). They are located on the imaginary axis, spaced by the temperature of the black hole. The fact that they all have positive imaginary part will single out the retarded propagator in position space.

10.2.2.2 Hybrid WKB for an asymptotically BTZ solution

We now consider the response function for a general, asymptotically extremal BTZ geometry. We assume that the scalar wave equation closely matches the BTZ wave equation (10.2.20) outside a certain radius. There are several ways to convert this equation to the standard Schrödinger form (10.1.4). We choose a version that leads to the simplest mode expansions:

$$K(r) = \frac{\Psi(r)}{r}, \quad x = \ln r, \quad x \in \mathbb{R}. \quad (10.2.26)$$

⁶Indeed, close to the horizon of the extremal BTZ geometry, a set of orthogonal Killing vectors is given by ∂_t and ∂_v . The conjugate momenta can be read off from (10.2.19): $\Phi = e^{-i(2\omega t + (p+\omega)v)} K(r)$. Therefore, 2ω is really the momentum conjugate to t near the black hole horizon.

The Schrödinger potential in the asymptotic region is

$$V(x) \sim V_{\text{BTZ}}(x) \equiv (\Delta - 1)^2 + 4\omega p e^{-2x} - 4\omega^2 r_H^2 e^{-4x}. \quad (10.2.27)$$

This potential approaches $(\Delta - 1)^2$ at the boundary $x \sim \infty$ and so $\mu = \Delta - 1 > 0$. The BTZ horizon would be at $x \rightarrow -\infty$. The BTZ potential has a unique classical turning point, x_+ , given by:

$$x_+ \equiv \frac{1}{2} \ln \left[\frac{2}{(\Delta - 1)^2} \left(|\omega| \sqrt{p^2 + r_H^2 (\Delta - 1)^2} - \omega p \right) \right]. \quad (10.2.28)$$

For general asymptotically BTZ geometries, we consider a regime of ω and p where the outermost classical turning point of $V(x)$, x_+ , is inside the BTZ region: $V(x) \sim V_{\text{BTZ}}(x)$, $x \gtrsim x_+$. This requires that the energy of the mode is higher than a certain value.

In the inner region, $x < x_+$, the potential can take a very complicated form. As explained in Section 10.1.3, the relevant quantity to describe the inner region is the quantity \mathcal{A} which has different expressions according to the form of the potential. Whenever x_+ is in the BTZ region, the other quantities that enter in the WKB hybrid formula for the response function (10.1.15) can be derived from $V_{\text{BTZ}}(x)$. The expression for I_+ , defined in (10.1.16), is an elementary integral leading to:

$$e^{-2I_+} = (\Delta - 1)^{2-2\Delta} |\omega|^{\Delta-1} (p^2 + r_H^2 (\Delta - 1)^2)^{\frac{\Delta-1}{2}} \times \exp \left(\Delta - 1 - \frac{2p}{r_H} \arctan \left[\frac{r_H (\Delta - 1)}{\sqrt{p^2 + r_H^2 (\Delta - 1)^2 - p}} \right] \right). \quad (10.2.29)$$

For $\Psi_E^{\text{grow}}(x)$ and $\Psi_E^{\text{dec}}(x)$, we simply use the growing and decaying scalar modes in an extremal-BTZ black hole (10.2.21). In our coordinate system, this gives

$$\begin{aligned} \Psi_E^{\text{grow}}(x) &= (-2i r_H \omega)^{\frac{\Delta}{2}-1} e^{(2-\Delta)x} \text{M} \left(-\frac{i p}{2r_H}, -\frac{\Delta-1}{2}, -2i r_H \omega e^{-2x} \right), \\ \Psi_E^{\text{dec}}(x) &= (-2i r_H \omega)^{-\frac{\Delta}{2}} e^{\Delta x} \text{M} \left(-\frac{i p}{2r_H}, \frac{\Delta-1}{2}, -2i r_H \omega e^{-2x} \right). \end{aligned} \quad (10.2.30)$$

It should be noted that these functions are actually real for real values of ω, p, r_H, Δ and x . We now have all the ingredients of (10.1.15), except for \mathcal{A} , which depends entirely on the details of the “inner region”.

As a special case, we can apply our WKB method to the BTZ geometry itself. Indeed, the BTZ potential only has one classical turning point and so the WKB response function is given by (10.2.11), and, in particular, we have $\mathcal{A} = \frac{1}{2} \text{sign}(\omega) i$ in (10.1.15). We therefore conclude that within the validity of the WKB approximation we must have

$$R_E^{\text{BTZ}}(\omega, p) \approx \frac{1}{2} \left(\sqrt{3} + \text{sign}(\omega) i \right) e^{-2I_+} - \frac{\Psi_E^{\text{grow}}(x_+)}{\Psi_E^{\text{dec}}(x_+)}, \quad (10.2.31)$$

where $R_E^{\text{BTZ}}(\omega, p)$ is given by (10.2.25). Taking the real and imaginary parts of this expression, we arrive at the approximate identities:

$$\frac{\sqrt{3}}{2} e^{-2I_+} - \frac{\Psi_E^{\text{grow}}(x_+)}{\Psi_E^{\text{dec}}(x_+)} \approx \text{Re} [R_E^{\text{BTZ}}], \quad \frac{\text{sign}(\omega)}{2} e^{-2I_+} \approx \text{Im} [R_E^{\text{BTZ}}], \quad (10.2.32)$$

where we have used the fact that e^{-2I_+} , $\Psi_E^{\text{grow}}(x_+)$ and $\Psi_E^{\text{dec}}(x_+)$ are all real. Using these expressions in (10.1.15) we arrive at the result advertised in (10.1.20) for a generic, asymptotically BTZ response function, R_{WKB} ,

$$R_{WKB}(\omega, p) \approx \text{Re} [R_E^{\text{BTZ}}(\omega, p)] + 2 \text{sign}(\omega) \mathcal{A} \text{Im} [R_E^{\text{BTZ}}(\omega, p)] , \quad (10.2.33)$$

This is our primary result for the general WKB analysis of asymptotically BTZ metrics. This formula has been computed for 2Δ non-integer but the analytic continuation to integer values of 2Δ is well-defined since we know the expression of R_E^{BTZ} for Δ integer from the literature. The formula (10.2.33) is only valid when the largest turning point is inside the BTZ region, in other words, in a regime of momenta where the waves stop oscillating at a distance which lies inside the BTZ region.

It is also important to note that in deriving (10.1.15), and in particularly in making the identifications (10.2.32) that led to (10.1.20) crucially requires both ω and p to be real. This will be very important for understanding the pole structure of the response function.

In addition to obtaining the formula (10.2.33), the application of the WKB technique to the BTZ metric also illustrates the method very simply and affords us the opportunity to assess the accuracy of the WKB approximation. Indeed, one can numerically evaluate and compare both sides of the approximate identities (10.2.32) using (10.2.28), (10.2.29), (10.2.30) and (10.2.25). The details of this can be found in Appendix A.12.1, where we show that, even for relatively small values of Δ , the accuracy is within a few percent and that the accuracy greatly improves as Δ increases.

10.2.3 Model response function in the interior: global AdS₃

The superstratum geometries are capped BTZ geometries which are smooth global AdS₃ geometries in the IR. In this section we briefly review the computation of the response function in global AdS₃ and we apply our WKB hybrid method to check the suitability of this method to such backgrounds. The global Lorentzian AdS₃ metric of radius ℓ may be written in the following forms:

$$\begin{aligned} ds^2 &= - (r^2 + 1) dt^2 + \frac{\ell^2 dr^2}{r^2 + 1} + r^2 dy^2 \\ &= - \frac{1}{4} (du - dv)^2 + r^2 du dv + \frac{\ell^2 dr^2}{r^2 + 1} , \end{aligned} \quad (10.2.34)$$

where $0 \leq y < 2\pi R_y$ and $u = y + t$ and $v = y - t$. The wave equation for a scalar field Φ of mass $m^2 \ell^2 = \Delta(\Delta - 2)$ with the Ansatz $\Phi = e^{-i(\omega u + p v)} K(r)$ is given by the Klein–Gordon equation:

$$\frac{1}{\ell^2 r} \partial_r (r (r^2 + 1) \partial_r K) - \left(\frac{\Delta(\Delta - 2)}{\ell^2} - \frac{(\omega - p)^2}{r^2 + 1} + \frac{(\omega + p)^2}{r^2} \right) K = 0 . \quad (10.2.35)$$

Moreover, we assume without loss of generality that $\Delta > 1$. For convenience, we set the radius ℓ to 1 which can be also reabsorbed by scaling $(\ell\omega, \ell p) \rightarrow (\omega, p)$.

10.2.3.1 Exact analysis for global AdS₃

The Klein–Gordon equation can be reduced to a standard hypergeometric equation whose solutions can be written as a linear combination of:

$$K_1(\omega, p; r) \equiv r^{(\omega+p)} (r^2 + 1)^{\frac{1}{2}(\omega-p)} {}_2F_1 \left(1 + \omega - \frac{1}{2}\Delta, \omega + \frac{1}{2}\Delta, \omega + p + 1; -r^2 \right) , \quad (10.2.36)$$

$$K_2(\omega, p; r) \equiv r^{-(\omega+p)} (r^2 + 1)^{\frac{1}{2}(\omega-p)} {}_2F_1 \left(1 - \frac{1}{2}\Delta - p, \frac{1}{2}\Delta - p, 1 - \omega - p; -r^2 \right) . \quad (10.2.37)$$

These functions are defined by their power expansion about $r = 0$ in which the generic term is $r^{2n \pm (\omega+p)}$, $n \in \mathbb{Z}, n \geq 0$. It is worth noting that in the neighbourhood of $r = 0$, the wave equation, (10.2.35),

becomes, at leading order, the Laplace equation of flat $\mathbb{R}^{2,1}$ written in polar coordinates:

$$\frac{1}{r} \partial_r (r \partial_r K) - \frac{(\omega + p)^2}{r^2} K = 0. \quad (10.2.38)$$

It is this equation that fixes the leading powers of r in (10.2.37). The solution that is regular at $r = 0$ is thus

$$K_{reg}(\omega, p; r) = \Theta(\omega + p) K_1(\omega, p; r) + \Theta(-(\omega + p)) K_2(\omega, p; r), \quad (10.2.39)$$

where Θ is the Heaviside step function.

One can also expand about infinity by using the inversion, $r \rightarrow \frac{1}{r}$, and one finds that an equivalent basis of solutions is given by:

$$\tilde{K}_1(\omega, p; r) \equiv r^{(\omega - p + \Delta - 2)} (r^2 + 1)^{\frac{1}{2}(p - \omega)} {}_2F_1\left(1 + p - \frac{1}{2}\Delta, 1 - \omega - \frac{1}{2}\Delta, 2 - \Delta; -r^{-2}\right), \quad (10.2.40)$$

$$\tilde{K}_2(\omega, p; r) \equiv r^{(\omega - p - \Delta)} (r^2 + 1)^{\frac{1}{2}(p - \omega)} {}_2F_1\left(p + \frac{1}{2}\Delta, \frac{1}{2}\Delta - \omega, \Delta; -r^{-2}\right). \quad (10.2.41)$$

These functions are defined by their expansions as $r \rightarrow \infty$:

$$\tilde{K}_1(\omega, p; r) = r^{(\Delta - 2)} \sum_{n=0}^{\infty} a_n r^{-2n}, \quad \tilde{K}_2(\omega, p; r) = r^{-\Delta} \sum_{n=0}^{\infty} b_n r^{-2n}. \quad (10.2.42)$$

Since $\Delta > 2$, \tilde{K}_1 and \tilde{K}_2 purely contain non-normalizable and normalizable modes. Note that if $\Delta \notin \mathbb{N}_{>2}$ then there can be no mixing of these series and so \tilde{K}_1 unambiguously represents the purely non-normalizable mode.

Finally, note that the wave equation (10.2.35) is invariant under $(\omega, p) \rightarrow -(\omega, p)$ and one can use the Euler transformation of the hypergeometric functions to verify that under this transformation $K_1 \leftrightarrow K_2$ while the \tilde{K}_j are individually invariant.

Response functions

To get the boundary-to-boundary Green function, or response function, for AdS_3 , one should expand K_{reg} in (10.2.39) around infinity. In particular, one finds for K_1 and K_2 :

$$K_1(\omega, p; r) \sim r^{-\Delta} \Gamma(1 + \omega + p) \left[\frac{\Gamma(1 - \Delta)}{\Gamma(1 + p - \frac{1}{2}\Delta) \Gamma(1 + \omega - \frac{1}{2}\Delta)} + r^{2(\Delta - 1)} \frac{\Gamma(\Delta - 1)}{\Gamma(p + \frac{1}{2}\Delta) \Gamma(\omega + \frac{1}{2}\Delta)} \right], \quad (10.2.43)$$

$$K_2(\omega, p; r) \sim r^{-\Delta} \Gamma(1 - \omega - p) \left[\frac{\Gamma(1 - \Delta)}{\Gamma(1 - \omega - \frac{1}{2}\Delta) \Gamma(1 - p - \frac{1}{2}\Delta)} + r^{2(\Delta - 1)} \frac{\Gamma(\Delta - 1)}{\Gamma(\frac{1}{2}\Delta - \omega) \Gamma(\frac{1}{2}\Delta - p)} \right]. \quad (10.2.44)$$

Taking the ratio of normalizable and non-normalizable parts yields to a response function for each of the solutions

$$R_1(\omega, p) = \frac{\Gamma(1 - \Delta) \Gamma(\omega + \frac{1}{2}\Delta) \Gamma(p + \frac{1}{2}\Delta)}{\Gamma(\Delta - 1) \Gamma(1 + \omega - \frac{1}{2}\Delta) \Gamma(1 + p - \frac{1}{2}\Delta)}, \quad (10.2.45)$$

$$R_2(\omega, p) = \frac{\Gamma(1 - \Delta) \Gamma(\frac{1}{2}\Delta - \omega) \Gamma(\frac{1}{2}\Delta - p)}{\Gamma(\Delta - 1) \Gamma(1 - \frac{1}{2}\Delta - \omega) \Gamma(1 - \frac{1}{2}\Delta - p)}.$$

The response function for smooth solutions in global AdS_3 is therefore:

$$R^{\text{AdS}_3}(\omega, p) = \Theta(\omega + p) R_1(\omega, p) + \Theta(-(\omega + p)) R_2(\omega, p). \quad (10.2.46)$$

These Green functions are “formal” in that they have poles that require careful interpretation. First, these functions are infinite when $\Delta \in \mathbb{N}_{>2}$. This arises because of the standard degeneration inherent in Frobenius’ method: the non-normalizable solution is no longer a power series but contains a logarithmic term that multiplies the normalizable solution. We avoid this issue by taking $\Delta \notin \mathbb{Z}$, and then analytically continuing in Δ when possible.

Second, the response function has also a tower of evenly spaced poles on the real axis corresponding to the frequencies and momenta where the regular solution (10.2.39) is normalizable. They correspond to the values where the arguments of the Gamma function in the numerators of (10.2.45) cross a negative integer value. To make the pole structure more manifest in the formulation of the response function, it is worth to rewrite R^{AdS_3} in a more compact but non-analytic expression

$$R^{\text{AdS}_3}(\omega, p) = \frac{\Gamma(1 - \Delta)}{\Gamma(\Delta - 1)} \frac{\Gamma(\tilde{\omega} + \frac{1}{2}\Delta)}{\Gamma(1 + \tilde{\omega} - \frac{1}{2}\Delta)} \frac{\Gamma(\tilde{p} + \frac{1}{2}\Delta)}{\Gamma(1 + \tilde{p} - \frac{1}{2}\Delta)}, \quad (10.2.47)$$

where we have defined

$$\tilde{\omega} \equiv \frac{|\omega + p| - |\omega - p|}{2}, \quad \tilde{p} \equiv \frac{|\omega + p| + |\omega - p|}{2}. \quad (10.2.48)$$

Since \tilde{p} is always positive, normalizable modes exist only in the range of frequency and momentum where $\tilde{\omega} + \frac{1}{2}\Delta < 0$. Those poles follows the following evenly spaced spectrum

$$|\omega_j - p_j| - |\omega_j + p_j| - \Delta = 2j, \quad j \in \mathbb{N}, \quad (10.2.49)$$

Moreover, by anticipating the comparison with the WKB answer, it is also useful to write down R^{AdS_3} in the range where poles exist, $\tilde{\omega} + \frac{1}{2}\Delta < 0$,

$$R^{\text{AdS}_3}(\omega, p) = \frac{\Gamma(1 - \Delta)}{\Gamma(\Delta - 1)} \frac{\Gamma(\frac{1}{2}\Delta - \tilde{\omega})}{\Gamma(1 - \tilde{\omega} - \frac{1}{2}\Delta)} \frac{\Gamma(\tilde{p} + \frac{1}{2}\Delta)}{\Gamma(1 + \tilde{p} - \frac{1}{2}\Delta)} \times \left[-\sin(\pi\Delta) \tan\left(\frac{\pi}{2}(2\tilde{\omega} + \Delta + 1)\right) - \cos(\pi\Delta) \right], \quad (10.2.50)$$

where the coefficient in front of the bracket is smooth in this range and where the tan term gives the spectrum.

The more subtle issue is how to integrate around all the poles in the response functions. Fortunately one can find a very thorough treatment of this issue in [198–200]. This involves careful combinations of analytic continuation, matching conditions and contour selection. Selecting different contours around poles either includes or excludes normalizable modes in the solution. This is reviewed in Appendix A.13.2, where we use a particular contour prescription to relate the formal momentum-space Green functions derived here to a position-space Green function of interest.

10.2.3.2 WKB treatment

Once again we use the metric (10.2.34) and the wave equation (10.2.35). We rescale the wave-function and change variable according to:

$$K(r) = \frac{\Psi(r)}{\sqrt{r^2 + 1}}, \quad x = \ln(r), \quad x \in \mathbb{R}, \quad (10.2.51)$$

and the wave equation takes the Schrödinger form (10.1.4) with

$$V_{\text{AdS}}(x) \equiv \frac{e^{2x}}{e^{2x} + 1} \left((\Delta - 1)^2 - \frac{(\omega - p)^2 - 1}{e^{2x} + 1} + \frac{(\omega + p)^2}{e^{2x}} \right). \quad (10.2.52)$$

The boundaries were at $r = 0$ and at $r = \infty$ and these are now at $x = +\infty$ and $x = -\infty$, where the potential limits to $\mu^2 \equiv (\Delta - 1)^2$ and $(\omega + p)^2$, respectively.

The potential is thus bounded by the value at infinity and the centrifugal barrier at $x = -\infty$ ($r = 0$). The two turning points, x_- and x_+ , and “classical region” $x_- < x < x_+$ only exists if the middle “energy term” in (10.2.52) is sufficiently negative. More precisely, to have classical turning points one must have

$$(\Delta - 1 + |\omega + p|)^2 < (\omega - p)^2 - 1 \quad \Leftrightarrow \quad (\Delta - 1)^2 + 4\omega p + 1 < -2(\Delta - 1)|\omega + p|. \quad (10.2.53)$$

If this is satisfied, then the two turning points are at real values of x and are given by:

$$e^{2x_{\pm}} = -\frac{1}{2(\Delta - 1)^2} \left(((\Delta - 1)^2 + 4\omega p + 1) \mp \sqrt{((\Delta - 1)^2 + 4\omega p + 1)^2 - 4(\Delta - 1)^2(p + \omega)^2} \right). \quad (10.2.54)$$

The WKB integrals are elementary and we find:

$$\Theta = \frac{\pi}{2} \left[-\Delta + 1 - |\omega + p| + \sqrt{(\omega - p)^2 - 1} \right], \quad (10.2.55)$$

and

$$\begin{aligned} e^{-2I_+} = & \left(\frac{e^{2x_+} - e^{2x_-}}{4} \right)^{\Delta-1} \left(\frac{e^{x_+} - e^{x_-}}{e^{x_+} + e^{x_-}} \right)^{(\Delta-1)e^{x_-} + x_+} \\ & \times \left(\frac{\sqrt{e^{x_+} + 1} + \sqrt{e^{x_-} + 1}}{\sqrt{e^{x_+} + 1} - \sqrt{e^{x_-} + 1}} \right)^{(\Delta-1)\sqrt{(e^{x_+} + 1)(e^{x_-} + 1)}}, \end{aligned} \quad (10.2.56)$$

As one would expect, (10.2.53) implies that $\Theta > 0$.

The exact asymptotic problem is just the wave equation in the global-AdS₃ background and so $\Psi_E^{\text{grow}}(x)$ and $\Psi_E^{\text{dec}}(x)$ are given by (10.2.41) and (10.2.51):

$$\begin{aligned} \Psi_E^{\text{grow}}(x) &= e^{(\Delta-2+\omega-p)x} (1 + e^{2x})^{(1-\omega+p)/2} {}_2F_1 \left(1 + p - \frac{\Delta}{2}, 1 - \omega - \frac{\Delta}{2}, 2 - \Delta, -e^{-2x} \right), \\ \Psi_E^{\text{dec}}(x) &= e^{(-\Delta+\omega-p)x} (1 + e^{2x})^{(1-\omega+p)/2} {}_2F_1 \left(p + \frac{\Delta}{2}, -\omega + \frac{\Delta}{2}, \Delta, -e^{-2x} \right). \end{aligned} \quad (10.2.57)$$

The WKB response function, R_{WKB}^{AdS} , can be then computed easily from the formula (10.1.15) with $\mathcal{A} = \tan \Theta$. This $\tan \Theta$ term is the only unbounded term and its poles correspond to the normalizable modes, when Θ crosses a value of type $\frac{\pi}{2}(2k + 1)$ with $k \in \mathbb{N}$. This reproduces very accurately the spectrum dependence of the exact response function, R^{AdS_3} (10.2.49). Indeed, in the range of parameters satisfying (10.2.53), we have that $\tilde{\omega} < 0$ and (10.2.50) takes the form

$$R^{\text{AdS}_3} = g_1(\omega, p) + g_2(\omega, p) \tan \Theta_E, \quad (10.2.58)$$

where $g_1(\omega, p)$ and $g_2(\omega, p)$ are two non-diverging functions given in (10.2.50) and the exact spectrum function Θ_E is

$$\Theta_E = \frac{\pi}{2} [-\Delta - 1 - |\omega + p| + |\omega - p|]. \quad (10.2.59)$$

We see that $\Theta \sim \Theta_E$ as long as $|\omega - p| \gg 1$ which is guaranteed from (10.2.53) if we assume that Δ is large. Moreover, in Appendix A.12.2 we perform a numerical exploration, using the expressions of I_+ , Ψ_E^{grow} and Ψ_E^{dec} above, that shows that

$$\frac{\sqrt{3}}{2} e^{-2I_+} - \frac{\Psi_E^{\text{grow}}(x_+)}{\Psi_E^{\text{dec}}(x_+)} \approx g_1(\omega, p), \quad \frac{1}{2} e^{-2I_+} \approx g_2(\omega, p), \quad (10.2.60)$$

which implies

$$R_{WKB}^{\text{AdS}} \sim R^{\text{AdS}_3}, \quad (10.2.61)$$

when Δ is large and when $|\omega - p|$ is also larger than $\Delta - 1 + |\omega + p|$ (for $\Delta \sim 5$ and $|\omega - p| - \Delta + 1 - |\omega + p| \sim 5$ the error of the WKB formula is already below 5%). Thus, our WKB technique provides an extremely accurate approximation to describe AdS-like response function.

10.3 The (1,0,n) Superstrata

In this section, we briefly review all the features of the metric of the (1,0,n) superstratum solution that are essential to our computation.

10.3.1 The metric

Asymptotically AdS_3 , (1,0,n) Superstrata have been introduced in the previous chapter. The fields involved in the metric can be derived from the general formulas of Section 4.2.5. In the present work, we are using the null coordinates

$$u = y - t, \quad v = y + t.$$

The six-dimensional metric is [30, 98, 99, 116]

$$\begin{aligned} ds_6^2 = & \sqrt{Q_1 Q_5} \Lambda \left[\frac{dr^2}{r^2 + a^2} - \frac{F_1(r)}{a^2(2a^2 + b^2)^2 F_2(r) R_y^2} \left(dv - \frac{a^2(a^4 + (2a^2 + b^2)r^2)}{F_1(r)} du \right)^2 \right. \\ & + \frac{a^2 r^2 (r^2 + a^2)}{F_1(r) R_y^2} du^2 + d\theta^2 + \frac{1}{\Lambda^2} \sin^2 \theta \left(d\varphi_1 + \frac{a^2}{(2a^2 + b^2) R_y} (du - dv) \right)^2 \\ & \left. + \frac{F_2(r)}{\Lambda^2} \cos^2 \theta \left(d\varphi_2 - \frac{1}{(2a^2 + b^2) F_2(r) R_y} [a^2(du + dv) + b^2 F_0(r) dv] \right)^2 \right], \end{aligned} \quad (10.3.1)$$

where

$$\begin{aligned} F_0(r) &\equiv 1 - \frac{r^{2n}}{(r^2 + a^2)^n}, & F_1(r) &\equiv a^6 - b^2(2a^2 + b^2)r^2 F_0(r), \\ F_2(r) &\equiv 1 - \frac{a^2 b^2}{2a^2 + b^2} \frac{r^{2n}}{(r^2 + a^2)^{n+1}}, & \Lambda &\equiv \sqrt{1 - \frac{a^2 b^2}{2a^2 + b^2} \frac{r^{2n}}{(r^2 + a^2)^{n+1}} \sin^2 \theta}. \end{aligned} \quad (10.3.2)$$

This has the form of an S^3 fibration, parametrized by $(\theta, \varphi_1, \varphi_2)$, over a 2+1-dimensional base space, parametrized by (t, u, v) . The metric parameters a , b and n are related to supergravity charges, Q_1, Q_5, Q_P, J_L and J_R or to the quantized charges, N_1, N_5, N_P, j_L and j_R via (4.2.74), (4.2.76) and (4.2.77). We consider the solutions which have a long BTZ-like throat. This requires

$$a^2 \ll \{Q_1, Q_5, Q_P\} \iff a \ll b. \quad (10.3.3)$$

The longest throat geometry is obtained by taking the minimum value of angular momentum $j_R = \frac{1}{2}$. Henceforth, we consider the solutions with $j_R = \frac{1}{2}$, and for such throats one has $N_1 N_5 = 1 + \frac{b^2}{2a^2} \sim \frac{b^2}{2a^2}$.

Thus, one can read off from the metric the two regions of the solutions which are depicted in Fig. 4.4:

- The smooth cap geometry: for $r \lesssim \sqrt{n} a$, the geometry is a S^3 fibration over a global AdS_3 space with a highly red-shifted time and a non-zero angular momentum along y ,

$$\begin{aligned} ds_6^2 = & \sqrt{Q_1 Q_5} \left[\frac{dr^2}{r^2 + a^2} - (r^2 + a^2) \frac{1}{a^2 R_y^2} d\tau^2 + \frac{r^2}{a^2 R_y^2} \left(dy + \frac{b^2}{2a^2} d\tau \right)^2 \right. \\ & \left. + d\theta^2 + \sin^2 \theta \left(d\varphi_1 - \frac{d\tau}{R_y} \right)^2 + \cos^2 \theta \left(d\varphi_2 - \frac{dy}{R_y} - \frac{b^2}{2a^2} \frac{d\tau}{R_y} \right)^2 \right] \end{aligned} \quad (10.3.4)$$

where $\tau = (1 + \frac{b^2}{2a^2})^{-1} t = (N_1 N_5)^{-1} t$. One can check that the local geometry at $r \sim 0$ is a smooth S^3 fibration over $\mathbb{R}^{1,2}$.

- The extremal-BTZ geometry: for $r \gtrsim \sqrt{n} a$, the geometry is S^3 fibration over extremal BTZ

$$ds_6^2 = \sqrt{Q_1 Q_5} \left[\frac{d\rho^2}{\rho^2} - \rho^2 dt^2 + \rho^2 dy^2 + \frac{n}{R_y^2} (dy + dt)^2 + d\theta^2 + \sin^2 \theta d\varphi_1^2 + \cos^2 \theta d\varphi_2^2 \right] \quad (10.3.5)$$

where $\rho = \frac{r}{\sqrt{Q_1 Q_5}}$. The left and right temperatures of the BTZ region are

$$T_L = \frac{\sqrt{n}}{2\pi R_y}, \quad T_R = 0. \quad (10.3.6)$$

The overall superstratum geometry is then the combination of a S^3 fibration over a BTZ geometry which ends with a highly red-shifted $\text{AdS}_3 \times S^3$. It is then natural to expect that wave perturbations will combine the features of those both geometries as it will be more precise in the next following sections.

10.3.2 The massless scalar wave perturbation

We rederived the minimally-coupled massless scalar wave equation (9.3.3) with the definition $(u, v) = (y - t, y + t)$. The separability allows to expand the eigenfunctions as:

$$\Phi = K(r) S(\theta) e^{-i \left(\frac{\Omega}{R_y} u + \frac{P}{R_y} v + q_1 \varphi_1 + q_2 \varphi_2 \right)}. \quad (10.3.7)$$

Note that we have reestablish the momentum conjugate (Ω, P) as opposed to (ω, p) . The reason for this will become apparent shortly. The wave equation reduces to one radial and one angular wave equation. The angular wave equation (9.3.6) and its solutions (9.3.11) are identical here. The radial equation becomes with the new coordinates:

$$\begin{aligned} \frac{1}{r} \partial_r (r (r^2 + a^2) \partial_r K(r)) + \left(\frac{a^2 (P - \Omega + q_1)^2}{r^2 + a^2} - \frac{a^2 (P + \Omega + q_2)^2}{r^2} \right) K(r) \\ + \frac{b^2 \Omega (-2a^2 P + F_0(r)(2a^2 (\Omega - q_1) + b^2 \Omega))}{a^2 (r^2 + a^2)} K(r) = m K(r), \end{aligned} \quad (10.3.8)$$

where m corresponds to the constant eigenvalue of the Laplacian operator along the S^3 related to the conformal weight of the wave, Δ , as $m \equiv \Delta(\Delta - 2)$. Without loss of generality, we consider that $\Delta > 1$. The regularity of the angular wave function constrains the wave quantum number (9.3.13). Moreover, the regularity of the modes at $r = 0$ requires [117]:

$$k \equiv \Omega + P \in \mathbb{Z}. \quad (10.3.9)$$

According to Section 9.3, the modes are essentially supported and determined by the AdS_3 cap geometry. When n is taken to be large, their discrete spectrum is given by (9.3.26)⁷

$$\left| \left(\frac{b^2}{a^2} + 1 \right) \Omega_j - P_j - q_1 \right| - |\Omega_j + P_j + q_2| - \Delta = 2j, \quad j \in \mathbb{N}, \quad (10.3.10)$$

where the index j is the mode number. This corresponds to the spectrum of an AdS_3 geometry computed in (10.2.49) with the additional quantum numbers q_1 and q_2 coming from vector-field reduction of the S^3 and the red-shifted frequency and momentum:

$$\omega = \left(1 + \frac{b^2}{2a^2} \right) \Omega, \quad p = P - \frac{b^2}{2a^2} \Omega, \quad (10.3.11)$$

⁷Note that this spectrum appears slightly different because of the redefinition $\{u, v\} = \{y - t, y + t\}$ compared to $\{t, t + y\}$ in the previous chapter.

These expressions provide a valuable insight into the physics of the deep Superstrata: their bound-state excitations (at least at large n) are simply those of a global AdS₃ geometry but with a red-shifted time (10.3.4). Since the Superstratum also asymptotes to a (non-red-shifted) global AdS₃ geometry at infinity one needs to interpolate between these two limits in order to compute the response function. This requires non-normalizable modes and the high-energy normalizable modes. For that purpose, we will apply the WKB strategy detailed in Section 10.1.3 and 10.2 and we will find that the interpolation along the throat is provided by the BTZ response function.

10.3.3 WKB analysis

The first step is to reduce the wave equation to Schrödinger form, just as we did in previous sections. We first rescale the wave function and change variables:

$$K(r) = \frac{\Psi(r)}{\sqrt{r^2 + a^2}}, \quad x = \ln\left(\frac{r}{a}\right), \quad x \in \mathbb{R}. \quad (10.3.12)$$

The radial wave equation gives

$$\frac{d^2}{dx^2} \Psi(x) - V(x) \Psi(x) = 0. \quad (10.3.13)$$

where $V(x)$ is given by:

$$V(x) \equiv \frac{e^{2x}}{e^{2x} + 1} \left[(\Delta - 1)^2 - \frac{1}{e^{2x} + 1} (B^2 - 1) + e^{-2x} A^2 + \frac{e^{-2x}}{(e^{-2x} + 1)^{n+1}} C \right], \quad (10.3.14)$$

and

$$A \equiv |\Omega + P + q_2|, \quad B \equiv \left| \Omega \left(1 + \frac{b^2}{a^2} \right) - P - q_1 \right|, \quad C \equiv \frac{b^2}{a^2} \Omega \left(2(\Omega - q_1) + \frac{b^2}{a^2} \Omega \right). \quad (10.3.15)$$

The general form of such potential is depicted in Fig.10.3. In this case we have $\mu = (\Delta - 1)$ and $V(-\infty) = A^2$.

We define x_{\pm} as the two turning points of the potential⁸, $V(x_{\pm}) = 0$. Zone II is the classically allowed region where $V(x) < 0$ and zone I and III are the classically forbidden regions with positive potential.

We compute the physical wave function $\Psi(x)$ at leading order in each zone by applying the WKB approximation as we did for a scalar wave in global AdS₃ in Section 10.2.1.2. We impose the regularity of the solution at $x = -\infty$ ($r = 0$) and we apply the junction rules with Airy functions to connect the three parts of the solution at the turning points. Therefore, the WKB approximation gives

$$\Psi_{\text{phys}}(x) = \begin{cases} \frac{1}{|V(x)|^{\frac{1}{4}}} \exp\left(-\int_x^{x_-} |V(z)|^{\frac{1}{2}} dz\right), & x < x_-, \\ \frac{1}{|V(x)|^{\frac{1}{4}}} \cos\left(\int_{x_-}^x |V(z)|^{\frac{1}{2}} dz + \frac{\pi}{4}\right), & x_- < x < x_+, \\ \frac{2 \cos \Theta}{|V(x)|^{\frac{1}{4}}} \left[\exp\left(\int_{x_+}^x |V(z)|^{\frac{1}{2}} dz\right) + \frac{\tan \Theta}{2} \exp\left(-\int_{x_+}^x |V(z)|^{\frac{1}{2}} dz\right) \right], & x > x_+, \end{cases} \quad (10.3.16)$$

where the WKB integral Θ is defined in (10.1.18). The validity of the WKB approximation is guaranteed when the condition given in (10.1.5) is satisfied. This imposes

$$|\Omega| \gtrsim \frac{2a^2}{b^2} \quad \text{and} \quad \Delta \gtrsim 1. \quad (10.3.17)$$

⁸If $A = 0$, then $x_- = -\infty$. This does not compromise our discussion in any way since $|V(x)|^{1/2}$ remains integrable at this location.

From the discrete spectrum of the modes (10.3.10), we expect that the WKB approximation will not be accurate for the first few modes. We will see how to deal this issue in the next sections. Moreover, the integral of $|V|^{\frac{1}{2}}$ cannot be performed analytically and one needs to divide our computation into different ranges of frequencies Ω and $k = \Omega + P$ to approximate its value.

To apply the WKB technique developed in Section 10.2 one needs to have a good understanding of the behavior of the superstratum potential, in particular to identify the interior and asymptotic potentials depending of the range of values of Ω and P . From now on, we will assume for simplicity that the wave perturbations are independent of φ_1 and φ_2 by setting $q_1 = q_2 = 0$. The inclusion of non-zero values of q_1 and q_2 is fairly straightforward. Moreover, we are interested in superstratum backgrounds with $1 \ll \sqrt{n} \ll \frac{b}{a} \sim \sqrt{N_1 N_5 / j_R}$. This assumption is not necessary for the computation as it was in Section 9.3.3. It simply allows the geometry to have a large cap region ($0 < r < \sqrt{n}a$) which can support the first few modes.

First, we observe that the term proportional to C in (10.3.14) is the core difference between superstratum potential and that of global-AdS₃, (10.2.52). This term is irrelevant as long as $e^{2x} \lesssim n$, or $r \lesssim \sqrt{n}a$, which exactly corresponds to the validity of the cap geometry (10.3.4). Above this transition, there are various possibilities that depend on the values of Ω and P . Before detailing those possibilities, we define three limits of potential

$$\begin{aligned} V^{\text{cap}}(x) &\equiv \frac{e^{2x}}{e^{2x} + 1} \left[(\Delta - 1)^2 - \frac{1}{e^{2x} + 1} \left(\left(\Omega \left(1 + \frac{b^2}{a^2} \right) - P \right)^2 - 1 \right) + e^{-2x} (\Omega + P)^2 \right], \\ V^{\text{BTZ}}(x) &\equiv (\Delta - 1)^2 + \frac{2b^2 P \Omega}{a^2} e^{-2x} - \frac{b^4 n \Omega^2}{a^4} e^{-4x}, \\ V^{\text{I-B}}(x) &\equiv (\Delta - 1)^2 + \frac{2b^2 P \Omega - a^2 \Delta (\Delta - 2)}{a^2} e^{-2x} - \frac{b^4 n \Omega^2}{a^4} e^{-4x}. \end{aligned} \quad (10.3.18)$$

The potential, $V^{\text{cap}}(x)$, is obtained by dropping C , and so:

$$V(x) \sim V^{\text{cap}}(x), \quad e^{2x} \lesssim n. \quad (10.3.19)$$

In the range $|\Omega| \lesssim \frac{2\sqrt{n}a^2}{b^2}$, we will show explicitly in Section 10.4.2 that the superstratum potential will be well approximated by $V^{\text{cap}}(x)$ also when $e^{2x} \gtrsim n$. Intuitively, this is due to the fact that the bump induced by the term proportional to C in (10.3.14) is subleading compared to the other terms in this range of frequency.

In the range $|\Omega| \gtrsim \frac{2\sqrt{n}a^2}{b^2}$, we can perform an expansion of the superstratum potential for $e^{2x} \gtrsim n$ which gives a BTZ-type of potential (10.2.27)

$$V(x) \sim (\Delta - 1)^2 + e^{-2x} [A^2 - B^2 + 1 + C - (\Delta - 1)^2] - e^{-4x} [-B^2 + 1 - (n + 1)C - (\Delta - 1)^2] \quad (10.3.20)$$

By carefully analyzing which terms in the coefficients in front of e^{-2x} and e^{-4x} are leading or subleading at large b/a and n , we can show that

$$\begin{aligned} V(x) &\sim V^{\text{BTZ}}(x), & n \lesssim e^{2x} \text{ and } k = \Omega + P \approx 0, \\ V(x) &\sim V^{\text{I-B}}(x), & n \lesssim e^{2x} \text{ and } k \sim 0. \end{aligned} \quad (10.3.21)$$

The two first potentials in (10.3.18) can be directly derived by computing the wave equations in the smooth cap region (10.3.4) and in the extremal-BTZ region (10.3.5). Thus, $V^{\text{cap}}(x)$ is the scalar potential in a global AdS₃ background given in (10.2.52) with red-shifted momentum and frequency, $\omega = \left(1 + \frac{b^2}{2a^2}\right) \Omega$ and $p = P - \frac{b^2}{2a^2} \Omega$. Similarly, $V^{\text{BTZ}}(x)$ matches the scalar potential in extremal BTZ (10.2.27) with the same red-shifted frequency. However, $V^{\text{I-B}}(x)$, where “I-B” means “intermediate BTZ,” does not correspond to a potential of a specific region in the superstratum background. Thus, according to (10.3.21), the wave perturbation with $k \sim 0$ will feel a potential which differs from the expectation of the BTZ region of the superstratum background.

10.4 Response function for (1,0,n) Superstrata

We are interested in computing the response function in (1,0,n)-superstratum solutions with $1 \ll \sqrt{n} \ll \frac{b}{a} \sim \sqrt{N_1 N_5 / j_R}$ and with $q_1 = q_2 = 0$. For that purpose, we apply the general WKB computation detailed in Section 10.1.3 to a scalar field perturbation to the superstratum background detailed in Section 10.3.

10.4.1 Summary of results

We will show that the response function in momentum space has four distinct regimes depending on Ω and $k = \Omega + P$ depicted in Fig.10.4:

- The cap regime. For small Ω , $|\Omega| \lesssim \frac{2\sqrt{n}a^2}{b^2}$, and at any k , the turning points x_{\pm} are both located inside the cap (10.3.19), so the wave only sees the cap geometry. The response function is given by the response function in Global AdS₃, R^{AdS_3} (10.2.46), with highly red-shifted frequency and momentum.
- The BTZ regime. For large Ω , $|\Omega| \gtrsim \frac{2\sqrt{n}a^2}{b^2}$, and for $k \approx 0$, the outermost turning point is no longer in the cap region and the wave starts to explore the extremal-BTZ region of the geometry. The response function in momentum space is a deformation by $\tan \Theta$ of the response function of extremal-BTZ, R^{BTZ} (10.2.25), as detailed in Section 10.2.2.
- The intermediate BTZ regime. For large Ω , $|\Omega| \gtrsim \frac{2\sqrt{n}a^2}{b^2}$, but for $k \sim 0$, the wave differs from the extremal-BTZ expectation. The response function in momentum space is similar to the one in the BTZ regime but with a “rescaled” momentum \hat{P} which differs from P only when $|\Omega| \lesssim \frac{a}{b}$:

$$\hat{P} \equiv P - \frac{a^2}{2b^2\Omega} \Delta(\Delta - 2). \quad (10.4.1)$$

- The centrifugal barrier regime. When $k\Omega > 0$ and $|k| > \frac{b^2}{a^2}|\Omega|$, the centrifugal barrier at the origin of the space is very high, nothing can penetrate the throat and the potential of the scalar perturbation is always positive. Correspondingly, there are no bound states. When $|\Omega| \lesssim \frac{2\sqrt{n}a^2}{b^2}$, this effect is well captured by the response function in global AdS₃. However, when $|\Omega| \gtrsim \frac{2\sqrt{n}a^2}{b^2}$, the wave is strongly repulsed outside the BTZ throat which is not captured by the BTZ response function. In this specific regime, the response function cannot be computed using the WKB hybrid method. We denote as $R^{\text{bar}}(\Omega, P)$ the response function in this regime.

We will show that in those four regimes we have according to the global-AdS₃ response function, $R^{\text{AdS}_3}(\omega, p)$ (10.2.46), and to the extremal-BTZ response function, $R^{\text{BTZ}}(\omega, p)$ (10.2.25),

$$R^{(1,0,n)}(\Omega, P) \sim \begin{cases} R^{\text{AdS}_3}\left(\frac{b^2\Omega}{2a^2}, P + (1 - \frac{b^2}{2a^2})\Omega\right), & |\Omega| \lesssim \frac{2\sqrt{n}a^2}{b^2}, \\ \text{Re} \left[R^{\text{BTZ}}\left(\frac{b^2\Omega}{2a^2}, \hat{P}\right) \right] + \text{sign}(\Omega) \tan \Theta \text{Im} \left[R^{\text{BTZ}}\left(\frac{b^2\Omega}{2a^2}, \hat{P}\right) \right], & \frac{2\sqrt{n}a^2}{b^2} \lesssim |\Omega|, P \sim \Omega, \\ \text{Re} \left[R^{\text{BTZ}}\left(\frac{b^2\Omega}{2a^2}, P\right) \right] + \text{sign}(\Omega) \tan \Theta \text{Im} \left[R^{\text{BTZ}}\left(\frac{b^2\Omega}{2a^2}, P\right) \right], & \frac{2\sqrt{n}a^2}{b^2} \lesssim |\Omega|, P \approx \Omega, \\ R^{\text{bar}}(\Omega, P), & \frac{2\sqrt{n}a^2}{b^2} \lesssim |\Omega|, \Omega k > 0, |k| > \frac{b^2|\Omega|}{a^2}. \end{cases} \quad (10.4.2)$$

The $\tan \Theta$ term which captures the microstate structure of the geometry when $\frac{2\sqrt{n}a^2}{b^2} \lesssim |\Omega|$ is given by the IR cap geometry. We will show that

$$\Theta \sim \frac{\pi}{2} [|\gamma\Omega - P| - \delta|\Omega + P| - \eta], \quad \frac{2\sqrt{n}a^2}{b^2} \lesssim |\Omega|, \quad (10.4.3)$$

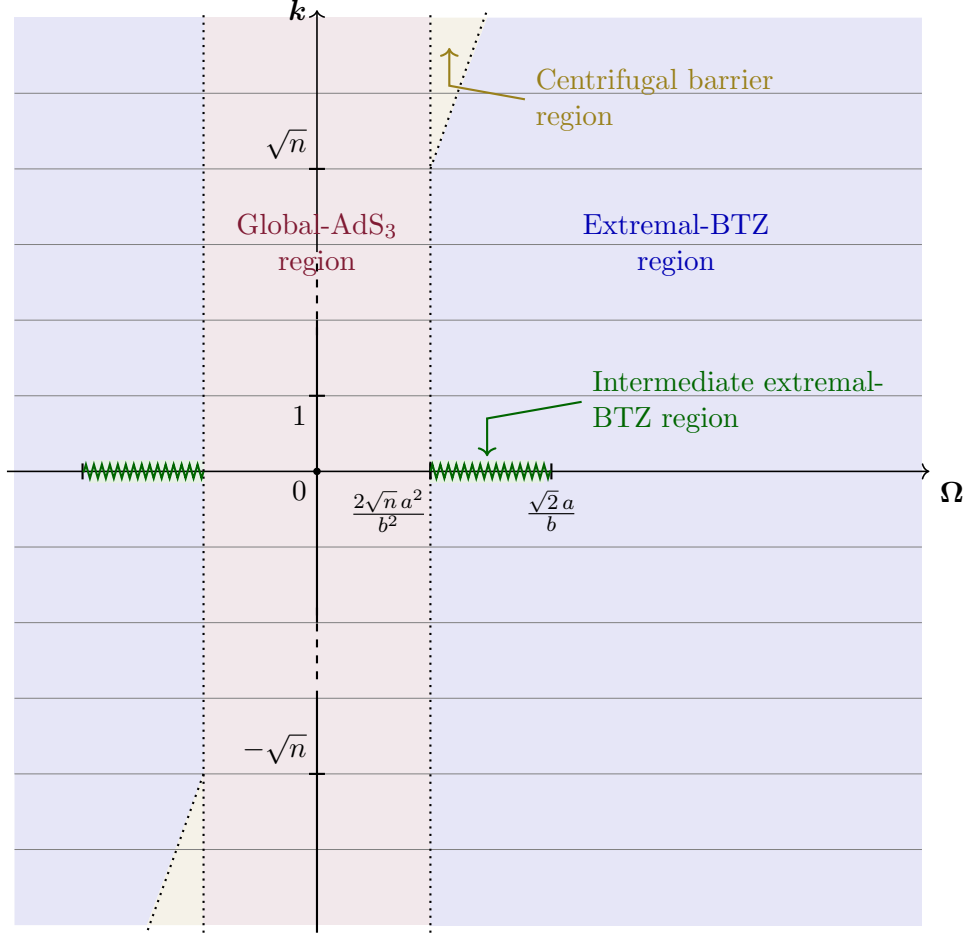


Figure 10.4: The four regimes for the $(1,0,n)$ -superstratum response function as a function of Ω and $k = \Omega + P$. For very small Ω , the wave goes far inside the throat and is essentially determined by the global- AdS_3 geometry at the cap. For larger frequencies, the wave starts to explore the extremal-BTZ region. The value of k changes only the centrifugal barrier felt very close to the origin. However, the value $k \sim 0$ yields to a third domain called “intermediate” extremal-BTZ (see subsection 10.4.4).

with $\gamma \sim b^2/a^2$, $\delta \sim 1$ and $\eta \sim |\Delta - 1|$. This is very close to the same spectrum function which is included inside $R^{\text{AdS}_3}(\frac{2a^2\Omega}{b^2}, P + (1 - \frac{b^2}{2a^2})\Omega)$ when $|\Omega| \lesssim \frac{2\sqrt{n}a^2}{b^2}$ and which can be derived from (10.2.59)

$$\Theta \sim \frac{\pi}{2} \left[\left| \left(\frac{b^2}{a^2} + 1 \right) \Omega - P \right| - |\Omega + P| - |\Delta - 1| \right], \quad |\Omega| \lesssim \frac{2\sqrt{n}a^2}{b^2} \quad (10.4.4)$$

In the next subsections, we will show how to obtain the first three lines of (10.4.2) using the hybrid WKB technique detailed in Section 10.1.3, and from (10.1.15) in particular. The only quantity which will not be computable with WKB is $R^{\text{bar}}(\Omega, P)$.

The expression for the response function of the Superstratum, (10.4.2), strongly reflects the intuitive physical picture of the Superstratum. There is an AdS cap at a very high red-shift relative to infinity. Thus the modes that explore the bottom of the throat produce a response function that looks like that of global AdS_3 but with highly blue-shifted modes relative to the frequencies at infinity. The AdS cap is connected to the asymptotic region at infinity by a long BTZ throat, and modes that explore this throat have a response function that is modulated by the BTZ response function.

In this way one will see what appears to be “absorptive behaviour” of the BTZ throat over short time scales, while over long time-scales one will see strong echoes from the cap, in agreement with unitarity requirements. Because of the explicit appearance of the BTZ response function, the Superstratum will also contain information about the left temperature of the extremal BTZ metric. This temperature governs the decay of the response function over time-scales much less than the echo return-time. We will discuss the position-space response functions in more detail in Section 10.5.

The remaining part, $R^{\text{bar}}(\Omega, P)$, of the response function is perhaps rather less interesting because the probe has so much energy and angular momentum that it simply cannot penetrate the throat of the Superstratum.

Finally we note that the response function has poles in the real (Ω, P) -plane. They appear through R^{AdS_3} and through $\tan \Theta$ in (10.4.2) and simply represent the bound states of the cap. Indeed, because of (10.4.3), these bound states are almost identical to those of a global AdS_3 . As explained in the introduction, the Superstratum cannot have quasi-normal modes. On the other hand, the BTZ response function, (10.2.25), has poles along the imaginary P -axis and these do indeed correspond to quasi-normal modes. The important point is that even though (10.4.2) involves the BTZ response function, the poles are specifically excluded because the approximation we made is only valid in the *real* (Ω, P) -plane. Thus the BTZ response function merely modulates the amplitude of the response function and does not (and cannot) introduce imaginary poles.

10.4.2 The cap regime

We consider that $|\Omega| \lesssim \frac{2\sqrt{n}a^2}{b^2}$. The graph in Fig.10.5 shows the superstratum potential $V(x)$ and the cap potential $V^{\text{cap}}(x)$ as a function of x for $\Omega = \frac{\sqrt{n}a^2}{2b^2}$, $\Delta = 5$ and $k = 1$. From the figure, the potentials look very close to each other. More rigorously, we have

$$\delta V(x) \equiv \left| \frac{V(x) - V_{\text{cap}}(x)}{V_{\text{cap}}(x)} \right| \lesssim \left(\frac{b^2 \Omega}{a^2(\Delta - 1)} \right)^2 (1 + e^{-2x})^{-n-2} e^{-2x}, \quad x \approx x_{\pm}. \quad (10.4.5)$$

Consequently, for $|\Omega| \lesssim \frac{2\sqrt{n}a^2}{b^2}$ and Δ large, we have $V(x) \sim V_{\text{cap}}(x)$ for any x . Moreover, $V_{\text{cap}}(x)$ is simply the potential of a scalar wave in a red-shifted global AdS_3 geometry as explained in the previous section. Thus one can reproduce the results of the Sections 10.2.3.1 and 10.2.3, where we have computed the WKB response function in a global AdS_3 background and where we have compared it to the exact function. The WKB computation can be applied only if the potential has classical turning points which is guaranteed for global AdS_3 when (10.2.53) is satisfied. For our red-shifted AdS_3 cap, this translates into the condition that $k\Omega > 0$ and $|k| > \frac{b^2|\Omega|}{a^2}$. Moreover, the WKB approximation has been shown to be accurate for values of Δ of order at least slightly higher than one and for $|\omega - p| = |(\frac{2b^2}{a^2} - 1)\Omega - P| \gg 1$. Thus, under all those assumptions and for $\frac{a^2}{b^2} \ll |\Omega| \lesssim \frac{2\sqrt{n}a^2}{b^2}$, the $(1,0,n)$ -superstratum response function is given by

$$R^{(1,0,n)}(\Omega, P) \sim R^{\text{AdS}_3} \left(\frac{2a^2 \Omega}{b^2}, P + \left(1 - \frac{b^2}{2a^2} \right) \Omega \right), \quad (10.4.6)$$

where $R^{\text{AdS}_3}(\omega, p)$ is given by (10.2.46).

One can actually relax the assumptions of validity of this expression. According to (10.4.5), one should have $|\Omega| \lesssim \frac{2\sqrt{n}a^2}{b^2}$ and Δ large so as to have $\delta V(x)$ small. The additional requirement that $|(\frac{2b^2}{a^2} - 1)\Omega - P| \gg 1$ is only necessary for the WKB approximation. Indeed, for $|(\frac{2b^2}{a^2} - 1)\Omega - P| \lesssim 1$, the $(1,0,n)$ -superstratum potential is even more closely approximated by the cap potential according to (10.4.5), and the identification (10.4.6) is thus even more accurate. Thus we have established the first line of (10.4.2).

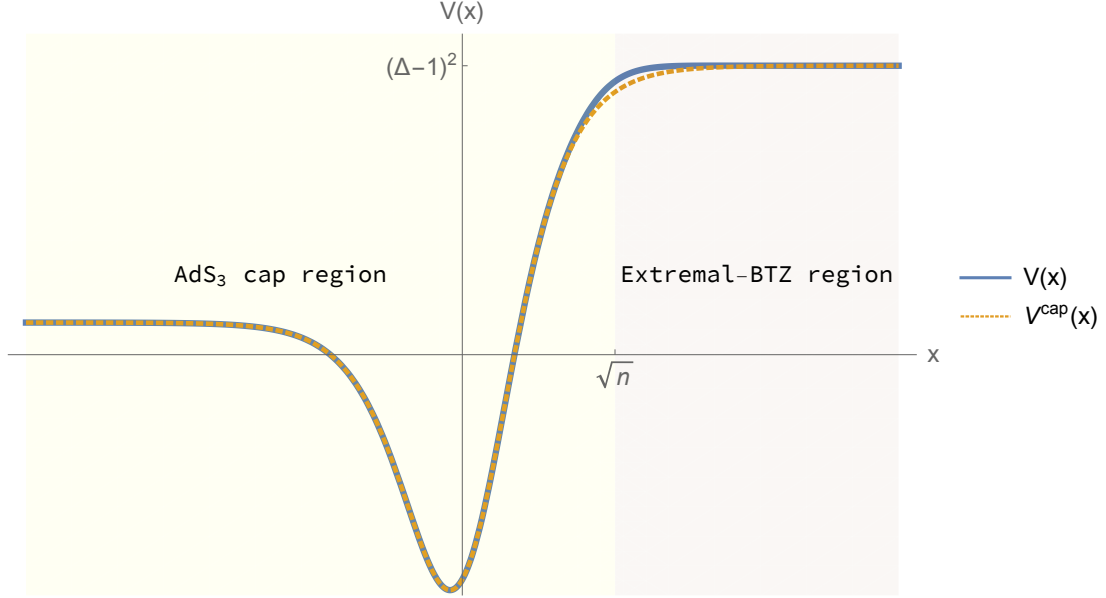


Figure 10.5: *The cap regime*: The superstratum potential $V(x)$ and the approximated potential $V^{\text{cap}}(x)$ when $|\Omega| \lesssim \frac{2\sqrt{n}a^2}{b^2}$.

For small frequencies, the response function is determined by the red-shifted global AdS_3 geometry at the cap. The spectrum of the normalizable modes is given by the real poles in (10.4.6) which corresponds to the spectrum of a highly red-shifted global AdS_3 . This is valid so long as $|\Omega| \lesssim \frac{2\sqrt{n}a^2}{b^2}$, which corresponds to the \sqrt{n} first modes. For higher frequencies, the scalar wave starts to explore the BTZ region of the geometry and then the response function will differ from the global- AdS_3 expectation as we will discuss in the next sections.

10.4.3 The extremal-BTZ regime

We assume that $\frac{2\sqrt{n}a^2}{b^2} \lesssim |\Omega|$ and that $P \approx \Omega$. As depicted in Fig.10.6, one can show that x_+ is therefore in the extremal-BTZ region, $x_+ \gtrsim \sqrt{n}$. One can then use all the machinery developed in Section 10.2 by considering $V_{\text{BTZ}}(x)$ as the asymptotic potential “ $V_{\text{asympt}}(x)$ ”. Moreover, $V_{\text{BTZ}}(x)$ corresponds to the potential one can compute in an extremal-BTZ black hole (10.2.18) at the left temperature $T_R = \frac{\sqrt{n}}{2\pi}$ and with a highly red-shifted coordinate u . One can apply the computation in Section 10.2.2.2 with $\omega = \frac{b^2}{2a^2} \Omega \sim N_1 N_5 \Omega / j_R$, $p = P$, $r_H = \sqrt{n}$ and $\mathcal{A} = \tan \Theta$ where Θ is defined in (10.1.18). The final result for the response function (10.1.20) gives

$$R^{(1,0,n)}(\Omega, P) \sim \text{Re} \left[R^{\text{BTZ}} \left(\frac{b^2 \Omega}{2a^2}, P \right) \right] + \text{sign}(\Omega) \tan \Theta \text{Im} \left[R^{\text{BTZ}} \left(\frac{b^2 \Omega}{2a^2}, P \right) \right], \quad (10.4.7)$$

where $R^{\text{BTZ}}(\omega, p)$ is the response function in momentum space of a scalar field in an extremal-BTZ black hole (10.2.25).

This expression shows how the superstratum response function matches the overall shape of the BTZ response function but with a deformation term, $\tan \Theta$. In the cap regime, $|\Omega| \lesssim \frac{2\sqrt{n}a^2}{b^2}$, Θ is given by (10.4.4). For $\frac{2\sqrt{n}a^2}{b^2} \lesssim |\Omega|$, finding an analytic expression for Θ is a harder task since the superstratum potential is no longer well approximated by $V_{\text{cap}}(x)$ or by any other explicitly integrable potential between the two turning point since $x_+ \gtrsim \sqrt{n}$. We therefore performed a numerical computation of Θ . Surprisingly, Θ is almost linear as a function of Ω and P as in the global- AdS_3 regime (see Fig.10.7 as

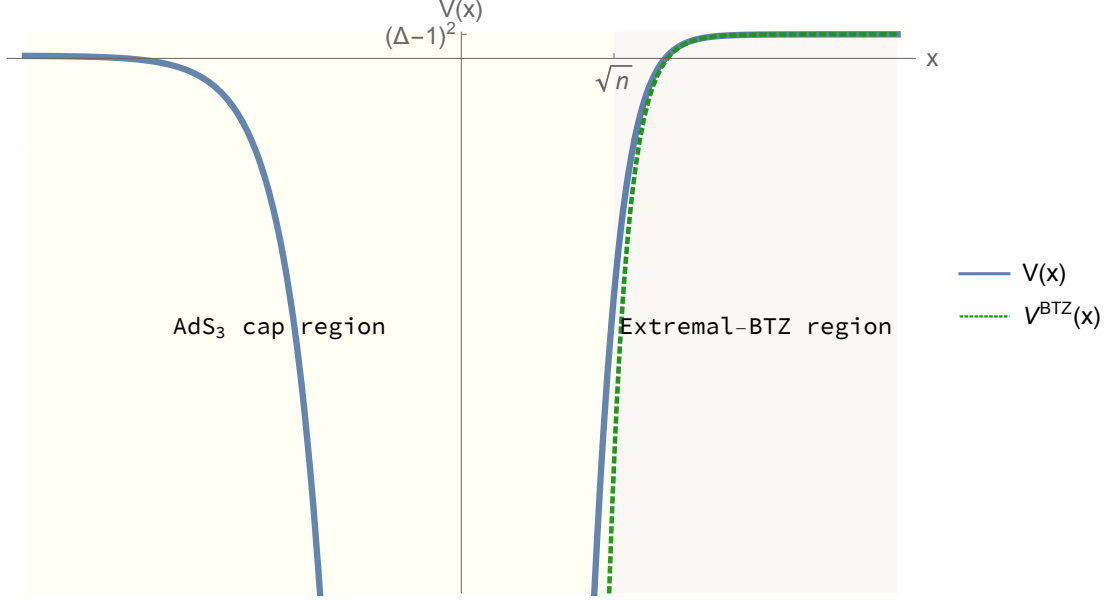


Figure 10.6: *The extremal-BTZ regime:* the superstratum potential $V(x)$ and the approximated potential $V^{\text{BTZ}}(x)$ when $\frac{2\sqrt{n}a^2}{b^2} \lesssim |\Omega|$ and $P \approx \Omega$.

an illustration). Moreover, this behaviour is similar to (10.4.4) with slightly different coefficients

$$\Theta \sim \frac{\pi}{2} [|\gamma\Omega - P| - \delta|\Omega + P| - \eta], \quad (10.4.8)$$

with $\gamma \sim \frac{b^2}{a^2}$, $\delta \sim 1$ and $\eta \sim |\Delta - 1|$. The spectrum of the $(1,0,n)$ -superstratum states is then very close to a linear function of Ω and P , even when the modes start to explore the BTZ throat. We can expect from those evenly spaced poles in the spectrum that the response function in position space will be periodic and not sporadic. This difference comes from the highly coherent nature of $(1,0,n)$ Superstrata which we will comment in more details in Section 10.6.

10.4.4 The intermediate extremal-BTZ regime

When $P \sim \Omega$ and $\frac{2\sqrt{n}a^2}{b^2} \lesssim \Omega$, the superstratum potential is not well approximated anymore by the BTZ potential since the term $a^2\Delta(\Delta - 2)$ is not subleading compared to $2b^2P\Omega$ as long as $|\Omega| \lesssim \frac{a}{b}$. We must then consider the “intermediate” extremal-BTZ potential $V^{\text{I-B}}(x)$ defined in (10.3.18). We use “intermediate” since a rescaling $\hat{P} \equiv P + \frac{a^2}{2b^2\Omega} \Delta(\Delta - 2)$ converts $V^{\text{I-B}}(x)$ to the BTZ potential, $V^{\text{BTZ}}(x)$, with \hat{P} instead of P . Thus, we can extrapolate easily the WKB computation of the previous section. For $\frac{2\sqrt{n}a^2}{b^2} \lesssim |\Omega|$ with $P \sim \Omega$, the response function is

$$R^{(1,0,n)}(\Omega, P) \sim \text{Re} \left[R^{\text{BTZ}} \left(\frac{b^2 \Omega}{2a^2}, \hat{P} \right) \right] + \text{sign}(\Omega) \tan \Theta \text{Im} \left[R^{\text{BTZ}} \left(\frac{b^2 \Omega}{2a^2}, \hat{P} \right) \right], \quad (10.4.9)$$

where Θ is still of the form of (10.4.8) in this regime of parameters. It is only when $\frac{a}{b} \lesssim \Omega$ that $\hat{P} \sim P$ and that superstratum response function can fully match the BTZ expectation as in previous section. Thus, our computation indicates an intermediate scale in momentum space, $\frac{a}{b} \sim \sqrt{N_1 N_5 / j_R}$, from where the superstratum response function starts to slightly differ from the BTZ expectation. This scale in position space is $t \sim \frac{b}{a} R_y$. The superstratum response function will slightly differ from the BTZ response function at $t \sim \frac{b}{a} R_y$ which is an order of magnitude below the usual scale $t \sim \frac{b^2}{a^2} R_y$ for generic black hole microstate.

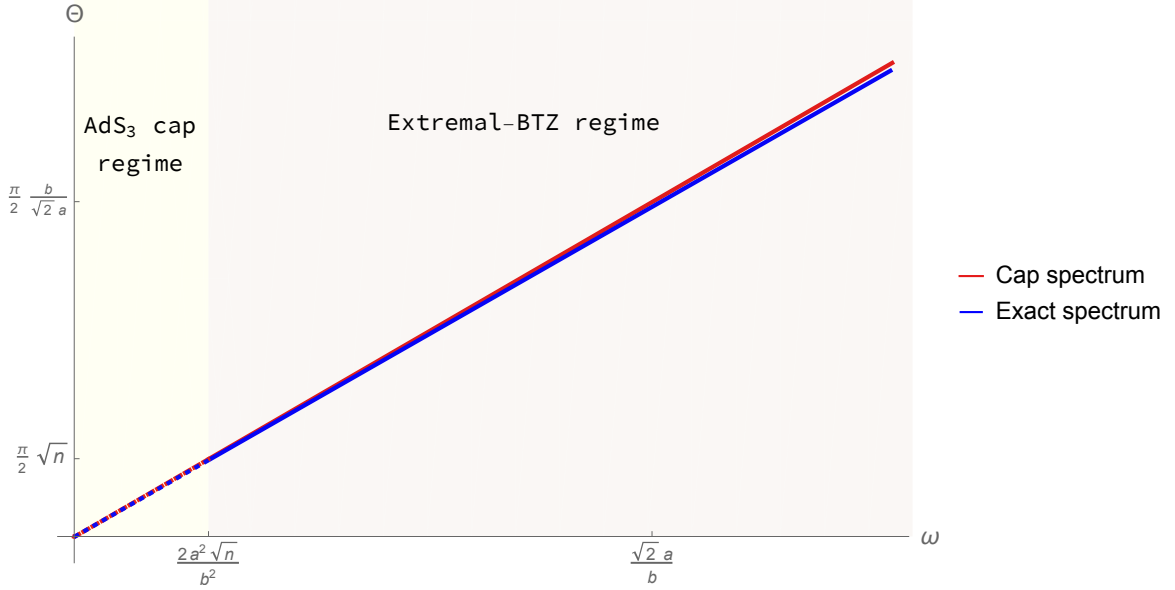


Figure 10.7: The spectrum function determined by the WKB function Θ (10.1.18) as a function of Ω . The graph in blue corresponds to the numerical value of Θ with the full $(1,0,n)$ -superstratum potential (10.3.14). The graph in red corresponds to the cap spectrum given by (10.4.4). The graphs have been computed for $\Delta = 3$, $k = 1$, $a = 1$, $b = 2 \cdot 10^3$ and $n = 750$ but different parameters give the same behaviours.

In [117, 118], geodesic motions of probe particles in capped BTZ background have been studied. The authors showed that a particle dropped from right outside the throat will suffer Planck-scale tidal forces at a distance $r \lesssim \sqrt{ab}$, way above the cap region. However, a similar computation in an extremal-BTZ geometry gives a constant and small tidal stress. The radial scale for a classical particle and our frequency scale for a scalar wave can be related by the usual lore that a classical particle lies where the potential of the wave equals the energy (on-shell condition). This corresponds to the radial distance where the potential vanishes in our convention and to the classical turning points. In the present regime of parameters, the turning point, x_+ is given by the intermediate-BTZ potential. From the result (10.2.28), the turning point in the x coordinate, $e^x = r/a$,

$$x_+ = \frac{1}{2} \ln \left[\frac{b^2}{a^2(\Delta-1)^2} \left(|\Omega| \sqrt{\hat{P}^2 + n(\Delta-1)^2} - \Omega \hat{P} \right) \right]. \quad (10.4.10)$$

Thus, for $P \sim \Omega \sim \frac{a}{b}$ we have

$$x_+ \sim \frac{1}{2} \ln \left[\frac{b}{a} \right] \quad \Rightarrow \quad r_+ \sim \sqrt{ab} \quad (10.4.11)$$

The frequency scale where the scalar waves start to differ from the extremal-BTZ expectation matches the radial scale where the tidal stresses of classical infalling particles reach the Planck scale.

10.4.5 The centrifugal-barrier regime

The WKB hybrid computation requires the existence of at least one turning point. Our attempts to extend the technique to strictly positive potentials have either failed or been inaccurate. When the potential is always positive, there is no classically allowed region and the scalar waves are either growing or decaying. The physical waves which are smooth at $x \sim -\infty$ are then necessarily growing at the boundary. As explained in Section 10.1.2.1, the WKB approximation is inefficient to extract the

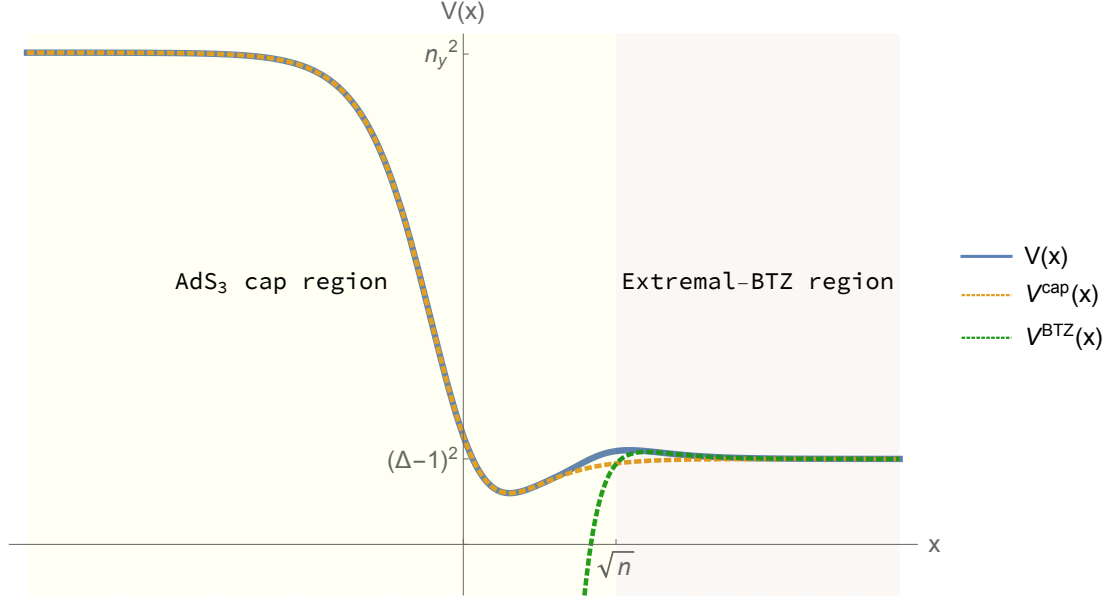


Figure 10.8: *The centrifugal-barrier regime*: the superstratum potential $V(x)$ and the approximated potential $V^{\text{BTZ}}(x)$ when $\frac{2\sqrt{n}a^2}{b^2} \lesssim |\Omega|$, $k\Omega > 0$ and $|k| > \frac{b^2|\Omega|}{a^2}$.

vev part from an only growing wave function. Moreover, this does not mean that the response function is zero. As an illustration, the scalar wave equation in global- AdS_3 has a range of frequencies and momenta where the potential is strictly positive (10.2.53). However, from a straightforward computation, the response function, (10.2.46), is not zero or even close to zero in this regime. Nevertheless, the momentum space response function has no poles in this regime.

The superstratum potential, (10.3.14), has no classical turning point when the centrifugal barrier at the origin given by A is larger than the penetration parameter given by B . A straightforward analysis shows that the potential has a large centrifugal barrier and is strictly positive when

$$k\Omega > 0 \quad \text{and} \quad |k| > \frac{b^2|\Omega|}{a^2}.$$

For small values of Ω , we have shown that the superstratum potential is well-approximated by the global- AdS_3 cap potential. Thus, the centrifugal-barrier regime is taken into account by the identification of the superstratum response function to the AdS_3 cap response function (10.4.6).

The issue occurs for large Ω , $\frac{2\sqrt{n}a^2}{b^2} \lesssim |\Omega|$, in the BTZ regime. The superstratum potential is no longer well-approximated by the cap potential and one cannot apply our WKB hybrid method to extract the response function from the asymptotic BTZ potential. As an illustration, the Figure 10.8 gives the behavior of the potentials in this regime.

However, we have good intuition that the response function in this regime does not have a significant impact on the physics of wave perturbations in superstratum backgrounds for different reasons. First, in momentum space, the relevant information is contained in the pole structure of the response function, particularly in their locations and in their envelopes. The centrifugal-barrier regime is essentially characterized by the absence of normalizable modes, i.e. the absence of poles. Thus, it will only reduce the expected zone where normalizable modes exist. Second, this regime corresponds to very high momentum k and has a small size in the two-dimensional momentum space given by k and Ω (Fir.10.4). Indeed, it is delimited by $|\Omega| \gtrsim \frac{2\sqrt{n}a^2}{b^2} \sim \frac{\sqrt{n}j_R}{N_1N_5}$ and by the sharp line $|k| > \frac{b^2|\Omega|}{a^2} \sim \frac{N_1N_5}{j_R}|\Omega|$.

Consequently, we neglect the response function in this regime and have good hope that it does not compromise the overall understanding of the response function in $(1,0,n)$ Superstratum.

In the next section, we will discuss the Fourier transform of the response function to position-space.

10.5 Position-space Green functions

We now return to our original goal of assessing to what extent the $(1, 0, n)$ Superstratum differs from the full black hole ensemble it is part of. While the calculations performed above are most natural in momentum space, an observer probing the microstate geometry from far away will be more interested in position space results.

There are many choices of correlation functions in a Lorentzian field theory, including the Feynman, Wightman, Advanced and Retarded propagators. These represent distinct physical quantities and are obtained by choosing different time orderings in position space, or by integrating in a particular way around poles of the momentum space propagator. To clarify the different two-point functions, we have examined in the Appendix two well-understood examples in some detail: global AdS (Appendix A.13.1) and extremal BTZ (Appendix A.13.2). In this section, we study the properties position space propagator in the superstratum background.

10.5.1 Position space Green function in $(1,0,n)$ Superstrata

The momentum space analysis of the superstratum two-point function leads to a rather unwieldy result (10.4.2), which makes the Fourier transform back to position space cumbersome. In this section, we sketch the overall profile of the Green function in position space.

There are three relevant time scales. We will argue that for time shorter than $\frac{b R_y}{a} \sim \sqrt{N_1 N_5} R_y$, the propagator is dominated by the extremal-BTZ response. Beyond that time, up to times of order $\frac{b^2 R_y}{\sqrt{n} a^2} \sim N_1 N_5 R_y / \sqrt{n}$, the correction from the intermediate regime will change the position space propagator away from the extremal BTZ expectation. Finally, at a time of order $\frac{b^2 R_y}{a^2} \sim N_1 N_5 R_y$ the discrete energy spectrum will become significant and will lead to slightly-deformed echoes from the cap.

First, let us argue that the contribution from $\tan \Theta$ to the extremal-BTZ response does not drastically alter the propagator at short time scales. We will model the full propagator in momentum space as $R^{\text{BTZ}}(\Omega, P) \cdot \tilde{g}(\Omega, P)$ ⁹, where \tilde{g} encodes the modulation from $\tan \Theta$. If the spectrum was perfectly linear, we could choose $\tilde{g}(\Omega, P) = \tan(\frac{b^2 \Omega}{a^2} \pm P)$. The position space propagator is then given by the convolution

$$G(u, v) = \int \frac{d\lambda d\kappa}{(2\pi)^2} R^{\text{BTZ}}(\lambda, \kappa) g(u - \lambda, v - \kappa) , \quad (10.5.1)$$

$$g(u, v) \propto \delta\left(\frac{b^2}{a^2} v \mp u\right) \sum_m \delta\left(u + \frac{2b^2}{a^2} m R_y\right) , \quad (10.5.2)$$

where g is the formal inverse Fourier transform of $\tan(\frac{b^2 \Omega}{a^2} \pm P)$. This implies that the position space propagator is periodic in the direction orthogonal to $u \mp \frac{a^2}{b^2} v$, repeating itself whenever u increases with $\frac{2b^2}{a^2} R_y$, or equivalently after t increases with $\frac{b^2}{a^2} \pm 1$ in that direction. After that time, the response is a perfect echo of the extremal BTZ answer. This was under the assumption that the energy spectrum is perfectly linear. Since the superstratum spectrum is slightly anharmonic, the consecutive echoes will instead be slightly more deformed and attenuated. This is represented by the large peak at $t \sim b^2/a^2$ in Figure 10.9.

⁹One should consider the imaginary part of R^{BTZ} . However, the Fourier transform of the imaginary part can be obtained from the Fourier transform of the function and its conjugate. One can then consider R^{BTZ} only for the ease of the discussion.

According to the second line of (10.4.2), the response is not really that of extremal BTZ, but rather with the replacement $P \rightarrow \hat{P} = P - \frac{a^2 \Delta(\Delta-2)}{b^2 \Omega}$. In the Fourier transform to position space, we can change basis to get

$$\int \frac{d\Omega d\hat{P}}{(2\pi)^2} e^{-i(\Omega u + \hat{P}v)/R_y} e^{-\frac{ia^2 \Delta(\Delta-2)v}{b^2 \Omega}} R^{\text{BTZ}}(\Omega, \hat{P}) . \quad (10.5.3)$$

Using the expression (10.2.25) for the momentum space BTZ propagator, this integral separates into the integral over \hat{P} , which is unaltered, and the integral over Ω

$$\int \frac{d\Omega}{2\pi} e^{-i\Omega u/R_y} e^{-\frac{ia^2 \Delta(\Delta-2)v}{b^2 R_y \Omega}} (-i\Omega)^{\Delta-1} = \left(\frac{-i b^2 u}{a^2 \Delta(\Delta-2)v} \right)^{-\Delta/2} J_{-\Delta} \left(2\sqrt{\frac{ia^2 \Delta(\Delta-2)v u}{b^2 R_y^2}} \right) , \quad (10.5.4)$$

where $J_{-\Delta}$ is the Bessel function of the first kind.¹⁰ When we expand it for small values of $v u$, we find

$$\frac{1}{\Gamma(1+\Delta)} \left(\frac{-u}{R_y} \right)^{-\Delta} \left(1 + \frac{ia^2 \Delta(\Delta-2)v u}{(1-\Delta)b^2 R_y^2} + \mathcal{O}(\frac{a^2 u v}{b^2})^2 \right) , \quad (10.5.6)$$

which follows the behavior of the extremal BTZ black hole up to time scales where $v u \sim \frac{b^2}{a^2} R_y^2$. This deviation first becomes significant at times of order $t = \frac{b}{a} R_y$, as depicted by the blue and red lines in Figure 10.9.

Finally, the response (10.4.2) differs from the extremal-BTZ response whenever $|\Omega| \lesssim \frac{\sqrt{n} a^2}{b^2}$. We can model this in two steps. First the momentum-space BTZ propagator is multiplied by a high-pass filter such as $\tilde{g}(\Omega, P) = \theta(\Omega - \frac{\sqrt{n} a^2}{b^2}) + \theta(-\Omega - \frac{\sqrt{n} a^2}{b^2})$. Second, we add the AdS₃ regime of (10.4.2). The first step is to apply (10.5.1) again, but with

$$g(u, v) = (2\pi)^2 \delta(u) \delta(v) - \frac{2}{u} \sin \left(\frac{\sqrt{n} a^2 u}{b^2} \right) \delta(v) . \quad (10.5.7)$$

The second function is very spread out, but it is also suppressed by $n^{1/4} a/b$. Its effect is suppressed by $1/\sqrt{N_1 N_5}$. To add the AdS₃ regime, we add the position space AdS₃ propagator with a low-pass filter $\tilde{g} = \theta(\Omega + \frac{\sqrt{n} a^2}{b^2}) - \theta(\Omega - \frac{\sqrt{n} a^2}{b^2})$, the Fourier transform of which is just the second term of (10.5.7). All in all, the position space propagator obtained by replacing the BTZ propagator with the AdS₃ propagator for energies $|\Omega| \lesssim \frac{\sqrt{n} a^2}{b^2}$ is

$$R^{\text{BTZ}}(u, v) + \frac{1}{\pi u} \int \frac{d\lambda}{2\pi} \left(R^{\text{AdS}}(\lambda, v) - R^{\text{BTZ}}(\lambda, v) \right) \sin \left(\frac{\sqrt{n} a^2 (u - \lambda)}{b^2} \right) . \quad (10.5.8)$$

The AdS₃ response function has the same poles as the $\tan \Theta$ term, and hence will contribute to the recurrences (10.5.2).

Notice that R^{BTZ} decays like $\exp(-\frac{\Delta r_H}{R_y} v)$ as long as $v \lesssim R_y/2$,¹¹ whereas the second term in (10.5.8) is of order $n^{1/4} a/b (v/R_y)^{-\Delta}$. This is significant, because it means that the second term is comparable to the first at high temperatures

$$r_H = \sqrt{n} \sim \frac{1}{\Delta} \log \left(\frac{b^2}{\sqrt{n} a^2} \right) . \quad (10.5.9)$$

¹⁰This identity follows from the integral representation of the Bessel function,

$$J_m(x) = \frac{1}{2\pi} \int_{-\pi}^{\pi} d\tau e^{ix \sin \tau - im\tau} , \quad \Omega = i\sqrt{\frac{a^2 \Delta(\Delta-2)v}{b^2 u}} e^{i\tau} . \quad (10.5.5)$$

The $i\epsilon$ -prescription used for the purpose of this illustration is therefore $-i\Omega \rightarrow -i\Omega + \text{sign}(u)\epsilon$.

¹¹This is where, for large values of r_H , the first image in Figure A.10 takes over. For small values of r_H , the exponential decay lasts as long as $\frac{r_H}{R_y} v \ll 1$, but in this regime, it does not become parametrically small.

For the superstratum geometry to accurately imitate a black hole at least at times of the order R_y , the temperature must be small enough that the second contribution in (10.5.8) is negligible. This requires $\Delta\sqrt{n} \ll \log(b^2/(\sqrt{n}a^2))$.

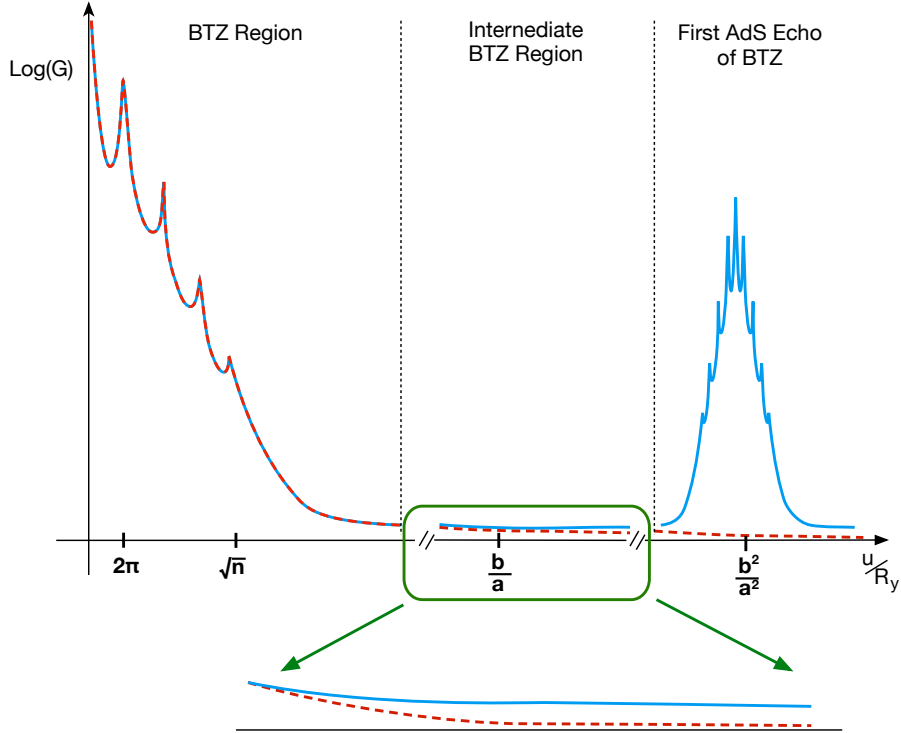


Figure 10.9: Schematic description of the $(1, 0, n)$ -superstratum Green’s function in position space (continuous line in blue) and its comparison to the extremal BTZ Green’s function (dashed line in red). At early times of order R_y , the behavior is very similar to that in Figure A.10, with polynomial fall off briefly interrupted by singularities at every $\Delta u = 2\pi R_y$ from the light-cone wrapping around the y -direction. (The singularities are cut off in the picture to clarify their relative weight.) At times of order $b R_y/a$, the behavior of the superstratum two-point function starts to deviate from that of extremal BTZ, following (10.5.6). Finally, at times of order $b^2 R_y/a^2$, the superstratum Green’s function features its first significant echo which is absent in BTZ. It is a slightly attenuated and deformed copy of the singularity around $u \approx 0$. Ever less significant echos will follow at times equal to integer multiples of $b^2 R_y/a^2$.

10.6 Final comment

This chapter contains the first computation of a correlator of two light operators in a geometry that has the same asymptotic region and the same throat as an extremal BTZ black hole, but differs from it at the scale of the horizon.

All the HHLL correlators that have been so far computed in the bulk [201, 202, 194, 203, 204] involve heavy states that are quite far away from the heavy states that one expects to contribute to the entropy of the BTZ black hole. In “microstate geometry” language, the geometries dual to these states have shallow throats that do not contain the AdS_2 very-near-horizon geometry characteristic of BTZ black holes. In contrast, the geometries dual to heavy states we consider have an arbitrarily long AdS_2 throat, and only differ from the BTZ black hole arbitrarily close to the horizon. This can also be

seen from the fact that the mass gap of these geometries is the same as the mass gap of the typical momentum-carrying states of the D1-D5 CFT.

Hence, one expects the HHLL four-point function we compute in the bulk to display thermal behavior for times smaller than the inverse mass gap, and thus to match the four-point function computed when the heavy state is taken to be the thermal state (dual in the bulk to the BTZ black hole). However, for longer times one expects to see non-thermal effects. Note that this expectation was first spelled out in the CFT, where it was argued that HHLL four-point function computed using typical heavy states are expected to differ at late times from the four-point functions computed using the thermal state. Our calculation confirms this from the bulk perspective, and moreover shows that this late-time non-thermal behavior happens exactly because the geometries dual in the bulk to typical low-mass-gap CFT states differ from the BTZ black hole at the scale of the horizon.

Seeing thermal behavior in the absence of a horizon appears to be quite counterintuitive, especially in light of the intuition that thermalization comes from absorption of stuff by the black hole and the common conceit that only solutions with a horizon can describe typical black hole microstates. Our result shows that the horizonless microstate geometries with long AdS_2 throats give rise, at short times, to exactly the same thermal behavior one finds in the black hole solution, while avoiding the information-loss problems associated to the presence of a horizon and restoring the information after long times.

This being said, the supergravity solutions that we use to compute HHLL correlators are quite far from the most generic horizonless supergravity solutions one can construct, and hence the late-time behavior of their correlators, while consistent with information recovery, is also not generic. Indeed, we have found that after times of order the central charge, $N_1 N_5$, the two-point function “comes back from the grave” to a value that is just a tiny bit smaller than its starting value, then decays thermally again, then comes back from the grave to a tiny smaller value, then decays again, etc.

It would be very interesting to try to extend our calculations to more generic superstrata, and to see whether one can obtain a behavior at long times that approximates closer thermal behavior. Unfortunately, the metric and fields of the most generic superstratum solutions are complicated functions of five variables! And while this represents a big achievement for the microstate geometry programme, computing holographic in such cohomogeneity-five solutions is way beyond the current analytical and numerical technology (even finding solutions to the wave equation is hard). The solutions we use are much simpler single-mode $(1, 0, n)$ superstrata, in which the wave equation is separable, and one can compute two-point functions without resorting to heavy numerics. As we have seen in the paper, even to compute two-point functions in our geometries we had to develop a new hybrid-WKB technology. To repeat our calculation for more complicated superstrata one would need to extend this hybrid-WKB technology to functions of two or more variables, which appears quite challenging.

Aside from the study of microstate geometries, the hybrid-WKB technology we have constructed will have applications in other areas of holography, as it is the only technique that can be used to compute holographic correlation functions in backgrounds where the wave equation is not solvable analytically.

Appendix

A.1 Integration in \mathbb{R}^3

We use the spherical coordinates (ρ, ϑ, ϕ) of \mathbb{R}^3 . We consider that there are n centers determined by a coordinate a_j on the z axis. The shifted spherical coordinates around the j^{th} center, $(\rho_j, \vartheta_j, \phi)$, are given by

$$\rho_j = \sqrt{\rho^2 + a_i^2 - 2\rho a_i \cos \vartheta} \quad \vartheta_j = \arccos\left(\frac{\rho \cos \vartheta - a_j}{\rho_j}\right). \quad (\text{A.1.1})$$

In this section, we give the mathematical library of solutions of the following equations

$$\begin{aligned} d_3 f^{(a)} + \star_3 d_3 t^{(a)} &= s^{(a)}, \\ \star_3 d_3 T^{(a)} &= S^{(a)}, \end{aligned} \quad (\text{A.1.2})$$

where $s^{(a)}$ and $S^{(a)}$ are source terms, $(f^{(a)}, t^{(a)})$ are a couple of a scalar and a one-form and $T^{(a)}$ is a one-form. We consider the following sources:

$$\begin{aligned} S^{(0)} &\equiv d_3 \left(\frac{1}{\rho} \right), \quad s_j^{(1)} = S_j^{(1)} \equiv d_3 \left(\frac{1}{\rho_j} \right), \quad S_j^{(2)} \equiv \frac{a_j}{\rho} d_3 \left(\frac{1}{\rho_j} \right) - \frac{a_j}{\rho_j} d_3 \left(\frac{1}{\rho} \right), \\ S_{ij}^{(3)} &\equiv \frac{a_i}{\rho_i} d_3 \left(\frac{1}{\rho_j} \right) - \frac{a_i}{\rho_j} d_3 \left(\frac{1}{\rho_i} \right), \quad S_{ij}^{(4)} \equiv \left(1 - \frac{a_i a_j}{\rho^2} \right) d_3 \left(\frac{\rho}{\rho_i \rho_j} \right), \\ S_{ijk}^{(5)} &\equiv \left(\frac{1}{a_i a_j} + \frac{1}{\rho^2} - \frac{1}{a_i a_k} - \frac{1}{a_j a_k} \right) \frac{\rho}{\rho_i \rho_j} d_3 \left(\frac{1}{\rho_k} \right) \\ &\quad + \left(\frac{1}{a_i a_k} + \frac{1}{\rho^2} - \frac{1}{a_i a_j} - \frac{1}{a_j a_k} \right) \frac{\rho}{\rho_i \rho_k} d_3 \left(\frac{1}{\rho_j} \right) \\ &\quad + \left(\frac{1}{a_j a_k} + \frac{1}{\rho^2} - \frac{1}{a_i a_j} - \frac{1}{a_i a_k} \right) \frac{\rho}{\rho_j \rho_k} d_3 \left(\frac{1}{\rho_i} \right) \\ &\quad + \left(-\frac{1}{\rho^2} + \frac{1}{a_i a_j} + \frac{1}{a_i a_k} + \frac{1}{a_j a_k} \right) \frac{\rho^2}{\rho_i \rho_j \rho_k} d_3 \left(\frac{1}{\rho} \right), \\ s_j^{(2)} &\equiv \frac{1}{\rho} d_3 \left(\frac{1}{\rho_j} \right), \quad s_j^{(3)} \equiv \frac{1}{\rho_j} d_3 \left(\frac{1}{\rho_j} \right), \quad s_{ij}^{(4)} \equiv \frac{1}{\rho_i} d_3 \left(\frac{1}{\rho_j} \right), \quad s_j^{(5)} \equiv \frac{1}{\rho \rho_j} d_3 \left(\frac{1}{\rho_j} \right), \\ s_{ij}^{(6)} &\equiv \frac{1}{\rho \rho_i} d_3 \left(\frac{1}{\rho_j} \right), \quad s_{ijk}^{(7)} \equiv \frac{1}{\rho_j \rho_k} d_3 \left(\frac{1}{\rho_i} \right) + \frac{1}{\rho_i \rho_k} d_3 \left(\frac{1}{\rho_j} \right) + \frac{1}{\rho_i \rho_j} d_3 \left(\frac{1}{\rho_k} \right), \\ s_{ijk}^{(8)} &\equiv \frac{1}{a_j a_k} \frac{1}{\rho_j \rho_k} d_3 \left(\frac{1}{\rho_i} \right) + \frac{1}{a_i a_k} \frac{1}{\rho_i \rho_k} d_3 \left(\frac{1}{\rho_j} \right) + \frac{1}{a_i a_j} \frac{1}{\rho_i \rho_j} d_3 \left(\frac{1}{\rho_k} \right) \\ s_{ijk}^{(9)} &\equiv \left(\frac{1}{\rho} + \frac{\rho}{a_j a_k} \right) \frac{1}{\rho_j \rho_k} d_3 \left(\frac{1}{\rho_i} \right) + \left(\frac{1}{\rho} + \frac{\rho}{a_i a_k} \right) \frac{1}{\rho_i \rho_k} d_3 \left(\frac{1}{\rho_j} \right) + \left(\frac{1}{\rho} + \frac{\rho}{a_i a_j} \right) \frac{1}{\rho_i \rho_j} d_3 \left(\frac{1}{\rho_k} \right), \end{aligned} \quad (\text{A.1.3})$$

The solutions of the equation sourced by $S^{(a)}$ are

$$\begin{aligned}
T^{(0)} &= \cos \vartheta d\phi, & T_j^{(1)} &= \cos \vartheta_j d\phi, & T_j^{(2)} &= \frac{\rho - a_j \cos \vartheta}{\rho_j} d\phi, \\
T_{ij}^{(3)} &= \frac{a_i}{a_j - a_i} \frac{\rho^2 + a_i a_j - (a_i + a_j) \rho \cos \vartheta}{\rho_i \rho_j} d\phi, & T_{ij}^{(4)} &= \frac{(\rho^2 + a_i a_j) \cos \vartheta - (a_i + a_j) \rho}{\rho_i \rho_j} d\phi, \\
T_{ijk}^{(5)} &= \frac{\rho^3 + \rho(a_i a_j + a_i a_k + a_j a_k) - (\rho^2(a_i + a_j + a_k) + a_i a_j a_k) \cos \vartheta}{\rho_i \rho_j \rho_k} d\phi.
\end{aligned} \tag{A.1.4}$$

The solutions of the equation sourced by $s^{(a)}$ are

$$\begin{aligned}
f_j^{(1)} &= \frac{1}{2\rho_j}, & t_j^{(1)} &= \frac{\cos \vartheta_j}{2} d\phi, & f_j^{(2)} &= \frac{\rho}{2\rho_j}, & t_j^{(2)} &= \frac{\rho - a_j \cos \vartheta}{2a_j \rho_j} d\phi, \\
f_j^{(3)} &= \frac{1}{2\rho_j^2}, & t_j^{(3)} &= 0, & f_{ij}^{(4)} &= \frac{1}{2} \frac{1}{\rho_i \rho_j}, & t_{ij}^{(4)} &= \frac{\rho^2 + a_i a_j - (a_i + a_j) \rho \cos \vartheta}{2(a_j - a_i) \rho_i \rho_j} d\phi, \\
f_i^{(5)} &= \frac{\cos \vartheta}{2a_i \rho_i^2}, & t_i^{(5)} &= \frac{\rho \sin^2 \vartheta}{2a_i \rho_i^2} d\phi, \\
f_{ij}^{(6)} &= \frac{\rho^2 + a_i a_j - 2a_j \rho \cos \vartheta}{2a_j(a_i - a_j) \rho_i \rho_j}, & t_{ij}^{(6)} &= \frac{\rho(a_i + a_j \cos 2\vartheta) - (\rho^2 + a_i a_j) \cos \vartheta}{2a_j(a_i - a_j) \rho_i \rho_j} d\phi, \\
f_{ijk}^{(7)} &= \frac{1}{\rho_i \rho_j \rho_k}, & t_{ijk}^{(7)} &= 0, & f_{ijk}^{(8)} &= \frac{\rho \cos \vartheta}{a_i a_j a_k \rho_i \rho_j \rho_k}, & t_{ijk}^{(8)} &= \frac{\rho^2 \sin^2 \vartheta}{a_i a_j a_k \rho_i \rho_j \rho_k} d\phi, \\
f_{ijk}^{(9)} &= \frac{\rho^2(a_i + a_j + a_k) + a_i a_j a_k}{2a_i a_j a_k \rho_i \rho_j \rho_k}, \\
t_{ijk}^{(9)} &= \frac{\rho^3 + \rho(a_i a_j + a_i a_k + a_j a_k) - (\rho^2(a_i + a_j + a_k) + a_i a_j a_k) \cos \vartheta}{2a_i a_j a_k \rho_i \rho_j \rho_k} d\phi.
\end{aligned} \tag{A.1.5}$$

One can also add a solution of the homogeneous equation, and we consider a such solution with components:

$$f^{(10)} = M, \quad \star_3 d_3 t^{(10)} = -dM, \tag{A.1.6}$$

where M is a harmonic function that generically can be of the form:

$$M = m + \frac{m_0}{\rho} + \sum_{j=1}^n \frac{m_j}{\rho_j}. \tag{A.1.7}$$

The corresponding $t^{(10)}$ is

$$t^{(10)} = \kappa d\phi - m_0 \cos \vartheta d\phi - \sum_{j=1}^n m_j \cos \vartheta_j d\phi. \tag{A.1.8}$$

Appendix of Chapter 5

A.2 Numerical analysis of the entropy parameter of four-GH-center solutions

The aspect ratios of the solutions are fixed to:

$$\begin{aligned}\frac{z_1}{z_2} &\approx 10^2 \\ \frac{z_2}{z_3} &\approx 10^2.\end{aligned}\tag{A.2.1}$$

By generating such solutions using numerics, we want to describe the evolution of the entropy parameter \mathcal{H} as a function of the nine degrees of freedom of the solutions $k_1, k_2, k_3, \frac{Q_2^{(1)}}{Q_1^{(3)}}, \frac{Q_3^{(2)}}{Q_1^{(2)}}, \frac{Q_2^{(3)}}{Q_3^{(1)}}, q_0, q_1$ and q_2 . We decompose our analysis in three parts. We first analyze the entropy parameter by varying the initial supertube charges $\frac{Q_2^{(1)}}{Q_1^{(3)}}, \frac{Q_3^{(2)}}{Q_1^{(2)}}$ and $\frac{Q_2^{(3)}}{Q_3^{(1)}}$, with all the other parameters fixed. Then, we analyze the entropy parameter when varying q_0, q_1 and q_2 . Finally, we analyze the entropy parameter as we vary the three initial dipole charges k_1, k_2 and k_3 .

Each of the graphs is made by generating 2500 solutions following the procedure detailed in Section 5.2.2. Because a configuration of parameters $k_1, k_2, k_3, \frac{Q_2^{(1)}}{Q_1^{(3)}}, \frac{Q_3^{(2)}}{Q_1^{(2)}}, \frac{Q_2^{(3)}}{Q_3^{(1)}}, q_0, q_1$ and q_2 can give different four-GH-center solutions, we take the final solution with the highest entropy parameter. Moreover, for readability reason, we smooth all the discrete graphs we initially obtained to have at the end a continuous curve.

- The graphs in Fig.A.1 show the variations of the entropy parameter with the three ratios of supertube charges. The other parameters have been fixed to

$$\begin{aligned}k_1 &= -k_2 = k_3 = 1, \\ q_0 &= q_1 = q_2 = 1.\end{aligned}\tag{A.2.2}$$

The entropy parameters can be greater than 15% in many domains of charge ratios and more than 25% in some small others.

- The graphs in Fig.A.2 illustrate the variation of the entropy parameter as a function of q_0, q_1 and q_2 . We suppressed the values zero in the graphs. They correspond to three-GH-center and one-supertube solutions. The six other parameters have been fixed to

$$\begin{aligned}k_1 &= -k_2 = k_3 = 1, \\ 9 \frac{Q_2^{(1)}}{Q_1^{(3)}} &= \frac{1}{2} \frac{Q_3^{(2)}}{Q_1^{(2)}} = \frac{Q_2^{(3)}}{Q_3^{(1)}} = 1.\end{aligned}\tag{A.2.3}$$

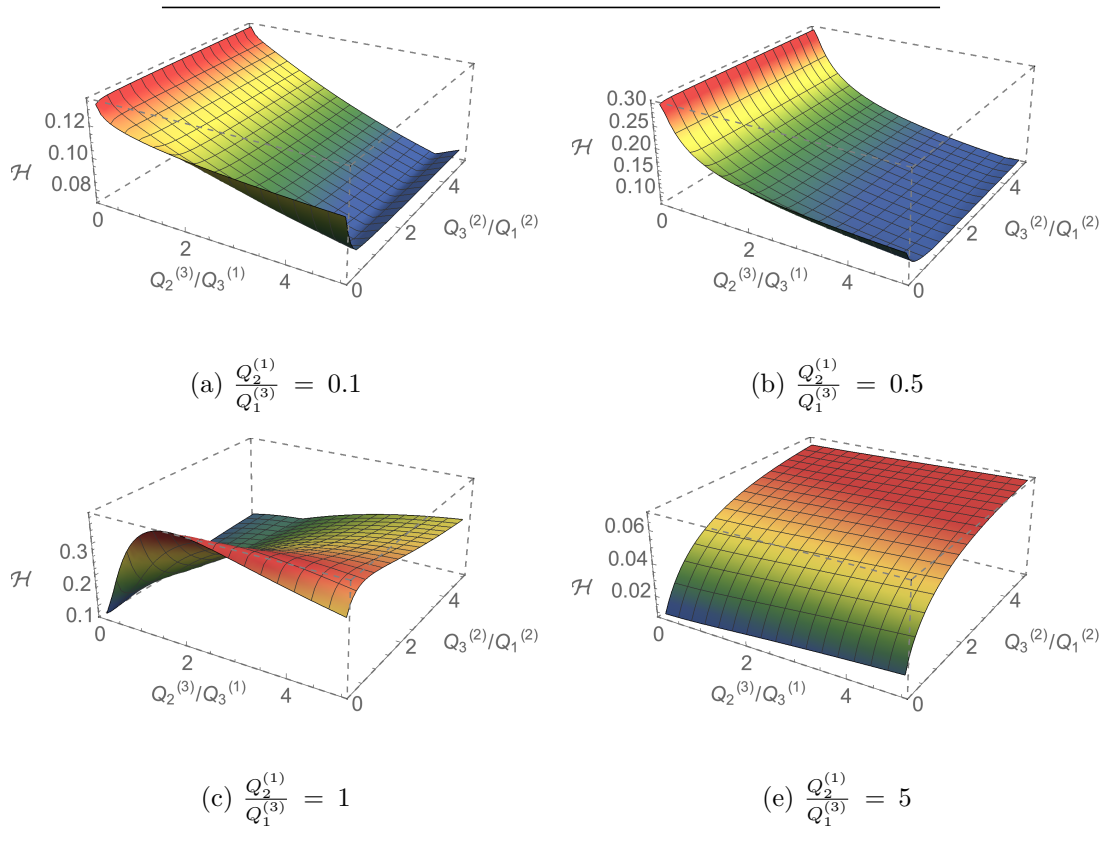


Figure A.1: The entropy parameter \mathcal{H} as a function of the charge ratios with q , q_1 , q_2 , k_1 , $-k_2$ and k_3 equal to 1.

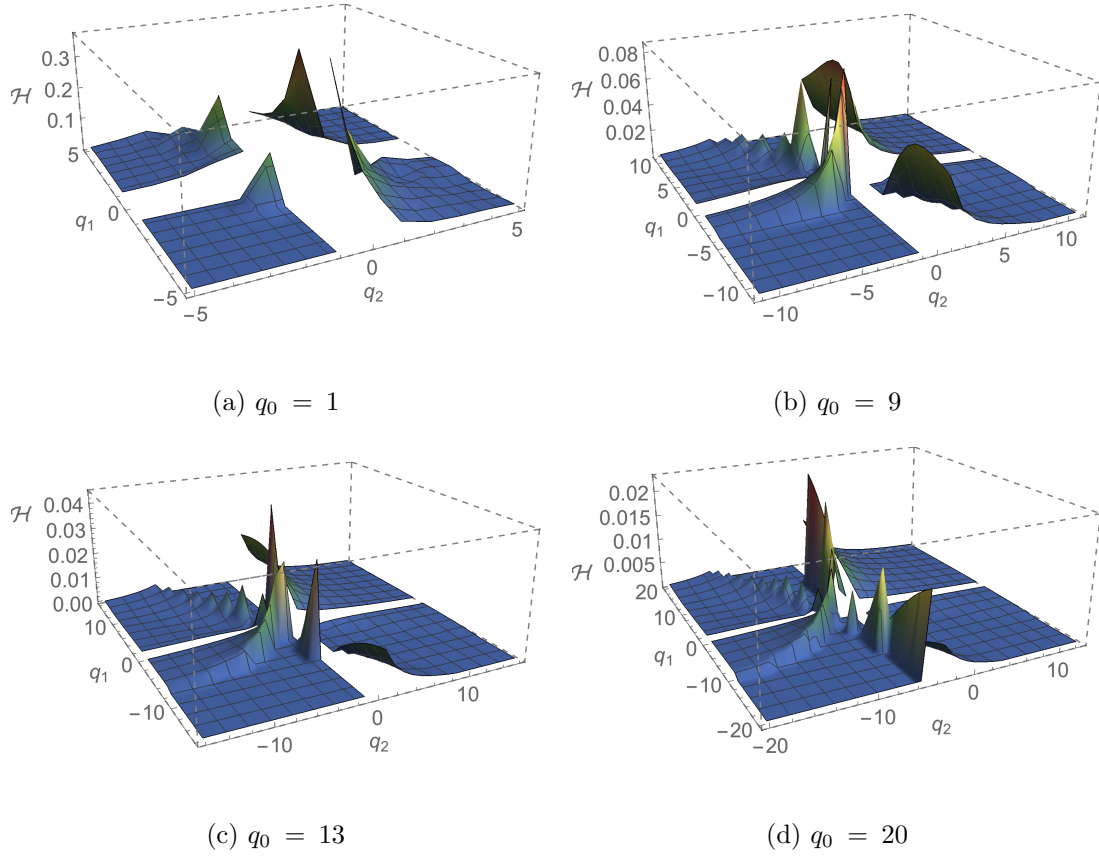


Figure A.2: The entropy parameter \mathcal{H} as a function of the charges of V, q_0 , q_1 and q_2 with $k_1, -k_2, k_3$ are equal to 1 and $\frac{Q_3^{(2)}}{Q_1^{(2)}} = 2$, $\frac{Q_2^{(3)}}{Q_3^{(1)}} = 1$ and $\frac{Q_2^{(1)}}{Q_1^{(3)}} = 0.9$.

However, we observed the same features for different values of charge ratios and dipole charges. The graphs show that for any value of q_0 the entropy is maximum when the absolute values of the charges are close to one. Furthermore the minimal Gibbons-Hawking charges (1,1,1 and -2) are the best choice to obtain four-GH-center solutions with low angular momentum. This is an unexpected feature. Indeed, in the five-center solution of [85], the GH charges are close to each other and large. Our solutions do not share this feature.

- For the initial supertube dipole charges, we observed that the sign configuration given by (A.2.2) (k_2 negative, k_1 and k_3 positive) is the optimal one. With the two other sign configurations, we did not find domains of charges where the entropy parameter is above 0.1. For the rest of the analysis we focus on configurations with k_2 negative and k_1 and k_3 positive. By doing a quick analysis, we observed that the entropy parameter does not depend on the absolute value of k_2 . The graphs in Fig. A.3 illustrate how the entropy parameter depends on the absolute value of the dipole charges k_1 and k_3 . We vary also one charge ratio, $\frac{Q_2^{(1)}}{Q_1^{(3)}}$, keeping the other parameters fixed:

$$\begin{aligned}
 q_0 &= q_1 = q_2 = 1, \\
 \frac{1}{2} \frac{Q_3^{(2)}}{Q_1^{(2)}} &= \frac{Q_2^{(3)}}{Q_3^{(1)}} = 1.
 \end{aligned}
 \tag{A.2.4}$$

We remark that the entropy parameter depends essentially on the ratio $\frac{k_1}{k_3}$ and the entropy is maximum and far from 0 for one particular value of $\frac{k_1}{k_3}$. We observed the same kind of graph for

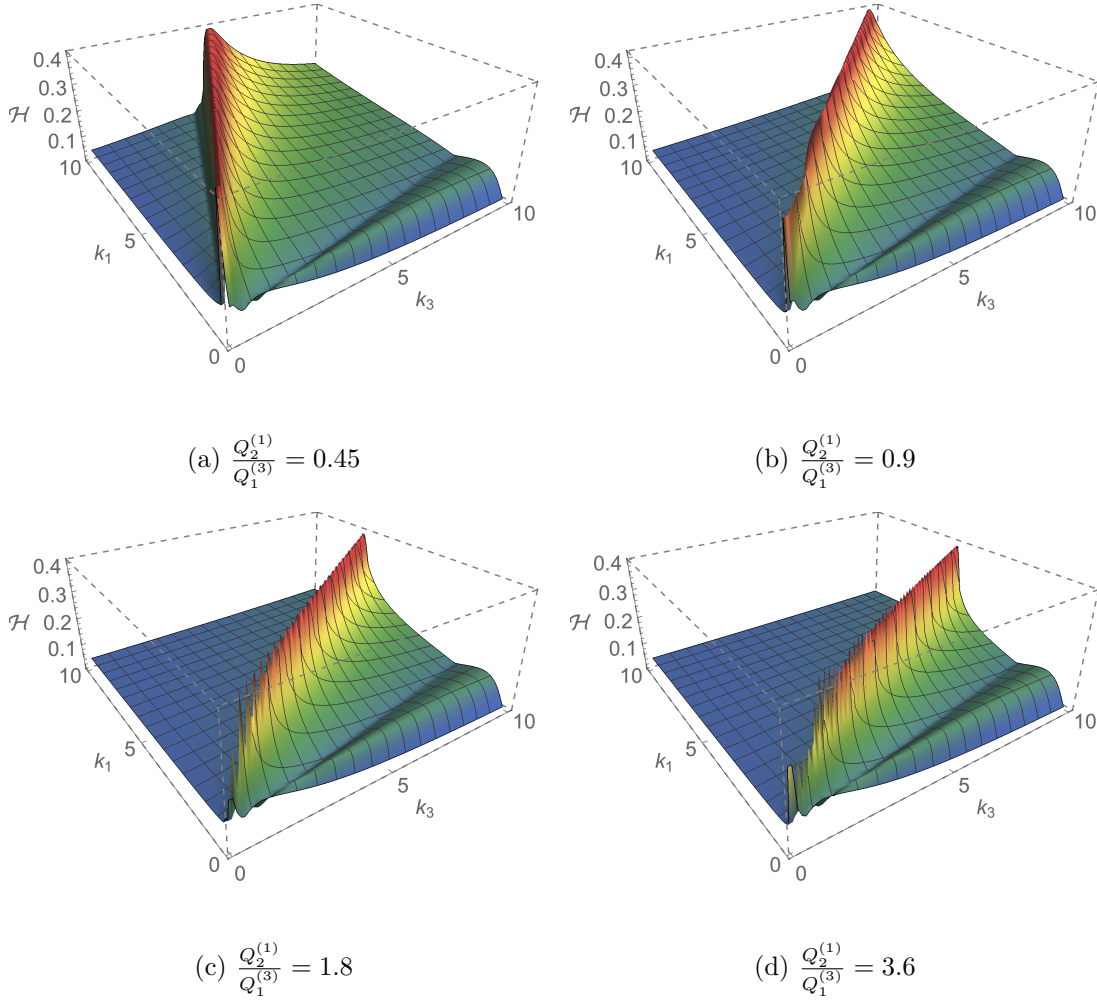


Figure A.3: The entropy parameter \mathcal{H} as a function of the dipole charges k_1 and k_3 and one charge ratio $\frac{Q_2^{(1)}}{Q_1^{(3)}}$ with q_0, q_1, q_2 equal to 1 and $\frac{Q_3^{(2)}}{Q_1^{(2)}} = 2, \frac{Q_2^{(3)}}{Q_3^{(1)}} = 1$

different values of charge ratios. If one varies the value of $\frac{Q_2^{(1)}}{Q_1^{(3)}}$, the particular value of $\frac{k_1}{k_3}$ changes but the maximum value of the entropy parameter remains the same whereas if one varies the two other charge ratios both change. The maximum value of entropy parameter we observed is 0.3.

To conclude, the numerical analysis shows that there exist large domains of supertube-charge ratios and supertube dipole charges where the entropy parameter of solutions satisfying (5.3.2) is maximal and around 0.3. The only necessary conditions to have an angular momentum significantly below the cc bound is that the Gibbons-Hawking charges must be minimal and the dipole charge configuration of the generating three-supertube solution must be k_1 and k_3 positive and k_2 negative. Moreover, increasing the difference in scale between the inter-center distances does not affect how the entropy parameter varies with $k_1, k_2, k_3, \frac{Q_2^{(1)}}{Q_1^{(3)}}, \frac{Q_3^{(2)}}{Q_1^{(2)}}, \frac{Q_2^{(3)}}{Q_3^{(1)}}, q_0, q_1$ and q_2 . It affects only the maximal value reachable as it was detailed in Section 5.3.1.

A.3 Numerical analysis of the entropy parameter of solutions with one Supertube and three Gibbons-Hawking centers

We proceed the same way to analyse the entropy parameter of solutions with three Gibbons-Hawking centers and one Supertube. We focus on solutions without scale differences between the inter-center distances (5.3.2). According to the method used to generate them (see Section 5.2.2), the solutions depends on eight free parameters and the aspect ratios (5.3.2). We will also decompose our analysis in three parts. We first vary the initial supertube charges $\frac{Q_2^{(1)}}{Q_1^{(3)}}$, $\frac{Q_3^{(2)}}{Q_1^{(2)}}$ and $\frac{Q_2^{(3)}}{Q_3^{(1)}}$, with all the other parameters fixed. Then, we analyze the entropy parameter as a function of q_0 and q_J , where J is 1, 2 or 3 depending on which center is the Supertube. Finally, we vary the three initial dipole charges k_1 , k_2 and k_3 . All the graphs have been generated as explained in the previous section.

- First of all, we noticed that the localization of the supertube center compared to the three Gibbons-Hawking centers has a significant impact on the entropy parameter. The best configuration is when the Supertube is not located between the Gibbons-Hawking centers. With our conventions, this means that the supertube center is the first center given by $(0, 0, z_1)$. Indeed, we have found several domains of charges and dipole charges where the entropy parameter is above 0.15 for the three possible supertube loci. However, we have found that \mathcal{H} has much higher values when the Supertube is located at the first center.
- The graphs in Fig.A.4 give the variations of the entropy parameter with the three initial charge ratios when the Supertube is located at the first center. We have fixed the other parameters to be

$$\begin{aligned} k_1 &= -k_2 = k_3 = 1, \\ q_0 &= -q_3 = 1. \end{aligned} \tag{A.3.1}$$

We observe that when the initial charge ratio $\frac{Q_2^{(1)}}{Q_1^{(3)}}$ is between 0.4 and 1 and when $\frac{Q_2^{(3)}}{Q_3^{(1)}}$ is small, the entropy parameter can reach 0.25. This is the upper bound we found for a configuration which satisfies (A.3.1) and (5.3.2).

- Regarding the variation of the entropy parameter as a function of q_0 and q_3 (q_2 is fixed to satisfy $\Sigma q_a = 1$), we have observed the same features as in solutions with four Gibbons-Hawking centers: the higher the absolute value of the Gibbons-Hawking charges is, the lower is the entropy parameter. The graph in Fig.A.5 shows the variation of the entropy parameter as a function of q_0 and q_3 for solutions satisfying (5.3.2) and with

$$\begin{aligned} k_1 &= -k_2 = k_3 = 1, \\ 5 \frac{Q_2^{(1)}}{Q_1^{(3)}} &= 60 \frac{Q_2^{(3)}}{Q_3^{(1)}} = \frac{1}{4} \frac{Q_3^{(2)}}{Q_1^{(2)}} = 1. \end{aligned} \tag{A.3.2}$$

We have observed similar variations for different initial charge ratios and dipole charges. Thus, $q_0 = 1$, $q_2 = 1$ and $q_3 = -1$ is the best configuration to optimize the entropy parameter.

- Varying the initial supertube dipole charges, we have again observed exactly the same features as in solutions with four Gibbons-Hawking centers. The best sign configuration is when k_2 is negative and when k_1 and k_3 are positive. Moreover, the entropy parameter does not depend significantly on the absolute value of k_2 and it only depends on $\frac{k_1}{k_3}$. It also reaches a maximum for a particular value of the ratio $\frac{k_1}{k_3}$. The value and the location of the maximum depends on the values of the supertube charge ratios. The graphs in Fig.A.6 illustrate these conclusions. We built solutions and computed their entropy as a function of the absolute value of the dipole charges k_1

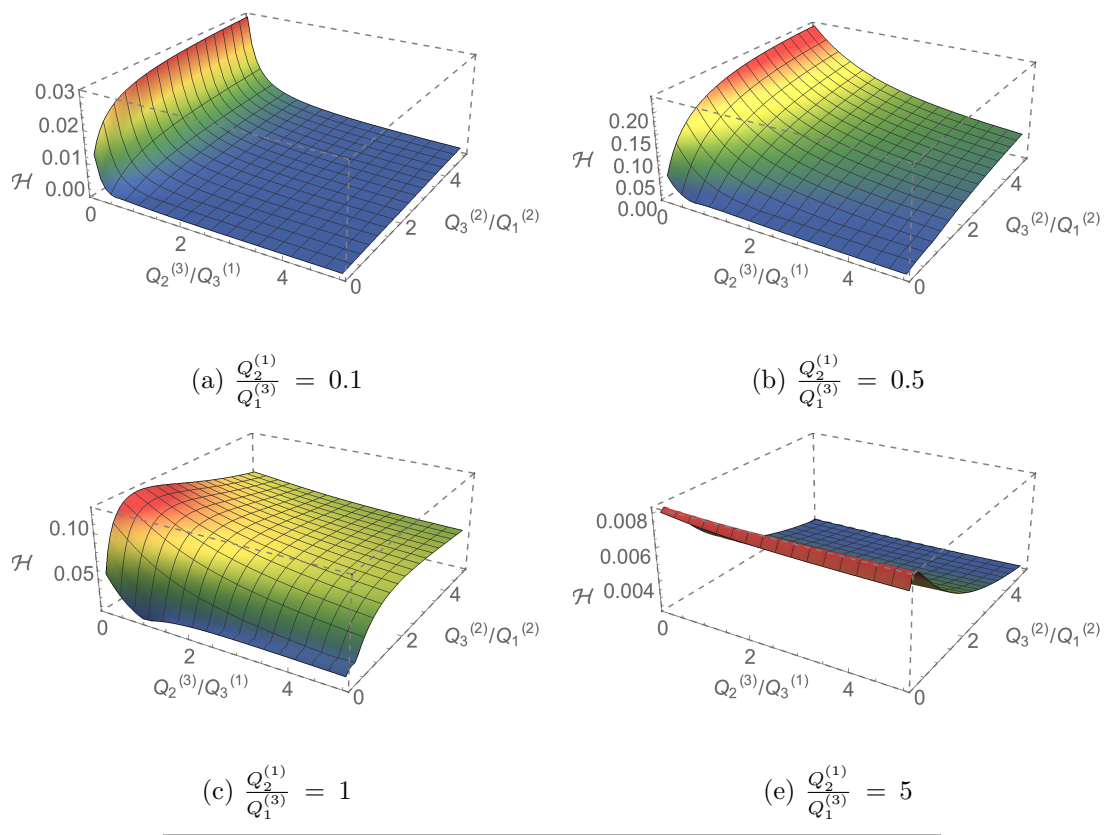


Figure A.4: The entropy parameter \mathcal{H} as a function of the charge ratios with q_0 , q_2 , k_1 , $-k_2$ and k_3 equal to 1.

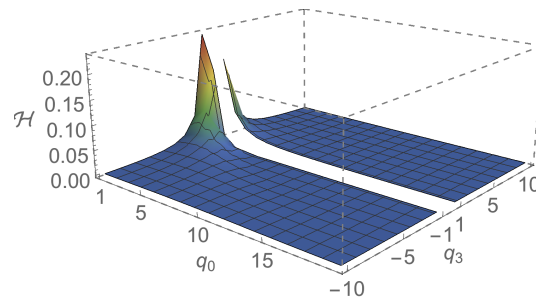


Figure A.5: The entropy parameter \mathcal{H} as a function of the charges of V, q_0 and q_3 with k_1 , $-k_2$, k_3 are equal to 1 and $\frac{Q_3^{(2)}}{Q_1^{(2)}} = 4$, $\frac{Q_2^{(3)}}{Q_3^{(1)}} = 0.06$ and $\frac{Q_2^{(1)}}{Q_1^{(3)}} = 0.5$.

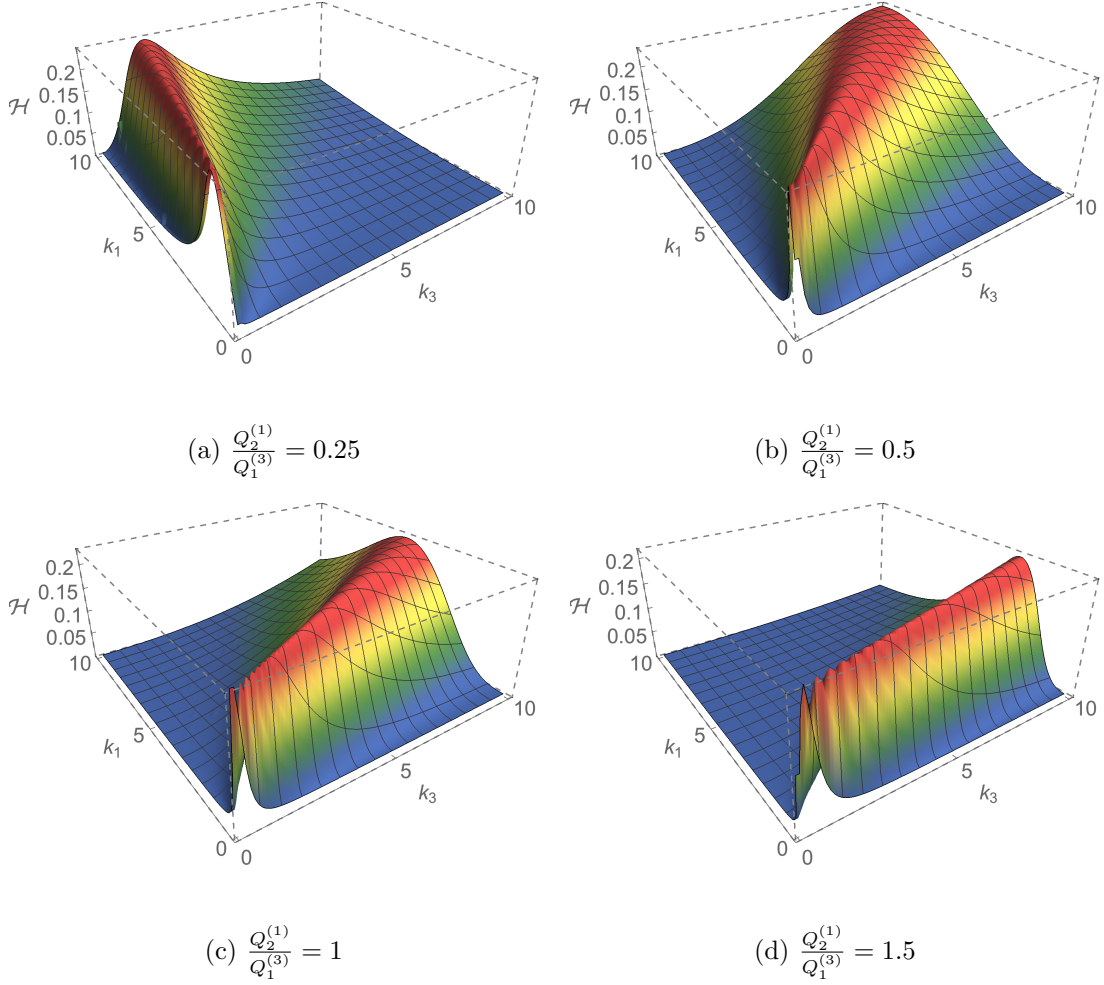


Figure A.6: The entropy parameter \mathcal{H} as a function of the dipole charges k_1 and k_3 and one charge ratio $\frac{Q_2^{(1)}}{Q_1^{(3)}}$ with q_0, q_1, q_2 equal to 1 and $\frac{Q_3^{(2)}}{Q_1^{(2)}} = 4$, $\frac{Q_2^{(3)}}{Q_3^{(1)}} = 0.06$

and k_3 and one charge ratio $\frac{Q_2^{(1)}}{Q_1^{(3)}}$. The other parameters have been fixed to

$$\begin{aligned} q_0 &= q_1 = q_2 = 1. \\ \frac{1}{4} \frac{Q_3^{(2)}}{Q_1^{(2)}} &= 60 \frac{Q_2^{(3)}}{Q_3^{(1)}} = 1. \end{aligned} \tag{A.3.3}$$

We have analyzed the entropy parameter for charge ratios different from the one above. The upper bound of all the maxima we observed is 0.25.

The numerical analysis shows that solutions with one Supertube and three Gibbons-Hawking centers do not need to have a scale difference between the inter-center distances to have an entropy parameter above 0.1. If one chooses minimal Gibbons-Hawking charges and k_2 negative, k_1 and k_3 positive, one can find domains of parameters where the entropy is around 0.2.

Appendix of Chapter 6

A.4 Analysis of three-center solutions

A.4.1 Analytic investigation of solutions with two Supertubes and one GH center

We review our method to construct zero angular momentum BPS multicenter solutions with global D0 and D4 charges being 0 and D6 and D2 charges being 1 starting from solutions with two supertube centers of different species and one GH center.

- We start with the full parameter space of solutions. The GH center is the 0^{th} center with charges q, κ_1, κ_2 and κ_3 . We consider also a two-charge Supertube of species 1 located at the 1^{st} center with charges $k_1, Q_1^{(2)}$ and $Q_1^{(3)}$ and a two-charge Supertube of species 2 located at the 2^{nd} center with charges $k_2, Q_2^{(1)}$ and $Q_2^{(3)}$. The general form of the eight harmonic function is:

$$\begin{aligned}
 V &= \frac{q}{r_0}, & M &= \frac{\kappa_1 \kappa_2 \kappa_3}{q^2 r_0} + \frac{Q_1^{(2)} Q_1^{(3)}}{k_1 r_1} + \frac{Q_2^{(1)} Q_2^{(3)}}{k_2 r_2}, \\
 K^1 &= \frac{\kappa_1}{r_0} + \frac{k_1}{r_1}, & L_1 &= -\frac{\kappa_2 \kappa_3}{q r_0} + \frac{Q_2^{(1)}}{r_2}, \\
 K^2 &= \frac{\kappa_2}{r_0} + \frac{k_2}{r_2}, & L_2 &= -\frac{\kappa_1 \kappa_3}{q r_0} + \frac{Q_1^{(2)}}{r_1}, \\
 K^3 &= \frac{\kappa_3}{r_0}, & L_3 &= -\frac{\kappa_1 \kappa_2}{q r_0} + \frac{Q_1^{(3)}}{r_1} + \frac{Q_2^{(3)}}{r_2}.
 \end{aligned} \tag{A.4.1}$$

First, we want to impose the values of the eight global D-brane charges. This reduces the number of free parameters to two. One can express everything in terms of k_1 and k_2 :

$$\begin{aligned}
 \{q, \kappa_1, \kappa_2, \kappa_3\} &= \{1, -k_1, -k_2, 0\} \\
 \{Q_1^{(2)}, Q_1^{(3)}\} &= \left\{1, \frac{k_1(1 + k_1 k_2)}{k_1 - k_2}\right\} \\
 \{Q_2^{(1)}, Q_2^{(3)}\} &= \left\{1, \frac{k_2(1 + k_1 k_2)}{k_2 - k_1}\right\}
 \end{aligned} \tag{A.4.2}$$

- For zero angular momentum three-center solutions, the bubble equations take the following simple form

$$\begin{aligned}
 \frac{\Gamma_{01}}{r_{01}} + \frac{\Gamma_{02}}{r_{02}} &= 0, \\
 -\frac{\Gamma_{01}}{r_{01}} + \frac{\Gamma_{12}}{r_{12}} &= 0, \\
 -\frac{\Gamma_{02}}{r_{02}} - \frac{\Gamma_{12}}{r_{12}} &= 0,
 \end{aligned} \tag{A.4.3}$$

which are easily solved by

$$r_{02} = -\frac{\Gamma_{02}}{\Gamma_{01}} r_{01}, \quad r_{12} = \frac{\Gamma_{12}}{\Gamma_{01}} r_{01}. \quad (\text{A.4.4})$$

We have used the notation $\Gamma_{IJ} = \langle \Gamma_I, \Gamma_J \rangle$. We notice that the solutions are invariant under rescaling of inter-center distances $r_{IJ} \rightarrow \lambda r_{IJ}$. That is why, r_{01} remains a free parameter all along the construction.

Furthermore, the solution corresponds to a physical center configuration if and only if it satisfies the triangle inequality

$$\begin{aligned} (r_{01} + r_{02} - r_{12})(r_{01} - r_{02} + r_{12})(-r_{01} + r_{02} + r_{12}) &\geq 0 \\ \iff \left(1 - \frac{\Gamma_{02}}{\Gamma_{01}} - \frac{\Gamma_{12}}{\Gamma_{01}}\right) \left(1 + \frac{\Gamma_{02}}{\Gamma_{01}} + \frac{\Gamma_{12}}{\Gamma_{01}}\right) \left(-1 - \frac{\Gamma_{02}}{\Gamma_{01}} + \frac{\Gamma_{12}}{\Gamma_{01}}\right) &\geq 0 \end{aligned} \quad (\text{A.4.5})$$

which constrains the two-dimensional parameter space of k_1 and k_2 significantly.

- The solution must have a positive quartic invariant (4.1.27) to guarantee the absence of closed timelike curve. One can either use the conjecture in [140] or the condition (4.1.28). Small number of centers makes the second option to be the simplest. We expand $Z_I V$ around each center. We find that $Z_I V \geq 0$ imposes

$$\begin{aligned} q Q_2^{(1)} \geq 0, \quad q Q_1^{(2)} \geq 0, \quad \frac{q Q_1^{(3)} - k_1 k_2}{r_{01}} + \frac{q Q_2^{(3)} - k_1 k_2}{r_{02}} &\geq 0, \\ q Q_1^{(3)} + k_1 k_2 \left(\frac{r_{01}}{r_{12}} - 1\right) \geq 0, \quad q Q_2^{(3)} + k_1 k_2 \left(\frac{r_{02}}{r_{12}} - 1\right) &\geq 0, \end{aligned} \quad (\text{A.4.6})$$

which further constrains the parameter space defined by k_1 and k_2 . We remind the reader that these conditions are not necessarily sufficient to be free of closed timelike curves. One needs to check once those conditions satisfied that the quartic invariant is indeed positive.

- Last but not least, one has to impose all the charges in the harmonic functions (A.4.1) to be integer.

After few simplifications, the equations (A.4.5) and (A.4.6) are satisfied if k_1 and k_2 satisfy

$$(k_1 > 0 \text{ and } -\frac{1}{k_1} \leq k_2 \leq 0) \text{ or } (k_1 < 0 \text{ and } 0 \leq k_2 \leq -\frac{1}{k_1}) \text{ or } (k_1 = 0 \text{ and } |k_2| \geq 1). \quad (\text{A.4.7})$$

Requiring each charge of the harmonic functions to be integer restricts (A.4.7) to six possible values $(k_1, k_2) = \{(0, 1), (0, -1), (1, 0), (1, -1), (-1, 0), (-1, 1)\}$.

We can repeat exactly the same procedure with solutions of two Supertubes of species 1 and 3 and solutions of two Supertubes of species 2 and 3. By carefully counting the redundancies, we have a final count of 12 inequivalent solutions. Their charge vectors as well as their center configuration are given in detail in Table 6.1. Their main and common features are that the center configurations are axisymmetric with a $U(1)$ symmetry and all centers carry D-brane charges of value -1, 0 or 1. Moreover, as explained in Section 6.1, for most of the solutions found, the two-charge-supertube centers are actually fluxed D-brane centers. The six first solutions in Table 6.1 have a GH center and two D4-brane centers with an induced D2 charge. The six other solutions have one GH center, one two-charge-supertube center and one simple D2-brane center with an induced D0 charge.

We have carefully checked that the quartic invariant is strictly positive for all solutions found and that they are not related by gauge transformations.

One can also wonder why we do not consider configurations with two supertube centers of the same species. This is straightforward to check that such configurations are strictly incompatible with the global D-brane charges we impose (6.1.1).

A.4.2 Numerical analysis of solutions with one Supertube and two GH centers and solutions with three GH centers

We review our numerical method which shows that there exists no valid solutions satisfying (6.1.1) with one Supertube and two GH centers or with three GH centers. The number of parameters of such solutions makes an analytic approach difficult. The steps of our numerical analysis were the following:

- First, we start with the most general solutions. The solutions with one Supertube and two GH centers form a family of 11 parameters whereas the solutions with three GH centers form a family of 12 parameters.
- We fix 8 parameters by imposing the global D-brane charges (6.1.1).
- We run the other free parameters from -500 to 500. Each value corresponds to one particular solution. For each one, firstly we check if the solution has integer charges, secondly if the solutions of the bubble equations can give physical center configurations (A.4.5), and thirdly if the quartic invariant is positive. Checking the positivity of the quartic invariant is the hardest part. We have principally used the conjecture postulated in [140]. This conjecture drastically simplifies the loop computations. It allows to check the positivity of the quartic invariant all over the \mathbb{R}^3 base space by checking an algebraic condition on a matrix derived from the bubble equations. This conjecture should work for multicenter solutions with GH centers only. However, one can mathematically consider supertube center as a limit of a GH center. For instance, one can obtain (4.1.65) from (4.1.58) by taking the limit $\epsilon \rightarrow 0$ with

$$q_a = -\epsilon k_1, \quad k_a^1 = k_1, \quad k_a^2 = \epsilon Q_a^{(3)}, \quad k_a^3 = \epsilon Q_a^{(2)}. \quad (\text{A.4.8})$$

Thus, we can extend the conjecture to our solutions.

We did not find any solutions satisfying all the conditions in the huge range of parameters we have scanned. Furthermore, from the previous section we have a good intuition that if a solution exists the charges should be small. Consequently, one can say that our numerical analysis suggests that there is no solution of three GH centers or one Supertube and two GH centers satisfying (6.1.1).

A.5 Analysis of four-center and five-center solutions

A.5.1 Analysis of four-center solutions

We perform a similar analysis as in Section A.4.2. The main goal is to scan a significant part of the parameter space looking for BPS four-center solutions satisfying (6.1.1).

- As before, we start with the most general solutions. The solutions with three Supertubes and one GH center form a family of 13 parameters, the solutions with two Supertubes and two GH centers form a family of 14 parameters, the solutions with one Supertube and three GH centers form a family of 15 parameters and the solutions with four GH centers form a family of 16 parameters, .
- We fix 8 parameters by imposing the global D-brane charges (6.1.1).
- We run the remaining parameters from -5 to 5 (the range of values is smaller than in Section A.4.2 due to the higher number of free parameters). For each value, we check if the solution is a valid BPS multicenter solution:
 - First, we check if all the harmonic-function charges are integer.
 - Second, we check if the solution of the bubble equation can give rise to a physical center configuration. Because we have four centers and not three, this step is more complex than the one in the previous section. Indeed, we have to check four triangle inequalities as (A.4.5)

for each face of the tetrahedron formed by the four centers plus an angle inequality at one vertex of the tetrahedron.

- Third, we check the absence of closed timelike curves as in the previous section.

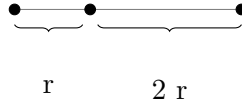
No solution have been found in the range of values. One can realistically extend this result to all four-center BPS solutions.

A.5.2 Analysis of five-center solutions

The number of parameters and the complexity of the constraints for five-center configurations make the numerical scan of the parameter space impossible. However, we have randomly generated some solutions and checked if they are valid and physical. The main idea is to fix as many parameters as possible using the equations (the global D-brane charges, the bubble equations) and pick random values for the other parameters and check if they satisfy all the inequations (the absence of closed timelike curves, the triangle inequalities etc...). We have generated a significant number ($\sim 10^3$) of five-center solutions focusing on solutions with low charges at the centers, we find no valid solutions. This tends to argue that no five-center solutions with pure D6 and D2 charges exist.

A.6 Configurations with $Q_{D6} = 2$

In this section, we give to the interested reader the charge vectors of the 18 three-center solutions with one GH center and two 16-supercharge centers with global D-brane charges $(Q_{D6}, Q_{D4}^1, Q_{D4}^2, Q_{D4}^3; Q_{D2}^1, Q_{D2}^2, Q_{D2}^3, Q_{D0}) = (2, 0, 0, 0; 1, 1, 1, 0)$. They are given in the Table A.1. The center configurations are axisymmetric and look like



with the GH center either in the middle or on the right depending on the solution considered.

Table A.1: The 18 multicenter solutions with global D-brane charges $(Q_{D6}, Q_{D4}^1, Q_{D4}^2, Q_{D4}^3; Q_{D2}^1, Q_{D2}^2, Q_{D2}^3, Q_{D0}) = (2, 0, 0, 0; 1, 1, 1, 0)$.

1	$\Gamma_0 = (2, 1, 0, -2; 0, 1, 0, 0)$ $\Gamma_1 = (0, -1, 0, 0; 0, 0, 1, 0)$ $\Gamma_2 = (0, 0, 0, 2; 1, 0, 0, 0)$	2	$\Gamma_0 = (2, 0, -1, 0; 0, 0, 0, 0)$ $\Gamma_1 = (0, 0, 0, 0; 0, 1, 0, -1)$ $\Gamma_2 = (0, 0, 1, 0; 1, 0, 1, 1)$
3	$\Gamma_0 = (2, 1, -2, 0; 0, 0, 1, 0)$ $\Gamma_1 = (0, 0, 2, 0; 1, 0, 0, 0)$ $\Gamma_2 = (0, -1, 0, 0; 0, 1, 0, 0)$	4	$\Gamma_0 = (2, 0, -2, 1; 1, 0, 0, 0)$ $\Gamma_1 = (0, 0, 0, -1; 0, 1, 0, 0)$ $\Gamma_2 = (0, 0, 2, 0; 0, 0, 1, 0)$
5	$\Gamma_0 = (2, -2, 0, 1; 0, 1, 0, 0)$ $\Gamma_1 = (0, 2, 0, 0; 0, 0, 1, 0)$ $\Gamma_2 = (0, 0, 0, -1; 1, 0, 0, 0)$	6	$\Gamma_0 = (2, 0, 0, -1; 0, 0, 0, 0)$ $\Gamma_1 = (0, 0, 0, 1; 1, 1, 0, 1)$ $\Gamma_2 = (0, 0, 0, 0; 0, 0, 1, -1)$
7	$\Gamma_0 = (2, 0, 1, -2; 1, 0, 0, 0)$ $\Gamma_1 = (0, 0, 0, 2; 0, 1, 0, 0)$ $\Gamma_2 = (0, 0, -1, 0; 0, 0, 1, 0)$	8	$\Gamma_0 = (2, -1, 0, 0; 0, 0, 0, 0)$ $\Gamma_1 = (0, 1, 0, 0; 0, 1, 1, 1)$ $\Gamma_2 = (0, 0, 0, 0; 1, 0, 0, -1)$
9	$\Gamma_0 = (2, -2, 1, 0; 0, 0, 1, 0)$ $\Gamma_1 = (0, 0, -1, 0; 1, 0, 0, 0),$ $\Gamma_2 = (0, 2, 0, 0; 0, 1, 0, 0)$	10	$\Gamma_0 = (2, 2, -1, 0; 0, 0, 1, 0)$ $\Gamma_1 = (0, -2, 0, 0; 0, 1, 0, 0)$ $\Gamma_2 = (0, 0, 1, 0; 1, 0, 0, 0)$
11	$\Gamma_0 = (2, 2, 0, -1; 0, 1, 0, 0)$ $\Gamma_1 = (0, 0, 0, 1; 1, 0, 0, 0)$ $\Gamma_2 = (0, -2, 0, 0; 0, 0, 1, 0)$	12	$\Gamma_0 = (2, 0, -1, 2; 1, 0, 0, 0)$ $\Gamma_1 = (0, 0, 0, -2; 0, 1, 0, 0)$ $\Gamma_2 = (0, 0, 1, 0; 0, 0, 1, 0)$

13	$\Gamma_0 = (2, 0, 2, -1; 1, 0, 0, 0)$ $\Gamma_1 = (0, 0, -2, 0; 0, 0, 1, 0)$ $\Gamma_2 = (0, 0, 0, 1; 0, 1, 0, 0),$	14	$\Gamma_0 = (2, -1, 2, 0; 0, 0, 1, 0)$ $\Gamma_1 = (0, 0, -2, 0; 1, 0, 0, 0)$ $\Gamma_2 = (0, 1, 0, 0; 0, 1, 0, 0)$
15	$\Gamma_0 = (2, -1, 0, 2; 0, 1, 0, 0)$ $\Gamma_1 = (0, 1, 0, 0; 0, 0, 1, 0)$ $\Gamma_2 = (0, 0, 0, -2; 1, 0, 0, 0)$	16	$\Gamma_0 = (2, 1, 0, 0; 0, 0, 0, 0)$ $\Gamma_1 = (0, 0, 0, 0; 1, 0, 0, 1)$ $\Gamma_2 = (0, -1, 0, 0; 0, 1, 1, -1)$
17	$\Gamma_0 = (2, 0, 0, 1; 0, 0, 0, 0)$ $\Gamma_1 = (0, 0, 0, 0; 0, 0, 1, 1)$ $\Gamma_2 = (0, 0, 0, -1; 1, 1, 0, -1)$	18	$\Gamma_0 = (2, 0, 1, 0; 0, 0, 0, 0)$ $\Gamma_1 = (0, 0, 0, 0; 0, 1, 0, 1)$ $\Gamma_2 = (0, 0, -1, 0; 1, 0, 1, -1)$

A.7 Three-node abelian quiver with general (a,b,c)

The case of a general Abelian 3-node quiver with closed loop and with vanishing FI parameters, is quite similar to $(a, b, c) = (2, 1, 1)$. It is described by the following quiver

$$\begin{array}{ccc}
 & \textcircled{1} & \\
 X_\alpha \nearrow & & \searrow Y_\beta \\
 \textcircled{1} & \xleftarrow{C_\gamma} & \textcircled{1}
 \end{array}, \tag{A.7.1}$$

with $\alpha = 1, \dots, a$, $\beta = 1, \dots, b$, $\gamma = 1, \dots, c$ where (a, b, c) is the unique triplet of integer intersection product $(a, b, c) \equiv (\langle \Gamma_i, \Gamma_j \rangle, \langle \Gamma_j, \Gamma_k \rangle, \langle \Gamma_k, \Gamma_i \rangle)$, i, j, k are three different integers between 0 and 2 in order to satisfy $a \geq b > 0$ and $c > 0$. The D-term equations are given by

$$\sum_{\alpha=1}^a |X_\alpha|^2 - \sum_{\gamma=1}^c |C_\gamma|^2 = 0 \tag{A.7.2}$$

$$\sum_{\beta=1}^b |Y_\beta|^2 - \sum_{\alpha=1}^a |X_\alpha|^2 = 0 \tag{A.7.3}$$

$$-\sum_{\beta=1}^b |Y_\beta|^2 + \sum_{\gamma=1}^c |C_\gamma|^2 = 0. \tag{A.7.4}$$

Again, we assume a generic cubic superpotential

$$W = w_{\alpha\beta\gamma} X_\alpha Y_\beta C_\gamma, \tag{A.7.5}$$

which gives the following F-term equations:

$$w_{\alpha\beta\gamma} Y_\beta C_\gamma = 0, \quad w_{\alpha\beta\gamma} X_\alpha C_\gamma = 0, \quad w_{\alpha\beta\gamma} X_\alpha Y_\beta = 0. \tag{A.7.6}$$

As argued in [158], the solution space consists of 3 chambers, in each of which only one of the three fields vanishes. However by D-term equations, this also implies vanishing of all three fields. So there

is only one chamber, consisting a single solution. Again, the solution preserves $U(1) \times U(1)$ gauge symmetry.

We briefly make comparison with [158], which considered same quiver, but with non-zero FI parameters, and came to rather different conclusions. For non-zero FI parameters, after setting one of the fields to zero, D-term equations define a product of projective spaces. On the other hand, setting a field to zero, solves two F-term equations automatically. The remaining one defines a complete intersection manifold in the product of projective spaces. Requiring the dimension of this manifold to be non-negative gives the condition $a + b \geq c + 2$ and permutations. When we set the FI parameters to zero, these projective spaces collapse to a point and so does the intersection manifold. As a result we do not have any condition on (a, b, c) . This is rather puzzling as physically one would have expected to get some version of triangle inequality. In particular, we would like to understand the Coulomb branch description of quivers with triangle inequality violating (a, b, c) .

Due to the above mentioned differences, the conclusions of [158] do not apply to quivers discussed in this paper.

Appendix of Chapter 8

A.8 The example of asymptotically $\text{WAdS}_3 \times \text{SqS}^3$ bubbling solution

In this section, we examine the IR geometry of the solution constructed in Section 8.2.4. We give the local $S^1 \times \mathbb{R}^4$ metric (8.2.15) at each of the four centers and the periodicities of the angles.

- At the origin of the space, $r \sim 0$:

The local metric is

$$ds_0^2 = \frac{5\Lambda^2}{18} \sqrt{\frac{7}{3}} \left[\frac{dr^2}{r} + \frac{5632}{1575} dy_0^2 + r (d\theta^2 + 2(1 + \cos \theta) d\phi_{L0}^2 + 2(1 - \cos \theta) d\phi_{R0}^2) \right], \quad (\text{A.8.1})$$

where y_0 , ϕ_{L0} and ϕ_{R0} are related to the angles at infinity y_∞ , ψ_∞ and ϕ by

$$\begin{aligned} y_0 &= y_\infty + \frac{9}{4} (\psi_\infty - \phi), \\ \phi_{L0} &= \frac{1}{8} (21 y_\infty + 31(\psi_\infty - \phi)) + \phi, \\ \phi_{R0} &= \frac{1}{8} (21 y_\infty + 31(\psi_\infty - \phi)). \end{aligned} \quad (\text{A.8.2})$$

We can read the periodicities from (8.2.23)

$$(y_0, \phi_{L0}, \phi_{R0}) = \begin{cases} (y_0, \phi_{L0}, \phi_{R0}) - \frac{20\pi T}{473} (51, 64, 64) \\ (y_0, \phi_{L0}, \phi_{R0}) + \frac{\pi}{2} (18, 31, 31) \\ (y_0, \phi_{L0}, \phi_{R0}) + 2\pi (0, 1, 0) \end{cases}. \quad (\text{A.8.3})$$

Using the procedure detailed in Section 8.2.2, this corresponds to a smooth discrete quotient of $S^1 \times \mathbb{R}^4$ if b is not divisible by 2 where b is the denominator of the irreducible fraction $T = \frac{a}{b}$.

- At the second center, $r_1 \sim 0$:

The local metric is

$$ds_1^2 = \frac{\Lambda^2}{23} \sqrt{\frac{155}{2}} \left[\frac{dr_1^2}{r_1} + \frac{15548}{837} dy_1^2 + r_1 (d\theta_1^2 + 2(1 + \cos \theta_1) d\phi_{L1}^2 + 2(1 - \cos \theta_1) d\phi_{R1}^2) \right], \quad (\text{A.8.4})$$

where y_1 , ϕ_{L1} and ϕ_{R1} are related to the angles at infinity y_∞ , ψ_∞ and ϕ by

$$\begin{aligned} y_1 &= y_\infty + \psi_\infty - \frac{5}{13}\phi, \\ \phi_{L1} &= \frac{1}{6}(21y_\infty + 31\psi_\infty - 23\phi) + \phi, \\ \phi_{R1} &= \frac{1}{6}(21y_\infty + 31\psi_\infty - 23\phi). \end{aligned} \quad (\text{A.8.5})$$

We can read the periodicities from (8.2.23)

$$(y_1, \phi_{L1}, \phi_{R1}) = \begin{cases} (y_1, \phi_{L1}, \phi_{R1}) - \frac{160\pi T}{1419} (3, 32, 32) \\ (y_1, \phi_{L1}, \phi_{R1}) + \frac{2\pi}{3} (6, 31, 31) \\ (y_1, \phi_{L1}, \phi_{R1}) + \frac{2\pi}{39} (24, 91, 52) \end{cases}. \quad (\text{A.8.6})$$

This corresponds to a smooth discrete quotient of $S^1 \times \mathbb{R}^4$ if b is not divisible by 13 where b is the denominator of the irreducible fraction $T = \frac{a}{b}$.

- At the third center, $r_5 \sim 0$:

The local metric is

$$\begin{aligned} ds_5^2 &= \frac{65\Lambda^2}{207} \sqrt{\frac{11}{6}} \left[\frac{dr_5^2}{r_5} + \frac{599081}{128700} dy_5^2 \right. \\ &\quad \left. + r_5 (d\theta_5^2 + 2(1 + \cos \theta_5) d\phi_{L5}^2 + 2(1 - \cos \theta_5) d\phi_{R5}^2) \right], \end{aligned} \quad (\text{A.8.7})$$

where y_5 , ϕ_{L5} and ϕ_{R5} are related to the angles at infinity y_∞ , ψ_∞ and ϕ by

$$\begin{aligned} y_5 &= y_\infty - \frac{3}{61}(3\psi_\infty - 13\phi), \\ \phi_{L5} &= \frac{1}{32}(21y_\infty + 31\psi_\infty - 17\phi) + \phi, \\ \phi_{R5} &= \frac{1}{32}(21y_\infty + 31\psi_\infty - 17\phi). \end{aligned} \quad (\text{A.8.8})$$

Then, we can read the periodicities from (8.2.23)

$$(y_5, \phi_{L5}, \phi_{R5}) = \begin{cases} (y_5, \phi_{L5}, \phi_{R5}) + \frac{320\pi T}{28853} (120, -61, -61) \\ (y_5, \phi_{L5}, \phi_{R5}) + \frac{\pi}{488} (-288, 1891, 1891) \\ (y_5, \phi_{L5}, \phi_{R5}) + \frac{\pi}{488} (480, 1403, 427) \end{cases}. \quad (\text{A.8.9})$$

This corresponds to a smooth discrete quotient of $S^1 \times \mathbb{R}^4$ if b is not divisible by 16 where b is the denominator of the irreducible fraction $T = \frac{a}{b}$.

- At the fourth center, $r_p \sim 0$:

The local metric is

$$\begin{aligned} ds_p^2 &= \frac{\Lambda^2}{207} \sqrt{\frac{145}{3}} \left[\frac{dr_p^2}{r_p} + \frac{66309}{232} dy_p^2 \right. \\ &\quad \left. + r_p (d\theta_p^2 + 2(1 + \cos \theta_p) d\phi_{Lp}^2 + 2(1 - \cos \theta_p) d\phi_{Rp}^2) \right], \end{aligned} \quad (\text{A.8.10})$$

where y_p , ϕ_{Lp} and ϕ_{Rp} are related to the angles at infinity y_∞ , ψ_∞ and ϕ by

$$\begin{aligned} y_p &= y_\infty - \frac{21}{31}(\psi_\infty + \phi) , \\ \phi_{Lp} &= \frac{1}{16}(21 y_\infty + 31 \psi_\infty + 15 \phi) + \phi , \\ \phi_{Rp} &= \frac{1}{16}(21 y_\infty + 31 \psi_\infty + 15 \phi) . \end{aligned} \quad (\text{A.8.11})$$

Then, we can read the periodicities from (8.2.23)

$$(y_p, \phi_{Lp}, \phi_{Rp}) = \begin{cases} (y_p, \phi_{Lp}, \phi_{Rp}) + \frac{640 \pi T}{14663} (3, -31, -31) \\ (y_p, \phi_{Lp}, \phi_{Rp}) + \frac{\pi}{124} (336, 961, 961) \\ (y_p, \phi_{Lp}, \phi_{Rp}) + \frac{\pi}{124} (336, 961, 713) \end{cases} . \quad (\text{A.8.12})$$

This corresponds to a smooth discrete quotient of $S^1 \times \mathbb{R}^4$ if b is not divisible by 8 where b is the denominator of the irreducible fraction $T = \frac{a}{b}$.

Therefore, the IR bubbling geometry is smooth if and only if $T = \frac{a}{b} \in \mathbb{Q}$ and b is not divisible by 2 or 13.

A.9 The example of asymptotically NHEK bubbling solution

In this section, we focus on the IR geometry of the solution constructed in 8.3.3. We give the local $S^1 \times \mathbb{R}^4$ metrics (8.2.15) around each of the four centers and the periodicities of the angles.

- At the origin of the space, $r \sim 0$:

The local metric is

$$\begin{aligned} ds_0^2 &= \frac{\Lambda^2}{240} \sqrt{\frac{675 - 67\sqrt{65}}{6}} \left[\frac{dr^2}{r} + \frac{49(2915 + 259\sqrt{65})}{10240} dy_0^2 \right. \\ &\quad \left. + r(d\theta^2 + 2(1 + \cos \theta) d\phi_{L0}^2 + 2(1 - \cos \theta) d\phi_{R0}^2) \right] , \end{aligned} \quad (\text{A.9.1})$$

where y_0 , ϕ_{L0} and ϕ_{R0} are related to the angles at infinity y_∞ , ψ_∞ and ϕ by

$$\begin{aligned} y_0 &= y_\infty + \frac{17}{7}(\psi_\infty - \phi) , \\ \phi_{L0} &= -6 y_\infty + 10(\phi - \psi_\infty) + \phi , \\ \phi_{R0} &= -6 y_\infty + 10(\phi - \psi_\infty) . \end{aligned} \quad (\text{A.9.2})$$

The periodicities derived from (8.3.8) are

$$(y_0, \phi_{L0}, \phi_{R0}) = \begin{cases} (y_0, \phi_{L0}, \phi_{R0}) + 2\pi \left(-\frac{33}{7\Lambda}, \frac{15}{\Lambda}, \frac{15}{\Lambda} \right) \\ (y_0, \phi_{L0}, \phi_{R0}) + 2\pi \left(\frac{34}{7}, -20, -20 \right) \\ (y_0, \phi_{L0}, \phi_{R0}) + 2\pi (0, 1, 0) \end{cases} . \quad (\text{A.9.3})$$

Using the procedure of Section 8.2.2, this is a smooth discrete quotient of $S^1 \times \mathbb{R}^4$ for any rational Λ .

- At the second center, $r_1 \sim 0$:

The local metric is

$$ds_1^2 = \frac{\Lambda^2}{420} \sqrt{\frac{-635 + 123\sqrt{65}}{2}} \left[\frac{dr_1^2}{r_1} + \frac{289(2575 + 303\sqrt{65})}{47360} dy_1^2 \right. \\ \left. + r_1 (d\theta_1^2 + 2(1 + \cos \theta_1) d\phi_{L1}^2 + 2(1 - \cos \theta_1) d\phi_{R1}^2) \right], \quad (\text{A.9.4})$$

where y_1 , ϕ_{L1} and ϕ_{R1} are related to the angles at infinity y_∞ , ψ_∞ and ϕ by

$$\begin{aligned} y_1 &= y_\infty + \frac{1}{17} (23\psi_\infty - 27\phi), \\ \phi_{L1} &= -6y_\infty - 10\psi_\infty + 12\phi, \\ \phi_{R1} &= -6y_\infty - 10\psi_\infty + 11\phi. \end{aligned} \quad (\text{A.9.5})$$

The periodicities are

$$(y_1, \phi_{L1}, \phi_{R1}) = \begin{cases} (y_1, \phi_{L1}, \phi_{R1}) - 2\pi \left(-\frac{27}{17\Lambda}, \frac{15}{\Lambda}, \frac{15}{\Lambda} \right) \\ (y_1, \phi_{L1}, \phi_{R1}) + 2\pi \left(\frac{46}{17}, -20, -20 \right) \\ (y_1, \phi_{L1}, \phi_{R1}) + 2\pi \left(-\frac{4}{17}, 2, 1 \right) \end{cases}. \quad (\text{A.9.6})$$

This is a smooth discrete quotient of $S^1 \times \mathbb{R}^4$.

- At the third center, $r_5 \sim 0$:

The local metric is

$$ds_5^2 = \frac{\Lambda^2}{560} \sqrt{\frac{9635 - 323\sqrt{65}}{6}} \left[\frac{dr_5^2}{r_5} + \frac{529(1215 + 223\sqrt{65})}{564480} dy_5^2 \right. \\ \left. + r_5 (d\theta_5^2 + 2(1 + \cos \theta_5) d\phi_{L5}^2 + 2(1 - \cos \theta_5) d\phi_{R5}^2) \right], \quad (\text{A.9.7})$$

where y_5 , ϕ_{L5} and ϕ_{R5} are related to the angles at infinity y_∞ , ψ_∞ and ϕ by

$$\begin{aligned} y_5 &= y_\infty + \frac{1}{23} (\psi_\infty + 3\phi), \\ \phi_{L5} &= -\frac{1}{21} (6y_\infty + 10\psi_\infty + 9\phi) + \phi, \\ \phi_{R5} &= -\frac{1}{21} (6y_\infty + 10\psi_\infty + 9\phi), \end{aligned} \quad (\text{A.9.8})$$

with the following periodicities

$$(y_5, \phi_{L5}, \phi_{R5}) = \begin{cases} (y_5, \phi_{L5}, \phi_{R5}) + 2\pi \left(\frac{51}{23\Lambda}, \frac{5}{7\Lambda}, \frac{5}{7\Lambda} \right) \\ (y_5, \phi_{L5}, \phi_{R5}) + 2\pi \left(\frac{2}{23}, -\frac{20}{21}, -\frac{20}{21} \right) \\ (y_5, \phi_{L5}, \phi_{R5}) + 2\pi \left(\frac{4}{23}, \frac{2}{21}, -\frac{19}{21} \right) \end{cases}. \quad (\text{A.9.9})$$

This corresponds to a smooth discrete quotient of $S^1 \times \mathbb{R}^4$.

- At the fourth center, $r_p \sim 0$:

The local metric is

$$ds_p^2 = \frac{4\Lambda^2}{9} \frac{1}{43675 + 5435\sqrt{65}} \left[\frac{dr_p^2}{r_p} + \frac{45(6145 + 737\sqrt{65})}{8} dy_p^2 + r_p (d\theta_p^2 + 2(1 + \cos \theta_p) d\phi_{Lp}^2 + 2(1 - \cos \theta_p) d\phi_{Rp}^2) \right], \quad (\text{A.9.10})$$

where y_p , ϕ_{Lp} and ϕ_{Rp} are related to the angles at infinity y_∞ , ψ_∞ and ϕ by

$$\begin{aligned} y_p &= y_\infty + \frac{3}{5}(\psi_\infty + \phi), \\ \phi_{Lp} &= -6y_\infty - 10\psi_\infty - 9\phi, \\ \phi_{Rp} &= -6y_\infty - 10\psi_\infty - 10\phi. \end{aligned} \quad (\text{A.9.11})$$

The periodicities are

$$(y_p, \phi_{Lp}, \phi_{Rp}) = \begin{cases} (y_p, \phi_{Lp}, \phi_{Rp}) - 2\pi \left(\frac{3}{5\Lambda}, \frac{15}{\Lambda}, \frac{15}{\Lambda} \right) \\ (y_p, \phi_{Lp}, \phi_{Rp}) + 2\pi \left(\frac{6}{5}, -20, -20 \right) \\ (y_p, \phi_{Lp}, \phi_{Rp}) + 2\pi \left(\frac{6}{5}, -19, -20 \right) \end{cases}. \quad (\text{A.9.12})$$

This corresponds to a smooth discrete quotient of $S^1 \times \mathbb{R}^4$. Thus, the IR bubbling geometry is smooth for any rational values of Λ .

Appendix of Chapter 9

A.10 Analytic solution of the wave equation for large n

In this appendix we give the full mathematical proof of our method to analytically solve the radial part of the free massless scalar wave equation (9.3.15) in a $(1, 0, n)$ -superstratum geometry with $n \gg 1$, working to leading order in the $1/n$ expansion. From the outset we impose the condition $\Delta \neq 1$ as required by the regularity of the angular wavefunction (9.3.13). For ease of presentation, we consider $P + q_2 \neq 0$. However, one can apply the same method when $P + q_2 = 0$.

We solve for $K(z)$ subject to

$$K(0) = 0, \quad K(1) = 0. \quad (\text{A.10.1})$$

To do so we divide the radial equation in two pieces:

$$\mathcal{L}[\tilde{\Omega}] K(z) - \frac{z^n}{1-z} \mathcal{E}[\tilde{\Omega}] K(z) = 0, \quad (\text{A.10.2})$$

where

$$\begin{aligned} \mathcal{L}[\tilde{\Omega}] &\equiv \partial_z (z \partial_z) + \frac{1}{4(1-z)} \left[\left(P + q_1 + \frac{b^2 \tilde{\Omega}}{2} \right)^2 - \frac{(P + q_2)^2}{z} - \frac{\Delta(\Delta - 2)}{1-z} \right], \\ \mathcal{E}[\tilde{\Omega}] &\equiv \frac{b^2 \tilde{\Omega} (4q_1 + b^2 \tilde{\Omega})}{16}, \end{aligned} \quad (\text{A.10.3})$$

where we remind the reader that q_1 , q_2 and Δ are integers.

The strategy will be to exploit the fact that $\mathcal{L}[\tilde{\Omega}]K = 0$ is analytically solvable, and that the second term in (A.10.2) can be treated (with some care) as subleading. We make a series expansion in $1/n^\nu$, where $\nu \equiv |\Delta - 1|$ was defined in (9.3.20),

$$\begin{aligned} K(z) &= K^{(1)}(z) + \frac{1}{n^\nu} K^{(2)}(z) + \frac{1}{n^{2\nu}} K^{(3)}(z) + \dots, \\ \tilde{\Omega} &= \Omega^{(1)} + \frac{1}{n^\nu} \Omega^{(2)} + \frac{1}{n^{2\nu}} \Omega^{(3)} + \dots \end{aligned} \quad (\text{A.10.4})$$

The powers of n in this expansion are chosen so that all $\Omega^{(J)}$ and $K^{(J)}(z)$ will turn out to be of order one when n is large.

We insert this expansion in the wave equation (A.10.2), and we arrange the series expansion in $1/n$ according to our strategy. That is, we put the leading part of the second term in (A.10.2) on the right-hand side of the second equation below:

$$\begin{aligned} \mathcal{L}[\Omega^{(1)}] K^{(1)}(z) &= 0, & K^{(1)}(0) &= K^{(1)}(1) = 0, \\ \mathcal{L}[\Omega^{(1)}] K^{(2)}(z) &= \frac{K^{(1)}(z)}{1-z} \left(n^\nu \mathcal{E}[\Omega^{(1)}] z^n - b^2 \Omega^{(2)} (P + q_1 + \frac{b^2}{2} \Omega^{(1)}) \right), & K^{(2)}(0) &= K^{(2)}(1) = 0, \end{aligned} \quad (\text{A.10.5})$$

and so on at higher order. We will carefully justify this arrangement of terms in what follows.

If one shows that each $K^{(J)}(z)$ and $\Omega^{(J)}$ are of order one when n is large, this guarantees that the series expansion (A.10.4) converges and that the principal features of the solution are captured by $K^{(1)}(z)$. The expansion is similar in spirit to the WKB approximation.

We will need to treat carefully the first term on the second line of (A.10.5). The main subtlety with this term is that even though $z^n \ll 1$ for $z \in [0, 1)$, the combination $\frac{z^n}{1-z}$ diverges as $z \rightarrow 1$. However, since $K^{(1)}(z)$ satisfies (A.10.5) then it behaves as $z \rightarrow 1$ as (9.3.19)

$$(1-z)^{\frac{1+|\Delta-1|}{2}}. \quad (\text{A.10.6})$$

Thus for $\Delta \geq 3$ and $\Delta \leq -1$, the combination $\frac{z^n}{1-z} K^{(1)}(z)$ tends to zero as $z \rightarrow 1$. For $\Delta = 2$ and $\Delta = 0$, $\frac{z^n}{1-z} K^{(1)}(z)$ tends to a finite value as $z \rightarrow 1$ (although the interval where $\frac{z^n}{1-z} K^{(1)}(z)$ is non-negligible is a set of measure zero in the large n limit). We will carefully analyze the equations and solutions for general Δ near $z \rightarrow 1$ in what follows.

Derivation of $K^{(1)}$

Let us solve the wave equation (A.10.5) for $K^{(1)}(z)$ without imposing any boundary condition. There is only one branch of regular solutions for $P + q_2 \in \mathbb{Z}^*$:

$$K^{(1)}(z) = \kappa^{(1)} z^{\frac{|P+q_2|}{2}} (1-z)^{-\frac{\Delta-2}{2}} {}_2F_1\left(\frac{\gamma-\delta}{2}, \frac{\gamma+\delta}{2}, \mu, z\right), \quad (\text{A.10.7})$$

with

$$\gamma = -\Delta + 2 + |P + q_2|, \quad \delta = P + q_1 + \frac{b^2 \Omega}{2}, \quad \mu = 1 + |P + q_2|, \quad (\text{A.10.8})$$

and where $\kappa^{(1)}$ is a constant.

- Condition $K^{(1)}(1) = 0$.

We compute the limit of $K^{(1)}$ (A.10.7) around $z = 1$ for the allowed values of Δ :

$$K^{(1)}(z) \underset{z \rightarrow 1}{\sim} \kappa^{(1)} \begin{cases} \frac{(\Delta-2)! \Gamma(\mu)}{\Gamma(\mu - \frac{\gamma+\delta}{2}) \Gamma(\mu - \frac{\gamma-\delta}{2})} (1-z)^{1-\frac{\Delta}{2}} + \mathcal{O}\left((1-z)^{\frac{\Delta}{2}}\right), & \Delta \geq -2, \\ \frac{(\Delta-2)! \Gamma(\mu)}{\Gamma(\frac{\gamma+\delta}{2}) \Gamma(\frac{\gamma-\delta}{2})} (1-z)^{\frac{\Delta}{2}} + \mathcal{O}\left((1-z)^{1-\frac{\Delta}{2}}\right), & \Delta \leq -4. \end{cases}$$

We see that the leading-order terms do not tend to zero as $z \rightarrow 1$, while the higher-order terms do. Thus, we must set the leading order terms to zero. This can be done by arranging a pole in one of the Gamma functions in the respective denominators:

$$\begin{aligned} \Delta \geq -2 & \Rightarrow \Gamma\left(\mu - \frac{\gamma \pm \delta}{2}\right) = \pm\infty \Rightarrow -\mu + \frac{\gamma \pm \delta}{2} = j \in \mathbb{N}, \\ \Delta \leq -4 & \Rightarrow \Gamma\left(\frac{\gamma \pm \delta}{2}\right) = \pm\infty \Rightarrow -\frac{\gamma \pm \delta}{2} = j \in \mathbb{N}. \end{aligned} \quad (\text{A.10.9})$$

Both conditions give the same two towers of permitted values of $\Omega^{(1)}$ labelled by j ,

$$\begin{aligned} \Omega_j^{(1)+} &= \frac{2}{b^2} \left[2j + 1 + |\Delta - 1| + |P + q_2| - (P + q_1) \right], \\ \Omega_j^{(1)-} &= -\frac{2}{b^2} \left[2j + 1 + |\Delta - 1| + |P + q_2| + (P + q_1) \right]. \end{aligned} \quad (\text{A.10.10})$$

As usual we restrict attention to the positive frequencies, $\Omega_j^{(1)} = \Omega_j^{(1)+}$. Thus, the radial wave functions are

$$K_j^{(1)}(z) = \kappa_j^{(1)} (1-z)^{\frac{1+|\Delta-1|}{2}} z^{\frac{|P+q_2|}{2}} \sum_{\ell=0}^j (-1)^\ell \binom{j}{\ell} \frac{(j+1+|\Delta-1|+|P+q_2|)_\ell}{(1+|P+q_2|)_\ell} z^\ell. \quad (\text{A.10.11})$$

- Condition $K^{(1)}(0) = 0$.

We observe that this condition is automatically satisfied by the radial wave function (A.10.11).

Derivation of $K^{(2)}$

From now on, $K^{(1)}$ is fixed to be a polynomial function of the tower labelled by j given in (A.10.11). We must now solve the following differential equation (A.10.5) to find $K_j^{(2)}$,

$$\begin{aligned} \mathcal{L}[\Omega_j^{(1)}] K_j^{(2)}(z) &= \frac{K_j^{(1)}(z)}{1-z} \left(n^\nu \mathcal{E}[\Omega_j^{(1)}] z^n - \gamma_j^{(2)} \right), \\ K_j^{(2)}(0) &= K_j^{(2)}(1) = 0, \end{aligned} \quad (\text{A.10.12})$$

where for convenience we have defined the constant $\gamma_j^{(2)}$ to be

$$\gamma_j^{(2)} \equiv b^2 \Omega_j^{(2)} \left(P + q_1 + \frac{b^2}{2} \Omega_j^{(1)} \right). \quad (\text{A.10.13})$$

This is the more involved step of the method. It is crucial to show that solutions of (A.10.12) do not diverge at the boundaries and are of order one when n is large. If one of these two conditions is not satisfied, the expansion (A.10.4) is ill-defined. We use the standard method of variation of parameters to solve the equation, since we already know that $K_j^{(1)}$ is a solution to the homogeneous equation. We find

$$K_j^{(2)}(z) = K_j^{(1)}(z) \int_0^z dy \frac{\mathcal{P}_j(y)}{y \left(K_j^{(1)}(y) \right)^2}, \quad (\text{A.10.14})$$

where \mathcal{P}_j is a polynomial defined by

$$\mathcal{P}_j(y) \equiv \int_0^y dx \frac{\left(K_j^{(1)}(x) \right)^2}{1-x} \left(n^\nu \mathcal{E}[\Omega_j^{(1)}] x^n - \gamma_j^{(2)} \right). \quad (\text{A.10.15})$$

At first sight, the integral (A.10.14) appears likely to be divergent. Indeed, the polynomial $y \left(K_j^{(1)}(y) \right)^2$ has $j+2$ distinct roots: a root of multiplicity $|P+q_2|+1$ at 0, a root of multiplicity $1+|\Delta-1|$ at 1, and j roots of multiplicity 2 between 0 and 1; let us call these intermediate roots α_ℓ for $\ell = 1, \dots, j$ (see Eq. (A.10.11)). We will see that assigning a specific value to $\gamma_j^{(2)}$ will make the function regular and bounded everywhere. Before dealing with the regularity issues at each zero, we first rewrite $\left(K_j^{(1)}(z) \right)^2$ in three convenient forms that will be useful in what follows:

$$\begin{aligned} \left(K_j^{(1)}(z) \right)^2 &= \kappa_j^2 (1-z)^{1+|\Delta-1|} z^{|P+q_2|} \prod_{\ell=1}^j (z - \alpha_\ell)^2 \\ &= \kappa_j^2 z^{|P+q_2|} (1-z) \sum_{\ell} a_\ell z^\ell \\ &= \kappa_j^2 (1-z)^{1+|\Delta-1|} \sum_{\ell} b_\ell (1-z)^\ell \end{aligned} \quad (\text{A.10.16})$$

where κ_j is a constant and where the sums on the second and third lines run from 0 to the appropriate maximum values of ℓ .

- At $z = 0$

The integral (A.10.14) appears to be ill-defined at $z = 0$. However, if we compute $\mathcal{P}_j(y)$ with the second formulation of $\left(K_j^{(1)}(z)\right)^2$ in (A.10.16), the regularity of the integral at 0 is explicit. We integrate (A.10.15):

$$\mathcal{P}_j(y) = \kappa_j y^{|P+q_2|+1} \sum_{\ell} a_{\ell} \left(\frac{n^{\nu} \mathcal{E}[\Omega_j^{(1)}]}{n + |P + q_2| + \ell} y^n - \frac{\gamma_j^{(2)}}{|P + q_2| + \ell} \right) y^{\ell}. \quad (\text{A.10.17})$$

Moreover, the denominator in (A.10.14) is

$$y \left(K_j^{(1)}(y)\right)^2 = \kappa_j y^{|P+q_2|+1} (1-y)^{1+|\Delta-1|} \prod_{\ell=0}^j (y - \alpha_{\ell})^2. \quad (\text{A.10.18})$$

By comparing those two expressions, it is straightforward to see that $\frac{\mathcal{P}_j(y)}{y \left(K_j^{(1)}(y)\right)^2}$ takes a finite value at $y = 0$ and is integrable at 0. Furthermore, if one takes the limit $z \rightarrow 0$ of the differential equation (A.10.12) one can show that $K_j^{(2)}$ has a zero of multiplicity $\frac{|P+q_2|}{2}$ at $z = 0$ exactly as $K_j^{(1)}$.

- At $z = \alpha_{\ell}$

Obviously, $z = \alpha_{\ell}$ is not a zero of $\mathcal{P}_j(y)$. So the argument above cannot be used here. However, around α_{ℓ} we have

$$\begin{aligned} \int_0^z \frac{\mathcal{P}_j(y)}{y \left(K_j^{(1)}(y)\right)^2} &\underset{z \rightarrow \alpha_{\ell}}{\sim} \int_0^z \frac{dy}{(y - \alpha_{\ell})^2} \underset{z \rightarrow \alpha_{\ell}}{\sim} \frac{1}{z - \alpha_{\ell}}, \\ K_j^{(1)}(z) &\underset{z \rightarrow \alpha_{\ell}}{\sim} (z - \alpha_{\ell}). \end{aligned} \quad (\text{A.10.19})$$

Thus, the product of the two is well-defined and $K_j^{(2)}$ is well-defined at $z = \alpha_{\ell}$.

- At $z = 1$

Proving the regularity of $K_j^{(2)}$ around 1 is less straightforward. The most direct argument we found is the following: we compute $\mathcal{P}_j(y)$ using the third expression of (A.10.16) and we prove that $\mathcal{P}_j(y)$ has a zero of multiplicity $1 + \nu$ at 1 for a specific value of $\Omega_j^{(2)}$ (A.10.4). We derive $\mathcal{P}_j(y)$ according to (A.10.16)

$$\begin{aligned} \mathcal{P}_j(y) &= \mathcal{P}_j(1) - \int_y^1 dx \frac{\left(K_j^{(1)}(x)\right)^2}{1-x} \left(n^{\nu} \mathcal{E}[\Omega_j^{(1)}] x^n - \gamma_j^{(2)} \right), \\ &= \mathcal{P}_j(1) + (1-y)^{1+\nu} \sum_{\ell} b'_{\ell} (1-y)^{\ell}. \end{aligned} \quad (\text{A.10.20})$$

where b'_{ℓ} can be computed from b_{ℓ} (A.10.16), $\mathcal{E}[\Omega_j^{(1)}]$, $\gamma_j^{(2)}$ and n . Consequently, if we fix $\Omega_j^{(2)}$ to satisfy $\mathcal{P}_j(1) = 0$, $\mathcal{P}_j(y)$ has indeed a zero of multiplicity $(1 + \nu)$ at 1 which guarantees that $K_j^{(2)}$ takes a finite value. Moreover by expanding (A.10.17) in powers of $1/n$ we find

$$\begin{aligned} \mathcal{P}_j(y) &\equiv n^{\nu} \mathcal{E}[\Omega_j^{(1)}] y^{n+1} \sum_{\alpha=0} \frac{(-1)^{\alpha}}{n^{\alpha}} (y \partial_y)^{\alpha} \left(\frac{\left(K_j^{(1)}(y)\right)^2}{1-y} \right) \\ &\quad - \gamma_j^{(2)} \int_0^y dx \frac{\left(K_j^{(1)}(x)\right)^2}{1-x}, \end{aligned} \quad (\text{A.10.21})$$

where $(y\partial_y)^\alpha$ means we derive and multiply α times. Evaluating this formula at $y = 1$ shows that there always exists a unique solution $\Omega_j^{(2)}$ of $\mathcal{P}_j(1) = 0$ and this value is of order one when n is large and $j \lesssim \sqrt{n}$. Furthermore, if one takes the limit of the differential equation (A.10.12) for this particular value of $\Omega_j^{(2)}$ one can show that the finite value $K_j^{(2)}(1)$ must be exactly 0 and the multiplicity of this zero is necessarily $\frac{1+\nu}{2}$ exactly as it is for $K_j^{(1)}$.

Finally, $K_j^{(2)}$ does not diverge in $[0, 1]$ and it is straightforward from (A.10.17) and (A.10.14) that $K_j^{(2)}(z)$ is of order one when n is large.

In a nutshell, we have shown that the second term of the series expansion (A.10.4) is well-defined: $K_j^{(2)}(z)$ is regular, $K_j^{(2)}(0) = K_j^{(2)}(1) = 0$ with the same multiplicity as $K_j^{(1)}$ and $\Omega_j^{(2)}$ and $K_j^{(2)}(z)$ are of order one when n is large and $j \lesssim \sqrt{n}$.

Higher-order terms

We finally discuss the higher-order terms of the $\frac{1}{n}$ -expansion $\{K_j^{(3)}, \dots; \Omega_j^{(3)}, \dots\}$. Each term of the expansion satisfies a differential equation of the form

$$\begin{aligned} \mathcal{L}[\Omega_j^{(1)}] K_j^{(J)}(z) &= (\dots) K_j^{(1)}(z) + (\dots) K_j^{(2)}(z) + \dots + (\dots) K_j^{(J-1)}(z), \\ K_j^{(J)}(0) &= K_j^{(J)}(1) = 0. \end{aligned} \tag{A.10.22}$$

If we know that each function $K_j^{(K)}(z)$ for $K < J$ is well-defined with zeroes at $z = 0$ and $z = 1$ with multiplicity $\frac{|p+q_2|}{2}$ and $\frac{1+\nu}{2}$ respectively, the same arguments as above can be used to prove that there exists a value for $\Omega_j^{(J)}$ where $K_j^{(J)}(z)$ is well-defined with the same kinds of zeroes at $z = 0$ and $z = 1$.

To conclude, we have solved the wave equation (9.3.22) in the limit where n is large. We have expanded the solutions for large n and demonstrated the consistency of this expansion. All the features of the tower of solutions are captured by the tower of leading-order terms $K_j^{(1)}$, as discussed in Section 9.3.3.

Appendix of Chapter 10

A.11 Potentials with arbitrarily many turning points

We consider a Schrödinger equation of the type (10.1.4) with a potential with arbitrarily many classical turning points where the potential vanishes. In this section, one will give the expression of the quantity \mathcal{A} which encodes the information about the potential $V(x)$ for $x < x_+$ as well as the physical boundary condition imposed as $x \rightarrow -\infty$ in the response function computed from the WKB hybrid technique (10.1.15):

- If $V(x)$ has an even number, $2k$, of turning points, $x_1, x_2 \dots x_{2k}$, one necessarily has $V(x) \geq 0$ in the “interior region,” $x < x_1$. The physical boundary condition as $x \rightarrow -\infty$ is that Ψ is smooth in this limit. Thus, we have

$$\mathcal{A} = 2 \frac{M_{22}}{M_{12}}, \quad (\text{A.11.1})$$

where M_{ij} are the matrix elements of the following matrix

$$M \equiv \begin{pmatrix} -\sin \Theta_{2k-1} & 2 \cos \Theta_{2k-1} \\ \frac{1}{2} \cos \Theta_{2k-1} & \sin \Theta_{2k-1} \end{pmatrix} \cdot \prod_{j=1}^{k-1} \begin{pmatrix} \frac{1}{2} e^{-\Theta_{2j}} \cos \Theta_{2j-1} & e^{-\Theta_{2j}} \sin \Theta_{2j-1} \\ -e^{\Theta_{2j}} \sin \Theta_{2j-1} & 2 e^{\Theta_{2j}} \cos \Theta_{2j-1} \end{pmatrix}, \quad (\text{A.11.2})$$

with

$$\Theta_i \equiv \int_{x_i}^{x_{i+1}} |V(z)|^{\frac{1}{2}} dz. \quad (\text{A.11.3})$$

The Θ_{2j} with even indexes correspond to the tunnelling factors where the potential is positive and the Θ_{2j-1} give the phase factors from the field oscillations. One should order the matrices in the product according to: $\prod_{j=1}^{k-1} M^{(j)} = M^{(k-1)} \cdot M^{(k-2)} \dots M^{(1)}$.

- If $V(x)$ has an odd number, $2k-1$, of turning points, $x_1, x_2 \dots x_{2k-1}$, one necessarily has $V(x) < 0$ for $x < x_1$. The interesting physical boundary conditions are those of a black hole in which the modes are required to be purely infalling as $x \rightarrow -\infty$. The prescription used for the modes as a function of the time-coordinate, u , is $\Psi(x, u) = \Psi(x) e^{-i\Omega u}$. Thus, we obtain

$$\mathcal{A} = 2 \frac{\bar{M}_{21}}{\bar{M}_{11}}, \quad (\text{A.11.4})$$

where \bar{M}_{ij} are the matrix elements of the following matrix

$$\bar{M} \equiv -\text{sign}(\Omega) \prod_{j=1}^{k-1} \begin{pmatrix} 2 e^{\Theta_{2j-1}} \cos \Theta_{2j} & -e^{-\Theta_{2j-1}} \sin \Theta_{2j} \\ e^{\Theta_{2j-1}} \sin \Theta_{2j} & \frac{1}{2} e^{-\Theta_{2j-1}} \cos \Theta_{2j} \end{pmatrix} \cdot \begin{pmatrix} e^{-i\frac{\pi}{4}} & e^{i\frac{\pi}{4}} \\ \frac{1}{2} e^{i\frac{\pi}{4}} & \frac{1}{2} e^{-i\frac{\pi}{4}} \end{pmatrix} \quad (\text{A.11.5})$$

with the same definitions for (A.11.3) and the same matrix product conventions.

A.12 Comparison of the exact and approximate response functions

A.12.1 The exact and approximate BTZ response functions

The exact response function of a scalar field in an extremal-BTZ black hole for Δ non-integer has been computed in Section 10.2.2. We want to check the accuracy of the WKB formula (10.1.15) to retrieve the response function of an asymptotically BTZ geometry. For that purpose, we compare the WKB response function computed in a full-BTZ geometry (see Section 10.2.2.2) with its exact result, (10.2.25), by plotting the error function

$$\text{Err} \equiv \left| \frac{R_{WKB}^{\text{BTZ}} - R_E^{\text{BTZ}}}{R_E^{\text{BTZ}}} \right|, \quad (\text{A.12.1})$$

as a function of ω and p for different values of Δ (see Fig. A.7). From the graphs Fig. A.7, we observe that the accuracy of the WKB response function depends strongly on the sign of ωp . For positive values of ωp , the WKB formula is extremely close to the exact result for any values of Δ whereas for negative values, larger values of Δ gives a better accuracy. Moreover, it is really surprising how the accuracy of the formula does not depend on the order of magnitude of ω and p ¹. The only condition of validity of the formula we derived is that the order of magnitude of Δ is slightly higher than 1 (for $\Delta \sim 5$ the error is already below 5% for any values of ω and p). This is usually required by the WKB condition on the potential (10.1.5).

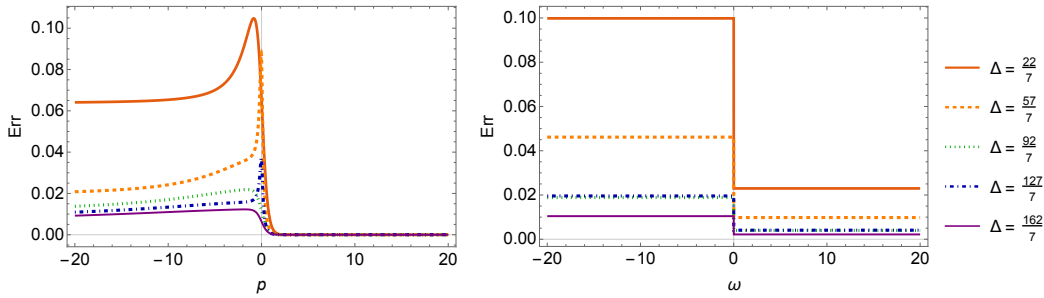


Figure A.7: The error function of the WKB formula (10.1.15), Err (A.12.1), for an extremal-BTZ geometry as a function of ω , p and Δ . The graph on the left gives Err as a function of p for different values of Δ and for $\omega = 1/2$ and $r_H = 1$. The graph on the right gives Err as a function of ω for the same values of Δ and for $p = 1/2$ and $r_H = 1$.

A.12.2 The exact and approximate AdS_3 response functions

Here we check the accuracy of the WKB formula (10.1.15) for global AdS_3 . The poles of the WKB response function which give the frequencies and momenta of the normalizable modes are given by Θ (10.2.55): $\Theta \in \frac{\pi}{2} \mathbb{Z}$. It is straightforward to see that it match the exact spectrum given by (10.2.59) if

$$\sqrt{(\omega - p)^2 - 1} \sim |\omega - p| \quad \Rightarrow \quad |\omega - p| \gg 1, \quad (\text{A.12.2})$$

which is directly satisfies in our regime of parameters (10.2.53) by the common validity condition of WKB: $\Delta \gg 1$.

Moreover, we can also compute the difference between the WKB result and the exact result as a function of ω and p as we did for BTZ. However, one cannot use the same error function (A.12.1) since

¹Usually the WKB approximation works for large values of momentum and frequencies.

now the response functions have poles and zeroes which are not exactly at the same location. It is preferable to compare smooth functions with no zero. Thus, we will compare the two exact functions $g_1(\omega, p)$ and $g_2(\omega, p)$, (10.2.58), to their WKB equivalents

$$g_1^{WKB}(\omega, p) \equiv \frac{\sqrt{3}}{2} e^{-2I_+} - \frac{\Psi_E^{\text{grow}}(x_+)}{\Psi_E^{\text{dec}}(x_+)}, \quad g_2^{WKB}(\omega, p) \equiv \frac{1}{2} e^{-2I_+}. \quad (\text{A.12.3})$$

We use a similar error function to (A.12.1)

$$\text{Err}_i \equiv \frac{g_i^{WKB} - g_i}{g_i}, \quad i = 1, 2. \quad (\text{A.12.4})$$

In Fig. A.8, we have plotted $\text{Err}_{1/2}$ for different values of Δ as a function of $\omega - p$ and $\omega + p$. As for BTZ, the WKB result proves to be highly accurate as soon as Δ is quite large and when $|\omega - p|$ is also larger than $\Delta - 1 + |\omega + p|$. Indeed for $\Delta \sim 5$ and $|\omega - p| - \Delta + 1 - |\omega + p| \sim 5$ the error of the WKB formula is already below 5%.

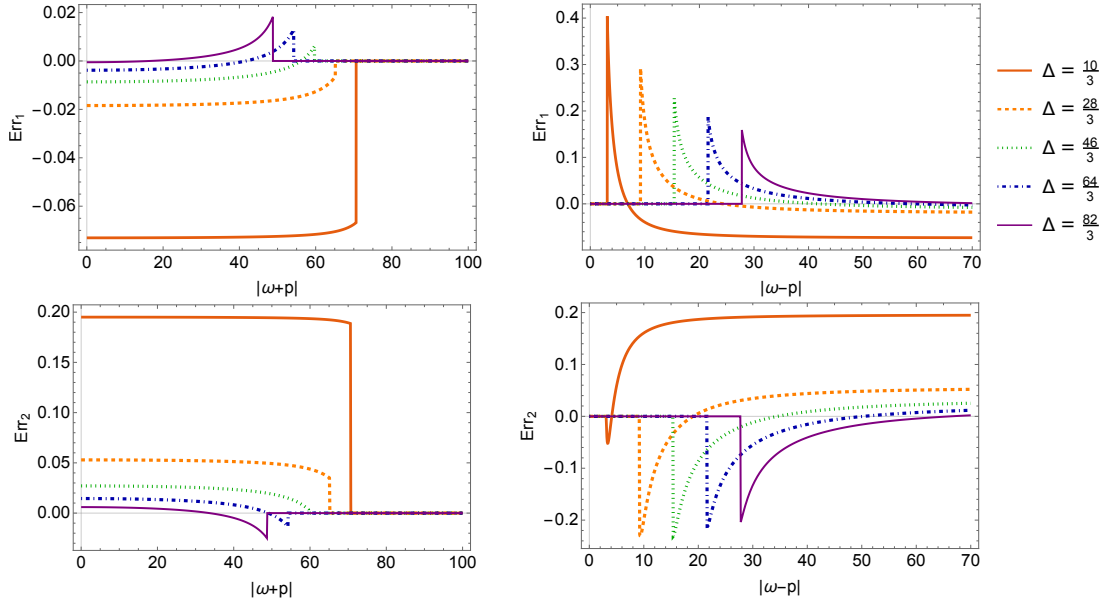


Figure A.8: The error functions of the WKB formula (10.1.15), $\text{Err}_{1/2}$ (A.12.4), for a Global AdS_3 geometry as a function of $|\omega - p|$, $|\omega + p|$ and Δ . The graphs on the left give $\text{Err}_{1/2}$ as a function of $|\omega - p|$ for different values of Δ and for $|\omega + p| = 1/2$. The graphs on the right give $\text{Err}_{1/2}$ as a function of $|\omega + p|$ for the same values of Δ and for $|\omega - p| = 80$. Each curve has a sharp ending point which corresponds to the point where (10.2.53) is not satisfied anymore.

A.13 Position-space Green functions

To clarify the different two-point functions, that is Feynman, Wightman, Advanced and Retarded propagators, one can obtain from the momentum space propagator, we examine two well-understood examples in some detail: global AdS and extremal BTZ.

A.13.1 Position space Green's functions in extremal BTZ

The inverse Fourier transform of the BTZ response function (10.2.25) separates into left-moving and right-moving part. This is possible because there is no *a priori* periodic identification of the y -circle,

neither on the bulk side nor on the boundary side of the duality is it enforced by regularity. The result is valid for quantized or continuous conjugate momentum. We will therefore perform the inverse transformation in p and ω independently, and impose spatial periodicity later.

The left-moving part of the propagator (10.2.25) has poles at $p = ir_H(\Delta + 2n)/l$ with corresponding residues $2r_H(-1)^m/(l m!)$ for $m \in \mathbb{Z}, m > 0$. Since they are in the upper imaginary p -plane, these poles are only picked up by the contour when it is closed in the upper half-plane. This happens only when $v < 0$, leading to the retarded propagator:

$$\begin{aligned}
\int \frac{dp}{2\pi} e^{-ip \frac{v}{R_y}} \frac{\Gamma(2-\Delta) \Gamma(\frac{1}{2}(\Delta + \frac{ilp}{r_H}))}{\Gamma(\Delta) \Gamma(1 - \frac{1}{2}(\Delta - \frac{ilp}{r_H}))} &= \theta(-v) \frac{\Gamma(2-\Delta)}{\Gamma(\Delta)} \sum_{m=0}^{\infty} \frac{4i\pi r_H e^{r_H v(\Delta+2m)/(l R_y)} (-1)^m}{2\pi l m! \Gamma(1-\Delta-m)} \\
&= \theta(-v) \frac{2il(1-\Delta)}{r_H \Gamma(\Delta)} e^{\frac{r_H \Delta v}{l R_y}} \sum_{m=0}^{\infty} \frac{(-1)^m \Gamma(1-\Delta) e^{\frac{2r_H m v}{l R_y}}}{\Gamma(m+1) \Gamma(1-\Delta-m)} \\
&= \theta(-v) \frac{2il(1-\Delta)}{r_H \Gamma(\Delta)} e^{\frac{r_H \Delta v}{l R_y}} \left(1 - e^{\frac{2r_H v}{l R_y}}\right)^{-\Delta} \\
&= -\frac{2il \theta(-v)}{r_H \Gamma(\Delta-1)} \left[-2 \sinh\left(\frac{r_H v}{l R_y}\right)\right]^{-\Delta} \tag{A.13.1}
\end{aligned}$$

Note that the series that appears is convergent since $|e^{2r_H v/(l R_y)}| < 1$.

For the right-moving part, $(-2i\omega l r_H)^{\Delta-1}$, we can split up the integral in $\omega > 0$ and $\omega < 0$. The first part gives the integral representation of the Γ function

$$\begin{aligned}
\int_0^{\infty} \frac{d\omega}{2\pi} e^{-i\omega \frac{u}{R_y}} (-2ilr_H \omega)^{\Delta-1} &= \frac{1}{2\pi} e^{-i\frac{\pi}{2}(\Delta-1)} (2lr_H)^{\Delta-1} \int_0^{\infty} d\omega e^{-i\omega \frac{u}{R_y}} \omega^{\Delta-1} \\
&= \frac{1}{2\pi} e^{-i\frac{\pi}{2}(\Delta-1)} (2lr_H)^{\Delta-1} \left(\frac{i u}{R_y}\right)^{-\Delta} \Gamma(\Delta). \tag{A.13.2}
\end{aligned}$$

The contribution from $\omega < 0$ gives exactly the complex conjugate of this result. Since it is purely imaginary for $u < 0$, the sum is only non-zero for positive u . Putting it all together we get

$$\begin{aligned}
R(u, v) &= -\frac{2i}{\pi l^2} (\Delta-1) (2lr_H)^{\Delta} \sin(\pi\Delta) \Theta(u) \Theta(-v) \left(\frac{u}{R_y}\right)^{-\Delta} \left[-2 \sinh\left(\frac{r_H v}{l R_y}\right)\right]^{-\Delta} \\
&= \frac{2(\Delta-1)}{\pi l^2} \Theta(t) (lr_H)^{\Delta} \left(\left[\sinh\left(\frac{r_H v}{l R_y} + i\epsilon\right) \left(\frac{u}{R_y} - i\epsilon\right) \right]^{-\Delta} \right. \\
&\quad \left. - \left[\sinh\left(-\frac{r_H v}{l R_y} + i\epsilon\right) \left(-\frac{u}{R_y} - i\epsilon\right) \right]^{-\Delta} \right). \tag{A.13.3}
\end{aligned}$$

In the final step we have rewritten the result as a commutator, to match with the definition of the retarded propagator.

As we remarked earlier, the BTZ metric (10.2.18) is defined for non-compact y with $-\infty < y < \infty$. One way to get the position-space Green function for a compactified y -circle, is to sum over images:

$$\begin{aligned}
R_c(u, v) &= \frac{2(\Delta-1)}{\pi l^2} \Theta(t) (lr_H)^{\Delta} \sum_{m \in \mathbb{Z}} \left(\left[\sinh\left(\frac{r_H(v-2\pi m R_y)}{l R_y} + i\epsilon\right) \left(\frac{u}{R_y} + 2\pi m - i\epsilon\right) \right]^{-2h} \right. \\
&\quad \left. - \left[\sinh\left(-\frac{r_H(v-2\pi m R_y)}{l R_y} + i\epsilon\right) \left(-\frac{u}{R_y} + 2\pi m - i\epsilon\right) \right]^{-2h} \right), \tag{A.13.4}
\end{aligned}$$

The result (A.13.4) is depicted in Figures A.9 and A.10.

The periodic images give rise to a quite different long-time behavior of the two-point function on the cylinder, as compared to that on the plane. Their impact is most dramatic in the left-moving

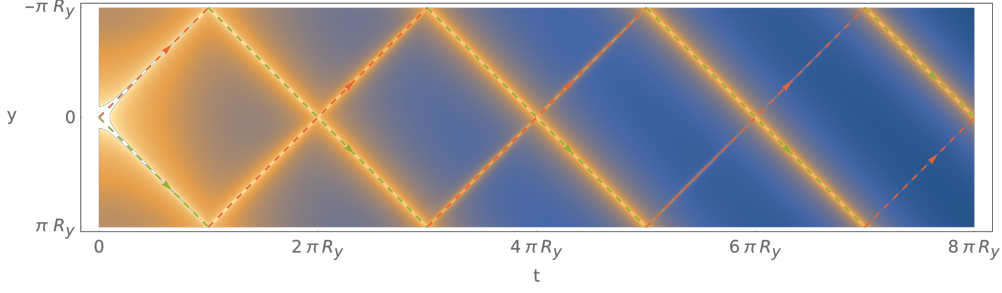


Figure A.9: Logarithmic densityplot of the two-point function (A.13.4) on a cylinder $(t, y) \cong (t, y + 2\pi R_y)$ with $h = 1$ and $r_H/(l R_y) = \pi/20$ (i.e. $\beta_L = 20$ and $\beta_R \rightarrow \infty$). The two-point function is sharply peaked on the light-cone (yellow), falling off polynomially in u (green arrows) and exponentially in v (red arrows). When following a light-ray (e.g. at constant v), the two-point function has peaks with u -periodicity $4\pi R_y$ whenever it meets the light-ray going in the other direction. Note that there are no reflecting boundary conditions in this figure, instead the y -circle is periodic.

section, i.e. when evolving in v while keeping u fixed. This is depicted in the second panel of Figure A.10 and in Figure A.11. As long as $\frac{r_H}{l R_y} v \lesssim 1$, the two-point function is dominated by the $m = 0$ image. Afterwards, the $m = 0$ image decays much faster than the total two-point function, and it is the “nearest” image (with $m \approx v/2\pi R_y$) is dominant.

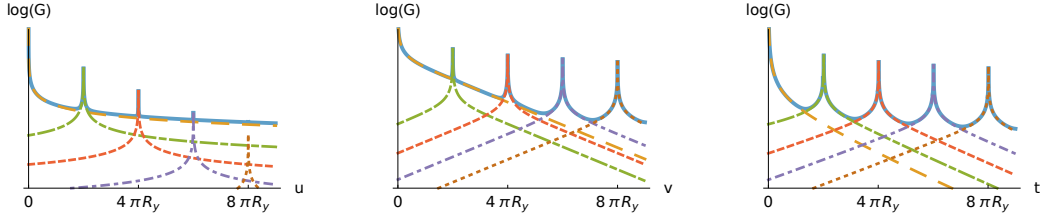


Figure A.10: Logarithmic plot of the two-point function (A.13.4) with $h = 1$ and $\frac{r_H}{a R_y} = \pi/8$ along three different directions (u , v and t) while keeping the orthogonal direction (v , u and y , resp.) constant, here: $R_y/20$. The total value of the two-point function is plotted (fat, blue) as well as the individual contributions from the $m = \{0, 1, 2, 3, 4\}$ modes (increasingly finely dashed lines). In the u direction, the behavior remains dominated by the $m = 0$ mode. The other modes appear briefly as poles on the light-cone. The behavior in the v direction is drastically different. Starting at v of order the inverse temperature, the $m = 0$ mode loses dominance to the “nearest” mode. The behavior in t shares properties of both u and v . The fall-off is exponential between the poles, but the exchange of dominance between the modes makes the long time behavior polynomial.

This observation can be made a bit more precise by considering when the m^{th} image becomes larger than the 0^{th} :

$$\left| \sinh\left(\frac{r_H}{l R_y} v\right) u \right|^{-\Delta} < \left| \sinh\left[\frac{r_H}{l R_y} (v - 2\pi R_y m)\right] (u + 2\pi R_y m) \right|^{-\Delta}. \quad (\text{A.13.5})$$

When $\frac{r_H}{l R_y} v \ll 1$, the left-hand side can be approximated by $(\frac{r_H}{l R_y} v u)^{-\Delta}$, which means that the m^{th} image only dominates when $|v - 2\pi R_y m| \lesssim |v| |u/2\pi R_y m|$, for small u . This is only true whenever the left-moving light-ray crosses the right-moving one. In the opposite regime $\frac{r_H}{l R_y} v \gg 1$, the exponential growth of the sinh-function takes over. The equation (A.13.5) reduces to

$$\sinh\left|\frac{r_H}{l R_y} (v - 2\pi R_y m)\right| < \left|\frac{u}{u + 2\pi R_y m}\right| e^{\frac{r_H}{l R_y} v}. \quad (\text{A.13.6})$$

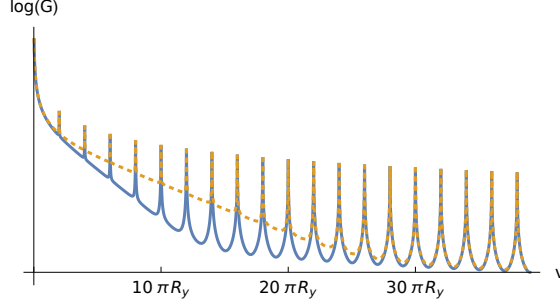


Figure A.11: Logarithmic plot of the two-point function (A.13.4) with $h = 1$ in the v -direction with $u = R_y/20$ held constant. The left-moving temperature is $\frac{r_H}{l R_y} = \pi/20$ for the solid blue line and $\frac{r_H}{l R_y} = \pi/40$ for the dotted orange line. The exponential fall-off (linear on this plot) is visible at early times, as long as the $m = 0$ mode dominates the propagator. In this regime, the other modes appear only briefly as poles. For v larger than $\pi\beta_L$, the behavior changes drastically. The propagator locally still behaves as an exponential, but the enveloping curve is polynomial at long times.

This inequality is first satisfied when v is roughly halfway between 0 and $2\pi R_y m$. In this regime, the two-point function is always dominated by the closest image. Thus, at long time scales, the behavior of the two-point function is drastically altered by the compact y -circle: the propagator is not suppressed as $e^{-2h \frac{r_H}{l R_y} v}$ but roughly as v^{-2h} .

A.13.2 Position space Green's functions in AdS_3

The Fourier transform of the AdS propagators R_1 and R_2 in (10.2.45) is more complicated because they have poles on the real ω and p axes. Unlike the BTZ case, the retarded propagator is no longer singled out by the location of the poles. Instead, there are some rather simple and direct routes to linking R_1 and R_2 to various Green functions by altering the contour prescription. We will focus on retarded two-point functions as before. Extracting the ω -dependent part of R_1 , we define²:

$$\tilde{I}_1(\omega) \equiv -i \Gamma(1 - \Delta) \frac{\Gamma(\frac{1}{2}\Delta + \omega)}{\Gamma(1 - \frac{1}{2}\Delta + \omega)}. \quad (\text{A.13.7})$$

and consider the Fourier transform to position space

$$I_1(u) \equiv \int \frac{d\omega}{2\pi} e^{-i\omega \frac{u}{R_y}} \tilde{I}_1(\omega + i\epsilon). \quad (\text{A.13.8})$$

where we have introduced $\epsilon > 0$ to make \tilde{I}_1 analytic in the upper complex ω plane. This is the appropriate continuation to calculate the retarded propagator, since it makes the inverse Fourier transform vanish for $\text{Re}(u) < 0$ where the contour can be deformed to $\text{Im}(\omega) \rightarrow \infty$. The Γ -function in the numerator has poles at $\omega = -i\epsilon - (\frac{1}{2}\Delta + m)$, with corresponding residues $(-1)^m/(m!)$ for any non-negative integer m . For $\text{Re}(u) > 0$, we can again express it as a sum over the residues:

$$\begin{aligned} I_1(u) &= -i \theta(u) \Gamma(1 - \Delta) \sum_{m=0}^{\infty} \frac{2i\pi e^{iu(\frac{1}{2}\Delta + m + i\epsilon)/R_y} (-1)^m}{2\pi m! \Gamma(1 - \Delta - m)} \\ &= \theta(u) \left[-2i \sin\left(\frac{u}{2R_y}\right) \right]^{-\Delta}. \end{aligned} \quad (\text{A.13.9})$$

²The p -dependent part of the response function is identical and the analysis can be done in a similar way.

Note that the series is convergent if $|e^{iu/R_y}| < 1$, which corresponds to $\text{Im}(u) > 0$, or, if one keeps u real, one must deform $u \rightarrow u + i\epsilon$:

$$I_1(u) = \theta(u) \left[-2i \sin\left(\frac{u+i\epsilon}{2R_y}\right) \right]^{-\Delta}. \quad (\text{A.13.10})$$

Up to an overall normalization, this is the left-moving part of the advanced Green function of the CFT on the cylinder.

Similarly, for the response function, R_2 , one can make the Fourier transform of

$$\tilde{I}_2(\omega) \equiv -i \Gamma(1-\Delta) \frac{\Gamma(\frac{1}{2}\Delta - \omega)}{\Gamma(1 - \frac{1}{2}\Delta - \omega)}, \quad (\text{A.13.11})$$

with the same $\omega \rightarrow \omega + i\epsilon$. One then finds

$$I_2(u) = \theta(u) \left[2i \sin\left(\frac{u-i\epsilon}{2R_y}\right) \right]^{-\Delta}. \quad (\text{A.13.12})$$

The shift $u \rightarrow u - i\epsilon$ arises because the sum over poles only converges if $|e^{-iu/R_y}| < 1$, which corresponds to $\text{Im}(u) < 0$. Thus the two response functions only differ by a phase and the space-time $i\epsilon$ prescription. To get the retarded Green function, one simply gives the poles in ω a small, *negative* imaginary part.

In the foregoing computation, we have taken a liberty by ignoring the periodicity of the y coordinate. Since this periodicity is fixed by smoothness in the origin of AdS_3 , we need to redo the computation more carefully. The Fourier transform of the response function, R_1 , is, more correctly, given by:

$$I_{full}(t, y) \equiv \sum_{k=-\infty}^{\infty} \int \frac{d\varpi}{2\pi} e^{-\frac{i\varpi t}{R_y}} e^{\frac{iky}{R_y}} \frac{\Gamma(1-\Delta) \Gamma(\frac{1}{2}(\Delta + k + \varpi)) \Gamma(\frac{1}{2}(\Delta + k - \varpi))}{\Gamma(\Delta - 1) \Gamma(1 - \frac{1}{2}(\Delta - k - \varpi)) \Gamma(1 - \frac{1}{2}(\Delta - k + \varpi))}, \quad (\text{A.13.13})$$

where $\varpi = (\omega - p)$ is the continuum momentum along t and $k = (\omega + p) \in \mathbb{Z}$ is the discrete Fourier mode around y .

There are now two sets of poles: $\varpi = \Delta + k + 2m$ and $\varpi = -\Delta - k - 2n$, $m \in \mathbb{Z}, m \geq 0$. For $2\Delta \notin \mathbb{Z}$, these poles never coincide. Moreover at these poles, the denominator always contains a factor of $\Gamma(1 + k + m)$, which means that there are only non-zero residues for $k + m \geq 0$. Thus the non-trivial residues separate into positive and negative frequencies: $\varpi = -\Delta - k - 2n < 0$ and $\varpi = \Delta + k + 2m > 0$.

A sum over the residues of the poles at $\varpi = \pm(\Delta + k + 2m)$ gives

$$\frac{\Gamma(1-\Delta)}{\Gamma(\Delta-1)} \sum_{k=-\infty}^{\infty} \sum_{m=0}^{\infty} (-1)^m \frac{\Gamma(k+m+\Delta)}{\Gamma(m+1)\Gamma(1-\Delta-m)\Gamma(1+k+m)} e^{\pm i(\Delta+k+2n)\frac{t}{R_y}} e^{\frac{iky}{R_y}} \quad (\text{A.13.14})$$

$$= e^{\pm \frac{i\Delta t}{R_y}} \left[\sum_{\ell=0}^{\infty} \frac{\Gamma(\ell+\Delta)}{\Gamma(\Delta-1)\Gamma(1+\ell)} e^{\pm \frac{i\ell(t\pm y)}{R_y}} \right] \left[\sum_{m=0}^{\infty} (-1)^m \frac{\Gamma(1-\Delta)}{\Gamma(m+1)\Gamma(1-\Delta-m)} e^{\pm \frac{im(t\mp y)}{R_y}} \right], \quad (\text{A.13.15})$$

where $\ell = (k + m)$ and we have used the fact that the residues vanish unless $\ell \geq 0$. Now use the identity

$$\Gamma(\Delta + \ell) = (-1)^\ell \frac{\Gamma(\Delta)\Gamma(1-\Delta)}{\Gamma(1-\Delta-\ell)} \quad (\text{A.13.16})$$

to rewrite the sum over residues as

$$\begin{aligned} & (\Delta - 1) e^{\pm \frac{i\Delta t}{R_y}} \left[\sum_{\ell=0}^{\infty} (-1)^\ell \frac{\Gamma(1-\Delta)}{\Gamma(1-\Delta-\ell)\Gamma(1+\ell)} e^{\pm \frac{i\ell(t\pm y)}{R_y}} \right] \\ & \quad \times \left[\sum_{m=0}^{\infty} (-1)^m \frac{\Gamma(1-\Delta)}{\Gamma(m+1)\Gamma(1-\Delta-m)} e^{\pm \frac{im(t\mp y)}{R_y}} \right] \\ & = (\Delta - 1) \left[\mp 2i \sin\left(\frac{t\pm(y+i\epsilon)}{2R_y}\right) \right]^{-\Delta} \left[\pm 2i \sin\left(\frac{t\mp(y+i\epsilon)}{2R_y}\right) \right]^{-\Delta} \end{aligned} \quad (\text{A.13.17})$$

This is the standard form of the CFT propagator on the cylinder defined by (t, y) , with $y \cong y + 2\pi R_y$. Whether one picks up the positive or negative frequency poles depends upon the sign of t in (A.13.13) and whether one integrates above or below the poles along the real axis (or, equivalently, whether one shifts the frequencies according to $\varpi \rightarrow \varpi \mp i\epsilon$). For example, the Feynman propagator is given by integrating above the positive frequency poles and below the negative frequency poles.

One should note that, in our discussion of the Green functions, we have ignored the Heaviside functions in (10.2.46) and worked with R_1 . To get the Feynman propagator from R^{AdS_3} requires a much more complicated set of contour deformations and analytic continuations. This is discussed in great detail in [198–200]. The important bottom line here is that the construction of Green functions in global AdS_3 is well-understood and, because the cap of Superstratum is a close approximation to the global AdS_3 with all the concomitant bound states and poles, the construction of Green functions will follow the same prescriptions that one uses in global AdS_3 itself.

Bibliography

- [1] **LIGO Scientific, Virgo**, B. P. Abbott *et al.*, “Observation of Gravitational Waves from a Binary Black Hole Merger,” *Phys. Rev. Lett.* **116** no. 6, (2016) 061102, [arXiv:1602.03837 \[gr-qc\]](#).
- [2] **Event Horizon Telescope**, K. Akiyama *et al.*, “First M87 Event Horizon Telescope Results. I. The Shadow of the Supermassive Black Hole,” *Astrophys. J.* **875** no. 1, (2019) L1.
- [3] J. M. Maldacena, “The large N limit of superconformal field theories and supergravity,” *Adv. Theor. Math. Phys.* **2** (1998) 231–252, [arXiv:hep-th/9711200](#).
- [4] E. D’Hoker and D. Z. Freedman, “Supersymmetric gauge theories and the AdS / CFT correspondence,” in *Strings, Branes and Extra Dimensions: TASI 2001: Proceedings*, pp. 3–158. 2002. [arXiv:hep-th/0201253 \[hep-th\]](#).
- [5] I. Bena, S. El-Showk, and B. Vercnocke, “Black Holes in String Theory,” *Springer Proc. Phys.* **144** (2013) 59–178.
- [6] A. Sen, “Extremal black holes and elementary string states,” *Mod. Phys. Lett. A* **10** (1995) 2081–2094, [arXiv:hep-th/9504147](#).
- [7] A. Dabholkar, “Exact counting of black hole microstates,” *Phys. Rev. Lett.* **94** (2005) 241301, [arXiv:hep-th/0409148](#).
- [8] A. Strominger and C. Vafa, “Microscopic Origin of the Bekenstein-Hawking Entropy,” *Phys. Lett. B* **379** (1996) 99–104, [arXiv:hep-th/9601029](#).
- [9] S. D. Mathur, “The fuzzball proposal for black holes: An elementary review,” *Fortsch. Phys.* **53** (2005) 793–827, [arXiv:hep-th/0502050](#).
- [10] J. Polchinski and M. J. Strassler, “The String dual of a confining four-dimensional gauge theory,” [arXiv:hep-th/0003136 \[hep-th\]](#).
- [11] B. C. Palmer and D. Marolf, “Counting supertubes,” *JHEP* **06** (2004) 028, [arXiv:hep-th/0403025](#).
- [12] V. S. Rychkov, “D1-D5 black hole microstate counting from supergravity,” *JHEP* **01** (2006) 063, [arXiv:hep-th/0512053](#).
- [13] D. Bak, Y. Hyakutake, and N. Ohta, “Phase moduli space of supertubes,” *Nucl. Phys. B* **696** (2004) 251–262, [arXiv:hep-th/0404104](#).
- [14] D. Bak, Y. Hyakutake, S. Kim, and N. Ohta, “A geometric look on the microstates of supertubes,” *Nucl. Phys. B* **712** (2005) 115–138, [arXiv:hep-th/0407253](#).
- [15] I. Bena and N. P. Warner, “Black holes, black rings and their microstates,” *Lect. Notes Phys.* **755** (2008) 1–92, [arXiv:hep-th/0701216](#).
- [16] K. Skenderis and M. Taylor, “The fuzzball proposal for black holes,” *Phys. Rept.* **467** (2008) 117–171, [arXiv:0804.0552 \[hep-th\]](#).
- [17] G. T. Horowitz and J. Polchinski, “A correspondence principle for black holes and strings,” *Phys. Rev. D* **55** (1997) 6189–6197, [arXiv:hep-th/9612146](#).
- [18] I. R. Klebanov and M. J. Strassler, “Supergravity and a confining gauge theory: Duality cascades and chi SB resolution of naked singularities,” *JHEP* **0008** (2000) 052, [arXiv:hep-th/0007191 \[hep-th\]](#).

- [19] H. Lin, O. Lunin, and J. M. Maldacena, “Bubbling AdS space and 1/2 BPS geometries,” *JHEP* **10** (2004) 025, [arXiv:hep-th/0409174](#).
- [20] S. D. Mathur, “The information paradox: A pedagogical introduction,” *Class. Quant. Grav.* **26** (2009) 224001, [arXiv:0909.1038 \[hep-th\]](#).
- [21] S. W. Hawking, M. J. Perry, and A. Strominger, “Soft Hair on Black Holes,” *Phys. Rev. Lett.* **116** no. 23, (2016) 231301, [arXiv:1601.00921 \[hep-th\]](#).
- [22] J. De Boer, S. F. Lokhande, E. Verlinde, R. Van Breukelen, and K. Papadodimas, “On the interior geometry of a typical black hole microstate,” [arXiv:1804.10580 \[hep-th\]](#).
- [23] P. Heidmann, “Four-center bubbled BPS solutions with a Gibbons-Hawking base,” *JHEP* **10** (2017) 009, [arXiv:1703.10095 \[hep-th\]](#).
- [24] I. Bena, P. Heidmann, and P. F. Ramirez, “A systematic construction of microstate geometries with low angular momentum,” *JHEP* **10** (2017) 217, [arXiv:1709.02812 \[hep-th\]](#).
- [25] I. Bena, P. Heidmann, and D. Turton, “AdS₂ holography: mind the cap,” *JHEP* **12** (2018) 028, [arXiv:1806.02834 \[hep-th\]](#).
- [26] P. Heidmann and S. Mondal, “The full space of BPS multicenter states with pure D-brane charges,” [arXiv:1810.10019 \[hep-th\]](#).
- [27] P. Heidmann, “Bubbling the NHEK,” *JHEP* **01** (2019) 108, [arXiv:1811.08256 \[hep-th\]](#).
- [28] P. Heidmann and N. P. Warner, “Superstratum Symbiosis,” [arXiv:1903.07631 \[hep-th\]](#).
- [29] I. Bena, P. Heidmann, R. Monten, and N. P. Warner, “Thermal Decay without Information Loss in Horizonless Microstate Geometries,” [arXiv:1905.05194 \[hep-th\]](#).
- [30] I. Bena, S. Giusto, R. Russo, M. Shigemori, and N. P. Warner, “Habemus Superstratum! A constructive proof of the existence of superstrata,” *JHEP* **05** (2015) 110, [arXiv:1503.01463 \[hep-th\]](#).
- [31] N. Ceplak, R. Russo, and M. Shigemori, “Supercharging Superstrata,” [arXiv:1812.08761 \[hep-th\]](#).
- [32] A. Einstein, “On the General Theory of Relativity,” *Sitzungsber. Preuss. Akad. Wiss. Berlin (Math. Phys.)* **1915** (1915) 778–786. [Addendum: *Sitzungsber. Preuss. Akad. Wiss. Berlin (Math. Phys.)* 1915, 799(1915)].
- [33] S. W. Hawking and G. F. R. Ellis, *The Large Scale Structure of Space-Time*. Cambridge Monographs on Mathematical Physics. Cambridge University Press, 2011.
- [34] R. M. Wald, *General Relativity*. Chicago Univ. Pr., Chicago, USA, 1984.
- [35] R. Penrose, “Gravitational collapse: The role of general relativity,” *Riv. Nuovo Cim.* **1** (1969) 252–276. [Gen. Rel. Grav. 34, 1141(2002)].
- [36] J. D. Bekenstein, “Black holes and the second law,” *Lett. Nuovo Cim.* **4** (1972) 737–740.
- [37] R. Penrose and R. M. Floyd, “Extraction of rotational energy from a black hole,” *Nature* **229** (1971) 177–179.
- [38] S. W. Hawking, “Particle Creation by Black Holes,” *Commun. Math. Phys.* **43** (1975) 199–220. Erratum: [Commun. Math. Phys. **46**, 206 (1976)].
- [39] S. R. Coleman and J. Mandula, “All Possible Symmetries of the S Matrix,” *Phys. Rev.* **159** (1967) 1251–1256.
- [40] E. Cremmer, B. Julia, and J. Scherk, “Supergravity Theory in Eleven-Dimensions,” *Phys. Lett.* **B76** (1978) 409–412. [,25(1978)].
- [41] W. Taylor, “TASI Lectures on Supergravity and String Vacua in Various Dimensions,” [arXiv:1104.2051 \[hep-th\]](#).

- [42] J. Polchinski, *String theory. Vol. 2: Superstring Theory and Beyond*. Cambridge Univ. Pr., 1998.
- [43] E. B. Bogomolny, “Stability of Classical Solutions,” *Sov. J. Nucl. Phys.* **24** (1976) 449. [*Yad. Fiz.*24,861(1976)].
- [44] M. K. Prasad and C. M. Sommerfield, “An Exact Classical Solution for the ’t Hooft Monopole and the Julia-Zee Dyon,” *Phys. Rev. Lett.* **35** (1975) 760–762.
- [45] J. P. Gauntlett and S. Pakis, “The Geometry of D = 11 killing spinors,” *JHEP* **0304** (2003) 039, [arXiv:hep-th/0212008 \[hep-th\]](#).
- [46] R. Blumenhagen, D. Lust, and S. Theisen, *Basic concepts of string theory*. Theoretical and Mathematical Physics. Springer, Heidelberg, Germany, 2013.
<http://www.springer.com/physics/theoretical%2C+mathematical+%26+computational+physics/book/978-3-642-29496-9>.
- [47] J. H. Schwarz and P. C. West, “Symmetries and Transformations of Chiral N=2 D=10 Supergravity,” *Phys. Lett.* **126B** (1983) 301–304.
- [48] J. H. Schwarz, “Covariant Field Equations of Chiral N=2 D=10 Supergravity,” *Nucl. Phys.* **B226** (1983) 269. [,269(1983)].
- [49] P. S. Howe and P. C. West, “The Complete N=2, D=10 Supergravity,” *Nucl. Phys.* **B238** (1984) 181–220.
- [50] L. J. Romans, “Massive N=2a Supergravity in Ten-Dimensions,” *Phys. Lett.* **B169** (1986) 374. [,374(1985)].
- [51] E. Witten, “String theory dynamics in various dimensions,” *Nucl. Phys.* **B443** (1995) 85–126, [arXiv:hep-th/9503124 \[hep-th\]](#). [,333(1995)].
- [52] M. Grana, “Flux compactifications in string theory: A Comprehensive review,” *Phys. Rept.* **423** (2006) 91–158, [arXiv:hep-th/0509003 \[hep-th\]](#).
- [53] T. H. Buscher, “A Symmetry of the String Background Field Equations,” *Phys. Lett.* **B194** (1987) 59–62.
- [54] I. V. Lavrinenko, H. Lu, C. N. Pope, and T. A. Tran, “U duality as general coordinate transformations, and space-time geometry,” *Int. J. Mod. Phys.* **A14** (1999) 4915–4942, [arXiv:hep-th/9807006 \[hep-th\]](#).
- [55] I. Antoniadis, S. Ferrara, and T. R. Taylor, “N=2 heterotic superstring and its dual theory in five-dimensions,” *Nucl. Phys.* **B460** (1996) 489–505, [arXiv:hep-th/9511108 \[hep-th\]](#).
- [56] M. Gunaydin, G. Sierra, and P. K. Townsend, “The Geometry of N=2 Maxwell-Einstein Supergravity and Jordan Algebras,” *Nucl. Phys.* **B242** (1984) 244–268.
- [57] M. Gunaydin, G. Sierra, and P. K. Townsend, “Gauging the d = 5 Maxwell-Einstein Supergravity Theories: More on Jordan Algebras,” *Nucl. Phys.* **B253** (1985) 573. [,573(1984)].
- [58] H. Nishino and E. Sezgin, “Matter and Gauge Couplings of N=2 Supergravity in Six-Dimensions,” *Phys. Lett.* **144B** (1984) 187–192.
- [59] S. Ferrara, F. Riccioni, and A. Sagnotti, “Tensor and vector multiplets in six-dimensional supergravity,” *Nucl. Phys.* **B519** (1998) 115–140, [arXiv:hep-th/9711059 \[hep-th\]](#).
- [60] J. B. Gutowski, D. Martelli, and H. S. Reall, “All supersymmetric solutions of minimal supergravity in six dimensions,” *Class. Quant. Grav.* **20** (2003) 5049–5078, [arXiv:hep-th/0306235](#).
- [61] M. Cariglia and O. A. P. Mac Conamhna, “The General form of supersymmetric solutions of N=(1,0) U(1) and SU(2) gauged supergravities in six-dimensions,” *Class. Quant. Grav.* **21** (2004) 3171–3196, [arXiv:hep-th/0402055 \[hep-th\]](#).

- [62] P. K. Townsend, “A New Anomaly Free Chiral Supergravity Theory From Compactification on K3,” *Phys. Lett.* **139B** (1984) 283–287.
- [63] S. Ferrara, R. Minasian, and A. Sagnotti, “Low-energy analysis of M and F theories on Calabi-Yau threefolds,” *Nucl. Phys.* **B474** (1996) 323–342, [arXiv:hep-th/9604097 \[hep-th\]](#).
- [64] A. Dabholkar and J. Park, “An Orientifold of type IIB theory on K3,” *Nucl. Phys.* **B472** (1996) 207–220, [arXiv:hep-th/9602030 \[hep-th\]](#).
- [65] E. G. Gimon and C. V. Johnson, “K3 orientifolds,” *Nucl. Phys.* **B477** (1996) 715–745, [arXiv:hep-th/9604129 \[hep-th\]](#).
- [66] E. G. Gimon and C. V. Johnson, “Multiple realizations of N=1 vacua in six-dimensions,” *Nucl. Phys.* **B479** (1996) 285–304, [arXiv:hep-th/9606176 \[hep-th\]](#).
- [67] L. E. Ibanez and A. M. Uranga, “D = 6, N=1 string vacua and duality,” in *Dualities in gauge and string theories. Proceedings, APCTP Winter School, Sorak Mountain Resort, Seoul, Sokcho, Korea, February 17-28, 1997*, pp. 230–282. 1997. [arXiv:hep-th/9707075 \[hep-th\]](#).
- [68] P. de Lange, D. R. Mayerson, and B. Vercnocke, “Structure of Six-Dimensional Microstate Geometries,” *JHEP* **09** (2015) 075, [arXiv:1504.07987 \[hep-th\]](#).
- [69] J. B. Gutowski and H. S. Reall, “General supersymmetric AdS(5) black holes,” *JHEP* **04** (2004) 048, [arXiv:hep-th/0401129 \[hep-th\]](#).
- [70] K. Behrndt, A. H. Chamseddine, and W. A. Sabra, “BPS black holes in N=2 five-dimensional AdS supergravity,” *Phys. Lett.* **B442** (1998) 97–101, [arXiv:hep-th/9807187 \[hep-th\]](#).
- [71] D. Klemm and W. A. Sabra, “Supersymmetry of black strings in D = 5 gauged supergravities,” *Phys. Rev.* **D62** (2000) 024003, [arXiv:hep-th/0001131 \[hep-th\]](#).
- [72] G. Gibbons and N. Warner, “Global structure of five-dimensional fuzzballs,” *Class. Quant. Grav.* **31** (2014) 025016, [arXiv:1305.0957 \[hep-th\]](#).
- [73] B. E. Niehoff and H. S. Reall, “Evanescent ergosurfaces and ambipolar hyperkähler metrics,” *JHEP* **04** (2016) 130, [arXiv:1601.01898 \[hep-th\]](#).
- [74] R. D. Sorkin, “Kaluza-klein monopole,” *Phys. Rev. Lett.* **51** (Jul, 1983) 87–90. <https://link.aps.org/doi/10.1103/PhysRevLett.51.87>.
- [75] D. J. Gross and M. J. Perry, “Magnetic monopoles in kaluza-klein theories,” *Nuclear Physics B* **226** no. 1, (1983) 29 – 48. <http://www.sciencedirect.com/science/article/pii/0550321383904625>.
- [76] F. Denef, “Supergravity flows and D-brane stability,” *JHEP* **0008** (2000) 050, [arXiv:hep-th/0005049 \[hep-th\]](#).
- [77] I. Bena, C.-W. Wang, and N. P. Warner, “The foaming three-charge black hole,” *Phys. Rev.* **D75** (2007) 124026, [arXiv:hep-th/0604110](#).
- [78] P. Berglund, E. G. Gimon, and T. S. Levi, “Supergravity microstates for BPS black holes and black rings,” *JHEP* **0606** (2006) 007, [arXiv:hep-th/0505167 \[hep-th\]](#).
- [79] I. Bena and N. P. Warner, “Bubbling supertubes and foaming black holes,” *Phys. Rev.* **D74** (2006) 066001, [arXiv:hep-th/0505166](#).
- [80] P. M. Crichigno, F. Porri, and S. Vandoren, “Bound states of spinning black holes in five dimensions,” *JHEP* **05** (2017) 101, [arXiv:1603.09729 \[hep-th\]](#).
- [81] I. Bena, N. Bobev, and N. P. Warner, “Spectral Flow, and the Spectrum of Multi-Center Solutions,” *Phys. Rev.* **D77** (2008) 125025, [arXiv:0803.1203 \[hep-th\]](#).
- [82] G. Dall’Agata, S. Giusto, and C. Ruef, “U-duality and non-BPS solutions,” *JHEP* **02** (2011) 074, [arXiv:1012.4803 \[hep-th\]](#).
- [83] I. Bena, N. Bobev, C. Ruef, and N. P. Warner, “Supertubes in Bubbling Backgrounds: Born-Infeld Meets Supergravity,” *JHEP* **07** (2009) 106, [arXiv:0812.2942 \[hep-th\]](#).

- [84] J. Breckenridge, R. C. Myers, A. Peet, and C. Vafa, “D-branes and spinning black holes,” *Phys.Lett.* **B391** (1997) 93–98, [arXiv:hep-th/9602065](#) [hep-th].
- [85] I. Bena, C.-W. Wang, and N. P. Warner, “Mergers and Typical Black Hole Microstates,” *JHEP* **11** (2006) 042, [arXiv:hep-th/0608217](#).
- [86] I. Bena, C.-W. Wang, and N. P. Warner, “Plumbing the Abyss: Black Ring Microstates,” *JHEP* **07** (2008) 019, [arXiv:0706.3786](#) [hep-th].
- [87] F. Denef, “Quantum quivers and Hall / hole halos,” *JHEP* **0210** (2002) 023, [arXiv:hep-th/0206072](#) [hep-th].
- [88] D. Mateos and P. K. Townsend, “Supertubes,” *Phys. Rev. Lett.* **87** (2001) 011602, [arXiv:hep-th/0103030](#).
- [89] D. Mateos, S. Ng, and P. K. Townsend, “Supercurves,” *Phys. Lett.* **B538** (2002) 366–374, [arXiv:hep-th/0204062](#) [hep-th].
- [90] R. Emparan, D. Mateos, and P. K. Townsend, “Supergravity supertubes,” *JHEP* **07** (2001) 011, [arXiv:hep-th/0106012](#).
- [91] D. Mateos, S. Ng, and P. K. Townsend, “Tachyons, supertubes and brane / anti-brane systems,” *JHEP* **03** (2002) 016, [arXiv:hep-th/0112054](#) [hep-th].
- [92] O. Lunin and S. D. Mathur, “AdS/CFT duality and the black hole information paradox,” *Nucl. Phys.* **B623** (2002) 342–394, [arXiv:hep-th/0109154](#).
- [93] P. A. Cano and T. Ortin, “All the supersymmetric solutions of ungauged $\mathcal{N} = (1, 0)$, $d = 6$ supergravity,” [arXiv:1804.04945](#) [hep-th].
- [94] H. Het Lam and S. Vandoren, “BPS solutions of six-dimensional $(1, 0)$ supergravity coupled to tensor multiplets,” *JHEP* **06** (2018) 021, [arXiv:1804.04681](#) [hep-th].
- [95] I. Bena, S. Giusto, M. Shigemori, and N. P. Warner, “Supersymmetric Solutions in Six Dimensions: A Linear Structure,” *JHEP* **1203** (2012) 084, [arXiv:1110.2781](#) [hep-th].
- [96] S. Giusto, L. Martucci, M. Petrini, and R. Russo, “6D microstate geometries from 10D structures,” *Nucl.Phys.* **B876** (2013) 509–555, [arXiv:1306.1745](#) [hep-th].
- [97] S. Giusto and R. Russo, “Superdescendants of the D1D5 CFT and their dual 3-charge geometries,” *JHEP* **1403** (2014) 007, [arXiv:1311.5536](#) [hep-th].
- [98] I. Bena, E. Martinec, D. Turton, and N. P. Warner, “Momentum Fractionation on Superstrata,” *JHEP* **05** (2016) 064, [arXiv:1601.05805](#) [hep-th].
- [99] I. Bena, S. Giusto, E. J. Martinec, R. Russo, M. Shigemori, D. Turton, and N. P. Warner, “Smooth horizonless geometries deep inside the black-hole regime,” *Phys. Rev. Lett.* **117** no. 20, (2016) 201601, [arXiv:1607.03908](#) [hep-th].
- [100] I. Bena, E. Martinec, D. Turton, and N. P. Warner, “M-theory Superstrata and the MSW String,” *JHEP* **06** (2017) 137, [arXiv:1703.10171](#) [hep-th].
- [101] I. Bena, S. Giusto, E. J. Martinec, R. Russo, M. Shigemori, D. Turton, and N. P. Warner, “Asymptotically-flat supergravity solutions deep inside the black-hole regime,” *JHEP* **02** (2018) 014, [arXiv:1711.10474](#) [hep-th].
- [102] S. Giusto and R. Russo, “Adding new hair to the 3-charge black ring,” *Class.Quant.Grav.* **29** (2012) 085006, [arXiv:1201.2585](#) [hep-th].
- [103] S. D. Mathur, A. Saxena, and Y. K. Srivastava, “Constructing ‘hair’ for the three charge hole,” *Nucl. Phys.* **B680** (2004) 415–449, [arXiv:hep-th/0311092](#).
- [104] M. Banados, C. Teitelboim, and J. Zanelli, “The Black hole in three-dimensional space-time,” *Phys. Rev. Lett.* **69** (1992) 1849–1851, [arXiv:hep-th/9204099](#).
- [105] O. Lunin and S. D. Mathur, “Metric of the multiply wound rotating string,” *Nucl. Phys.* **B610** (2001) 49–76, [arXiv:hep-th/0105136](#).

- [106] O. Lunin, J. M. Maldacena, and L. Maoz, “Gravity solutions for the D1-D5 system with angular momentum,” [arXiv:hep-th/0212210](#) [[hep-th](#)].
- [107] I. Kanitscheider, K. Skenderis, and M. Taylor, “Fuzzballs with internal excitations,” *JHEP* **06** (2007) 056, [arXiv:0704.0690](#) [[hep-th](#)].
- [108] S. D. Mathur and D. Turton, “Oscillating supertubes and neutral rotating black hole microstates,” *JHEP* **1404** (2014) 072, [arXiv:1310.1354](#) [[hep-th](#)].
- [109] I. Bena, S. F. Ross, and N. P. Warner, “Coiffured Black Rings,” *Class.Quant.Grav.* **31** (2014) 165015, [arXiv:1405.5217](#) [[hep-th](#)].
- [110] N. Seiberg and E. Witten, “The D1/D5 system and singular CFT,” *JHEP* **04** (1999) 017, [arXiv:hep-th/9903224](#).
- [111] F. Larsen and E. J. Martinec, “U(1) charges and moduli in the D1-D5 system,” *JHEP* **06** (1999) 019, [arXiv:hep-th/9905064](#).
- [112] S. D. Mathur and D. Turton, “Microstates at the boundary of AdS,” *JHEP* **05** (2012) 014, [arXiv:1112.6413](#) [[hep-th](#)].
- [113] J. R. David, G. Mandal, and S. R. Wadia, “Microscopic formulation of black holes in string theory,” *Phys. Rept.* **369** (2002) 549–686, [arXiv:hep-th/0203048](#).
- [114] I. Kanitscheider, K. Skenderis, and M. Taylor, “Holographic anatomy of fuzzballs,” *JHEP* **04** (2007) 023, [arXiv:hep-th/0611171](#).
- [115] M. Baggio, J. de Boer, and K. Papadodimas, “A non-renormalization theorem for chiral primary 3-point functions,” *JHEP* **07** (2012) 137, [arXiv:1203.1036](#) [[hep-th](#)].
- [116] I. Bena, D. Turton, R. Walker, and N. P. Warner, “Integrability and Black-Hole Microstate Geometries,” *JHEP* **11** (2017) 021, [arXiv:1709.01107](#) [[hep-th](#)].
- [117] A. Tyukov, R. Walker, and N. P. Warner, “Tidal Stresses and Energy Gaps in Microstate Geometries,” *JHEP* **02** (2018) 122, [arXiv:1710.09006](#) [[hep-th](#)].
- [118] I. Bena, E. J. Martinec, R. Walker, and N. P. Warner, “Early Scrambling and Capped BTZ Geometries,” [arXiv:1812.05110](#) [[hep-th](#)].
- [119] M. Cvetič and A. A. Tseytlin, “Nonextreme black holes from nonextreme intersecting M-branes,” *Nucl. Phys.* **B478** (1996) 181–198, [arXiv:hep-th/9606033](#) [[hep-th](#)].
- [120] J. Breckenridge, D. Lowe, R. C. Myers, A. Peet, A. Strominger, *et al.*, “Macroscopic and microscopic entropy of near extremal spinning black holes,” *Phys.Lett.* **B381** (1996) 423–426, [arXiv:hep-th/9603078](#) [[hep-th](#)].
- [121] M. Cvetič and D. Youm, “General Rotating Five Dimensional Black Holes of Toroidally Compactified Heterotic String,” *Nucl. Phys.* **B476** (1996) 118–132, [arXiv:hep-th/9603100](#).
- [122] M. Cvetič and F. Larsen, “Near horizon geometry of rotating black holes in five dimensions,” *Nucl. Phys.* **B531** (1998) 239–255, [arXiv:hep-th/9805097](#).
- [123] O. J. C. Dias, R. Emparan, and A. Maccarrone, “Microscopic theory of black hole superradiance,” *Phys. Rev.* **D77** (2008) 064018, [arXiv:0712.0791](#) [[hep-th](#)].
- [124] M. Guica and A. Strominger, “Microscopic Realization of the Kerr/CFT Correspondence,” *JHEP* **02** (2011) 010, [arXiv:1009.5039](#) [[hep-th](#)].
- [125] W. Song and A. Strominger, “D-brane Construction of the 5D NHEK Dual,” *JHEP* **07** (2012) 176, [arXiv:1105.0431](#) [[hep-th](#)].
- [126] S. El-Showk and M. Guica, “Kerr/CFT, dipole theories and nonrelativistic CFTs,” *JHEP* **12** (2012) 009, [arXiv:1108.6091](#) [[hep-th](#)].
- [127] I. Bena, M. Guica, and W. Song, “Un-twisting the NHEK with spectral flows,” *JHEP* **1303** (2013) 028, [arXiv:1203.4227](#) [[hep-th](#)].

- [128] I. Bredberg, T. Hartman, W. Song, and A. Strominger, “Black Hole Superradiance From Kerr/CFT,” *JHEP* **04** (2010) 019, [arXiv:0907.3477 \[hep-th\]](#).
- [129] D. Anninos, W. Li, M. Padi, W. Song, and A. Strominger, “Warped AdS(3) Black Holes,” *JHEP* **03** (2009) 130, [arXiv:0807.3040 \[hep-th\]](#).
- [130] D. Orlando and L. I. Uruchurtu, “Warped anti-de Sitter spaces from brane intersections in type II string theory,” *JHEP* **06** (2010) 049, [arXiv:1003.0712 \[hep-th\]](#).
- [131] W. Song and A. Strominger, “Warped AdS3/Dipole-CFT Duality,” *JHEP* **05** (2012) 120, [arXiv:1109.0544 \[hep-th\]](#).
- [132] K. Goldstein and S. Katmadas, “Almost BPS black holes,” *JHEP* **05** (2009) 058, [arXiv:0812.4183 \[hep-th\]](#).
- [133] I. Bena, S. Giusto, C. Ruef, and N. P. Warner, “Multi-Center non-BPS Black Holes - the Solution,” *JHEP* **11** (2009) 032, [arXiv:0908.2121 \[hep-th\]](#).
- [134] I. Bena, G. Dall’Agata, S. Giusto, C. Ruef, and N. P. Warner, “Non-BPS Black Rings and Black Holes in Taub-NUT,” *JHEP* **06** (2009) 015, [arXiv:0902.4526 \[hep-th\]](#).
- [135] O. Vasilakis and N. P. Warner, “Mind the Gap: Supersymmetry Breaking in Scaling, Microstate Geometries,” *JHEP* **1110** (2011) 006, [arXiv:1104.2641 \[hep-th\]](#).
- [136] G. Bossard and S. Katmadas, “A bubbling bolt,” *JHEP* **1407** (2014) 118, [arXiv:1405.4325 \[hep-th\]](#).
- [137] I. Bena, G. Bossard, S. Katmadas, and D. Turton, “Non-BPS multi-bubble microstate geometries,” *JHEP* **02** (2016) 073, [arXiv:1511.03669 \[hep-th\]](#).
- [138] I. Bena, G. Bossard, S. Katmadas, and D. Turton, “Bolting Multicenter Solutions,” *JHEP* **01** (2017) 127, [arXiv:1611.03500 \[hep-th\]](#).
- [139] I. Bena, N. Bobev, S. Giusto, C. Ruef, and N. P. Warner, “An Infinite-Dimensional Family of Black-Hole Microstate Geometries,” *JHEP* **1103** (2011) 022, [arXiv:1006.3497 \[hep-th\]](#).
- [140] J. Avila, P. F. Ramirez, and A. Ruiperez, “One Thousand and One Bubbles,” *JHEP* **01** (2018) 041, [arXiv:1709.03985 \[hep-th\]](#).
- [141] F. Denef and G. W. Moore, “Split states, entropy enigmas, holes and halos,” *JHEP* **11** (2011) 129, [arXiv:hep-th/0702146 \[hep-th\]](#).
- [142] J. Manschot, B. Pioline, and A. Sen, “Wall Crossing from Boltzmann Black Hole Halos,” *JHEP* **07** (2011) 059, [arXiv:1011.1258 \[hep-th\]](#).
- [143] A. Chowdhury, R. S. Garavuso, S. Mondal, and A. Sen, “BPS State Counting in N=8 Supersymmetric String Theory for Pure D-brane Configurations,” *JHEP* **10** (2014) 186, [arXiv:1405.0412 \[hep-th\]](#).
- [144] A. Chowdhury, R. S. Garavuso, S. Mondal, and A. Sen, “Do All BPS Black Hole Microstates Carry Zero Angular Momentum?,” *JHEP* **04** (2016) 082, [arXiv:1511.06978 \[hep-th\]](#).
- [145] D. Shih, A. Strominger, and X. Yin, “Counting dyons in N=8 string theory,” *JHEP* **06** (2006) 037, [arXiv:hep-th/0506151 \[hep-th\]](#).
- [146] R. Dijkgraaf, G. W. Moore, E. P. Verlinde, and H. L. Verlinde, “Elliptic genera of symmetric products and second quantized strings,” *Commun. Math. Phys.* **185** (1997) 197–209, [arXiv:hep-th/9608096 \[hep-th\]](#).
- [147] J. M. Maldacena, G. W. Moore, and A. Strominger, “Counting BPS black holes in toroidal Type II string theory,” [arXiv:hep-th/9903163 \[hep-th\]](#).
- [148] J. R. David, D. P. Jatkar, and A. Sen, “Dyon spectrum in generic N=4 supersymmetric Z(N) orbifolds,” *JHEP* **01** (2007) 016, [arXiv:hep-th/0609109 \[hep-th\]](#).
- [149] F. Denef, B. R. Greene, and M. Raugas, “Split attractor flows and the spectrum of BPS D-branes on the quintic,” *JHEP* **05** (2001) 012, [arXiv:hep-th/0101135 \[hep-th\]](#).

- [150] F. Denef, “(Dis)assembling special Lagrangians,” [arXiv:hep-th/0107152 \[hep-th\]](#).
- [151] B. Bates and F. Denef, “Exact solutions for supersymmetric stationary black hole composites,” *JHEP* **1111** (2011) 127, [arXiv:hep-th/0304094 \[hep-th\]](#).
- [152] V. Balasubramanian, E. G. Gimon, and T. S. Levi, “Four Dimensional Black Hole Microstates: From D-branes to Spacetime Foam,” *JHEP* **0801** (2008) 056, [arXiv:hep-th/0606118 \[hep-th\]](#).
- [153] I. Bena and N. P. Warner, “Resolving the Structure of Black Holes: Philosophizing with a Hammer,” [arXiv:1311.4538 \[hep-th\]](#).
- [154] M. Bianchi, J. F. Morales, L. Pieri, and N. Zinnato, “More on microstate geometries of 4d black holes,” *JHEP* **05** (2017) 147, [arXiv:1701.05520 \[hep-th\]](#).
- [155] A. Sen, “Arithmetic of Quantum Entropy Function,” *JHEP* **08** (2009) 068, [arXiv:0903.1477 \[hep-th\]](#).
- [156] A. Dabholkar, J. Gomes, S. Murthy, and A. Sen, “Supersymmetric Index from Black Hole Entropy,” *JHEP* **04** (2011) 034, [arXiv:1009.3226 \[hep-th\]](#).
- [157] M. R. Douglas and G. W. Moore, “D-branes, quivers, and ALE instantons,” [arXiv:hep-th/9603167 \[hep-th\]](#).
- [158] I. Bena, M. Berkooz, J. de Boer, S. El-Showk, and D. Van den Bleeken, “Scaling BPS Solutions and pure-Higgs States,” *JHEP* **1211** (2012) 171, [arXiv:1205.5023 \[hep-th\]](#).
- [159] A. Dabholkar, S. Murthy, and D. Zagier, “Quantum Black Holes, Wall Crossing, and Mock Modular Forms,” [arXiv:1208.4074 \[hep-th\]](#).
- [160] J. P. Gauntlett, J. B. Gutowski, C. M. Hull, S. Pakis, and H. S. Reall, “All supersymmetric solutions of minimal supergravity in five- dimensions,” *Class. Quant. Grav.* **20** (2003) 4587–4634, [arXiv:hep-th/0209114 \[hep-th\]](#).
- [161] I. Bena, S. F. Ross, and N. P. Warner, “On the Oscillation of Species,” *JHEP* **1409** (2014) 113, [arXiv:1312.3635 \[hep-th\]](#).
- [162] M. Guica, T. Hartman, W. Song, and A. Strominger, “The Kerr/CFT Correspondence,” *Phys. Rev.* **D80** (2009) 124008, [arXiv:0809.4266 \[hep-th\]](#).
- [163] S. Detournay, T. Hartman, and D. M. Hofman, “Warped Conformal Field Theory,” *Phys. Rev.* **D86** (2012) 124018, [arXiv:1210.0539 \[hep-th\]](#).
- [164] I. Bena, L. Heurtier, and A. Puhm, “AdS₃: the NHEK generation,” *JHEP* **05** (2016) 120, [arXiv:1510.08055 \[hep-th\]](#).
- [165] S. Giusto, O. Lunin, S. D. Mathur, and D. Turton, “D1-D5-P microstates at the cap,” *JHEP* **1302** (2013) 050, [arXiv:1211.0306 \[hep-th\]](#).
- [166] B. Chakrabarty, D. Turton, and A. Virmani, “Holographic description of non-supersymmetric orbifolded D1-D5-P solutions,” *JHEP* **11** (2015) 063, [arXiv:1508.01231 \[hep-th\]](#).
- [167] G. Bossard, S. Katmadas, and D. Turton, “Two Kissing Bolts,” [arXiv:1711.04784 \[hep-th\]](#).
- [168] J. E. McClintock, R. Shafee, R. Narayan, R. A. Remillard, S. W. Davis, *et al.*, “The Spin of the Near-Extreme Kerr Black Hole GRS 1915+105,” *Astrophys. J.* **652** (2006) 518–539, [arXiv:astro-ph/0606076 \[astro-ph\]](#).
- [169] J. M. Maldacena, A. Strominger, and E. Witten, “Black hole entropy in M-theory,” *JHEP* **12** (1997) 002, [arXiv:hep-th/9711053](#).
- [170] F. Benini, K. Hristov, and A. Zaffaroni, “Exact microstate counting for dyonic black holes in AdS₄,” *Phys. Lett.* **B771** (2017) 462–466, [arXiv:1608.07294 \[hep-th\]](#).
- [171] F. Azzurli, N. Bobev, P. M. Crichigno, V. S. Min, and A. Zaffaroni, “A universal counting of black hole microstates in AdS₄,” *JHEP* **02** (2018) 054, [arXiv:1707.04257 \[hep-th\]](#).

- [172] A. Strominger, “AdS(2) quantum gravity and string theory,” *JHEP* **01** (1999) 007, [arXiv:hep-th/9809027 \[hep-th\]](#).
- [173] R. K. Gupta and A. Sen, “Ads(3)/CFT(2) to Ads(2)/CFT(1),” *JHEP* **04** (2009) 034, [arXiv:0806.0053 \[hep-th\]](#).
- [174] V. Balasubramanian, J. de Boer, M. M. Sheikh-Jabbari, and J. Simon, “What is a chiral 2d CFT? And what does it have to do with extremal black holes?,” *JHEP* **02** (2010) 017, [arXiv:0906.3272 \[hep-th\]](#).
- [175] V. Balasubramanian, J. Parsons, and S. F. Ross, “States of a chiral 2d CFT,” *Class. Quant. Grav.* **28** (2011) 045004, [arXiv:1011.1803 \[hep-th\]](#).
- [176] A. Castro and W. Song, “Comments on AdS₂ Gravity,” [arXiv:1411.1948 \[hep-th\]](#).
- [177] M. Cvetič and I. Papadimitriou, “AdS₂ holographic dictionary,” *JHEP* **12** (2016) 008, [arXiv:1608.07018 \[hep-th\]](#). [Erratum: JHEP01,120(2017)].
- [178] J. M. Maldacena, J. Michelson, and A. Strominger, “Anti-de Sitter fragmentation,” *JHEP* **02** (1999) 011, [arXiv:hep-th/9812073 \[hep-th\]](#).
- [179] A. Almheiri and J. Polchinski, “Models of AdS₂ backreaction and holography,” *JHEP* **11** (2015) 014, [arXiv:1402.6334 \[hep-th\]](#).
- [180] A. Kitaev, “A simple model of quantum holography.” Talks at KITP, April 7, 2015 and May 27, 2015. <http://online.kitp.ucsb.edu/online/entangled15/kitaev>, <http://online.kitp.ucsb.edu/online/entangled15/kitaev2>.
- [181] J. Maldacena and D. Stanford, “Remarks on the Sachdev-Ye-Kitaev model,” *Phys. Rev.* **D94** no. 10, (2016) 106002, [arXiv:1604.07818 \[hep-th\]](#).
- [182] J. S. Cotler, G. Gur-Ari, M. Hanada, J. Polchinski, P. Saad, S. H. Shenker, D. Stanford, A. Streicher, and M. Tezuka, “Black Holes and Random Matrices,” *JHEP* **05** (2017) 118, [arXiv:1611.04650 \[hep-th\]](#).
- [183] V. Balasubramanian, B. Craps, B. Czech, and G. Srofi, “Echoes of chaos from string theory black holes,” *JHEP* **03** (2017) 154, [arXiv:1612.04334 \[hep-th\]](#).
- [184] A. Kitaev and S. J. Suh, “The soft mode in the Sachdev-Ye-Kitaev model and its gravity dual,” [arXiv:1711.08467 \[hep-th\]](#).
- [185] I. Bena, N. Bobev, and N. P. Warner, “Bubbles on Manifolds with a U(1) Isometry,” *JHEP* **08** (2007) 004, [arXiv:0705.3641 \[hep-th\]](#).
- [186] O. Lunin, “Bubbling geometries for AdS₂ × S²,” *JHEP* **10** (2015) 167, [arXiv:1507.06670 \[hep-th\]](#).
- [187] A. Sen, “State Operator Correspondence and Entanglement in AdS₂/CFT₁,” *Entropy* **13** (2011) 1305–1323, [arXiv:1101.4254 \[hep-th\]](#).
- [188] A. Castro, D. Grumiller, F. Larsen, and R. McNees, “Holographic Description of AdS(2) Black Holes,” *JHEP* **11** (2008) 052, [arXiv:0809.4264 \[hep-th\]](#).
- [189] C. Chamon, R. Jackiw, S.-Y. Pi, and L. Santos, “Conformal quantum mechanics as the CFT₁ dual to AdS₂,” *Phys. Lett.* **B701** (2011) 503–507, [arXiv:1106.0726 \[hep-th\]](#).
- [190] R. Jackiw and S. Y. Pi, “Conformal Blocks for the 4-Point Function in Conformal Quantum Mechanics,” *Phys. Rev.* **D86** (2012) 045017, [arXiv:1205.0443 \[hep-th\]](#). [Erratum: Phys. Rev. D86,089905(2012)].
- [191] J. M. Bardeen and G. T. Horowitz, “The Extreme Kerr throat geometry: A Vacuum analog of AdS(2) × S²,” *Phys. Rev.* **D60** (1999) 104030, [arXiv:hep-th/9905099 \[hep-th\]](#).
- [192] A. Sen, “Black Hole Entropy Function, Attractors and Precision Counting of Microstates,” *Gen. Rel. Grav.* **40** (2008) 2249–2431, [arXiv:0708.1270 \[hep-th\]](#).

- [193] H. K. Kunduri and J. Lucietti, “Classification of near-horizon geometries of extremal black holes,” *Living Rev. Rel.* **16** (2013) 8, [arXiv:1306.2517 \[hep-th\]](#).
- [194] A. Bombini, A. Galliani, S. Giusto, E. Moscato, and R. Russo, “Unitary 4-point correlators from classical geometries,” *Eur. Phys. J. C* **78** no. 1, (2018) 8, [arXiv:1710.06820 \[hep-th\]](#).
- [195] S. Raju and P. Shrivastava, “A Critique of the Fuzzball Program,” [arXiv:1804.10616 \[hep-th\]](#).
- [196] K. Skenderis, “Lecture notes on holographic renormalization,” *Class. Quant. Grav.* **19** (2002) 5849–5876, [arXiv:hep-th/0209067 \[hep-th\]](#).
- [197] D. T. Son and A. O. Starinets, “Minkowski space correlators in AdS / CFT correspondence: Recipe and applications,” *JHEP* **09** (2002) 042, [arXiv:hep-th/0205051 \[hep-th\]](#).
- [198] K. Skenderis and B. C. van Rees, “Real-time gauge/gravity duality,” *Phys. Rev. Lett.* **101** (2008) 081601, [arXiv:0805.0150 \[hep-th\]](#).
- [199] K. Skenderis and B. C. van Rees, “Real-time gauge/gravity duality: Prescription, Renormalization and Examples,” *JHEP* **05** (2009) 085, [arXiv:0812.2909 \[hep-th\]](#).
- [200] B. C. van Rees, “Real-time gauge/gravity duality and ingoing boundary conditions,” *Nucl. Phys. Proc. Suppl.* **192-193** (2009) 193–196, [arXiv:0902.4010 \[hep-th\]](#).
- [201] A. Galliani, S. Giusto, E. Moscato, and R. Russo, “Correlators at large c without information loss,” *JHEP* **09** (2016) 065, [arXiv:1606.01119 \[hep-th\]](#).
- [202] A. Galliani, S. Giusto, and R. Russo, “Holographic 4-point correlators with heavy states,” *JHEP* **10** (2017) 040, [arXiv:1705.09250 \[hep-th\]](#).
- [203] A. Bombini and A. Galliani, “AdS₃ four-point functions from $\frac{1}{8}$ -BPS states,” [arXiv:1904.02656 \[hep-th\]](#).
- [204] J. Tian, J. Hou, and B. Chen, “Holographic Correlators on Integrable Superstrata,” [arXiv:1904.04532 \[hep-th\]](#).

Titre: Les micro-états de trous noirs en Théorie des Cordes: noire est la couleur, régulières sont les géométries?

Mots clés: Théorie des Cordes, Trous noirs, AdS/CFT, Supergravité, Fuzzballs.

Résumé: Les trous noirs sont produits par effondrement gravitationnel d'étoiles supermassives et contiennent en leur centre une singularité de l'espace-temps habillée d'un horizon auquel rien ne peut s'échapper. Ils se situent la frontière théorique commune entre la Relativité Générale et la Mécanique Quantique, ce qui en fait le principal laboratoire théorique et expérimental pour tester les théories quantiques de la gravité comme la Théorie des Cordes.

L'entropie d'un trou noir est énorme, de l'ordre de sa masse au carré. Comme tout objet entropique, une description microscopique en termes de dégénérescence d'états devrait exister. De plus, le trou noir s'évapore par rayonnement d'Hawking et l'information l'intérieur semble perdue, ce qui compromet la principe d'unitarité, pierre angulaire de la Mécanique Quantique.

Par conséquent, la Théorie des Cordes doit fournir les degrés de liberté nécessaires pour décrire la nature de micro-état de trous noirs, elle doit également trouver un mécanisme résolvant la singularité et le paradoxe de la perte d'information.

Cette thèse porte sur la physique des trous noirs travers le "fuzzball proposal" et le "microstate geometry program". La majeure partie de la discussion se déroulera dans la limite de basse énergie de la Théorie des Cordes, c'est-à-dire

en Supergravité. Le "proposal" stipule qu'il existe " e^S " solutions non singulières sans horizon qui ressemblent un trou noir large distance mais qui diffèrent proximité de l'horizon. Sur la base de cette affirmation, la solution de trou noir classique correspond la description statistique d'un système de solutions qui ont la même géométrie que le trou noir l'extérieur de l'horizon, mais qui se terminent par des géométries régulières, dites "fuzzy". La proposition soulève plusieurs questions : Comment la singularité est-elle résolue ? De telles géométries peuvent-elles être construites en Supergravité ? Comment l'information s'échappe-t-elle de l'ensemble des micro-états ?

La thèse est décomposée en trois parties. La première partie présente les bases et donne un aperçu du "microstate geometry program". La deuxième partie regroupe cinq travaux qui se consacrent construire de larges familles de micro-états de trous noirs supersymétriques ou non supersymétriques. La dernière partie passe en revue deux travaux. L'un d'eux étudie le processus de diffusion dans les micro-états. Cela permet d'élucider comment le principe d'unicité est restaurée et comment l'information s'échappe des micro-états. La seconde traite du rôle des micro-états dans le contexte de la correspondance AdS_2/CFT_1 et donne l'ébauche d'une preuve pour le "fuzzball proposal".

Title: Black-hole microstates in String Theory: black is the color but smooth are the geometries?

Keywords: String Theory, Black holes, AdS/CFT, Supergravity, Fuzzballs.

Abstract: Black holes are produced by gravitational collapse of supermassive stars and consist of a spacetime singularity dressed by a horizon from which nothing can escape. They lie at the common theoretical border between General Relativity and Quantum Mechanics, making them the main theoretical and experimental laboratory for testing quantum theories of gravity as String theory.

The entropy of a black hole is huge, of the order of its mass squared. As any entropic object, a microscopic description in terms of large degeneracy of states should exist. Moreover, black hole evaporates through thermal Hawking's radiation and the information in the interior seems lost, that compromises the unitary principle, a cornerstone of Quantum Mechanics.

Therefore, String Theory must provide the degrees of freedom necessary to describe the microstate nature of black holes, it must also find a mechanism resolving the singularity and the information loss paradox.

This thesis addresses black-hole physics through the lens of the fuzzball proposal and the microstate geometry program. The major part of the discussion will be conducted in the low-energy limit of String Theory, that is in Supergravity. The proposal states that there exist " e^S " horizonless non-singular solutions that resemble a black hole at large distance but differ in the vicinity of the horizon.

Based on this statement, the classical black-hole solution corresponds to the average description of a system of solutions which match the black-hole geometry outside the horizon but cap off as "fuzzy" smooth geometries in the infrared. The proposal leads to several questions: How is the singularity resolved? Can " e^S " such geometries be built in Supergravity? How does the information escape from the ensemble of microstates?

The thesis is decomposed in three parts. The first part introduces the basic materials and gives a review of the microstate geometry program. The second part gathers five works that all consist in constructing large classes of smooth horizonless microstate geometries of supersymmetric or non-supersymmetric black holes. The last part review two works. One is investigating the scattering process in microstate geometries. This helps to elucidate how unitarity is restored and how information escapes from black-hole backgrounds. The second one addresses the role of microstate geometries in the context of the AdS_2/CFT_1 correspondence and gives a beginning of proof for the fuzzball proposal.

